



HAL
open science

Behavioral and pharmacological enhancement of neural plasticity in the adult visual cortex

Maëva Gacoin

► **To cite this version:**

Maëva Gacoin. Behavioral and pharmacological enhancement of neural plasticity in the adult visual cortex. Neuroscience. Université Claude Bernard - Lyon I, 2023. English. NNT : 2023LYO10015 . tel-04480271

HAL Id: tel-04480271

<https://theses.hal.science/tel-04480271>

Submitted on 27 Feb 2024

HAL is a multi-disciplinary open access archive for the deposit and dissemination of scientific research documents, whether they are published or not. The documents may come from teaching and research institutions in France or abroad, or from public or private research centers.

L'archive ouverte pluridisciplinaire **HAL**, est destinée au dépôt et à la diffusion de documents scientifiques de niveau recherche, publiés ou non, émanant des établissements d'enseignement et de recherche français ou étrangers, des laboratoires publics ou privés.



THESE de DOCTORAT DE L'UNIVERSITE LYON 1

**Ecole Doctorale : ED 476-NSCo
Neurosciences et Cognition**

Discipline: Neurosciences

Soutenue publiquement le 06/02/2023, par :
Maëva Gacoïn

**Amélioration comportementale et pharmacologique de la
plasticité neuronale dans le cortex visuel adulte**

--

**Behavioral and pharmacological enhancement of neural
plasticity in the adult visual cortex**

Devant le jury composé de :

Procyk, Emmanuel, D.R., SBRI, Lyon

Président

Cottureau, Benoît, D.R., CERCO, Toulouse

Rapporteur

Wardak, Claire, C.R., IBrain, Tours

Rapporteuse

Cristofori, Irene, Maître de conférences, ISCMJ/ UCBL, Lyon

Examinatrice

Pouget, Pierre, C.R., ICM, Paris

Examineur

Procyk, Emmanuel, D.R., SBRI, Lyon

Examineur

Ben Hamed, Suliann, D.R., ISCMJ, Lyon

Directrice de thèse

Desmurget, Michel, D.R., ISCMJ, Lyon

Co-directeur de thèse

Université Claude Bernard – LYON 1

| | |
|-----------------------------------------------------------------|------------------------|
| Président de l'Université | M. Frédéric FLEURY |
| Président du Conseil Académique | M. Hamda BEN HADID |
| Vice-Président du Conseil d'Administration | M. Didier REVEL |
| Vice-Président du Conseil des Etudes et de la Vie Universitaire | M. Philippe CHEVALLIER |
| Vice-Président de la Commission de Recherche | M. Petru MIRONESCU |
| Directeur Général des Services | M. Pierre ROLLAND |

COMPOSANTES SANTE

| | |
|---------------------------------------------------------------------|----------------------------------------|
| Département de Formation et Centre de Recherche en Biologie Humaine | Directrice : Mme Anne-Marie SCHOTT |
| Faculté d'Odontologie | Doyenne : Mme Dominique SEUX |
| Faculté de Médecine et Maïeutique Lyon Sud - Charles Mérieux | Doyenne : Mme Carole BURILLON |
| Faculté de Médecine Lyon-Est | Doyen : M. Gilles RODE |
| Institut des Sciences et Techniques de la Réadaptation (ISTR) | Directeur : M. Xavier PERROT |
| Institut des Sciences Pharmaceutiques et Biologiques (ISBP) | Directrice : Mme Christine VINCIGUERRA |

COMPOSANTES & DEPARTEMENTS DE SCIENCES & TECHNOLOGIE

| | |
|-----------------------------------------------------------------------------|---------------------------------------------------|
| Département Génie Electrique et des Procédés (GEP) | Directrice : Mme Rosaria FERRIGNO |
| Département Informatique | Directeur : M. Behzad SHARIAT |
| Département Mécanique | Directeur M. Marc BUFFAT |
| Ecole Supérieure de Chimie, Physique, Electronique (CPE Lyon) | Directeur : Gérard PIGNAULT |
| Institut de Science Financière et d'Assurances (ISFA) | Directeur : M. Nicolas LEBOISNE |
| Institut National du Professorat et de l'Education | Administrateur Provisoire : M. Pierre CHAREYRON |
| Institut Universitaire de Technologie de Lyon 1 | Directeur : M. Christophe VITON |
| Observatoire de Lyon | Directrice : Mme Isabelle DANIEL |
| Polytechnique Lyon | Directeur : Emmanuel PERRIN |
| UFR Biosciences | Administratrice provisoire : Mme Kathrin GIESELER |
| UFR des Sciences et Techniques des Activités Physiques et Sportives (STAPS) | Directeur : M. Yannick VANPOULLE |
| UFR Faculté des Sciences | Directeur : M. Bruno ANDRIOLETTI |

Remerciements

Je souhaite tout d'abord exprimer ma gratitude aux membres du jury évaluateurs de mon travail de thèse, pour leur temps et leur précieuse évaluation. A titre individuels, je remercie Claire Wardak et Benoît Cotterau d'avoir accepté d'en être les rapporteurs et Irene Cristofori, Pierre Pouget et Emmanuel Procyk d'avoir accepté d'en être les examinateurs.

Merci à toi Suliann, en premier lieu de m'avoir accueillie au sein de ton équipe pour travailler sur ce projet passionnant, d'avoir accepté de me superviser et de m'avoir fait confiance. Je loue tout particulièrement ton expertise à laquelle j'aspire, ta patience et ton enthousiasme scientifique. Enfin je te suis chaleureusement reconnaissante pour ton encadrement et ton mentorat ainsi que pour nos échanges, tant sur le plan scientifique qu'humain.

Merci au membres évaluateurs de mon comité de suivi de thèse, Jean-Baptiste Durand et Emmanuel Procyk, pour vos retours tout au long de ma thèse et pour vos conseils bienveillants.

J'adresse également mes chaleureux remerciements à Mathilda, ma binôme de labo. J'ai en effet eu la chance d'évoluer avec toi dès le début de ma thèse et je te suis très reconnaissante pour le temps passé à me former au travail avec les animaux, les acquisitions de données, les analyses... tu as eu un rôle-clef dans ce travail mais aussi dans mon évolution scientifique. Merci pour ton soutien, ces galères partagées, ces moments de joies et ces discussions scientifiques (et moins scientifiques), c'est un honneur de travailler avec une chercheuse telle que toi.

Je tiens à remercier les celles et ceux qui m'ont apporté une précieuse assistance technique tout au long de ma thèse. Un immense merci à Franck Lamberton et Danièle Ibarrola (CERMEP) pour leur assistance et leur professionnalisme sans faille qui m'ont permis de mener à bien les acquisitions IRM et dont je garde bonnes notes des conseils prodigués. Toujours à propos d'IRM, un grand merci à Quentin pour tes réparations et ta disponibilité sur l'antenne IRM. Je remercie également le personnel animalier, Fidji, Laurence, Marion, Marylou et Chloé pour leur précieux travail. Merci également à Emilie Ecuier pour l'assistance vétérinaire. Merci à l'équipe informatique Johan, Sylvain, Marco et Thomas d'assurer le bon fonctionnement matériel. Enfin, un grand merci à toi Serge pour l'assistance technique et la mise en place des tâches en entraînement et à l'IRM.

Je remercie également les membres de l'équipe passés et présents. Merci à ceux avec lesquels j'ai eu l'opportunité de collaborer directement, dont Simon, pour ton assistance aux analyses IRM et tes conseils ; Mojtaba for your eagerness to learn and your joyfulness, I know Sam and Scooby are in good hands with you ; Nassim, pour ton aide sur les acquisitions du projet comportemental sur l'humain et ton sérieux ; Julian, pour tes conseils techniques et ta gentillesse; Maxime, que j'ai pu former aux acquisitions IRM et qui m'y a bien aidée ; et ceux qui se sont succédés dans notre bureau place, Fabio « c'est pas facile », Yann pour l'aide avec l'imagerie de diffusion et sa formidable pédagogie, Valentin et Michael, bien que brièvement, mais aussi les autres membres de l'équipe pour les échanges scientifiques et de sympathie, Axel pour partager nos histoires de singes et me motiver à aller faire de l'escalade, Slimane dont la gentillesse qui n'a d'égale que son brio, Wei-An, Souhir, Achille, Clément, Sameh, Carine, Fardin, Celia, Camilla, Maryam, Gwendoline, ... Un merci tout particulier à Justine d'avoir enclenché ce projet de façon si bien organisée, de m'avoir assistée à distance de bon cœur et d'avoir pris part à la correction de ce manuscrit.

Merci aux membres de l'ISC, passés et présents qui rendent la vie quotidienne plus agréable. Merci tout d'abord aux directeurs de laboratoire, Angela Sirigu lorsque je suis arrivée, et Pier Francesco Ferrari. Merci à Sandra pour son aide technique lors de la préparation de la fluoxétine, mais aussi Holly et Alice qui m'ont permis de travailler ensemble dans la bonne humeur, Rossella, pour m'avoir cuisiné la meilleure amatriciana, Vale, pour tes encouragements au boulot et à l'escalade Marie (pauses thé), Nico, pour ta bonne humeur, Sofie, que je suis déjà triste de quitter, mais aussi, Rémi J, Rémi P., Tadeusz, Nico, Seb, Felipe, Jacopo, Sameer, Maciek, Giulia, Sanaz et toutes les belles personnes que j'ai eu la chance d'y croiser, même pour le temps d'un baby-foot.

Je remercie également mes amis du même quartier ou de l'autre bout de l'Europe qui m'ont soutenue et encouragée tout au long de ma thèse. Merci à Ambre, Claire (et Valentin et Elisabeth), Max, Valention pour leur soutien inconditionnel, mais aussi Elo, Mo (et Anthony et Hector) et Ju, Aurélien qui refuse de se faire oublier pour mon plus grand bien, les copains Gphy Julien, Quentin, Maud, Adrien, Guillaume, Marion, mais aussi, Benoît et Sylvanie, Irina, Vincent (et Calixte et Iris), Philippe, ...

Je ne saurais exprimer suffisamment toute ma reconnaissance et ma gratitude à ma famille qui m'a donné beaucoup d'amour et de soutiens, bien au-delà de ma thèse et malgré la distance. Merci à vous tous !

Je remercie évidemment Etienne, mon co-équipier au quotidien, pour la douceur et la joie qu'il a su y semer.

J'exprime enfin ma plus chaleureusement reconnaissance aux primates qui seront le moins à même de me lire mais qui sont pourtant présents, entre les lignes, tout au long de ce manuscrit. Au-delà de l'aspect scientifique, leur personnalité (l'un farceur et l'autre sérieux), nos rencontres, ce qu'ils m'ont appris, tout est là. Sam, Scooby merci pour tout.

Résumé

Au cours de son développement précoce, sur une courte période de temps appelée période critique, les structures et les fonctions du cerveau sont très sensibles aux entrées sensorielles. Cette sensibilité est soutenue par un état de plasticité accrue et résulte d'une forte excitabilité du cerveau. Une fois la période critique terminée, en raison d'une inhibition massive destinée à équilibrer l'hyperexcitabilité, et plus le cerveau mûrit jusqu'à l'âge adulte, cette plasticité s'affaiblit. Un certain degré de plasticité subsiste après cette période critique initiale et joue un rôle essentiel dans l'apprentissage et la réparation du cerveau. Cependant, l'efficacité plus faible de la plasticité dans le cerveau adulte peut entraver la récupération, comme dans le cas de l'amblyopie adulte. Des études antérieures sur des rongeurs ont démontré qu'une classe spécifique de neuromodulateurs peut augmenter l'apprentissage perceptif et ainsi améliorer la plasticité visuelle. Dans la présente thèse, nous cherchons à comprendre les mécanismes neuronaux sous-jacents de la plasticité visuelle lorsque l'apprentissage perceptif est couplé à un neuromodulateur, chez des primates non humains adultes. Pour caractériser un tel effet, nous avons utilisé l'imagerie par résonance magnétique fonctionnelle (IRMf), la pharmacologie et des observations comportementales. Nous avons ainsi conçu une étude longitudinale pour caractériser l'état basal du cerveau (point temporel T1), puis ses changements en termes de connectivité fonctionnelle et de schémas d'activation après une manipulation comportementale descendante, c'est-à-dire une manipulation de récompense biaisant la prise de décision en faveur de parties spécifiques du champ visuel (point temporel 2). Enfin, nous avons caractérisé les changements survenant lorsque cette manipulation comportementale basée sur la récompense était couplée à une administration de neuromodulateurs (point temporel 3). Afin d'améliorer la plasticité, ce neuromodulateur doit rétablir l'excitabilité neuronale. Nous avons donc émis l'hypothèse qu'un inhibiteur sélectif de la recapture de la sérotonine (ISRS), et plus particulièrement la fluoxétine, qui diminue les niveaux de GABA dans le cerveau, entraînant ainsi une diminution globale (bien que complexe) de l'inhibition corticale, contribuerait à renforcer la plasticité dans le cerveau adulte. L'apprentissage perceptif en présence de fluoxétine a produit des signatures comportementales et neurales marquées de l'apprentissage, indiquant ainsi une plasticité accrue. Dans une première étude (comportementale), impliquant trois tâches visuelles distinctes couplant des mécanismes top-down et bottom-up, nous avons démontré que sous fluoxétine la vision de la luminance est dégradée ainsi que la résolution spatiale visuelle, alors que la sensibilité à la récompense augmente. Dans une deuxième étude (IRMf), nous avons examiné les changements de connectivité fonctionnelle du cerveau après un apprentissage extensif de nouvelles contingences spatiales basé sur la récompense et avec l'impact de la fluoxétine. Nous mettons en évidence que la décorrélation générale entre les voies visuelles ventrales et dorsales observées après un apprentissage perceptif basé sur la récompense est renforcée en présence de l'ISRS. Nous proposons que ces changements corticaux sous-tendent la sensibilité accrue aux emplacements spatiaux récompensés observée au niveau comportemental et contribuent à la maximisation du résultat comportemental. Notre

troisième et dernière étude (IRMf), soutient davantage ce point de vue, en montrant que si les schémas d'activations dans V2 suivent la carte de priorité spatiale construite par l'apprentissage basé sur la récompense, ces effets sont fortement renforcés par la fluoxétine. De manière assez remarquable, ces changements sont spécifiques aux représentations corticales du champ visuel inférieur. Nous montrons en outre que la fluoxétine dégrade le codage de la résolution spatiale dans le cortex visuel, ce qui appuie nos observations comportementales de l'étude 1.

Dans l'ensemble, nous décrivons les mécanismes neuronaux et de réseau par lesquels la fluoxétine contribue à la réintégration de la plasticité corticale visuelle dans le cerveau adulte et leurs corrélats comportementaux. Ceci a des implications majeures dans le domaine clinique dans le contexte de la récupération sensorielle et cognitive ou de l'apprentissage.

Mots-clés : Plasticité visuelle à l'âge adulte, fluoxétine, IRMf, comportement, récompense, carte de priorité spatiale, macaques rhésus.

Abstract

During its early development, on a short time-window called the critical period, the brain structures and functions are very sensitive to sensory inputs. This sensitivity is supported by a state of enhanced plasticity and results from a high excitability of the brain. Once the critical period closes, due to a massive inhibition to balance the hyper-excitability, and the more the brain matures into adulthood, this plasticity becomes weaker. Some degree of plasticity remains after this initial critical period and plays a critical role in learning and brain repair. However, the weaker efficiency of plasticity in the adult brain can hinder recovery such as in adult amblyopia. Previous studies on rodents have demonstrated that a specific class of neuromodulators can increase perceptual learning and thus enhance visual plasticity. In the present thesis, we seek to understand the underlying neural mechanisms of visual plasticity when the perceptual learning is coupled with a neuromodulator, in adult non-human primates. To characterize such an effect, we used functional magnetic resonance imaging (fMRI), pharmacology and behavioral observations. We thus designed a longitudinal study to characterize the brain basal state (time point T1), then its changes in functional connectivity and activation patterns after a behavioral top-down manipulation, i.e. a reward manipulation biasing decision making in favor of specific parts of the visual field (time point 2). Finally, we characterized the changes occurring when this behavioral reward-based manipulation was coupled with a neuromodulator intake (time point 3). In order to enhance a plasticity, this neuromodulator has to re-instate neural excitability. We thus hypothesized that a selective serotonin reuptake inhibitor (SSRI), and specifically fluoxetine, which decreases GABA levels in the brain, hence resulting in a global (though complex) decrease of cortical inhibition, would contribute to enhance plasticity in the adult brain. Perceptual learning in the presence of fluoxetine produced marked behavioral and neural signatures of learning, thus indicating an enhanced plasticity. In a first study (behavioral), involving three distinct visual tasks coupling top-down and bottom-up mechanisms, we demonstrated that under fluoxetine luminance vision is degraded as well visual spatial resolution, while sensitivity to reward increases. In a second study (fMRI), we investigated the whole brain functional connectivity changes following an extensive reward-based learning of novel spatial contingencies and with the impact of fluoxetine. We highlight that the general decorrelation between the ventral and dorsal visual pathways observed following reward-based perceptual learning is further enhanced in the presence of the SSRI. We propose that these cortical changes underlie the enhanced sensitivity to rewarded spatial locations observed at the behavioral level and contribute to the maximization of behavioral outcome. Our third and last study (fMRI), further supports this view, by showing that while activations patterns in V2 track the spatial priority map constructed through the reward-based learning, these effects are greatly enhanced by fluoxetine. Quite remarkably, these changes are specific to the lower visual field cortical representations. We additionally show that fluoxetine degrades spatial resolution coding in the visual cortex, supporting our behavioral observations in study 1.

Overall, we describe the neural and network mechanisms through which fluoxetine contribute to the reinstatement of visual cortical plasticity in the adult brain and their behavioral correlates. This has major implications in the clinical field in the context of sensory and cognitive recovery or learning.

Keywords: Visual plasticity in adulthood, fluoxetine, fMRI, behavior, reward, spatial priority map, rhesus macaques.

Preface

The present Ph.D. thesis manuscript is an account of my research work on the topic of the behavioral and pharmacological enhancement of plasticity in the adult macaque visual cortex, that I had the opportunity to conduct at the Institut des Sciences Cognitives – Marc Jeannerod, in the team *Neural basis of spatial cognition and action*, under the supervision of its leader, Suliann Ben Hamed. To that extent, I conducted a longitudinal protocol involving fMRI methods.

In a first part of the manuscript, I define the topic and set the frames of our studies in an **Introduction**. The **Chapter I**, aims at characterizing behaviorally the effect of pharmacology intake in the visual system through three tasks. The **Chapter II** lays on findings of the first chapter and focuses more particularly on the functional connectivity of the brain to understand the underlying neural bases of behavioral and pharmacological manipulations of the visual system. The **Chapter III** focuses on the visual area as we here study the retinotopy evolution across the longitudinal protocol and the activity of this area according to our manipulations. Then, I discuss these results and present the perspectives and ongoing projects in link with this thesis work in a **Discussion & perspectives** part. In a last part, I present **three appendices** summarizing the ongoing advance of research project I had the opportunity to be a contributor of. The first one is a project dedicated on multisensory integration in the macaque brain in a social context leading to three papers. The second is a longitudinal study of the early social adversity effect in the juvenile macaque. The third one is a methodological study on diffusion MRI technique.

Even though I am the main contributor of the 3 presented studies, from the design to the writing, passing-by data acquisitions and analyses, I was only able to accomplish my work thanks to the guidance I received, the teamwork and my fellow collaborators. Thus, the pronoun *we* is used.

Abbreviation list

%SC: Percent signal change

5-HT: 5-hydroxytryptamine

ACC: Anterior cingulate cortex

ADHD: Attention-deficit-hyperactivity-disorder

BOLD: Blood oxygenation level dependent

Ca²⁺: Calcium

D4: 4-quadrants peripheral detection task

D8: 8-quadrants peripheral detection task

DLPFC: Dorsolateral prefrontal cortex

E/I: Excitation/Inhibition balance

FC: Functional connectivity

FEF: Frontal eye fields

fMRI: Functional magnetic resonance imaging

FX: Fixed effect

GABA: γ -Aminobutyric acid

IPS: Intraparietal sulcus

IT: Inferior temporal cortex

MION: Monocrystalline iron-oxide nanoparticles

MT: Middle temporal area

LIP: Lateral intraparietal sulcus

LTP: Long-term potentiation

LDP: Long-term depression

LS: Lateral sulcus

OD: Ocular dominance

OFC: Orbitofrontal cortex

PCC: Posterior cingulate cortex

RDX: Random effect

ROI: Region of interest

RT: Reaction time

SERT: Serotonin transporter

SPL: Superior parietal cortex

SSRI: Selective serotonin reuptake inhibitor

T1-3: Time-point 1-3

V1 : Visual area V1; primary visual area

V2 : Visual area V2

V3 : Visual area V3

V4 : Visual area V4

VL PFC: Ventrolateral prefrontal cortex

List of publications

ARTICLES

Published

Journal articles related to the thesis:

1. **Socially meaningful visual context either enhances or inhibits vocalization processing in the macaque brain.** (Appendix n°1, pp. 205-221)

Mathilda Froesel, **Maëva Gacoïn**, Simon Clavagnier, Marc Hauser, Quentin Goudard, Suliann Ben Hamed. (2022)

Nature communications, <https://doi.org/10.1038/s41467-022-32512-9>

Contributions: Stimuli preparation, data acquisitions.

2. **Automated video-based heartrate tracking.** (Appendix n°1, p. 193-203)

Mathilda Froesel, Quentin Goudard, Marc Hauser, **Maëva Gacoïn**, & Suliann Ben Hamed. (2020)

Scientific reports, <https://doi.org/10.1038/s41598-020-74954-5>

Contributions: Data acquisitions.

3. **An evolutionary gap in primate default mode network organization.**

Clément M. Garin, Yuki Hori, Stefan Everling, Christopher T. Whitlow, Finnegan J Calabro, Beatriz Luna, Mathilda Froesel, **Maëva Gacoïn**, Suliann Ben Hamed, Marc Dhenain, Christos Constantinidis (2022).

Cell reports, <https://doi.org/10.1016/j.celrep.2022.110669>

Contributions: Data acquisitions, data pre-processing.

4. **Toward next-generation primate neuroscience: A collaboration-based strategic plan for integrative neuroimaging.**

Michael Milham, Chris Petkov, Pascal Belin, Suliann Ben Hamed, Henry Evrard, ..., **Maëva Gacoïn**, ... & Michael Ortiz-Rios. (2022)

Neuron, <https://doi.org/10.1016/j.neuron.2021.10.015>

Contributions: Data acquisitions, data pre-processing.

External laboratories collaboration:

5. **Adrenergic prolongation of action potential duration in rainbow trout myocardium via inhibition of the delayed rectifier potassium current.**

Denis V Abramochkin, T Eliot Haworth, Vladislav S Kuzmin, Irina Dzhumaniiazova, Ksenia B Pustovit, **Maëva Gacoïn**, Holly A Shiels. (2022)

Comparative Biochemistry and Physiology Part A: Molecular & Integrative Physiology, <https://doi.org/10.1016/j.cbpa.2022.111161>

Contributions: Data acquisitions.

Under revision

6. **Fluoxetine increases luminance perceptual thresholds while enhancing motivation and reward sensitivity** (Chapter 1, study n°1, pp. 63-100)

Maëva Gacoin, Suliann Ben Hamed. (2022)

bioRxiv, <https://doi.org/10.1101/2022.11.11.516168>

Contributions: Study concept and design, stimuli preparation, methodology, animal training, data acquisitions, investigation, writing – original draft, writing – review & editing.

7. **Macaque amygdala, claustrum and pulvinar support the cross-modal association of social audiovisual stimuli based on meaning.** (Appendix n°1, pp. 223-251)

Mathilda Froesel, Maëva Gacoin, Simon Clavagnier, Marc Hauser, Quentin Goudard, Suliann Ben Hamed. (2022)

bioRxiv, <https://doi.org/10.1101/2022.09.28.509981>

Contributions: Stimuli preparation, data acquisitions.

In preparation

8. **Effect of Fluoxetine and behavioral training on resting-state connectivity of the macaque visual cortex with the rest of the brain.** (Chapter 2, study n°2, pp. 107-144)

Maëva Gacoin, Mathilda Froesel, Simon Clavagnier, Maxime Gaudet-Trafit, Suliann Ben Hamed

Contributions: Study concept and design, stimuli preparation, methodology, animal training, data acquisitions, investigation, writing – original draft.

9. **Effects of Fluoxetine and behavioral training on the retinotopic organization of the macaque visual cortex.** (Chapter 3, study n°3, pp. 147-171)

Maëva Gacoin, Mathilda Froesel, Simon Clavagnier, Justine Cléry, Maxime Gaudet-Trafit, Suliann Ben Hamed

Contributions: Study concept and design, stimuli preparation, methodology, animal training, data acquisitions, investigation, writing – original draft.

10. **Effect of a transient visual scotoma on visual perception and top-down attentional control in adults humans.**

Maëva Gacoin, Nassim Daghghi, Simon Clavagnier and Suliann Ben Hamed

Contributions: Study concept and design, stimuli preparation, methodology, data acquisitions, investigation.

11. **Developmental changes of pulvino-cortical connectivity in macaques**

Mathilda Froesel*, Simon Clavagnier*, Holly Rayson, **Maëva Gacoin**, Alice Massera, Pier Francesco Ferrari, & Suliann Ben Hamed

Contributions: Data acquisitions.

12. **Maturation of defensive peripersonal space cortical functional connectivity following early social adversity.**

Mathilda Froesel, Simon Clavagnier, Holly Rayson, **Maëva Gacoin**, Alice Massera, Pier Francesco Ferrari, & Suliann Ben Hamed.

Contributions: Data acquisitions.

13. **High Definition Triggered Three-Dimensional Diffusion MRI of Anesthetized Rhesus Macaque Brain** (Appendix n°3, pp. 258-292)

Yann Bihan-Poudec, Slimane Tounekti, Thomas Troalen, Mathilda Froesel, Franck Lambertson, **Maëva Gacoin**, Nathalie Richard, Suliann Ben Hamed, Bassem Hiba

Contributions: Data acquisitions.

PRESENTATIONS

1. **Fluoxetine enhances perceptual learning and luminance perception during adulthood.**

Maëva Gacoin, Suliann Ben Hamed. (2022)

FENS (Poster)

2. **Developmental changes of pulvino-cortical connectivity in macaques.** (Appendix n°2, pp. 254-257)

Mathilda Froesel*, Simon Clavagnier*, Holly Rayson, **Maëva Gacoin**, Alice Massera, Pier Francesco Ferrari, & Suliann Ben Hamed. (2022)

FENS (Poster)

3. **Early social adversity in non-human primates interferes with the developmental trajectory of amygdalo-cortical functional connectivity.** (Appendix n°2, pp. 254-257)

Simon Clavagnier*, Holly Rayson*, Mathilda Froesel*, **Maëva Gacoin**, Alice Massera, Pier Francesco Ferrari, & Suliann Ben Hamed. (2022)

FENS (Poster)

4. **Reward spatial contingencies reshape visual activations in the primate visual cortex.**

Maëva Gacoin, Mathilda Froesel, Simon Clavagnier, Justine Cléry, Wei-An Sheng, Maxime Gaudet-Trafit, Suliann Ben Hamed. (2021)

NeuroFrance (Poster)

5. **Neural Correlates of Integration of audio-visual information of congruent social meaning in monkeys.**

Mathilda Froesel, **Maëva Gacoin**, Simon Clavagnier, Marc Hauser, Quentin Goudard & Suliann Ben Hamed. (2021)

NeuroFrance (Poster)

6. **Automated video-based heart rate tracking for the anesthetized and behaving monkey.**
Mathilda Froesel*, Quentin Goudard*, Marc Hauser, **Maëva Gacoin** & Suliann Ben Hamed (2021)
Doctoral school NSCo (Poster)

CONFERENCES HOSTING AT THE *Institut des Sciences Cognitives* – *Marc Jeannerod*

1. “What to do with a PhD in Neurosciences outside academia?”
2. “Gender Bias : understand it to overcome it”
3. Practical sessions organization: “BIDS setting up”

MEDIA AND PUBLIC OUTREACH

1. **La rêverie est-elle le propre de l’homme ?**
Maëva Gacoin & Mathilda Froesel. (2022)

Cortex Mag, <https://www.cortex-mag.net/la-reverie-est-il-le-propre-de-lhomme/>

2. **Comme nous, les macaques analysent les signaux de leur environnement en fonction du contexte socio-émotionnel.**
Mathilda Froesel & **Maëva Gacoin**. (2022)

Cortex Mag, <https://www.cortex-mag.net/comme-nous-les-macaques-analysent-les-signaux-de-leur-environnement-en-fonction-du-contexte-socio-emotionnel/>

Table of contents

| | |
|--------------------------------------------------------------------------------------------------------------------------------------------------------------------------|------------|
| REMERCIEMENTS | 3 |
| RÉSUMÉ | 6 |
| ABSTRACT | 8 |
| PREFACE | 10 |
| ABBREVIATION LIST | 11 |
| LIST OF PUBLICATIONS | 12 |
| INTRODUCTION | 20 |
| The visual system: development and plasticity | 22 |
| 1. From light to information processing in the visual system | 22 |
| 2. What is neuronal plasticity? | 23 |
| 3. The critical period in the developing primary visual system | 26 |
| 4. Inducing plasticity in the adult brain: the case of amblyopia..... | 28 |
| Induction of visual plasticity in the adult brain | 30 |
| 1. At cellular and molecular levels..... | 30 |
| 2. Cognitive mechanisms | 30 |
| 3. A general point on neurotransmitters | 33 |
| 1. Glutamatergic modulation..... | 33 |
| 2. Cholinergic modulations. | 33 |
| 3. Noradrenergic modulations. | 34 |
| 4. Dopaminergic modulations. | 34 |
| 4. Serotonin | 34 |
| Hypotheses summary | 40 |
| Choice of the macaque as model | 41 |
| Thesis overview | 42 |
| References | 43 |
| CHAPTER I: Behavioral characterization of the effects of fluoxetine on visual perception | 60 |
| General introduction to the chapter I | 62 |
| Study n°1 | 62 |
| Perspectives of the chapter I | 99 |
| CHAPTER II: Perceptual learning induced by a spatial priority map coupled with chronic fluoxetine administration: a resting state fmri study in the macaque | 102 |
| General introduction to the chapter II | 104 |
| Abstract | 105 |

| | |
|----------------------------------------------------------------------------------------------------------------------------------------------------------------------------|------------|
| Introduction | 106 |
| Material and Methods | 107 |
| 1. Animals and ethical approval | 107 |
| 2. Surgery | 107 |
| 3. Fluoxetine preparation..... | 107 |
| 4. Fluoxetine administration..... | 108 |
| 5. Experimental setup | 108 |
| 6. MRI acquisitions parameters..... | 108 |
| 7. Behavioral tasks | 109 |
| 8. Preprocessing | 114 |
| 9. Data analysis | 114 |
| Results | 116 |
| 1. Fluoxetine-induced changes in cortical functional connectivity following reward-based spatial learning..... | 116 |
| 2. Effects of fluoxetine and reward-based learning on cortical FC..... | 121 |
| 3. Ventral & dorsal pathways comparison: effect of the reward..... | 126 |
| 4. Lateralization reward-induced bias in FC in the dorsal visual pathway | 128 |
| Discussion | 129 |
| 1. Coupled effects of fluoxetine and reward output on general brain connectivity | 130 |
| 2. The reward saliency establishes correlations between visual areas | 131 |
| 3. Inhibition of the ventral pathway when under-rewarded | 132 |
| 4. Reinforcement of the dorso-ventral decorrelation under fluoxetine | 133 |
| Conclusion | 134 |
| Supplementary figures | 136 |
| References | 138 |
| Perspectives of the chapter II | 143 |
| CHAPTER III: Chronic fluoxetine administration enhances the decoupling between dorsal and ventral v2 induced by a reward-based training of a spatial priority map.. | 144 |
| General introduction to the chapter III | 146 |
| Abstract | 147 |
| Introduction | 147 |
| Material and Methods | 149 |
| 1. Behavioral tasks | 149 |
| 2. Data analysis | 151 |
| Results | 153 |
| 1. Retinotopic mapping | 153 |
| 2. Changes in percent signal changes as a function of reward-based learning | 158 |
| 3. Effect of fluoxetine on reward-based learning effects on cortical activations..... | 161 |

| | |
|---------------------------------------------------------------------------------------------------------------|------------|
| Discussion | 163 |
| 1. Reward-based alteration of the spatial priority map does not alter retinotopic maps. | 163 |
| 2. Dorsal ROIs activations modulation following reward manipulation | 164 |
| 3. Increased task specific training effect due to fluoxetine administration..... | 164 |
| Conclusion | 165 |
| References | 166 |
| Perspectives of the chapter III | 170 |
| DISCUSSION & PERSPECTIVES | 172 |
| General discussion | 173 |
| Perspectives | 176 |
| 1. Functional and structural effects of fluoxetine on cortical plasticity | 177 |
| 2. Behavioral effects of fluoxetine on visual perception..... | 180 |
| References | 183 |
| APPENDICES | 190 |
| Appendix 1 : Cortical and subcortical neural bases of audio-visual social processing in macaques | 192 |
| References | 192 |
| Appendix 2: Effect of early social deprivation on the development of <i>Macaca mulatta</i> | 253 |
| References | 253 |
| Appendix 3: Diffusion imaging | 257 |
| References | 257 |

INTRODUCTION

| | |
|--------------------------------------------------------|----|
| The visual system: development and plasticity..... | 22 |
| Induction of visual plasticity in the adult brain..... | 30 |
| Hypotheses summary | 40 |
| Choice of the macaque as model..... | 41 |
| Thesis overview..... | 42 |
| References | 43 |

The visual system: development and plasticity

1. From light to information processing in the visual system

The visual system is composed of the eyes as main sensory organ, and multiple central nervous system components. All these components in their integrity allow us to perceive incoming visual information and develop a variety of visual cognitive functions such as localization, identification, categorization, and many more.

When light first hits the cornea, photoreceptors of the retina, rods and cones, are excited (Chichilnisky and Wandell, 1995) and light is converted in colors and contrasts. Ganglion cells then project to the cortex the converted light into electrical signal through the optic nerve to the optic chiasm. Here, the projecting axons from the retinas of both eyes join or cross medially, and after this partial decussation, they form the lateralized optic tracts (for review, see Petros et al., 2008). Retinal projections are allocated to each brain hemisphere in the optic chiasm. From there, information of the right visual hemifield are sent contralaterally to the left hemisphere and vice versa for the left hemifield (Jeffery, 2001). The central part of the visual field is sent to both cortical hemispheres. For example, an information in the right hemifield perceived by the left eye will be projected ipsilaterally in the left hemisphere whereas the same information perceived by the right eye will cross the optic chiasm to be projected contralaterally to the left hemifield (**Figure 1**). Importantly, the space where both hemifields are seen by both eyes is called the binocular visual field (Hubel and Wiesel, 1959). Thanks to binocular vision, primates, the eyes of which face forward in the face and have overlapping representations of the visual field, can process the visual information into stereopsis (or stereoscopic vision) that contributes to depth perception and enhance the field of view (Poggio and Poggio, 1984; Read, 2021).

Figure 1: Allocation of visual information in the human brain (Motz et al., 2012)

While some axons of the optic tract project directly to the midbrain or to the superior colliculus, most of them innervate the right and left lateral geniculate nuclei (LGN) (Watanabe and Rodieck, 1989) located in the dorsal thalamus. From there, visual information is then forwarded to the primary visual cortex (V1), also known as the striate cortex (Chatterjee and Callaway, 2003), that covers the occipital pole of the occipital lobe. In one of their key experiment, Hubel and Wiesel (1977) have demonstrated that after injecting radioactive proline in a macaque eye, a region within layer IV of the striate cortex present stripes corresponding to each eyes nerve endings, revealing for the first time the existence of ocular dominance columns. These ocular dominance columns alternate systematically between left eye and right eye dominance and are at the root of the coding of depth (Cléry et al., 2015).

Beyond V1, information is processed in the visual extrastriate areas, which are organized in two separate streams (Goodale and Milner, 1992; Ungerleider and Haxby, 1994). The dorsal visual stream or “where” pathway is essential for the spatial localization of objects and movement processing. It projects from visual area V3, to middle temporal regions (MT or V5), then to the posterior parietal cortex to end in the dorsolateral prefrontal cortex (DLPFC). The ventral visual stream or “what” pathway is directed toward visual area V4, to the inferior temporal cortex and to the ventrolateral prefrontal cortex (VLPFC) and aims at categorizing and recognizing objects (Mishkin and Ungerleider, 1982; Ungerleider and Haxby, 1994; Goodale and Westwood, 2004; Ungerleider and Pessoa, 2008).

Thanks to the parallel processing within these visual pathways, feedback and feedforward connectivity within these pathways, as well as direct reciprocal connection between them at several levels of the visual hierarchy, the brain combines stimuli to identify information from visual objects according to their color, form, movement, luminosity and spatial location. This complex system continuously evolves through life, and is subject to both refinement (e.g. through development or learning) and impairment (e.g. through lesions or aging) thanks to neuronal plasticity.

2. What is neuronal plasticity?

1. Definition and history

The brain and its function are not fixed in adulthood. This is due to neuronal plasticity. This term, according to many scientists, first pointed toward the regenerative capacity of the peripheral nervous system. Then, in 1964, Marian Diamond published the first scientific evidence of anatomical brain plasticity, driven by environmental enrichment (Diamond et al., 1964).

During the same period, David Hubel and Torsten Wiesel made a crucial discovery in their work with kittens. The experiment consisted of suturing only one eye and recording cortical brain maps. Hubel and Wiesel (Hubel and Wiesel, 1963; Wiesel and Hubel, 1963a, 1963b) found that the part of the kitten's brain associated with the closed eye was not as dormant as expected. Instead, it processed visual

information from the open eye. Hence, researchers often describe neuroplasticity as “The ability to make adaptive changes related to the structure and function of the nervous system.” (Zilles, 1992).

In 2002, Wall and colleagues traced the mechanisms underlying neuroplasticity (Wall et al., 2002). According to their findings, the reorganization occurs at all levels of the processing hierarchy; this produces the map changes they observed in the cerebral cortex. Crucial for learning, memory, development, behavioral adaptability and repair, brain plasticity is now considered as **the ability of neurons to be modulated in response to experience**.

2. Experience and activity dependent plasticity

Experience-dependent plasticity. Much of our knowledge about how activity affects the development of neural circuits comes from studies of mammalian visual systems, where differences in the input of each eye affects connectivity patterns in the visual cortex. In addition to early visual regions, changes in the structure and size of the human cerebral cortex, from infancy to late adolescence, suggest that experience-dependent critical periods may influence connectivity and complex behaviors (for review, see Nithianantharajah and Hannan, 2006). In humans, postnatal changes in cortical size may reflect a consequence of experience and activity on the differential development of some cortical regions but not others.

Activity-dependent plasticity. Experience-dependent plasticity is in part implemented thanks to activity-dependent plasticity. Activity-dependent plasticity is a form of functional and structural neuroplasticity that arises from the use of cognitive functions and personal experience; hence, it is the biological basis for learning and the formation of new memories (for review, see Ganguly and Poo, 2013). By experimentation on rats, it was found that visual experience during vigilant states leads to increased responsiveness and plastic changes in the visual cortex (Tsanov and Manahan-Vaughan, 2007). Moreover, depressed states were found to negatively alter the stimulus so the response was not robust. This experiment proves that even the visual cortex is capable of achieving activity-dependent plasticity, as it is reliant on both visual exploration and the arousal state of the animal. There are many mechanisms involved in activity-dependent plasticity. These include long-term potentiation (LTP), long-term depression (LTD), synaptic elimination, neurogenesis, and synaptogenesis (Bruehl-Jungerman et al., 2007).

3. Synaptic plasticity

Hebbian theory. Hebbian theory is a neuroscientific theory that states that the increase in efficiency of synapses is the result of repeated and persistent stimulation of a postsynaptic cell by a presynaptic cell. This is an attempt to explain synaptic plasticity, the adaptation of neurons in the brain during learning (Hebb, 1949; Viana Di Prisco, 1984).

Regardless of the widespread use of Hebbian models for long-term development, Hebb's principle does not cover all forms of long-term synaptic plasticity. Hebb recognized no rules for

inhibitory synapses, nor did he make predictions for anti-causal spike sequences (presynaptic neurons activated after postsynaptic neurons). Synaptic alterations can occur not only between activated neurons A and B, but also in neighboring synapses. These forms of heterosynaptic and homeostatic plasticity are considered as non-Hebbian. This apparent randomness of synaptic connections enables a network of neurons to continuously try out new network configurations while maintaining its functionality (Kappel et al., 2015).

Short-term synaptic plasticity. Release of neurotransmitters are enhanced by short-term potentiation, which are themselves the results of actions of calcium (Ca^{2+}) in the presynaptic terminal. This type of synaptic plasticity lasts for seconds to minutes, no more. It is mostly observed during repeated activation of chemical synapses. We distinguish several forms of short-term synaptic plasticity such as facilitation, depression, potentiation and augmentation. Their mechanisms all involve a repetitive synaptic activity and can trigger each other. Although their relative contributions vary from synapse to synapse, these forms of short-term synaptic plasticity collectively cause transmission at all chemical synapses to change dynamically because of the recent history of synaptic activity (for review, see Zucker and Regehr, 2002).

Long-term synaptic plasticity. Other types of synaptic activity can also produce a long-lasting increase in synaptic strength (long-term potentiation, LTP) or a decrease of it (long-term depression, LDP). These two mechanisms only define the direction of change in synaptic efficacy and are also Ca^{2+} dependent (Paulsen and Sejnowski, 2000). At least some of the synaptic changes produced by these forms of plasticity are postsynaptic and caused by changes in neurotransmitter receptor transport, although changes in neurotransmission may also occur. In V1, it has been shown that the push-pull mechanism (receptors coupled to the G-protein G_s promote the expression of LTP at the expense of LTD, and G_q -coupled receptors promote LTD at the expense of LTP) paired to monocular stimulation and pharmacology action on G_s or G_q coupled receptors can modulate the neuronal response and remain stable even in adulthood (Gu, 2002; Hong et al., 2020).

Long-lasting synaptic plasticity may act as a neural mechanism for many forms of brain plasticity, such as learning new behaviors or acquiring new memories of a recent history of synaptic activity. Plasticity is however more active during development during a particular period (for review, see Espinosa and Stryker, 2012), and is crucial to refine visual, somatosensory and auditory systems. This period of sensitivity is referred to as the critical period (Wiesel, 1982; Berardi et al., 2000).

3. The critical period in the developing primary visual system

1. Early sensory experience shapes the visual system

The critical period is a temporal window in which neural connections are particularly sensitive in response to an external stimulus and varies widely among animal species (**Figure 2b**). Hence, the more complex the brain and the longer the life of the animal are, the more extended the critical period will be (**Figure 2a**) (Berardi et al., 2000). Thus, in the visual cortex, experience shapes synaptic circuits during a period of enhanced plasticity that follows eye opening (Hubel and Wiesel, 1970; Lehmann and Löwel, 2008).

Figure 2: Life span and critical period relationship (Berardi et al., 2000)

On another side, studies of the visual systems of kittens and non-human primates have demonstrated that even a few days of abnormal visual experiences during the critical period can lead to visual impairment. Indeed, as discussed earlier, in their landmark experiments, Hubel and Wiesel showed that by depriving kittens of normal visual experience during the critical period by eyelid suture, the circuitry of the neurons in their visual cortex is irreversibly altered. However, if the same experiment is conducted in an adult cat, little to no impairment occur (Hubel and Wiesel, 1963; Wiesel and Hubel, 1963a, 1963b).

Accordingly, the normal functional development can be altered by manipulating the visual input, using methods such as dark rearing (Duffy and Mitchell, 2013) or monocular deprivation, the later permitting to manipulate ocular dominance (OD) of cortical neurons. In the latter, changes in visual inputs alter the natural dominance of the contralateral eye (for review, see Espinosa and Stryker, 2012; Hensch and Quinlan, 2018). Since it is typical of the critical period, OD has been characterized among rodents, ferrets, cats, monkeys and humans (Banks et al., 1975; Olson and Freeman, 1980; Harwerth et al., 1986; Fagiolini et al., 1994; Huang et al., 1999; Issa et al., 1999) as a marker of this time window and even induce molecular changes (Cnops et al., 2008). The decline of OD plasticity after the critical period requires “brakes” on plasticity mediated by specific molecular mechanisms to close the critical period and their continuous application to keep it closed (Bavelier et al., 2010). In this context, excitation/inhibition (E/I) balance has been proposed to play a key role as a brake on cortical plasticity and GABAergic neuromodulation has been proposed to play a key role in this respect.

2. Excitation/ inhibition (E/I) and the role of the GABAergic circuit

There are two main types of γ -Aminobutyric acid (GABA) receptors: an ionotropic GABA_A receptor that induces hyperpolarization in mature cells (Kaila et al., 2014) and a metabotropic GABA_B receptor (Wu et al., 2016), which are G-protein coupled receptors interacting with potassium and calcium channels. In the developing brain, GABA acts as an excitatory neurotransmitter. However in the mature brain, it rather inhibits the target cells. The GABA binding to GABA_B receptors either cause a postsynaptic potassium release inducing a slow inhibitory potential or inhibits presynaptic calcium channels, which leads to a decreasing of neurotransmitter release (Ulrich and Bettler, 2007). GABA is involved in several cognitive functions (Schmidt-Wilcke et al., 2018; Kim et al., 2019), such as impulsivity (Boy et al., 2011; Yoon et al., 2016), working memory (Duncan et al., 2014; Yoon et al., 2016) and motor function (Stinear and Byblow, 2003; Zoghi et al., 2003; Duncan et al., 2014). The inhibiting role of GABA is also crucial to modulate the end of the critical period and to trigger the plasticity of ocular dominance (OD) (Hensch et al., 1998; Fagiolini and Hensch, 2000).

In adults, E/I balance measured in V1 during resting state has been proven to modulate the deprivation state of OD (Pizzorusso, 2002; Harauzov et al., 2010; Heimel et al., 2011). More specifically, in rats, it has been shown that a reduced intracortical inhibition triggers OD plasticity in the adult visual cortex due to monocular deprivation is accompanied by an enhancement of activity-dependent potentiation of synaptic efficacy but not of activity-dependent depression (Harauzov et al., 2010). A transplantation of embryonic inhibitory neurons into the visual cortex of mice allowed to reactivate visual cortical plasticity, hence opened a new critical period after a deprivation during the initial critical period (Davis et al., 2015). In human adults, GABA has also been measured thanks to magnetic resonance spectroscopy in V1 (Lunghi et al., 2015). In this study, after binocular rivalry and monocular deprivation, the team observed a high correlation between the GABA concentration in the

visual cortex and the perceptual enhancement of the deprived eye. Specifically, pre or post-synaptic GABA_B receptors inhibit both excitatory and inhibitory neurons, so the activation of these receptors plays a role in the information exchange between brain areas managing both synaptic plasticity and rhythmicity (for review, see Sanchez-Vives et al., 2021). Therefore, reducing the cortical inhibition of GABA has a role in visual plasticity and in the reopening of the critical period.

In addition, GABA concentration reduction is associated with several neurodevelopmental disorders (Chattopadhyaya and Di Cristo, 2012) such as attention-deficit-hyperactivity-disorder (ADHD) (Edden et al., 2012). Indeed, in animal studies, GABA is involved in attentional regulation (Katzner et al., 2011; Paine et al., 2011; McGarrity et al., 2017) and in visuo-spatial attention (Petersen et al., 1987; Pezze et al., 2014). Human studies show that high GABA concentration improves attentional selectivity in the visual cortex (van Loon et al., 2013; Sandberg et al., 2014), by suppressing task-irrelevant information or by enhancing the specificity of neural representations (Sandberg et al., 2014; Frangou et al., 2019). GABA is then shown to be involved in top-down and bottom-up visual attentional processing. It shapes visual attention by suppressing bottom-up signals while improving attentional selectivity in early visual areas (van Loon et al., 2013) which are influenced by top-down signals (Sandberg et al., 2014).

4. Inducing plasticity in the adult brain: the case of amblyopia

The impaired circuitry of the critical period caused by abnormal visual experience or pre-natal alteration of the visual system can decrease the visual representation quality and be the cause of pathologies such as amblyopia or congenital cataract. The latter for example, is very rare at young age and is caused by genetic mutation affecting lens development, hence a visual deprivation of the affected eye, inducing a form of amblyopia (Churchill and Graw, 2011; Rong et al., 2015).

Amblyopia ('lazy eye') is a developmental disorder caused by physiological alterations in the visual cortex in stages of the postnatal visual system development resulting in eyesight deficiencies and affects 2-5% of children (Powell and Hatt, 2009). It has two main causes (Tailor et al., 2016): either a difference in the optical properties of the two eyes, reflected in a different spectacle prescription for the right and the left eye (anisometropia) or/and strabismus (misalignment of the visual axes). The imbalanced input between the two eyes results in low stereoscopy (Greenwood et al., 2012), suppression of the central part of the visual field (corresponding to the overlap between the two hemifields, **Figure 1**) (Hess et al., 2014), reduction in contrast sensitivity and perceptual spatial distortions (Barrett et al., 2004), these effects have been shown in both humans and other animals (for review, see Kiorpes, 2006).

Amblyopia is relatively easy to correct until the age of 8 years by improving the quality of visual input in the affected eye (for review, see Daw, 1998; Mitchell and Mackinnon, 2002; Simons, 2005) but becomes increasingly resistant to reversal with age. However some mechanisms are known to enhance plasticity in the adult visual cortex, such as local inhibition, transplants or neuromodulation (for review,

see Hensch and Quinlan, 2018). In particular, the release of the intracortical inhibitory brake (**Figure 3**) is considered crucial to re-instate a juvenile-like plasticity in adulthood and initiate recovery from amblyopia in the adult brain (Bavelier et al., 2010; Baroncelli et al., 2011).

Hence, OD is also of clinical significance to the recovery of vision in patients with amblyopia or strabismus (Hoyt, 2005). For example, an experiment conducted in non-amblyopic human adults using monocular deprivation for 150min causes effects on the deprived eye for 90min (Lunghi et al., 2011), while a replication of this protocol locates the local binocular changes in layer IV for area V1 (Zhou et al., 2014). Another significant study using brain imaging reveals the nature of neuroplastic changes at play during short-term monocular deprivation on healthy humans adults, showing interocular inhibitory interactions prior to binocular combination (Chadnova et al., 2017). Thus, even at a smaller scale, the adult visual system remains plastic even after the critical period (Karni and Bertini, 1997; for review, see Castaldi et al., 2020), making the study of enhancement of visual plasticity in adulthood crucial.

Figure 3: Evolving plastic capacity across the lifespan (blue arrows) suggests possible mechanisms for enhancing learning and recovery of function in adulthood (red arrows). (Bavelier et al., 2010)

Induction of visual plasticity in the adult brain

1. At cellular and molecular levels

Critical period is likely to be triggered again in adulthood thanks to cellular and molecular manipulations. For example, introducing immature astrocytes in adult cats reopens a period of high plasticity, reminiscent of the early life visual critical period (Müller and Best, 1989). In the mouse visual cortex, astrocytes control critical-period closure. Indeed, a study showed that mice etched with immature astrocytes had high plasticity compared to control mice with monocular deficiency when culture medium was injected or mice that were not injected. Thus, astrocytes not only influence the activity of individual synapses but are also important in the experience-dependent wiring of brain circuits, as well as in critical period closure (Ribot et al., 2021). In addition, some proteins such as Tau (a microtubule-associated protein that has been involved in glaucoma) may limit visual plasticity in adult mice. It has been found to be involved in the adaptive plastic mechanisms operating in the adult visual brain subjected to sensory experience changes (Rodriguez et al., 2020).

Yet very promisingly, such experiments remain invasive and are still studied in animal models such as rodents. While this field remain of high interest, attention modulation and pharmacological manipulation have also been shown to contribute to enhanced plasticity in adulthood.

2. Cognitive mechanisms

1. The role of attention: bottom-up & top-down pathways

Among all types of attention, the visuospatial selective attention refers to the cognitive process that permits to focus on a specific part of the visual field in order to prioritize relevant information while ignoring the irrelevant ones (Itti and Koch, 2001; Di Bello et al., 2022). In the brain, two networks are involved in controlling attention. They are the **top-down attention**, which is the voluntary guidance of attention led by self-intention, often guided by an external factor, prior knowledge, willful plans, and current goals, and the **bottom-up attention** which is involuntary guidance of attention by a salient stimulus relative to the background (Corbetta and Shulman, 2002; Yantis, 2002; Ibos et al., 2013; Astrand et al., 2015).

Brain regions involved in top-down & bottom-up attention. Bottom-up processing of visual information starts from V1 (Katsuki and Constantinidis, 2014) and projects to higher cortical areas through the ventral and dorsal pathways (Mishkin et al., 1983; Ungerleider and Pessoa, 2008). On the other hand, top-down mechanisms go from higher cognitive functions associated regions, such as prefrontal areas, like the frontal eye fields (FEF), and parietal areas, like the intraparietal sulcus (IPS),

which are associated with gaze, and modulate neuronal activity down to early visual areas (MT, V4-V1) (Hopfinger et al., 2000; Noudoost et al., 2010; Wardak et al., 2011; Ibos et al., 2013; Miller and Buschman, 2013; Astrand et al., 2015; Esterman et al., 2015; Meehan et al., 2017; Thiele and Bellgrove, 2018). Subcortical regions are also involved in the visual attentional control such as the superior colliculus, the thalamus, the lateral geniculate nucleus (LGN) and the pulvinar (Schneider, 2011; Fiebelkorn and Kastner, 2020).

Priority map & statistical learning. The close connection of these networks (Buschman and Miller, 2007; Katsuki and Constantinidis, 2014; Richter et al., 2017) allows the integration of both selection history with current goals with the salience to shape a priority map, like reward-based history effects (Awh et al., 2012; Failing and Theeuwes, 2018; Theeuwes et al., 2022). Indeed, visual attention and working memory processes have a strong interaction (Awh et al., 2006; Chelazzi et al., 1998; Theeuwes et al., 2009), the encoding of which is refined by the level of attentional prioritization (Klyszejko et al., 2014) and is affected by both reward and punishment stimuli related to prior experiences (Kahnt et al., 2014; Watson et al., 2019). The integration of bottom-up and top-down factors in visual attention leads to the principle of the priority map (Serences and Yantis, 2006, 2004; Bisley and Goldberg, 2010; Di Bello et al., 2022) which tends to increase the activity in the frontoparietal network (Corbetta and Shulman, 2002; Katsuki and Constantinidis, 2012, 2014). Indeed, when a distractor is presented prior to a target, there is a concurrent increased activity in the visual cortex, thus triggering the frontal and parietal areas concerned by the target to come (Luck et al., 1997; Kastner et al., 1999; Ress et al., 2000; Müller and Kleinschmidt, 2003). In addition, neurons with a large receptive fields may encode multiple objects (either distractor, cue or target) to identify their size and location (Ito et al., 1995; Lueschow et al., 1994). If two objects compete in this receptive field, and more specifically in visual area V4 and the inferotemporal cortex, the most salient one affects normally the neurons response, while the less salient suppresses any kind of response (Moran and Desimone, 1985; Chelazzi et al., 1998). Moreover, in order to optimize one's behavior, it has been shown that FEF and IPS conversely suppresses distractors processing and enhances spatial target selection from the early visual areas level (Di Bello et al., 2020), under attentional guidance (Gaillard et al., 2020; Di Bello et al., 2022). The amplified attentional effect caused by stimuli competition, in comparison with no competition, has been widely documented (Shiu and Pashler, 1994; Kastner et al., 1998; Reynolds et al., 1999; Awh and Pashler, 2000; Doshier and Lu, 2000; Kastner and Ungerleider, 2001; Awh et al., 2003). Interestingly, the more the receptive field has objects, the less fine information spread and priority set –up are (Wise and Desimone, 1988; Miller et al., 1993a), although a voluntary shift of attention to navigate between the hierarchically organized receptive fields may occur (Serences and Yantis, 2006). The spatial priority map can also be altered by statistical learning (Ferrante et al., 2018), and enhanced by objects reward competitiveness (Chelazzi et al., 2014).

2. Other behavioral manipulations

1. *Perceptual learning*

Perceptual learning is the most dominant form of cortical plasticity in adulthood. It involves implicit memory thanks to experience and practice, in order to produce repetitive sensory interventions. It has been widely studied in the search for a treatment for amblyopia in adulthood (for review, see Levi and Li, 2009). For example, even in adulthood, extensive and repeated practice of a simple discrimination task affects both stimuli representation in early and late visual areas (Adab et al., 2014). Practice thus leads to long-lasting improvement of performance through neural processing in the visual cortex by using the stimulus information more efficiently, as shown in studies on amblyopia for example (Kiorpes, 2006).

2. *Cross-modal plasticity*

Other ways to induce plasticity non-invasively involve multisensory learning and integration (Bavelier and Neville, 2002; Ewall et al., 2021). Indeed, most studies focus on one sensory modality while the brain is now considered as a connectome. As a result, sensory interactions are worth considering in the context of plasticity (for review, see Shimojo, 2001). Most often, it is associated with a deprivation in early stages of development, such as blindness.

Motor. It has been shown that motor exercise coupled to visual experience such as the monocular deprivation can trigger short-term homeostatic plasticity in adults (Lunghi and Sale, 2015). Although the effect of motor exercise on the effect of monocular deprivation is still a topic of controversy (Zhou et al., 2017; Finn et al., 2019), evidence shows that neurons in mouse visual cortex respond more during locomotion than when still (Niell and Stryker, 2010; Kaneko and Stryker, 2014) yet these effects are smaller in non-human species such as monkeys (Cook and Maunsell, 2002; Reynolds and Chelazzi, 2004).

Somatosensory. Because it shares similar mechanisms to restore firing rate after sensory deprivation as those described in the visual system, somatosensory area stimulation is investigated to restore homeostatic plasticity. In a study by Gainey and Feldman (2017), it has been proposed that activity-dependent plasticity interacts with Hebbian synaptic plasticity in a context of sensory deprivation, very similar in rodents somatosensory and visual cortices. Moreover, patients with a visual hemispatial neglect (a deficit of attention) of their own body (most often, their arm and hand) caused by a lesion in an hemisphere may be rewired thanks to somatosensory stimulation of the vestibular system (Kerckhoff, 2003).

Auditory. A tracer study in primates by Falchier et al., (2002) shows that V1 receives projections from nonvisual extrastriate cortical areas such as auditory and polysensory area of the temporal lobe cortices, showing multimodal integration at early stage in the visual cortical pathway. Once this milestone is laid, we can wonder whether audio-visual inputs can drive plasticity in V1. A recent

imaging study (two-photons, Ca²⁺ and voltage) on mice goes further in investigating this interaction and showed that this cross-modal plasticity not only exists, but is persistent over days (Knöpfel et al., 2019). Indeed average activity of multimodal neurons increases in response to a tone previously paired to a visual stimulus but decrease in response to unpaired tone to visual stimuli, altogether showing that V1 processes congruent auditory and visual stimuli by strengthening functional associations in multisensory neurons (Aller et al., 2021). Vice-versa, visual stimulation can enhance the performance in an auditory working memory task (Albouy et al., 2022). An imaging study in the intraparietal sulcus (IPS) has also shown a better sensitivity to numerosity displayed in the form of differential number of beeps, in blind individuals than on blindfolded sighted participants (Kanjlia et al., 2021). This testify for the extended adaptability of the brain in a condition that is usually considered as an impairment.

All in all, the study of cross-modal plasticity is rather recent and is also being studied to propose therapies in schizophrenia (Wijtenburg et al., 2021). However, these effects being caused by sensory modulation remain too low to induce long-lasting effects, compared with a pharmacological manipulation involving the neurotransmitters.

3. A general point on neurotransmitters

Another way to restore plasticity through alteration of the excitation-inhibition balance is to play on neuromodulators, to favor excitation. Indeed, a coupling of Hebbian plasticity, such as LTD and LTP, and neuromodulators highly infers on the individual behavioral state (for review, see Gu, 2002) and can even reverse definitively the effects of a monocular deprivation among adults (Hong et al., 2020). They all have their own action mechanisms to modulate plasticity. However, the key target of molecular signaling in plasticity is the inhibition of GABAergic neurons. Through their post synaptic receptors, they are very sensitive to critical period alterations.

1. Glutamatergic modulation.

Glutamatergic modulators, and more precisely AMPA (α -amino-3-hydroxy-5-methyl-4-isoxazolepropionic acid) and NMDA (N-méthyl-D-aspartate) receptors, are involved in synaptic plasticity. Activated by glycine or glutamate, they are important molecules in the short- and long-term potentiation between neurons. Indeed, when their activity increases, this leads to signaling modification in the post-synaptic cell. Hence, pre and post synaptic receptors coordination results in plasticity, strengthened by correlated activity.

2. Cholinergic modulations.

The involvement of acetylcholine circuitry on the E/I balance by reducing the size and the diffusion of receptive fields excitation in the visual cortex has been shown in humans (Silver et al., 2008), rats (Kimura et al., 1999) and marmosets (Roberts et al., 2005). We can then argue that cholinergic signaling plays a role in neuronal plasticity. Accordingly, it has been shown that cholinergic

modulations promote remyelination, a crucial structural factor of the plasticity, and so the rewiring of old and new connections (Fields, 2015; for review, see Fields et al., 2017).

3. Noradrenergic modulations.

The central noradrenergic system is responsible for saliency (Rogawski and Aghajanian, 1980), improvement in the treatment of sensory information (Waterhouse and Navarra, 2019), attentional processes/visuo-spatial attention (Reynaud et al., 2019) but also spatial and recognition memory, cognitive flexibility and arousal. The principal source of noradrenaline in the central nervous system is the locus coeruleus which can modulate the activity of cortical GABAergic cells in the neocortex and hippocampus (Kawaguchi and Shindou, 1998). More precisely, it mediates plasticity in the attentional neural network (Coull et al., 1999). In addition, the increase in the local availability of noradrenaline enhances neuronal plasticity, by accelerating cortical recovery from the effects of prior monocular deprivation in cats and has been proposed as a treatment for amblyopia (Kasamatsu, 1982, 1991; Gordon et al., 1988).

4. Dopaminergic modulations.

Dopamine is widely studied to be involved in Parkinson disease (PD), its deficit resulting from the degradation of the dopaminergic neurons being one of the causes of this neurodegenerative pathology. However, an exercise-induced increase in the dopamine D2 receptor expression, protein and binding in the striatum, may restore motor learning both in healthy and PD patients (for review, see Jakowec et al., 2016), which corresponds to a form of plasticity. Dopamine is also linked to motivation and its depletion can lead to depressive state (Pessiglione et al., 2018). However, endogenous dopamine in the brain regulates the critical period synaptic plasticity through learning and memory (Jay, 2003). Since it strongly interacts with the serotonergic system (Cools, 2008; Dremencov et al., 2009; Fischer et al., 2015) we now seek to understand more the latter system involvement into plasticity mechanisms.

Serotonergic neuromodulation being a focus of the present Ph.D. thesis manuscript, it is considered in an independent section in extensive details.

4. Serotonin

1. A brief history of serotonin identification

Serotonin was identified in 1946 under the name Enteramine by the pharmacologist Vittorio Erspamer in the enterochromaffin cells of the digestive tract (Erspamer and Asero, 1952), which he found to cause smooth muscle contractions. Meanwhile, in 1948 Maurice Rapport and Irvine Page (Rapport et al., 1948a, 1948b, 1948c), who were interested in hypertensive substances, isolated and characterized a vasoconstrictor substance that occurs in blood clotting. They named it "serotonin" by contracting the Latin word "serum," its source, and the Greek "tonic," its effect on blood vessels. The following year he analyzed it as 5-hydroxytryptamine (5-HT) and Enteramine has later been identified

as corresponding to this specific molecule (Reid and Rand, 1952). The presence of serotonin in the central nervous system was suggested not much longer after its initial identification (Twarog and Page, 1953) for its role as a neurotransmitter (Brodie and Shore, 1957). Later on, serotonin has been found to be at a higher concentration in specific nerve ending of neurons of the pineal gland in rats, compared to others structures of the brain (Michaelson and Whittaker, 1963; Zieher and De Robertis, 1963), paving the way to map specific nuclei that contain serotonin, now known as the serotonergic system (Dahlstroem and Fuxe, 1964). Nowadays, serotonin, or 5-hydroxytryptamine (5-HT), is characterized as a biogenic amine neurotransmitter, derived from the amino acid L-tryptophan, that is involved in a wide range of behaviors, including emotional states and mental arousal. Although more than 90% of the body serotonin lies in the platelets or the enterochromaffin cells of the gastrointestinal mucosa (Berger et al., 2009), its role in the central nervous system is to modulate efficiency of synaptic transmission (Twarog and Page, 1953). The serotonin system regulates physiology (Muller and Jacobs, 2010) and many behaviors, such as impulsivity, attention, emotions, reward processing and decision-making (Abi-Dargham et al., 1997; Clarke et al., 2004; Cools et al., 2008; Dayan and Huys, 2009; Homberg, 2012; Nakamura, 2013) and its dysfunction is involved in Parkinson's disease, autism, drug addiction and schizophrenia (Abi-Dargham et al., 1997; Huot et al., 2011; Nakamura, 2013).

2. Characteristics of the serotonergic system

1. *The raphe nuclei*

Nuclei subdivision. The raphe nuclei are a set of subcortical structures of the brain, they are present in the medulla oblongata, the pontine and the midbrain (Dahlstroem and Fuxe, 1964). They are often divided into two groups: the rostral nuclei are located near the upper part of the brain stem and the caudal ones are located closer to the lower region of the brain stem.

Most of the serotonergic neurons of the brain are located in the rostral group. It contains the caudal linear nucleus, the dorsal raphe nucleus (Ren et al., 2018) and the median raphe nucleus, and these two latter contain the most abundant serotonergic population (Dahlstroem and Fuxe, 1964). The caudal group that involves a minor cluster of serotonergic neurons contains the raphe nucleus magnus, the dark raphe nucleus and the pale raphe nucleus, which is the smallest of all raphe nuclei. The dorsal raphe and the median raphe nuclei display ascending projections targeting a large number of forebrain regions (Azmitia and Segal, 1978; Ishimura et al., 1988; Vertes and Linley, 2008) to regulate sleep and wakefulness while they actually receive a similar input (Vertes and Linley, 2008).

Raphe nuclei projections. Serotonin is distributed from the raphe nuclei throughout the brain and the spinal cord by distributed efferent and afferent projections (Pollak Dorocic et al., 2014). Indeed, serotonergic neurons of the dorsal raphe nucleus project rostrally into the cerebral hemispheres (**Figure 4**), raphe nuclei in the pontine branch project into the brainstem and cerebellum and those in the medulla oblongata go to the spinal cord. Afferences of the raphe nuclei come from the cortex, the cerebellum, the hypothalamus and the locus coeruleus. The ascending efferences are widely distributed to the frontal

cortex, the hypothalamus, the thalamus, the basal ganglia and the locus coeruleus (Ren et al., 2018). The descending efferences are distributed to the nuclei of the cranial nerves, to the spinal cord.

Figure 4: Serotonergic projection in the central nervous system (Dales & Purves, 2018)

Serotonin synthesis. There are five biogenic amine neurotransmitters: the three catecholamines (dopamine, norepinephrine, and epinephrine), histamine and serotonin. All the catecholamines are derived from a common precursor, the amino acid tyrosine. Serotonin is synthesized in serotonergic terminals from L-tryptophan (Clark et al., 1954; Tyce, 1990), which crosses the blood-brain barrier, and is released by serotonergic neurons of the raphe nuclei in the brainstem (for review, see Mohammad-Zadeh et al., 2008; Walker and Tadi, 2022). More precisely, tryptophan is transported in the serotonergic neuron by a plasma membrane transporter and hydroxylated in a reaction catalyzed by the enzyme tryptophan-5-hydroxylase (Meriney and Fanselow, 2019). Since tryptophan cannot be endogenously synthesized, the synthesis of serotonin is limited by the dietary tryptophan intake and the rate of the tryptophan-5-hydroxylase activity. In the central nervous system, presynaptic neurons such as the pineal gland, catecholaminergic neurons and serotonergic neurons synthesize and store the serotonin. After being released in the synaptic cleft, serotonin can bind either to its specific postsynaptic receptors or to autosynaptic receptors (**Figure 5**). This latter binding induces a negative feedback, thus preventing some more release of serotonin in the synaptic cleft rather enhancing its storage in the synapse (Cerrito and Raiteri, 1979).

Figure 5: Serotonergic synapse and metabolism of 5-HT from synthesis, storage, release to uptake via serotonin transporters (Ni & Watts, 2003)

2. Serotonergic receptors

The effects of serotonin in the body are mediated by seven types of 5-HT receptors (5-HT₁ to 5-HT₇) (Hoyer et al., 1994), which have different affinities to agonists and antagonists according to their subtypes. At least fourteen 5-HT receptor subtypes has been identified (Hoyer et al., 1994; Hoyer and Martin, 1997) and the two most widely studied receptors are 5-HT_{1a} and 5-HT_{2a}, for their dense expression in the human brain (Beliveau et al., 2017; Carhart-Harris and Nutt, 2017; Hansen et al., 2022). Six of these receptors' subtypes are metabotropic, with a monomeric structure typical of G-protein-coupled receptors. The nature of these receptors determines the excitatory or the inhibitory effect of serotonin on other neurons. These receptors are involved in a wide range of behaviors, such as circadian rhythms, motor behaviors, emotions control and arousal. In the central nervous system, impairments in the function of these receptors are associated with numerous psychiatric disorders (Berger et al., 2009), such as depression, anxiety disorders and schizophrenia. Drugs acting on 5-HT receptors are effective treatments for several of these conditions.

3. Serotonin transporters and reuptake

After the neuronal depolarization followed by the serotonin release in the synaptic cleft, it is removed from it by its selective serotonin transporter (SERT), which is a monoamine transporter (Torres et al., 2003). It is located in the presynaptic neuron, in the plasma membrane, and this reuptake thus decreases the concentration of synaptic serotonin (Ni and Watts, 2006). The high concentration of serotonin in the synaptic cleft contributes to an increase in the strength and duration of signaling on the postsynaptic serotonin receptor. In order to regulate this availability, two presynaptic mechanisms are at play, which are the binding of serotonin to its auto receptors and the increased activity of SERT. While SERT are responsible at removing serotonin from the synaptic cleft, the negative feedback

induced by the serotonin reuptake prevents some further serotonin synaptic release (Cerrito and Raiteri, 1979).

This reuptake can be inhibited by the selective serotonin reuptake inhibitors (SSRIs). They are a class of drugs that inhibit the ability of SERT to reuptake serotonin into presynaptic terminals: the principle of SSRIs is to prevent serotonin recapture by binding specifically to the SERT. Thus, serotonin remains longer around the synapse, increasing neuron stimulation and the serotonergic system activity, while a positive feedback loop is at play, releasing more serotonin in the synaptic cleft (Owens, 1996). Several SSRIs are antidepressants, such as fluoxetine, citalopram and its enantiomer escitalopram, fluvoxamine, paroxetine and sertraline.

3. Serotonin functions

1. *Physiological and emotional role: some examples*

Wakefulness and sleep regulation. Serotonin neurons that travel from the dorsal raphe nucleus to other brainstem nuclei play an important role in the regulation of sleep and wake cycles, and is especially involved during the sleep/wake shift (Siegel, 2004; Sakurai, 2007). Indeed, these neurons show a high degree of activity in moments of alertness but are generally inactive during the rapid eye movement sleep. Circadian rhythms are also influenced by the connection that the supra-chiasmatic nucleus establishes with the anterior nucleus and with the middle nucleus of the raphe.

Pain perception. The dorsal raphe nucleus and the nucleus magnus are involved in natural pain inhibition processes. The spinal cord circuits responsible for the transmission of pain signals are partially inhibited by projections from these nuclei (Ossipov et al., 2010).

Appetite control. Serotonin regulates appetite and food intake by diminishing hunger sensation while preserving satiety (Blundell and Halford, 1998). In the latter study, the anorexic valence is even associated with serotonergic drugs and it was shown later that there is indeed a strong pharmacological specificity regarding these effects on the 5HT_{2C} receptor (Halford and Harrold, 2012).

Depressive mood. Serotonin depletion affects the mood and has a role in depressive state, SSRI are thus proposed as anti-depressants (Pehrson et al., 2015). On a molecular and cellular level, depressive behavior alters dopamine neuron excitability and the GABAergic synaptic plasticity, leading to a misinterpretation of reward (Russo and Nestler, 2013). Recent findings also showed the coupled role of SSRI with physical exercise or learning to potentially stimulate a neuroplasticity and enhance the depression treatment (Kraus et al., 2017).

2. *Effect on social behavior*

Serotonin intake promotes prosocial behavior among primates (Raleigh et al., 1980), such as cooperation, while decreasing anti-social behavior, such as aggression and isolation (for review, see

Steenbergen et al., 2016). In addition, serotonin modulation had been linked to the establishment of social hierarchies, whether studying the relation between SERT availability and neural responses in humans related to learning of social dominance hierarchies (Janet et al., 2022) or by stimulating serotonin receptors with serotonin agonists injections and observing any behavioral changes in mammals (Sandi and Haller, 2015; Terranova et al., 2016). For example, among vervet monkeys, a male who occupies a dominant position in the social hierarchy consequently presents a high serotonin concentration in the blood (Raleigh, 1984) and reversely, suppression of serotonin signaling can induce its subordination (Raleigh et al., 1991). In addition, an input of tryptophan in macaques, thus increasing central serotonin concentration, alters saccades and social gaze toward other macaque faces, (Weinberg-Wolf et al., 2021). Serotonin decrease has also linked social learning deficits and depression, through the modulation of the social reward value learning (Frey and McCabe, 2020). Thus, SSRIs have been proposed in a treatment in social behavior disorders such as social phobia (Van Ameringen et al., 1999).

3. Effect on attentional control

In the brain, serotonin signaling has a role in attention, reducing the ability to ignore a distracting stimulus while not affecting sustained attention (Carter et al., 2005; Wingen et al., 2008), and more particularly in processing top-down attentional control (Scholes et al., 2007; Enge et al., 2011, 2014). Indeed, there is a high concentration of 5-HT_{2A} receptors in the pre-frontal cortex (PFC) (Puig and Gullledge, 2011) and as the latter region is responsible for learning, working memory and motivation, 5-HT has been found to be involved in these functions (Meneses and Liy-Salmeron, 2012).

Serotonin is also known to be involved in the inhibition of prepotent responses and on impulsivity (Brown et al., 2012; Worbe et al., 2014; Meyniel et al., 2016) while also having a role in attentional processing (Carter et al., 2005; Scholes et al., 2007; Wingen et al., 2008; Enge et al., 2014; Li et al., 2018). These effects remain highly dependent on the baseline attentional state of the individual and an adjunction of serotonin in the brain may even have contrary effects whether we have a high or a low baseline attention (Weinberg-Wolf et al., 2018). Thus, while SSRI decrease activity in brain regions associated with sustained attention, no clear behavioral effect has been reported (Wingen et al., 2008).

4. Focus on fluoxetine

The antidepressant fluoxetine (Prozac) is an SSRI that does not affect the reuptake of catecholamines, such as dopamine. In mice, it has recently been proposed as a therapy to treat mature visual system impairments, such as degeneration of retinal pigmented epithelium cells involved in macular degeneration (Ambati et al., 2021). Still in rodents, fluoxetine treatment coupled to a shift in OD by monocular deprivation participated to re-instate juvenile-like plasticity (Umemori et al., 2018). This supports the idea that fluoxetine can alter E/I balance to reinstate the characteristic plasticity of the critical period, to heal vision damages or ischemic brain injuries such as stroke (Chollet et al., 2011; Mead et al., 2020; for review, see Schneider et al., 2021). Indeed, serotonin decreases inhibition, hence

modulating the homeostatic response of visual circuits (Baroncelli et al., 2010; Guidotti et al., 2012), in favor of excitation in the E/I balance. This observation has been confirmed in rats, fluoxetine decreasing inhibition in the adult visual cortex in landmark studies (Vetencourt et al., 2008, 2011) by decreasing extracellular GABA concentrations. In addition, fluoxetine also participates in degrading “brakes” such as parvalbumin-positive interneurons in the frontal cortex (Guirado et al., 2014; Ng et al., 2015), essential in synaptic stabilization, even in single dosing (**Figure 6**). Once this plastic environment is instated, the cortex being hyperexcitable (Guirado et al., 2009), behavioral manipulation of the visual system such as monocular deprivation can indeed lead to shifts in OD, similar to those observed during the critical period. The repetitive fluoxetine administration at chronic dosing coupled to an experience-dependent modulation then induces long lasting effects in the visual system (Hong et al., 2021), due to the rise of inhibition levels, similar to the end of the critical period (**Figure 6**). Indeed, while being induced by top-down and bottom-up modulations, and since it has a strong affinity for receptors 5HT_{2a,c}, highly concentrated in PFC and visual areas (Pälvimäki et al., 1996; Beliveau et al., 2017), fluoxetine stimulates the homeostatic balance thus allowing a persistent consolidation of synaptic changes.

Figure 6: Differential effects of SSRI such as Fluoxetine according to the dose schedule (Schneider et al., 2021). While a single dosing participates in reopening the critical period and enhancing cortical plasticity, a chronic intake of this SSRI restores the E/I balance, completing the rewiring process and consolidating a long-lasting novel circuit

Hypotheses summary

Section 2 has covered the importance of enhancing visual plasticity in adulthood and the different approaches that allow to reach this goal. On a molecular and cellular scale, the mechanisms at play during visual plasticity in the adult brain are very juvenile-like. Although we cannot pretend to re-

open a critical period, some plasticity at the adult age remains and it has now been widely shown that it can be enhanced. The means we discussed here range from the molecular to the behavioral cross-modal manipulation. In the follow research achievement, we focus on the hypothesis that a coupling of attentional pathway modulation combined with pharmacology (Fluoxetine) will potentiate adult plasticity and we will seek a better understanding of the process at play during visual plasticity in adulthood.

Indeed, the use of a SSRI, and more particularly of fluoxetine to that extent is highly promising, yet, its precise effect on the primate brain has been surprisingly little documented. We here hypothesize and test for 1) a behavioral effect of fluoxetine on visual perception and on top-down control of visual processing; 2) an antero-posterior connectivity decoupling due to behavioral training and a top-down manipulation of spatial saliency; 3) an enhancement of this effect due to fluoxetine administration. Overall, reporting an improved perceptual learning thanks to pharmacology coupled to behavioral manipulation, would permit to decipher the mechanism at play in this specific enhancement of visual plasticity in adulthood.

To reach this goal, we first characterized the behavioral effects of fluoxetine on three different visual tasks. We then designed a longitudinal protocol, which involves three measurement time points thanks to magnetic resonance imaging (MRI) techniques such as functional MRI (fMRI), myelin mapping and GABA spectroscopy. The first measurement point was a control (T1). The second was recorded after behavioral training involving top-down modulations of attention of hemifields using reward biases (T2). The third measurement consisted in the same manipulation but reversed in space, with the addition of Fluoxetine administration (T3).

Choice of the macaque as model

To conduct this longitudinal study, coupling both imaging techniques and pharmacology, we designed protocols that require a controlled environment to ensure the observed effects are indeed a result of either the behavioral or the pharmacological manipulation. Indeed, the plasticity we seek to observe is very subtle. In addition, both our behavioral and pharmacological protocols require periods of daily training and Fluoxetine administration, requiring from subjects reliability and availability.

Both of these criterions are quite difficult to meet on a 4-years longitudinal study when working with human subjects. For that reason, we decided to conduct this project on a non-human primate model of cognition (macaques). Because they can learn complex behavioral tasks and share a similar visual system with humans (contrary to rodents), we decided to carry our experiments on rhesus macaques (*Macaca mulatta*). Indeed, this specie is the phylogenetically closest to human that we can study in a laboratory environment and consequently is very well documented both functionally and anatomically. Thus, since we use neuro-imaging techniques, we already benefit from strong and numerous comparison

points and from an established literature to optimize our protocols. The same arguments apply regarding pharmacology studies. Even though macaques and humans physiologic system differ, they share major similarities, including their response to Fluoxetine. In addition, macaques can be trained to daily Fluoxetine administration thanks to positive reinforcement. Such training eases their manipulation to scan them thanks to MRI technique.

In the context of this thesis, we also work with macaques not only as a model for human physiology but also for a better understanding of this primate specie. Indeed, some data collected during this thesis allowed to contribute to a primate imaging exchange database. In another project, we characterize the neural response to socio-emotionnal stimuli in a context of audio-visual integration (**Appendix 1**). Macaques were also a well-suited model for a developmental study (**Appendix 2**) as they grow faster than humans, and to develop new methodologies, (**Appendix 1 & 3**).

Thus, to design and conduct experiments to either confirm or reject our working hypotheses, the rhesus macaque (*Macaca mulatta*) stands out as an ideal experimental model. This thesis project involves two adult male rhesus macaques, aged 9 (Samourai) and 8 (Scooby) at the beginning of the study.

Thesis overview

The first chapter (study n°1) is a behavioral study of the SSRI fluoxetine on adults macaques. It involved three distinct visual tasks coupling top-down and bottom-up mechanisms to characterize its effect on the visual system. We hypothesized and demonstrated that, under fluoxetine as observed in an alteration of the spatial priority map task, luminance vision is degraded as well visual spatial resolution, while sensitivity to reward increases. In the second chapter (study n°2), we link the observed behavior to its underlying brain network mechanisms by having a closer look at the functional connectivity of the visual system, thanks to fMRI on awake macaques. We here describe our longitudinal protocol that occurred in 3 steps: control (T1), behavioral reward manipulation (T2), behavioral reward manipulation combined to fluoxetine intake (T3). By using the paradigm of the altered spatial priority map task, we thus designed a dual-choice saccadic task that imbalances the salience in the visual field that constitutes the behavioral manipulation in T2 and T3 time-points. We thus investigated the whole brain functional connectivity changes following this extensive reward-based learning of novel spatial contingencies and with the impact of fluoxetine. In the third chapter (study n°3), we hypothesized that we could support the observed functional networks modulations observed in the second chapter (study n°2) through T1, T2 and T3 by zooming in further on the visual areas retinotopy and activity, thanks to fMRI on awake macaques.

References

- Abi-Dargham, A., Laruelle, M., Aghajanian, G.K., Charney, D., Krystal, J., 1997. The role of serotonin in the pathophysiology and treatment of schizophrenia. *J Neuropsychiatry Clin Neurosci* 9, 1–17. <https://doi.org/10.1176/jnp.9.1.1>
- Adab, H.Z., Popivanov, I.D., Vanduffel, W., Vogels, R., 2014. Perceptual Learning of Simple Stimuli Modifies Stimulus Representations in Posterior Inferior Temporal Cortex. *Journal of Cognitive Neuroscience* 26, 2187–2200. https://doi.org/10.1162/jocn_a_00641
- Albouy, P., Martinez-Moreno, Z.E., Hoyer, R.S., Zatorre, R.J., Baillet, S., 2022. Supramodality of neural entrainment: Rhythmic visual stimulation causally enhances auditory working memory performance. *Science Advances* 8, eabj9782. <https://doi.org/10.1126/sciadv.abj9782>
- Aller, M., Mihalik, A., Noppeney, U., 2021. Audiovisual adaptation is expressed in spatial and decisional codes (preprint). *Neuroscience*. <https://doi.org/10.1101/2021.02.15.431309>
- Ambati, M., Apicella, I., Wang, S., Narendran, S., Leung, H., Pereira, F., Nagasaka, Y., Huang, P., Varshney, A., Baker, K.L., Marion, K.M., Shadmehr, M., Stains, C.I., Werner, B.C., Satta, S.R., Taylor, E.W., Sutton, S.S., Magagnoli, J., Gelfand, B.D., 2021. Identification of fluoxetine as a direct NLRP3 inhibitor to treat atrophic macular degeneration. *Proceedings of the National Academy of Sciences* 118, e2102975118. <https://doi.org/10.1073/pnas.2102975118>
- Astrand, E., Ibos, G., Duhamel, J.-R., Hamed, S.B., 2015. Differential Dynamics of Spatial Attention, Position, and Color Coding within the Parietofrontal Network. *J. Neurosci.* 35, 3174–3189. <https://doi.org/10.1523/JNEUROSCI.2370-14.2015>
- Awh, E., Belopolsky, A.V., Theeuwes, J., 2012. Top-down versus bottom-up attentional control: a failed theoretical dichotomy. *Trends in Cognitive Sciences* 16, 437–443. <https://doi.org/10.1016/j.tics.2012.06.010>
- Awh, E., Matsukura, M., Serences, J.T., 2003. Top-down control over biased competition during covert spatial orienting. *Journal of Experimental Psychology: Human Perception and Performance* 29, 52–63. <https://doi.org/10.1037/0096-1523.29.1.52>
- Awh, E., Pashler, H., 2000. Evidence for split attentional foci. *Journal of Experimental Psychology: Human Perception and Performance* 26, 834–846. <https://doi.org/10.1037/0096-1523.26.2.834>
- Awh, E., Vogel, E.K., Oh, S.-H., 2006. Interactions between attention and working memory. *Neuroscience* 139, 201–208. <https://doi.org/10.1016/j.neuroscience.2005.08.023>
- Azmitia, E.C., Segal, M., 1978. An autoradiographic analysis of the differential ascending projections of the dorsal and median raphe nuclei in the rat. *Journal of Comparative Neurology* 179, 641–667. <https://doi.org/10.1002/cne.901790311>
- Banks, M.S., Aslin, R.N., Letson, R.D., 1975. Sensitive Period for the Development of Human Binocular Vision. *Science* 190, 675–677. <https://doi.org/10.1126/science.1188363>
- Baroncelli, L., Maffei, L., Sale, A., 2011. New Perspectives in Amblyopia Therapy on Adults: A Critical Role for the Excitatory/Inhibitory Balance. *Frontiers in Cellular Neuroscience* 5.
- Baroncelli, L., Sale, A., Viegi, A., Maya Vetencourt, J.F., De Pasquale, R., Baldini, S., Maffei, L., 2010. Experience-dependent reactivation of ocular dominance plasticity in the adult visual cortex. *Experimental Neurology* 226, 100–109. <https://doi.org/10.1016/j.expneurol.2010.08.009>
- Barrett, B.T., Bradley, A., McGraw, P.V., 2004. Understanding the Neural Basis of Amblyopia. *Neuroscientist* 10, 106–117. <https://doi.org/10.1177/1073858403262153>

- Bavelier, D., Levi, D.M., Li, R.W., Dan, Y., Hensch, T.K., 2010. Removing Brakes on Adult Brain Plasticity: From Molecular to Behavioral Interventions. *Journal of Neuroscience* 30, 14964–14971. <https://doi.org/10.1523/JNEUROSCI.4812-10.2010>
- Bavelier, D., Neville, H.J., 2002. Cross-modal plasticity: where and how? *Nat Rev Neurosci* 3, 443–452. <https://doi.org/10.1038/nrn848>
- Beliveau, V., Ganz, M., Feng, L., Ozenne, B., Højgaard, L., Fisher, P.M., Svarer, C., Greve, D.N., Knudsen, G.M., 2017. A High-Resolution *In Vivo* Atlas of the Human Brain's Serotonin System. *J. Neurosci.* 37, 120–128. <https://doi.org/10.1523/JNEUROSCI.2830-16.2016>
- Berardi, N., Pizzorusso, T., Maffei, L., 2000. Critical periods during sensory development. *Current Opinion in Neurobiology* 10, 138–145. [https://doi.org/10.1016/S0959-4388\(99\)00047-1](https://doi.org/10.1016/S0959-4388(99)00047-1)
- Berger, M., Gray, J.A., Roth, B.L., 2009. The Expanded Biology of Serotonin. *Annu Rev Med* 60, 355–366. <https://doi.org/10.1146/annurev.med.60.042307.110802>
- Bisley, J.W., Goldberg, M.E., 2010. Attention, Intention, and Priority in the Parietal Lobe. *Annual Review of Neuroscience* 33, 1–21. <https://doi.org/10.1146/annurev-neuro-060909-152823>
- Blundell, J.E., Halford, J.C.G., 1998. Serotonin and Appetite Regulation. *Mol Diag Ther* 9, 473–495. <https://doi.org/10.2165/00023210-199809060-00005>
- Boy, F., Evans, C.J., Edden, R.A.E., Lawrence, A.D., Singh, K.D., Husain, M., Sumner, P., 2011. Dorsolateral Prefrontal γ -Aminobutyric Acid in Men Predicts Individual Differences in Rash Impulsivity. *Biological Psychiatry, Genetic and Environmental Contributors to Disturbed Cortical Development in Developmental Disorders* 70, 866–872. <https://doi.org/10.1016/j.biopsych.2011.05.030>
- Brodie, B.B., Shore, P.A., 1957. A CONCEPT FOR A ROLE OF SEROTONIN AND NOREPINEPHRINE AS CHEMICAL MEDIATORS IN THE BRAIN. *Annals of the New York Academy of Sciences* 66, 631–642. <https://doi.org/10.1111/j.1749-6632.1957.tb40753.x>
- Brown, H.D., Amodeo, D.A., Sweeney, J.A., Ragozzino, M.E., 2012. The selective serotonin reuptake inhibitor, escitalopram, enhances inhibition of prepotent responding and spatial reversal learning. *J Psychopharmacol* 26, 1443–1455. <https://doi.org/10.1177/0269881111430749>
- Buschman, T.J., Miller, E.K., 2007. Top-Down Versus Bottom-Up Control of Attention in the Prefrontal and Posterior Parietal Cortices. *Science* 315, 1860–1862. <https://doi.org/10.1126/science.1138071>
- Carhart-Harris, R., Nutt, D., 2017. Serotonin and brain function: a tale of two receptors. *J Psychopharmacol* 31, 1091–1120. <https://doi.org/10.1177/0269881117725915>
- Carter, O.L., Burr, D.C., Pettigrew, J.D., Vollenweider, F.X., 2005. Using psilocybin to investigate the relationship between attention, working memory and the serotonin 5-HT_{1A} and 5-HT_{2A} receptors. *Journal of Vision* 5, 683. <https://doi.org/10.1167/5.8.683>
- Castaldi, E., Lunghi, C., Morrone, M.C., 2020. Neuroplasticity in adult human visual cortex. *Neuroscience & Biobehavioral Reviews* 112, 542–552. <https://doi.org/10.1016/j.neubiorev.2020.02.028>
- Cerrito, F., Raiteri, M., 1979. Serotonin release is modulated by presynaptic autoreceptors. *European Journal of Pharmacology* 57, 427–430. [https://doi.org/10.1016/0014-2999\(79\)90506-5](https://doi.org/10.1016/0014-2999(79)90506-5)
- Chadnova, E., Reynaud, A., Clavagnier, S., Hess, R.F., 2017. Short-term monocular occlusion produces changes in ocular dominance by a reciprocal modulation of interocular inhibition. *Sci Rep* 7, 41747. <https://doi.org/10.1038/srep41747>
- Chatterjee, S., Callaway, E.M., 2003. Parallel colour-opponent pathways to primary visual cortex. *Nature* 426, 668–671. <https://doi.org/10.1038/nature02167>
- Chattopadhyaya, B., Di Cristo, G., 2012. GABAergic Circuit Dysfunctions in Neurodevelopmental Disorders. *Frontiers in Psychiatry* 3.

- Chelazzi, L., Duncan, J., Miller, E.K., Desimone, R., 1998. Responses of Neurons in Inferior Temporal Cortex During Memory-Guided Visual Search. *Journal of Neurophysiology* 80, 2918–2940. <https://doi.org/10.1152/jn.1998.80.6.2918>
- Chelazzi, L., E to inova, J., Calletti, R., Lo Gerfo, E., Sani, I., Della Libera, C., Santandrea, E., 2014. Altering Spatial Priority Maps via Reward-Based Learning. *Journal of Neuroscience* 34, 8594–8604. <https://doi.org/10.1523/JNEUROSCI.0277-14.2014>
- Chichilnisky, E.-J., Wandell, B.A., 1995. Photoreceptor sensitivity changes explain color appearance shifts induced by large uniform backgrounds in dichoptic matching. *Vision Research* 35, 239–254. [https://doi.org/10.1016/0042-6989\(94\)00122-3](https://doi.org/10.1016/0042-6989(94)00122-3)
- Chollet, F., Tardy, J., Albucher, J.-F., Thalamas, C., Berard, E., Lamy, C., Bejot, Y., Deltour, S., Jaillard, A., Niclot, P., Guillon, B., Moulin, T., Marque, P., Pariente, J., Arnaud, C., Loubinoux, I., 2011. Fluoxetine for motor recovery after acute ischaemic stroke (FLAME): a randomised placebo-controlled trial. *The Lancet Neurology* 10, 123–130. [https://doi.org/10.1016/S1474-4422\(10\)70314-8](https://doi.org/10.1016/S1474-4422(10)70314-8)
- Churchill, A., Graw, J., 2011. Clinical and experimental advances in congenital and paediatric cataracts. *Philosophical Transactions of the Royal Society B: Biological Sciences* 366, 1234–1249. <https://doi.org/10.1098/rstb.2010.0227>
- Clark, C.T., Weissbach, H., Udenfriend, S., 1954. 5-HYDROXYTRYPTOPHAN DECARBOXYLASE: PREPARATION AND PROPERTIES. *Journal of Biological Chemistry* 210, 139–148. [https://doi.org/10.1016/S0021-9258\(18\)65440-7](https://doi.org/10.1016/S0021-9258(18)65440-7)
- Clarke, H.F., Dalley, J.W., Crofts, H.S., Robbins, T.W., Roberts, A.C., 2004. Cognitive Inflexibility After Prefrontal Serotonin Depletion. *Science* 304, 878–880. <https://doi.org/10.1126/science.1094987>
- Cléry, J., Guipponi, O., Wardak, C., Ben Hamed, S., 2015. Neuronal bases of peripersonal and extrapersonal spaces, their plasticity and their dynamics: Knowns and unknowns. *Neuropsychologia* 70, 313–326. <https://doi.org/10.1016/j.neuropsychologia.2014.10.022>
- Cnops, L., Hu, T.-T., Burnat, K., Arckens, L., 2008. Influence of Binocular Competition on the Expression Profiles of CRMP2, CRMP4, Dyn I, and Syt I in Developing Cat Visual Cortex. *Cerebral cortex (New York, N.Y. : 1991)* 18, 1221–31. <https://doi.org/10.1093/cercor/bhm157>
- Cook, E.P., Maunsell, J.H.R., 2002. Dynamics of neuronal responses in macaque MT and VIP during motion detection. *Nat Neurosci* 5, 985–994. <https://doi.org/10.1038/nn924>
- Cools, R., 2008. Role of Dopamine in the Motivational and Cognitive Control of Behavior. *Neuroscientist* 14, 381–395. <https://doi.org/10.1177/1073858408317009>
- Cools, R., Roberts, A.C., Robbins, T.W., 2008. Serotonergic regulation of emotional and behavioural control processes. *Trends in Cognitive Sciences* 12, 31–40. <https://doi.org/10.1016/j.tics.2007.10.011>
- Corbetta, M., Shulman, G.L., 2002. Control of goal-directed and stimulus-driven attention in the brain. *Nat Rev Neurosci* 3, 201–215. <https://doi.org/10.1038/nrn755>
- Coull, J.T., Büchel, C., Friston, K.J., Frith, C.D., 1999. Noradrenergically Mediated Plasticity in a Human Attentional Neuronal Network. *NeuroImage* 10, 705–715. <https://doi.org/10.1006/nimg.1999.0513>
- Dahlstroem, A., Fuxe, K., 1964. EVIDENCE FOR THE EXISTENCE OF MONOAMINE-CONTAINING NEURONS IN THE CENTRAL NERVOUS SYSTEM. I. DEMONSTRATION OF MONOAMINES IN THE CELL BODIES OF BRAIN STEM NEURONS. *Acta Physiol Scand Suppl SUPPL 232*:1-55.
- Davis, M.F., Figueroa Velez, D.X., Guevarra, R.P., Yang, M.C., Habeeb, M., Carathedathu, M.C., Gandhi, S.P., 2015. Inhibitory Neuron Transplantation into Adult Visual Cortex Creates a New Critical

- Period that Rescues Impaired Vision. *Neuron* 86, 1055–1066. <https://doi.org/10.1016/j.neuron.2015.03.062>
- Daw, N.W., 1998. Critical Periods and Amblyopia. *Archives of Ophthalmology* 116, 502–505. <https://doi.org/10.1001/archophth.116.4.502>
- Dayan, P., Huys, Q.J.M., 2009. Serotonin in affective control. *Annu Rev Neurosci* 32, 95–126. <https://doi.org/10.1146/annurev.neuro.051508.135607>
- Di Bello, F., Ben Hadj Hassen, S., Astrand, E., Ben Hamed, S., 2022. Prefrontal Control of Proactive and Reactive Mechanisms of Visual Suppression. *Cerebral Cortex* 32, 2745–2761. <https://doi.org/10.1093/cercor/bhab378>
- Di Bello, F., Ben Hadj Hassen, S., Astrand, E., Ben Hamed, S., 2020. Selection and suppression of visual information in the macaque prefrontal cortex (preprint). *Neuroscience*. <https://doi.org/10.1101/2020.03.25.007922>
- Diamond, M.C., Krech, D., Rosenzweig, M.R., 1964. The effects of an enriched environment on the histology of the rat cerebral cortex. *Journal of Comparative Neurology* 123, 111–119. <https://doi.org/10.1002/cne.901230110>
- Doshier, B.A., Lu, Z.-L., 2000. Noise Exclusion in Spatial Attention. *Psychol Sci* 11, 139–146. <https://doi.org/10.1111/1467-9280.00229>
- Dremencov, E., Mansari, M.E., Blier, P., 2009. Effects of sustained serotonin reuptake inhibition on the firing of dopamine neurons in the rat ventral tegmental area. *Journal of Psychiatry and Neuroscience* 34, 223–229.
- Duffy, K.R., Mitchell, D.E., 2013. Darkness Alters Maturation of Visual Cortex and Promotes Fast Recovery from Monocular Deprivation. *Current Biology* 23, 382–386. <https://doi.org/10.1016/j.cub.2013.01.017>
- Duncan, N.W., Wiebking, C., Northoff, G., 2014. Associations of regional GABA and glutamate with intrinsic and extrinsic neural activity in humans—A review of multimodal imaging studies. *Neuroscience & Biobehavioral Reviews* 47, 36–52. <https://doi.org/10.1016/j.neubiorev.2014.07.016>
- Edden, R.A.E., Crocetti, D., Zhu, H., Gilbert, D.L., Mostofsky, S.H., 2012. Reduced GABA Concentration in Attention-Deficit/Hyperactivity Disorder. *Archives of General Psychiatry* 69, 750–753. <https://doi.org/10.1001/archgenpsychiatry.2011.2280>
- Elodie Bruel-Jungerman, Claire Rampon, Serge Laroche, 2007. Adult Hippocampal Neurogenesis, Synaptic Plasticity and Memory: Facts and Hypotheses. *Reviews in the Neurosciences* 18, 93–114. <https://doi.org/10.1515/REVNEURO.2007.18.2.93>
- Enge, S., Fleischhauer, M., Lesch, K.-P., Reif, A., Strobel, A., 2014. Variation in Key Genes of Serotonin and Norepinephrine Function Predicts Gamma-Band Activity during Goal-Directed Attention. *Cerebral Cortex* 24, 1195–1205. <https://doi.org/10.1093/cercor/bhs398>
- Enge, S., Fleischhauer, M., Lesch, K.-P., Strobel, A., 2011. On the role of serotonin and effort in voluntary attention: Evidence of genetic variation in N1 modulation. *Behavioural Brain Research* 216, 122–128. <https://doi.org/10.1016/j.bbr.2010.07.021>
- Erspamer, V., Asero, B., 1952. Identification of Enteramine, the Specific Hormone of the Enterochromaffin Cell System, as 5-Hydroxytryptamine. *Nature* 169, 800–801. <https://doi.org/10.1038/169800b0>
- Espinosa, J.S., Stryker, M.P., 2012. Development and Plasticity of the Primary Visual Cortex. *Neuron* 75, 230–249. <https://doi.org/10.1016/j.neuron.2012.06.009>

- Esterman, M., Liu, G., Okabe, H., Reagan, A., Thai, M., DeGutis, J., 2015. Frontal eye field involvement in sustaining visual attention: Evidence from transcranial magnetic stimulation. *NeuroImage* 111, 542–548. <https://doi.org/10.1016/j.neuroimage.2015.01.044>
- Ewall, G., Parkins, S., Lin, A., Jaoui, Y., Lee, H.-K., 2021. Cortical and Subcortical Circuits for Cross-Modal Plasticity Induced by Loss of Vision. *Front. Neural Circuits* 15, 665009. <https://doi.org/10.3389/fncir.2021.665009>
- Fagiolini, M., Hensch, T.K., 2000. Inhibitory threshold for critical-period activation in primary visual cortex. *Nature* 404, 183–186. <https://doi.org/10.1038/35004582>
- Fagiolini, M., Pizzorusso, T., Berardi, N., Domenici, L., Maffei, L., 1994. Functional postnatal development of the rat primary visual cortex and the role of visual experience: Dark rearing and monocular deprivation. *Vision Research* 34, 709–720. [https://doi.org/10.1016/0042-6989\(94\)90210-0](https://doi.org/10.1016/0042-6989(94)90210-0)
- Failing, M., Theeuwes, J., 2018. Selection history: How reward modulates selectivity of visual attention. *Psychon Bull Rev* 25, 514–538. <https://doi.org/10.3758/s13423-017-1380-y>
- Falchier, A., Clavagnier, S., Barone, P., Kennedy, H., 2002. Anatomical Evidence of Multimodal Integration in Primate Striate Cortex. *J. Neurosci.* 22, 5749–5759. <https://doi.org/10.1523/JNEUROSCI.22-13-05749.2002>
- Ferrante, O., Patacca, A., Di Caro, V., Della Libera, C., Santandrea, E., Chelazzi, L., 2018. Altering spatial priority maps via statistical learning of target selection and distractor filtering. *Cortex* 102, 67–95. <https://doi.org/10.1016/j.cortex.2017.09.027>
- Fiebelkorn, I.C., Kastner, S., 2020. Functional Specialization in the Attention Network. *Annu Rev Psychol* 71, 221–249. <https://doi.org/10.1146/annurev-psych-010418-103429>
- Fields, R.D., 2015. A new mechanism of nervous system plasticity: activity-dependent myelination. *Nat Rev Neurosci* 16, 756–767. <https://doi.org/10.1038/nrn4023>
- Fields, R.D., Dutta, D.J., Belgrad, J., Robnett, M., 2017. Cholinergic signaling in myelination. *Glia* 65, 687–698. <https://doi.org/10.1002/glia.23101>
- Finn, A.E., Baldwin, A.S., Reynaud, A., Hess, R.F., 2019. Visual plasticity and exercise revisited: No evidence for a “cycling lane.” *Journal of Vision* 19, 21. <https://doi.org/10.1167/19.6.21>
- Fischer, A.G., Jocham, G., Ullsperger, M., 2015. Dual serotonergic signals: a key to understanding paradoxical effects? *Trends in Cognitive Sciences* 19, 21–26. <https://doi.org/10.1016/j.tics.2014.11.004>
- Frangou, P., Emir, U.E., Karlaftis, V.M., Nettekoven, C., Hinson, E.L., Larcombe, S., Bridge, H., Stagg, C.J., Kourtzi, Z., 2019. Learning to optimize perceptual decisions through suppressive interactions in the human brain. *Nat Commun* 10, 474. <https://doi.org/10.1038/s41467-019-08313-y>
- Frey, A.-L., McCabe, C., 2020. Effects of serotonin and dopamine depletion on neural prediction computations during social learning. *Neuropsychopharmacol.* 45, 1431–1437. <https://doi.org/10.1038/s41386-020-0678-z>
- Gaillard, C., Ben Hadj Hassen, S., Di Bello, F., Bihan-Poudec, Y., VanRullen, R., Ben Hamed, S., 2020. Prefrontal attentional saccades explore space rhythmically. *Nat Commun* 11, 925. <https://doi.org/10.1038/s41467-020-14649-7>
- Gainey, M.A., Feldman, D.E., 2017. Multiple shared mechanisms for homeostatic plasticity in rodent somatosensory and visual cortex. *Philosophical Transactions of the Royal Society B: Biological Sciences* 372, 20160157. <https://doi.org/10.1098/rstb.2016.0157>
- Ganguly, K., Poo, M., 2013. Activity-Dependent Neural Plasticity from Bench to Bedside. *Neuron* 80, 729–741. <https://doi.org/10.1016/j.neuron.2013.10.028>

- Goodale, M.A., Milner, A.D., 1992. Separate visual pathways for perception and action. *Trends in Neurosciences* 15, 20–25. [https://doi.org/10.1016/0166-2236\(92\)90344-8](https://doi.org/10.1016/0166-2236(92)90344-8)
- Goodale, M.A., Westwood, D.A., 2004. An evolving view of duplex vision: separate but interacting cortical pathways for perception and action. *Current Opinion in Neurobiology* 14, 203–211. <https://doi.org/10.1016/j.conb.2004.03.002>
- Gordon, B., Allen, E., Trombley, P., 1988. The role of norepinephrine in plasticity of visual cortex. *Progress in Neurobiology* 30, 171–191. [https://doi.org/10.1016/0301-0082\(88\)90005-6](https://doi.org/10.1016/0301-0082(88)90005-6)
- Greenwood, J.A., Tailor, V.K., Sloper, J.J., Simmers, A.J., Bex, P.J., Dakin, S.C., 2012. Visual Acuity, Crowding, and Stereo-Vision Are Linked in Children with and without Amblyopia. *Investigative Ophthalmology & Visual Science* 53, 7655–7665. <https://doi.org/10.1167/iovs.12-10313>
- Gu, Q., 2002. Neuromodulatory transmitter systems in the cortex and their role in cortical plasticity. *Neuroscience* 111, 815–835. [https://doi.org/10.1016/S0306-4522\(02\)00026-X](https://doi.org/10.1016/S0306-4522(02)00026-X)
- Guidotti, G., Calabrese, F., Auletta, F., Olivier, J., Racagni, G., Homberg, J., Riva, M.A., 2012. Developmental Influence of the Serotonin Transporter on the Expression of Npas4 and GABAergic Markers: Modulation by Antidepressant Treatment. *Neuropsychopharmacology* 37, 746–758. <https://doi.org/10.1038/npp.2011.252>
- Guirado, R., Perez-Rando, M., Sanchez-Matarredona, D., Castrén, E., Nacher, J., 2014. Chronic fluoxetine treatment alters the structure, connectivity and plasticity of cortical interneurons. *International Journal of Neuropsychopharmacology* 17, 1635–1646. <https://doi.org/10.1017/S1461145714000406>
- Guirado, R., Varea, E., Castillo-Gómez, E., Gómez-Climent, M.A., Rovira-Esteban, L., Blasco-Ibáñez, J.M., Crespo, C., Martínez-Guijarro, F.J., Nacher, J., 2009. Effects of chronic fluoxetine treatment on the rat somatosensory cortex: Activation and induction of neuronal structural plasticity. *Neuroscience Letters* 457, 12–15. <https://doi.org/10.1016/j.neulet.2009.03.104>
- Halford, J.C.G., Harrold, J.A., 2012. 5-HT_{2C} Receptor Agonists and the Control of Appetite, in: Joost, H.-G. (Ed.), *Appetite Control, Handbook of Experimental Pharmacology*. Springer, Berlin, Heidelberg, pp. 349–356. https://doi.org/10.1007/978-3-642-24716-3_16
- Hansen, J.Y., Shafiei, G., Markello, R.D., Smart, K., Cox, S.M.L., Nørgaard, M., Beliveau, V., Wu, Y., Gallezot, J.-D., Aumont, É., Servaes, S., Scala, S.G., DuBois, J.M., Wainstein, G., Bezgin, G., Funck, T., Schmitz, T.W., Spreng, R.N., Galovic, M., Koeppe, M.J., Duncan, J.S., Coles, J.P., Fryer, T.D., Aigbirhio, F.I., McGinnity, C.J., Hammers, A., Soucy, J.-P., Baillet, S., Guimond, S., Hietala, J., Bedard, M.-A., Leyton, M., Kobayashi, E., Rosa-Neto, P., Ganz, M., Knudsen, G.M., Palomero-Gallagher, N., Shine, J.M., Carson, R.E., Tuominen, L., Dagher, A., Misic, B., 2022. Mapping neurotransmitter systems to the structural and functional organization of the human neocortex. *Nat Neurosci* 1–13. <https://doi.org/10.1038/s41593-022-01186-3>
- Harauzov, A., Spolidoro, M., DiCristo, G., Pasquale, R.D., Cancedda, L., Pizzorusso, T., Viegi, A., Berardi, N., Maffei, L., 2010. Reducing Intracortical Inhibition in the Adult Visual Cortex Promotes Ocular Dominance Plasticity. *J. Neurosci.* 30, 361–371. <https://doi.org/10.1523/JNEUROSCI.2233-09.2010>
- Harwerth, R.S., Smith, E.L., Duncan, G.C., Crawford, M.L., Von Noorden, G.K., 1986. Multiple sensitive periods in the development of the primate visual system. *Science* 232, 235–238. <https://doi.org/10.1126/science.3952507>
- Hebb, D.O., 1949. *The organization of behavior; a neuropsychological theory*, *The organization of behavior; a neuropsychological theory*. Wiley, Oxford, England.
- Heimel, J.A., van Versendaal, D., Levelt, C.N., 2011. The Role of GABAergic Inhibition in Ocular Dominance Plasticity. *Neural Plasticity* 2011, e391763. <https://doi.org/10.1155/2011/391763>

- Hensch, T.K., Fagiolini, M., Mataga, N., Stryker, M.P., Baekkeskov, S., Kash, S.F., 1998. Local GABA Circuit Control of Experience-Dependent Plasticity in Developing Visual Cortex. *Science* 282, 1504–1508. <https://doi.org/10.1126/science.282.5393.1504>
- Hensch, T.K., Quinlan, E.M., 2018. Critical periods in amblyopia. *Visual Neuroscience* 35, E014. <https://doi.org/10.1017/S0952523817000219>
- Hess, R.F., Thompson, B., Baker, D.H., 2014. Binocular vision in amblyopia: structure, suppression and plasticity. *Ophthalmic Physiol Opt* 34, 146–162. <https://doi.org/10.1111/opo.12123>
- Homberg, J.R., 2012. Serotonin and decision making processes. *Neuroscience & Biobehavioral Reviews* 36, 218–236. <https://doi.org/10.1016/j.neubiorev.2011.06.001>
- Hong, S.Z., Huang, S., Severin, D., Kirkwood, A., 2020. Pull-push neuromodulation of cortical plasticity enables rapid bi-directional shifts in ocular dominance. *eLife* 9, e54455. <https://doi.org/10.7554/eLife.54455>
- Hong, S.Z., Mesik, L., Grossman, C.D., Cohen, J.Y., Lee, B., Lee, H.-K., Hell, J.W., Kirkwood, A., 2021. Norepinephrine Potentiates and Serotonin Depresses Visual Cortical Responses by Transforming Eligibility Traces (preprint). *Neuroscience*. <https://doi.org/10.1101/2021.06.22.449441>
- Hopfinger, J.B., Buonocore, M.H., Mangun, G.R., 2000. The neural mechanisms of top-down attentional control. *Nat Neurosci* 3, 284–291. <https://doi.org/10.1038/72999>
- Hoyer, D., Clarke, D.E., Fozard, J.R., Hartig, P.R., Martin, G.R., Mylecharane, E.J., Saxena, P.R., Humphrey, P.P., 1994. International Union of Pharmacology classification of receptors for 5-hydroxytryptamine (Serotonin). *Pharmacol Rev* 46, 157–203.
- Hoyer, D., Martin, G., 1997. 5-HT Receptor Classification and Nomenclature: Towards a Harmonization with the Human Genome. *Neuropharmacology* 36, 419–428. [https://doi.org/10.1016/S0028-3908\(97\)00036-1](https://doi.org/10.1016/S0028-3908(97)00036-1)
- Hoyt, C.S., 2005. Amblyopia: A Neuro-Ophthalmic View. *Journal of Neuro-Ophthalmology* 25, 227–231. <https://doi.org/10.1097/01.wno.0000177304.67715.ba>
- Huang, Z.J., Kirkwood, A., Pizzorusso, T., Porciatti, V., Morales, B., Bear, M.F., Maffei, L., Tonegawa, S., 1999. BDNF Regulates the Maturation of Inhibition and the Critical Period of Plasticity in Mouse Visual Cortex. *Cell* 98, 739–755. [https://doi.org/10.1016/S0092-8674\(00\)81509-3](https://doi.org/10.1016/S0092-8674(00)81509-3)
- Hubel, D.H., Wiesel, T.N., 1970. The period of susceptibility to the physiological effects of unilateral eye closure in kittens. *The Journal of Physiology* 206, 419–436. <https://doi.org/10.1113/jphysiol.1970.sp009022>
- Hubel, D.H., Wiesel, T.N., 1963. Receptive fields of cells in striate cortex of very young, visually inexperienced kittens. *Journal of Neurophysiology* 26, 994–1002. <https://doi.org/10.1152/jn.1963.26.6.994>
- Hubel, D.H., Wiesel, T.N., 1959. Receptive fields of single neurones in the cat's striate cortex. *J Physiol* 148, 574–591.
- Hubel, D.H., Wiesel, T.N., LeVay, S., Barlow, H.B., Gaze, R.M., 1977. Plasticity of ocular dominance columns in monkey striate cortex. *Philosophical Transactions of the Royal Society of London. B, Biological Sciences* 278, 377–409. <https://doi.org/10.1098/rstb.1977.0050>
- Huot, P., Fox, S.H., Brotchie, J.M., 2011. The serotonergic system in Parkinson's disease. *Progress in Neurobiology* 95, 163–212. <https://doi.org/10.1016/j.pneurobio.2011.08.004>
- Ibos, G., Duhamel, J.-R., Hamed, S.B., 2013. A Functional Hierarchy within the Parietofrontal Network in Stimulus Selection and Attention Control. *J. Neurosci.* 33, 8359–8369. <https://doi.org/10.1523/JNEUROSCI.4058-12.2013>

- Ishimura, K., Takeuchi, Y., Fujiwara, K., Tominaga, M., Yoshioka, H., Sawada, T., 1988. Quantitative analysis of the distribution of serotonin-immunoreactive cell bodies in the mouse brain. *Neuroscience Letters* 91, 265–270. [https://doi.org/10.1016/0304-3940\(88\)90691-X](https://doi.org/10.1016/0304-3940(88)90691-X)
- Issa, N.P., Trachtenberg, J.T., Chapman, B., Zahs, K.R., Stryker, M.P., 1999. The Critical Period for Ocular Dominance Plasticity in the Ferret's Visual Cortex. *J. Neurosci.* 19, 6965–6978. <https://doi.org/10.1523/JNEUROSCI.19-16-06965.1999>
- Ito, M., Tamura, H., Fujita, I., Tanaka, K., 1995. Size and position invariance of neuronal responses in monkey inferotemporal cortex. *Journal of Neurophysiology* 73, 218–226. <https://doi.org/10.1152/jn.1995.73.1.218>
- Itti, L., Koch, C., 2001. Computational modelling of visual attention. *Nat Rev Neurosci* 2, 194–203. <https://doi.org/10.1038/35058500>
- Jakowec, M.W., Wang, Z., Holschneider, D., Beeler, J., Petzinger, G.M., 2016. Engaging cognitive circuits to promote motor recovery in degenerative disorders. exercise as a learning modality. *Journal of Human Kinetics* 52, 35–51. <https://doi.org/10.1515/hukin-2015-0192>
- Janet, R., Ligneul, R., Losecaat-Vermeer, A.B., Philippe, R., Bellucci, G., Derrington, E., Park, S.Q., Dreher, J.-C., 2022. Regulation of social hierarchy learning by serotonin transporter availability. *Neuropsychopharmacol.* 1–8. <https://doi.org/10.1038/s41386-022-01378-2>
- Jay, T.M., 2003. Dopamine: a potential substrate for synaptic plasticity and memory mechanisms. *Progress in Neurobiology* 69, 375–390. [https://doi.org/10.1016/S0301-0082\(03\)00085-6](https://doi.org/10.1016/S0301-0082(03)00085-6)
- Jeffery, G., 2001. Architecture of the Optic Chiasm and the Mechanisms That Sculpt Its Development. *Physiological Reviews* 81, 1393–1414. <https://doi.org/10.1152/physrev.2001.81.4.1393>
- Kahnt, T., Park, S.Q., Haynes, J.-D., Tobler, P.N., 2014. Disentangling neural representations of value and salience in the human brain. *Proc Natl Acad Sci USA* 111, 5000–5005. <https://doi.org/10.1073/pnas.1320189111>
- Kaila, K., Ruusuvuori, E., Seja, P., Voipio, J., Puskarjov, M., 2014. GABA actions and ionic plasticity in epilepsy. *Current Opinion in Neurobiology, SI: Inhibition: Synapses, Neurons and Circuits* 26, 34–41. <https://doi.org/10.1016/j.conb.2013.11.004>
- Kaneko, M., Stryker, M.P., 2014. Sensory experience during locomotion promotes recovery of function in adult visual cortex. *eLife* 3, e02798. <https://doi.org/10.7554/eLife.02798>
- Kanjlia, S., Feigenson, L., Bedny, M., 2021. Neural basis of approximate number in congenital blindness. *Cortex* 142, 342–356. <https://doi.org/10.1016/j.cortex.2021.06.004>
- Kappel, D., Habenschuss, S., Legenstein, R., Maass, W., 2015. Network Plasticity as Bayesian Inference. *PLOS Computational Biology* 11, e1004485. <https://doi.org/10.1371/journal.pcbi.1004485>
- Karni, A., Bertini, G., 1997. Learning perceptual skills: behavioral probes into adult cortical plasticity. *Current Opinion in Neurobiology* 7, 530–535. [https://doi.org/10.1016/S0959-4388\(97\)80033-5](https://doi.org/10.1016/S0959-4388(97)80033-5)
- Kasamatsu, T., 1991. Chapter 42 - Adrenergic regulation of visuocortical plasticity: a role of the locus coeruleus system, in: Barnes, C.D., Pompeiano, O. (Eds.), *Progress in Brain Research, Neurobiology of the Locus Coeruleus*. Elsevier, pp. 599–616. [https://doi.org/10.1016/S0079-6123\(08\)63837-6](https://doi.org/10.1016/S0079-6123(08)63837-6)
- Kasamatsu, T., 1982. Enhancement of neuronal plasticity by activating the norepinephrine system in the brain: a remedy for amblyopia. *Hum Neurobiol* 1, 49–54.
- Kastner, S., De Weerd, P., Desimone, R., Ungerleider, L.G., 1998. Mechanisms of Directed Attention in the Human Extrastriate Cortex as Revealed by Functional MRI. *Science* 282, 108–111. <https://doi.org/10.1126/science.282.5386.108>

- Kastner, S., Pinsk, M.A., De Weerd, P., Desimone, R., Ungerleider, L.G., 1999. Increased Activity in Human Visual Cortex during Directed Attention in the Absence of Visual Stimulation. *Neuron* 22, 751–761. [https://doi.org/10.1016/S0896-6273\(00\)80734-5](https://doi.org/10.1016/S0896-6273(00)80734-5)
- Kastner, S., Ungerleider, L.G., 2001. The neural basis of biased competition in human visual cortex. *Neuropsychologia* 39, 1263–1276. [https://doi.org/10.1016/S0028-3932\(01\)00116-6](https://doi.org/10.1016/S0028-3932(01)00116-6)
- Katsuki, F., Constantinidis, C., 2014. Bottom-Up and Top-Down Attention: Different Processes and Overlapping Neural Systems. *Neuroscientist* 20, 509–521. <https://doi.org/10.1177/1073858413514136>
- Katsuki, F., Constantinidis, C., 2012. Early involvement of prefrontal cortex in visual bottom-up attention. *Nat Neurosci* 15, 1160–1166. <https://doi.org/10.1038/nn.3164>
- Katzner, S., Busse, L., Carandini, M., 2011. GABAA Inhibition Controls Response Gain in Visual Cortex. *J. Neurosci.* 31, 5931–5941. <https://doi.org/10.1523/JNEUROSCI.5753-10.2011>
- Kawaguchi, Y., Shindou, T., 1998. Noradrenergic Excitation and Inhibition of GABAergic Cell Types in Rat Frontal Cortex. *J. Neurosci.* 18, 6963–6976. <https://doi.org/10.1523/JNEUROSCI.18-17-06963.1998>
- Kerkhoff, G., 2003. Modulation and rehabilitation of spatial neglect by sensory stimulation, in: *Progress in Brain Research, Neural Control of Space Coding and Action Production*. Elsevier, pp. 257–271. [https://doi.org/10.1016/S0079-6123\(03\)42018-9](https://doi.org/10.1016/S0079-6123(03)42018-9)
- Kim, G.H., Kang, I., Jeong, H., Park, S., Hong, H., Kim, J., Kim, J.Y., Edden, R.A.E., Lyoo, I.K., Yoon, S., 2019. Low Prefrontal GABA Levels Are Associated With Poor Cognitive Functions in Professional Boxers. *Frontiers in Human Neuroscience* 13.
- Kimura, F., Fukuda, M., Tsumoto, T., 1999. Acetylcholine suppresses the spread of excitation in the visual cortex revealed by optical recording: possible differential effect depending on the source of input. *European Journal of Neuroscience* 11, 3597–3609. <https://doi.org/10.1046/j.1460-9568.1999.00779.x>
- Kiorpes, L., 2006. Visual Processing in Amblyopia: Animal Studies. *Strabismus* 14, 3–10. <https://doi.org/10.1080/09273970500536193>
- Klyszejko, Z., Rahmati, M., Curtis, C.E., 2014. Attentional priority determines working memory precision. *Vision Research* 105, 70–76. <https://doi.org/10.1016/j.visres.2014.09.002>
- Knöpfel, T., Sweeney, Y., Radulescu, C.I., Zabouri, N., Doostdar, N., Clopath, C., Barnes, S.J., 2019. Audio-visual experience strengthens multisensory assemblies in adult mouse visual cortex. *Nat Commun* 10, 5684. <https://doi.org/10.1038/s41467-019-13607-2>
- Kraus, C., Castrén, E., Kasper, S., Lanzenberger, R., 2017. Serotonin and neuroplasticity – Links between molecular, functional and structural pathophysiology in depression. *Neuroscience & Biobehavioral Reviews* 77, 317–326. <https://doi.org/10.1016/j.neubiorev.2017.03.007>
- Lehmann, K., Löwel, S., 2008. Age-Dependent Ocular Dominance Plasticity in Adult Mice. *PLOS ONE* 3, e3120. <https://doi.org/10.1371/journal.pone.0003120>
- Levi, D.M., Li, R.W., 2009. Perceptual learning as a potential treatment for amblyopia: A mini-review. *Vision Research, Perceptual Learning* 49, 2535–2549. <https://doi.org/10.1016/j.visres.2009.02.010>
- Li, X., Chen, W., Pan, K., Li, H., Pang, P., Guo, Y., Shu, S., Cai, Y., Pei, L., Liu, D., Afewerky, H.K., Tian, Q., Zhu, L.-Q., Lu, Y., 2018. Serotonin receptor 2c-expressing cells in the ventral CA1 control attention via innervation of the Edinger–Westphal nucleus. *Nat Neurosci* 21, 1239–1250. <https://doi.org/10.1038/s41593-018-0207-0>
- Luck, S.J., Chelazzi, L., Hillyard, S.A., Desimone, R., 1997. Neural Mechanisms of Spatial Selective Attention in Areas V1, V2, and V4 of Macaque Visual Cortex. *Journal of Neurophysiology* 77, 24–42. <https://doi.org/10.1152/jn.1997.77.1.24>

- Lueschow, A., Miller, E.K., Desimone, R., 1994. Inferior Temporal Mechanisms for Invariant Object Recognition. *Cerebral Cortex* 4, 523–531. <https://doi.org/10.1093/cercor/4.5.523>
- Lunghi, C., Burr, D.C., Morrone, C., 2011. Brief periods of monocular deprivation disrupt ocular balance in human adult visual cortex. *Current Biology* 21, R538–R539. <https://doi.org/10.1016/j.cub.2011.06.004>
- Lunghi, C., Emir, U.E., Morrone, M.C., Bridge, H., 2015. Short-Term Monocular Deprivation Alters GABA in the Adult Human Visual Cortex. *Current Biology* 25, 1496–1501. <https://doi.org/10.1016/j.cub.2015.04.021>
- Lunghi, C., Sale, A., 2015. A cycling lane for brain rewiring. *Current Biology* 25, R1122–R1123. <https://doi.org/10.1016/j.cub.2015.10.026>
- McGarrity, S., Mason, R., Fone, K.C., Pezze, M., Bast, T., 2017. Hippocampal Neural Disinhibition Causes Attentional and Memory Deficits. *Cerebral Cortex* 27, 4447–4462. <https://doi.org/10.1093/cercor/bhw247>
- Mead, G.E., Legg, L., Tilney, R., Hsieh, C.F., Wu, S., Lundström, E., Rudberg, A.S., Kutlubayev, M., Dennis, M.S., Soleimani, B., Barugh, A., Hackett, M.L., Hankey, G.J., 2020. Fluoxetine for stroke recovery: Meta-analysis of randomized controlled trials. *International Journal of Stroke* 15, 365–376. <https://doi.org/10.1177/1747493019879655>
- Meehan, T.P., Bressler, S.L., Tang, W., Astafiev, S.V., Sylvester, C.M., Shulman, G.L., Corbetta, M., 2017. Top-down cortical interactions in visuospatial attention. *Brain Struct Funct* 222, 3127–3145. <https://doi.org/10.1007/s00429-017-1390-6>
- Meneses, A., Liy-Salmeron, G., 2012. Serotonin and emotion, learning and memory. *Reviews in the Neurosciences* 23, 543–553. <https://doi.org/10.1515/revneuro-2012-0060>
- Meriney, S., Fanselow, E., 2019. *Synaptic Transmission*. Academic Press.
- Meyniel, F., Goodwin, G.M., Deakin, J.W., Klinge, C., MacFadyen, C., Milligan, H., Mullings, E., Pessiglione, M., Gaillard, R., 2016. A specific role for serotonin in overcoming effort cost. *eLife* 5, e17282. <https://doi.org/10.7554/eLife.17282>
- Michaelson, I.A., Whittaker, V.P., 1963. The subcellular localization of 5-hydroxytryptamine in guinea pig brain. *Biochemical Pharmacology* 12, 203–211. [https://doi.org/10.1016/0006-2952\(63\)90185-0](https://doi.org/10.1016/0006-2952(63)90185-0)
- Miller, E.K., Buschman, T.J., 2013. Cortical circuits for the control of attention. *Current Opinion in Neurobiology, Macrocircuits* 23, 216–222. <https://doi.org/10.1016/j.conb.2012.11.011>
- Miller, E.K., Li, L., Desimone, R., 1993. Activity of neurons in anterior inferior temporal cortex during a short-term memory task. *J. Neurosci.* 13, 1460–1478. <https://doi.org/10.1523/JNEUROSCI.13-04-01460.1993>
- Mishkin, M., Ungerleider, L.G., 1982. Contribution of striate inputs to the visuospatial functions of parieto-occipital cortex in monkeys. *Behavioural Brain Research* 6, 57–77. [https://doi.org/10.1016/0166-4328\(82\)90081-X](https://doi.org/10.1016/0166-4328(82)90081-X)
- Mishkin, M., Ungerleider, L.G., Macko, K.A., 1983. Object vision and spatial vision: two cortical pathways. *Trends in Neurosciences* 6, 414–417. [https://doi.org/10.1016/0166-2236\(83\)90190-X](https://doi.org/10.1016/0166-2236(83)90190-X)
- Mitchell, D.E., Mackinnon, S., 2002. The present and potential impact of research on animal models for clinical treatment of stimulus deprivation amblyopia. *Clinical and Experimental Optometry* 85, 5–18. <https://doi.org/10.1111/j.1444-0938.2002.tb03067.x>
- Mohammad-Zadeh, L.F., Moses, L., Gwaltney-Brant, S.M., 2008. Serotonin: a review. *Journal of Veterinary Pharmacology and Therapeutics* 31, 187–199. <https://doi.org/10.1111/j.1365-2885.2008.00944.x>

- Moran, J., Desimone, R., 1985. Selective Attention Gates Visual Processing in the Extrastriate Cortex. *Science* 229, 782–784. <https://doi.org/10.1126/science.4023713>
- Motz, B.A., James, K.H., Busey, T.A., 2012. The Lateralizer: a tool for students to explore the divided brain. *Advances in Physiology Education* 36, 220–225. <https://doi.org/10.1152/advan.00060.2012>
- Müller, C.M., Best, J., 1989. Ocular dominance plasticity in adult cat visual cortex after transplantation of cultured astrocytes. *Nature* 342, 427–430. <https://doi.org/10.1038/342427a0>
- Müller, N.G., Kleinschmidt, A., 2003. Dynamic Interaction of Object- and Space-Based Attention in Retinotopic Visual Areas. *J. Neurosci.* 23, 9812–9816. <https://doi.org/10.1523/JNEUROSCI.23-30-09812.2003>
- Nakamura, K., 2013. The role of the dorsal raphe nucleus in reward-seeking behavior. *Frontiers in Integrative Neuroscience* 7.
- Ng, K.L., Gibson, E.M., Hubbard, R., Yang, J., Caffo, B., O'Brien, R.J., Krakauer, J.W., Zeiler, S.R., 2015. Fluoxetine Maintains a State of Heightened Responsiveness to Motor Training Early After Stroke in a Mouse Model. *Stroke* 46, 2951–2960. <https://doi.org/10.1161/STROKEAHA.115.010471>
- Ni, W., Watts, S.W., 2006. 5-HYDROXYTRYPTAMINE IN THE CARDIOVASCULAR SYSTEM: FOCUS ON THE SEROTONIN TRANSPORTER (SERT). *Clin Exp Pharmacol Physiol* 33, 575–583. <https://doi.org/10.1111/j.1440-1681.2006.04410.x>
- Niell, C.M., Stryker, M.P., 2010. Modulation of Visual Responses by Behavioral State in Mouse Visual Cortex. *Neuron* 65, 472–479. <https://doi.org/10.1016/j.neuron.2010.01.033>
- Nithianantharajah, J., Hannan, A.J., 2006. Enriched environments, experience-dependent plasticity and disorders of the nervous system. *Nat Rev Neurosci* 7, 697–709. <https://doi.org/10.1038/nrn1970>
- Noudoost, B., Chang, M.H., Steinmetz, N.A., Moore, T., 2010. Top-down control of visual attention. *Current Opinion in Neurobiology, Cognitive neuroscience* 20, 183–190. <https://doi.org/10.1016/j.conb.2010.02.003>
- Olson, C.R., Freeman, R.D., 1980. Profile of the sensitive period for monocular deprivation in kittens. *Exp Brain Res* 39, 17–21. <https://doi.org/10.1007/BF00237065>
- Ossipov, M.H., Dussor, G.O., Porreca, F., 2010. Central modulation of pain. *J Clin Invest* 120, 3779–3787. <https://doi.org/10.1172/JCI43766>
- Owens, M.J., 1996. Molecular and cellular mechanisms of antidepressant drugs. *Depression and Anxiety* 4, 153–159. [https://doi.org/10.1002/\(SICI\)1520-6394\(1996\)4:4<153::AID-DA1>3.0.CO;2-G](https://doi.org/10.1002/(SICI)1520-6394(1996)4:4<153::AID-DA1>3.0.CO;2-G)
- Paine, T.A., Slipp, L.E., Carlezon, W.A., 2011. Schizophrenia-Like Attentional Deficits Following Blockade of Prefrontal Cortex GABAA Receptors. *Neuropsychopharmacol* 36, 1703–1713. <https://doi.org/10.1038/npp.2011.51>
- Pälvimäki, E.-P., Majasuo, H., Laakso, A., Kuoppamäki, M., Syvälahti, E., Roth, B.L., Hietala, J., 1996. Interactions of selective serotonin reuptake inhibitors with the serotonin 5-HT_{2C} receptor. *Psychopharmacology* 126, 234–240. <https://doi.org/10.1007/BF02246453>
- Paulsen, O., Sejnowski, T.J., 2000. Natural patterns of activity and long-term synaptic plasticity. *Curr Opin Neurobiol* 10, 172–179.
- Pehrson, A.L., Leiser, S.C., Gulinello, M., Dale, E., Li, Y., Waller, J.A., Sanchez, C., 2015. Treatment of cognitive dysfunction in major depressive disorder—a review of the preclinical evidence for efficacy of selective serotonin reuptake inhibitors, serotonin–norepinephrine reuptake inhibitors and the multimodal-acting antidepressant vortioxetine. *European Journal of Pharmacology, Mood disorders-preclinical, clinical and translational aspects* 753, 19–31. <https://doi.org/10.1016/j.ejphar.2014.07.044>

- Pessiglione, M., Vinckier, F., Bouret, S., Daunizeau, J., Le Bouc, R., 2018. Why not try harder? Computational approach to motivation deficits in neuro-psychiatric diseases. *Brain* 141, 629–650. <https://doi.org/10.1093/brain/awx278>
- Petersen, S.E., Robinson, D.L., Morris, J.D., 1987. Contributions of the pulvinar to visual spatial attention. *Neuropsychologia* 25, 97–105. [https://doi.org/10.1016/0028-3932\(87\)90046-7](https://doi.org/10.1016/0028-3932(87)90046-7)
- Petros, T.J., Rebsam, A., Mason, C.A., 2008. Retinal Axon Growth at the Optic Chiasm: To Cross or Not to Cross. *Annu. Rev. Neurosci.* 31, 295–315. <https://doi.org/10.1146/annurev.neuro.31.060407.125609>
- Pezze, M., McGarrity, S., Mason, R., Fone, K.C., Bast, T., 2014. Too Little and Too Much: Hypoactivation and Disinhibition of Medial Prefrontal Cortex Cause Attentional Deficits. *J. Neurosci.* 34, 7931–7946. <https://doi.org/10.1523/JNEUROSCI.3450-13.2014>
- Pizzorusso, T., 2002. Reactivation of Ocular Dominance Plasticity in the Adult Visual Cortex. *Science* 298, 1248–1251. <https://doi.org/10.1126/science.1072699>
- Poggio, G.F., Poggio, T., 1984. The Analysis of Stereopsis. *Annu. Rev. Neurosci.* 7, 379–412. <https://doi.org/10.1146/annurev.ne.07.030184.002115>
- Pollak Dorocic, I., Fürth, D., Xuan, Y., Johansson, Y., Pozzi, L., Silberberg, G., Carlén, M., Meletis, K., 2014. A Whole-Brain Atlas of Inputs to Serotonergic Neurons of the Dorsal and Median Raphe Nuclei. *Neuron* 83, 663–678. <https://doi.org/10.1016/j.neuron.2014.07.002>
- Powell, C., Hatt, S.R., 2009. Vision screening for amblyopia in childhood. *Cochrane Database Syst Rev* CD005020. <https://doi.org/10.1002/14651858.cd005020.pub3>
- Puig, M.V., Gullledge, A.T., 2011. Serotonin and Prefrontal Cortex Function: Neurons, Networks, and Circuits. *Mol Neurobiol* 44, 449–464. <https://doi.org/10.1007/s12035-011-8214-0>
- Raleigh, M.J., 1984. Social and Environmental Influences on Blood Serotonin Concentrations in Monkeys. *Arch Gen Psychiatry* 41, 405. <https://doi.org/10.1001/archpsyc.1984.01790150095013>
- Raleigh, M.J., Brammer, G.L., Yuwiler, A., Flannery, J.W., McGuire, M.T., Geller, E., 1980. Serotonergic influences on the social behavior of vervet monkeys (*Cercopithecus aethiops sabaeus*). *Experimental Neurology* 68, 322–334. [https://doi.org/10.1016/0014-4886\(80\)90089-8](https://doi.org/10.1016/0014-4886(80)90089-8)
- Raleigh, M.J., McGuire, M.T., Brammer, G.L., Pollack, D.B., Yuwiler, A., 1991. Serotonergic mechanisms promote dominance acquisition in adult male vervet monkeys. *Brain Research* 559, 181–190. [https://doi.org/10.1016/0006-8993\(91\)90001-C](https://doi.org/10.1016/0006-8993(91)90001-C)
- Rapport, M.M., Green, Arda.Alden., Page, I.H., 1948a. SERUM VASOCONSTRICTOR (SEROTONIN): III. CHEMICAL INACTIVATION. *Journal of Biological Chemistry* 176, 1237–1241. [https://doi.org/10.1016/S0021-9258\(18\)57136-2](https://doi.org/10.1016/S0021-9258(18)57136-2)
- Rapport, M.M., Green, Arda.Alden., Page, I.H., 1948b. PARTIAL PURIFICATION OF THE VASOCONSTRICTOR IN BEEF SERUM. *Journal of Biological Chemistry* 174, 735–741. [https://doi.org/10.1016/S0021-9258\(18\)57355-5](https://doi.org/10.1016/S0021-9258(18)57355-5)
- Rapport, M.M., Green, Arda.Alden., Page, I.H., 1948c. SERUM VASOCONSTRICTOR (SEROTONIN): IV. ISOLATION AND CHARACTERIZATION. *Journal of Biological Chemistry* 176, 1243–1251. [https://doi.org/10.1016/S0021-9258\(18\)57137-4](https://doi.org/10.1016/S0021-9258(18)57137-4)
- Read, J.C.A., 2021. Binocular Vision and Stereopsis Across the Animal Kingdom. *Annu. Rev. Vis. Sci.* 7, 389–415. <https://doi.org/10.1146/annurev-vision-093019-113212>
- Reid, G., Rand, M., 1952. Pharmacological Actions of Synthetic 5-Hydroxytryptamine (Serotonin, Thrombocytin). *Nature* 169, 801–802. <https://doi.org/10.1038/169801a0>

- Ren, J., Friedmann, D., Xiong, J., Liu, C.D., Ferguson, B.R., Weerakkody, T., DeLoach, K.E., Ran, C., Pun, A., Sun, Y., Weissbourd, B., Neve, R.L., Huguenard, J., Horowitz, M.A., Luo, L., 2018. Anatomically Defined and Functionally Distinct Dorsal Raphe Serotonin Sub-systems. *Cell* 175, 472-487.e20. <https://doi.org/10.1016/j.cell.2018.07.043>
- Ress, D., Backus, B.T., Heeger, D.J., 2000. Activity in primary visual cortex predicts performance in a visual detection task. *Nat Neurosci* 3, 940–945. <https://doi.org/10.1038/78856>
- Reynaud, A.J., Froesel, M., Guedj, C., Ben Hadj Hassen, S., Cléry, J., Meunier, M., Ben Hamed, S., Hadj-Bouziane, F., 2019. Atomoxetine improves attentional orienting in a predictive context. *Neuropharmacology* 150, 59–69. <https://doi.org/10.1016/j.neuropharm.2019.03.012>
- Reynolds, J.H., Chelazzi, L., 2004. ATTENTIONAL MODULATION OF VISUAL PROCESSING. *Annu. Rev. Neurosci.* 27, 611–647. <https://doi.org/10.1146/annurev.neuro.26.041002.131039>
- Reynolds, J.H., Chelazzi, L., Desimone, R., 1999. Competitive Mechanisms Subserve Attention in Macaque Areas V2 and V4. *J. Neurosci.* 19, 1736–1753. <https://doi.org/10.1523/JNEUROSCI.19-05-01736.1999>
- Ribot, J., Breton, R., Calvo, C.-F., Moulard, J., Ezan, P., Zapata, J., Samama, K., Moreau, M., Bemelmans, A.-P., Sabatet, V., Dingli, F., Loew, D., Milleret, C., Billuart, P., Dallérac, G., Rouach, N., 2021. Astrocytes close the mouse critical period for visual plasticity. *Science* 373, 77–81. <https://doi.org/10.1126/science.abf5273>
- Richter, C.G., Thompson, W.H., Bosman, C.A., Fries, P., 2017. Top-Down Beta Enhances Bottom-Up Gamma. *J. Neurosci.* 37, 6698–6711. <https://doi.org/10.1523/JNEUROSCI.3771-16.2017>
- Roberts, M.J., Zinke, W., Guo, K., Robertson, R., McDonald, J.S., Thiele, A., 2005. Acetylcholine Dynamically Controls Spatial Integration in Marmoset Primary Visual Cortex. *Journal of Neurophysiology* 93, 2062–2072. <https://doi.org/10.1152/jn.00911.2004>
- Rodriguez, L., Joly, S., Zine-Eddine, F., Mdzomba, J.B., Pernet, V., 2020. Tau modulates visual plasticity in adult and old mice. *Neurobiology of Aging* 95, 214–224. <https://doi.org/10.1016/j.neurobiolaging.2020.07.024>
- Rogawski, M.A., Aghajanian, G.K., 1980. Modulation of lateral geniculate neurone excitability by noradrenaline microiontophoresis or locus coeruleus stimulation. *Nature* 287, 731–734. <https://doi.org/10.1038/287731a0>
- Rong, X., Ji, Y., Fang, Y., Jiang, Y., Lu, Y., 2015. Long-Term Visual Outcomes of Secondary Intraocular Lens Implantation in Children with Congenital Cataracts. *PLOS ONE* 10, e0134864. <https://doi.org/10.1371/journal.pone.0134864>
- Russo, S.J., Nestler, E.J., 2013. The brain reward circuitry in mood disorders. *Nat Rev Neurosci* 14, 609–625. <https://doi.org/10.1038/nrn3381>
- Sakurai, T., 2007. The neural circuit of orexin (hypocretin): maintaining sleep and wakefulness. *Nat Rev Neurosci* 8, 171–181. <https://doi.org/10.1038/nrn2092>
- Sanchez-Vives, M.V., Barbero-Castillo, A., Perez-Zabalza, M., Reig, R., 2021. GABAB receptors: modulation of thalamocortical dynamics and synaptic plasticity. *Neuroscience* 456, 131–142. <https://doi.org/10.1016/j.neuroscience.2020.03.011>
- Sandberg, K., Blicher, J.U., Dong, M.Y., Rees, G., Near, J., Kanai, R., 2014. Occipital GABA correlates with cognitive failures in daily life. *NeuroImage* 87, 55–60. <https://doi.org/10.1016/j.neuroimage.2013.10.059>
- Sandi, C., Haller, J., 2015. Stress and the social brain: behavioural effects and neurobiological mechanisms. *Nat Rev Neurosci* 16, 290–304. <https://doi.org/10.1038/nrn3918>

- Schmidt-Wilcke, T., Fuchs, E., Funke, K., Vlachos, A., Müller-Dahlhaus, F., Puts, N.A.J., Harris, R.E., Edden, R.A.E., 2018. GABA—from Inhibition to Cognition: Emerging Concepts. *Neuroscientist* 24, 501–515. <https://doi.org/10.1177/1073858417734530>
- Schneider, C.L., Majewska, A.K., Busza, A., Williams, Z.R., Mahon, B.Z., Sahin, B., 2021. Selective serotonin reuptake inhibitors for functional recovery after stroke: similarities with the critical period and the role of experience-dependent plasticity. *J Neurol* 268, 1203–1209. <https://doi.org/10.1007/s00415-019-09480-0>
- Schneider, K.A., 2011. Subcortical Mechanisms of Feature-Based Attention. *J Neurosci* 31, 8643–8653. <https://doi.org/10.1523/JNEUROSCI.6274-10.2011>
- Scholes, K.E., Harrison, B.J., O’Neill, B.V., Leung, S., Croft, R.J., Pipingas, A., Phan, K.L., Nathan, P.J., 2007. Acute Serotonin and Dopamine Depletion Improves Attentional Control: Findings from the Stroop Task. *Neuropsychopharmacol* 32, 1600–1610. <https://doi.org/10.1038/sj.npp.1301262>
- Serences, J.T., Yantis, S., 2006. Selective visual attention and perceptual coherence. *Trends in Cognitive Sciences* 10, 38–45. <https://doi.org/10.1016/j.tics.2005.11.008>
- Serences, J.T., Yantis, S., 2004. Attentional Priority Maps in Human Cortex: (537052012-668). <https://doi.org/10.1037/e537052012-668>
- Shimojo, S., 2001. Sensory modalities are not separate modalities: plasticity and interactions. *Current Opinion in Neurobiology* 11, 505–509. [https://doi.org/10.1016/S0959-4388\(00\)00241-5](https://doi.org/10.1016/S0959-4388(00)00241-5)
- Shiu, L., Pashler, H., 1994. Negligible effect of spatial precuing on identification of single digits. *Journal of Experimental Psychology: Human Perception and Performance* 20, 1037–1054. <https://doi.org/10.1037/0096-1523.20.5.1037>
- Siegel, J.M., 2004. The Neurotransmitters of Sleep 4.
- Silver, M.A., Shenhav, A., D’Esposito, M., 2008. Cholinergic Enhancement Reduces Spatial Spread of Visual Responses in Human Early Visual Cortex. *Neuron* 60, 904–914. <https://doi.org/10.1016/j.neuron.2008.09.038>
- Simons, K., 2005. Amblyopia Characterization, Treatment, and Prophylaxis. *Survey of Ophthalmology* 50, 123–166. <https://doi.org/10.1016/j.survophthal.2004.12.005>
- Steenbergen, L., Jongkees, B.J., Sellaro, R., Colzato, L.S., 2016. Tryptophan supplementation modulates social behavior: A review. *Neuroscience & Biobehavioral Reviews* 64, 346–358. <https://doi.org/10.1016/j.neubiorev.2016.02.022>
- Stinear, C.M., Byblow, W.D., 2003. Role of Intracortical Inhibition in Selective Hand Muscle Activation. *Journal of Neurophysiology* 89, 2014–2020. <https://doi.org/10.1152/jn.00925.2002>
- Taylor, V., Bossi, M., Greenwood, J.A., Dahmann-Noor, A., 2016. Childhood amblyopia: current management and new trends. *Br Med Bull* 119, 75–86. <https://doi.org/10.1093/bmb/ldw030>
- Terranova, J.I., Song, Z., Larkin, T.E., Hardcastle, N., Norvelle, A., Riaz, A., Albers, H.E., 2016. Serotonin and arginine–vasopressin mediate sex differences in the regulation of dominance and aggression by the social brain. *Proceedings of the National Academy of Sciences* 113, 13233–13238. <https://doi.org/10.1073/pnas.1610446113>
- Theeuwes, J., Belopolsky, A., Olivers, C.N.L., 2009. Interactions between working memory, attention and eye movements. *Acta Psychologica*, Spatial working memory and imagery: From eye movements to grounded cognition 132, 106–114. <https://doi.org/10.1016/j.actpsy.2009.01.005>
- Theeuwes, J., Bogaerts, L., van Moorselaar, D., 2022. What to expect where and when: how statistical learning drives visual selection. *Trends in Cognitive Sciences* 26, 860–872. <https://doi.org/10.1016/j.tics.2022.06.001>

- Thiele, A., Bellgrove, M.A., 2018. Neuromodulation of Attention. *Neuron* 97, 769–785. <https://doi.org/10.1016/j.neuron.2018.01.008>
- Torres, G.E., Gainetdinov, R.R., Caron, M.G., 2003. Plasma membrane monoamine transporters: structure, regulation and function. *Nat Rev Neurosci* 4, 13–25. <https://doi.org/10.1038/nrn1008>
- Tsanov, M., Manahan-Vaughan, D., 2007. The Adult Visual Cortex Expresses Dynamic Synaptic Plasticity That Is Driven by the Light/Dark Cycle. *J. Neurosci.* 27, 8414–8421. <https://doi.org/10.1523/JNEUROSCI.1101-07.2007>
- Twarog, B.M., Page, I.H., 1953. Serotonin Content of Some Mammalian Tissues and Urine and a Method for Its Determination. *American Journal of Physiology-Legacy Content* 175, 157–161. <https://doi.org/10.1152/ajplegacy.1953.175.1.157>
- Tyce, G.M., 1990. Origin and metabolism of serotonin. *J Cardiovasc Pharmacol* 16 Suppl 3, S1-7.
- Ulrich, D., Bettler, B., 2007. GABAB receptors: synaptic functions and mechanisms of diversity. *Current Opinion in Neurobiology, Signalling mechanisms* 17, 298–303. <https://doi.org/10.1016/j.conb.2007.04.001>
- Umemori, J., Winkel, F., Didio, G., Llach Pou, M., Castrén, E., 2018. iPlasticity: Induced juvenile-like plasticity in the adult brain as a mechanism of antidepressants: Antidepressant-induced plasticity. *Psychiatry Clin. Neurosci.* 72, 633–653. <https://doi.org/10.1111/pcn.12683>
- Ungerleider, L.G., Haxby, J.V., 1994. ‘What’ and ‘where’ in the human brain. *Current Opinion in Neurobiology* 4, 157–165. [https://doi.org/10.1016/0959-4388\(94\)90066-3](https://doi.org/10.1016/0959-4388(94)90066-3)
- Ungerleider, L.G., Pessoa, L., 2008. What and where pathways. *Scholarpedia* 3, 5342. <https://doi.org/10.4249/scholarpedia.5342>
- Van Ameringen, M., Mancini, C., Oakman, J.M., Farvolden, P., 1999. Selective Serotonin Reuptake Inhibitors in the Treatment of Social Phobia. *Mol Diag Ther* 11, 307–315. <https://doi.org/10.2165/00023210-199911040-00006>
- van Loon, A.M., Knapen, T., Scholte, H.S., St. John-Saaltink, E., Donner, T.H., Lamme, V.A.F., 2013. GABA Shapes the Dynamics of Bistable Perception. *Current Biology* 23, 823–827. <https://doi.org/10.1016/j.cub.2013.03.067>
- Vertes, R.P., Linley, S.B., 2008. Efferent and afferent connections of the dorsal and median raphe nuclei in the rat, in: Monti, J.M., Pandi-Perumal, S.R., Jacobs, B.L., Nutt, D.J. (Eds.), *Serotonin and Sleep: Molecular, Functional and Clinical Aspects*. Birkhäuser, Basel, pp. 69–102. https://doi.org/10.1007/978-3-7643-8561-3_3
- Vetencourt, J.F.M., Sale, A., Viegi, A., Baroncelli, L., De Pasquale, R., F. O’Leary, O., Castrén, E., Maffei, L., 2008. The Antidepressant Fluoxetine Restores Plasticity in the Adult Visual Cortex. *Science* 320, 385–388. <https://doi.org/10.1126/science.1150516>
- Vetencourt, J.F.M., Tiraboschi, E., Spolidoro, M., Castrén, E., Maffei, L., 2011. Serotonin triggers a transient epigenetic mechanism that reinstates adult visual cortex plasticity in rats: Epigenetics of serotonin-induced adult cortical plasticity. *European Journal of Neuroscience* 33, 49–57. <https://doi.org/10.1111/j.1460-9568.2010.07488.x>
- Viana Di Prisco, G., 1984. Hebb synaptic plasticity. *Progress in Neurobiology* 22, 89–102. [https://doi.org/10.1016/0301-0082\(84\)90021-2](https://doi.org/10.1016/0301-0082(84)90021-2)
- Walker, E.P., Tadi, P., 2022. Neuroanatomy, Nucleus Raphe, in: *StatPearls*. StatPearls Publishing, Treasure Island (FL).
- Wall, J.T., Xu, J., Wang, X., 2002. Human brain plasticity: an emerging view of the multiple substrates and mechanisms that cause cortical changes and related sensory dysfunctions after injuries of sensory

- inputs from the body. *Brain Research Reviews* 39, 181–215. [https://doi.org/10.1016/S0165-0173\(02\)00192-3](https://doi.org/10.1016/S0165-0173(02)00192-3)
- Wardak, C., Olivier, E., Duhamel, J.-R., 2011. The relationship between spatial attention and saccades in the frontoparietal network of the monkey. *European Journal of Neuroscience* 33, 1973–1981. <https://doi.org/10.1111/j.1460-9568.2011.07710.x>
- Watanabe, M., Rodieck, R.W., 1989. Parasol and midget ganglion cells of the primate retina. *Journal of Comparative Neurology* 289, 434–454. <https://doi.org/10.1002/cne.902890308>
- Waterhouse, B.D., Navarra, R.L., 2019. The locus coeruleus-norepinephrine system and sensory signal processing: A historical review and current perspectives. *Brain Research, Behavioral Consequences of Noradrenergic Actions in Sensory Networks* 1709, 1–15. <https://doi.org/10.1016/j.brainres.2018.08.032>
- Watson, P., Pearson, D., Wiers, R.W., Le Pelley, M.E., 2019. Prioritizing pleasure and pain: attentional capture by reward-related and punishment-related stimuli. *Current Opinion in Behavioral Sciences, Pain and Aversive Motivation* 26, 107–113. <https://doi.org/10.1016/j.cobeha.2018.12.002>
- Weinberg-Wolf, H., Fagan, N.A., Anderson, G.M., Tringides, M., Dal Monte, O., Chang, S.W.C., 2018. The effects of 5-hydroxytryptophan on attention and central serotonin neurochemistry in the rhesus macaque. *Neuropsychopharmacol* 43, 1589–1598. <https://doi.org/10.1038/s41386-017-0003-7>
- Weinberg-Wolf, H., Fagan, N.A., Dal Monte, O., Chang, S.W.C., 2021. Increasing central serotonin with 5-HTP disrupts the inhibition of social gaze in non-human primates (preprint). *Neuroscience*. <https://doi.org/10.1101/2021.02.26.431901>
- Wiesel, T.N., 1982. The postnatal development of the visual cortex and the influence of environment. *Bioscience Reports* 2, 351–377. <https://doi.org/10.1007/BF01119299>
- Wiesel, T.N., Hubel, D.H., 1963a. Effects of visual deprivation on morphology and physiology of cells in the cat's lateral geniculate body. *Journal of Neurophysiology* 26, 978–993. <https://doi.org/10.1152/jn.1963.26.6.978>
- Wiesel, T.N., Hubel, D.H., 1963b. Single-cell responses in striate cortex of kittens deprived of vision in one eye. *Journal of Neurophysiology* 26, 1003–1017. <https://doi.org/10.1152/jn.1963.26.6.1003>
- Wijtenburg, S.A., West, J., Korenic, S.A., Kuhney, F., Gaston, F.E., Chen, H., Rowland, L.M., 2021. Multimodal Neuroimaging Study of Visual Plasticity in Schizophrenia. *Front. Psychiatry* 12, 644271. <https://doi.org/10.3389/fpsy.2021.644271>
- Wingen, M., Kuypers, K.P.C., van de Ven, V., Formisano, E., Ramaekers, J.G., 2008. Sustained attention and serotonin: a pharmaco-fMRI study. *Human Psychopharmacology: Clinical and Experimental* 23, 221–230. <https://doi.org/10.1002/hup.923>
- Wise, S.P., Desimone, R., 1988. Behavioral Neurophysiology: Insights into Seeing and Grasping. *Science* 242, 736–741. <https://doi.org/10.1126/science.3187520>
- Worbe, Y., Savulich, G., Voon, V., Fernandez-Egea, E., Robbins, T.W., 2014. Serotonin Depletion Induces 'Waiting Impulsivity' on the Human Four-Choice Serial Reaction Time Task: Cross-Species Translational Significance. *Neuropsychopharmacol* 39, 1519–1526. <https://doi.org/10.1038/npp.2013.351>
- Wu, F., Liu, M., Chen, C., Chen, J., Tan, Q., 2016. Effects of Dietary Gamma Aminobutyric Acid on Growth Performance, Antioxidant Status, and Feeding-related Gene Expression of Juvenile Grass Carp, *Ctenopharyngodon idellus*. *Journal of the World Aquaculture Society* 47, 820–829. <https://doi.org/10.1111/jwas.12327>
- Yantis, S., 2002. Stimulus-Driven and Goal-Directed Attentional Control, in: Cantoni, V., Marinaro, M., Petrosino, A. (Eds.), *Visual Attention Mechanisms*. Springer US, Boston, MA, pp. 125–134. https://doi.org/10.1007/978-1-4615-0111-4_12

Yoon, J.H., Grandelis, A., Maddock, R.J., 2016. Dorsolateral Prefrontal Cortex GABA Concentration in Humans Predicts Working Memory Load Processing Capacity. *J. Neurosci.* 36, 11788–11794. <https://doi.org/10.1523/JNEUROSCI.1970-16.2016>

Zhou, J., Reynaud, A., Hess, R.F., 2014. Real-time modulation of perceptual eye dominance in humans. *Proc. R. Soc. B.* 281, 20141717. <https://doi.org/10.1098/rspb.2014.1717>

Zhou, J., Reynaud, A., Kim, Y.J., Mullen, K.T., Hess, R.F., 2017. Chromatic and achromatic monocular deprivation produce separable changes of eye dominance in adults. *Proceedings of the Royal Society B: Biological Sciences* 284, 20171669. <https://doi.org/10.1098/rspb.2017.1669>

Zieher, L.M., De Robertis, E., 1963. Subcellular localization of 5-hydroxytryptamine in rat brain. *Biochemical Pharmacology* 12, 596–598. [https://doi.org/10.1016/0006-2952\(63\)90141-2](https://doi.org/10.1016/0006-2952(63)90141-2)

Zilles, K., 1992. Neuronal plasticity as an adaptive property of the central nervous system. *Annals of Anatomy - Anatomischer Anzeiger* 174, 383–391. [https://doi.org/10.1016/S0940-9602\(11\)80255-4](https://doi.org/10.1016/S0940-9602(11)80255-4)

Zoghi, M., Pearce, S.L., Nordstrom, M.A., 2003. Differential Modulation of Intracortical Inhibition in Human Motor Cortex during Selective Activation of an Intrinsic Hand Muscle. *The Journal of Physiology* 550, 933–946. <https://doi.org/10.1113/jphysiol.2003.042606>

Zucker, R.S., Regehr, W.G., 2002. Short-Term Synaptic Plasticity. *Annu. Rev. Physiol.* 64, 355–405. <https://doi.org/10.1146/annurev.physiol.64.092501.114547>

CHAPTER I

BEHAVIORAL CHARACTERIZATION OF THE EFFECTS OF FLUOXETINE ON VISUAL PERCEPTION

| | |
|--------------------------------------------|-----|
| General introduction to the chapter I..... | 63 |
| Study n°1 | 64 |
| Perspectives of the chapter I..... | 100 |

General introduction to the chapter I

The introduction of this thesis displays the importance of enhancing the visual plasticity in the adult and how to reach this goal. Accordingly, the most common way to trigger this plasticity is to act on the excitation/inhibition balance, in favor of a higher excitability. As a result, sensory inputs will be more likely to influence the brain on both functional and structural levels, in order to induce long-lasting changes. Among all strategies investigated to re-instantiate this plasticity, the modulation of neurotransmitters, and more particularly, of serotonin, are very promising. Indeed, a general increase of serotonin concentration and signaling in the brain is expected to reduce GABA levels, thus decreasing GABA_A receptors activity. Since the GABA has an inhibiting role in the mammalian brain, the previously described cascade of actions is expected to lead to a reduction of inhibition, which is expected to act in favor of an increase of excitation in the excitation/inhibition balance. Since the serotonin cannot cross the blood-brain barrier, all the means to increase its action in the brain are indirect. Modulation of serotonin levels can be achieved by intakes of the direct precursor of serotonin synthesis or serotonin receptors agonist. Here, we took a particular interest in SSRIs, at third way to modulate serotonin levels. Indeed, this pharmacological class, which is mostly known for their antidepressant role, constitutes the most efficient ways to increase serotonin in the central nervous system.

In this first chapter, which also constitutes the first empirical study I present from my Ph.D. work (**study n°1**), we will therefore focus on the SSRI fluoxetine impact on visual perception through behavioral and physiological observations. Indeed, prior to the investigation of its effects on the neural correlates associated with visual plasticity and the underlying mechanisms at play, our approach aimed at first understanding the behavioral effects on vision and top-down processes. Such a process allowed us to first, validate the effect of fluoxetine in the context of visual plasticity to corroborate the literature, but more importantly, to bring another perspective on understanding the low to high-level features involved in such a plasticity enhanced by SSRI intake. These features range from luminance perception to motivation, including reward sensitivity and attention orientation. Thus, we set up three active tasks, involving respectively target detection, spatial discrimination and choice according to the reward output. We describe these tasks and the behavioral effects of fluoxetine in these tasks in **study n°1**. Thanks to those, along with physiological validations such as pupil increase under fluoxetine, we additionally highlighted the fact that under fluoxetine, monkey work longer while reaching higher performances. Very interestingly, we also showed a differential reaction times differences between placebo and fluoxetine conditions, depending on the task, thus testifying of a high-level cognitive effect of fluoxetine.

Study n°1: Fluoxetine increases luminance perceptual thresholds while enhancing motivation and reward sensitivity. **Maëva Gacoin**, Suliann Ben Hamed. *BiorXiv*: doi: <https://biorxiv.org/cgi/content/short/2022.11.11.516168v1> (in revision)

1 Fluoxetine degrades luminance perceptual thresholds 2 while enhancing motivation and reward sensitivity

3 Maëva Gacoin¹, Suliann Ben Hamed¹

4 1. Institut des Sciences Cognitives Marc Jeannerod, UMR5229 CNRS Université de Lyon, 67
5 Boulevard Pinel, 69675 Bron Cedex, France

6
7 Corresponding author: Maëva Gacoin (maeva.gacoin@isc.cnrs.fr), Suliann Ben Hamed
8 (benhamed@isc.cnrs.fr)

9 Abstract

10 Selective serotonin reuptake inhibitors (SSRIs) increase serotonin activity in the brain. While they are
11 mostly known for their antidepressant properties, they have been shown to improve visual functions
12 in amblyopia and impact cognitive functions ranging from attention to motivation and sensitivity to
13 reward. Yet, a clear understanding of the specific action of serotonin to each of bottom-up sensory
14 and top-down cognitive control components and their interaction is still missing. To address this
15 question, we characterize, in two adult male macaques, the behavioral effects of fluoxetine, a specific
16 SSRI, on visual perception under varying bottom-up (luminosity, distractors) and top-down
17 (uncertainty, reward biases) constraints while they are performing three different visual tasks. We first
18 manipulate target luminosity in a visual detection task, and we show that fluoxetine degrades
19 luminance perceptual thresholds. We then use a target detection task in the presence of spatial
20 distractors, and we show that under fluoxetine, monkeys display both more liberal responses as well
21 as a degraded perceptual spatial resolution. In a last target selection task, involving free choice in the
22 presence of reward biases, we show that monkeys display an increased sensitivity to reward outcome
23 under fluoxetine. In addition, we report that monkeys produce, under fluoxetine, more trials and less
24 aborts, increased pupil size, shorter blink durations, as well as task-dependent changes in reaction
25 times. Overall, while low level vision appears to be degraded by fluoxetine, performance in the visual
26 tasks are maintained under fluoxetine due to enhanced top-down control based on task outcome and
27 reward maximization.

28 Keywords

29 Fluoxetine, serotonin, macaque, visual perception, luminosity, response criterion, reward sensitivity

1 Introduction

2 While selective serotonin reuptake inhibitors (SSRIs) are mostly known for their antidepressant
3 properties (Bauer et al., 2008), serotonin concentration in the brain impacts multiple sensory and
4 cognitive functions ranging from retinal (for review, see Masson 2019; Pootanakit and Brunken 2000)
5 and visual functions (Lansner et al., 2019), to higher order cognitive functions such as sustained
6 attention (Carter et al., 2005; Enge et al., 2011; Li et al., 2018; Scholes et al., 2007; Wingen et al., 2008),
7 impulsivity (Brown et al., 2012; Meyniel et al., 2016; Worbe et al., 2014), working memory and learning
8 (Meneses and Liy-Salmeron, 2012) and emotional and affective processing (Bar-Haim et al., 2007;
9 Harmer, 2008; Harmer et al., 2006; Pérez-Edgar et al., 2010). Serotonin has also been proposed to play
10 a crucial role in remodeling visual cortical circuits (Maya-Vetencourt et al. 2008; 2011; Umemori et al.
11 2018) as well as in cognitive flexibility (Clarke et al., 2004). In this context, the specific contribution of
12 serotonin to low-level visual luminosity perception on the one hand and to the top-down control
13 mechanisms of visual perception on the other hand, such as attentional selection and distractor
14 suppression (Di Bello et al., 2022) or reward-based decision making (Homberg, 2012; Seymour et al.,
15 2012) is still a matter of research.

16 Serotonin brain concentrations can be modulated by increasing the circulating levels of tryptophan, its
17 precursor, by the action of selective serotonin agonists, or yet by the action of SSRIs. These bind
18 selectively to serotonin transporters and inhibit their ability to reuptake serotonin into presynaptic
19 terminals, resulting in an increase in the levels of extracellular serotonin (Wong et al., 1995; Clark et
20 al., 1996). Thus, increased release in serotonin enhances the neurotransmitter likelihood to bind to a
21 post-synaptic receptor. In addition, the decrease of serotonin reuptake also inhibits the negative
22 feedback regulation, resulting in increased serotonin release in the synaptic cleft (Cerrito and Raiteri,
23 1979). A particular SSRI, fluoxetine (Prozac), expresses a strong binding to receptors 5-HT_{2c} (Ni and
24 Miledi, 1997; Pälvimäki et al., 1996) and 5-HT_{2a} (Koch, 2002), the latter having the highest
25 concentration in the visual system (Beliveau et al., 2017; Hansen et al., 2022), as well as in the pre-
26 frontal cortex (Puig and Gullledge, 2011). In particular, serotonin modulates the neuronal activity in
27 the visual system, in a dose- and specie dependent-manner, such that increase or depletion of 5-HT
28 regulates the switch between single-spike activity and rhythmic burst firing specifically in brain regions
29 involved in visual processing, such as the retina, the visual cortex, and the thalamus (Brunken et al.,
30 1993; McCormick and Wang, 1991; Monckton and McCormick, 2002; Moreau et al., 2013). In addition,
31 fluoxetine decreases extracellular GABA levels (Vetencourt et al., 2008; Baroncelli et al., 2011, Beshara
32 et al., 2016; Santana et al., 2004) thus leading to enhanced cortical excitability through a reduction of
33 global inhibition. Relevant to the study of the effects of serotonin on top-down and bottom-up visual

1 processes, GABA_A receptor concentrations are higher in the visual cortex than in the rest of the brain
2 and higher in the ventral part of the striate and extrastriate cortex than in its dorsal part (Kaulen et al.,
3 2022). However, the link between GABA_A receptor concentrations and cognitive readout is not
4 straightforward. Indeed, GABA concentrations in the prefrontal cortex are negatively related to
5 attentional blink magnitude while GABA concentrations in the posterior parietal cortex are positively
6 correlated with attentional blink magnitude and GABA concentrations in the visual cortex do not
7 contribute to attentional blink magnitude (Kihara et al., 2016). All this taken together indicates
8 complex interactions between serotonin circulating levels and behavioral and cognitive markers of
9 visual perception.

10 In the present work, we precisely characterize the effects of fluoxetine on visual perception under
11 varying bottom-up (luminosity, distractors) and top-down (uncertainty, reward biases) constraints,
12 while two monkeys perform three different visual tasks. The first task is a visual detection task in the
13 presence of target stimuli of varying luminosity and mostly involves bottom-up visual processes. This
14 task thus allows to characterize the effects of fluoxetine on luminosity perceptual thresholds. The
15 second task is a visual detection task in the presence of spatial distractors and involves a combination
16 of bottom-up visual processes and top-down target selection and reactive distractor suppression
17 mechanisms (Di Bello et al., 2022). This task thus allows to characterize the effects of fluoxetine on
18 perception under spatial uncertainty. The third task is a free choice task in the presence of reward
19 biases (Chelazzi et al., 2014). This task thus allows to characterize the effects of fluoxetine on reward-
20 based decision making. Overall, we report longer time on the task, increased pupil size and shorter
21 blink durations under fluoxetine, increased luminance perceptual thresholds, such that higher levels
22 of luminosity are needed to reach a 50% correct detection, more liberal decision thresholds thus
23 producing more responses to both targets and distractors, a degraded perceptual spatial resolution
24 under spatial uncertainty, and an enhanced sensitivity to both the positive incentive of high rewards
25 as well as to the negative outcome of low rewards. We finally show that fluoxetine can either speed
26 up or slow down manual reaction times, depending on the nature of the task. Overall, we show that
27 the effects of fluoxetine on perception result from interference with both bottom-up perceptual
28 mechanisms, namely degraded luminosity thresholds or degraded spatial resolution and top-down
29 perceptual mechanisms, namely relaxed decision thresholds and increased sensitivity to reward
30 outcomes. In other words, while low level vision appears to be degraded by fluoxetine, performance
31 in the visual tasks may be maintained under fluoxetine due to enhanced top-down control based on
32 task outcome and reward maximization.

1 Results

2 *Under fluoxetine, monkeys work longer and produce less aborts*

3 Based on serum concentration decay time in macaques (half-life <16h, Sawyer and Howell, 2011) and
4 to the reported threshold for behavioral effects (Fontenot et al., 2009; Chen et al., 2012), monkeys
5 were injected with 2.5mg/kg of Fluoxetine or an equivalent volume of saline. On each session, subjects
6 were allowed to work for as long as they were motivated to. Monkeys were considered as less
7 motivated and were brought back to their home cage when their compliance to the central fixation
8 constrain in the task decreased beyond a certain threshold (85% overall fixation in a block of 280 trials
9 for both the luminance detection task and the target detection task with distractors and 75% for the
10 saccadic reward competition task).

11 For all three tasks, a significant increase in the number of trials as well as a significant decrease in abort
12 trials (i.e. trials discontinued prior to the onset of task response signal) is observed when monkeys are
13 on fluoxetine compared to placebo sessions (Figure 1). Specifically, during the luminance detection
14 task, both monkeys M1 and M2 performed more trials per session in fluoxetine sessions as compared
15 to placebo sessions (M1: median number of trials per session +/- s.e.: placebo: 1257,67+/-233,98;
16 fluoxetine: 1914,33+/-13,95; Wilcoxon non-parametric test, p=0,024 M2: placebo: 289,25+/-62,33;
17 fluoxetine: 387+/-14,81; p=0,034) and less aborted trials (M1: median %Abort: placebo: 50,60+/-0,03;
18 fluoxetine: 35,53+/-0,01; p=0,005; M2: placebo: 90,16+/-0,02; fluoxetine: 84,83+/-0,02; p=0,045). This
19 was also true for the detection task with distractors (M1: median number of trials per session +/- s.e.:
20 placebo: 970,5+/-72,85; fluoxetine: 1443,5+/-69,01; p=0,001; M2: placebo: 270,8+/-44,04; fluoxetine:
21 496,9+/-86,39; p=0,009; M1: median %Abort: placebo: 23,71+/-0,01; fluoxetine: 22,7+/-0,01; p=0,016;
22 M2: placebo: 18,93+/-0,01; fluoxetine: 16,47+/-0,01; p 0,027). However, we did not observe this effect
23 for the saccadic reward competition task (M1: median number of trials per session +/- s.e.: placebo:
24 936+/-109,10; fluoxetine: 1128+/-94,99; p=0,124; M2: placebo: 624+/-87,64; fluoxetine: 792+/-94,99;
25 p=0,109; M1: median %Abort: placebo: 29,46+/-0,05; fluoxetine: 27,80+/-0,020; p=0,456; M2:
26 placebo: 44,15+/-0,02; fluoxetine: 37,78+/-0,02; p=0,128). Overall, fluoxetine thus enhances both the
27 motivation of the monkeys to work (more trials) as well as their compliance on the task (less aborts).
28 Please note that, due to the nature of the tasks, performance defined as the percentage of correct
29 trials cannot be computed.

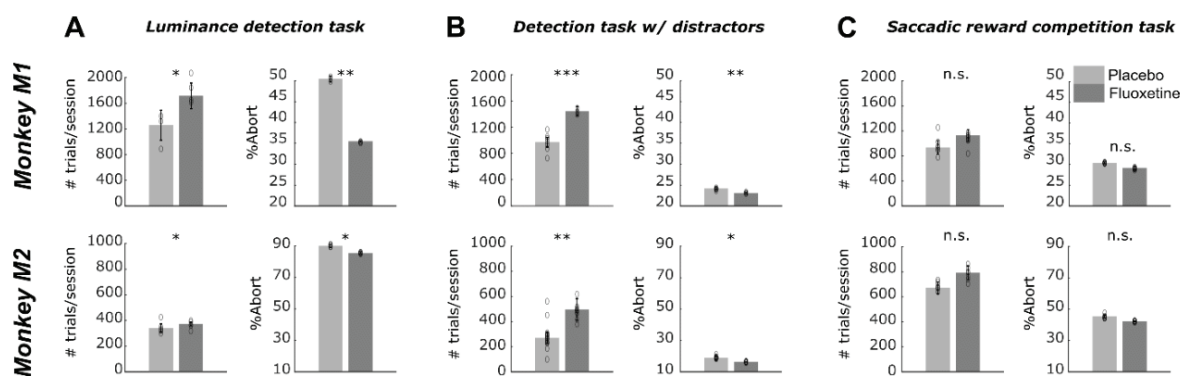


Figure 1: Effect of fluoxetine on on-task motivation (# of trials) and on-task compliance (% aborts), on the Luminance detection task (A), the detection task with distractors (B) and the saccadic reward competition task (C). For all plots, median +/- s.e. of the median are represented. Placebo data are represented in light gray and fluoxetine data are represented in dark gray. Statistical significance is represented as follows: *, p<0.001; **, p<0.01; *, p<0.05; n.s., p>0.05.**

Under fluoxetine, perceptual thresholds are increased

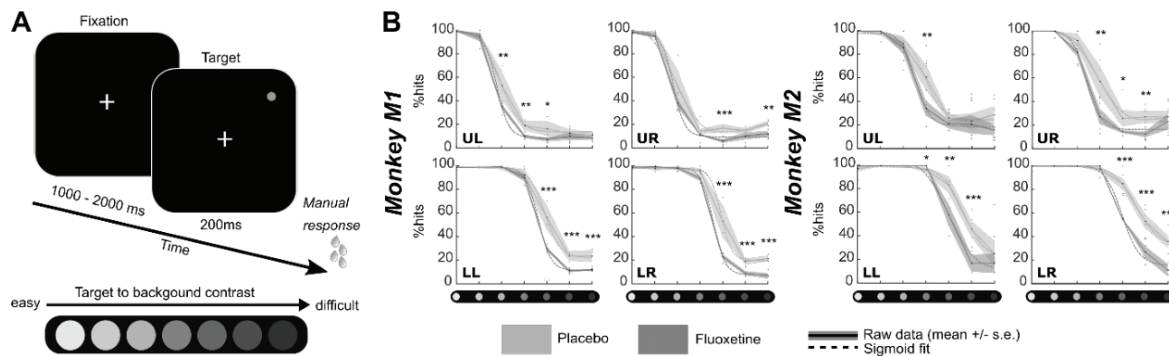
In order to assess the effect of fluoxetine on perceptual thresholds, we had monkeys detect targets of varying luminosities ranging from very high luminance to very low, in seven steps (Figure 2). Targets could appear in one of four locations on the screen (upper left, upper right, lower left, lower right). It is to be noted that this experiment was conducted twice, at a 10 months' interval and all observations reported below are reproduced (supplemental figure S1).

Both monkeys had a hit rate of 100% in both the placebo and fluoxetine conditions for the high luminosity targets, indicating that they were well trained and highly motivated in this task. Behavioral performance (% Hits, i.e. correct responses) were extracted as a function of target location and target luminosity for each monkey and each session and fitted with a sigmoid fit (Figure 2b, supplemental figure S1).

Two different effects of fluoxetine can be described. First, fluoxetine increases perceptual thresholds such that lower luminosity targets are less perceived under fluoxetine relative to placebo condition. This is quantified by a shift in the p^{50} (i.e. point of perceptual indecision) of sigmoid fits in the fluoxetine relative to the placebo condition towards higher luminosities ($\overline{p^{50}}$, median +/- s.e. fluoxetine, M1: placebo: $4,76 \pm 0,01$; fluoxetine: $4,23 \pm 0,04$; Wilcoxon non-parametric test, $p=0,026$; M2: placebo: $3,90 \pm 0,03$; fluoxetine: $3,71 \pm 0,02$; $p=0,002$).

Second, under fluoxetine, monkeys had lower hit rates than on placebo condition, producing significantly less hits for lower luminosity targets (Figure 1B). A two-way ANOVA on target position x condition indicates a significant effect of condition and quadrant with no interaction for both monkeys (M1: target position, $F(1,83)=78,365$, $p<0,001$; condition, $F(3,249)=77,638$, $p<0,001$; interaction,

1 $F(3,249)= 1,639, p= 0,181$; M2: target position, $F(1,76)= 40,803, p<0,001$; condition, $F(3,228)= 41,768,$
 2 $p<0,001$; interaction, $F(3,228)= 1,702, p= 0,167$). Post-hoc Wilcoxon tests indicate that this holds
 3 significant in M1 for three quadrants out of four and in M2, for one quadrant out of four (Figure 1B).
 4 This indicates that their perception for low luminosity target is strongly degraded under fluoxetine.
 5 Alternatively, this possibly indicates that monkeys become more conservative under fluoxetine, i.e.
 6 they select more carefully their responses to minimize errors. These hypotheses are evaluated in the
 7 next section, using a second behavioral task.



8

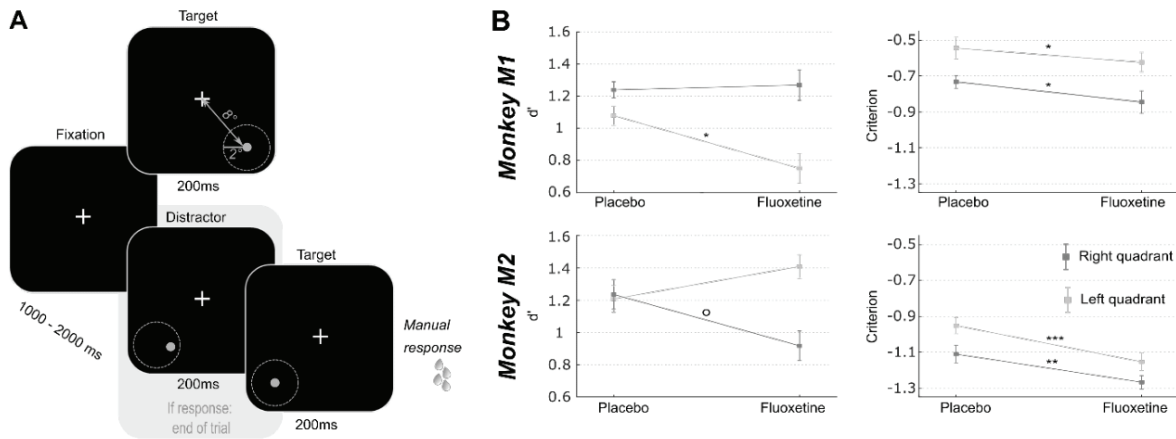
9 **Figure 2: Effect of fluoxetine on perceptual thresholds in a luminance detection task.** (A) Monkeys had to detect a target
 10 presented in one of four quadrants. Target luminosity ranged from high to low luminosity in 7 steps. Monkeys were rewarded
 11 for a speeded detection of target presentation. Targets were presented at four different locations, in the upper left (UL),
 12 upper right (UR), lower right (LR) and lower left (LL) quadrants, at 8° of eccentricity from the center of the screen, for 200ms.
 13 (B) For both monkeys, % of hits were computed independently for each target luminosity. Dots represent individual sessions,
 14 continuous lines represent average % hits across all sessions (+/-s.e.) and dashed lines represent sigmoid fit of the data.
 15 Placebo data are represented in light gray and fluoxetine data are represented in dark gray. Behavioral data are represented
 16 independently for each target position. Statistical significance is represented as follows: ***, $p<0.001$; **, $p<0.01$; *, $p<0.05$;
 17 n.s., $p>0.05$.

18 *Under spatial uncertainty, fluoxetine relaxes perceptual decision thresholds and degrades perceived*
 19 *spatial resolution*

20 In order to further investigate the effects of fluoxetine on perceptual sensitivity and response decision
 21 thresholds described in the previous experiment, we had monkeys perform luminosity target detection
 22 task in the presence of spatial distractors (Figure 3a). In this task, targets and distractors were only
 23 distinguishable by their spatial position, and were set at a perceptual threshold of 70%, as
 24 characterized in the luminance detection task (Figure 2). Targets and distractors could either be
 25 presented in the lower left or in the lower right quadrants. As for the previous task, this experiment
 26 was conducted twice, at a 10 months' interval and all observations reported below are reproduced.

27 Based on the monkeys' response in this task (Hits: correct target detections; Misses: no response to
 28 target presentation; False alarms: erroneous responses to distractors and Correct rejections: correct
 29 no response to distractors), we calculated the criterion (reflecting the willingness to respond that the
 30 signal is present in an ambiguous situation, independently of the subject's sensitivity to the signal) and

1 d-prime (reflects the actual sensitivity of the subject to the signal) over all sessions in both the
2 fluoxetine and placebo conditions. A high criterion corresponds to a conservative behavior (i.e. less
3 responses but mostly correct) while a low criterion corresponds to a liberal behavior (i.e. more
4 responses but more false alarms). A high d' indicates the signal is easily detected in the face of noise
5 while a low d' reflects a difficulty to detect the signal. Because reaction times differed between left
6 and right targets, these trials were considered independently. This spatial uncertainty task was very
7 difficult; thus, overall criteria were negative. Yet, for both monkeys and both hemifields, we observe a
8 significant decrease in criterion after fluoxetine administration compared to the placebo condition
9 (Figure 3b, M1: right: fluoxetine, median \pm s.e. of median, $-0,84\pm 0,05$; placebo: $-0,73\pm 0,03$;
10 Wilcoxon non-parametric test, $p=0,047$, left: fluoxetine, $-0,62\pm 0,04$; placebo: $-0,54\pm 0,06$; $p=0,012$;
11 M2: right: fluoxetine, $-1,27\pm 0,04$; placebo: $-1,11\pm 0,05$; $p= 0,002$, left: fluoxetine, $-1,15\pm 0,05$;
12 placebo: $-0,95\pm 0,05$; $p<0,001$). Under fluoxetine, both subjects lowered their response decision
13 thresholds, so that they allowed themselves more mistakes. This effect was present irrespective of
14 whether distractors were closest to the target location, closest to the center of the visual field or
15 further away in the periphery (supplemental figure S2a and S2b, Two-way ANOVA condition \times
16 distractor location, M1: condition, $F(1,91)= 4,266$, $p=0,041$; location, $F(2,182)= 12,772$, $p<0,001$;
17 interaction, $F(2,182)= 0,139$, $p=0,870$; M2: condition, $F(1,62)= 19,484$, $p<0,001$; location, $F(2,124)=$
18 $11,389$, $p<0,001$; interaction, $F(2,124)= 0,829$, $p= 0,439$, this analysis cumulates both test and retest
19 tasks to increase samples per distractor location categories). In this task, changes in d-prime (assessing
20 sensitivity to spatial location) were inconsistent across subjects and across hemifields (M1: right:
21 fluoxetine, median \pm s.e.: $1,27\pm 0,07$; placebo: $1,24\pm 0,05$; Wilcoxon non-parametric test, $p=0,323$;
22 left: fluoxetine, $0,75\pm 0,06$; placebo: $-0,54\pm 0,06$; $p=0,020$; M2: right: fluoxetine, $0,92\pm 0,09$;
23 placebo: $1,23\pm 0,09$; $p= 0,065$; left: fluoxetine, $1,41\pm 0,07$; placebo: $1,21\pm 0,08$; $p= 0,250$). Because
24 fluoxetine is expected to change excitatory/inhibitory balance in favor of excitation through its effect
25 on GABAergic circuitry and thus change the coding spatial resolution in the visual cortex (Hendry and
26 Jones, 1988), we reasoned that changes in spatial d-primes might depend on the actual distance of the
27 distractors to the target. For both monkeys, fluoxetine resulted in significantly decreased d-primes for
28 close distractors but not for intermediate and far distractors (Figure S2b, intermediate distractors, M1:
29 Wilcoxon non-parametric test, $p=0,126$; M2, $p=0,470$; close distractors, M1: $p=0,041$; M2, $p=0,043$; far
30 distractors, M1: $p= 0,155$; M2: $p=0,481$). Post-hoc analyses however indicate that this effect was
31 driven, in both monkeys, by a right quadrant effect. This suggests a degraded spatial resolution in the
32 visual cortex, compatible with a related excitatory/inhibitory balance under fluoxetine.



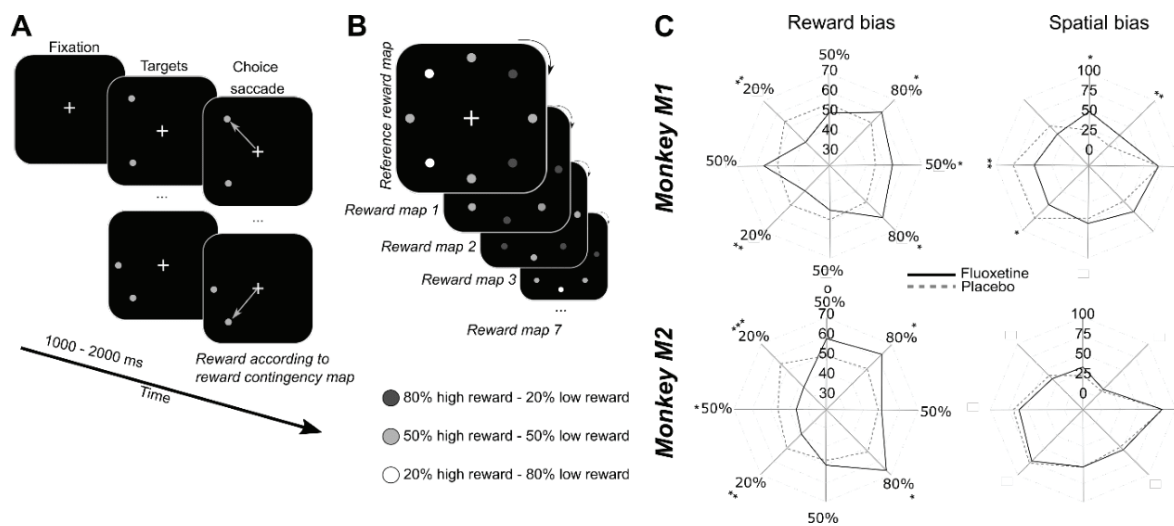
1

2 **Figure 3: Effect of fluoxetine on spatial sensitivity d' and response criterion in a target detection task in the presence**
 3 **of spatial distractors.** (A) Monkeys had to detect a target presented in one of two quadrants (lower left or lower right). Target
 4 luminosity was kept high and presented at a fixed location, at 8° of eccentricity from the center of the screen, for 200ms.
 5 Monkeys were rewarded for a speeded detection of target presentation. On 75% of the trials, targets were preceded by a
 6 distractor, undistinguishable from the target except for its spatial location. These distractors were located within a circle of
 7 2° of eccentricity around the target. Responses to these distractors interrupted the trial and monkeys were not rewarded. (B)
 8 For both monkeys, d' and criterion were computed independently for each target (left, light gray; right, dark gray). Median
 9 +/- s.e. of median are presented for placebo and fluoxetine conditions. Statistical significance is represented as follows: ***,
 10 $p < 0.001$; **, $p < 0.01$; *, $p < 0.05$; °, $p < 0.07$.

11 **Fluoxetine results in increased sensitivity to reward during free choice**

12 Decision-making in non-human primates is most often guided by reward expectation. Recent fMRI
 13 observations suggest that spatial biases induced by reward incentives are subtended by a cortical
 14 network that is functionally distinct from spatial biases induced by spatial attention (Zubair et al.,
 15 2021). Additionally, in ecological conditions, foraging often takes place in a changing environment,
 16 where the actual location of rewards change dynamically with time and the actions taken in this
 17 environment. Continuously updating expected reward locations is thus crucial. We extensively trained
 18 the two macaques included in the present study on a saccadic reward competition in a stable
 19 environment (Figure 4a). On every trial, the monkeys had to make a saccade to one of two possible
 20 targets. Each successful saccade was rewarded, but the delivered reward depended on which target
 21 was selected on this specific trial. Some targets were associated with an 80% probability of high reward
 22 and a 20% probability of low reward (High expected reward). Some targets were associated with the
 23 opposite reward contingencies: 20% probability of high reward and 80% probability of low reward (Low
 24 expected rewards). Some others yet were associated with 50% probability of high or low reward
 25 (Intermediate expected reward). Reward contingencies were fixed from one trial to the next, and were
 26 spatially organized such that each High or Low expected reward target was neighbored by
 27 Intermediate expected reward targets. Prior to our measurements, monkeys were training on the
 28 contingency map task, in a fixed reference configuration. They were then trained under a daily
 29 rotational change in this overlearned contingency map for four weeks. In order to evaluate the effect

1 of fluoxetine on reward-based decision-making in a changing environment, we then performed acute
 2 fluoxetine (or placebo) injections while the monkeys performed the saccade reward competition task
 3 described above, to the exception that reward contingency maps varied from one day to the next in a
 4 pseudo-random manner (Figure 4b). In addition to engage monkeys in active inference of the reward
 5 contingency maps on each day, this manipulation allowed to dissociate possible effects of fluoxetine
 6 on each of reward and spatial biases. On every week, a placebo session was recorded. The next day,
 7 monkeys received an acute injection of 2,5mg/kg of fluoxetine. They then worked on the remaining
 8 weekdays on the same task, but these days were considered as washout days. Because subjects,
 9 whether human or non-human, have individual reward sensitivities as well as individual spatial response
 10 biases, we independently characterize the effects of fluoxetine on reward and spatial biases as
 11 presented next.



12

13 **Figure 4: Effect of fluoxetine on saccadic choices towards targets of different reward contingencies.** (A) Monkeys had to
 14 fixate a central cross on a screen 60cm away from their eyes. After an interval of 1 to 2 secs, two stimuli appeared
 15 simultaneously at two different locations out of eight. All of the 8 possible target locations were organized along a virtual
 16 circle of 8° of eccentricity from the fixation cross, equidistant one from the other. Monkeys were rewarded to make a saccadic
 17 eye movement to any of the two targets. (B) Each target was associated with two possible reward quantities, but with a
 18 different probability. High expected reward targets were associated with 80% of high reward probability and 20% of low
 19 reward probability. Low expected reward targets were associated with 20% of high reward probability and 80% of low
 20 reward probability. Intermediate expected reward targets were associated with 50% of high reward probability and 50% of low
 21 reward probability. Reward contingencies between neighbors were kept constant as follows: 80% high reward (HR) – 50% HR
 22 – 80% HR – 50% HR – 20%HR – 50% HR – 20% HR – 50% HR. However, the actual location of high and low rewarding targets
 23 changed pseudo-randomly from one day to the next. Thus, monkeys had to learn the new reward contingencies every day.
 24 We did not evaluate how much monkeys built a representation of the reference contingency map. (C) Polar plots represent
 25 the probability that monkeys choose any given target either as a function of the reward contingency map (i.e. irrespective of
 26 actual spatial position, left) or as a function of the spatial map (i.e. irrespective of actual reward contingency maps, right).
 27 Median are presented for placebo (dashed lines) and fluoxetine (continuous lines) conditions. Statistical significance is
 28 represented as follows: ***, p<0.001; **, p<0.01; *, p<0.05.

29 **Effect of fluoxetine on reward biases.** In order to assess the effect of fluoxetine on reward-induced
 30 biases, we computed for each individual reward contingency, a reward selectivity index (RSI) as
 31 follows. For each rewarded contingency, we estimate the median proportion of instances in which this

1 contingency was chosen, irrespective of the reward contingency associated with the other singleton in
2 the pair, as well as irrespective of spatial positions. Thus, RSI reflects preference for a given reward
3 contingency irrespective of other sources of variation in the trial. Hence, a high RSI indicates that
4 monkeys prefer this contingency relative to the others. An increase in reward selectivity index under
5 fluoxetine indicates that the preference for this specific spatial position is enhanced. In both monkeys,
6 we observe a significant increase in the RSI on the highly rewarded items (80% of high reward
7 probability (M1: 80%HR₁: fluoxetine, median +/- s.e.: 60,33+/-3,40; placebo: 52,34+/-1,72; Wilcoxon
8 non-parametric test, p=0,028; 80%HR₂: fluoxetine, 60,37+/-6,24; placebo: 48,22+/-1,94; p=0,044. M2:
9 80%HR₁: fluoxetine, 62,62+/-4,91; placebo: 51,45+/-1,59; p=0,026; 80%HR₂: fluoxetine, 66,44+/-5,04;
10 placebo: 52,22+/-2,09; p=0,011) and for M1, an increase on the intermediate reward items (50% of
11 high reward probability, M1: 50%HR₈₀₋₈₀: fluoxetine, median +/- s.e.: 54,08+/-4,45; placebo: 44,90+/-
12 0,54; p=0,0314) neighboring them (Figure 4c, left). This indicates an increase in the monkeys'
13 preference for these rewards under fluoxetine. We also observe, for both monkeys, a significant
14 decrease in the RSI on both the low reward items (20% of high reward probability, M1: 20%HR₁:
15 fluoxetine, median +/- s.e.: 38+/-4,50; placebo: 53,85+/-2,50; p=0,005; 20%HR₂: fluoxetine, 39,18+/-
16 2,84; placebo: 49,97+/-2,25; p=0,006. M2: 20%HR₁: fluoxetine, 37,15+/-4,32; placebo: 55,08+/-0,89;
17 p<0,001; 20%HR₂: fluoxetine, 38,88+/-3,66; placebo: 49,96+/-1,74; p=0,009) and for M2 on the
18 intermediate reward items (50% of high reward probability, M2: 50%HR₂₀₋₂₀: fluoxetine, median +/-
19 s.e.: 36,24+/-5,16; placebo: 46,18+/-1,88; p=0,048) neighboring them (Figure 4c). This indicates a
20 decrease in the monkeys' preference for these rewards under fluoxetine. Thus, overall, this
21 demonstrates that fluoxetine significantly alters reward-based decision making such that subjects are
22 more sensitive to the positive incentive of high reward probabilities as well as to the negative outcome
23 of low reward probabilities.

24 ***Effect of fluoxetine on spatial biases.*** In order to assess the effect of fluoxetine on intrinsic spatial
25 biases, we computed for each individual target position, a spatial selectivity index (SSI) as follows. For
26 each spatial location, we estimated the median proportion of instances in which this position was
27 chosen, irrespective of the spatial position of the other singleton in the pair, as well as irrespective of
28 reward contingencies. Hence, a high SSI indicates that monkeys prefer this contingency relative to the
29 others. An increase in spatial selectivity index under fluoxetine indicates that the preference for this
30 specific reward contingency is enhanced. Under fluoxetine, Monkey M1 shows a decreased SSI
31 specifically for the left targets relative to the placebo and an increased SSI in upper positions (Figure
32 4c, right). Because spatial positions on the left hemifield were associated with a high SSI in the placebo
33 condition relative to the right targets, this indicates that the monkeys often preferred targets on this

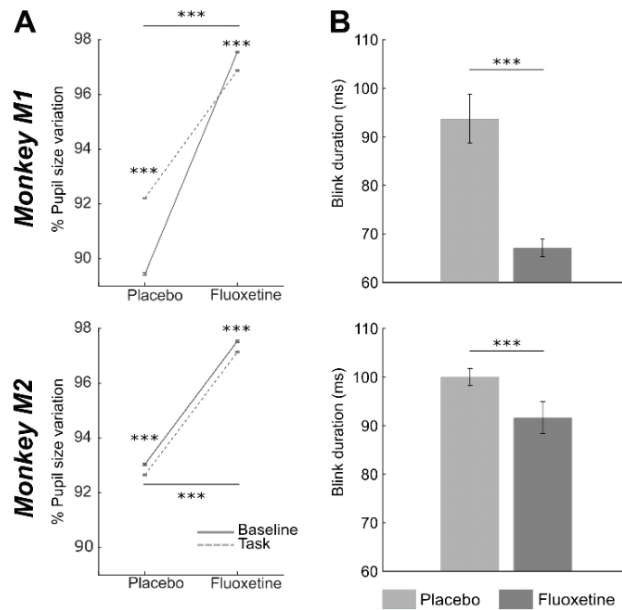
1 side on the placebo condition and that this spatial bias decreased under fluoxetine (M1: Middle-left:
2 fluoxetine, median +/- s.e.: 47,39+/-6,13; placebo: 77,36+/-6,78; Wilcoxon non-parametric test,
3 p=0,003; Low-left: fluoxetine, 50,34+/-7,99; placebo: 76,58+/-8,21; p=0,020). Likewise, Monkey M1
4 had a low SSI toward upper positions in placebo position relative to lower positions targets and this
5 spatial bias decreased under fluoxetine (M1: Up: fluoxetine, median +/- s.e.: 49,29+/-7,65; placebo:
6 22,99+/-8,51; p=0,020; Up-right: fluoxetine, 33,07+/-5,38; placebo: 13,29+/-3,37; p=0,004). Thus, in
7 this monkey, fluoxetine resulted in a reduction in overall spatial biases. Monkey M2 show no significant
8 difference in SSIs between the placebo and the fluoxetine condition (Figure 4c, right).

9 *Pupil size is enlarged and blink duration decreased under fluoxetine*

10 Changes in perceptual thresholds as described in the first luminance detection task can be accounted
11 for by local changes in excitatory/inhibitory balance in the visual cortex. However, this can also be
12 accounted for by changes in oculomotor functions such as pupil size changes and blink duration
13 (LeDoux et al., 1998). We thus quantified these two parameters independently in the fluoxetine and
14 placebo conditions.

15 Overall, pupil size significantly increases under fluoxetine relative to placebo, both at rest and in the
16 task (Figure 5A, two-way ANOVA, condition x epoch: M1: main condition effect, $F(1,2999)= 1910$,
17 $p<0,001$; main epoch effect: $F(1,2999)= 64926$, $p<0,001$; interaction: $F(1,83)= 6027$, $p<0,001$; M2: main
18 condition effect, $F(1,2999)= 58539$, $p<0,001$; main epoch effect: $F(1,2999)= 57$, $p<0,001$; interaction:
19 $F(1,2999)= 55$, $p<0,001$). This observation is in agreement with what has already been described in the
20 literature (Cazettes et al., 2021; McGuirk and Silverstone, 1990). However, enlarged pupil size is
21 associated with enhanced visual acuity (Leibowitz, 1952). Thus, this observation on pupil size is at odds
22 with our observation of degraded perceptual thresholds in the luminance detection task.

23 We also measured eye blink statistics as a proxy of attentional engagement. Blink rate in the task was
24 not affected by fluoxetine (M1: Median+/-s.e., fluoxetine= 0,18+/-0,001 blinks/sec; placebo= 0,19+/-
25 0,02 blink/sec; Wilcoxon test, $p= 0,152$; M2: fluoxetine= 0,13+/-0,01 blink/sec; placebo= 0,13+/-0,01
26 blink/sec; Wilcoxon test, $p= 0,290$). However, blink duration was significantly shorter under fluoxetine
27 relative to placebo (Figure 5B, Wilcoxon test, M1: $p<0,001$; M2: $p<0,001$). Because epochs of blinking
28 have been shown to interfere with cognition (Irwin, 2014), shorter eye blink under fluoxetine might be
29 associated with stronger involvement in the task.



1

2 **Figure 5: Effect of fluoxetine on pupil size and eye blink duration.** (A) Median +/-s.e. of %pupil size change relative to the
3 entire task, for monkeys M1 (top) and M2 (bottom), during rest (baseline, continuous line) and after target presentation (task,
4 dashed lines), in the placebo and fluoxetine conditions. (B) Median +/-s.e. of blink duration, for monkeys M1 (top) and M2
5 (bottom), in the placebo and fluoxetine conditions. Statistical significance is represented as follows: ***, $p < 0.001$; **, $p < 0.01$;
6 *, $p < 0.05$.

7

8 *Paradoxical effects of fluoxetine on manual reaction times*

9 Reaction times (RT) correspond to a complex behavioral variable that is subject to modulations by
10 multiple cognitive functions ranging from spatial attention (Wardak et al., 2011, 2012a), to temporal
11 expectation and anticipation (Cravo et al., 2013; Wardak et al., 2012b), decision making (Fujimoto et
12 al., 2021; Hanks et al., 2006; Noorani and Carpenter, 2016), perception (Song et al., 2008),
13 reinforcement learning (Viejo et al., 2018), arousal (Davranche et al., 2006; Eason et al., 1969; Fujimoto
14 et al., 2021), reward (Epstein et al., 2011; Firestone and Douglas, 1975; Procyk et al., 2000; Simen et
15 al., 2009), to name a few. In the following, we characterize the effect of fluoxetine on RT distributions.
16 For the sake of clarity, in the following, we focus on manual reaction times in the two first tasks, as
17 saccadic reaction time from the saccadic reward choice task are confounded by possible spatial and
18 reward biases. We used the LATER model in order to classify reaction times in anticipatory reaction
19 times and controlled reaction times (supplemental figure S3).

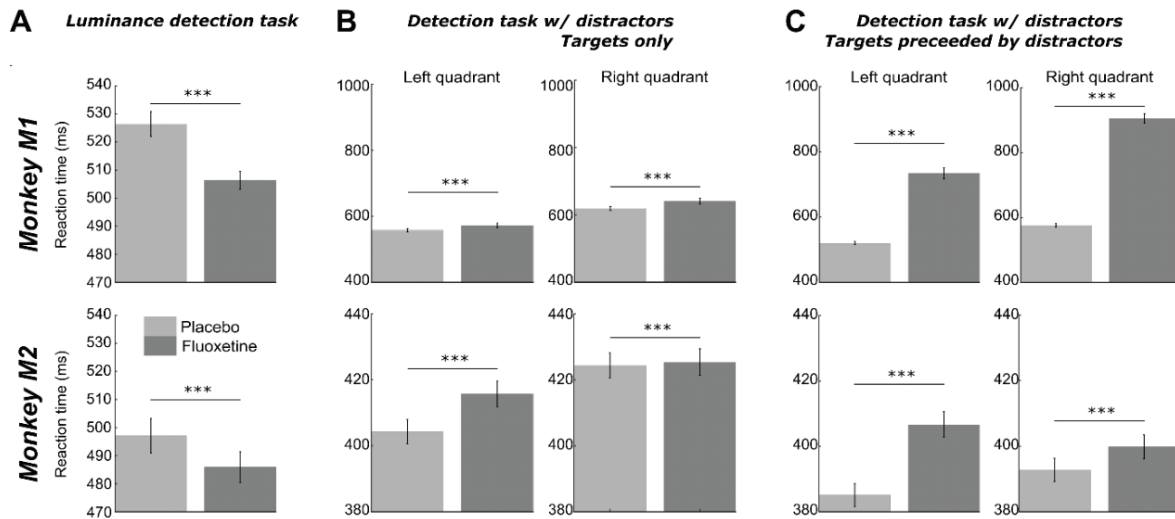
20 For the luminance detection task, because reaction times vary as a function of target luminance, we
21 focused on the trials with two highest target luminance. On these trials, both monkeys had a 100% hit
22 rate. We pooled the trials corresponding to the two easiest targets on all four positions. We report, in
23 both monkeys, a significant decrease in controlled reaction time under fluoxetine relative to placebo
24 (Figure 6, M1: median RT +/- s.e., placebo = 526,4ms +/- 4,38; fluoxetine = 506,4ms +/- 3,21; $p < 0,001$).

1 M2 median RT +/- s.e., placebo = 497,1ms +/- 6,19; fluoxetine = 485,9 +/- 5,49; $p < 0,001$). Fluoxetine
2 did not have the same impact on the rate of anticipatory responses in each monkey. M1 had fewer
3 anticipations in the fluoxetine condition (2,89%) relative to the placebo condition (7,83%, $p < 0,001$) and
4 faster responses in the fluoxetine condition (median RT +/- s.e., 263,8ms +/- 2,99) relative to the
5 placebo condition (329,3ms +/- 4,30; $p < 0,001$). In M2, anticipation rate was not significantly different
6 in the fluoxetine condition (7,08%) relative to the placebo condition (6.06%, $p = 0,344$) and these
7 anticipatory responses were slower in the fluoxetine condition (median RT +/- s.e., 286,7ms +/- 6,16)
8 relative to the placebo condition (234,4ms +/- 4,67; $p = 0,029$).

9 For the target detection task in the presence of distractors, we report the opposite observations.
10 Indeed, RT increased under fluoxetine in target only trials (M1: median RT +/- s.e., placebo_{RIGHT} =
11 619,3ms +/- 5,77; placebo_{LEFT} = 557,9ms +/- 5,24; fluoxetine_{RIGHT} = 641,1ms +/- 8,29; fluoxetine_{LEFT} =
12 572,5ms +/- 6,90; $p_{\text{PLACEBO-FLUOX}} < 0,001$. M2 median RT +/- s.e., placebo_{RIGHT} = 424,4ms +/- 3,80 ;
13 placebo_{LEFT} = 404,3ms +/- 3,62; fluoxetine_{RIGHT} = 425,4ms +/- 4,03; fluoxetine_{LEFT} = 415,7 ms +/- 3,91;
14 $p_{\text{PLACEBO-FLUOX}} < 0,001$). On these trials, we also report less percentage of anticipatory responses under
15 fluoxetine relative to placebo (M1, left quadrant, placebo = 3,62%, fluoxetine = 1,25%, $p < 0,001$; right
16 quadrant, placebo = 8,86%, fluoxetine = 1,25%, $p = 0,008$; M2, left quadrant, placebo = 1,79%,
17 fluoxetine = 0,55%, $p < 0,001$; right quadrant, placebo = 0,92%, fluoxetine = 0,59%, $p < 0,001$).

18 On trials with a distractor preceding target presentation, RT also increased under fluoxetine in target
19 only trials (M1: median RT +/- s.e., placebo_{RIGHT} = 575,5ms +/- 5,50; placebo_{LEFT} = 520,15ms +/- 4,78;
20 fluoxetine_{RIGHT} = 906ms +/- 14,46; fluoxetine_{LEFT} = 733,7ms +/- 16,23; $p_{\text{PLACEBO-FLUOX}} < 0,001$. M2 median
21 RT +/- s.e., placebo_{RIGHT} = 392,8ms +/- 3,49 ; placebo_{LEFT} = 385,1ms +/- 3,52; fluoxetine_{RIGHT} = 399,8ms
22 +/- 3,70; fluoxetine_{LEFT} = 406,7 ms +/- 3,85; $p_{\text{PLACEBO-FLUOX}} < 0,001$). In addition, we observe a marked
23 increase of the overall percentage of anticipatory responses (M1, left quadrant, placebo = 25,74%,
24 fluoxetine = 91,75%, $p < 0,001$; right quadrant, placebo = 47,49%, fluoxetine = 97,74%, $p < 0,001$. M2,
25 left quadrant, placebo = 9,71%, fluoxetine = 10,06%, $p < 0,001$; right quadrant, placebo = 3,37%,
26 fluoxetine = 25,48%, $p < 0,001$), and significantly more when distractor is preceding the target compared
27 to target only trials under fluoxetine than in the placebo condition (Two-way ANOVA condition
28 distractor presence, M1: left quadrant, condition, $F(1,8) = 3586,177$, $p < 0,001$; location, $F(1,8) =$
29 $1123,003$, $p < 0,001$; interaction, $F(1,8) = 857,459$, $p < 0,001$; right quadrant, condition, $F(1,8) = 132,883$,
30 $p < 0,001$; location, $F(1,8) = 847,965$, $p < 0,001$; interaction, $F(1,8) = 1258,187$, $p < 0,001$;M2: left quadrant,
31 condition, $F(1,15) = 2342,318$, $p < 0,001$; location, $F(1,15) = 3669,967$, $p < 0,001$; interaction, $F(1,15) =$
32 $1463,787$, $p < 0,001$; right quadrant, condition, $F(1,15) = 595,421$ $p < 0,001$; location, $F(1,15) = 2481,401$,
33 $p < 0,001$; interaction, $F(1,15) = 358,152$, $p < 0,001$). Overall, on this task, we thus report a paradoxical

1 effect of fluoxetine, associated with more anticipatory RTs on distractor trials, indicating a stronger
 2 release of proactive inhibitory mechanisms (Wardak et al., 2012a, 2012b; Criaud et al., 2012), while at
 3 the same time we report longer controlled RT on these same trials, indicating stronger cognitive
 4 control.



5
 6 **Figure 6: Effect of fluoxetine on controlled reaction times.** Median +/-s.e. of reaction times, for monkeys M1 (top) and M2
 7 (bottom), in the placebo and fluoxetine conditions in the luminance task (A, all positions collapsed, high luminance targets
 8 only), in the detection tasks with distractors, on target only trials (B), and in trials with distractors (C). Statistical significance
 9 is represented as follows: ***, $p < 0.001$; **, $p < 0.01$; *, $p < 0.05$.

10 Discussion

11 In the present work, we precisely characterize the effects of fluoxetine on behavioral and physiological
 12 metrics while monkeys are performing three different visual tasks. We report a set of specific effects
 13 of fluoxetine as well as several non-specific effects of fluoxetine, including longer time on the task and
 14 shorter blink durations. Luminance perceptual thresholds are increased, such that higher levels of
 15 luminosity are needed to reach a 50% correct detection. Under sensory uncertainty, decision
 16 thresholds are released and perceptual spatial resolution is degraded. We additionally show that
 17 fluoxetine increases sensitivity to reward outcome. Last, we show that fluoxetine can either speed up
 18 or slow down manual reaction times, depending on the nature of the task. In the following, we discuss
 19 these observations in the light of the current knowledge on fluoxetine.

20 Fluoxetine interferes with retinal functions

21 We here show that fluoxetine results in increased visual perceptual thresholds, higher levels of
 22 luminosity being required to achieve similar detection thresholds as in placebo. This can be accounted
 23 for by the reported role of serotonin (5-hydroxytryptamine or 5-HT) in the physiology and development

1 of the retinal of vertebrates (for review, see Masson, 2019; Pootanakit and Brunken, 2000). 5-HT is
2 synthesized as a precursor for melanopsin in both photoreceptors and amacrine cells (Millar et al.,
3 1988; Pourcho, 1996; Vaney, 1986) and its uptake occurs in bipolar and retinal ganglion cells (RGC). In
4 particular, amacrine cells are major transporters of rod signals to RGC, playing a role in increasing their
5 slow potential information (Nelson, 1982; Smith and Vardi, 1995). Accordingly, in fish, fluoxetine
6 enhances serotonin accumulation in bipolar cells (Schuette and Chappell, 1998). A similar 5-HT uptake
7 is described in cat RGC following the injection of a serotonergic neurotoxin (Wassle et al., 1987). This
8 results in the suppression of spontaneous spike firing in RGC, thus decreasing melanopsin driven
9 response (Hughes et al., 2016). Overall, the coupled retinal effect of the SSRI on decreasing melanopsin
10 and the rods transporter activity of amacrine cells is thus responsible for luminance perception
11 depletion, and possibly accounts for our experimental observation of a p^{50} indecision threshold shifted
12 toward higher luminosities.

13 *Fluoxetine interferes with pupil and blink physiology*

14 SSRIs have been shown to result in increased pupil dilation (Hughes et al., 2016; Schmitt et al., 2002).
15 In particular, patients treated with fluoxetine have bigger pupillary diameters and slower pupillary
16 contraction (Rodriguez et al., 2020). It is unclear whether these effects are also associated with low
17 level changes in visual accommodation (Rodriguez et al., 2020). Enlarged pupil diameter has been
18 associated with higher thresholds at detecting the frequency at which a flickering light is perceived as
19 a steady light source (Schmitt et al., 2002) as well as with enhanced letter identification report at very
20 short presentation timings (Lansner et al., 2019). This suggests larger pupil size impacts perception and
21 possibly also accounts for our experimental observation of a p^{50} indecision threshold shifted toward
22 higher luminosities.

23 To our knowledge, there are no reports that fluoxetine impacts blink duration. Capitão et al., (2015)
24 show that fluoxetine modulates emotional processing, suppressing for example the motion-
25 potentiated startle effect. Here, we show a significant decrease in blink duration, in the absence of
26 change in blink frequency. In the context of our task, these blinks are considered as spontaneous rather
27 than reflex blinks in response to external events. Spontaneous blinks have been shown to correlate
28 with the activation of a network involving somatosensory primary and secondary areas, as well as
29 parietal, cingulate, insular, as well as striate and extrastriate visual areas (Guipponi et al., 2015).
30 Shorter blinks possibly correlate with weaker activations in this network. This remains to be explored
31 as well as the possible link between blink duration and perception.

1 *Fluoxetine enhances motivation on task*

2 Reward is a key motivational factor and reward processing is known to regulate cognitive functions
3 such as attention, memory, decision making and learning (Arnsten and Rubia, 2012; for review, see
4 Hélié et al., 2017). Fluoxetine is proposed to mediate these cognitive functions through the reward
5 valuation pathways. Indeed, Inhibition of central serotonin reuptake decreases probabilistic learning
6 (Chamberlain et al., 2006) and SSRI enhances reward processing in healthy adults (Macoveanu, 2014;
7 McCabe et al., 2010; Scholl et al., 2017). The serotonergic cells of the dorsal raphe nucleus project
8 to both the bed nucleus of the stria terminalis, an anxiety-related structure, the ventral tegmental
9 area, a reward-related structure, and are shown to respond to emotional salience (Paquelet et al.,
10 2022). The activity of this neuronal population is additionally shown to correlate with learning rate,
11 both in a context of expected and unexpected uncertainty (Grossman et al., 2022). Fluoxetine has also
12 been associated with a reduction of effort cost, or to an increased valuation of reward. Indeed, a study
13 in healthy humans shows that subjects who received a SSRI put more effort to get a reward (Meyniel
14 et al., 2016). Last, fluoxetine has been shown to decrease both hunger and thirst (McGuirk and
15 Silverstone, 1990). In spite of this convergent evidence for a role of serotonergic pathway on
16 motivation through reward processing and valuation, caution is required as it has been shown that
17 changes in sensitivity to the reward under SSRI is highly dose-dependent (Bari et al., 2010).

18 We report that monkeys make more trials and produce less abort trials under fluoxetine relative to the
19 placebo condition. These observations are reproduced in three different behavioral tasks and both
20 monkeys. This could be accounted for by an enhanced motivation to work. This enhanced motivation
21 could be due to increased hunger or thirst. This however seems unlikely, as in humans, fluoxetine has
22 been shown to decrease hunger and thirst rather than increase them (McGuirk and Silverstone, 1990).
23 A general effect of fluoxetine on effort and reward valuation is more plausible (Meyniel et al., 2016).
24 Accordingly, we observe that both monkeys expressed, in addition to an increase in the number of task
25 trials, a higher willingness to initiate working sessions, at all stages of experimental preparation and
26 execution (higher willingness to come out of the cage, and go in monkey chair, faster eye calibration,
27 no signs of restlessness at the end of the working session that would indicate that the monkey wants
28 to go back to its home cage).

29 In the free choice task, we manipulated reward contingency and we measured the monkeys' sensitivity
30 to reward. Fluoxetine significantly altered reward based-decision making such that subjects were more
31 sensitive to the positive incentive of high reward probability as well as to the negative outcome of low
32 reward probabilities. In other words, monkeys' decision-making was more impacted by expected

1 reward under fluoxetine. Thus, not only did monkeys put more effort to get a reward under fluoxetine
2 (Meyniel et al., 2016), but they also better used reward information in order to guide their behavior.

3 *Fluoxetine interferes with attention*

4 Shorter blinks (Hsieh and Tai, 2013) as well as enlarged pupil (Aston-Jones and Cohen, 2005; Wang et
5 al., 2018) have been associated with higher arousal. Improved arousal could thus be at the origin of
6 the enhanced commitment to the task. Beyond this non-specific arousal effect, enhanced performance
7 in task could also be due to enhanced attention, taking place independently from motivational factors.
8 Indeed, it has been shown that 5-HTP (the immediate serotonin precursor) uptake increases attention
9 in low baseline attention individuals (Weinberg-Wolf et al., 2018). Likewise, fluoxetine is shown to
10 selectively modulate, prefrontal synaptic growth during macaque brain development (Golub et al.,
11 2017). It is also shown to activate other cortical structures involved in sustained attention, such as the
12 thalamus and caudate nucleus in healthy subjects but no behavioral effect on sustained attention has
13 been reported (Wingen et al., 2008) and the dorsolateral prefrontal cortex in attention deficit
14 hyperactivity disorder and autism spectrum disorder patients (Chantiluke et al., 2015; Hollander et al.,
15 2005; Quintana et al., 2007; Riggs et al., 2007; Strawn et al., 2015). Last, frontoparietal inhibitory
16 mechanisms have been shown to be closely linked with individual differences in attentional processing
17 such that GABA concentrations in the prefrontal cortex are negatively related to attentional blink
18 magnitude while GABA concentrations in the posterior parietal cortex are positively correlated with
19 attentional blink magnitude (Kihara et al., 2016). In other words, the functional roles of the GABAergic
20 system in selective attention differ between the prefrontal and the parietal cortex. In contrast, GABA
21 concentrations in the visual cortex do not contribute to neither attentional blink magnitude nor to
22 first-target accuracy during a rapid serial visual presentation (Kihara et al., 2016). The GABA-mediated
23 effects of fluoxetine are complex. Indeed, fluoxetine increases the cerebrospinal fluid GABA levels
24 (Gören et al., 2007), indirectly affecting the GABA levels in the brain (Beshara et al., 2016; Santana et
25 al., 2004). This results in a change in the excitatory/inhibitory balance in the brain to the benefit of a
26 stronger inhibition (Yin et al., 2021). However, all this taken together suggests a specific impact of
27 fluoxetine on the fronto-parietal attentional network (Ibos et al., 2013). A direct role of fluoxetine on
28 the correlated activation of the fronto-parietal attentional network is observed in the same macaques
29 as those included in the present study, during the performance of a perceptual task during an fMRI
30 protocol (Gacoin, PhD dissertation). This thus confirms the impact of fluoxetine on the cortical
31 substrates of the attentional function.

32 Attentional control on perception involves both changes in perceptual sensitivity and changes and the
33 decision response threshold. The neuronal activity in the prefrontal cortex has been associated to both

1 (Luo and Maunsell, 2018), while the neuronal activity of extrastriate cortex has mostly been associated
2 with changes in sensitivity (Martinez-Trujillo and Gulli, 2018). Here, in a spatial decision task involving
3 a spatial uncertainty, we report both a change in response criterion, monkeys becoming more liberal,
4 as well as a loss of spatial resolution in visual processing. In line with the observations by Kihara et al.
5 (2016), we predict that GABA concentrations in the prefrontal cortex are negatively related to response
6 criterion magnitude, thus accounting for our experimental observations under fluoxetine. This predicts
7 a decrease in functional connectivity between the prefrontal and parietal cortex under fluoxetine.

8 *Fluoxetine and reaction times*

9 Reaction times (RT) are modulated by multiple cognitive functions ranging from spatial attention
10 (Wardak et al., 2012a, 2011), to temporal expectation and anticipation (Cravo et al., 2013; Wardak et
11 al., 2012b), decision making (Fujimoto et al., 2021; Hanks et al., 2006; Noorani and Carpenter, 2016),
12 perception (Song et al., 2008), reinforcement learning (Viejo et al., 2018), arousal (Davranche et al.,
13 2006; Eason et al., 1969; Fujimoto et al., 2021) and reward processing (Epstein et al., 2011; Firestone
14 and Douglas, 1975; Procyk et al., 2000; Simen et al., 2009). RTs have recently been found to be
15 prolonged in the context of decision-making under SSRIs (Khalighinejad et al., 2022). We here
16 reproduce this observation (prolonged RTs under fluoxetine) in a detection task under spatial
17 uncertainty as well as in a task involving free choice based on reward incentives. However, we report
18 the opposite trend (i.e. speeded up RTs under fluoxetine) in a luminance detection task. We propose
19 to interpret this paradoxical effect in the context of stochastic resonance. A recent study by (Groen et
20 al., 2018) shows that adding noise to the visual cortex using transcranial random noise stimulation
21 enhanced decision-making when stimuli were just below perceptual threshold, but not when they
22 were well below or above threshold. Stretching this observation, we would like to propose that the
23 observed paradoxical effects of fluoxetine on RT depend on the specific noise functions associated
24 with each task, noise being defined as both neuronal noise possibly effected by fluoxetine due to
25 changes in the excitatory/inhibitory balance in the brain (Yin et al., 2021), as well as task related noise
26 or uncertainty, be it spatial uncertainty or reward-related uncertainty.

27 *Fluoxetine and cognitive flexibility*

28 Cognitive flexibility corresponds to the ability animals have to dynamically change their behavioral
29 strategy as a function of the external contingencies as well as their internal drives. Prefrontal serotonin
30 levels have been associated with enhanced behavioral flexibility (Clarke et al., 2004). Here, we show
31 that under fluoxetine, in a free choice task in which reward contingencies change daily and thus have
32 to be relearned, fluoxetine resulted in a stronger implementation of reward outcome in the choice

1 strategy of the monkeys. This thus indicates that monkeys were more flexible in adapting their
2 response choice from one day to the next and from one trial to the next, confirming an enhanced level
3 of cognitive flexibility.

4 *GABA-, Dopamine- and noradrenaline-mediated effects of fluoxetine on perception*

5 Perception relies on both lower level visual mechanisms and higher order attentional mechanisms. As
6 discussed in a previous section, frontoparietal inhibitory mechanisms are closely linked with individual
7 differences in attentional processing (Kihara et al. 2016), such that the functional roles of the
8 GABAergic system in selective attention differs between the prefrontal and the parietal cortex. In
9 contrast, GABA concentrations in the visual cortex do not contribute to neither attentional blink
10 magnitude nor to first-target accuracy during a rapid serial visual presentation (Kihara et al. 2016). It
11 is unclear whether visual cortex GABA concentrations affect perceptual luminosity thresholds
12 independently of top-down attentional processes. GABA_A receptor distribution is not homogenous
13 throughout the brain (Kaulen et al., 2022). In particular, GABA_A receptor concentrations are higher in
14 the ventral part of the striate and extrastriate cortex than in its dorsal part (Kaulen et al., 2022). Due
15 to this GABA_A inhomogeneity, predicting the cognitive effects of systemic fluoxetine neuromodulation
16 is complex. For example, this bias in GABA_A receptor concentrations between dorsal and ventral
17 occipital cortex possibly contributes the well documented functional asymmetry between the upper
18 and lower visual fields (Carlsen et al., 2007, 2007; Chen et al., 2005; Khan and Lawrence, 2005; Liu et
19 al., 2006; Maehara et al., 2004; Qu et al., 2006; Rizzolatti et al., 1987) and higher spatial resolution in
20 the lower visual field (Levine and McAnany, 2005; Sample et al., 1997). This asymmetry has been
21 proposed to have an evolutionary origin (Previc, 1990) due to the fact that hand and tool manipulation
22 mostly occurs in the lower visual field (Levine and McAnany, 2005). In our own data, the luminance
23 detection task, we observe that under fluoxetine, monkeys produce less responses to very low
24 luminosities, specifically in the lower visual field (which is coded by the dorsal part of the occipital
25 cortex). We propose that in the upper visual field, due to the higher GABA_A receptor concentrations in
26 the ventral part of the striate and extrastriate cortex, noise cancellation is efficient including in the
27 absence of fluoxetine. Due to the lower GABA_A receptor concentrations in the ventral part of the
28 striate and extrastriate cortex, noise cancellation in this part of the visual field is enhanced under
29 fluoxetine.

30 This highlights the complexity of predicting the specific effects of fluoxetine on cognition. To bring
31 further complexity to this question, at high doses, fluoxetine has been shown to enhance synaptic
32 dopamine and noradrenaline in the rat prefrontal cortex and in the hypothalamus (Bymaster et al.,
33 2002; Itti and Koch, 2001; Pälvimäki et al., 1996; Perry and Fuller, 1997; Pinna et al., 2009), influencing

1 the mesocortical dopaminergic pathway (Gobert et al., 2000). Overall, we show that fluoxetine
2 interferes with bottom-up perceptual mechanisms, namely degraded luminosity thresholds and
3 degraded spatial resolution as well as on top-down perceptual mechanisms, namely relaxed decision
4 thresholds and increased sensitivity to reward outcomes. In other words, fluoxetine degrades low level
5 visual functions while at the same time maintaining performance in the visual tasks due to enhanced
6 top-down control based on task outcome and reward maximization.

7 **Material and methods**

8 ***Animals and ethical approval***

9 Two healthy adult male rhesus macaques (*macaca mulatta*) took part in the study (M1: 11kgs, 12 years;
10 M2: 8,5kgs, 13 years). The project was authorized by the French Ministry for Higher Education and
11 Research (# 2016120910476056 and #1588- 2015090114042892) in accordance with the French
12 transposition texts of Directive 2010/63/UE. This authorization was based on an ethical evaluation by
13 the French Committee on the Ethics of Experiments in Animals (C2EA) CELYNE registered at the
14 national level as C2EA number 42.

15 ***Surgery***

16 The animals were implanted with a peek MRI-compatible headset covered by dental acrylic. The
17 anesthesia for the surgery was induced by Zoletil (Tiletamine-Zolazepam, Virbac, 5 mg/kg) and
18 maintained by isoflurane (Belamont, 1–2%). Post-surgery analgesia was ensured thanks to Temgesic
19 (buprenorphine, 0.3 mg/ml, 0.01 mg/kg). During recovery, proper analgesic and antibiotic coverage
20 was provided. The surgical procedures conformed to European and National Institutes of Health
21 Guidelines for the Care and Use of Laboratory Animals.

22 ***Fluoxetine preparation***

23 Fluoxetine hydrochloride is a selective 5-HT reuptake inhibitor. It binds to the human 5-HT transporter
24 with a K_i of 0.9 nmol/l and is between 150- and 900-fold selective for 5-HT1A, 5-HT2A et 5-HT2C over
25 H1, α_1 , α_2 -adrenergic, and muscarinic receptors (Ambati et al., 2021). The fluoxetine (N-Methyl-3-[(4-
26 trifluoromethyl) phenoxy]-3-phenylpropylamine hydrochloride) used in the present study has a
27 molecular weight of 345,78 g/mol. Powder galenic form (BioTechne©, ToCris BioScience) was diluted
28 in a saline vehicle (NaCl) as follows. In order to inject the smallest possible volume to the monkeys, we
29 dissolved fluoxetine in a saline solution at a concentration of 8 mg/mL, vortexed 10 seconds and heated
30 the suspension at 60°C in bain-marie to increase solubility while not degrading the active compound.

1 When needed, this preparation was frozen at -20°C so as to avoid the molecule degradation and
2 heated back to body temperature when necessary.

3 *Fluoxetine administration*

4 In order to reduce the stress potentially induced by the injection, monkeys were progressively trained
5 to spontaneously receive subcutaneous saline injections with clicker training. In contrast with
6 intramuscular injections, subcutaneous injections allow a slow distribution of injected product, thus a
7 longer half-life in the body. Injection site and side of injection was changed daily. Injection sites were
8 carefully monitored and sanitized. Once animals reached stable performance and were habituated to
9 subcutaneous injections, behavioral data collection started under either placebo (saline) or fluoxetine
10 injections (2,5mg/kg/day). This Fluoxetine concentration was chosen based on its specific serum
11 concentration decay time in macaques (half-life <16h, Sawyer and Howell, 2011) and the reported
12 threshold for behavioral effects (Fontenot et al., 2009; Chen et al., 2012). Two different injection
13 schedules were used. Acute schedule involving, over a full working week, one day of saline injection,
14 followed by one day of fluoxetine, followed by three days of saline injections (Free choice task).
15 Chronical injections involved daily fluoxetine injections during one full month (Luminance perceptual
16 task and target detection task under spatial uncertainty). The effect of this latter schedule was
17 compared to that of one month of saline injections. Monkeys were always injected in the morning, at
18 the same time, and behavioral data was collected 4 to 6 hours later based on the pharmacokinetics of
19 fluoxetine (Sawyer and Howell, 2011). Table 1 describes the number of placebo and fluoxetine sessions
20 collected for each task, under each injection schedule, as well as general trial statistics.

21 *Experimental setup*

22 Monkeys sat in a primate chair in sphinx position head-fixated thanks to a surgically implanted head
23 post. They were positioned in front of a screen. The eye to screen distance was of 60cm and screen
24 resolution was 1200x1900pixels with a 60Hz refresh rate. Gaze location was sampled at 120Hz using
25 an infrared video-eye tracking system (ISCAN). Eye Movement data Acquisition Software interfaced
26 with an inhouse program for stimulus delivery and experimental control (Presentation©). Monkey
27 hand responses were produced by releasing a bar, the effect of which was to restore the continuity of
28 an infra-red optic beam.

29 *Behavioral tasks*

30 Animals had free access to food and were maintained under a water regulation schedule individually
31 optimized to keep a stable motivation and performance. They were trained on three different

1 behavioral tasks. In all of these tasks, monkeys had to fixate a central fixation point on a screen for a
2 variable duration (1-to-2 secs) while stimuli (size: 0.5°; duration: 100ms) were presented at an
3 eccentricity of 8°.

4 **Luminance detection task.** This task aims at assessing changes in luminance perception thresholds
5 under fluoxetine as compared to saline placebo injections. Monkeys had to fixate a central cross. One
6 thousand to 2000ms from fixation onset, a 200ms target appeared randomly at one of the four possible
7 following positions: (6v2, 6v2), (-6v2, 6v2), (-6v2, -6v2) or (6v2, -6v2). This task was designed to be
8 dominated by bottom-up perceptual processes as we did not use any spatial cue to indicate to the
9 monkeys the position of the upcoming target (Reynolds et al., 2000; Carrasco et al., 2004; Ibos et al.,
10 2009; Reynolds and Chelazzi, 2004). The luminance of the target varied from the background
11 luminance, from easy to hard, on a scale of seven equidistant luminance values (figure 1). Each target
12 position was sampled for each luminance 10 times per session. Monkeys were rewarded for producing
13 a hand response to target presentation, within a response time window of [150ms- 1000ms]. Misses
14 or false alarms are not rewarded. Note that by construction the task does not produce correct
15 rejections. This task was tested twice, in two sets of recording sessions spaced by ten months and a
16 wash out period of at least two consecutive months in between (first data collection: M1: 7 sessions,
17 M2: 10 sessions; second data collection: M1: 3 sessions, M2: 4 sessions (table 1). Individual
18 psychometric luminance perception curves are constructed for each of the four target positions
19 independently for the placebo and the fluoxetine conditions. In the results, we discuss the data
20 collected during the first data collection sessions. The data from the second data collection sessions
21 are presented in supplementary material (figure S1). They are not significantly different from those
22 reported for the first sessions, indicating a stable and reproducible effect in time.

23 **Target detection task in the presence of distractors.** The previous task allows to identify possible
24 changes in individual perception thresholds. However, changes in such metrics can be due to bottom-
25 up changes in perceptual sensitivity (or d') or to changes in individual subject response criterion.
26 In order to refine our understanding of the effect of fluoxetine on perception and decision-making, we
27 used a peripheral target detection task in the presence of spatial distractors (Figure 2). Monkeys had
28 to fixate a central cross. One thousand to 2000ms from fixation onset, a 200ms target appeared
29 randomly at one of the four possible following positions: (6v2, 6v2), (-6v2, 6v2), (-6v2, -6v2) or (6v2, -
30 6v2). Target luminance was defined as target luminance associated with a 70% correct detection
31 threshold in the placebo sessions of the luminance task. Prior to actual target presentation, a 200ms
32 spatial distractor could randomly appear within of virtual circle of 2° around the expected target
33 location (as learned from the previous task). Distractors were identical to the target and only differed

1 in their position. Distractors were present in 3:4 of the trials. Monkeys were rewarded for producing a
 2 hand response to target presentation, within a response time window of [150ms- 1000ms]. Data on
 3 this task were collected from 8 (M1) & 15 (M2) placebo sessions and 4 (M1) & 10 (M2) fluoxetine
 4 sessions (table 1).

5 **Saccadic reward competition task.** In order to investigate the possible contribution of fluoxetine to
 6 the implementation of reward biases and learning, we used a saccadic competitive task, towards
 7 stimuli the spatial position of which was associated, with a specific reward probability schedule (Figure
 8 3). The specific spatial reward contingencies changed from one session to the next. Monkeys had to
 9 fixate a central cross. One thousand to 2000ms from fixation onset, two identical stimuli were
 10 presented. Stimuli were drawn from a virtual array of eight stimuli organized along a circle of 8° of
 11 eccentricity. From one session to the other, each location in this virtual array was associated with a
 12 different reward probability (stable across trials of the same session), which the monkeys discovered
 13 at the beginning of the session, thus building a reward based spatial priority map (Chelazzi et al., 2014;
 14 Della Libera et al., 2017), then exploited during the rest of the session. Possible high reward
 15 probabilities were 80%, 50% and 20%, according to a fixed spatial relationship, such that the extreme
 16 reward probabilities (80% and 20%) were neighbored intermediate reward probability targets (50%)
 17 (figure 3). Monkeys had to make a saccade to one of the two presented stimuli and were rewarded
 18 according to the reward probability associated with the chosen target location. The spatial reward
 19 contingency map was rotated from one day to the next, leading to seven different spatial reward
 20 contingency maps, played several times over independent sessions (as the initial spatial contingency
 21 map on which initial training was performed was not used). For this experiment, we used a 3-week
 22 chronic saline injection schedule followed by and 8-week chronic fluoxetine injection schedule.

| | Monkey 1 | | | | Monkey 2 | | | |
|-----------------------------------------------|-------------------------------------------------|--------------------------------------------------|-------------------------------------------------|-------------------------------------------------|------------------------------------------------|-------------------------------------------------|------------------------------------------------|-------------------------------------------------|
| | Placebo | | Fluoxetine | | Placebo | | Fluoxetine | |
| | Acute | Chronic | Acute | Chronic | Acute | Chronic | Acute | Chronic |
| Luminance detection task | | # Sess. =3; Med. # tr.= 1257 +/- 233.98 | | # Sess. =4; Med. # tr.= 1914 +/- 13.96 | | # Sess. =5; Med. # tr.= 289 +/- 62.33 | | # Sess. =5; Med. # tr.= 387 +/- 14.81 |
| Target detection task with distractors | | # Sess. =8; Med. # tr.= 970 +/- 72.85 | | # Sess. =4; Med. # tr.= 1443 +/- 69.01 | | # Sess. =15; Med. # tr.= 271 +/- 44.04 | | # Sess. =10; Med. # tr.= 497 +/- 86.39 |
| Saccadic reward competition task | # Sess. =7; Med. # tr.= 936 +/- 109.10 | | # Sess. =7; Med. # tr.= 1128 +/- 94.99 | | # Sess. =7; Med. # tr.= 624 +/- 87.64 | | # Sess. =7; Med. # tr.= 792 +/- 94.99 | |

1 **Table 1. Description of number of sessions and trial statistics.** Number of sessions and trial statistics (median + se) are
2 described per type of tasks (luminance detection task, target detection task with distractors and saccadic reward competition
3 task), condition (Placebo and Fluoxetine) and monkeys. Injections for the saccadic reward competition task, were performed
4 acutely (one day per week). For the other tasks, injections were performed according to a chronic injection schedule.

5

6 *Data analysis*

7 All analyses are implemented in Matlab® using ad-hoc scripts.

8 **Extracted behavioral and physiological measures.** For each task and each session, we quantified
9 *session length* (overall number of trials) and overall *behavioral performance* (percentage of correct
10 trials relative to the sum of correct and miss trials). For the luminance detection task, we computed
11 the behavioral performance independently for each target contrast level to right and left targets. We
12 then fit a sigmoid model to the data. Using a sigmoid function (R P (2022). *Sigm_fit*
13 (https://www.mathworks.com/matlabcentral/fileexchange/42641-sigm_fit), MATLAB Central File
14 Exchange. Retrieved August 30, 2022), we determined the *p50* (target luminance associated with a
15 50% chance performance), the *slope* (sensitivity to contrast changes) and the *baseline* (response level
16 to noise) for each mean number of trials per session (see table 1), in both placebo and fluoxetine
17 condition. On the two target detection tasks, *manual reaction times* (RT) were extracted, defined as
18 the time between target presentation and hand lever release (Figure 6, for RT distributions). Pupil size
19 variation (McGuirk and Silverstone, 1990; Phillips et al., 2000; Dumont et al., 2005) and blinks were
20 identified (Wilson et al., 1983; Semlitsch et al., 1993) and we quantified, for each session, the
21 distribution of *blink duration* and *pupil size variations* (Figure 5). We quantified durations of all blinks
22 while monkeys were engaged in tasks in both placebo and fluoxetine conditions and determined the
23 median value. As for measuring pupil dilation, we estimated pupil size during a period of 3 seconds of
24 rest before task initiation while monkeys were sat in the dark, and during a period of 3 seconds during
25 task execution, sampled after target presentation. Percentage pupil size variation in placebo and
26 fluoxetine conditions were computed by estimating the average pupil size on these two epochs and
27 normalizing it by average pupil size over the entire task duration.

28 **RT analyses.** All RTs above 1000ms were excluded from the analysis. RT distributions were then
29 analyzed using the Later model (Noorani and Carpenter, 2016). This model distributes data according
30 to their frequency of distribution. The LATER model allows to segregate RTs in two categories:
31 controlled and anticipated/express responses. We thus segregated, for each task, RT as a function of
32 target position, and we used the LATER model analysis in order to identify the cutoff between
33 anticipatory and controlled responses (Table 2).

34

1

| | <i>Monkey 1</i> | | | | <i>Monkey 2</i> | | | |
|--------------------------------------------------------------------------|-----------------|--------------|-------------------|--------------|-----------------|--------------|-------------------|--------------|
| | <i>Placebo</i> | | <i>Fluoxetine</i> | | <i>Placebo</i> | | <i>Fluoxetine</i> | |
| | <i>Left</i> | <i>Right</i> | <i>Left</i> | <i>Right</i> | <i>Left</i> | <i>Right</i> | <i>Left</i> | <i>Right</i> |
| <i>Luminance detection task</i> | 444ms | | 373ms | | 374ms | | 391ms | |
| <i>Detection task with distractors – targets only</i> | 431ms | 512ms | 390ms | 516ms | 290ms | 303ms | 328ms | 278ms |
| <i>Detection task with distractors – targets preceded by distractors</i> | 415ms | 466ms | 700ms | 836ms | 333ms | 339ms | 363ms | 292ms |

2 **Table 2. RT threshold between anticipatory and controlled responses as defined by the LATER model.** This threshold was
3 defined independently for each monkey, each task and each target position, except for the luminance detection task, for
4 which all four positions were considered together.

5

6 **Signal Detection Theory.** In the target detection task in the presence of distractors, we used signal-
7 detection-theory and computed the monkey’s sensitivity to the location of the target relative to the
8 distractors randomly presented around the target location (d' , reflecting bottom-up sensory features)
9 as well as their response criterion (reflecting top-down control in the decision-making process). These
10 metrics were independently computed per session (see table 1).

11 **Spatial (SSI) and reward (RSI) selectivity index.** In the saccadic reward competition task, we calculated,
12 for each session (Table 1), the choice performance of a given singleton for each possible pair of stimuli.
13 We then calculated, for each session, and each spatial position the SSI as follows. For each position i ,
14 we computed the median choice percentage SSI $_i$ that a singleton at position i was chosen, irrespective
15 of the second singleton in the pair and irrespective of their associated rewards. In other words, it is
16 the median, over all pairs containing singleton i , of the percentage of times i was actually chosen. SSI $_i$
17 thus reflects the average preference of the monkey for singleton i .

18 Likewise, we computed the RSI as follows. For each reward contingency i , we computed the median
19 choice percentage RSI $_i$ that a singleton with that specific reward contingency i was chosen, irrespective
20 of the reward associated with the second singleton in the pair, and irrespective of their spatial position.
21 RSI $_i$ thus reflects the average preference of the monkey for a given reward contingency i .

22 **Statistical analyses**

23 All statistical analyses are non-parametric Wilcoxon or Kruskal-Wallis tests, except when two-way
24 ANOVAs are required. P -value < 0.05 were considered as statistically significant. All statistical analyses
25 are implemented in Matlab® using ad-hoc scripts.

1 **Data availability**

2 The data that support the findings of this study are available from the corresponding author upon
3 reasonable request. A Source Data file provides the raw data used to create all of the figures of this
4 paper.

5 **Code availability**

6 The code that supports the findings of this study is available from the corresponding author upon
7 reasonable request.

8 **Acknowledgements**

9 With financial support from UNADEV (National Union for Blind and Visually Impaired People) in
10 partnership with ITMO NNP (Multi-Organism Thematic Institute Neurosciences, cognitive sciences,
11 neurology and psychiatry) / AVIESAN (national alliance for life science and health) as part of research
12 on vision disorders to S.B.H. as well as LABEX CORTEX funding (ANR-11-LABX-0042) from the Université
13 de Lyon, within the program Investissements d’Avenir (ANR-11-IDEX-0007) operated by the French
14 National Research Agency (ANR). We thank Fidji Francioly and Laurence Boes for animal care. We thank
15 Serge Pinède and Julian Amengual for technical assistance on the project.

16 **Author Contribution Statement**

17 Conceptualization, S.B.H., M.G; Stimuli preparation, M.G; Data Acquisition, M.G.; Methodology, M.G.,
18 S.B.H.; Investigation, M.G., S.B.H.; Writing – Original Draft, M.G., S.B.H.; Writing – Review & Editing,
19 M.G., S.B.H.; Funding Acquisition, S.B.H.; Supervision, S.B.H.

20 **Competing interest statement**

21 The authors declare no competing interests.

22 **Ethics declaration**

23 Animal experiments were authorized by the French Ministry for Higher Education and Research
24 (project no. 2016120910476056 and 1588-2015090114042892) in accordance with the French
25 transposition texts of Directive 2010/63/UE. This authorization was based on ethical evaluation by the
26 French Committee on the Ethics of Experiments in Animals (C2EA) CELYNE registered at the national
27 level as C2EA number 42.

1 References

- 2 Ambati, M., Apicella, I., Wang, S., Narendran, S., Leung, H., Pereira, F., Nagasaka, Y., Huang, P.,
3 Varshney, A., Baker, K.L., Marion, K.M., Shadmehr, M., Stains, C.I., Werner, B.C., Sadda, S.R.,
4 Taylor, E.W., Sutton, S.S., Magagnoli, J., Gelfand, B.D., 2021. Identification of fluoxetine as a
5 direct NLRP3 inhibitor to treat atrophic macular degeneration. *Proceedings of the National
6 Academy of Sciences* 118, e2102975118. <https://doi.org/10.1073/pnas.2102975118>
- 7 Arnsten, A.F.T., Rubia, K., 2012. Neurobiological Circuits Regulating Attention, Cognitive Control,
8 Motivation, and Emotion: Disruptions in Neurodevelopmental Psychiatric Disorders. *Journal of
9 the American Academy of Child & Adolescent Psychiatry* 51, 356–367.
10 <https://doi.org/10.1016/j.jaac.2012.01.008>
- 11 Aston-Jones, G., Cohen, J.D., 2005. An integrative theory of locus coeruleus-norepinephrine function:
12 adaptive gain and optimal performance. *Annu Rev Neurosci* 28, 403–450.
13 <https://doi.org/10.1146/annurev.neuro.28.061604.135709>
- 14 Bar-Haim, Y., Lamy, D., Pergamin, L., Bakermans-Kranenburg, M.J., van IJzendoorn, M.H., 2007. Threat-
15 related attentional bias in anxious and nonanxious individuals: A meta-analytic study.
16 *Psychological Bulletin* 133, 1–24. <https://doi.org/10.1037/0033-2909.133.1.1>
- 17 Bari, A., Theobald, D.E., Caprioli, D., Mar, A.C., Aidoo-Micah, A., Dalley, J.W., Robbins, T.W., 2010.
18 Serotonin Modulates Sensitivity to Reward and Negative Feedback in a Probabilistic Reversal
19 Learning Task in Rats. *Neuropsychopharmacol* 35, 1290–1301.
20 <https://doi.org/10.1038/npp.2009.233>
- 21 Baroncelli, L., Maffei, L., Sale, A., 2011. New Perspectives in Amblyopia Therapy on Adults: A Critical
22 Role for the Excitatory/Inhibitory Balance. *Frontiers in Cellular Neuroscience* 5.
- 23 Bauer, M., Monz, B.U., Montejo, A.L., Quail, D., Dantchev, N., Demyttenaere, K., Garcia-Cebrian, A.,
24 Grassi, L., Perahia, D.G.S., Reed, C., Tylee, A., 2008. Prescribing patterns of antidepressants in
25 Europe: Results from the Factors Influencing Depression Endpoints Research (FINDER) study.
26 *European Psychiatry* 23, 66–73. <https://doi.org/10.1016/j.eurpsy.2007.11.001>
- 27 Beliveau, V., Ganz, M., Feng, L., Ozenne, B., Højgaard, L., Fisher, P.M., Svarer, C., Greve, D.N., Knudsen,
28 G.M., 2017. A High-Resolution *In Vivo* Atlas of the Human Brain's Serotonin System. *J.
29 Neurosci.* 37, 120–128. <https://doi.org/10.1523/JNEUROSCI.2830-16.2016>
- 30 Beshara, S., Beston, B.R., Pinto, J.G.A., Murphy, K.M., 2016. Effects of Fluoxetine and Visual Experience
31 on Glutamatergic and GABAergic Synaptic Proteins in Adult Rat Visual Cortex. *eNeuro* 2,
32 ENEURO.0126-15.2015. <https://doi.org/10.1523/ENEURO.0126-15.2015>
- 33 Brown, H.D., Amodeo, D.A., Sweeney, J.A., Ragozzino, M.E., 2012. The selective serotonin reuptake
34 inhibitor, escitalopram, enhances inhibition of prepotent responding and spatial reversal
35 learning. *J Psychopharmacol* 26, 1443–1455. <https://doi.org/10.1177/0269881111430749>
- 36 Brunken, W.J., Jin, X.T., Pis-Lopez, A.M., 1993. Chapter 4 The properties of the serotonergic system
37 in the retina. *Progress in Retinal Research* 12, 75–99. [https://doi.org/10.1016/0278-4327\(93\)90005-E](https://doi.org/10.1016/0278-4327(93)90005-E)
- 39 Bymaster, F.P., Zhang, W., Carter, P.A., Shaw, J., Chernet, E., Phebus, L., Wong, D.T., Perry, K.W., 2002.
40 Fluoxetine, but not other selective serotonin uptake inhibitors, increases norepinephrine and
41 dopamine extracellular levels in prefrontal cortex. *Psychopharmacology* 160, 353–361.
42 <https://doi.org/10.1007/s00213-001-0986-x>
- 43 Capitão, L.P., Murphy, S.E., Browning, M., Cowen, P.J., Harmer, C.J., 2015. Acute fluoxetine modulates
44 emotional processing in young adult volunteers. *Psychol Med* 45, 2295–2308.
45 <https://doi.org/10.1017/S0033291715000240>
- 46 Carlsen, A.N., Maslovat, D., Chua, R., Franks, I.M., 2007. Perceptual processing time differences owing
47 to visual field asymmetries. *NeuroReport* 18, 1067–1070.
48 <https://doi.org/10.1097/WNR.0b013e3281ac22f1>
- 49 Carrasco, M., Ling, S., Read, S., 2004. Attention alters appearance. *Nat Neurosci* 7, 308–313.
50 <https://doi.org/10.1038/nn1194>

- 1 Carter, O.L., Burr, D.C., Pettigrew, J.D., Vollenweider, F.X., 2005. Using psilocybin to investigate the
2 relationship between attention, working memory and the serotonin 5-HT_{1A} and 5-HT_{2A}
3 receptors. *Journal of Vision* 5, 683. <https://doi.org/10.1167/5.8.683>
- 4 Cazettes, F., Reato, D., Morais, J.P., Renart, A., Mainen, Z.F., 2021. Phasic Activation of Dorsal Raphe
5 Serotonergic Neurons Increases Pupil Size. *Current Biology* 31, 192-197.e4.
6 <https://doi.org/10.1016/j.cub.2020.09.090>
- 7 Cerrito, F., Raiteri, M., 1979. Serotonin release is modulated by presynaptic autoreceptors. *European*
8 *Journal of Pharmacology* 57, 427–430. [https://doi.org/10.1016/0014-2999\(79\)90506-5](https://doi.org/10.1016/0014-2999(79)90506-5)
- 9 Chamberlain, S.R., Müller, U., Blackwell, A.D., Clark, L., Robbins, T.W., Sahakian, B.J., 2006.
10 Neurochemical Modulation of Response Inhibition and Probabilistic Learning in Humans.
11 *Science* 311, 861–863. <https://doi.org/10.1126/science.1121218>
- 12 Chantiluke, K., Barrett, N., Giampietro, V., Brammer, M., Simmons, A., Rubia, K., 2015. Disorder-
13 dissociated effects of fluoxetine on brain function of working memory in attention deficit
14 hyperactivity disorder and autism spectrum disorder. *Psychological Medicine* 45, 1195–1205.
15 <https://doi.org/10.1017/S0033291714002232>
- 16 Chelazzi, L., E to inova, J., Calletti, R., Lo Gerfo, E., Sani, I., Della Libera, C., Santandrea, E., 2014. Altering
17 Spatial Priority Maps via Reward-Based Learning. *Journal of Neuroscience* 34, 8594–8604.
18 <https://doi.org/10.1523/JNEUROSCI.0277-14.2014>
- 19 Chen, Y., Wyatt, H.J., Swanson, W.H., 2005. Pupillary evaluation of retinal asymmetry: Development
20 and initial testing of a technique. *Vision Research* 45, 2549–2563.
21 <https://doi.org/10.1016/j.visres.2005.04.003>
- 22 Chen, Y.-A., Huang, W.-S., Lin, Y.-S., Cheng, C.-Y., Liu, R.-S., Wang, S.-J., Li, I.-H., Huang, S.-Y., Shiue, C.-
23 Y., Chen, C.-Y., Ma, K.-H., 2012. Characterization of 4-[¹⁸F]-ADAM as an imaging agent for SERT
24 in non-human primate brain using PET: a dynamic study. *Nuclear Medicine and Biology* 39,
25 279–285. <https://doi.org/10.1016/j.nucmedbio.2011.08.002>
- 26 Clark, R.N., Ashby Jr., C.R., Dewey, S.L., Ramachandran, P.V., Strecker, R.E., 1996. Effect of acute and
27 chronic fluoxetine on extracellular dopamine levels in the caudate-putamen and nucleus
28 accumbens of rat. *Synapse* 23, 125–131. [https://doi.org/10.1002/\(SICI\)1098-
29 2396\(199607\)23:3<125::AID-SYN1>3.0.CO;2-A](https://doi.org/10.1002/(SICI)1098-2396(199607)23:3<125::AID-SYN1>3.0.CO;2-A)
- 30 Clarke, H.F., Dalley, J.W., Crofts, H.S., Robbins, T.W., Roberts, A.C., 2004. Cognitive Inflexibility After
31 Prefrontal Serotonin Depletion. *Science* 304, 878–880.
32 <https://doi.org/10.1126/science.1094987>
- 33 Cravo, A.M., Rohenkohl, G., Wyart, V., Nobre, A.C., 2013. Temporal Expectation Enhances Contrast
34 Sensitivity by Phase Entrainment of Low-Frequency Oscillations in Visual Cortex. *Journal of*
35 *Neuroscience* 33, 4002–4010. <https://doi.org/10.1523/JNEUROSCI.4675-12.2013>
- 36 Criaud, M., Wardak, C., Ben Hamed, S., Ballanger, B., Boulinguez, P., 2012. Proactive Inhibitory Control
37 of Response as the Default State of Executive Control. *Frontiers in Psychology* 3.
- 38 Davranche, K., Audiffren, M., Denjean, A., 2006. A distributional analysis of the effect of physical
39 exercise on a choice reaction time task. *Journal of Sports Sciences* 24, 323–329.
40 <https://doi.org/10.1080/02640410500132165>
- 41 Della Libera, C., Calletti, R., Eštočinová, J., Chelazzi, L., Santandrea, E., 2017. Reward-based plasticity of
42 spatial priority maps: Exploiting inter-subject variability to probe the underlying neurobiology.
43 *Cognitive Neuroscience* 8, 85–101. <https://doi.org/10.1080/17588928.2016.1213226>
- 44 Di Bello, F., Ben Hadj Hassen, S., Astrand, E., Ben Hamed, S., 2022. Prefrontal Control of Proactive and
45 Reactive Mechanisms of Visual Suppression. *Cerebral Cortex* 32, 2745–2761.
46 <https://doi.org/10.1093/cercor/bhab378>
- 47 Dumont, G.J.H., De Visser, S.J., Cohen, A.F., Van Gerven, J.M.A., 2005. Biomarkers for the effects of
48 selective serotonin reuptake inhibitors (SSRIs) in healthy subjects. *British Journal of Clinical*
49 *Pharmacology* 59, 495–510. <https://doi.org/10.1111/j.1365-2125.2005.02342.x>

- 1 Eason, R.G., Harter, M.R., White, C.T., 1969. Effects of attention and arousal on visually evoked cortical
2 potentials and reaction time in man. *Physiology & Behavior* 4, 283–289.
3 [https://doi.org/10.1016/0031-9384\(69\)90176-0](https://doi.org/10.1016/0031-9384(69)90176-0)
- 4 Enge, S., Fleischhauer, M., Lesch, K.-P., Strobel, A., 2011. On the role of serotonin and effort in
5 voluntary attention: Evidence of genetic variation in N1 modulation. *Behavioural Brain*
6 *Research* 216, 122–128. <https://doi.org/10.1016/j.bbr.2010.07.021>
- 7 Epstein, J.N., Langberg, J.M., Rosen, P.J., Graham, A., Narad, M.E., Antonini, T.N., Brinkman, W.B.,
8 Froehlich, T., Simon, J.O., Altaye, M., 2011. Evidence for higher reaction time variability for
9 children with ADHD on a range of cognitive tasks including reward and event rate
10 manipulations. *Neuropsychology* 25, 427–441. <https://doi.org/10.1037/a0022155>
- 11 Firestone, P., Douglas, V., 1975. The effects of reward and punishment on reaction times and
12 autonomic activity in hyperactive and normal children. *J Abnorm Child Psychol* 3, 201–216.
13 <https://doi.org/10.1007/BF00916751>
- 14 Fontenot, M.B., Musso, M.W., McFatter, R.M., Anderson, G.M., 2009. Dose-Finding Study of Fluoxetine
15 and Venlafaxine for the Treatment of Self-Injurious and Stereotypic Behavior in Rhesus
16 Macaques (*Macaca mulatta*). *Journal of the American Association for Laboratory Animal*
17 *Science* 48, 9.
- 18 Fujimoto, A., Murray, E.A., Rudebeck, P.H., 2021. Interaction between decision-making and
19 interoceptive representations of bodily arousal in frontal cortex (preprint). *Neuroscience*.
20 <https://doi.org/10.1101/2021.02.04.429750>
- 21 Gobert, A., Rivet, J.-M., Lejeune, F., Newman-Tancredi, A., Adhumeau-Auclair, A., Nicolas, J.-P.,
22 Cistarelli, L., Melon, C., Millan, M.J., 2000. Serotonin_{2C} receptors tonically suppress the activity
23 of mesocortical dopaminergic and adrenergic, but not serotonergic, pathways: A combined
24 dialysis and electrophysiological analysis in the rat. *Synapse* 36, 205–221.
25 [https://doi.org/10.1002/\(SICI\)1098-2396\(20000601\)36:3<205::AID-SYN5>3.0.CO;2-D](https://doi.org/10.1002/(SICI)1098-2396(20000601)36:3<205::AID-SYN5>3.0.CO;2-D)
- 26 Golub, M.S., Hackett, E.P., Hogrefe, C.E., Leranth, C., Elsworth, J.D., Roth, R.H., 2017. Cognitive
27 performance of juvenile monkeys after chronic fluoxetine treatment. *Developmental*
28 *Cognitive Neuroscience* 26, 52–61. <https://doi.org/10.1016/j.dcn.2017.04.008>
- 29 Gören, M.Z., Küçükbrahimoglu, E., Berkman, K., Terzioglu, B., 2007. Fluoxetine Partly Exerts its Actions
30 Through GABA: A Neurochemical Evidence. *Neurochem Res* 32, 1559–1565.
31 <https://doi.org/10.1007/s11064-007-9357-2>
- 32 Groen, O. van der, Tang, M.F., Wenderoth, N., Mattingley, J.B., 2018. Stochastic resonance enhances
33 the rate of evidence accumulation during combined brain stimulation and perceptual decision-
34 making. *PLOS Computational Biology* 14, e1006301.
35 <https://doi.org/10.1371/journal.pcbi.1006301>
- 36 Grossman, C.D., Bari, B.A., Cohen, J.Y., 2022. Serotonin neurons modulate learning rate through
37 uncertainty. *Current Biology* 32, 586–599.e7. <https://doi.org/10.1016/j.cub.2021.12.006>
- 38 Guipponi, O., Odouard, S., Pinède, S., Wardak, C., Ben Hamed, S., 2015. fMRI Cortical Correlates of
39 Spontaneous Eye Blinks in the Nonhuman Primate. *Cerebral Cortex* 25, 2333–2345.
40 <https://doi.org/10.1093/cercor/bhu038>
- 41 Hanks, T.D., Ditterich, J., Shadlen, M.N., 2006. Microstimulation of macaque area LIP affects decision-
42 making in a motion discrimination task. *Nat Neurosci* 9, 682–689.
43 <https://doi.org/10.1038/nn1683>
- 44 Hansen, J.Y., Shafiei, G., Markello, R.D., Smart, K., Cox, S.M.L., Nørgaard, M., Beliveau, V., Wu, Y.,
45 Gallezot, J.-D., Aumont, É., Servaes, S., Scala, S.G., DuBois, J.M., Wainstein, G., Bezgin, G.,
46 Funck, T., Schmitz, T.W., Spreng, R.N., Galovic, M., Koepp, M.J., Duncan, J.S., Coles, J.P., Fryer,
47 T.D., Aigbirhio, F.I., McGinnity, C.J., Hammers, A., Soucy, J.-P., Baillet, S., Guimond, S., Hietala,
48 J., Bedard, M.-A., Leyton, M., Kobayashi, E., Rosa-Neto, P., Ganz, M., Knudsen, G.M., Palomero-
49 Gallagher, N., Shine, J.M., Carson, R.E., Tuominen, L., Dagher, A., Masic, B., 2022. Mapping
50 neurotransmitter systems to the structural and functional organization of the human
51 neocortex. *Nat Neurosci* 1–13. <https://doi.org/10.1038/s41593-022-01186-3>

- 1 Harmer, C.J., 2008. Serotonin and emotional processing: Does it help explain antidepressant drug
2 action? *Neuropharmacology, Current Research on Serotonin: From Gene to Function to*
3 *Therapy* 55, 1023–1028. <https://doi.org/10.1016/j.neuropharm.2008.06.036>
- 4 Harmer, C.J., Mackay, C.E., Reid, C.B., Cowen, P.J., Goodwin, G.M., 2006. Antidepressant Drug
5 Treatment Modifies the Neural Processing of Nonconscious Threat Cues. *Biological Psychiatry*
6 59, 816–820. <https://doi.org/10.1016/j.biopsych.2005.10.015>
- 7 Hélie, S., Shamloo, F., Novak, K., Foti, D., 2017. The roles of valuation and reward processing in
8 cognitive function and psychiatric disorders. *Annals of the New York Academy of Sciences*
9 1395, 33–48. <https://doi.org/10.1111/nyas.13327>
- 10 Hendry, S.H.C., Jones, E.G., 1988. Activity-dependent regulation of GABA expression in the visual cortex
11 of adult monkeys. *Neuron* 1, 701–712. [https://doi.org/10.1016/0896-6273\(88\)90169-9](https://doi.org/10.1016/0896-6273(88)90169-9)
- 12 Hollander, E., Phillips, A., Chaplin, W., Zagursky, K., Novotny, S., Wasserman, S., Iyengar, R., 2005. A
13 Placebo Controlled Crossover Trial of Liquid Fluoxetine on Repetitive Behaviors in Childhood
14 and Adolescent Autism. *Neuropsychopharmacol* 30, 582–589.
15 <https://doi.org/10.1038/sj.npp.1300627>
- 16 Homberg, J.R., 2012. Serotonin and decision making processes. *Neuroscience & Biobehavioral Reviews*
17 36, 218–236. <https://doi.org/10.1016/j.neubiorev.2011.06.001>
- 18 Hsieh, C.-S., Tai, C.-C., 2013. An Improved and Portable Eye-Blink Duration Detection System to Warn
19 of Driver Fatigue. *Instrumentation Science & Technology* 41, 429–444.
20 <https://doi.org/10.1080/10739149.2013.796560>
- 21 Hughes, S., Foster, R.G., Peirson, S.N., Hankins, M.W., 2016. Inhibitory effects of fluoxetine on
22 photosensitive retinal ganglion cells. *Investigative Ophthalmology & Visual Science* 57, 4660.
- 23 Ibos, G., Duhamel, J.-R., Hamed, S.B., 2013. A Functional Hierarchy within the Parietofrontal Network
24 in Stimulus Selection and Attention Control. *J. Neurosci.* 33, 8359–8369.
25 <https://doi.org/10.1523/JNEUROSCI.4058-12.2013>
- 26 Ibos, G., Duhamel, J.-R., Hamed, S.B., 2009. The Spatial and Temporal Deployment of Voluntary
27 Attention across the Visual Field. *PLOS ONE* 4, e6716.
28 <https://doi.org/10.1371/journal.pone.0006716>
- 29 Itti, L., Koch, C., 2001. Computational modelling of visual attention. *Nat Rev Neurosci* 2, 194–203.
30 <https://doi.org/10.1038/35058500>
- 31 Kaulen, N., Rajkumar, R., Régio Brambilla, C., Mauler, J., Ramkiran, S., Orth, L., Sbaihat, H., Lang, M.,
32 Wyss, C., Rota Kops, E., Scheins, J., Neumaier, B., Ermert, J., Herzog, H., Langen, K.-J., Lerche,
33 C., Shah, N.J., Veselinović, T., Neuner, I., 2022. mGluR5 and GABAA receptor-specific
34 parametric PET atlas construction—PET/MR data processing pipeline, validation, and
35 application. *Human Brain Mapping* 43, 2148–2163. <https://doi.org/10.1002/hbm.25778>
- 36 Khalighinejad, N., Manohar, S., Husain, M., Rushworth, M.F.S., 2022. Complementary roles of
37 serotonergic and cholinergic systems in decisions about when to act. *Current Biology*.
38 <https://doi.org/10.1016/j.cub.2022.01.042>
- 39 Khan, M.A., Lawrence, G.P., 2005. Differences in visuomotor control between the upper and lower
40 visual fields. *Exp Brain Res* 164, 395–398. <https://doi.org/10.1007/s00221-005-2325-7>
- 41 Kihara, K., Kondo, H.M., Kawahara, J.I., 2016. Differential Contributions of GABA Concentration in
42 Frontal and Parietal Regions to Individual Differences in Attentional Blink. *J Neurosci* 36, 8895–
43 8901. <https://doi.org/10.1523/JNEUROSCI.0764-16.2016>
- 44 Koch, S., 2002. R-fluoxetine Increases Extracellular DA, NE, As Well As 5-HT in Rat Prefrontal Cortex
45 and Hypothalamus An in vivo Microdialysis and Receptor Binding Study. *Neuropsychopharmacology* 27, 949–959. [https://doi.org/10.1016/S0893-133X\(02\)00377-9](https://doi.org/10.1016/S0893-133X(02)00377-9)
- 46 Lansner, J., Jensen, C.G., Petersen, A., Fisher, P.M., Frokjaer, V.G., Vangkilde, S., Knudsen, G.M., 2019.
47 Three weeks of SSRI administration enhances the visual perceptual threshold - a randomized
48 placebo-controlled study. *Psychopharmacology* 236, 1759–1769.
49 <https://doi.org/10.1007/s00213-018-5158-3>
- 50

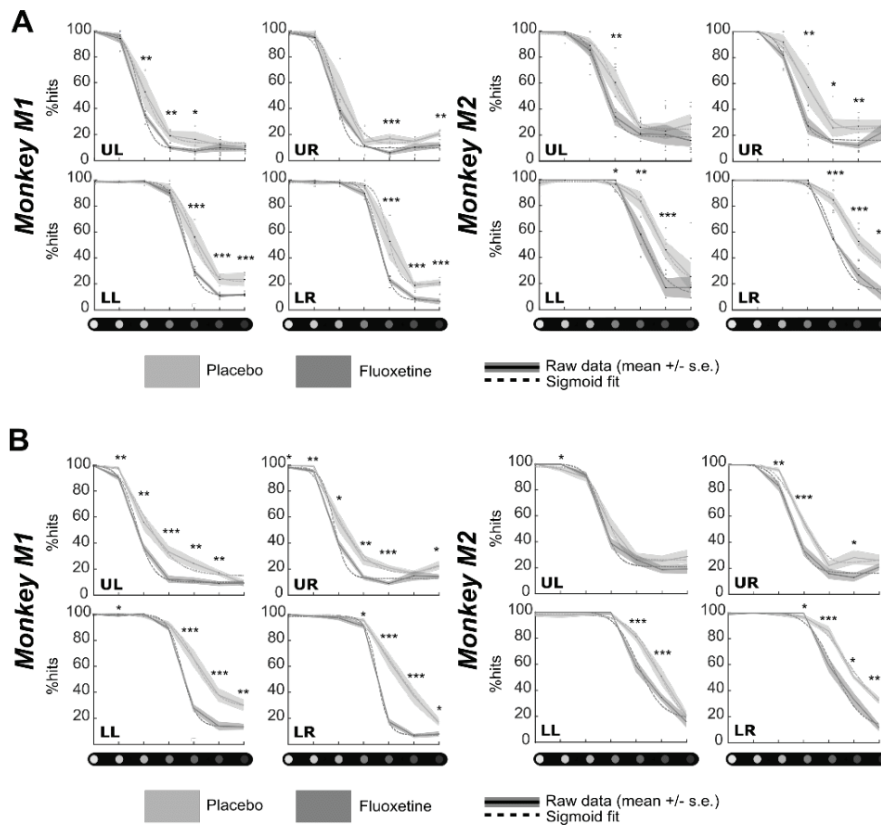
- 1 LeDoux, M.S., Lorden, J.F., Smith, J.M., Mays, L.E., 1998. Serotonergic modulation of eye blinks in cat
2 and monkey. *Neuroscience Letters* 253, 61–64. [https://doi.org/10.1016/S0304-](https://doi.org/10.1016/S0304-3940(98)00616-8)
3 [3940\(98\)00616-8](https://doi.org/10.1016/S0304-3940(98)00616-8)
- 4 Leibowitz, H., 1952. The Effect of Pupil Size on Visual Acuity for Photometrically Equated Test Fields at
5 Various Levels of Luminance*. *J. Opt. Soc. Am., JOSA* 42, 416–422.
6 <https://doi.org/10.1364/JOSA.42.000416>
- 7 Levine, M.W., McAnany, J.J., 2005. The relative capabilities of the upper and lower visual hemifields.
8 *Vision Research* 45, 2820–2830. <https://doi.org/10.1016/j.visres.2005.04.001>
- 9 Li, X., Chen, W., Pan, K., Li, H., Pang, P., Guo, Y., Shu, S., Cai, Y., Pei, L., Liu, D., Afewerky, H.K., Tian, Q.,
10 Zhu, L.-Q., Lu, Y., 2018. Serotonin receptor 2c-expressing cells in the ventral CA1 control
11 attention via innervation of the Edinger–Westphal nucleus. *Nat Neurosci* 21, 1239–1250.
12 <https://doi.org/10.1038/s41593-018-0207-0>
- 13 Liu, T., Heeger, D.J., Carrasco, M., 2006. Neural correlates of the visual vertical meridian asymmetry.
14 *Journal of Vision* 6, 12. <https://doi.org/10.1167/6.11.12>
- 15 Luo, T.Z., Maunsell, J.H.R., 2018. Attentional Changes in Either Criterion or Sensitivity Are Associated
16 with Robust Modulations in Lateral Prefrontal Cortex. *Neuron* 97, 1382–1393.e7.
17 <https://doi.org/10.1016/j.neuron.2018.02.007>
- 18 Macoveanu, J., 2014. Serotonergic modulation of reward and punishment: Evidence from
19 pharmacological fMRI studies. *Brain Research* 1556, 19–27.
20 <https://doi.org/10.1016/j.brainres.2014.02.003>
- 21 Maehara, G., Okubo, M., Michimata, C., 2004. Effects of background color on detecting spot stimuli in
22 the upper and lower visual fields. *Brain and Cognition* 55, 558–563.
23 <https://doi.org/10.1016/j.bandc.2004.04.003>
- 24 Martinez-Trujillo, J., Gulli, R.A., 2018. Dissecting Modulatory Effects of Visual Attention in Primate
25 Lateral Prefrontal Cortex Using Signal Detection Theory. *Neuron* 97, 1208–1210.
26 <https://doi.org/10.1016/j.neuron.2018.03.012>
- 27 Masson, J., 2019. Serotonin in retina. *Biochimie, 70 years of Serotonin* 161, 51–55.
28 <https://doi.org/10.1016/j.biochi.2018.11.006>
- 29 McCabe, C., Mishor, Z., Cowen, P.J., Harmer, C.J., 2010. Diminished Neural Processing of Aversive and
30 Rewarding Stimuli During Selective Serotonin Reuptake Inhibitor Treatment. *Biological*
31 *Psychiatry* 67, 439–445. <https://doi.org/10.1016/j.biopsych.2009.11.001>
- 32 McCormick, D.A., Wang, Z., 1991. Serotonin and noradrenaline excite GABAergic neurones of the
33 guinea-pig and cat nucleus reticularis thalami. *The Journal of Physiology* 442, 235–255.
34 <https://doi.org/10.1113/jphysiol.1991.sp018791>
- 35 McGuirk, J., Silverstone, T., 1990. The effect of the 5-HT re-uptake inhibitor fluoxetine on food intake
36 and body weight in healthy male subjects. *Int J Obes* 14, 361–372.
- 37 Meneses, A., Liy-Salmeron, G., 2012. Serotonin and emotion, learning and memory. *Reviews in the*
38 *Neurosciences* 23, 543–553. <https://doi.org/10.1515/revneuro-2012-0060>
- 39 Meyniel, F., Goodwin, G.M., Deakin, J.W., Klinge, C., MacFadyen, C., Milligan, H., Mullings, E.,
40 Pessiglione, M., Gaillard, R., 2016. A specific role for serotonin in overcoming effort cost. *eLife*
41 5, e17282. <https://doi.org/10.7554/eLife.17282>
- 42 Millar, T.J., Winder, C., Ishimoto, I., Morgan, I.G., 1988. Putative serotonergic bipolar and amacrine
43 cells in the chicken retina. *Brain Res* 439, 77–87. [https://doi.org/10.1016/0006-](https://doi.org/10.1016/0006-8993(88)91463-1)
44 [8993\(88\)91463-1](https://doi.org/10.1016/0006-8993(88)91463-1)
- 45 Monckton, J.E., McCormick, D.A., 2002. Neuromodulatory Role of Serotonin in the Ferret Thalamus.
46 *Journal of Neurophysiology* 87, 2124–2136. <https://doi.org/10.1152/jn.00650.2001>
- 47 Moreau, A.W., Amar, M., Callebert, J., Fossier, P., 2013. Serotonergic modulation of LTP at excitatory
48 and inhibitory synapses in the developing rat visual cortex. *Neuroscience* 238, 148–158.
49 <https://doi.org/10.1016/j.neuroscience.2013.02.013>
- 50 Nelson, R., 1982. All amacrine cells quicken time course of rod signals in the cat retina. *Journal of*
51 *Neurophysiology* 47, 928–947. <https://doi.org/10.1152/jn.1982.47.5.928>

- 1 Ni, Y.G., Miledi, R., 1997. Blockage of 5HT_{2c} serotonin receptors by fluoxetine (Prozac). *Proc. Natl.*
2 *Acad. Sci. U.S.A.* 94, 2036–2040. <https://doi.org/10.1073/pnas.94.5.2036>
- 3 Noorani, I., Carpenter, R.H.S., 2016. The LATER model of reaction time and decision. *Neuroscience &*
4 *Biobehavioral Reviews* 64, 229–251. <https://doi.org/10.1016/j.neubiorev.2016.02.018>
- 5 Pälvimäki, E.-P., Majasuo, H., Laakso, A., Kuoppamäki, M., Syvälahti, E., Roth, B.L., Hietala, J., 1996.
6 Interactions of selective serotonin reuptake inhibitors with the serotonin 5-HT_{2C} receptor.
7 *Psychopharmacology* 126, 234–240. <https://doi.org/10.1007/BF02246453>
- 8 Paquelet, G.E., Carrion, K., Lacefield, C.O., Zhou, P., Hen, R., Miller, B.R., 2022. Single-cell activity and
9 network properties of dorsal raphe nucleus serotonin neurons during emotionally salient
10 behaviors. *Neuron* 110, 2664-2679.e8. <https://doi.org/10.1016/j.neuron.2022.05.015>
- 11 Pérez-Edgar, K., Bar-Haim, Y., McDermott, J.M., Gorodetsky, E., Hodgkinson, C.A., Goldman, D., Ernst,
12 M., Pine, D.S., Fox, N.A., 2010. Variations in the serotonin-transporter gene are associated with
13 attention bias patterns to positive and negative emotion faces. *Biological Psychology* 83, 269–
14 271. <https://doi.org/10.1016/j.biopsycho.2009.08.009>
- 15 Perry, K.W., Fuller, R.W., 1997. Fluoxetine increases norepinephrine release in rat hypothalamus as
16 measured by tissue levels of MHPG-SO₄ and microdialysis in conscious rats. *J. Neural*
17 *Transmission* 104, 953–966. <https://doi.org/10.1007/BF01285563>
- 18 Phillips, M.A., Bitsios, P., Szabadi, E., Bradshaw, C.M., 2000. Comparison of the antidepressants
19 reboxetine, fluvoxamine and amitriptyline upon spontaneous pupillary fluctuations in healthy
20 human volunteers. *Psychopharmacology* 149, 72–76.
21 <https://doi.org/10.1007/s002139900334>
- 22 Pinna, G., Costa, E., Guidotti, A., 2009. SSRIs act as selective brain steroidogenic stimulants (SBSSs) at
23 low doses that are inactive on 5-HT reuptake. *Current Opinion in Pharmacology, Neurosciences*
24 9, 24–30. <https://doi.org/10.1016/j.coph.2008.12.006>
- 25 Pootanakit, K., Brunken, W.J., 2000. 5-HT_{1A} and 5-HT₇ receptor expression in the mammalian retina.
26 *Brain Research* 875, 152–156. [https://doi.org/10.1016/S0006-8993\(00\)02553-1](https://doi.org/10.1016/S0006-8993(00)02553-1)
- 27 Pourcho, R.G., 1996. Neurotransmitters in the retina. *Curr Eye Res* 15, 797–803.
28 <https://doi.org/10.3109/02713689609003465>
- 29 Previc, F.H., 1990. Functional specialization in the lower and upper visual fields in humans: Its
30 ecological origins and neurophysiological implications. *Behavioral and Brain Sciences* 13, 519–
31 542. <https://doi.org/10.1017/S0140525X00080018>
- 32 Procyk, E., Ford Dominey, P., Amiez, C., Joseph, J.-P., 2000. The effects of sequence structure and
33 reward schedule on serial reaction time learning in the monkey. *Cognitive Brain Research* 9,
34 239–248. [https://doi.org/10.1016/S0926-6410\(00\)00002-1](https://doi.org/10.1016/S0926-6410(00)00002-1)
- 35 Puig, M.V., Gullledge, A.T., 2011. Serotonin and Prefrontal Cortex Function: Neurons, Networks, and
36 Circuits. *Mol Neurobiol* 44, 449–464. <https://doi.org/10.1007/s12035-011-8214-0>
- 37 Qu, Z., Song, Y., Ding, Y., 2006. Asymmetry between the upper and lower visual fields: An event-related
38 potential study. *CHINESE SCI BULL* 51, 536–541. <https://doi.org/10.1007/s11434-006-0536-3>
- 39 Quintana, H., Butterbaugh, G.J., Purnell, W., Layman, A.K., 2007. Fluoxetine Monotherapy in Attention-
40 Deficit/Hyperactivity Disorder and Comorbid Non-Bipolar Mood Disorders in Children and
41 Adolescents. *Child Psychiatry Hum Dev* 37, 241–253. <https://doi.org/10.1007/s10578-006-0032-7>
- 42
- 43 Reynolds, J.H., Chelazzi, L., 2004. ATTENTIONAL MODULATION OF VISUAL PROCESSING. *Annu. Rev.*
44 *Neurosci.* 27, 611–647. <https://doi.org/10.1146/annurev.neuro.26.041002.131039>
- 45 Reynolds, J.H., Pasternak, T., Desimone, R., 2000. Attention Increases Sensitivity of V4 Neurons.
46 *Neuron* 26, 703–714. [https://doi.org/10.1016/S0896-6273\(00\)81206-4](https://doi.org/10.1016/S0896-6273(00)81206-4)
- 47 Riggs, P.D., Mikulich-Gilbertson, S.K., Davies, R.D., Lohman, M., Klein, C., Stover, S.K., 2007. A
48 Randomized Controlled Trial of Fluoxetine and Cognitive Behavioral Therapy in Adolescents
49 With Major Depression, Behavior Problems, and Substance Use Disorders. *Archives of*
50 *Pediatrics & Adolescent Medicine* 161, 1026–1034.
51 <https://doi.org/10.1001/archpedi.161.11.1026>

- 1 Rizzolatti, G., Riggio, L., Dascola, I., Umiltá, C., 1987. Reorienting attention across the horizontal and
2 vertical meridians: Evidence in favor of a premotor theory of attention. *Neuropsychologia* 25,
3 31–40. [https://doi.org/10.1016/0028-3932\(87\)90041-8](https://doi.org/10.1016/0028-3932(87)90041-8)
- 4 Rodriguez, L., Joly, S., Zine-Eddine, F., Mdzomba, J.B., Pernet, V., 2020. Tau modulates visual plasticity
5 in adult and old mice. *Neurobiology of Aging* 95, 214–224.
6 <https://doi.org/10.1016/j.neurobiolaging.2020.07.024>
- 7 Sample, P.A., Irak, I., Martinez, G.A., Yamagishi, N., 1997. Asymmetries in the Normal Short-wavelength
8 Visual Field: Implications for Short-wavelength Automated Perimetry. *American Journal of*
9 *Ophthalmology* 124, 46–52. [https://doi.org/10.1016/S0002-9394\(14\)71643-5](https://doi.org/10.1016/S0002-9394(14)71643-5)
- 10 Santana, N., Bortolozzi, A., Serrats, J., Mengod, G., Artigas, F., 2004. Expression of Serotonin1A and
11 Serotonin2A Receptors in Pyramidal and GABAergic Neurons of the Rat Prefrontal Cortex.
12 *Cerebral Cortex* 14, 1100–1109. <https://doi.org/10.1093/cercor/bhh070>
- 13 Sawyer, E.K., Howell, L.L., 2011. Pharmacokinetics of Fluoxetine in Rhesus Macaques following Multiple
14 Routes of Administration. *PHA* 88, 44–49. <https://doi.org/10.1159/000329417>
- 15 Schmitt, J.A., Riedel, W.J., Vuurman, E.F., Kruijzinga, M., Ramaekers, J.G., 2002. Modulation of the
16 Critical Flicker Fusion effects of serotonin reuptake inhibitors by concomitant pupillary
17 changes. *Psychopharmacology* 160, 381–386. <https://doi.org/10.1007/s00213-001-0993-y>
- 18 Scholes, K.E., Harrison, B.J., O'Neill, B.V., Leung, S., Croft, R.J., Pipingas, A., Phan, K.L., Nathan, P.J.,
19 2007. Acute Serotonin and Dopamine Depletion Improves Attentional Control: Findings from
20 the Stroop Task. *Neuropsychopharmacol* 32, 1600–1610.
21 <https://doi.org/10.1038/sj.npp.1301262>
- 22 Scholl, J., Kolling, N., Nelissen, N., Browning, M., Rushworth, M.F.S., Harmer, C.J., 2017. Beyond
23 negative valence: 2-week administration of a serotonergic antidepressant enhances both
24 reward and effort learning signals. *PLOS Biology* 15, e2000756.
25 <https://doi.org/10.1371/journal.pbio.2000756>
- 26 Schuette, E., Chappell, R.L., 1998. Excitatory Amino Acids and Serotonin Uptake Blockers Reveal two
27 Physiologically Distinct Serotonin Systems in the Retina of the Skate, Raja Erinacea.
28 *International Journal of Neuroscience* 95, 115–132.
29 <https://doi.org/10.3109/00207459809000655>
- 30 Semlitsch, H.V., Anderer, P., Saletu, B., Binder, G.A., Decker, K.A., 1993. Acute effects of the novel
31 antidepressant venlafaxine on cognitive event-related potentials (P300), eye blink rate and
32 mood in young healthy subjects. *International Clinical Psychopharmacology* 8, 155–166.
33 <https://doi.org/10.1097/00004850-199300830-00004>
- 34 Seymour, B., Daw, N.D., Roiser, J.P., Dayan, P., Dolan, R., 2012. Serotonin Selectively Modulates
35 Reward Value in Human Decision-Making. *J. Neurosci.* 32, 5833–5842.
36 <https://doi.org/10.1523/JNEUROSCI.0053-12.2012>
- 37 Simen, P., Contreras, D., Buck, C., Hu, P., Holmes, P., Cohen, J.D., 2009. Reward rate optimization in
38 two-alternative decision making: Empirical tests of theoretical predictions. *Journal of*
39 *Experimental Psychology: Human Perception and Performance* 35, 1865–1897.
40 <https://doi.org/10.1037/a0016926>
- 41 Smith, R.G., Vardi, N., 1995. Simulation of the Aii amacrine cell of mammalian retina: Functional
42 consequences of electrical coupling and regenerative membrane properties. *Visual*
43 *Neuroscience* 12, 851–860. <https://doi.org/10.1017/S095252380000941X>
- 44 Song, S., Howard, J.H., Howard, D.V., 2008. Perceptual sequence learning in a serial reaction time task.
45 *Exp Brain Res* 189, 145–158. <https://doi.org/10.1007/s00221-008-1411-z>
- 46 Strawn, J.R., Welge, J.A., Wehry, A.M., Keeshin, B., Rynn, M.A., 2015. Efficacy and Tolerability of
47 Antidepressants in Pediatric Anxiety Disorders: A Systematic Review and Meta-Analysis.
48 *Depression and Anxiety* 32, 149–157. <https://doi.org/10.1002/da.22329>
- 49 Umemori, J., Winkel, F., Didio, G., Llach Pou, M., Castrén, E., 2018. iPlasticity: Induced juvenile-like
50 plasticity in the adult brain as a mechanism of antidepressants: Antidepressant-induced
51 plasticity. *Psychiatry Clin. Neurosci.* 72, 633–653. <https://doi.org/10.1111/pcn.12683>

- 1 Vaney, D.I., 1986. Morphological identification of serotonin-accumulating neurons in the living retina.
2 Science 233, 444–446. <https://doi.org/10.1126/science.3726538>
- 3 Vetencourt, J.F.M., Sale, A., Viegi, A., Baroncelli, L., De Pasquale, R., F. O’Leary, O., Castrén, E., Maffei,
4 L., 2008. The Antidepressant Fluoxetine Restores Plasticity in the Adult Visual Cortex. Science
5 320, 385–388. <https://doi.org/10.1126/science.1150516>
- 6 Vetencourt, J.F.M., Tiraboschi, E., Spolidoro, M., Castrén, E., Maffei, L., 2011. Serotonin triggers a
7 transient epigenetic mechanism that reinstates adult visual cortex plasticity in rats: Epigenetics
8 of serotonin-induced adult cortical plasticity. European Journal of Neuroscience 33, 49–57.
9 <https://doi.org/10.1111/j.1460-9568.2010.07488.x>
- 10 Viejo, G., Girard, B., Procyk, E., Khamassi, M., 2018. Adaptive coordination of working-memory and
11 reinforcement learning in non-human primates performing a trial-and-error problem solving
12 task. Behavioural Brain Research, SI: MCC 2016 355, 76–89.
13 <https://doi.org/10.1016/j.bbr.2017.09.030>
- 14 Wang, C.-A., Baird, T., Huang, J., Coutinho, J.D., Brien, D.C., Munoz, D.P., 2018. Arousal Effects on Pupil
15 Size, Heart Rate, and Skin Conductance in an Emotional Face Task. Frontiers in Neurology 9.
- 16 Wardak, C., Ben Hamed, S., Olivier, E., Duhamel, J.-R., 2012a. Differential effects of parietal and frontal
17 inactivations on reaction times distributions in a visual search task. Frontiers in Integrative
18 Neuroscience 6.
- 19 Wardak, C., Olivier, E., Duhamel, J.-R., 2011. The relationship between spatial attention and saccades
20 in the frontoparietal network of the monkey. European Journal of Neuroscience 33, 1973–
21 1981. <https://doi.org/10.1111/j.1460-9568.2011.07710.x>
- 22 Wardak, C., Ramanoël, S., Guipponi, O., Boulinguez, P., Ben Hamed, S.B., 2012b. Proactive inhibitory
23 control varies with task context. European Journal of Neuroscience 36, 3568–3579.
24 <https://doi.org/10.1111/j.1460-9568.2012.08264.x>
- 25 Wassle, H., Voigt, T., Patel, B., 1987. Morphological and immunocytochemical identification of
26 indoleamine- accumulating neurons in the cat retina. J. Neurosci. 7, 1574–1585.
27 <https://doi.org/10.1523/JNEUROSCI.07-05-01574.1987>
- 28 Weinberg-Wolf, H., Fagan, N.A., Anderson, G.M., Tringides, M., Dal Monte, O., Chang, S.W.C., 2018.
29 The effects of 5-hydroxytryptophan on attention and central serotonin neurochemistry in the
30 rhesus macaque. Neuropsychopharmacol 43, 1589–1598. [https://doi.org/10.1038/s41386-
31 017-0003-7](https://doi.org/10.1038/s41386-017-0003-7)
- 32 Wilson, W.H., Higano, H., Papadatos, Y., Kelwala, S., Ban, T.A., 1983. A double-blind placebo controlled
33 study to compare the autonomic effects of fluvoxamine with those of amitriptyline and
34 doxepin in healthy volunteers. Br J Clin Pharmacol 15, 385S-392S.
- 35 Wingen, M., Kuypers, K.P.C., van de Ven, V., Formisano, E., Ramaekers, J.G., 2008. Sustained attention
36 and serotonin: a pharmaco-fMRI study. Human Psychopharmacology: Clinical and
37 Experimental 23, 221–230. <https://doi.org/10.1002/hup.923>
- 38 Wong, D.T., Bymaster, F.P., Engleman, E.A., 1995. Prozac (fluoxetine, lilly 110140), the first selective
39 serotonin uptake inhibitor and an antidepressant drug: Twenty years since its first publication.
40 Life Sciences 57, 411–441. [https://doi.org/10.1016/0024-3205\(95\)00209-O](https://doi.org/10.1016/0024-3205(95)00209-O)
- 41 Worbe, Y., Savulich, G., Voon, V., Fernandez-Egea, E., Robbins, T.W., 2014. Serotonin Depletion Induces
42 ‘Waiting Impulsivity’ on the Human Four-Choice Serial Reaction Time Task: Cross-Species
43 Translational Significance. Neuropsychopharmacol 39, 1519–1526.
44 <https://doi.org/10.1038/npp.2013.351>
- 45 Yin, Y.-Y., Wang, Y.-H., Liu, W.-G., Yao, J.-Q., Yuan, J., Li, Z.-H., Ran, Y.-H., Zhang, L.-M., Li, Y.-F., 2021.
46 The role of the excitation:inhibition functional balance in the mPFC in the onset of
47 antidepressants. Neuropharmacology 191, 108573.
48 <https://doi.org/10.1016/j.neuropharm.2021.108573>
- 49 Zubair, M., Arsenault, J.T., Vanduffel, W., 2021. Stimulus-Effector Associations Modulate Activity in
50 Early Visual Cortex of Monkeys. <https://doi.org/10.2139/ssrn.3985609>
- 51

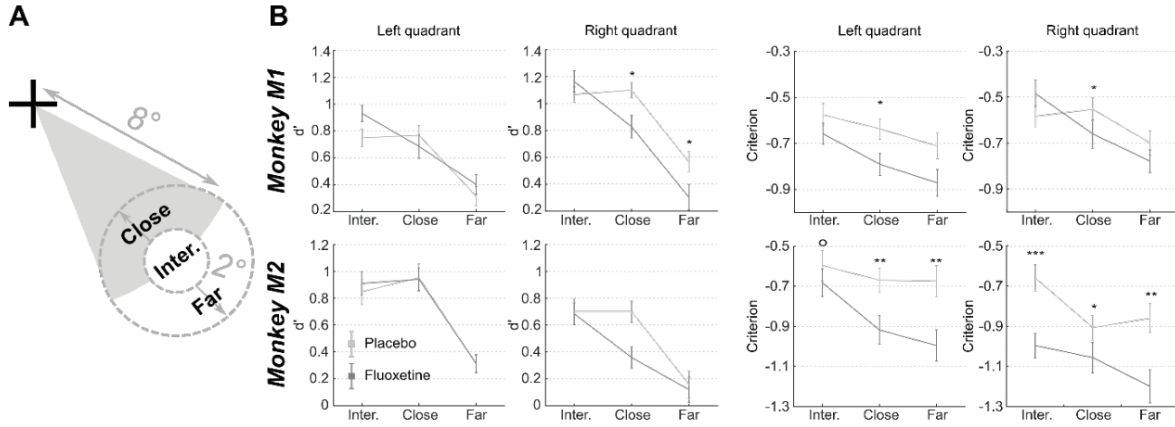
1 **Supplementary material**



2

3 **Figure S1: Effect of Fluoxetine on perceptual thresholds in a luminance detection task.** For both monkeys, % of hits were
4 computed independently for each target luminosity. Dots represent individual sessions, continuous lines represent average
5 % hits across all sessions (+/-s.e.) and dashed lines represent sigmoid fit of the data. Placebo data are represented in light
6 gray and Fluoxetine data are represented in dark gray. Behavioral data are represented independently for each target
7 position. Statistical significance is represented as follows: ***, $p < 0.001$; **, $p < 0.01$; *, $p < 0.05$; n.s., $p > 0.05$. (A) First
8 experiment (same data as in figure 2). (B) Second identical experiment at 10 months' interval.

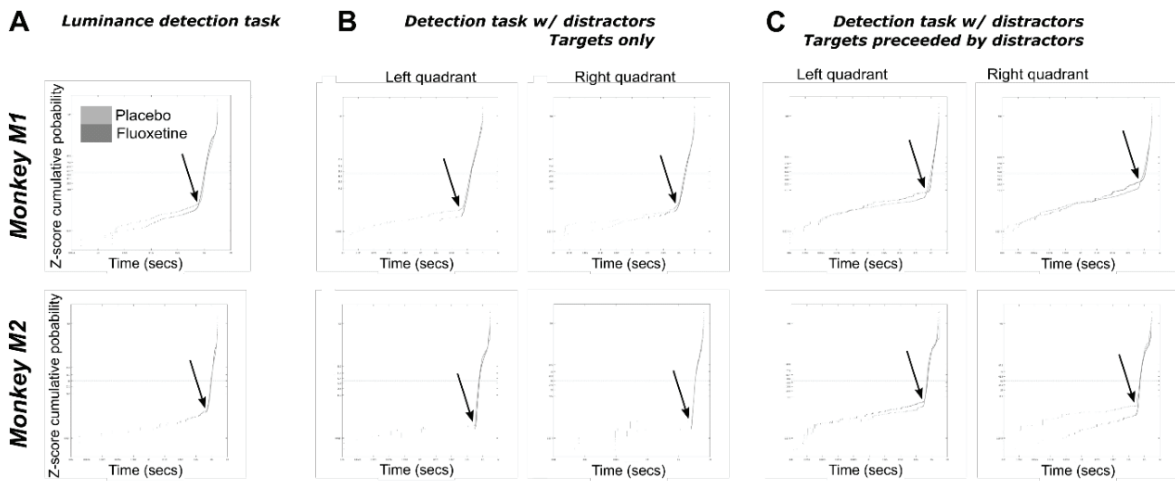
9



1

2 **Figure S2: Effect of Fluoxetine on spatial sensitivity d' and response criterion in a target detection task in the presence**
 3 **of spatial distractors, as a function of target distractor distance. (A) Spatial categorization of target to distractor distances.**
 4 (B) For both monkeys, d' and criterion were computed independently for each target and for each target to distractor
 5 distance. Median +/- s.e. of median are presented for placebo and Fluoxetine conditions. Statistical significance is represented
 6 as follows: ***, $p < 0.001$; **, $p < 0.01$; *, $p < 0.05$; °, $p < 0.07$. Figure 3 represents this data irrespective of target to distractor
 7 distance.

8



9

10 **Figure S3: Identification of limit between anticipatory and controlled RT using the LATER model, for monkeys M1 (top) and**
 11 **M2 (bottom), in the placebo (light gray) and Fluoxetine (dark gray) conditions in the luminance task (A, all positions collapsed,**
 12 **high luminance targets only), in the detection tasks with distractors, on target only trials (B), and in trials with distractors (C).**

Perspectives of the chapter I

In this study and first chapter, we focused on the effects of fluoxetine on both bottom-up and top-down mechanisms along with an interest on the interaction of these two cortical mechanisms. We showed that fluoxetine not only increases perceptual low-level luminance threshold, but is also actively involved in the high-level mechanisms to increase a potential perceptual learning, such as motivation and an enhanced reward sensitivity. In the manner of a compensatory process such as those observed during an ocular dominance plasticity induced by a monocular deprivation, we hypothesize that these high-level mechanisms are also enhanced as a response to cope with decreased luminance vision.

Noteworthy questions arise from these conclusions. We can first wonder about the learning rate across sessions given the required flexibility from macaques. Indeed, while they learn the new contingency map on the dual-choice saccadic task, we could compare the number of necessary trials needed to learn the new map and whether this learning remains static in the aftermath, in the manner of a plateau phase, depending on the conditions. Preliminary analysis indicate that learning is indeed faster under fluoxetine. Still on the same task, we can also investigate the performances, working duration and learning rate on wash-out days, following the fluoxetine intake. The data is available but have not been analyzed as yet. Since the pharmacokinetics of fluoxetine is expected to allow a behavioral effect up to 24-hours following fluoxetine administration (although this is expected to be subject-dependent), we would be interested to see if the reported behavioral effects are dose-dependent, or even if there would be a behavioral imprinting of such behaviors even in a washed-out organism (on the third day after fluoxetine administration for example), signing a persistence of plasticity in time. We are currently investigating this point. Other topics of matter concern attention orientation. Indeed, we report in study 1 that reaction times are modulated by fluoxetine in a task-dependent manner. In order to address directly this question, one idea would be to implement a new detection task with a cue prior to the target. Because attention orientation modulates visual contrasts, we did not consider implementing such a task while designing the study; the observations would indeed have been confounded by the impaired luminance perception induced by fluoxetine, therefore a conclusion would have been difficult to draw. Study 1 provides information on how to now design such a study. Among the different perspectives this study offers, an important one concerns the study of the fluoxetine on social perception. Indeed, I took a particular interest in parallel to my thesis project to investigate the neural correlates of socio-emotional contexts (**Appendix n°1**). Thus, I also acquired behavioral and fMRI data (*not presented in this manuscript*) of macaques while they were viewing dynamic images of interacting macaques and macaques faces with different emotional valences, and non-social scenes in placebo and fluoxetine condition. For the behavioral task, we expect to observe visual exploration of such scenes, thanks to eyetracker recordings, in both conditions. As shown by recent studies, fluoxetine plays a role in social gaze in macaques. Indeed, although the role of serotonin has been widely documented in several species,

Chapter I

an interesting perspective would be to characterize the role of fluoxetine in socially rewarding events and its relevance to enhance social information exploration. These data are still under investigation.

In **study 1**, we have thus studied behavioral effects of fluoxetine on the visual system and provided hypotheses on how fluoxetine is expected to modulate underlying neural correlates. In the next study, we will thus investigate the cortical functional connectivity changes under fluoxetine neuromodulation, in the context of a priority map alteration thanks to a reward-based learning task. We expect this to shed light on how fluoxetine biases visual perception in the occipital cortex under the influence of enhanced sensitivity to reward.

Chapter I

CHAPTER II

PERCEPTUAL LEARNING INDUCED BY A SPATIAL PRIORITY MAP COUPLED WITH CHRONIC FLUOXETINE ADMINISTRATION: A RESTING STATE fMRI STUDY IN THE MACAQUE

| | |
|----------------------------------------------|-----|
| General introduction to the chapter II | 104 |
| Abstract | 105 |
| Introduction | 106 |
| Material and Methods..... | 107 |
| Results | 116 |
| Discussion | 129 |
| Conclusion..... | 134 |
| Supplementary figures..... | 136 |
| References | 138 |
| Perspectives of the chapter II | 143 |

Chapter II

General introduction to the chapter II

In the chapter I, we characterized the behavioral effects of fluoxetine on the visual system using three different behavioral tasks. One of the major outcomes was that, under fluoxetine, macaques are more sensitive to reward in the context of a dual-choice saccadic task. Indeed, when the decision-making process involves differential reward values, monkeys chose more often the most rewarded location under fluoxetine than under placebo condition, while avoiding the least rewarding location more often. As our goal is to enhance visual plasticity in the adult brain, we exploited this particular task in order to design our induction of plasticity protocols. Furthermore, this task allows to manipulate reward values independently per hemifield. Hence, each macaques can be its own control as we can perform within-subjects inter-hemispheric comparisons at each conditions. As a result, we thus designed our longitudinal protocol of plasticity enhancement followed by imaging campaigns according to 3 time-points: a control condition (T1), a biasing of hemifields reward associated value thanks to an intense training on the dual-choice task (T2) and the reversed (along the vertical meridian) biasing of hemifields reward associated value thanks to the dual-choice task training coupled with chronic fluoxetine administration (T3).

In the light of our previous findings and the literature, we first expected to observe functional connectivity modulations in this chapter. We here discuss, based on resting state fMRI data collected at the three time points described above, how reward-based training with or without fluoxetine modifies cortical functional connectivity within the networks involved in top-down and bottom-up visual perception processes.

Study n°2: Perceptual learning induced by a spatial priority map coupled with chronic fluoxetine administration: a resting state study. **Maëva Gacoïn**, Mathilda Froesel, Simon Clavagnier, Maxime Gaudet-Trafit & Suliann Ben Hamed. (in prep.)

Perceptual learning induced by a spatial priority map coupled to chronic fluoxetine administration: a resting state study

Maëva Gacoin, Mathilda Froesel, Simon Clavagnier, Maxime Gaudet-Trafit & Suliann Ben Hamed. *In prep*

Abstract

While the brain synaptic connectivity is considered as stabilized in the adult brain, numerous studies state that a certain degree of plasticity remains and that this plasticity can be enhanced thanks to appropriate behavioral and pharmacological manipulations. The general principle of these manipulations is to render the brain more excitable to these environmental stimulations by playing on the excitation/inhibition balance of the brain. While glutamate has an excitatory action, the GABA is known to have an inhibition action. In the present study, our goal was to investigate the network correlates of a re-instantiation of plasticity thanks to intense reward-based behavioral training, on its own or combined with fluoxetine, an SSRI (anti-depressant) known to reduce GABA levels in the brain. Using resting state fMRI functional data collected in two awake macaques, in a control baseline condition, after behavioral manipulation and after behavioral manipulation combined with fluoxetine, we measured ROI-to-ROI and ROI-to-whole cortex functional connectivity, and we determined the specific effects of fluoxetine on this network. We first showed that fluoxetine action on the fronto-parieto-occipital connectivity is dependent on reward outcome. Then, we described that fluoxetine reweighs functional connectivity in favor of the dorsal visual stream by decreasing the functional connectivity to brain areas associated with the ventral visual stream in brain hemisphere associated with a high reward. Finally, we demonstrated that this reweighing is accompanied by a suppression of functional connectivity within the ventral visual stream with fluoxetine in brain hemisphere associated with a low reward. We propose that this massive changes in brain functional connectivity account for the behavioral observations described in Study 1.

Introduction

In the adult, brain synaptic connectivity is considered as stabilized to allow optimal interaction with the environment. This also involves less adaptability to new events or new cortical or bodily configurations (e.g. under learning or trauma). In order to improve learning and recovery of visual functions in adulthood, studies on the developmental critical period have concluded that manipulating the excitation/inhibition balance allows to enhance a form of plasticity (Bavelier et al., 2010). Indeed, even at a smaller scale, the adult visual system remains plastic beyond the critical period (Karni and Bertini, 1997; for review, see Castaldi et al., 2020). Perceptual learning is the most dominant form of cortical plasticity in the adult brain. It involves implicit memory consolidated by experience and practice, and can be elicited by repetitive sensory interventions. Indeed, extensive and repeated practice of a simple discrimination tasks, thus involving visual attention, affects both stimuli representation in early and late visual areas (Adab et al., 2014). The effects of this bottom-up manipulation, i.e. signal coming from primary areas to high order areas, can be enhanced by coupling it to top-down mechanisms of attention, such as a goal-directed attention toward a reward of high value. This is mostly driven by the visual attention network (Buschman and Miller, 2007; Ibos et al., 2013; Katsuki and Constantinidis, 2014; Richter et al., 2017). The cortical regions implement a priority map (Serences and Yantis, 2006, 2004; Bisley and Goldberg, 2010), which corresponds to an enhanced real-time representation of the locations of highest behavioral salience in the visual field relative to other sensory input of non interest, due to specific sensory selection and suppression mechanisms (Di Bello et al., 2022). Accordingly, strong, fine-grained and long-lasting plastic changes can be induced by altering the spatial priority map thanks to reward-based attentional learning (Chelazzi et al., 2013, 2014).

In healthy human adults, it has been shown that serotonin selective reuptake inhibitors (SSRIs), which increase serotonin availability in the synaptic cleft, enhance reward processing (Macoveanu, 2014; McCabe et al., 2010; Scholl et al., 2017) and that general serotonin increase in the brain modulates effort costs, thus improving learning efficiency (Meyniel et al., 2016). At the same time, inhibition of central serotonin reuptake decreases probabilistic learning (Chamberlain et al., 2006). In this context, we demonstrated in a previous study (Gacoin and Ben Hamed, 2022) that a particular SSRI, fluoxetine, enhances selectivity to reward when learning a priority map, choosing more frequently the most rewarding position and ignoring more the less rewarding ones. How serotonin availability impacts the spatial priority maps and interferes with parieto-frontal and occipital function is yet unknown.

In the present study, we specifically focus on reward-based learning of spatial priority maps and we address the question of whether and how fluoxetine interferes with this process. To do so, we recorded awake resting state fMRI data in two adult macaque monkeys (*Macaca mulatta*) after training them on specific tasks involving a reward-based learning of a spatial priority map, in the presence or absence of fluoxetine injections. In order to characterize the training effect, we used a dual-choice task

in the presence of a fixed reward contingency spatial map, i.e. in a task in which each target position is associated with specific probabilities of getting either a low or a high reward (Chelazzi et al., 2014). We used atlas-based regions of interest ROI to ROI connectivity analyses and task driven ROI analysis and we precisely characterized the whole brain effects of reward-based spatial prioritization as well as the whole brain effects of chronic fluoxetine administration on the brain and its interaction with reward-based prioritization.

Material and Methods

1. Animals and ethical approval

Two healthy adult male rhesus macaques (*macaca mulatta*) took part in the study (M1: 11kgs, 12 years; M2: 8,5kgs, 13 years). The project was authorized by the French Ministry for Higher Education and Research (# 2016120910476056) in accordance with the French transposition texts of Directive 2010/63/UE. This authorization was based on an ethical evaluation by the French Committee on the Ethics of Experiments in Animals (C2EA) CELYNE registered at the national level as C2EA number 42.

2. Surgery

The animals were implanted with a peek MRI-compatible headset covered by dental acrylic. The anesthesia for the surgery was induced by Zoletil (Tiletamine-Zolazepam, Virbac, 5 mg/kg) and maintained by isoflurane (Belamont, 1–2%). Post-surgery analgesia was ensured thanks to Temgesic (buprenorphine, 0.3 mg/ml, 0.01 mg/kg). During recovery, proper analgesic and antibiotic coverage was provided. The surgical procedures conformed to European and National Institutes of Health Guidelines for the Care and Use of Laboratory Animals.

3. Fluoxetine preparation

Fluoxetine hydrochloride is a selective 5-HT reuptake inhibitor. It binds to the human 5-HT transporter with a K_i of 0.9 nmol/l and is between 150- and 900-fold selective for 5-HT_{1A}, 5-HT_{2A} et 5-HT_{2C} over H₁, α_1 , α_2 -adrenergic, and muscarinic receptors (Ambati et al., 2021). The fluoxetine (N-Methyl-3-[(4-trifluoromethyl) phenoxy]-3-phenylpropylamine hydrochloride) used in the present study has a molecular weight of 345,78 g/mol. Powder galenic form (BioTechne©, ToCris BioScience) was diluted in a saline vehicle (NaCl) as follows. We diluted 50mg of fluoxetine in 6mL of saline, vortexed 10 seconds and heated the suspension at 60°C in bain-marie. When needed, it was frozen at -20°C so as to avoid the molecule degradation and heated back to body temperature when necessary.

4. Fluoxetine administration

In order to reduce the potential stress induced by the injection, monkeys were progressively trained to spontaneously receive subcutaneous saline injections with clicker training. In contrast with intramuscular injections, subcutaneous injections allow a slow distribution of injected product, which is here relevant to observe the fluoxetine effect during the whole duration of the acquisition session that can last up to 2 to 3 hours. The injection schedule during the training period and the fMRI acquisition period was chronic. Chronic injections involved daily fluoxetine injections (2,5mg/kg/day, Chen et al. 2012) and the training period lasted six weeks excluding weekends. Injection site and side of injection was changed daily to avoid discomfort to the animals as much as possible. Injection sites were carefully monitored and sanitized. Monkeys were injected in the morning, 4-6 hours prior to fMRI acquisition session or a training session duration, to allow the fluoxetine to fully take effect. Once animals reached stable performance on behavioral tasks during the training (more than 85% of overall fixation for detection tasks and retinotopic mapping tasks and more than 75% of overall fixation for saccadic reward competition task) and were habituated to subcutaneous injections, fMRI data collection started, still under fluoxetine injections.

5. Experimental setup

Monkeys sat in an MRI-compatible primate chair (Vanduffel et al., 2001) in sphinx position, head-fixed thanks to a surgically implanted head post. They were positioned in front of a translucent screen. Visual stimuli were retro-projected onto this translucent screen. The eye to screen distance was of 60cm and screen resolution was 1200x1900pixels with a 60Hz refresh rate. Gaze location was sampled at 1000Hz using a pupil-corneal reflection video-tracking system (EyeLink at 1000 Hz, SR-Research). Eye Movement data Acquisition Software interfaced with an in-house program for stimulus delivery and experimental control (based on Presentation©). For the detection task, monkey hand responses were produced by releasing a bar, the effect of which was to restore the continuity of an infrared optic beam. For the saccadic reward competition task, monkey had to select the choice target with an eye movement towards it.

6. MRI acquisitions parameters

In this study, in-vivo MRI scans were performed on a 3T Magnetom Prisma system (Siemens Healthineers, Erlangen, Germany).

1. Structural MRI

Monkeys were first anesthetized with an intramuscular injection of ketamine (10 mg/kg). Then, they were intubated and maintained under 1-2% of isoflurane. During the scan, animals were placed in a sphinx position in a Kopf MRI-compatible stereotaxic frame (Kopf Instruments, Tujunga, CA). Two

L11 coils were placed on each side of the skull and a L7 coil was placed on the top of it. Two T1-weighted anatomical images and one T2-weighted anatomical images were acquired for each subject using a magnetization-prepared rapid gradient-echo (MPRAGE) pulse sequence. Spatial resolution was set to 0.5 mm, with TR= 3000 ms, TE=5.38 ms, Inversion Time (TI)=1100 ms, flip angle=8°, bandwidth=130 Hz/pixel, 192 slices.

2. Functional MRI

Before each scanning session, a contrast agent, composed of monocrySTALLINE iron oxide nanoparticles, Molday ION™ (MION), was injected into the animal's saphenous vein (9-11 mg/kg) to increase the signal to noise ratio (Leite et al., 2002; Vanduffel et al., 2001). We acquired gradient-echoplanar images covering the whole brain (repetition time:2.00 s; echo time: 18 ms; 37 sagittal slices; resolution: 1.25x1.25x1.38 mm anisotropic voxels) with an eight-channel phased-array receive coil; and a saddle-shaped, radial transmit-only surface coil (MRI Coil Laboratory, Laboratory for Neuro- and Psychophysiology, Katholieke Universiteit Leuven, Leuven, Belgium, see Kolster et al. 2014). The same sequence was used for both the resting state and a set of active tasks.

7. Behavioral tasks

Animals had free access to food and were maintained under a water regulation schedule individually optimized to keep a stable motivation and performance. They were trained on four different behavioral tasks.

1. Plasticity induction schedule

On a first time point (time point 1 or T1), we trained both monkeys on an active peripheral detection task and on a retinotopic mapping task. They were then scanned at the fMRI while performing these tasks. On a second time point (time point 2 or T2) monkey learned a specific spatial reward contingency map thanks to a saccadic reward competition task. They were then scanned at the fMRI while performing the same tasks as in T1 as well as on this newly learned task. On a third time point (time point 3 or T3), monkeys were trained on a reversed spatial contingency map (relative to the vertical meridian) while receiving fluoxetine injections. Monkeys received chronic fluoxetine injection while being trained to the behavioral task, and still received it according to the same schedule during the period they were performing tasks at the MRI. They were then scanned at the MRI while performing the same tasks as in T2 (but with the reversed spatial reward contingency map relative to T2) (**Figure 1**). At each time point, fMRI resting state data (awake) were acquired prior to all other tasks.

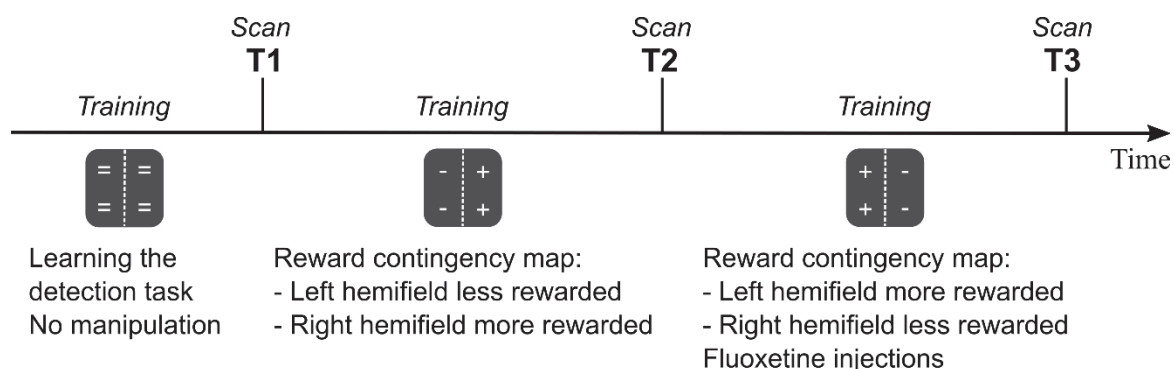


Figure 1: Experimental timeline of the three different time-points (T). T1 is the control condition and stimuli are all associated with the same amount of reward. T2 is the reward manipulation according to the hemifield condition. Here, stimuli on the left hemifield were overall associated with less reward than on T1 condition and reversely, stimuli on the right hemifield were overall associated with more reward than on T1 condition. T3 is also a reward manipulation condition where the overall amount of reward were reversed compared to the T2 condition. In addition, monkeys received chronic fluoxetine, both during the reversal learning that this condition involves and during the scanning session.

2. Training: Saccadic reward competition task

In order to investigate the possible contribution of fluoxetine to the implementation of reward biases and learning, we used a saccadic competitive task in which the targets were presented in different spatial positions (see **Figure 2, A**). Monkeys had to fixate a central cross. They had to maintain an overall 75% fixation or more during the whole acquisition. One thousand to 2000ms from fixation onset, two identical stimuli (targets) were presented. Stimuli were drawn from a virtual array of eight stimuli organized along a circle of 8° of eccentricity. Each location in this virtual array was associated with a different reward probability, thus building a reward based spatial priority map (Chelazzi et al., 2014). Possible reward probabilities were 80% (high), 50% (medium) and 20% (low), according to a fixed spatial relationship, such that the extreme reward probabilities (80% and 20%) were neighbored by intermediate reward probability targets (50%). Monkeys had to make a saccade to one of the two presented stimuli and were rewarded according to the reward probability associated with the chosen target location. Monkeys were trained for this task prior to the scanning sessions. Overall, during T2, the reward probability was higher on the right hemifield and lower on the left hemifield and was reversed for T3, with the most rewarded hemifield on the left and the least rewarded hemifield on the right (see **Figure 2, B**). In addition, for T3, there were 6 weeks of chronic injections of fluoxetine suspension prior to go to the MRI during the training period and chronic fluoxetine injections were maintained during the fMRI acquisitions. Monkeys also performed this task during fMRI acquisitions (166 volumes each) at T2 and T3, to reinforce the learning right after the resting state acquisition. This data will however not be presented in the present thesis manuscript.

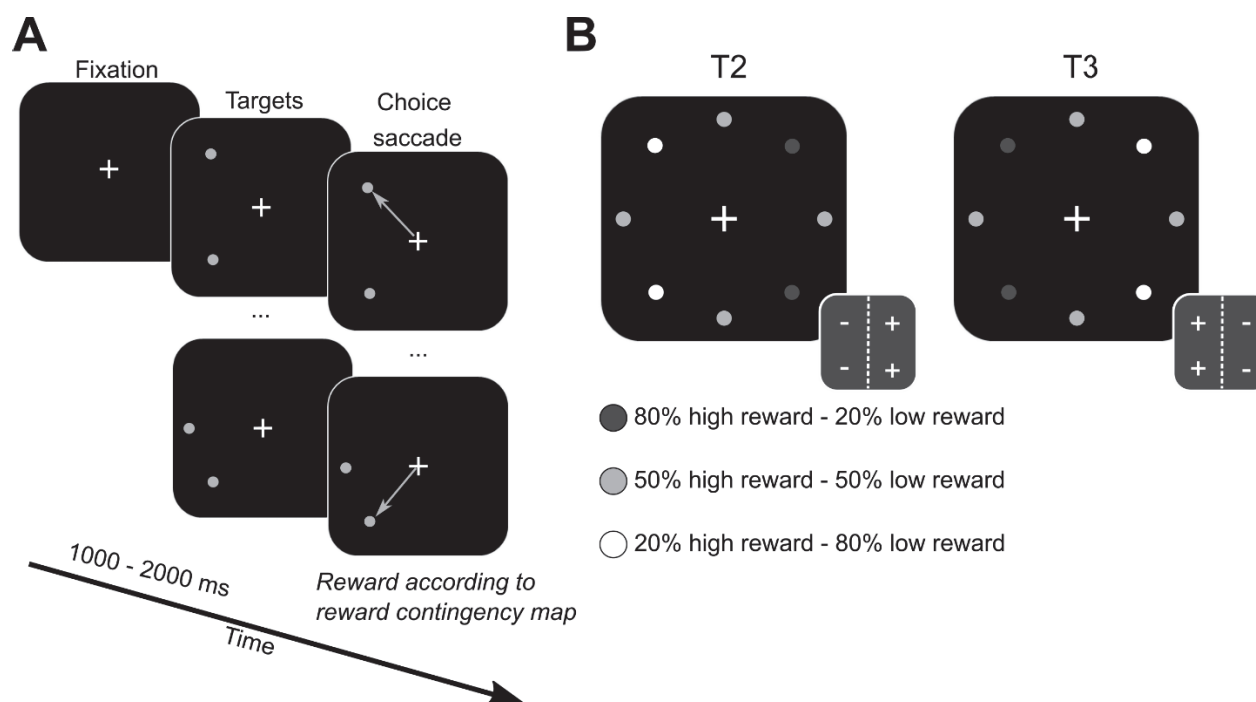


Figure 2: Saccadic choice towards targets of different reward contingencies. This task directs attention toward saliency region in the spatial map. We generate this saliency by altering the spatial priority map with statistical reward-based learning. (A) Monkeys had to fixate a central cross on a screen 60cm away from their eyes. After an interval of 1 to 2 secs, two stimuli appeared simultaneously at two different locations out of eight. All of the 8 possible target locations are organized along a virtual circle of 8° of eccentricity from the fixation cross, equidistant one from the other. Monkeys are rewarded to make a saccadic eye movement to any of the two targets. (B) Each target was associated with two possible reward quantities, but with a different probability. High-expected reward targets were associated with 80% of high reward probability and 20% of low reward probability. Low-expected reward targets were associated with 20% of high reward probability and 80% of low reward probability. Intermediate expected reward targets were associated with 50% of high reward probability and 50% of low reward probability. Reward contingencies between neighbors were kept constant as follows: 80% high reward (HR) – 50% HR – 80% HR – 50% HR – 20%HR – 50% HR – 20% HR – 50% HR. In T2 condition, 80% HR probabilities were on the right up and low positions (overall more rewarded on the right hemifield) and 20% HR were on left up and low position (overall less rewarded on the left visual hemifield). In T3 condition, 80% HR probabilities were on the left up and low positions (overall more rewarded on the left hemifield) and 20% HR were on right up and low position (overall less rewarded on the right visual hemifield). We did not evaluate the reversal learning speed.

3. MRI: Resting state

Animals sat in the scanner, in the dark with no external stimulation but the sound of the MRI. They were trained to remain still during the scanning period and no fixation was required. They had however to keep their eyes open. Each resting-state acquisition represents 240 volumes. Acquired data (T1: M1, 3360 volumes, in 14 acquisitions; M2, 3120 volumes in 13 acquisitions. T2: M1, 4560 volumes in 19 acquisitions; M2, 6480 volumes in 27 acquisitions. T3: M1, 3120 volumes in 13 acquisitions; M2, 6720 volumes in 28 acquisitions) were then sorted according to their quality. Data selection was based on amplitude of movement, time of open eyes during the scanning and individual scan SNR levels. We

selected 7 runs (highest value for M1 in T2) so we decided to work on 7 acquisitions of the best quality per time-point per monkey.

4. MRI: Retinotopic mapping

Monkeys had to fixate the central cross while stimuli were being displayed on the screen. They had to maintain an overall 85% fixation or more during the whole acquisition. These stimuli were expanding annuli rings, to measure eccentricity, ranging from 0,5 to 15° of eccentricity (**Figure 3, A**), and wedges to measure polar angles, counter clockwise. The stimuli were not overlapping. We displayed wedges in the upper and lower visual field in two distinct tasks (**Figure 3, B**). In the eccentricity task, the radial thickness for the first smaller ring displayed was 0,25° and their radial thickness expanded according to a $\log(r)$ law to approximate the human cortical magnification factor. We presented two cycles of stimuli each time for both retinotopic tasks. The stimuli were dynamic, consisting in a flickering and colorful image (Rima et al., 2020) with a homogenous spatial frequency and luminance. Each annuli task acquisition represented 118 volumes and both wedges tasks were 114 and 112 volumes length. Although here this task allowed us to determine regions of interest (ROI), we provide a more detailed discussion and analysis of its outputs in chapter 3 of this thesis manuscript.

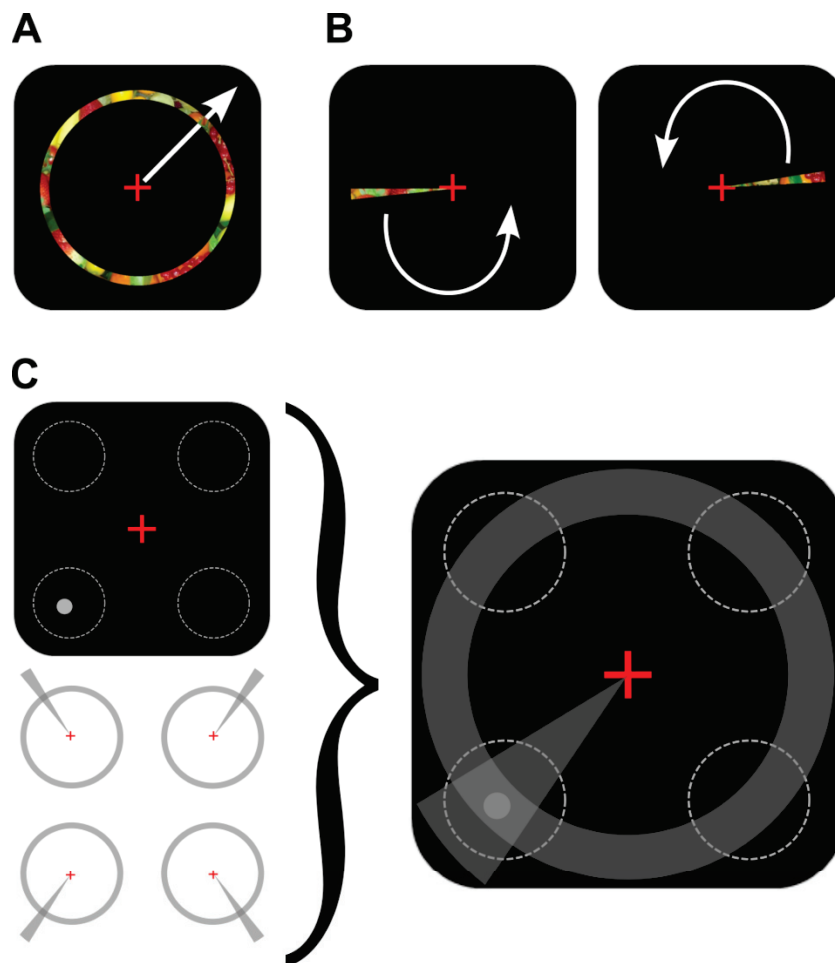


Figure 3: Retinotopic mapping and conjunction with the peripheral detection task. (A) Eccentricity mapping. Monkeys had to fixate a central cross while expanding dynamic and colorful annuli rings were displayed from 0,5° to 15° of their visual

field of view. These annuli rings were displayed for two cycles during the task. (B) Polar angles mapping. Monkeys had to fixate a central cross while counter clockwise wedges covering $0,5^\circ$ to 15° of the visual field of view from the central cross were displayed. These wedges were displayed for two cycles in two distinct tasks: the first one (left panel) covered the lower visual field of view and the second one (right panel) covered the upper visual field of view. (C) In order to determine the visual area seeds, we compared the fMRI activations in the brain in response to the stimuli in the peripheral detection task, with the conjunction of the activation to annuli rings and wedges that corresponded to the coordinates of the stimuli zones.

5. MRI: Peripheral detection task

The peripheral target detection task (here, the 4-quadrants peripheral detection task or D4 task) consists in fixating a central cross while each 1000ms to 2000ms, a target randomly appears for 200ms within a virtual 2° circle with a center placed at 8° of eccentricity from the central cross (**Figure 4, A**). They had to maintain an overall 85% fixation or more during the whole acquisition. The target can either appear in the up-right, up-left, down-right or down-left quadrant ($(6\sqrt{2}, 6\sqrt{2})$, $(-6\sqrt{2}, 6\sqrt{2})$, $(-6\sqrt{2}, -6\sqrt{2})$ or $(6\sqrt{2}, -6\sqrt{2})$, **Figure 4, B**). Monkeys were rewarded for producing a hand response at target presentation within a time window of [150ms – 1000ms]. Monkeys were trained to this task prior to be scanned until they reach 85% of correct trial of stable performances. In this task, reward was equally distributed among different target positions. Each peripheral detection task acquisition represents 166 volumes. Although this task permitted us to determine regions of interest (ROI) in the visual cortex, we provide a more detailed discussion and analysis of its outputs in chapter 3 of this thesis manuscript.

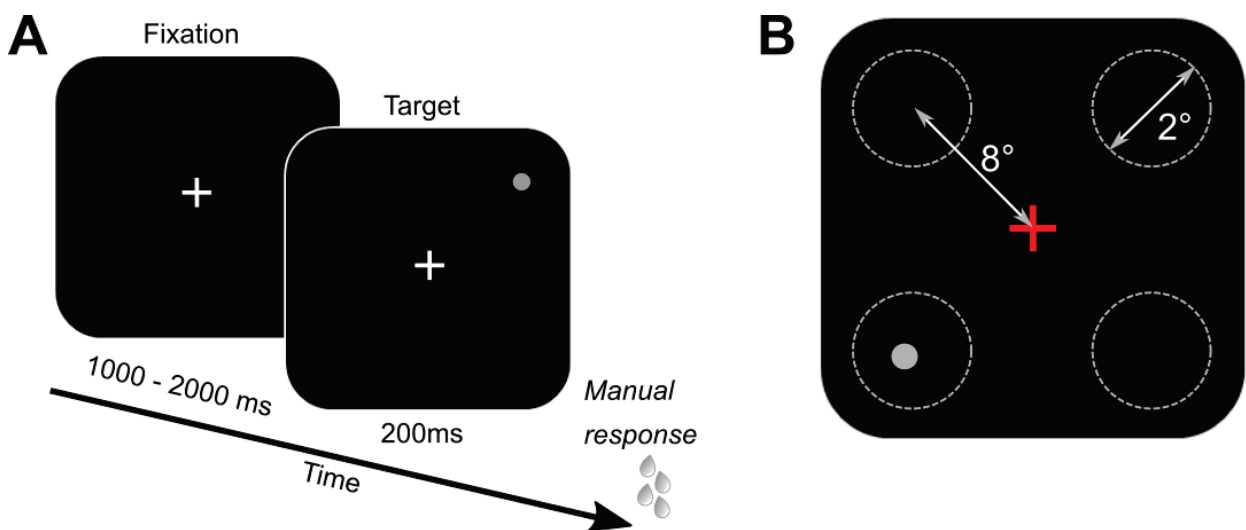


Figure 4: Peripheral detection task description. (A) Monkeys had to fixate a central cross on a screen 60cm away from their eyes. After an interval of 1 to 2 secs, a stimulus appeared in their peripheral vision. After a manual response within the response time window, they received a reward. (B) Stimuli could appear in a virtual circle of 2° of diameter, placed 8° away from the central cross, at four possible locations.

8. Preprocessing

1. Structural MRIs

Anatomical images were processed following these steps: The T1-weighted anatomical images were merged and reoriented thanks to Freesurfer. An FSL coregistration of the T2-weighted anatomical images was performed to the merged T1. On both of these images a Gaussian local low pass filter AONLM (adapted from Manjón et al., 2010) have been performed. This was followed by a normalization in the NMT space, followed by an automated brain extraction with FSL (Jenkinson et al., 2012; Smith et al., 2013), and ANTS (Avants et al., 2009) and a manual correction with ITK-SNAP (Yushkevich and Gerig, 2017) allowing to filter normed cropped brain. The segmentation of grey, white matter and CSF was then performed using a N4 bias field correction and Atropos loop. The results were back registered in the native space and hand corrected before creating surfaces with Freesurfer. Surfaces were then implemented in workbench where flat maps were have been created.

2. Functional MRIs

The five first images of functional sequences were removed to allow for signal stabilization. Functional volumes were corrected for head motion within and across sessions and slice timed. The reference slice for slice timing was the first one. They were linearly detrended, coregistered on the T2w anatomical image in its native spatial resolution with the software JIP (<http://www.nitrc.org/projects/jip>) and normalized to the template space F99 with FSL. A spatial smoothing was applied with a 3-mm FWHM Gaussian Kernel.

9. Data analysis

All analyses are implemented in Matlab® using ad-hoc scripts. Data were processed through a pipeline based on a combination of different packages: AFNI (Cox, 1996), FSL (Jenkinson et al., 2012; Smith et al., 2013), ANTS (Avants et al., 2009) and Workbench (<https://www.humanconnectome.org/software/get-connectome-workbench>). The T1-weighted and T2-weighted anatomical images were processed according to the HCP pipeline (Autio et al., 2020; Glasser et al., 2013) and were normalized into the MY19 Atlas (Donahue et al., 2016).

1. Functional connectivity network matrices

In order to have an understanding of the brain functional networks involved after training (T2) and fluoxetine administration coupled to training (T3) in comparison with the control condition (T1), we computed the functional connectivity network matrices thanks to FSLnet (<https://fsl.fmrib.ox.ac.uk/fsl/fslwiki/FSLNets>). We ran our analyses for each time point, pooling data of the seven best resting-state acquisitions of both monkeys (i.e. 14 resting states acquisitions per time point). The data we selected are the same for all the analyses we present in this chapter. We selected these data based on the combination of their signal-to-noise ratio, MION injection and head motion.

The reference atlas used was the CHARM-2, which parcellates the brain into 34 functional brain regions (17 regions per hemisphere). Once we obtained the 34x34 matrices of functional connectivity strengths between pairs of brain regions at each time point, we directly compared left and right hemispheres in T2 and T3 separately to describe training on reward effects. We also computed the difference between the brain regions in the high reward hemispheres between T2 and T3 (right hemisphere T3 – left hemisphere T2) and concomitantly for the low reward hemispheres (left hemisphere T3 – right hemisphere T2). This analysis allowed us to specifically characterize the combined effects of fluoxetine and training. We then ran a post-hoc t-test statistical analysis on the different functional connectivity matrices (T2, T3 and the differences) and only significant correlation strengths and differences are reported (for $p < 0,05$, $df=13$).

2. Region of interest (ROI) definition

We identified the four visual ROIs thanks to the retinotopic mapping using the conjunction of activations to the annuli and wedges corresponding to the location of the target locations presented in the peripheral detection task (**Figure 3, C**). The analysis of this task was performed with SPM12 (Wellcome Department of Imaging Neuroscience, London; www.fil.ion.ucl.ac.uk/spm) (Ashburner et al., 1994). Fixed effects of the Generalized Linear Model (GLM) corresponded to the different target positions in the four quadrant of the screen, i.e. left-up, right-up, left-down, right-down. Head motion and eye movements were included as covariates of no interest and we used a specific MION hemodynamic response function (HRF) to fit the modulation of the signal. This analysis was performed on both monkeys and the three different conditions (T1, T2 and T3). The ROIs selection was done taking the activation peaks of the contrast *target location vs fixation* at the statistical threshold of $p < 0.05$ corrected for multiple comparison using family-wise error (FWE) correction. We then created four 3mm diameter spheres centered around the local peak of activation in the right ventral V2, left ventral V2, right dorsal V2, left dorsal V2, respectively corresponding to a target presented in the left-up quadrant, right-up quadrant, left-down quadrant, right-down quadrant. We provide a more detailed description of these ROIs definitions in the chapter 3 of the present thesis manuscript. In addition, we defined left and right hemisphere dorso-lateral prefrontal cortex (DLPFC) ventral (DLPFCv, Brodmann area 46v) and dorsal (DLPFCd, Brodmann area 46d) seeds thanks to the D99 parcellation atlas. We created four 3mm diameter spheres that we used as seeds for the seed-to-brain analysis.

3. Resting state analysis

A seed-to brain analysis was performed for each monkey and each run of each condition (T1, T2 and T3) using each visual and DLPFC ROI as a seed thank to AFNI (Cox, 1996). We then obtain correlation maps which we compared using a group- linear mixed-effects (LME) modelling analysis (Chen et al., 2013; Song et al., 2021). We used this statistical method to determine if there was a condition effect (fixed effect) while taking into account variability assigned to the subjects and runs (random effects).

Results

At the behavioral level, we show that fluoxetine enhances reward sensitivity during visually guided decision-making (Gacoin and Ben Hamed, 2022). Our goal here is to identify the neural correlates of these behavioral observations and to characterize whether and how fluoxetine 1) modulates functional cortical connectivity patterns and 2) interferes with reward-based decision-making cortical processes. To address these questions, we first implemented a hypothesis-free approach using atlas-based ROI-to-ROI analyses of cortical functional connectivity. We then used the outcome of these analyses to perform hypotheses-driven tests, based on ROIs derived from individual subject cortical activations during visual detection tasks.

1. Fluoxetine-induced changes in cortical functional connectivity following reward-based spatial learning

We used the CHARM-2 cortical atlas (17 left and 17 right cortical regions, Jung et al., 2020) and we computed the functional connectivity between all pairs of cortical regions (both intra- and interhemispheric) at all scanning time points (T1, baseline awake resting-state; T2, awake resting-state following reward-based spatial learning; T3, awake resting-state following reward-based spatial learning with fluoxetine injections; **Figure 5**). We observe that, on T1, within hemisphere ROI-to-ROI functional connectivity matrices (FCM for short) are remarkably reproducible. This also holds true for across hemisphere maps, speaking for the quality of our data (statistical assessment will be consolidated in the final version of this work) (**Figure 5, B**). In the following, we describe several changes in functional cortical connectivity induced by either reward-based spatial learning and/or fluoxetine. It is important to note at this stage that, given our experimental protocol, we cannot describe the general cortical effects of fluoxetine on FC independently reward-based learning effects under fluoxetine.

In an independent study, (study n°1 of the present thesis manuscript: Gacoin and Ben Hamed, 2022), we show that fluoxetine improves reward selectivity. In the following, we seek to identify the neural basis of this behavioral observation and the effect of fluoxetine onto brain FC, depending on which hemifield was most rewarded (**Figure 5, C**). **Figure 5C** displays raw T2 and T3 correlation matrices (**Figure 5C**, larger maps, left and middle panels). The upper row represents FC whole brain maps for the high reward hemispheres of T2 and T3 respectively. The lower row represents FC whole brain maps for the low reward hemispheres of T2 and T3 respectively. Statistically significant FC are highlighted and smaller insets represent only significant FC (**Figure 5C**, smaller insets, left and middle panels, enlarged insets are presented in **Figure S1**). T3-T2 FC differences matrices show brain areas with statistical differences between T2 and T3 (**Figure 5C**, right panels, larger maps). Thus, a high FC in the T3-T2 differences matrix indicates that the T3 FC was significantly higher than the T2 FC in this

cortical area. Whole maps are presented as smaller insets. In the following tables, we report pairs of brain regions with significant comparisons between the significant FC and their direction.

1. Fluoxetine enhances FC within the dorsal visual pathway of the high reward hemisphere

We first describe fluoxetine enhancement of FC on reward manipulation for the high reward hemifield (**Figure 5C**, upper panel and Table 1). We report a marked enhancement of FC between T2 and T3 between the motor cortex and the somato-sensory cortex; the medial temporal lobe and the superior temporal region; the superior temporal region and the auditory cortex, as well as the floor of lateral sulcus; FC shifting significantly from a significant correlation to a yet higher FC (Table 1, dark red). We report a marked enhancement of FC between ACC and IPL under fluoxetine, FC shifting from a non-significant correlation to a positive correlation between T2 and T3 conditions (Table 1, orange). We similarly report an enhancement of FC between LPFC and middle temporal visual area (MT) and extrastriate regions, between motor cortex and IPL and SPL; as well as between the somato-sensory cortex and IPL. We report a marked enhancement of FC between T2 and T3 between somato-sensory cortex and inferior temporal cortex (IT) as well as between IT and the auditory cortex and the floor of the lateral sulcus (LS), FC shifting from a significant decorrelation to a non-significant FC (Table 1, light blue). Finally, we report a marked enhancement of FC between T2 and T3 between the motor cortex and IT, FC shifting from a significant decorrelation to a higher yet still significantly negative FC (Table 1, dark blue). Thus, half of the described FCs were not existent in T2 condition but became significant in T3 condition. Overall, we show that fluoxetine enhances FC within the dorsal visual pathway of the high reward hemisphere.

| Connectivity | ACC | | LPFC | | Motor cortex | | | | Somato-sensory | | Medial temporal | IT | | Superior temporal | |
|--------------|-------|-------|--------------|---------|--------------|-------|----------------|-------|----------------|--------------------------|-----------------|-------------|----------|-------------------|---------|
| | IPL | MT | Extra-strate | IT | IPL | SPL | Somato sensory | IT | IPL | Superior Temporal Region | Auditory | Floor of LS | Auditory | Floor of LS | |
| T2 →T3 | 0 → + | 0 → + | 0 → + | - - → - | 0 → + | 0 → + | + → +++ | - → 0 | 0 → + | + → +++ | - → 0 | 0 → 0 | - → + | 0 → +++ | 0 → +++ |

Table 1: Significant enhancement of FC between brain regions between T2 and T3 (see also Figure 7C), in the high reward hemisphere.

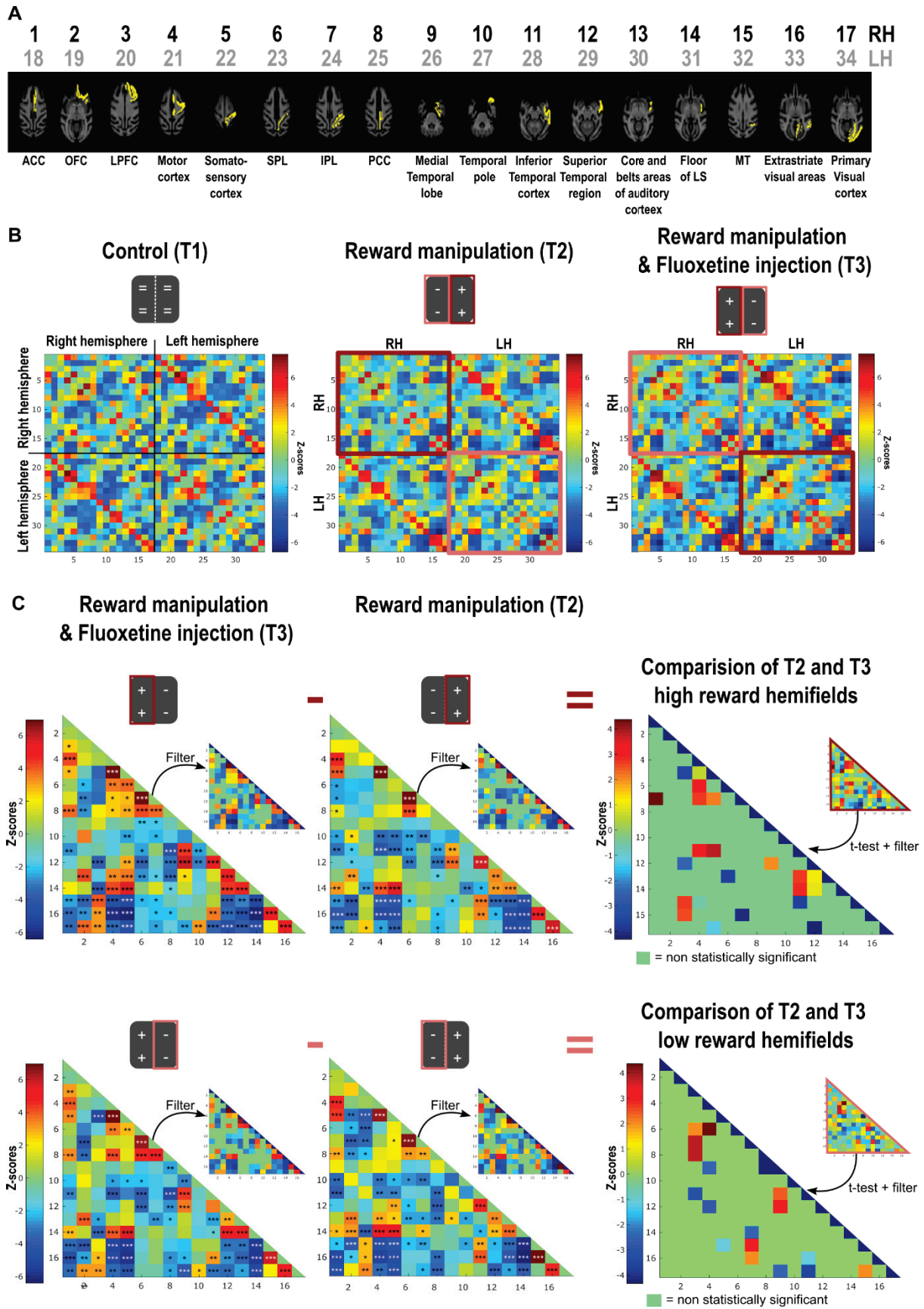


Figure 5: FSL-Net functional connectivity matrices (FCM). (A) The CHARM-2 functional atlas parcellates the cortex in 34 regions, 17 in the right hemisphere (1:17) and 17 in the left hemisphere (18:34). This panel represents the cortical location of each of these cortical regions - mapped onto the right hemisphere, for the sake of readability. (B) FCM in T1 (baseline awake

resting-state), T2 (awake resting-state following the learning of a spatial reward contingency map with higher rewards in the right visual hemifield) and T3 conditions (awake resting-state following the learning of a spatial reward contingency map with higher rewards in the left hemifield associated with fluoxetine injections). Dark red square: high reward hemifield regions (contralateral to the high reward visual hemifield); Light red square: low reward hemifield regions (contralateral to the low reward visual hemifield). Z-scores are color coded. (C) Comparison of T2 and T3 high (top row, right T2 hemisphere vs. left T3 hemisphere) and low (bottom row, left T2 hemisphere vs. right T3 hemisphere) reward hemifields. Left column represents FCM for T3. Middle column represents FCM for T2. Right column represents FCM difference between T2 and T3. In the left and middle columns, significant FC are indicated in main maps (***, $p < 0.001$; **, $p < 0.01$; * $p < 0.05$). Smaller inset maps represent only significant FC. In the right column, significant FC are indicated in smaller inset maps (***, $p < 0.001$; **, $p < 0.01$; * $p < 0.05$). Main maps represent only significant FC. Z-scores are color coded. ACC: anterior cingulate cortex; OFC: orbitofrontal cortex; LPFC: lateral prefrontal cortex; SPL: superior parietal lobule; IPL: inferior parietal cortex; PCC: posterior cingulate cortex; LS: lateral sulcus; MT: middle temporal area.

2. Fluoxetine enhances FC within the dorsal visual pathway of the low reward hemisphere

Next, we shift our focus on the enhancement effects of fluoxetine on reward manipulation in the low reward hemisphere (**Figure 5, C**, lower panel and Table 3). We report a marked enhancement of FC between medial temporal lobe and IT and the superior temporal region under fluoxetine, FC shifting from a non-significant correlation to a positive correlation between T2 and T3 conditions (Table 3, orange). We report also a marked enhancement of FC between T2 and T3 between somato-sensory cortex and inferior temporal cortex (IT) as well as between LPFC and IPL and PCC; IPL and MT and extrastriate visual areas; FC shifting from a significant decorrelation to a non-significant FC (Table 3, light blue). Finally, we report a shift between a significant decorrelation to significant correlation between T2 and T3 under fluoxetine between motor cortex and SPL (table 3). Overall, this suggests that fluoxetine enhances FC within the dorsal visual pathway of the low reward hemisphere.

| Connectivity | LPFC | | | Motor cortex | IPL | | Medial temporal | | MT |
|--------------|------|-----|-----|--------------|-----|--------------|-----------------|--------------------------|----|
| | SPL | IPL | PCC | SPL | MT | Extrastriate | IT | Superior Temporal region | V1 |
| T2 →T3 | | | | | | | | | |

Table 3: Significant enhancement of FC between brain regions between T2 and T3 (see also Figure 7C), in the low reward hemisphere.

3. Fluoxetine decorrelates FC between prefrontal and parietal areas and striate and extrastriate cortex in the low reward hemisphere

We now describe fluoxetine depression of FC on reward manipulation for the low reward hemifield (**Figure 5C**, upper panel and Table 4). We report a marked depression of FC between T2 and

T3 between LPFC and IT; Motor cortex and superior temporal region, and also medial temporal lobe; PCC and medial temporal lobe; IT and V1, FC shifting from a non-significant to a significant decorrelation FC (Table 4, light blue). We additionally report a marked depression of FC between T2 and T3 between IPL and floor of LS; medial temporal lobe and V1; FC shifting from a significant decorrelation to a higher yet still significantly negative FC (Table 4, dark blue). Thus, half of the described FCs were not existent in T2 condition but became significant in T3 condition. Finally, we report a decreased correlation between T2 and T3 condition between IT and extrastriate visual areas, FC shifting from a significant correlation to a lower yet still significantly positive FC (Table 4, red). Overall, fluoxetine decorrelates FC between prefrontal and parietal areas and striate and extrastriate cortex in the low reward hemisphere.

| Connectivity | LPFC | Motor Cortex | | IPL | PCC | Medial temporal | IT | |
|--------------|----------|-------------------|-----------------|-------------|----------------------|-----------------|----------|--------------|
| | IT | Superior temporal | Medial temporal | Floor of LS | Medial Temporal lobe | V1 | V1 | Extrastriate |
| T2 →T3 | 0 ↓ - | 0 ↓ - | 0 ↓ - | - ↓ - | 0 ↓ - | - ↓ - | 0 ↓ - | +++ ↓ + |

Table 4: Significant depression of FC between brain regions between T2 and T3 (see also Figure 7C), in the low reward hemisphere.

4. Fluoxetine enhances motor cortex interhemispheric functional connectivity

Acute fluoxetine intake modulates cerebral motor activity (Capitão et al., 2020; Loubinoux et al., 1999) and is also involved in motor recovery mechanisms after a stroke in patients being rehabilitated (Chollet et al., 2011; Dam et al., 1996). In a mouse model, fluoxetine intake can maintain the level of responsiveness to motor training after a stroke by reducing inhibitory interneuron expression in the premotor cortex (Ng et al., 2015). Accordingly, we here report a strong inter-hemispheric connectivity between the motor (4, 21) and the somatosensory cortex (5, 22) at all time points (**Figure 5, B**), but more so in T3 where the FC increases significantly between these two regions in the high reward hemisphere ($p < 0.05$, see Table 1). This enhanced functional connectivity in the motor network (Biswal et al., 1995) under fluoxetine supports our observation for faster reactions times in a standard visual detection task under fluoxetine (Gacoin and Ben Hamed, 2022, luminance threshold task, and see also Chapter 3).

In the following, we will focus on more specific visual striate and prefrontal areas.

2. Effects of fluoxetine and reward-based learning on cortical FC

The hypothesis free analysis described above points towards changes in functional connectivity between the striate cortex and parietal and prefrontal areas under fluoxetine in the context of reward-based learning. Due to our longitudinal task design, we were in a position to specifically identify 4 seeds in the occipital cortex (using the D4 task, see chapter 3), corresponding to cortical regions encoding 4 positions of the visual field, two of which were associated to higher reward probabilities prior to the resting state scanning and two to lower reward probabilities (organized along a left/right schema). These task-based seeds are all reliably located in area V2 (as defined by independent retinotopic mapping at each time-point) at a spatial eccentricity matching the D4 task quadrants (as confirmed by independent retinotopic mapping at each time-point). We used each of these 4 seeds to ran an LME seed-to-whole brain analyses across both monkeys. This method allows to evaluate the fixed condition effect (time-points) on the seed to brain connectivity for the visual seeds extracted from the active D4 task performed by the monkeys in the scanner (chapter 3), irrespective of other sources of variability such as inter-individual or intra-individual run variability. In the following, we first validate the FC of these seeds at the control time-point (T1) then we report the changes in FC due to reward-based learning behavioral training (T2), and finally, we report the changes in FC due to reward-based learning behavioral training under fluoxetine (T3). Due to the observed FC spatial maps, we report on dorsal and ventral visual V2 seeds, respectively activated by the low and upper visual fields, separately. All delineation of visual areas V1, V2, V3 presented here where obtained thanks to retinotopy mappings performed on each of the two macaques at T1, T2 and T3 (see chapter 3). Both global fixed effects (GFX) of right and left V2 dorsal seeds are significant (Left: GFX, χ^2 , $p=0,025$; Right: GFX, χ^2 , $p=0,049$). Only the GFX of right V2 ventral seed is significant (Left: GFX, χ^2 $p=0,230$; Right: GFX, χ^2 $p=0,030$). This is due to an unexpected functional activations in D4, in V2v left of Monkey 2.

1. Seed-to-brain in the visual cortex: control (T1)

We first focus on the left hemisphere. In the control condition (**Figure 6A, left panel**), the V2 dorsal (V2d) seed (FX, χ^2 , T1: $p<0,001$) shows significant FC with striate and extrastriate areas, as well with the other seeds locations on both left and right hemisphere (see green dots on the figure). The FC of this V2d seed is strongest with its homolog right V2d seed. On both hemispheres, we report significant FC with visual areas V3d and V6. On the left hemisphere, this seed has significant FC with the visual area V4, the lateral intraparietal sulcus (IPS) and the dorsal part of the dorso-lateral prefrontal cortex (DLPFC, bilaterally). The right V2d seed in the control condition (FX, χ^2 , T1: $p<0,001$), has a cortical FC map very similar to that of the left V2d. Indeed, the strongest connectivity of the right V2d seed in the control condition (**Figure 6A, right panel**) is also towards the contralateral V2d seed. This right V2d seed also has a significant FC with the ipsilateral V2v seed but not with the contralateral one (see green dots on the figure). Strikingly, the rest of the spatial functional connectivity map is very similar to the left V2d seed map. Indeed, the right V2d seed also correlates with ipsilateral and

contralateral V3d, as well as with contralateral IPS. We also report an ipsilateral connectivity with the prefrontal cortex, in dorsal part of the DLPFC. The left ventral V2 (V2v) seed, has significant FC with the V2d seed location ipsilaterally (**Figure 7A, left panel**; FX, χ^2 , T1: $p < 0,001$), but not with the right hemisphere seed positions. We report ipsilateral FC with V2, V3 and V4 areas but not with the DLPFC as we saw with the dorsal seed. The right V2v seed (**Figure 7A, right panel**; FX, χ^2 , T1: $p < 0,001$) has significant FC with the three other V2 seeds regions, with the DLPFC, and extrastriate visual regions on both hemispheres, very analogous to what we observe for the ipsilateral V2d seed connectivity. Thus, left V2v seed singles out casting doubt on our reported results on this seed. Overall, and except for the V2v left seed, we here described the expected connectivity for both V2d seeds in a control condition (Smith et al., 2009).

2. Seed-to-brain in the visual cortex: effect of training (T2)

Here, we present the functional connectivity maps of the visual seeds after manipulating the reward associated with 8 possible spatial target stimuli (T2 condition). In T2, on average, the right visual hemifield was more rewarded and the left visual hemifield was less rewarded than control condition.

The left V2d seed in the T2 condition (**Figure 6B, left panel**) significantly correlates with the other V2 seeds (see green dots on the figure, FX, χ^2 , T2: $p < 0,001$). It also correlates on both hemispheres with the middle temporal region (MT), V2 and the DLPFC. We also note that this seed has enhanced FC ipsilaterally with the lateral intraparietal sulcus (LIP). At first glance, we report the same FC as with left V2d, as compared to the right V2d seed (**Figure 6, B, right panel**; FX, χ^2 , T2: $p < 0,001$). The V2v seed correlation maps present analogous connectivity with the rest of the brain (FX, χ^2 , T2: $p < 0,001$) as the two dorsal seeds. The left V2v seed (rewarded seed, **Figure 7, B, left panel**) correlates with both V2d seeds, as well as with ipsilateral V2, V3d, IPS, MT and DLPFC. Interestingly, right V2v seed (**Figure 7, B, right panel**; FX, χ^2 , T2: $p < 0,001$) has significant FC with these same regions as well as with ipsilateral V1, IPS and DLPFC.

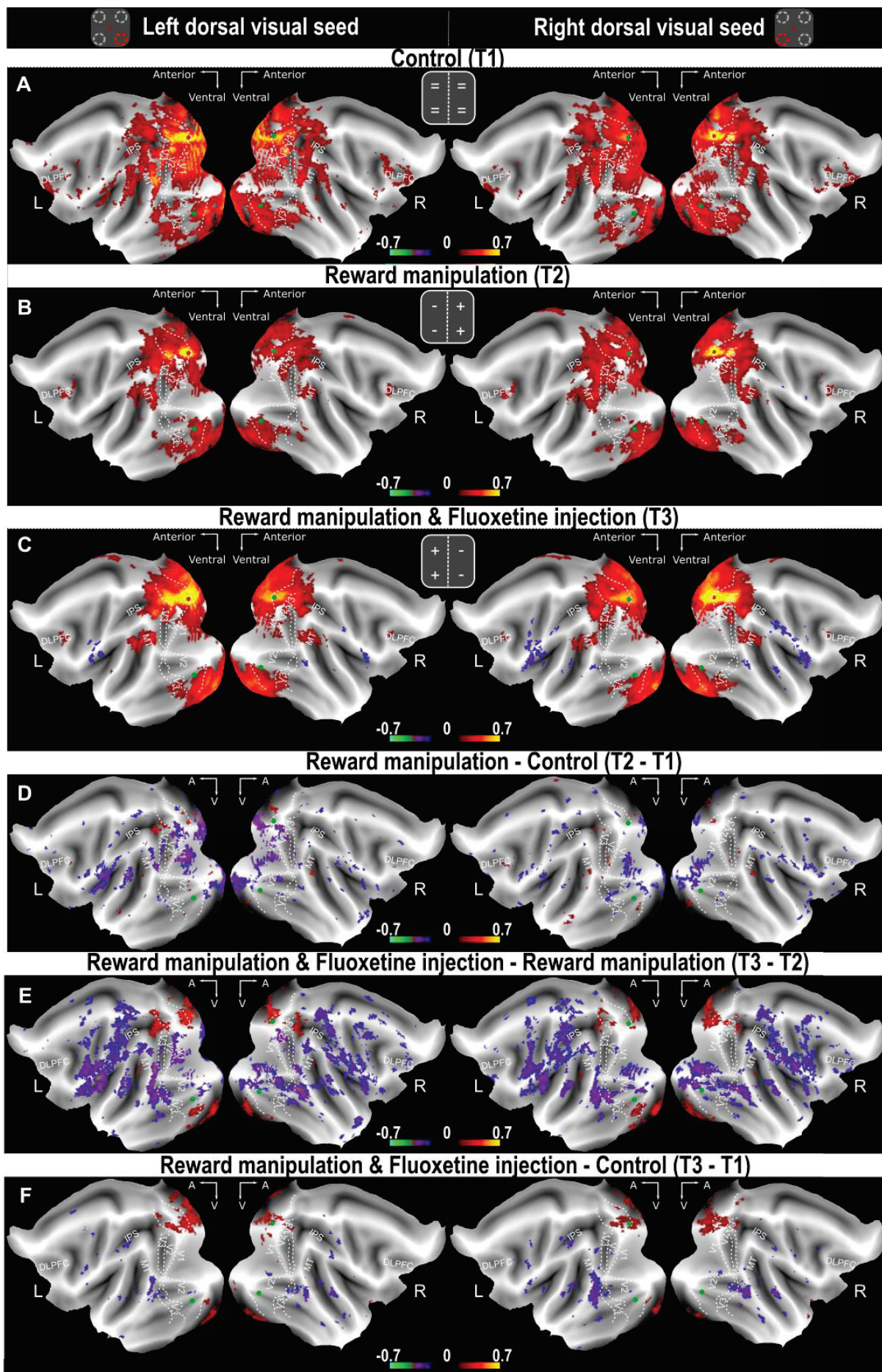


Figure 6: Flat maps of seed to brain connectivity for left and right hemispheres seeds in dorsal V2. Group cortical functional connectivity spatial maps for the left and right dorsal V2 seeds (in red). Other V2 seeds are represented in green, visual areas V1, V2 and V3 are outlined and the intra-parietal sulcus (IPS), the middle temporal region (MT) and the dorso-lateral prefrontal region (DLPFC) are labelled. All the presented flat maps are coregistered in the Yerkes functional atlas space. (A) Dorsal V2 seed to brain connectivity (left V2 seed, left panel; right V2 seed, right panel) for the control condition (T1). (B) Dorsal V2 seed to brain connectivity (left V2 seed, left panel; right V2 seed, right panel) for the reward manipulation condition (T2). Monkey's behavior and perception was biased by the learning of a specific spatial reward contingency map. In this condition, the most overall rewarded hemifield was the right one and the less overall rewarded hemifield was the left one. (C) Dorsal V2 seed to brain connectivity (left V2 seed, left panel; right V2 seed, right panel) for the reward manipulation associated to fluoxetine injection condition (T3). Monkey's behavior and perception was biased by the learning of a specific spatial reward contingency map while they were administered with chronic fluoxetine. In this condition, the most overall rewarded hemifield was the left one and the less overall rewarded hemifield was the right one. (D) Difference of T2 and T1 seed to brain connectivity maps. On the differential connectivity maps, red-yellow shades indicate a higher connectivity for T2 compared to T1 and purple-blue shades mean a lower connectivity for T2 compared to T1. (E) Differences of T3 and T2 seed to brain connectivity maps. (F) Differences of T3 and T1 seed to brain connectivity maps. The presented maps are Z-scores. Z-score levels are indicated by color scales.

We report few differences for the V2v seeds when comparing control and training conditions (**Figure 7D**; Left: FX, χ^2 , T2-T1: $p = 0.001$; Right: FX, χ^2 , T2-T1: $p = 0.024$). However, when looking at the differential connectivity maps for the dorsal seeds (**Figure 6D**), we first note a stronger and wider difference between T2 and T1 condition for the left seed (**left panel**, FX, χ^2 , T2-T1: $p < 0,001$) than with the right seed (**right panel**, T2-T1: $p < 0,001$). Indeed, the connectivity is stronger in T2 condition than in T1, from the left V2 seed toward V1, V3a, ventral visual area V4 and temporal brain regions. This connectivity difference between seeds of both hemispheres may reflect the training effect.

3. Seed-to-brain in the visual cortex: effect of pharmacology (T3)

T3 allows to quantify the combined effects of fluoxetine administration and of reward-based training with a reversed association of rewards as a function of the hemifields. Thus, the right hemifield is less rewarding than it was in T1 while the left hemifield is more rewarding than in T1.

The left V2d seed (**Figure 6C, left panel**) still correlates with the right V2d seed, but hardly with V2v seeds (see green dots on the figure, FX, χ^2 , T3: $p < 0,001$). While there is an increased connectivity strength for striate and V2 areas, there is also a refinement of projections, toward MT and the DLPFC. We report the same observations for the right V2d seed, except that it does not correlate anymore to the left V2v seed region (**Figure 6C, right panel**), with decorrelations toward temporal areas as well (FX, χ^2 , $p < 0,001$). Likewise, left V2v seed (**Figure 7C, left panel**; FX, χ^2 , T3: $p < 0,001$) does not functionally connects anymore to V2d seeds, while the right V2v is only connected to its homolog ipsilateral V2d seed (**Figure 7, C, right panel**; Right: FX, χ^2 , T3: $p < 0,001$).

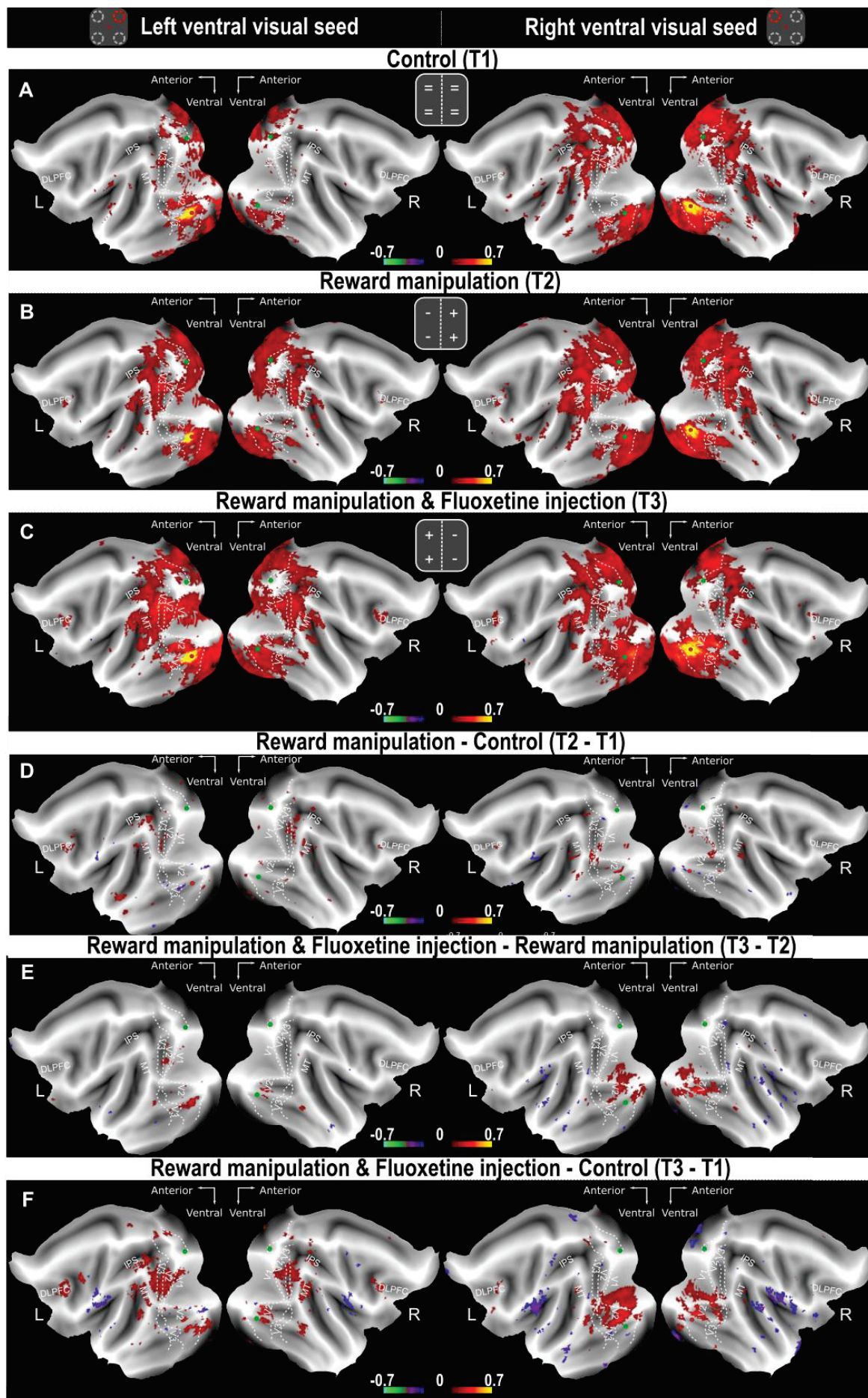


Figure 7: Flat maps of seed to brain connectivity for left and right hemispheres seeds in ventral V2. Group cortical functional connectivity spatial maps for the left and right ventral V2 seeds (in red). Other V2 seeds are represented in green, visual areas V1, V2 and V3, the intra-parietal sulcus (IPS), the middle temporal region (MT) and the dorso-lateral prefrontal region (DLPFC). (A) Ventral V2 seed to brain connectivity (left V2 seed, left panel; right V2 seed, right panel) for the control condition (T1). (B) Ventral V2 seed to brain connectivity (left V2 seed, left panel; right V2 seed, right panel) for the reward manipulation condition (T2). (C) Ventral V2 seed to brain connectivity (left V2 seed, left panel; right V2 seed, right panel) for the reward manipulation associated to fluoxetine injection condition (T3). (D) Difference of T2 and T1 seed to brain connectivity maps. (E) Differences of T3 and T2 seed to brain connectivity maps. (F) Differences of T3 and T1 seed to brain connectivity maps.

On the differential connectivity maps for V2d seeds between T3 and T2 conditions (characterizing the net effect of fluoxetine in the context of reward processing in occipital cortex, **Figure 6E**; Left: T3-T2: FX, χ^2 , $p=0,002$; Right: FX, χ^2 , T3-T2: $p=0,002$), we report little differences between V2d seeds differential connectivity. The T2 condition connectivity for dorsal seeds were overall stronger than in T3. On the contrary, for V2v seeds (**Figure 7E**), the connectivity was stronger in T3 than in T2 condition. Indeed, for left V2v (FX, χ^2 , T3-T2: $p=0,020$), we note a stronger T3 connectivity than T2 for parietal and prefrontal regions, whereas this strong connectivity for right V2v seed (FX, χ^2 , T3-T2: $p<0,001$) is more localized in ventral visual areas.

Comparisons of connectivity maps for V2d seeds between T3 and the control condition T1 (characterizing the effect of fluoxetine on reward processing in occipital cortex **Figure 6, F**) show once again few differences. Indeed, for the left V2d (FX, χ^2 , T3-T1: $p<0,001$) and the right V2d (FX, χ^2 , T3-T1: $p<0,001$), we report stronger connectivity in T1 condition than in T3 condition in dorsal V1. Similarly, there is a stronger connectivity toward V1 ventral area too in T3 condition compared to the control condition when we look at the V2v seeds connectivity (**Figure 7F**; Left: FX, χ^2 , T3-T1 : $p<0,001$; Right: FX, χ^2 , T3-T1 : $p<0,001$).

Overall, we show that FC striate cortex connectivity is mostly affected by reward and only marginally affected by fluoxetine. This finding is quite unexpected. In the following, we thus hypothesize that behavioral observation of fluoxetine effects in the context of reward-based learning are driven by top-down cortical effects differentially affected the dorsal and ventral cortical visual pathways.

3. Ventral & dorsal pathways comparison: effect of the reward

In order to probe whether and how fluoxetine impacts top-down control from the DLPFC during reward-based learning, we defined a dorsal (dark blue) and a ventral (light blue) DLPFC seed (respectively the DLPFCd and DLPFCv seeds) thanks to the D99 macaque atlas. We present ventral and dorsal DLPFC seeds FC with the rest of the brain (contours, **Figure 8**; DLPFCd, left: RDX, χ^2 , $p=0,610$; DLPFCd, right: RDX, χ^2 , $p=0,086$; DLPFCv, left: RDX, χ^2 , $p=0,357$; DLPFCv, right: RDX, χ^2 , $p=0,999$). The global fixed effect of conditions was not significant. As the T3 connectivity is close

to the T1 for the right DLPFC and as the left hemisphere present common spatial patterns in at least two out of the three conditions these results are not that surprising.

1. Seed-to-brain in the DLPFCv & DLPFCd: control (T1)

In the control condition (**Figure S2A**; DLPFCd, left : FDX, χ^2 , T1: $p < 0,001$; DLPFCd, right : FDX, χ^2 , T1: $p < 0,001$; DLPFCv, left : FDX, χ^2 , T1: $p < 0,001$; DLPFCv, right : FDX, χ^2 , T1: $p < 0,001$), we report that the DLPFCd seed from both hemisphere has, as expected, marked FC with the dorsal visual pathway, thus with IPS, MT and early visual areas. In contrast, and in agreement with previous literature, DLPFCv seeds have marked FC with the ventral visual pathway, including the temporal lobe and the ventral early visual areas.

2. Seed-to-brain in the DLPFCv & DLPFCd: effect of training (T2)

For the T2 condition (**Figure 8B**), in which the right hemifield is more rewarding compared to T1 condition, we observe that, for the left seeds, both DLPFCd and DLPFCv have significant FC with the dorsal visual pathway areas (**Figure 8A, left panel**; DLPFCd, left: FDX, χ^2 , T2: $p < 0,001$; DLPFCv, left: FDX, χ^2 , T2: $p < 0,001$), including the premotor cortex, LIP in the IPS, MT and lower visual cortical areas. However, when we look at the connectivity of DLPFC seeds for the right hemisphere, which is here less rewarding than in T1 condition (**Figure 8A, right panel**; DLPFCd, right: FDX, χ^2 , T2: $p < 0,001$; DLPFCv, right: FDX, χ^2 , T2: $p < 0,001$), we observe the same connectivity pattern for the DLPFCd as in T1, on both hemispheres, but no correlation at all with the DLPFCv seed. This shift of prefrontal FC in favor of the dorsal visual pathway due to reward-based learning confirms our observations that the V2 seeds are mostly correlated with dorsal visual pathway seeds.

3. Seed-to-brain in the DLPFCd & DLPFCv: effect of pharmacology (T3)

In the T3 condition, we here again observe that the DLPFCd seed of the left hemisphere (**Figure 8C**; DLPFCd, left: FDX, χ^2 , T3: $p < 0,001$; DLPFCv, left: FDX, χ^2 , T3: $p < 0,001$; DLPFCd, right: FDX, χ^2 , T3: $p < 0,001$; DLPFCv, right: FDX, χ^2 , T3: $p < 0,001$), which corresponds to the most rewarded hemisphere compared to T1, correlates with both IPS, MT and dorsal visual areas. However, the DLPFCv seeds correlate with this pathway only contralaterally, hence, with the hemisphere which corresponds to the most rewarded hemifield. In addition, the right DLPFCv connects to the ventral visual pathway (e.g. V4, LS, bilaterally) and to the contralateral DLPFC, while the right DLPFCd seed connects with V1 areas. This result is highly contrasting with our observation on the T1 and T2 condition.

Overall, we thus observe that reward-based learning decreases FC of DLPFCv with the rest of the brain, while at the same time, it enhanced FC of DLPFCd to the dorsal visual pathway. Specifically, a lateralized reward bias enhances DLPFCd connectivity to visual cortex ipsilaterally and more so in the rewarded hemisphere. This effect is further potentiated by fluoxetine. In the following, we focus on this lateralization reward-induced bias in FC.

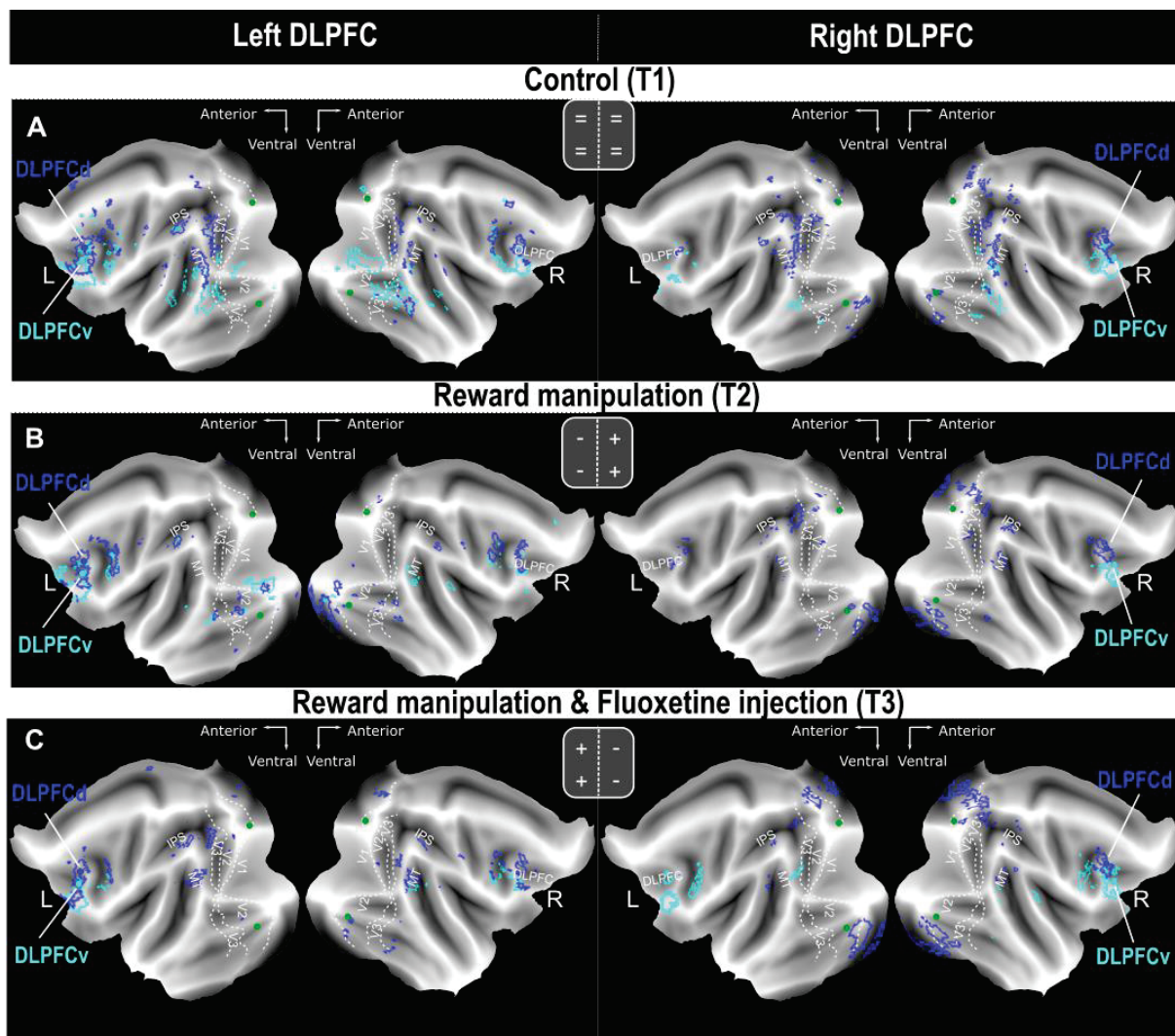


Figure 8: Flat maps of seed to brain connectivity for ventral and dorsal DLPFC seeds in both hemispheres. The dorsal DLPFC (DLPFCd) seed connectivity with the rest of the brain is represented in dark blue. The ventral DLPFC (DLPFCv) seed connectivity with the rest of the brain is in light blue. Seed to brain connectivity of DLPFCd and DLPFCv for both hemispheres (A) in the control condition (T1); (B) in the reward manipulation condition (T2); (C) in the reward manipulation associated to fluoxetine injection condition (T3).

4. Lateralization reward-induced bias in FC in the dorsal visual pathway

We here compare the connectivity of left and right DLPFCd seeds with the rest of the brain.

1. Seed-to-brain in the DLPFCd: control (T1)

In the control condition T1 (**Figure S2A**), we first observe very similar FC of DLPFC to the rest of the brain for both seeds, bilaterally. Indeed, both right and left DLPFCd seeds project to the contralateral seed. On the left hemisphere, they both have enhanced FC with V3 and V4 area. Interestingly, they also both have enhanced FC with IPS, the left DLPFCd FC being slightly more anterior than the right DLPFCd one. In the left hemisphere, both seeds have enhanced FC with V3 and V4 area,

as well as FEF. This largely corresponds to the expected FC of DLPFCd with the parietal and extrastriate cortex.

2. Seed-to-brain in the DLPFCd: effect of training (T2)

In the T2 condition (**Figure S2, B**), we here again observe that the DLPFCd seeds are functionally connected to each other with a higher strength from the left seed. In addition, the left DLPFCd correlates most with prefrontal areas such as FEF and parietal areas such as LIP on both hemispheres. In contrast, the right DLPFCd which hemispheres corresponds to the less rewarded hemifield in this condition, connects more with posterior areas such as V3, V2 and V1. We thus note here that the training and the reward contingency associated to each hemifield/hemisphere results in an asymmetric functional connectivity of the DLPFC with the rest of the brain.

3. Seed-to-brain in the DLPFCd: effect of pharmacology (T3)

The latter effect is found to be strengthened in the T3 condition (**Figure S2C**). Indeed, while the right DLPFCd still functionally correlates with the left hemisphere DLPFC, the reciprocal is not true anymore. Furthermore, while it still projects toward MT ipsilaterally and to early visual areas on both hemispheres, the left DLPFCd has no connectivity with the prefrontal areas on the right hemisphere. As a result, while reproducing the observations of T2, we show that fluoxetine results in an enhancement of the asymmetric of functional connectivity of the DLPFC with the rest of the brain under reward-based learning.

Discussion

Using atlas-based ROI to ROI connectivity analyses, we show that fluoxetine increases local connectivity in temporal regions, while inhibiting its connectivity with prefrontal and visual areas. Moreover, we also characterize a dorso-ventral decoupling between brain regions under fluoxetine. When investigating specifically the reward effect (low or high) according to hemifields, we note that a low reward income coupled with the SSRI leads to an inhibition of the ventral pathway connectivity and a less connected dorsal pathway. The ventral stream is responsible for object identification while the dorsal stream is essential for spatial location (Mishkin and Ungerleider, 1982; Ungerleider and Haxby, 1994; Goodale and Westwood, 2004; Ungerleider and Pessoa, 2008). We thus here hypothesize that when under-rewarded, fluoxetine amplifies the inhibition of the object identity to optimize the decision-making process, while still keeping track of the object position in order to target the most relevant position.

Looking closer at the specific seed-to-brain connectivity of visual areas and of both ventral and dorsal DLPFC, involved in decision-making process, we further support this hypothesis. Indeed, the results highlight that fluoxetine intake coupled with priority map learning can refine occipito-frontal connectivity. While the occipito-frontal connectivity is strengthened when the subjects are over-rewarded, we also observe a decrease of DLPFCv connectivity in the hemisphere coding for the low

rewarding stimuli. Thus, we here observe a re-allocation of the top-down pathway FC in the over rewarded hemifield, and an increase in the intra-prefrontal and inter-hemispheric connectivity, possibly permitting to optimize the choices to the task, to increase perceptual learning and enhance visual plasticity.

1. Coupled effects of fluoxetine and reward output on general brain connectivity

Overall, we report more significant correlations between brain regions for the most rewarding hemifield in fluoxetine condition. We note that the coupled effect of training and fluoxetine creates a positive correlation between LPFC and visual areas, while the same prefrontal region presents a reinforced decorrelation with temporal regions (**Figure 9**). This finding is associated with an increased correlation within temporal regions, which also decorrelates with visual areas.

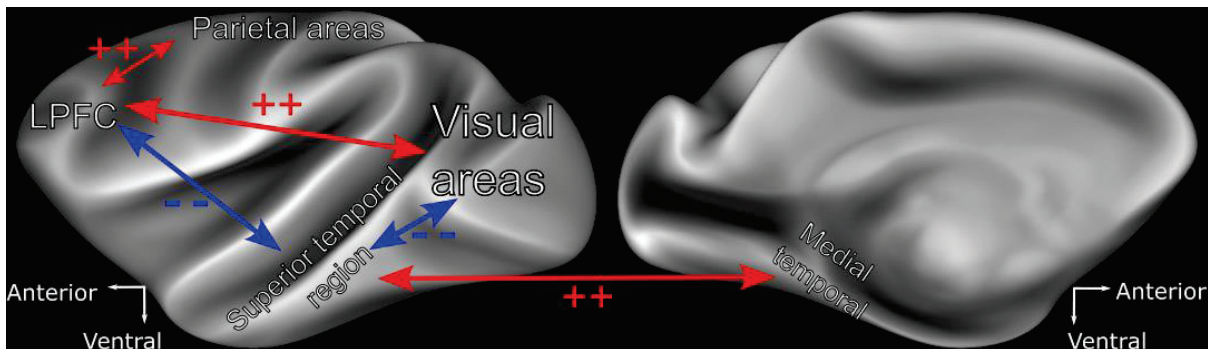


Figure 9: Representation of fluoxetine effect on FC strengths between brain regions in the context of a high reward (here associated with left hemisphere). Blue arrows represent an accentuation of negative correlation and red arrows positive difference of correlation between T2 and T3.

In the least rewarded hemifields, we note that fluoxetine increased the connectivity between LPFC and parietal regions, while the later, and specifically IPL increased its connectivity with visual areas. MT and V1 also decreased their reciprocal decorrelation (**Figure 10**). As observed for the most rewarded hemifields, temporal regions connectivity with each other was also strengthened. This effect could be accounted to be solely caused by fluoxetine and not by the specific training. Likewise, IT has a decreased connectivity with LPFC and visual areas. So does medial temporal lobe with V1 and PCC.

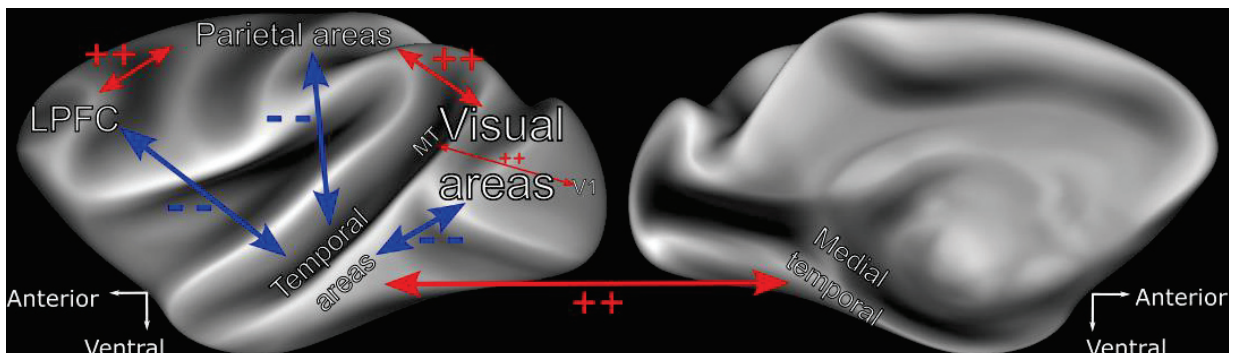


Figure 10: Representation of fluoxetine effect on correlations directions between brain regions in the context of a low reward (here associated with left hemisphere). Blue arrows represent negative difference of correlation and red arrows positive difference of correlation between T2 and T3. Thick red arrows represent an increase of positive connectivity while thin red arrow represent a decrease of negative connectivity.

We first report that regardless of the stimuli value, fluoxetine associated with training on a perceptual task in the present of spatial reward biases reinforce temporal regions connectivity with themselves, while decoupling their interactions with visual and prefrontal areas. We thus here observe a dorso-ventral decoupling, most pronounced in the low rewarded hemisphere. In this case, there was a decorrelation between the temporal region and parietal areas.

Furthermore, we show that there is a specific antero-posterior synchronization in the high rewarded condition (from none to connectivity from V2 to MT et LPFC, **Figure 5**), illustrated by a higher connectivity between the LPFC and visual areas whereas in low reward condition the control from the prefrontal areas passes through parietal areas and we observe an increased visual areas connectivity with itself (V1 and MT). We thus hypothesize that the specific effect of fluoxetine is an increased perceptual learning by creating a positive connectivity between prefrontal region and extrastriate visual areas and MT, leading to a specific and direct selection of the visual bottom up pathway associated with high reward, and a decoupling of these early and late cortical regions from parietal functions.

2. The reward saliency establishes correlations between visual areas

The present study shows the neural correlates of an altered spatial priority map in T2 condition, controlled by a reward-based learning task that orients spatial attention (Itti et al., 1998; Fecteau and Munoz, 2006). Two targets of different reward value probabilities competed (Chelazzi et al., 2014). Contrary to studies that associated a stimulus feature with a reward value (Libera and Chelazzi, 2006; Della Libera and Chelazzi, 2009; Raymond and O'Brien, 2009; Rutherford et al., 2010; for review, see Anderson, 2016), we here worked with stimuli that were strictly identically in appearance and duration. The only criterion that differentiates one stimulus from another in the present study is its spatial location. Thus, the effects of the reward manipulation observed here are specifically associated with spatial locations. This paradigm allowed us to manipulate hemifields according to the overall value of the reward probability. Moreover, it has been shown that reinforced spatial priority map learning allows a discrete, precise and long-lasting alteration of the attentional priority map (Chelazzi et al., 2014, 2013). Accordingly, we focused on the four occipital brain areas activated by the specific display of the manipulated spatial locations, which are found to be in V2.

At control condition, we first observe that one V2 seed, the left ventral one, is less correlated to the three others and conversely. Seeds were placed according to activation locations in V2 for both monkeys in response to peripheral detection task. In T1 condition, activations were at the same location

for both monkeys, except for the V2 left ventral one, where one of the monkey presents a slightly more ventral activation than was the other. We thus hypothesize that the observed decreased connectivity toward the other three seeds is driven by an inter-individual variability. However, in the T2 condition, we observe a rewiring of this particular seed with the three others. This could be accounted for by training. Indeed, this hemisphere coded here for the most rewarded hemifield. As the visuospatial selective attention induced in the spatial priority map task refers to the cognitive process, it permits to focus on a specific part of the visual field, in order to prioritize relevant information while ignoring the irrelevant ones (Itti and Koch, 2001). Moreover, by looking at the dorsal V2 seeds to brain connectivity differences between T2 and T1 conditions, we note a particularly stringent temporo-occipital decorrelation induced by the training, in the most rewarded hemisphere. However, when we consider these differences for the ventral V2 seeds, the effect is different. Here, the V2 seeds located in the most rewarded hemisphere in T2 condition has higher FC with IPS, FEF and to posterior DLPFC regions in comparison with T1 condition. In humans, the latter region is well known to support action selection based on sensory input (Koechlin et al., 2003). This strong ipsilateral correlation testifies here of the influence of training. In addition, the DLPFC systematically correlated with V2 seeds on both hemispheres for T2 and T3 conditions. We here observed that plastic changes occurred ipsilaterally in the brain, in agreement with the different spatial representations and attentional valences. To take a closer look at this ventro-dorsal difference, we further investigated the DLPFC connectivity using both DLPFCd and DLPFCv seeds.

3. Inhibition of the ventral pathway when under-rewarded

In the control condition, on both hemispheres, DLPFCd and DLPFCv respectively correlate with dorsal and ventral pathways described in the literature in the basal state (Jung et al., 2022). When focusing particularly on the connectivity maps corresponding to the overall most rewarded hemisphere we see a modification of this pattern. Indeed, both left DLPFCd and DLPFCv seeds share a connectivity with FEF and IPS, both involved in eye movement, and in visual attention control, and ventral striate and extrastriate areas. Since this pattern is reproduced contralaterally mostly from the DLPFCd seed, we here hypothesize that the reward training induces a connectivity reinforcement in favor of the dorsal pathway which is associated with object spatial location (Mishkin and Ungerleider, 1982; Goodale and Milner, 1992; Ungerleider and Haxby, 1994; Goodale and Westwood, 2004; Ungerleider and Pessoa, 2008). More strikingly, when observing the seed to brain connectivity of DLPFC for the less rewarded hemifield, we note an absence of DLPFCv connectivity relative to T1, while the DLPFCd follows the same dorsal visual pathway functional connectivity.

We hypothesize that the described effect here, results from a-task related inhibition of the ventral visual pathway, which is responsible for object recognition. Furthermore, the DLPFCd plays a role in motor planning, multi-tasking, and maintaining goals whereas the DLPFCv is preferentially involved in

the visuospatial identity-related information of attended signals and cues. Indeed, once the value of the object and the spatial saliency map has been learned, both dorsal and ventral visual pathways are expected to be involved in response to more rewarding stimuli. The task used for the training involves the association between reward value and position (Serences and Yantis, 2006). This association thus serves to construct the spatial priority map and guide reward-based decision making. We confirm this hypothesis by noting that the DLPFCd expresses stronger FC with ipsilateral early visual areas on the hemisphere coding for the least rewarding stimuli.

4. Reinforcement of the dorso-ventral decorrelation under fluoxetine

In the T3 condition, we still observe that both DLPFCd and DLPFCv seeds from the hemisphere coding for the more rewarding hemifield have strong connectivity with the rest of the brain. However, we note that for the hemisphere coding for the least rewarding stimuli, DLPFCv seed have a contralateral connectivity, which is different from the T2 condition. Here DLPFCv always correlates with FEF, for it is responsible for working memory, cognitive flexibility, planning, inhibition and abstract reasoning (Miller and Cummings, 2013). Thus, this suggests that with fluoxetine, bilateral DLPFC is engaged in refining the reward selectivity, enhancing the perceptual learning of the spatial priority map.

Moreover, in the T3 condition, we note a stronger connectivity toward V1. This is especially evident when looking at differential correlation maps involving the T3 condition for V2 seed to brain connectivity maps. Indeed, the visual areas have systematically a stronger connectivity within themselves, mostly dorsally for the right hemisphere encoding for the overall most rewarded hemifield. Our observations might correspond to the effect of perpetual learning increased by a hyper excitability of the brain. Indeed GABA_A receptor concentrations are higher in the visual cortex than in the rest of the brain and more particularly, higher in the ventral part of the striate and extrastriate cortex than in its dorsal part (Kaulen et al., 2022). However, fluoxetine decreases extracellular GABA levels (Vetencourt et al., 2008; Baroncelli et al., 2011, Beshara et al., 2016; Santana et al., 2004), while also having a strong affinity with 5-HT_{2a} receptors, present in high concentration in the visual cortex (Beliveau et al., 2017; Hansen et al., 2022). Since GABA is responsible for more inhibition (Ulrich and Bettler, 2007), there is then a global decrease of inhibition, this decrease being stronger in the ventral part of the visual cortex, thus resulting in more excitability.

In addition, we observe a complete decorrelation of V2v seeds and V2d seeds, solely in T3 condition and regardless of the rewarding hemifield. This is in agreement with the DLPFC seeds observation accounting for a potential overall effect of a ventro-dorsal decorrelation following reward-based training with fluoxetine.

Conclusion

We here show that fluoxetine action on the fronto-occipital connectivity is dependent on reward outcome. Indeed, we first characterize a decoupling between areas of the dorsal and ventral visual pathways with fluoxetine, thus amplifying the reward sensitivity effects already present in T2 condition. Thus, fluoxetine appears to reweigh functional connectivity in favor of the dorsal visual stream by decreasing the FC to brain areas associated with the ventral visual stream in brain hemisphere associated with a high reward (**Figure 11, A**). Additionally, there is a suppression of FC within the ventral visual stream with fluoxetine in brain hemisphere associated with a low reward (**Figure 11, B**), indicating a specific effect of Fluoxetine on spatial processing as compared to identify processing. We hypothesize that this new FC configuration contributes to a refinement of the decision-making process, in order to maximize behavioral outcome. Overall, we demonstrated here the underlying neural and network mechanisms that support the behavioral role of fluoxetine in enhancing reward-based perceptual learning.

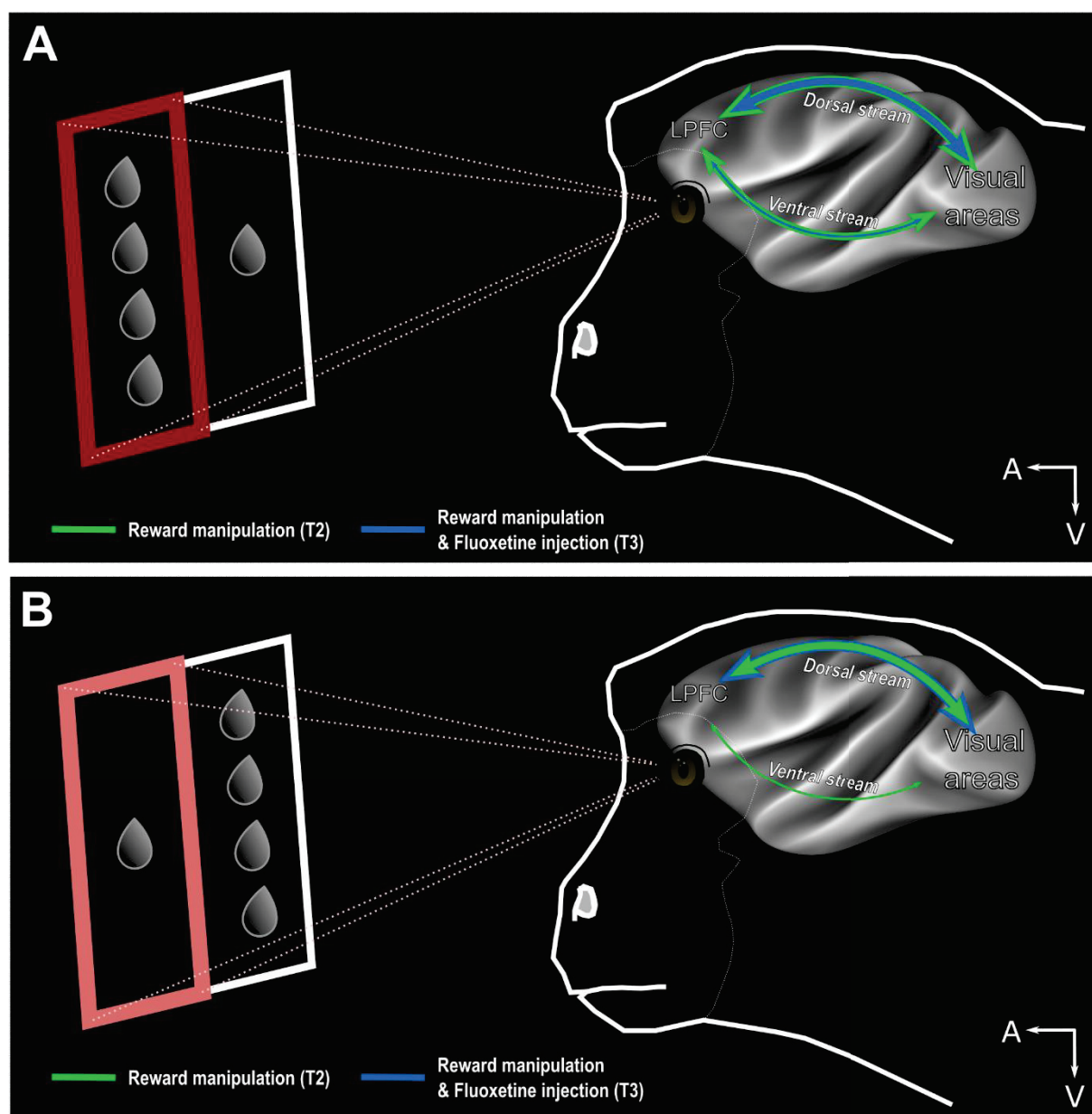


Figure 11: Summary: Schematic representation of the dorsal stream and the ventral stream connectivity according to the reward in T2 condition (green) and T3 condition (blue). (A) Dorsal and ventral visual stream connectivity strength on the high reward hemifields. (B) Dorsal and ventral visual stream connectivity strength on the low reward hemifields.

Supplementary figures

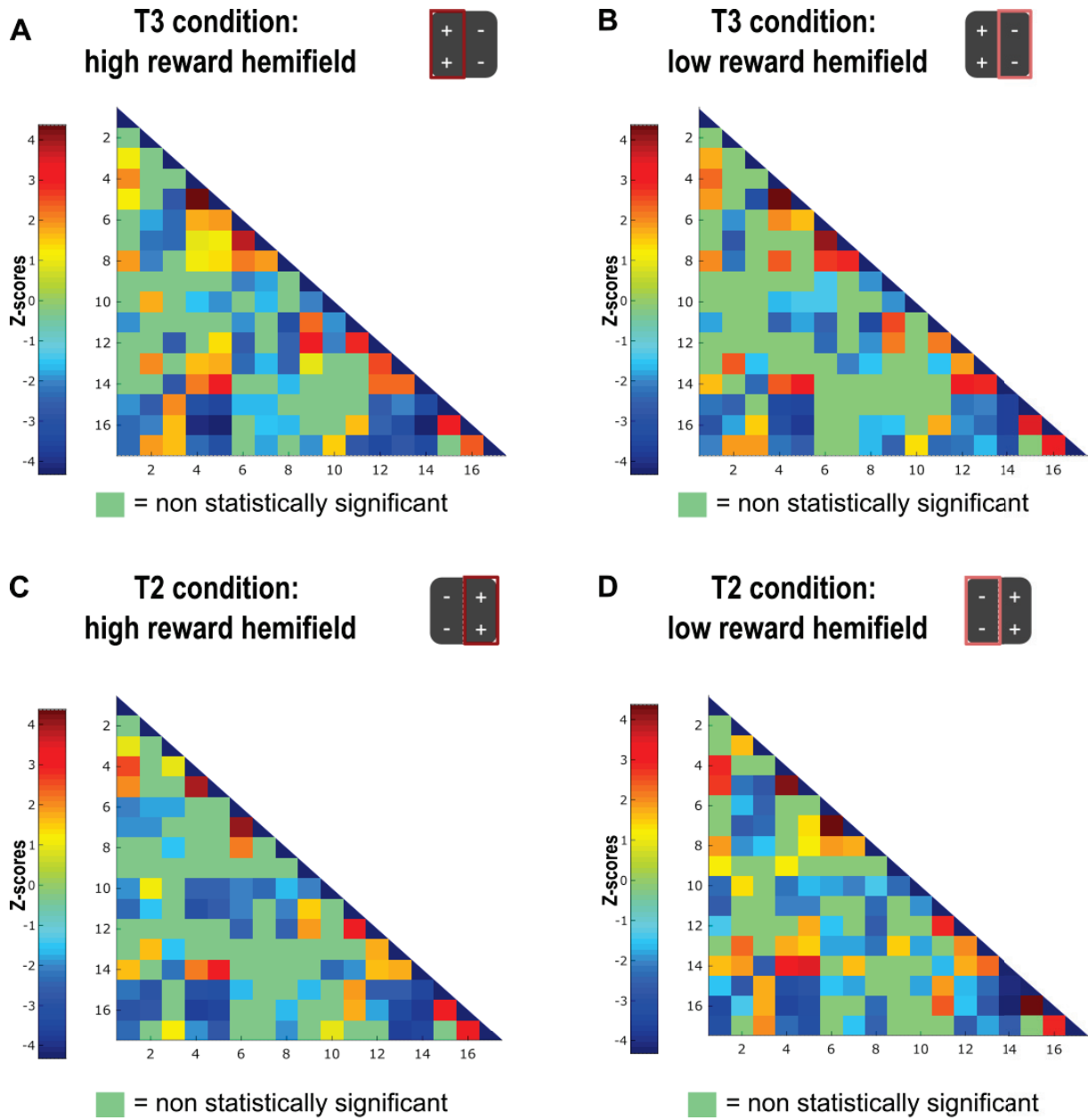


Figure S1: Functional connectivity matrices after a post-hoc statistical test filtering. The 17x17 matrices correspond to the FC Z-scores between brain regions as described in Figure 5, A. Filtered FC matrix for (A) the high reward hemifield in T3 condition, (B) the low reward hemifield in T3 condition, (C) the high reward hemifield in T2 condition and (D) the low reward hemifield in T2 condition.

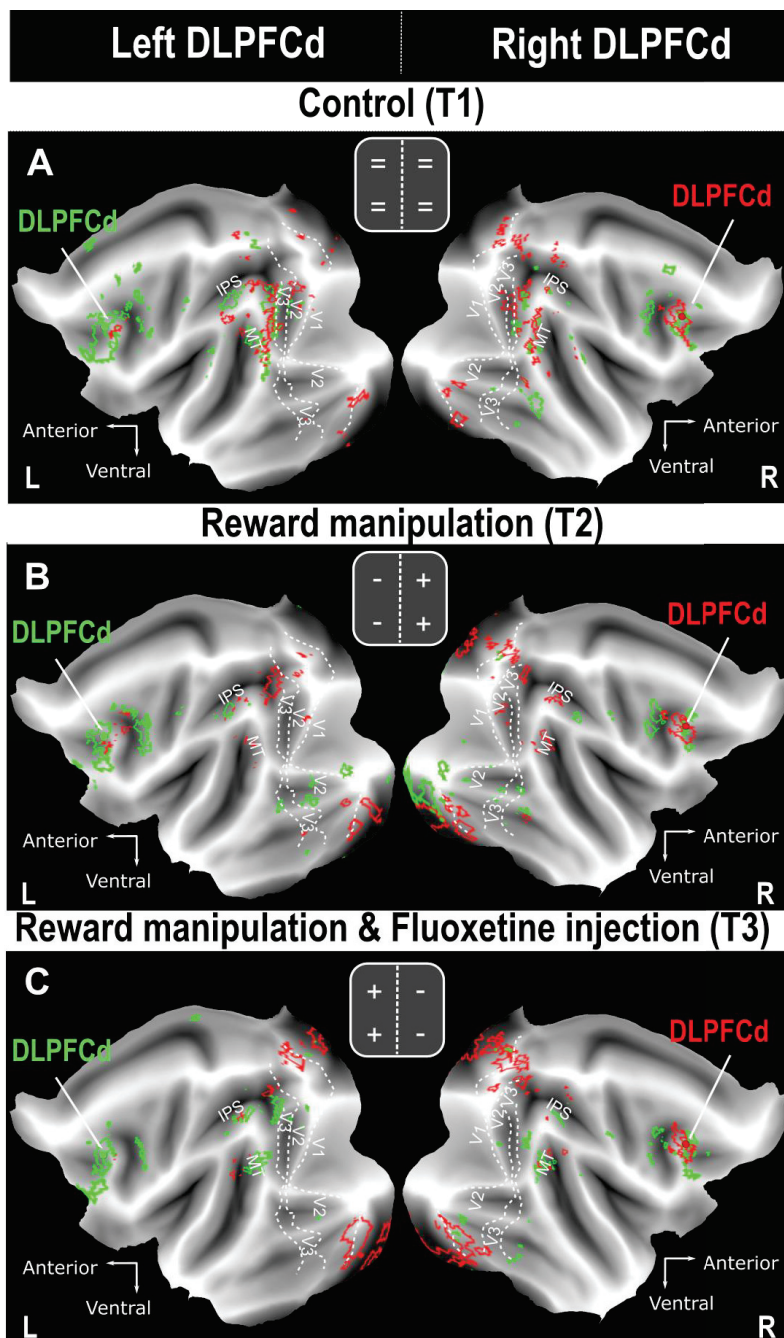


Figure S2: Flat maps of seed to brain functional connectivity for right and left DLPFCd seeds. We, here compare on a same flat map on both hemispheres the connectivity between right DLPFCd (in red) and left DLPFCd (in green) seeds with the rest of the brain. Seed to brain connectivity of right and left DLPFCd seeds for both hemispheres (A) in the control condition (T1), (B) in the reward manipulation condition (T2) and (C) in the reward manipulation associated to fluoxetine injection condition (T3).

References

- Adab, H.Z., Popivanov, I.D., Vanduffel, W., Vogels, R., 2014. Perceptual Learning of Simple Stimuli Modifies Stimulus Representations in Posterior Inferior Temporal Cortex. *Journal of Cognitive Neuroscience* 26, 2187–2200. https://doi.org/10.1162/jocn_a_00641
- Ambati, M., Apicella, I., Wang, S., Narendran, S., Leung, H., Pereira, F., Nagasaka, Y., Huang, P., Varshney, A., Baker, K.L., Marion, K.M., Shadmehr, M., Stains, C.I., Werner, B.C., Sadda, S.R., Taylor, E.W., Sutton, S.S., Magagnoli, J., Gelfand, B.D., 2021. Identification of fluoxetine as a direct NLRP3 inhibitor to treat atrophic macular degeneration. *Proceedings of the National Academy of Sciences* 118, e2102975118. <https://doi.org/10.1073/pnas.2102975118>
- Anderson, B.A., 2016. The attention habit: how reward learning shapes attentional selection. *Annals of the New York Academy of Sciences* 1369, 24–39. <https://doi.org/10.1111/nyas.12957>
- Ashburner, J., Barnes, G., Chen, C.-C., Daunizeau, J., Flandin, G., Friston, K., Gitelman, Glauche, V., Henson, R., Hutton, C., Kiebel, S., Kilner, J., Litvak, V., Mattout, J., Moran, R., Penny, W., Phillips, C., Rosa, M., Klaas, S., 1994. *Statistical Parametric Mapping*.
- Autio, J.A., Glasser, M.F., Ose, T., Donahue, C.J., Bastiani, M., Ohno, M., Kawabata, Y., Urushibata, Y., Murata, K., Nishigori, K., Yamaguchi, M., Hori, Y., Yoshida, A., Go, Y., Coalson, T.S., Jbabdi, S., Sotiropoulos, S.N., Kennedy, H., Smith, S., Van Essen, D.C., Hayashi, T., 2020. Towards HCP-Style macaque connectomes: 24-Channel 3T multi-array coil, MRI sequences and preprocessing. *NeuroImage* 215, 116800. <https://doi.org/10.1016/j.neuroimage.2020.116800>
- Avants, B.B., Tustison, N., Johnson, H., n.d. *Advanced Normalization Tools (ANTs)* 41.
- Baroncelli, L., Maffei, L., Sale, A., 2011. New Perspectives in Amblyopia Therapy on Adults: A Critical Role for the Excitatory/Inhibitory Balance. *Frontiers in Cellular Neuroscience* 5.
- Bavelier, D., Levi, D.M., Li, R.W., Dan, Y., Hensch, T.K., 2010. Removing Brakes on Adult Brain Plasticity: From Molecular to Behavioral Interventions. *Journal of Neuroscience* 30, 14964–14971. <https://doi.org/10.1523/JNEUROSCI.4812-10.2010>
- Beliveau, V., Ganz, M., Feng, L., Ozenne, B., Højgaard, L., Fisher, P.M., Svarer, C., Greve, D.N., Knudsen, G.M., 2017. A High-Resolution *In Vivo* Atlas of the Human Brain's Serotonin System. *J. Neurosci.* 37, 120–128. <https://doi.org/10.1523/JNEUROSCI.2830-16.2016>
- Beshara, S., Beston, B.R., Pinto, J.G.A., Murphy, K.M., 2016. Effects of Fluoxetine and Visual Experience on Glutamatergic and GABAergic Synaptic Proteins in Adult Rat Visual Cortex. *eNeuro* 2, ENEURO.0126-15.2015. <https://doi.org/10.1523/ENEURO.0126-15.2015>
- Bisley, J.W., Goldberg, M.E., 2010. Attention, Intention, and Priority in the Parietal Lobe. *Annual Review of Neuroscience* 33, 1–21. <https://doi.org/10.1146/annurev-neuro-060909-152823>
- Biswal, B., Zerrin Yetkin, F., Haughton, V.M., Hyde, J.S., 1995. Functional connectivity in the motor cortex of resting human brain using echo-planar mri. *Magnetic Resonance in Medicine* 34, 537–541. <https://doi.org/10.1002/mrm.1910340409>
- Buschman, T.J., Miller, E.K., 2007. Top-Down Versus Bottom-Up Control of Attention in the Prefrontal and Posterior Parietal Cortices. *Science* 315, 1860–1862. <https://doi.org/10.1126/science.1138071>
- Capitão, L.P., Chapman, R., Filippini, N., Wright, L., Murphy, S.E., James, A., Cowen, P.J., Harmer, C.J., 2020. Neural effects of a single dose of fluoxetine on resting-state functional connectivity in adolescent depression. *J Psychopharmacol* 34, 1461–1465. <https://doi.org/10.1177/0269881120959608>

Chapter II

- Castaldi, E., Lunghi, C., Morrone, M.C., 2020. Neuroplasticity in adult human visual cortex. *Neuroscience & Biobehavioral Reviews* 112, 542–552. <https://doi.org/10.1016/j.neubiorev.2020.02.028>
- Chamberlain, S.R., Müller, U., Blackwell, A.D., Clark, L., Robbins, T.W., Sahakian, B.J., 2006. Neurochemical Modulation of Response Inhibition and Probabilistic Learning in Humans. *Science* 311, 861–863. <https://doi.org/10.1126/science.1121218>
- Chelazzi, L., E to inova, J., Calletti, R., Lo Gerfo, E., Sani, I., Della Libera, C., Santandrea, E., 2014. Altering Spatial Priority Maps via Reward-Based Learning. *Journal of Neuroscience* 34, 8594–8604. <https://doi.org/10.1523/JNEUROSCI.0277-14.2014>
- Chelazzi, L., Perlato, A., Santandrea, E., Della Libera, C., 2013. Rewards teach visual selective attention. *Vision Research, Visual Attention 2013 Volume II* 85, 58–72. <https://doi.org/10.1016/j.visres.2012.12.005>
- Chen, G., Saad, Z.S., Britton, J.C., Pine, D.S., Cox, R.W., 2013. Linear mixed-effects modeling approach to fMRI group analysis. *NeuroImage* 73, 176–190. <https://doi.org/10.1016/j.neuroimage.2013.01.047>
- Chen, Y.-A., Huang, W.-S., Lin, Y.-S., Cheng, C.-Y., Liu, R.-S., Wang, S.-J., Li, I.-H., Huang, S.-Y., Shiue, C.-Y., Chen, C.-Y., Ma, K.-H., 2012. Characterization of 4-[18F]-ADAM as an imaging agent for SERT in non-human primate brain using PET: a dynamic study. *Nuclear Medicine and Biology* 39, 279–285. <https://doi.org/10.1016/j.nucmedbio.2011.08.002>
- Chollet, F., Tardy, J., Albucher, J.-F., Thalamas, C., Berard, E., Lamy, C., Bejot, Y., Deltour, S., Jaillard, A., Niclot, P., Guillon, B., Moulin, T., Marque, P., Pariente, J., Arnaud, C., Loubinoux, I., 2011. Fluoxetine for motor recovery after acute ischaemic stroke (FLAME): a randomised placebo-controlled trial. *The Lancet Neurology* 10, 123–130. [https://doi.org/10.1016/S1474-4422\(10\)70314-8](https://doi.org/10.1016/S1474-4422(10)70314-8)
- Cox, R.W., 1996. AFNI: software for analysis and visualization of functional magnetic resonance neuroimages. *Comput. Biomed. Res.* 29, 162–173. <https://doi.org/10.1006/cbmr.1996.0014>
- Dam, M., Tonin, P., De Boni, A., Pizzolato, G., Casson, S., Ermani, M., Freo, U., Piron, L., Battistin, L., 1996. Effects of Fluoxetine and Maprotiline on Functional Recovery in Poststroke Hemiplegic Patients Undergoing Rehabilitation Therapy. *Stroke* 27, 1211–1214. <https://doi.org/10.1161/01.STR.27.7.1211>
- Della Libera, C., Chelazzi, L., 2009. Learning to Attend and to Ignore Is a Matter of Gains and Losses. *Psychol Sci* 20, 778–784. <https://doi.org/10.1111/j.1467-9280.2009.02360.x>
- Di Bello, F., Ben Hadj Hassen, S., Astrand, E., Ben Hamed, S., 2022. Prefrontal Control of Proactive and Reactive Mechanisms of Visual Suppression. *Cerebral Cortex* 32, 2745–2761. <https://doi.org/10.1093/cercor/bhab378>
- Donahue, C.J., Sotiropoulos, S.N., Jbabdi, S., Hernandez-Fernandez, M., Behrens, T.E., Dyrby, T.B., Coalson, T., Kennedy, H., Knoblauch, K., Essen, D.C.V., Glasser, M.F., 2016. Using Diffusion Tractography to Predict Cortical Connection Strength and Distance: A Quantitative Comparison with Tracers in the Monkey. *J. Neurosci.* 36, 6758–6770. <https://doi.org/10.1523/JNEUROSCI.0493-16.2016>
- Fecteau, J.H., Munoz, D.P., 2006. Saliency, relevance, and firing: a priority map for target selection. *Trends in Cognitive Sciences* 10, 382–390. <https://doi.org/10.1016/j.tics.2006.06.011>
- Gacoin, M., Hamed, S.B., 2022. Fluoxetine degrades luminance perceptual thresholds while enhancing motivation and reward sensitivity. <https://doi.org/10.1101/2022.11.11.516168>
- Glasser, M.F., Sotiropoulos, S.N., Wilson, J.A., Coalson, T.S., Fischl, B., Andersson, J.L., Xu, J., Jbabdi, S., Webster, M., Polimeni, J.R., Van Essen, D.C., Jenkinson, M., 2013. The minimal p

- reprocessing pipelines for the Human Connectome Project. *NeuroImage, Mapping the Connectome* 80, 105–124. <https://doi.org/10.1016/j.neuroimage.2013.04.127>
- Goodale, M.A., Milner, A.D., 1992. Separate visual pathways for perception and action. *Trends in Neurosciences* 15, 20–25. [https://doi.org/10.1016/0166-2236\(92\)90344-8](https://doi.org/10.1016/0166-2236(92)90344-8)
- Goodale, M.A., Westwood, D.A., 2004. An evolving view of duplex vision: separate but interacting cortical pathways for perception and action. *Current Opinion in Neurobiology* 14, 203–211. <https://doi.org/10.1016/j.conb.2004.03.002>
- Hansen, J.Y., Shafiei, G., Markello, R.D., Smart, K., Cox, S.M.L., Nørgaard, M., Beliveau, V., Wu, Y., Gallezot, J.-D., Aumont, É., Servaes, S., Scala, S.G., DuBois, J.M., Wainstein, G., Bezgin, G., Funck, T., Schmitz, T.W., Spreng, R.N., Galovic, M., Koepp, M.J., Duncan, J.S., Coles, J.P., Fryer, T.D., Aigbirhio, F.I., McGinnity, C.J., Hammers, A., Soucy, J.-P., Baillet, S., Guimond, S., Hietala, J., Bedard, M.-A., Leyton, M., Kobayashi, E., Rosa-Neto, P., Ganz, M., Knudsen, G.M., Palomero-Gallagher, N., Shine, J.M., Carson, R.E., Tuominen, L., Dagher, A., Misic, B., 2022. Mapping neurotransmitter systems to the structural and functional organization of the human neocortex. *Nat Neurosci* 1–13. <https://doi.org/10.1038/s41593-022-01186-3>
- Ibos, G., Duhamel, J.-R., Hamed, S.B., 2013. A Functional Hierarchy within the Parietofrontal Network in Stimulus Selection and Attention Control. *J. Neurosci.* 33, 8359–8369. <https://doi.org/10.1523/JNEUROSCI.4058-12.2013>
- Itti, L., Koch, C., 2001. Computational modelling of visual attention. *Nat Rev Neurosci* 2, 194–203. <https://doi.org/10.1038/35058500>
- Itti, L., Koch, C., Niebur, E., 1998. A model of saliency-based visual attention for rapid scene analysis. *IEEE Trans. Pattern Anal. Machine Intell.* 20, 1254–1259. <https://doi.org/10.1109/34.730558>
- Jenkinson, M., Beckmann, C.F., Behrens, T.E.J., Woolrich, M.W., Smith, S.M., 2012. FSL. *Neuroimage* 62, 782–790. <https://doi.org/10.1016/j.neuroimage.2011.09.015>
- Jung, B., Taylor, P.A., Seidlitz, J., Sponheim, C., Perkins, P., Ungerleider, L.G., Glen, D., Messinger, A., 2020. A comprehensive macaque fMRI pipeline and hierarchical atlas. <https://doi.org/10.1101/2020.08.05.237818>
- Jung, J., Lambon Ralph, M.A., Jackson, R.L., 2022. Subregions of DLPFC Display Graded yet Distinct Structural and Functional Connectivity. *J. Neurosci.* 42, 3241–3252. <https://doi.org/10.1523/JNEUROSCI.1216-21.2022>
- Karni, A., Bertini, G., 1997. Learning perceptual skills: behavioral probes into adult cortical plasticity. *Current Opinion in Neurobiology* 7, 530–535. [https://doi.org/10.1016/S0959-4388\(97\)80033-5](https://doi.org/10.1016/S0959-4388(97)80033-5)
- Katsuki, F., Constantinidis, C., 2014. Bottom-Up and Top-Down Attention: Different Processes and Overlapping Neural Systems. *Neuroscientist* 20, 509–521. <https://doi.org/10.1177/1073858413514136>
- Kaulen, N., Rajkumar, R., Régio Brambilla, C., Mauler, J., Ramkiran, S., Orth, L., Sbaihat, H., Lang, M., Wyss, C., Rota Kops, E., Scheins, J., Neumaier, B., Ermert, J., Herzog, H., Langen, K.-J., Lerche, C., Shah, N.J., Veselinović, T., Neuner, I., 2022. mGluR5 and GABAA receptor-specific parametric PET atlas construction—PET/MR data processing pipeline, validation, and application. *Human Brain Mapping* 43, 2148–2163. <https://doi.org/10.1002/hbm.25778>
- Koechlin, E., Ody, C., Kouneiher, F., 2003. The Architecture of Cognitive Control in the Human Prefrontal Cortex. *Science* 302, 1181–1185. <https://doi.org/10.1126/science.1088545>
- Kolster, H., Janssens, T., Orban, G.A., Vanduffel, W., 2014. The retinotopic organization of macaque occipitotemporal cortex anterior to V4 and caudoventral to the middle temporal (MT) cluster. *J. Neurosci.* 34, 10168–10191. <https://doi.org/10.1523/JNEUROSCI.3288-13.2014>

Chapter II

- Leite, F.P., Tsao, D., Vanduffel, W., Fize, D., Sasaki, Y., Wald, L.L., Dale, A.M., Kwong, K.K., Orban, G.A., Rosen, B.R., Tootell, R.B.H., Mandeville, J.B., 2002. Repeated fMRI Using Iron Oxide Contrast Agent in Awake, Behaving Macaques at 3 Tesla. *NeuroImage* 16, 283–294. <https://doi.org/10.1006/nimg.2002.1110>
- Libera, C.D., Chelazzi, L., 2006. Visual Selective Attention and the Effects of Monetary Rewards. *Psychol Sci* 17, 222–227. <https://doi.org/10.1111/j.1467-9280.2006.01689.x>
- Loubinoux, I., Boulanouar, K., Ranjeva, J.-P., Carel, C., Berry, I., Rascol, O., Celsis, P., Chollet, F., 1999. Cerebral Functional Magnetic Resonance Imaging Activation Modulated by a Single Dose of the Monoamine Neurotransmission Enhancers Fluoxetine and Fenozolone during Hand Sensorimotor Tasks. *J Cereb Blood Flow Metab* 19, 1365–1375. <https://doi.org/10.1097/00004647-199912000-00010>
- Macoveanu, J., 2014. Serotonergic modulation of reward and punishment: Evidence from pharmacological fMRI studies. *Brain Research* 1556, 19–27. <https://doi.org/10.1016/j.brainres.2014.02.003>
- Manjón, J.V., Coupé, P., Martí-Bonmatí, L., Collins, D.L., Robles, M., 2010. Adaptive non-local means denoising of MR images with spatially varying noise levels. *Journal of Magnetic Resonance Imaging* 31, 192–203. <https://doi.org/10.1002/jmri.22003>
- McCabe, C., Mishor, Z., Cowen, P.J., Harmer, C.J., 2010. Diminished Neural Processing of Aversive and Rewarding Stimuli During Selective Serotonin Reuptake Inhibitor Treatment. *Biological Psychiatry* 67, 439–445. <https://doi.org/10.1016/j.biopsych.2009.11.001>
- Meyniel, F., Goodwin, G.M., Deakin, J.W., Klinge, C., MacFadyen, C., Milligan, H., Mullings, E., Pessiglione, M., Gaillard, R., 2016. A specific role for serotonin in overcoming effort cost. *eLife* 5, e17282. <https://doi.org/10.7554/eLife.17282>
- Miller, B.L., Cummings, J.L., 2013. *The Human Frontal Lobes, Second Edition: Functions and Disorders*. Guilford Publications.
- Mishkin, M., Ungerleider, L.G., 1982. Contribution of striate inputs to the visuospatial functions of parieto-preoccipital cortex in monkeys. *Behavioural Brain Research* 6, 57–77. [https://doi.org/10.1016/0166-4328\(82\)90081-X](https://doi.org/10.1016/0166-4328(82)90081-X)
- Ng, K.L., Gibson, E.M., Hubbard, R., Yang, J., Caffo, B., O'Brien, R.J., Krakauer, J.W., Zeiler, S.R., 2015. Fluoxetine Maintains a State of Heightened Responsiveness to Motor Training Early After Stroke in a Mouse Model. *Stroke* 46, 2951–2960. <https://doi.org/10.1161/STROKEAHA.115.010471>
- Raymond, J.E., O'Brien, J.L., 2009. Selective Visual Attention and Motivation: The Consequences of Value Learning in an Attentional Blink Task. *Psychol Sci* 20, 981–988. <https://doi.org/10.1111/j.1467-9280.2009.02391.x>
- Richter, C.G., Thompson, W.H., Bosman, C.A., Fries, P., 2017. Top-Down Beta Enhances Bottom-Up Gamma. *J. Neurosci.* 37, 6698–6711. <https://doi.org/10.1523/JNEUROSCI.3771-16.2017>
- Rima, S., Cottureau, B.R., Héjja-Brichard, Y., Trotter, Y., Durand, J.-B., 2020. Wide-field retinotopy reveals a new visuotopic cluster in macaque posterior parietal cortex. *Brain Struct Funct* 225, 2447–2461. <https://doi.org/10.1007/s00429-020-02134-2>
- Rutherford, H.J.V., O'Brien, J.L., Raymond, J.E., 2010. Value associations of irrelevant stimuli modify rapid visual orienting. *Psychonomic Bulletin & Review* 17, 536–542. <https://doi.org/10.3758/PBR.17.4.536>
- Santana, N., Bortolozzi, A., Serrats, J., Mengod, G., Artigas, F., 2004. Expression of Serotonin1A and Serotonin2A Receptors in Pyramidal and GABAergic Neurons of the Rat Prefrontal Cortex. *Cerebral Cortex* 14, 1100–1109. <https://doi.org/10.1093/cercor/bhh070>

Chapter II

- Scholl, J., Kolling, N., Nelissen, N., Browning, M., Rushworth, M.F.S., Harmer, C.J., 2017. Beyond negative valence: 2-week administration of a serotonergic antidepressant enhances both reward and effort learning signals. *PLOS Biology* 15, e2000756. <https://doi.org/10.1371/journal.pbio.2000756>
- Serences, J.T., Yantis, S., 2006. Selective visual attention and perceptual coherence. *Trends in Cognitive Sciences* 10, 38–45. <https://doi.org/10.1016/j.tics.2005.11.008>
- Serences, J.T., Yantis, S., 2004. Attentional Priority Maps in Human Cortex: (537052012-668). <https://doi.org/10.1037/e537052012-668>
- Smith, S.M., Beckmann, C.F., Andersson, J., Auerbach, E.J., Bijsterbosch, J., Douaud, G., Duff, E., Feinberg, D.A., Griffanti, L., Harms, M.P., Kelly, M., Laumann, T., Miller, K.L., Moeller, S., Petersen, S., Power, J., Salimi-Khorshidi, G., Snyder, A.Z., Vu, A.T., Woolrich, M.W., Xu, J., Yacoub, E., Uğurbil, K., Van Essen, D.C., Glasser, M.F., 2013. Resting-state fMRI in the Human Connectome Project. *NeuroImage, Mapping the Connectome* 80, 144–168. <https://doi.org/10.1016/j.neuroimage.2013.05.039>
- Smith, S.M., Fox, P.T., Miller, K.L., Glahn, D.C., Fox, P.M., Mackay, C.E., Filippini, N., Watkins, K.E., Toro, R., Laird, A.R., Beckmann, C.F., 2009. Correspondence of the brain's functional architecture during activation and rest. *Proceedings of the National Academy of Sciences* 106, 13040–13045. <https://doi.org/10.1073/pnas.0905267106>
- Song, X., García-Saldivar, P., Kindred, N., Wang, Y., Merchant, H., Meguerditchian, A., Yang, Y., Stein, E.A., Bradberry, C.W., Ben Hamed, S., Jedema, H.P., Poirier, C., 2021. Strengths and challenges of longitudinal non-human primate neuroimaging. *Neuroimage* 236, 118009. <https://doi.org/10.1016/j.neuroimage.2021.118009>
- Ulrich, D., Bettler, B., 2007. GABAB receptors: synaptic functions and mechanisms of diversity. *Current Opinion in Neurobiology, Signalling mechanisms* 17, 298–303. <https://doi.org/10.1016/j.conb.2007.04.001>
- Ungerleider, L.G., Haxby, J.V., 1994. 'What' and 'where' in the human brain. *Current Opinion in Neurobiology* 4, 157–165. [https://doi.org/10.1016/0959-4388\(94\)90066-3](https://doi.org/10.1016/0959-4388(94)90066-3)
- Ungerleider, L.G., Pessoa, L., 2008. What and where pathways. *Scholarpedia* 3, 5342. <https://doi.org/10.4249/scholarpedia.5342>
- Vanduffel, W., Fize, D., Mandeville, J.B., Nelissen, K., Van Hecke, P., Rosen, B.R., Tootell, R.B.H., Orban, G.A., 2001. Visual Motion Processing Investigated Using Contrast Agent-Enhanced fMRI in Awake Behaving Monkeys. *Neuron* 32, 565–577. [https://doi.org/10.1016/S0896-6273\(01\)00502-5](https://doi.org/10.1016/S0896-6273(01)00502-5)
- Vetencourt, J.F.M., Sale, A., Viegi, A., Baroncelli, L., De Pasquale, R., F. O'Leary, O., Castrén, E., Maffei, L., 2008. The Antidepressant Fluoxetine Restores Plasticity in the Adult Visual Cortex. *Science* 320, 385–388. <https://doi.org/10.1126/science.1150516>
- Yushkevich, P.A., Gerig, G., 2017. ITK-SNAP: An Intractive Medical Image Segmentation Tool to Meet the Need for Expert-Guided Segmentation of Complex Medical Images. *IEEE Pulse* 8, 54–57. <https://doi.org/10.1109/MPUL.2017.2701493>

Perspectives of the chapter II

We have here analyzed this data with the specific aim of understanding cortical functional connectivity changes between our manipulations in T2 and T3 conditions compared to the T1 condition. In order to complete this study, other brains regions connectivity would be interesting to study further. Indeed, a first limitation of this study was the parcellation of the CHARM-2 atlas we used. While its outcome permitted us to carry out this study, some regions of interest in this study were not represented with the required spatial resolution. These include the frontal eye field (FEF), or the lateral intraparietal sulcus (LIP), which are both involved in visual attention. Indeed, these regions are identified using the hypothesis driven LME approach. It would be of stronger value to also identify them using a hypothesis free approach.

It would also be extremely useful to expand out frame of view, and consider subcortical regions such as the pulvinar or the striatum, which are known to be modulated by serotonin, to name a few. In addition, since we manipulated the serotonin levels in the brain in the T3 condition, we expect a modulation of the dorsal raphe nucleus functional connectivity with the entire brain in contrast with T2 and T1 condition. We might face technical limitations there, as the raphe nuclei are located in a region of low signal-to-noise ratio with the type of MRI coils we use, yet it is worth exploring. We also expect modulation of the reward network from the T2 condition, in link with our observations on the DLPFC. This network is known to involve the ventral tegmental area (VTA), the hippocampus, the amygdala and the nucleus acumbens. Altogether, these further analyses would allow to have a complete overview of the effect of coupled behavioral and fluoxetine manipulation on the functional brain networks involved in visual plasticity induction in the adult brain.

CHAPTER III

CHRONIC FLUOXETINE ADMINISTRATION ENHANCES THE DECOUPLING BETWEEN DORSAL AND VENTRAL V2 INDUCED BY A REWARD-BASED TRAINING OF A SPATIAL PRIORITY MAP

| | |
|----------------------------------------------|-----|
| General introduction to the chapter III..... | 146 |
| Abstract | 147 |
| Introduction | 147 |
| Material and Methods..... | 149 |
| Results | 153 |
| Discussion | 163 |
| Conclusion..... | 165 |
| References | 166 |
| Perspectives of the chapter III..... | 170 |

General introduction to the chapter III

We have reported in the previous chapter the reweighing mechanisms of the brain functional connectivity, first in the context of a behavioral manipulation driven by the reward, and then, when this behavioral manipulation is coupled with a pharmacological manipulation of central serotonin levels using fluoxetine. This functional connectivity re-organization occurred at three different levels: between the left and right hemisphere, due to the behavioral manipulation; between the dorsal and ventral visual processing streams, due to the behavioral manipulation and amplified by the use of fluoxetine; between the prefronto-parieto-occipital regions, due the action of fluoxetine. These observations from the chapter II on whole brain connectivity scale deserve further investigation, on a smaller scale, by now specifically focusing on visual areas.

In the present chapter III, we define regions of interest (ROIs), thanks to the cross-validation between ROIs defined based on retinotopic mapping at the three same time-points T1, T2 and T3 described in the chapter II and ROIs defined based on the activation peaks in two detection tasks, differing in the level of spatial noise included in each of them. We compare the percent signal changes (%SC) within these ROIs, 1) as a function of their associated reward manipulation, 2) the pharmacological manipulation and 3) the nature of the task. We first observed that fluoxetine amplifies, in the context of reward-based learning, solely the responses of ROIs of the dorsal V2, thus confirming the decoupling between dorsal and ventral V2 observed in chapter III. We further show that the dorsal V2 activations recruit more cortical volume than the dorsal V2 activations under fluoxetine. We propose that these observations account for the behavioral effects of fluoxetine reported in chapter I, namely, a differential effect of fluoxetine on visual perception between the upper and the lower visual field as well as a degraded perception.

Study n°3: Chronic fluoxetine administration enhances the decoupling between dorsal and ventral V2 induced by a reward-based training of a spatial priority map. **Maëva Gacoïn**, Mathilda Froesel, Simon Clavagnier, Maxime Gaudet-Trafit & Suliann Ben Hamed. (*In prep*)

Chronic fluoxetine administration enhances the decoupling between dorsal and ventral V2 induced by a reward-based training of a spatial priority map

Maëva Gacoin, Mathilda Froesel, Simon Clavagnier, Maxime Gaudet-Trafit & Suliann Ben Hamed. *In prep*

Abstract

In a previous study of functional brain connectivity, we hypothesized that in the context of visual perception driven by the learning of spatial reward biases, fluoxetine amplifies the decoupling of the ventral and dorsal visual stream areas, and enhances correlation within the latter, thus probably optimizing spatial decision-making processes. In order to measure more precisely our manipulations (behavioral and pharmacological) effects on the visual cortex, we here used three metrics. First, the retinotopic mapping allowed us to assess the repeatability of the V1/V2/V3 delineation across our longitudinal project and to confirm our regions of interest localization in the V2 area, obtained thanks to peak of activation in two detection tasks. This allowed to estimate percentage signal change in these ROIs in each time point. The second metric corresponds to the overall activated V2 cortical volume compared to a fixation condition in these ROIs. We first observed that fluoxetine amplifies, in the context of reward-based learning, solely the responses of ROIs of the dorsal V2, thus confirming the decoupling between dorsal and ventral V2 observed in chapter III. We further show, thanks to the third metric; that the dorsal V2 activations recruit more cortical volume than the dorsal V2 activations under fluoxetine. We propose that these observations account for the behavioral effects of fluoxetine, namely, a differential effect of fluoxetine on visual perception between the upper and the lower visual field as well as a degraded perception.

Introduction

In the brain, the blood oxygen level depends on the neural activity expressed within the recorded area. The more this region is active, the more it consumes oxygen and needs blood input, due to a specific neurovascular coupling process, the underlying mechanisms of which are still under investigation. The principle of functional magnetic resonance imaging (fMRI) is to measure variations in blood oxygenation in response to underlying neural activity, hence called blood oxygenation level dependent (BOLD) signal (Logothetis and Wandell, 2004; Ogawa et al., 1990). Here we use monocrySTALLINE iron-oxide nanoparticles (MION) contrast agent-based hemodynamics response function, thus its response is inverted when compared with a BOLD response (Leite et al., 2002). In the previous study (chapter II, study n°2), we show that a reward-based learning induced by a spatial priority map with and without fluoxetine injection increases the local connectivity in temporal regions, while inhibiting its connectivity with prefrontal and visual areas. Moreover, we also characterized a decoupling between the dorsal and

the ventral visual pathway brain regions under fluoxetine. Since the ventral stream is responsible for object identification while the dorsal stream is essential for spatial location (Mishkin and Ungerleider, 1982; Ungerleider and Haxby, 1994; Goodale and Westwood, 2004; Ungerleider and Pessoa, 2008), we hypothesized that when visual perception is driven by reward, fluoxetine amplifies the inhibition of the object identity to optimize the decision-making process, while enhancing the localization of the object in order to target the most relevant position.

While serotonin selective reuptake inhibitors (SSRIs) are known to increase the behavioral sensitivity to reward (Macoveanu 2014; McCabe et al. 2010; Scholl et al. 2017; Gacoin and Ben Hamed 2022), the precise underlying neural and network correlates of this effect are still unknown. Moreover, while we show that there is a global decoupling between the dorsal and the ventral visual pathway brain regions due to the training and amplified when coupled with fluoxetine administration by looking at the functional connectivity, the precise origin of this decoupling in the visual system remains unclear. We thus here had monkeys perform an active task while in the fMRI in the presence and absence of fluoxetine, in order to identify specific task related changes in cortical responses. We also performed a systematic retinotopic mapping of striate and extrastriate visual areas in order to precisely characterize both local changes in visual representation as well as network changes in the cortical networks involved in visual decision-making.

To measure the enhanced plasticity effect in the visual cortex by our two manipulations, both behavioral and pharmacological, we thus used three metrics. The first one is the retinotopic mapping. Indeed the neurons of the visual cortex present particular receptive fields so that neighboring points of a seen visual scene are encoding by neighboring activations in the visual cortex (Brewer et al., 2002; Vanduffel et al., 2002; Fize et al., 2003; Kolster et al., 2009; Arcaro et al., 2011; Kolster et al., 2014; Janssens et al., 2014; Arcaro and Livingstone, 2017). We thus measured retinotopy across time-points (control condition, reward-based manipulation and reward-based manipulation coupled to fluoxetine injection) in a longitudinal fMRI study on two adult macaques, in order to first validate the repeatability of our measurement. We report the same V1/V2/V3 delineations across time-points. We use this information to validate sites of activation induced by the viewing of peripheral targets in two distinct peripheral detection tasks.

These two detection tasks allowed us to measure enhanced cortical plasticity in the visual cortex as a function of our conditions as evidences by differences in percent of signal change (%SC) relative to fixation and changes in volume activation size. These two metrics correlate with the cortical GABA level in the visual areas (Bhattacharyya et al., 2017) and can be taken as a proxy to assess the excitation/inhibition ratio with and without fluoxetine following reward-based training. We first see that %SC increases in both detection tasks and regardless of the SSRI when a more rewarding target is presented, but only in the dorsal visual areas (low visual field), in agreement with our functional

connectivity results. Since fluoxetine decreases cortical GABA levels (Vetencourt et al., 2008; Baroncelli et al., 2011, Beshara et al., 2016; Santana et al., 2004), and dorsal visual regions contain less GABA receptors (Kaulen et al., 2022), these regions are likely to be excited by learning, possibly accounting for our observations. These observations are task specific as GABA is also linked with enhanced intrinsic noise in tasks involving a spatial uncertainty (Hammett et al., 2020). All this taken together possibly accounts for our behavioral observations (Chapter 1) or a degraded spatial resolution in vision.

Material and Methods

Note that data from the study n°3 were acquired along with data presented in chapter II of the present thesis manuscript. Thus, animals and ethical approval, the two monkeys performing the tasks, surgery, fluoxetine preparation and administration, MRI experimental setup and acquisitions parameters, behavioral tasks and MRI preprocessing were the same. For reading comfort, we will not describe those again, but expand on it when necessary.

1. Behavioral tasks

1. Training: Saccadic reward competition task

Monkeys were trained on three different tasks as described in **Figure 1**. The saccadic reward competition task is the same that we presented and discussed in chapter II. Monkeys had to fixate a central cross. One thousand to 2000ms from fixation onset, two identical stimuli (target) were presented. Stimuli were drawn from a virtual array of eight stimuli organized along a circle of 8° of eccentricity (**Figure 1, A**). Each location in this virtual array was associated with a different reward probability, thus building a reward based spatial priority map (Chelazzi et al., 2014). Possible reward probabilities were 80% (high), 50% (medium) and 20% (low), according to a fixed spatial relationship, such that the extreme reward probabilities (80% and 20%) were neighbored by intermediate reward probability targets (50%). Monkeys had to make a saccade to one of the two presented stimuli and were rewarded according to the reward probability associated with the chosen target location. Monkeys were trained for this task prior to be scanned. Overall, during T2, the reward amount was higher on the right hemifield and lower on the left hemifield and was reversed for T3, with the most rewarded hemifield on the left and the least rewarded hemifield on the right. In addition, for T3, there were injections of chronic saline solution for 6 weeks followed by 6 weeks of chronic injection of fluoxetine suspension.

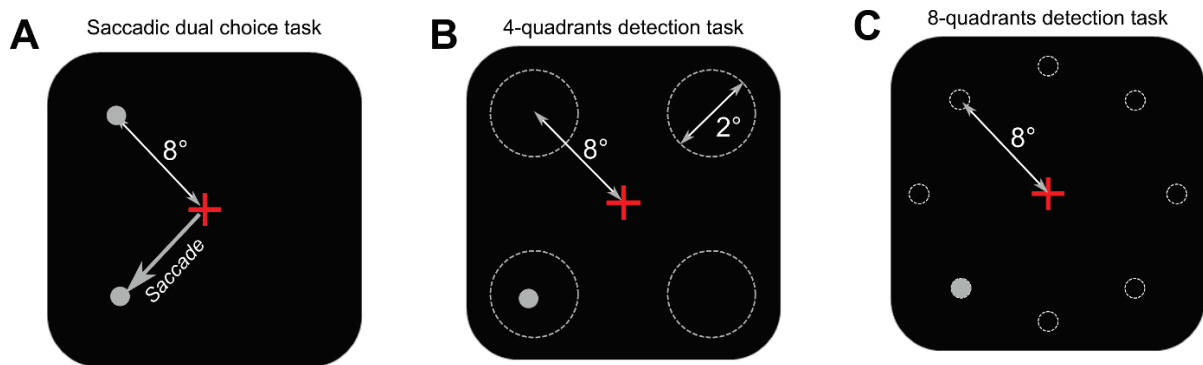


Figure 1: Active tasks. Prior to the MRI scans, monkeys were trained to perform these 3 active tasks, along with resting state tasks and retinotopic mapping tasks previously described in chapter 2. (A) Saccadic dual choice tasks, the monkey responds with a saccade and receives a reward amount according to the target position. (B) 4-quadrants detection task, the monkey responds with the hand by releasing a lever and receives the same amount of reward regardless of the stimuli position. Targets can appear with a virtual circle of 2° . (C) 8-quadrants detection task. Monkeys had to fixate a central cross on a screen 60cm away from their eyes. After an interval of 1 to 2 secs, stimuli would appear at one of the eight potential positions, at 8° of eccentricity from the fixation cross. If the monkey makes a hand response by releasing a lever, it gets a reward. This task uses the same 8 positions as in task (A) and follows the same paradigm as in task (B), except that there is no spatial noise. Note that none of the dashed line circles were actually displayed to the monkeys.

2. MRI: Retinotopic mapping

The neurons organization of the visual areas (from V1 to MT) are referred to as topographic and retinotopic maps or visuotopic retinal mapping. Indeed, they form a 2D representation of the visual scene formed on the retina such that neighboring regions are formed by neighboring neurons of neighboring receptive fields. We determined the retinotopic maps thanks to fMRI, which is a powerful tool to investigate those topographies in the macaque visual cortex (Brewer et al., 2002; Vanduffel et al., 2002; Fize et al., 2003; Kolster et al., 2009; Arcaro et al., 2011; Kolster et al., 2014; Janssens et al., 2014; Arcaro and Livingstone, 2017). During acquisitions, we stimulated our subjects retina by circular images (annuli) or polar angled lines (wedges) displayed while they were fixating a central point (Bridge, 2011; DeYoe et al., 1996), 60cm away from their eyes. Both of the stimuli types were covering an eccentricity from $0,5^\circ$ to 15° of the peripheral field of view, were flickering, colorful and consisted in an image representing a portion of an appetent scene to keep the macaques attentive. In the eccentricity task, the radial thickness for the first smaller ring displayed was $0,25^\circ$ and their radial thickness expanded according to a $\log(r)$ law to approximate the human cortical magnification factor. We here used the retinotopic mapping and its boundaries to define functional visual brain regions. Thus, in primates, V1 and V2 areas are delineated by the vertical meridian of their visual field projected on the cortex convex gyri folds (Rajimehr and Tootell, 2009). The horizontal meridian delineates boundaries between V2 and V3 areas. The combination of annuli rings and wedges allowed us to identify precise visual field maps (DeYoe et al., 1996; Engel et al., 1997; Sereno et al., 1995). Each annuli task acquisition represented 118 volumes and both wedges tasks were 114 and 112 volumes in length.

3. MRI: Peripheral detection tasks

The peripheral target detection task consisted in fixating a central cross while each 1000ms to 2000ms, a target randomly appeared for 200ms on a screen located 60cm away from the eyes of the monkeys at an eccentricity of 8° away from the central cross. If they responded manually by releasing a lever within a time window of [150ms – 1000ms], they were rewarded. Monkeys were trained to these tasks prior to be scanned until they reach 85% of correct trial of stable performances. In these tasks, reward was equally distributed among different target positions. Peripheral detection tasks are thus active tasks. For this study we displayed two distinct peripheral detection tasks. Each peripheral detection task acquisition represented 166 volumes each.

The first one is the 4-quadrants peripheral detection task (D4, **Figure 1, B**) that we already presented in chapter II. In this task, targets could appear in 4 possible locations, up-right, up-left, down-right or down-left quadrant ($(6\sqrt{2}, 6\sqrt{2})$, $(-6\sqrt{2}, 6\sqrt{2})$, $(-6\sqrt{2}, -6\sqrt{2})$ or $(6\sqrt{2}, -6\sqrt{2})$) within a virtual circle of 2° . Note that stimuli properties, such as their size, would not change according to the eccentricity. With this spatial noise, we here aimed at understanding the peripheral spatial vision whilst inducing behavioral and pharmacological plasticity. Indeed, we hypothesized that it could be enhanced or degraded according to our manipulations (d'Almeida et al., 2013; Chang et al., 2015; Striem-Amit et al., 2015).

The second task is the 8-quadrants peripheral detection task (D8, **Figure 1, C**). In this task, targets could appear in 8 possible locations: the 4 same as in the 4-quadrants detection task plus 4 others on the vertical and horizontal meridians, all on a virtual 8° circle of eccentricity from the central fixation cross. Note that these 8 positions are also the same as in the saccadic reward competition task. Contrary to the 4-quadrants peripheral detection task, there were no spatial noise. This task thus served as a reference for the D4 task described above.

2. Data analysis

We selected data based on the session signal-to-noise ratio, the success rate and fixation quality on the different tasks, low head and body motion from the monkey and for the overall quality of the scan. Although we acquired many more data, this filtering allowed us to have the best possible quality of analysis. We here present data acquired on annuli task (T1: M1, 1534 volumes; M2, 1888 volumes. T2: M1, 2490 volumes; M2, 1180 volumes. T3: M1, 1652 volumes; M2, 2006 volumes), polar angle task for the lower visual field task (T1: M1, 1824 volumes; M2, 1482 volumes. T2: M1, 1710 volumes; M2, 1026 volumes. T3: M1, 1938 volumes; M2, 1824 volumes), polar angle task for the higher visual field task (T1: M1, 1344 volumes; M2, 1008 volumes. T2: M1, 1680 volumes; M2, 1120 volumes. T3: M1, 1680 volumes; M2, 1904 volumes), 4-quadrants peripheral detection task (T1: M1, 4980 volumes; M2, 1494 volumes. T2: M1, 2158 volumes; M2, 1660 volumes. T3 : M1, 3320 volumes; M2, 3154

volumes.) and 8-quadrants peripheral detection task (T2: M1, 2988 volumes; M2, 2988 volumes. T3: M1, 2988 volumes; M2, 3320 volumes).

1. Retinotopic data: average phase maps and conjunction

We followed the same pre-processing steps as described in chapter II methods on the acquired retinotopic mapping tasks data, to determine a conjunction between wedges and annuli, and to determine retinotopic average phase maps. For the latter, we worked on the data prior their smoothing, to avoid any potential inference of signal. We removed linear tendencies to obtain all data under the same format with AFNI (Cox, 1996). We then used phase-encoded mapping method and calculated a fast Fourier transform on the time-series (Alvarez et al., 2015; Sereno et al., 1995). Finally, we determined a mask thanks to the F-statistic map, by applying a filter, being more or less stringent according to the situation, and applied it to our phase-encoded map such that only relevant brain areas were identified.

Thanks to our high spatial resolution, we could determine precisely on which annuli rings and wedges polar angles the stimuli used in the D4 or D8 task fall, and thus identify the expected spatial position of the corresponding brain activations to the targets of the peripheral detection tasks. We thus selected 4 pairs (one per position on our reference 4-positions ($6\sqrt{2}$, $6\sqrt{2}$), ($-6\sqrt{2}$, $6\sqrt{2}$), ($-6\sqrt{2}$, $-6\sqrt{2}$) or ($6\sqrt{2}$, $-6\sqrt{2}$), **Figure 1, B**) of annuli rings and wedges. We determined these pairs based on their eccentricity and angle, matching the target locations in task D4. Once we identified the annuli rings and wedges of interest, we extracted the corresponding contrast from a first-level statistical batch obtained with SPM12 (Wellcome Department of Imaging Neuroscience, London; www.fil.ion.ucl.ac.uk/spm) (Ashburner et al., 1994) on the smoothed pre-processed data. Head motion and eye movements were included as covariate of no interest and we used a hemodynamic response function (HRF) specific to our contrast agent (MION) to fit the modulation of the signal (Leite et al., 2002; Vanduffel et al., 2001). The ROI selections was done taking the activation peaks of the contrast *annuli or wedges of interest vs fixation* at the statistical threshold of $p < 0.05$ (t-score = 4,6) corrected for multiple comparison using family-wise error correction (FWE). Once obtained, we masked the annuli ROI by the corresponding wedge ROI and displayed the contours of the obtained conjunction. This analysis was performed on both monkeys and the three different conditions (T1, T2 and T3).

2. ROI definition and percent signal change

Data from the 4-quadrants peripheral detection task (D4) and from the 8-quadrants peripheral detection task (D8) were pre-processed as described in chapter II methods. The analysis of this task were performed with SPM12. Fixed effects of the Generalized Linear Model (GLM) were the different target positions in the four quadrants of the screen, i.e. left-up, right-up, left-down, right-down. Head motion and eye movements were included as covariate of no interest and we used a specific MION HRF to fit the modulation of the signal. This analysis was performed on both monkeys and the three different conditions (T1, T2 and T3). The ROIs selections was done taking the activation peaks of the contrast

target location vs fixation at the statistical threshold of $p < 0.05$ corrected for multiple comparison using FWE correction. ROIs were defined for each position and at each time-point as 3mm diameter spheres centered around the local peak of activation. Once we validated the localization of each ROI thanks to the conjunction of annuli and wedges coordinates specific of this time-point, macaque and position (**Figure 9**), we extracted the activity profiles with the Marsbar SPM toolbox (<http://marsbar.sourceforge.net>). The mean percent of signal change (%SC, +/- standard error of the mean across runs) was calculated for each condition (the targets positions) relative to the fixation baseline. We also calculated activation volumes, by measuring the total number of activated voxels with the activation peak ROI given by the target location vs. fixation contrast. This method is used to quantify fMRI activation (Al-Asmi et al., 2003; Krasnow et al., 2003; Hou et al., 2006).

3. Statistical analysis

%SC were compared using Wilcoxon non-parametric paired tests.

Results

1. Retinotopic mapping

Our first hypothesis regarding this study was that global topographical retinotopic mapping would not change according to training or coupled with fluoxetine administration, boundaries between visual cortical regions being defined early on during brain development and early life visual critical period. Hence, our aim is here to assess of the repeatability of the retinotopic mapping across time.

1. Eccentricity mapping

The eccentricity map provides information of the spread of visual areas from V1 to MT. On the control condition T1 (**Figure 2**), we first note that although the maps quality is suboptimal, due to a weak coverage of V1 (from blue-central field of view-, to yellow on the central circular color map), the retinotopic map of eccentricity is well localized in visual areas for both monkeys and on both hemispheres.

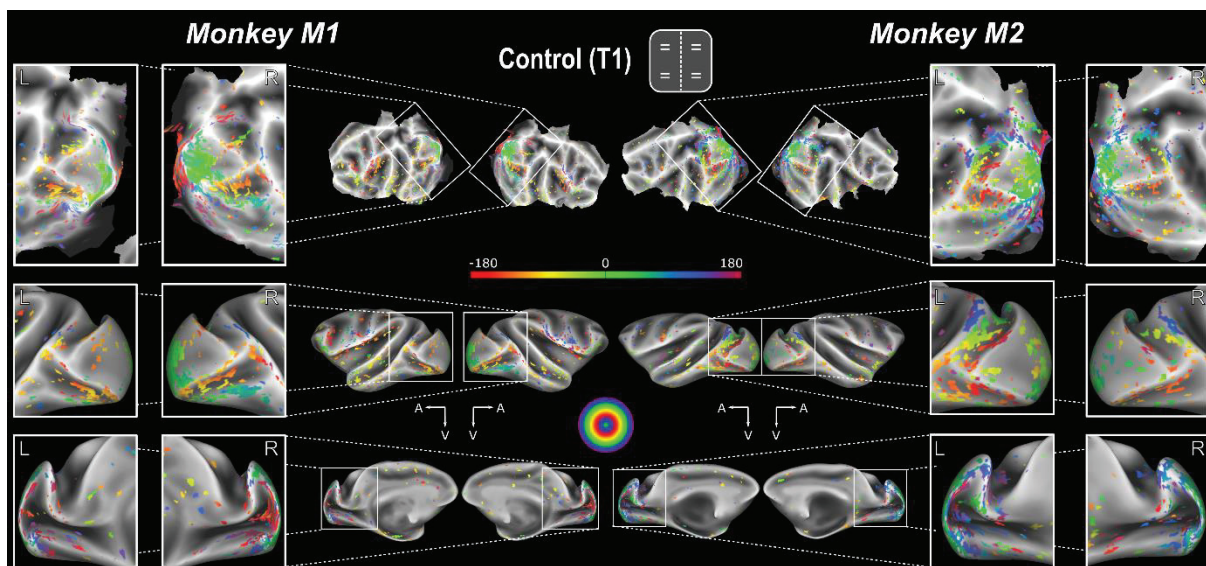


Figure 2: Retinotopic organization in V1 to MT areas as a function of eccentricity in condition T1 for monkey M1 and monkey M2 in their respective native spaces. The following indications are valid for all eccentricity retinotopic maps figures. Both hemispheres are shown. The upper panel is a flat map representation of the projected retinotopy on the cortical surface. The middle panel is a lateral view of this projection and the lower panel is a medial view of it. Left most and right most panels represent enlarged view of the central maps, centered on the occipital cortex. Each annulus circle is represented by a different color on the central circular color wheel, and finds its correspondence on the brain surfaces. Presented scales are t-scores.

We then repeated the mapping after the reward-based training in T2 condition (**Figure 3**). The maps of monkey M2 are still problematic. For monkey M1, we see more clearly the central field of view, (here from red to yellow on the central circular color map) on V1, then extending to higher order visual areas (from green to dark purple on the central circular color map).

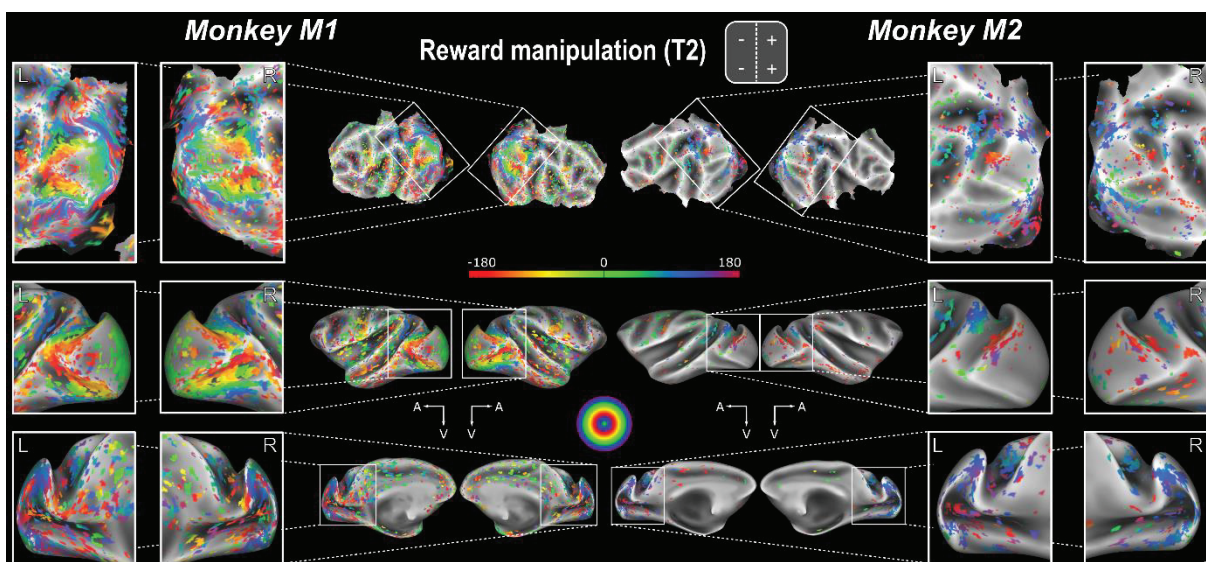


Figure 3: Retinotopic organization in V1 to MT areas according to the eccentricity in condition T2 for monkey M1 and monkey M2 in their respective native spaces. All as in Figure 2.

Finally, when measuring the eccentricity retinotopic mapping in T3 condition, we obtain a well-defined result (**Figure4_AnnuliT3**). We here see that for both monkeys, the whole panel of the central circular color map is covered. It indeed extends from V1 to MT area. On the medial view, we can note the delineation from green to blue that corresponds to the visual eccentricity that we defined in our active tasks. Activations for these targets should hence be within these delineations. Moreover, we also note that the eccentricity maps differ between subjects. In the following, we will assess the repeatability of our retinotopic map boundaries, based on V1, V2 and V3 areas delineation.

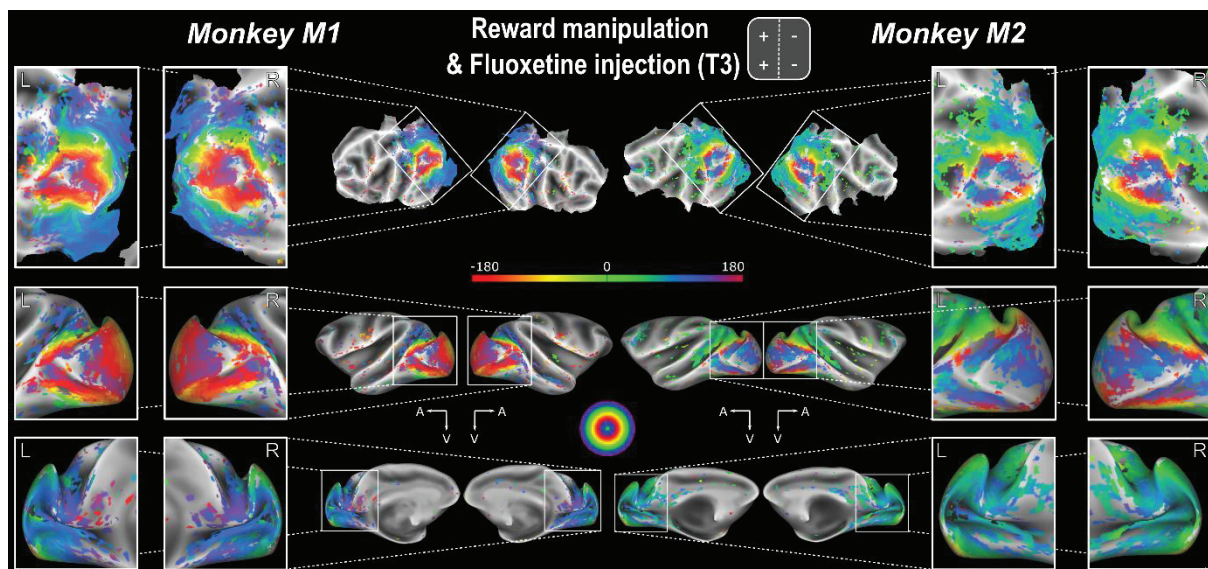


Figure 4: Retinotopic organization in V1 to MT areas according to the eccentricity in condition T3 for monkey M1 and M2 in their respective native spaces. All as in Figure2

2. Polar angle mapping

We here display the polar angle retinotopic mapping for both monkeys at each time-points T1, T2 and T3. The stimulations on the left hemifield are projected on the right hemisphere and conversely. The upper visual field stimulations are displayed ventrally and conversely (**Figure 5**). This fine categorization allowed us to define visual areas V1, V2 and V3 thanks to the meridians.

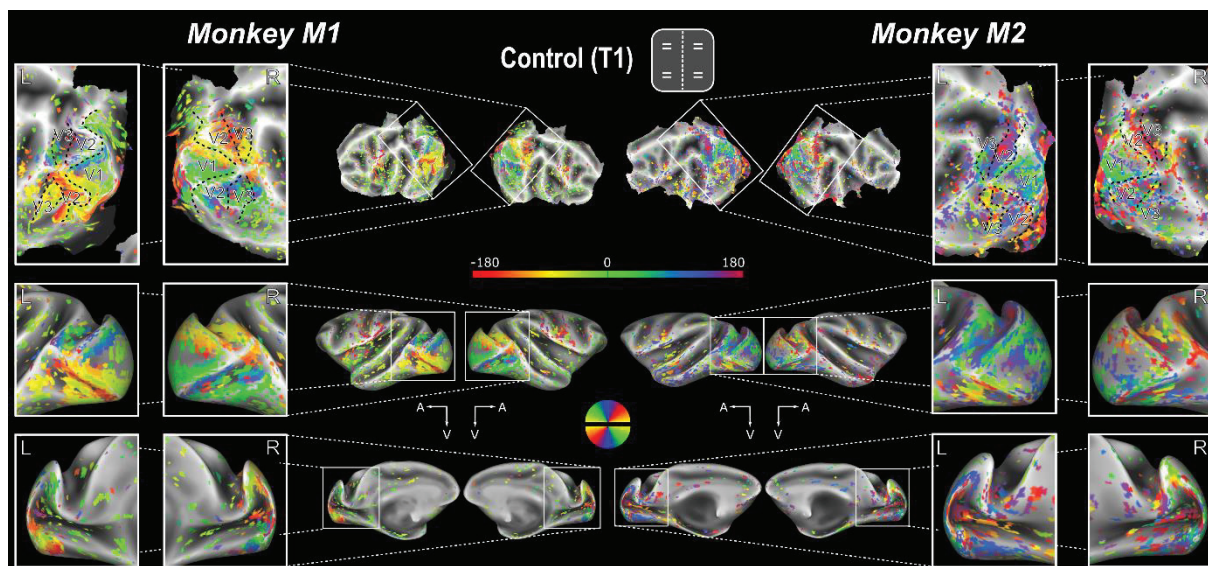


Figure 5: Retinotopic organization in V1 to MT areas as a function of polar angles in condition T1 for monkeys M1 and M2 in their respective native spaces. The following indications are valid for all polar angles retinotopic maps figures. Both hemispheres are shown. The upper panel is a flat map representation of the projected retinotopy on the cortical surface. The middle panel is a lateral view of this projection and the lower panel is a medial view of it. Left most and right most panels represent enlarged view of the central maps, centered on the occipital cortex. Each wedge is represented by a different color on the central circular color wheel, and finds its correspondence on the brain surfaces. Black dashed line on the flat maps are a custom V1/V2/V3 areas delineation according to the retinotopic mapping. Presented scales are t-scores.

Although less extended in peripheral visual areas as we saw from the eccentricity mapping in T2, the polar angle retinotopic mapping of T2 condition (**Figure 6**) allowed us to delineate our visual areas of interest both ventrally and dorsally.

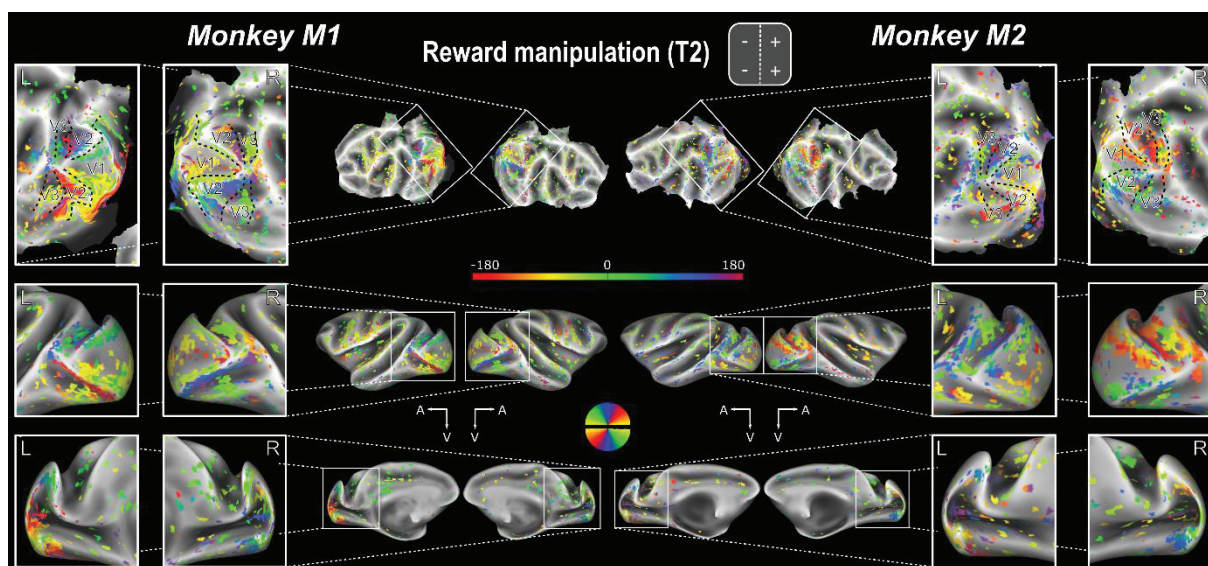


Figure 6: Retinotopic organization in V1 to MT areas according to polar angles in condition T2 for monkeys M1 and M2 in their respective native spaces. All as in Figure 5.

Again, on T3 condition (**Figure 7**), the mapping was well defined and the delineation are clearer for both monkeys. To this point, we noted no particular hemispheric retinotopic mapping difference due to the training.

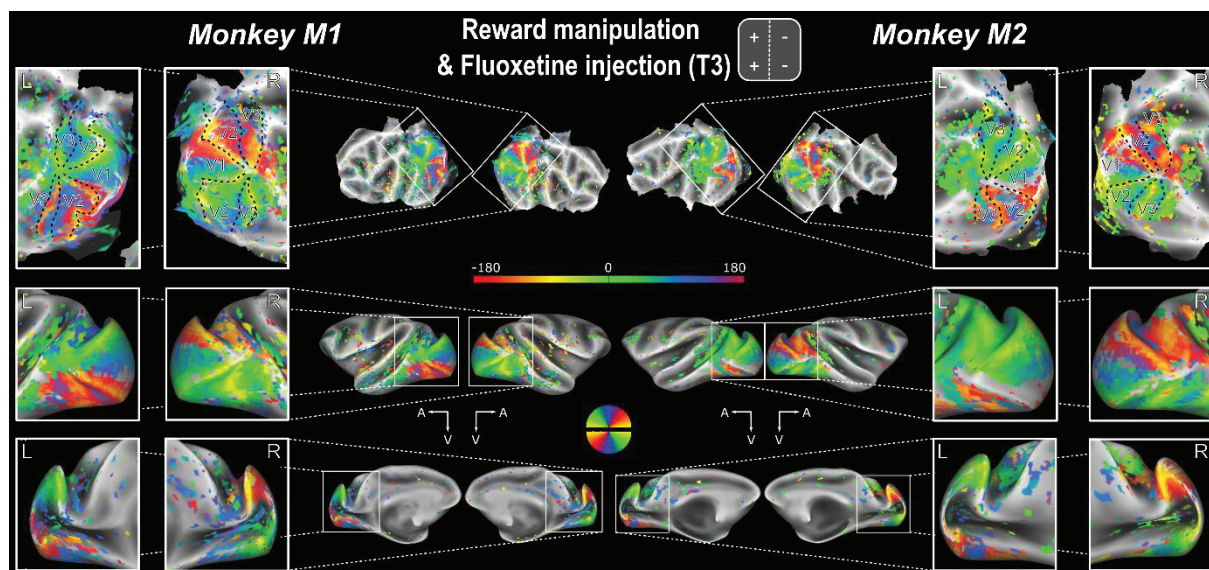


Figure 7: Retinotopic organization in V1 to MT areas according to polar angles in condition T3 for monkeys M1 and M2 in their respective native spaces. All as in Figure 5.

The aforementioned delineation comparison across time-points (**Figure 8**) show no pattern of difference and all areal limits are very stable in time. This is expected due to the fact that these areas are defined early on in brain development and early visual experience. Additionally, this speaks for the high repeatability of our experimental observations.

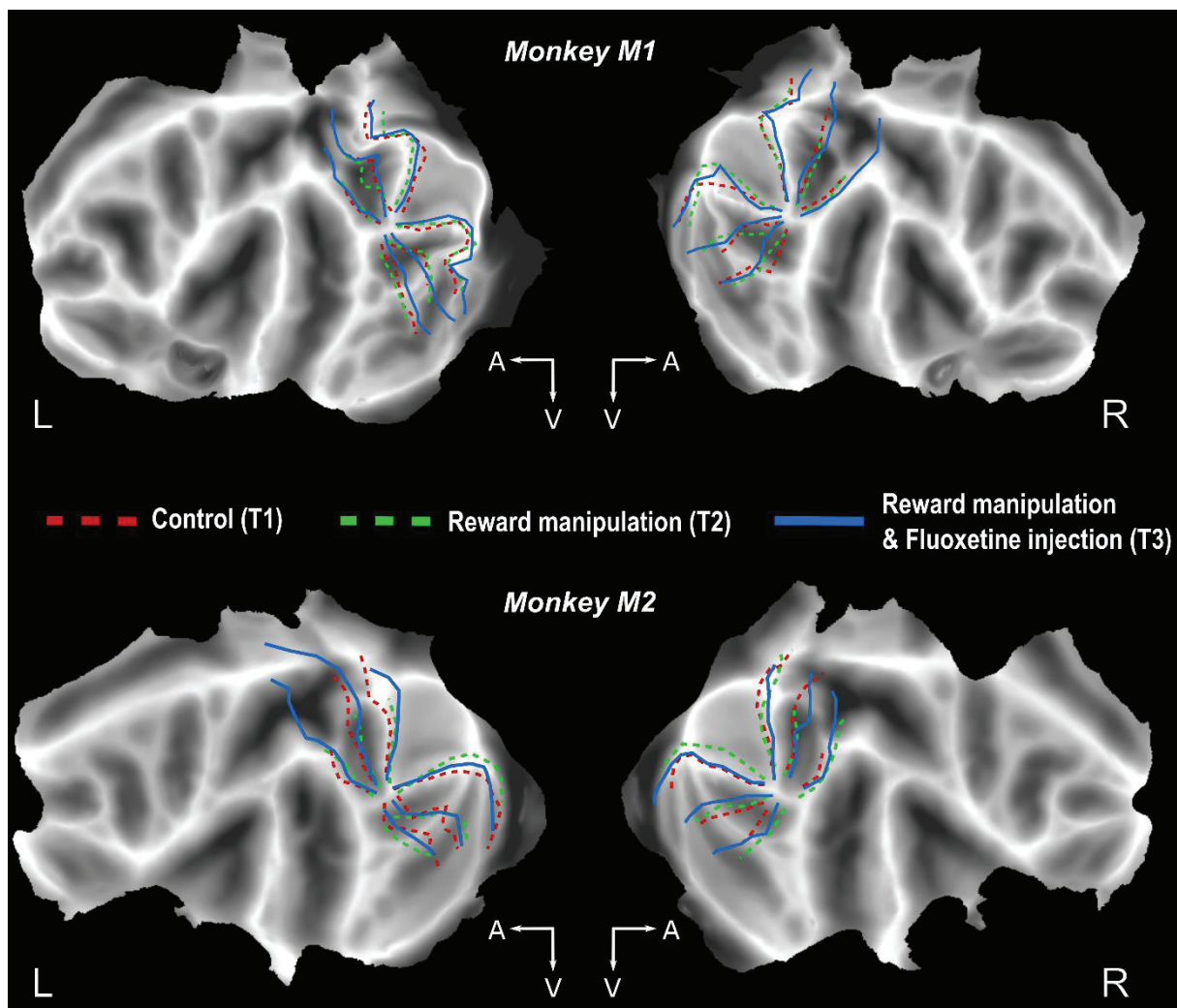


Figure 8: Flat maps representations of conditions comparison (T1, T2 and T3) of V1/V2/V3 delineation of the brain cortical surface established thanks to the polar angle retinotopic mapping for both monkeys M1 and M2 in their respective native spaces and on both hemispheres. Red dashed lines represent delineation of the T1 control condition. Green dashed lines represent delineation of the T2 reward manipulation condition. Blue continue line represent delineation of the T3 reward manipulation coupled to fluoxetine injection.

2. Changes in percent signal changes as a function of reward-based learning

We here present the percent signal changes (%SC) induced by target onset in the peripheral detection tasks, relative to periods of fixation (**Figure 9**). Figure 9, represents %SC for each given time-point, each target position and each monkey, for both target detection tasks (D4 and D8). Next to each %SC histogram, a medial view of the cortical surface of each monkey in their respective native space shows the contours of the dedicated conjunction (in black) and activations induced by the appearance of each peripheral target of interest (in red for D4 and in blue for D8). When the conjunction contour was not statistically significant, we used another time-point conjunction contour. The center of ROIs used to calculate %SC were taken on the localization of the activation. Note that all the %SC displayed here and

significantly different from the fixation baseline at all four locations (up left, UL; up right, UR; down left, DL; down right, DR), for both monkeys (**M1**: Wilcoxon two-sided non-parametric test: T1, D4: UL: $Z=1,889$, $p=0,049$, $n=30$; UR: $Z=3,783$, $p < 0,001$, $n=30$; DL: $Z=2,363$, $p=0,018$, $n=30$; DR: $Z=2,837$, $p=0,005$, $n=30$. T2, D4: UL: $Z=3,179$; $p=0,001$; $n=13$; UR: $Z=3,891$, $p < 0,001$, $n=13$; DL: $Z=2,466$, $p=0,014$, $n=13$; DR: $Z=3,179$, $p=0,001$, $n=13$. T2, D8, for the same quadrants as in D4: UL: $Z=2,418$, $p=0,016$, $n=18$; UR: $Z=4,853$, $p < 0,001$, $n=18$; DL: $Z=4,853$, $p < 0,001$, $n=18$; DR: $Z=3,636$, $p < 0,001$, $n=18$. T3, D4: UL: $Z=4,612$, $p < 0,001$, $n=20$; UR: $Z=4,036$, $p < 0,001$, $n=20$; DL: $Z=2,877$, $p=0,004$, $n=20$; DR: $Z=4,036$, $p < 0,001$, $n=20$. T3, D8, for the same quadrants as in D4: UL: $Z=4,244$, $p < 0,001$, $n=18$; UR: $Z=3,027$, $p=0,003$, $n=18$; DL: $Z=2,418$, $p=0,016$, $n=18$; DR: $Z=4,244$, $p < 0,001$, $n=18$. **M2**: T1, D4: UL: $Z=1,841$, $p=0,033$, $n=9$; UR: $Z=2,256$, $p=0,012$, $n=9$; DL: $Z=1,989$, $p=0,023$, $n=9$; DR: $Z=2,044$, $p=0,021$, $n=9$. T2, D4: UL: $Z=3,190$, $p=0,001$, $n=10$; UR: $Z=2,383$, $p=0,017$, $n=10$; DL: $Z=2,383$, $p=0,017$, $n=10$; DR: $Z=2,383$, $p=0,017$, $n=10$. T2, D8, for the same quadrants as in D4: UL: $Z=3,027$, $p=0,003$, $n=18$; UR: $Z=3,027$, $p=0,003$, $n=18$; DL: $Z=3,635$, $p < 0,001$, $n=18$; DR: $Z=3,635$, $p < 0,001$, $n=18$. T3, D4: UL: $Z=2,059$, $p=0,039$, $n=19$; UR: $Z=2,059$, $p=0,039$, $n=19$; DL: $Z=3,245$, $p=0,001$, $n=19$; DR: $Z=3,245$, $p=0,001$, $n=19$. T3, D8, for the same quadrants as in D4: UL: $Z=2,877$, $p=0,004$, $n=20$; UR: $Z=4,034$, $p < 0,001$, $n=20$; DL: $Z=2,299$, $p=0,022$, $n=20$; DR: $Z=4,612$, $p < 0,001$, $n=20$).

On the first time-point T1 (**Figure 9, A**), we computed %SC for the D4 task for both monkeys. For both monkeys, activations were either located into the conjunction or close to it, at the exception of the right hemisphere ventral activation for M1. We report no significant difference of %SC between the four quadrants for both monkeys at T1, nor between the up-down locations within each hemisphere (Wilcoxon two-sided non-parametric test: M1: UL-DL: $Z=0,547$, $p=0,582$; UR-DR: $Z=0,243$, $p=0,810$. M2: UL-DL: $Z=0,859$, $p=0,390$; UR-DR: $Z=0,644$, $p=0,522$) or right-left differences (M1: UL-UR: $Z=0,679$, $p=0,496$; DL-DR: $Z=0,075$, $p=0,944$. M2: UL-UR: $Z=1,643$, $p=0,101$; DL-DR: $Z=1,303$, $p=0,194$).

On the second time-point T2 (**Figure 9, B**), the right hemifield was overall more rewarded than the left hemifield. On this time point, the D4 activation in the ventral right hemisphere of M2 was not significant (dashed lines). We thus positioned the center of our ROI on the activation in the corresponding annuli/wedge conjunction, indicated by the red arrow. %PSC were not significantly different between right hemisphere and left hemisphere ventral ROIs, which map onto the upper visual field left and right targets in both monkeys (M1: UL-UR: $Z=1,293$, $p=0,197$. M2: UL-UR: $Z=0,314$, $p=0,787$). However, there was a significant difference between %SC of D4 right hemisphere and left hemisphere dorsal ROIs, which map onto the lower visual field left and right targets in both monkeys (M1: DL-DR: $Z=2,277$, $p=0,023$. M2: DL-DR: $Z=2,045$, $p=0,021$).

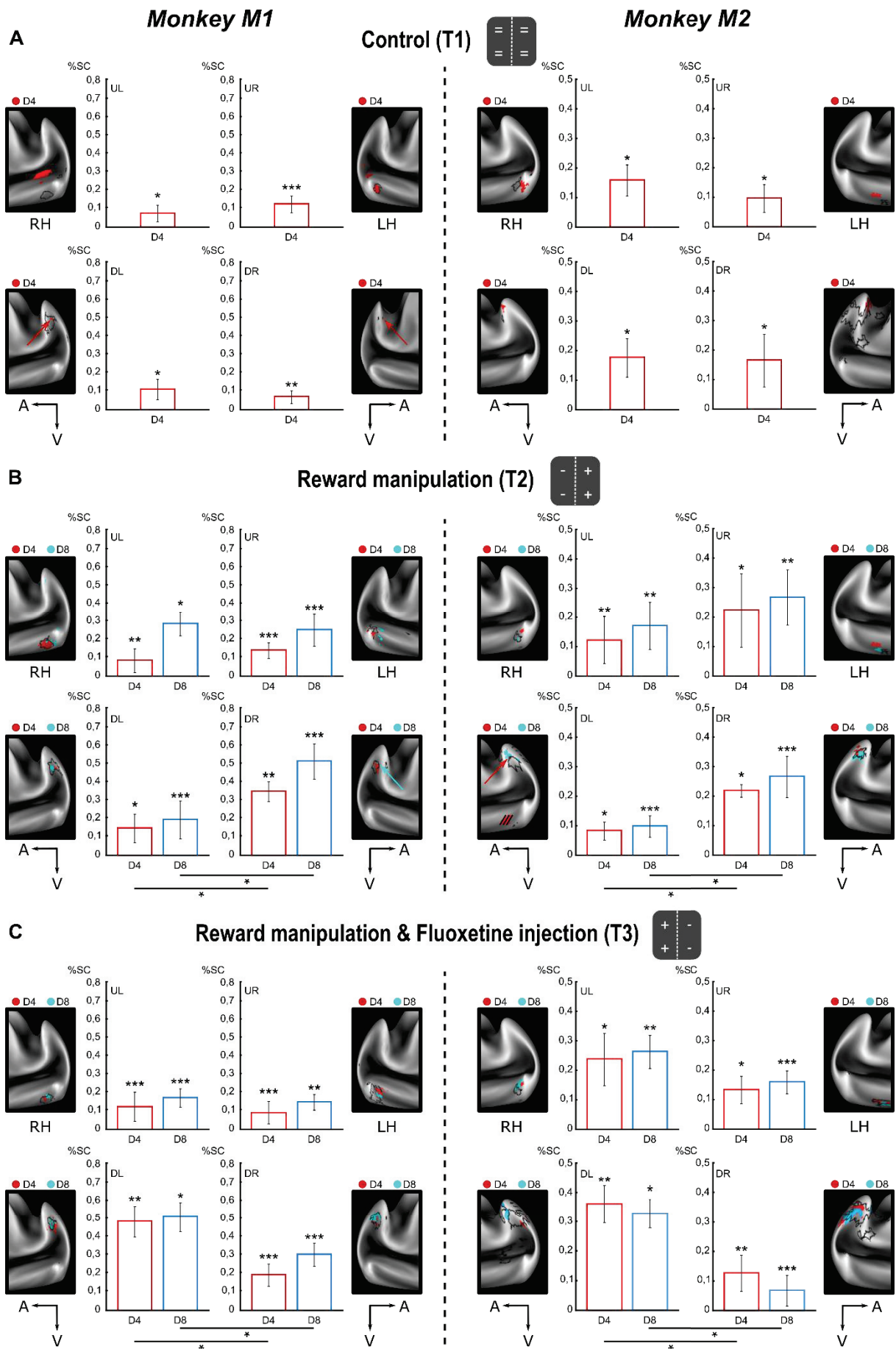


Figure 9: %SC and their corresponding ROIs on medial inflated brain view of the occipital cortex for monkeys M1 and M2. ROIs were defined on cortical activations to target onset relative to fixation, in either D4 task (in red) or in D8 task (in blue/cyan). Conjunctions of annuli rings and wedges at D4 target positions are indicated by their contours in black line. %SC data are presented as median +/- s.e. (A) For control, condition T1. (B) For reward manipulation, condition T2. (C) For reward manipulation coupled to fluoxetine injection, condition T3. Statistical significance is represented as follows: ***, $p < 0.001$; **, $p < 0.01$; *, $p < 0.05$; n.s., $p > 0.05$.

We report the same results regarding the D8 task (M1: UL-UR: $Z=0,467$, $p=0,638$; DL-DR: $Z=1,778$, $p=0,037$. M2: UL-UR: $Z=0,292$, $p=0,772$; DL-DR: $Z=1,709$, $p=0,044$). In both D4 and D8 tasks and for both monkeys, %SC is thus significantly higher in the left dorsal hemisphere (lower right visual field, the most rewarded hemifield) than in the right dorsal hemisphere (lower left visual field, the least rewarded hemifield).

On the third time-point T3 (**Figure 9, C**), the left hemifield was overall more rewarded and the right hemifield was overall less rewarded. %PSC were not significantly different between right hemisphere and left hemisphere ventral ROIs, which correspond to the upper visual fields left and right targets in both monkeys (M1: UL-UR: $Z=1,293$, $p=0,098$. M2: UL-UR: $Z=0,345$, $p=0,363$). However, as in T2 condition, there was a significant difference between %SC of D4 right hemisphere and left hemisphere dorsal ROIs, which correspond to the lower visual fields left and right targets in both monkeys (M1: DL-DR: $Z=1,714$, $p=0,044$. M2: DL-DR: $Z=1,717$, $p=0,043$). We report the same results regarding the D8 task (M1: UL-UR: $Z=0,152$, $p=0,440$; DL-DR: $Z=1,782$, $p=0,037$. M2: UL-UR: $Z=0,568$, $p=0,284$; DL-DR: $Z=1,676$, $p=0,046$). In both D4 and D8 tasks and for monkeys, %SC is thus significantly higher in the right dorsal hemisphere (lower left visual field, the most rewarded hemifield) than in the left dorsal hemisphere (lower right visual field, the least rewarded hemifield).

3. Effect of fluoxetine on reward-based learning effects on cortical activations

Given the nature of the tasks, i.e., the spatial effect, we also looked at the %SC differences between D4 and D8 tasks for each position for T2 and T3 conditions in both monkeys (**Figure 10, A**). A three-way ANOVA on target position x condition x monkey indicates a significant effect of condition and position with a position x condition interaction for both monkeys in D4 task (monkey, $F(1,9) = 3,223$, $p=0,106$; condition, $F(1,9)= 7,223$, $p=0,025$; target position, $F(3,27)= 5,547$, $p=0,004$; monkey x condition, $F(1,9) = 4,523$, $p=0,062$; monkey x target position, $F(3,27) = 1,787$, $p=0,173$; condition x target position, $F(3,27) = 4,567$, $p=0,010$; monkey x condition x target position, $F(3,27) = 3,362$, $p=0,033$) and in D8 task (monkey, $F(1,17) = 1,490$, $p=0,239$; condition, $F(1,17)= 5,926$, $p=0,026$; target position, $F(3,51)= 3,428$, $p=0,024$; monkey x condition, $F(1,17) = 3,441$, $p=0,081$; monkey x target position, $F(3,51) = 0,998$, $p=0,401$; condition x target position, $F(3,51) = 2,831$, $p=0,047$; monkey x condition x target position, $F(3,51) = 2,945$, $p=0,041$).

The main condition effect reflects the fact that under fluoxetine %SC is increased as can be seen in **Figure 9**. Indeed, we report a significant difference of %SC between T2 and T3 conditions for both D4 and D8 tasks. This observation thus accounts for a reward- and spatial-independent effect of fluoxetine on V2 activations.

In addition, fluoxetine effect statistically interacts with the positions (**Figure 10, A**). Post-hoc Wilcoxon two-sided non-parametric test indicates an increase of %SC for the most rewarded position in the low visual field in D4 task for the T3 condition compared to T2 condition (M1: DR_{T2-T3}: $Z=2,027$, $p=0,021$; M2: DR_{T2-T3}: $Z=1,621$, $p=0,052$). And, only for M1 on D8 task, a decrease of %SC for the least rewarded position in the upper visual field accompanied by a %SC increase for the least rewarded position in the lower visual field for the T3 condition compared to T2 condition (M1: UL_{T2-T3}: $Z=1,885$, $p=0,030$; UD_{T2-T3}: $Z=2,286$, $p=0,011$). We thus showed here that in addition to a general effect, fluoxetine also increases %SC of the ROI coding for the most rewarding position of the lower visual field (when comparing T3 to T2 condition).

To understand these specific local tasks effects, we further quantified the size of the D4 and D8 activations at each of the four same target positions (**Figure 10, B**). Indeed, although %SC were calculated from spherical ROIs of 3mm of diameter centered on the cortical activation induced by the target displaying, those activations were not all of the same size (D4 and D8 activations by targets are presented in red and blue, medial inflated brain view in **Figure 9**). Given that each activation ROI was selected by taking the activation peaks of the contrast target location vs fixation at the statistical threshold of $p<0.05$ corrected for multiple comparison using FWE correction, we thus have one value per position, per condition, per task. Nonetheless, we can still observe that in T3 condition, activation ROIs contain more voxels for the lower visual field than in T2 condition. There is a task dependent effect as well here, for increases in the T3 condition compared to the T2 condition are greater in the D4 task. We here observe that fluoxetine has a task dependent effect and also that it appears to affect more ROIs that correspond to the lower field of view. In addition, the enlarged activation size suggests a degraded spatial resolution as observed at the behavioral level, as cortex might ambiguously code for multiple overlapping information (the previously encoded location prior to the reward-based learning, as well as the novel positions acquired through learning). This observation will have to be further consolidated.

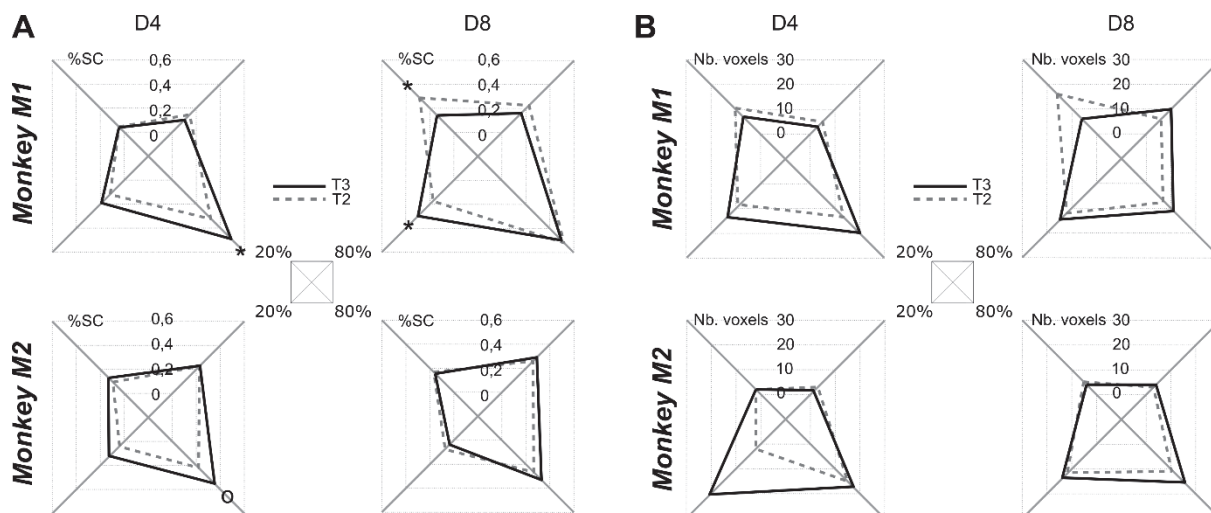


Figure 10: %SC comparison and number of voxels comparison between T2 and T3 condition in D4 and D8 tasks for both monkeys, on the least and most rewarded positions. T2 condition is represented in gray dashed lines. T3 condition is represented in black full lines. In order to compare both conditions, we consider the positions according to their assigned reward outcome, not their spatial localization. Thus T3 maps are left-right flipped to match T2 reward manipulation maps. (A) Representation of %SC according to the stimulus position in D4 and D8 tasks. %SC data are presented as median and were extracted from 3mm of diameter spherical ROIs centered on the cortical activation induced by the target displaying. Statistical significance is represented as follows: ***, $p < 0.001$; **, $p < 0.01$; *, $p < 0.05$; o, $p > 0.06$; n.s., $p > 0.05$. (B) Representation of number of voxels per activations induced by targets displaying in D4 and D8 tasks.

Discussion

1. Reward-based alteration of the spatial priority map does not alter retinotopic maps

We can first report, as expected, that each hemifield has a contralateral hemifield representation (Jeffery, 2001) and that, regardless of our maps quality, the eccentricity representation goes from the occipital pole (fovea) to the anterior calcarine (periphery). Moreover, the foveal region is represented by a larger zone in V1 than in the peripheral regions, which is also referred to as the cortical magnification (for review, see Wandell and Winawer, 2011). We can also note that compared to V1 and V2 areas, V3 ranges on a small cortical surface (Gattass et al., 1988). Thus, V1, V2 and V3 areas delineations are in agreement with previous MRI studies (Van Essen et al., 1984; Fize et al., 2003; Janssens et al., 2014; Arcaro and Livingstone, 2017) with distinct anatomical locations for dorsal and ventral parts for V2 and V3 areas (Lyon and Kaas, 2002). We also report an inter-individual variability on V1 borders between macaques, thus validating our protocol of modulating the peripheral visual field in V2 areas. Indeed, V1 borders observed with phase-encoded retinotopic mapping (that we also referred here as average phase mapping) are not likely to be reproducible across subjects (Dumoulin et al., 2003; Stensaas et al., 1974), due to differential development during the visual critical period.

We thus here validated the retinotopic maps of striate and extrastriate areas according to the literature, and showed that we reproduced these results across the conditions. This is in agreement with our prediction that we were not expecting to observe global topographic deformation or contours variations due to our reward-based alteration of the spatial priority map manipulation, but rather local modulations of levels of activations.

2. Dorsal ROIs activations modulation following reward manipulation

Thanks to imaging and electrophysiological techniques, it is well-known that spatial attention increases brain activations in the contralateral hemisphere to the displayed target (Heinze et al., 1994; Mangun et al., 1993; Vandenberghe et al., 1996; Woldorff et al., 1997), and more specifically in the extrastriate cortex (Clark and Hillyard, 1996). This effect can be enhanced with training, based on the introduction of spatial reward biases, such as the one that we induced in T2 and T3 conditions. When comparing the %SC of all D8 task positions, in the ROI specific for the most rewarded target (80% HR) of the low visual field, we observed first that the activation strength is very specific to the ROI position. Indeed, our reward-based training allowed precise identification of the target in space according to its value (Chelazzi et al., 2013, 2014) and the D8 task permitted to verify it in the present context. We here first observed that in agreement with our findings in chapter II, study n°2, and very interestingly, local differences between two hemispheres of activations strength only occurred in the dorsal V2 area, the %SC being higher for areas corresponding to the most rewarding positions than the areas corresponding to the least rewarding positions. This effect could be related to the behavioral biases reported in chapter I, in the lower visual hemifield (lower hemifield bias in the luminance perception performances on the peripheral detection task (Gacoïn and Ben Hamed, 2022)). This lower hemifield functional bias could also be related to the enhanced functional connectivity in the dorsal fronto-occipital visual pathway, and decrease of the functional connectivity in the ventral fronto-occipital visual pathway. These hypotheses remain to be consolidated. .

3. Increased task specific training effect due to fluoxetine administration

We have here observed a major influence of the reward on the cortical activity, at very precise positions and seemingly long lasting since they appear for tasks that present no particular reward bias. Moreover, we have observed that %SC and activation volume profiles follow the same trend. While these two metrics correlate, they are also useful to measure GABA concentration in a given region (Bhattacharyya et al., 2017). There is an inverse correlation between GABA concentration and fMRI signal amplitude in the visual cortex, thus the higher the %SC, the lower the GABA concentration (Muthukumaraswamy et al., 2009; Donahue et al., 2010; Violante et al., 2013) and conversely when observing the activation volume (Bhattacharyya et al., 2017). We propose, since the %SC and activation

volume are stronger in the dorsal V2 than in the ventral V2, that there is a lower concentration of GABA receptors in the dorsal part of the visual cortex than in its ventral part (for GABA_A receptors, Kaulen et al., 2022). In addition, we saw that in T3 condition, thus the reward-based training with fluoxetine administration, activation volume increased in the V2 dorsal part (thus the lower visual field) and tended to decrease in the ventral V2 part (thus the higher visual field). Hence, still reasoning on this anticorrelation between GABA concentration and activation volume, we propose that this effect can be accounted for, by the fact that fluoxetine decreases extracellular GABA levels (Vetencourt et al., 2008; Baroncelli et al., 2011, Beshara et al., 2016; Santana et al., 2004). Consequently, we here observe an enhanced cortical excitability through a reduction of global inhibition in the dorsal V2 part. The excitation/inhibition balance in favor of excitation is stronger in the dorsal V2 part.

We propose that this excitability favored by fluoxetine administration coupled to the reward-based training is responsible of the increased %SC in T3 condition compared to the T2 condition toward the most rewarding target in the low visual hemifield. This effect appears to be responsible for a greater sensitivity for reward, as SSRI enhances reward processing in healthy adults (Macoveanu, 2014; McCabe et al., 2010; Scholl et al., 2017), an effect that we also observe in chapter I, study n°1 (Gacoin and Ben Hamed, 2022). Interestingly, %SC increasing for the high rewarded position in the lower visual field is more specific to D4 task than D8 task in both monkeys. We have previously shown (Gacoin and Ben Hamed, 2022) that fluoxetine induced a degraded spatial resolution in the visual cortex, and we measured this effect specifically in the lower visual field. Indeed, we here observed a decreased GABA concentration on the dorsal V2 part. While the increase of cortical GABA levels are known to reduce intrinsic noise in the visual cortex (Hammett et al., 2020), we can expect that conversely, a decrease of cortical GABA level increases this intrinsic noise. Thus increases %SC in T3 condition in the D4 task, match degraded spatial resolution behavioral observation. Another hypothesis would be that an increased activation volume would decrease spatial resolution due to enlarged receptive fields and thus a less precise for that location. It is important to note here that these effects are not general effects of fluoxetine but rather are selectively observed at spatial locations subject to a behaviorally-induced learning-based plasticity.

Conclusion

Overall, we showed in the present study that although the long-lasting reward-based manipulation of spatial attention does not deform the retinotopic mapping in V1, V2 and V3 areas, the levels of activations at the very localization of cortical activation of peripheral targets are higher in the dorsal V2 areas for the most rewarded hemifield than it is for the low rewarded hemifield. We here hypothesized that, thanks to the natures of D4 and D8 tasks, we could observe the neural effect of degraded spatial resolution induced by fluoxetine administration that we observed behaviorally. Indeed, by using the %SC and activation metrics, which show an increase for the dorsal V2 regions that activates

in response to the display of low visual field target, we were able to conclude to a decreased cortical GABA level in the dorsal visual field for the T3 condition, in comparison with the T2 condition. Due to the increased excitability, this effect was exacerbated for the most rewarding position, and explains a degraded spatial resolution for the D4 task. These effects are not general effects of fluoxetine but are rather selectively observed at spatial locations subject to a behaviorally induced learning-based plasticity.

References

- Al-Asmi, A., Bénar, C.-G., Gross, D.W., Khani, Y.A., Andermann, F., Pike, B., Dubeau, F., Gotman, J., 2003. fMRI Activation in Continuous and Spike-triggered EEG–fMRI Studies of Epileptic Spikes. *Epilepsia* 44, 1328–1339. <https://doi.org/10.1046/j.1528-1157.2003.01003.x>
- Alvarez, I., de Haas, B., Clark, C.A., Rees, G., Schwarzkopf, D.S., 2015. Comparing different stimulus configurations for population receptive field mapping in human fMRI. *Front. Hum. Neurosci.* 9. <https://doi.org/10.3389/fnhum.2015.00096>
- Arcaro, M.J., Livingstone, M.S., 2017. Retinotopic Organization of Scene Areas in Macaque Inferior Temporal Cortex. *J. Neurosci.* 37, 7373–7389. <https://doi.org/10.1523/JNEUROSCI.0569-17.2017>
- Arcaro, M.J., Pinsk, M.A., Li, X., Kastner, S., 2011. Visuotopic Organization of Macaque Posterior Parietal Cortex: A Functional Magnetic Resonance Imaging Study. *J. Neurosci.* 31, 2064–2078. <https://doi.org/10.1523/JNEUROSCI.3334-10.2011>
- Ashburner, J., Barnes, G., Chen, C.-C., Daunizeau, J., Flandin, G., Friston, K., Gitelman, Glauche, V., Henson, R., Hutton, C., Kiebel, S., Kilner, J., Litvak, V., Mattout, J., Moran, R., Penny, W., Phillips, C., Rosa, M., Klaas, S., 1994. Statistical Parametric Mapping.
- Bhattacharyya, P.K., Phillips, M.D., Stone, L.A., Lowe, M.J., 2017. Activation volume vs BOLD signal change as measures of fMRI activation – its impact on GABA – fMRI activation correlation. *Magn Reson Imaging* 42, 123–129. <https://doi.org/10.1016/j.mri.2017.06.009>
- Bourne, J.A., Morrone, M.C., 2017. Plasticity of Visual Pathways and Function in the Developing Brain: Is the Pulvinar a Crucial Player? *Front. Syst. Neurosci.* 11. <https://doi.org/10.3389/fnsys.2017.00003>
- Brewer, A.A., Press, W.A., Logothetis, N.K., Wandell, B.A., 2002. Visual Areas in Macaque Cortex Measured Using Functional Magnetic Resonance Imaging. *J. Neurosci.* 22, 10416–10426. <https://doi.org/10.1523/JNEUROSCI.22-23-10416.2002>
- Bridge, H., 2011. Mapping the visual brain: how and why. *Eye (Lond)* 25, 291–296. <https://doi.org/10.1038/eye.2010.166>
- Chang, L.-H., Yotsumoto, Y., Salat, D.H., Andersen, G.J., Watanabe, T., Sasaki, Y., 2015. Reduction in the retinotopic early visual cortex with normal aging and magnitude of perceptual learning. *Neurobiology of Aging* 36, 315–322. <https://doi.org/10.1016/j.neurobiolaging.2014.08.025>
- Chelazzi, L., E to inova, J., Calletti, R., Lo Gerfo, E., Sani, I., Della Libera, C., Santandrea, E., 2014. Altering Spatial Priority Maps via Reward-Based Learning. *Journal of Neuroscience* 34, 8594–8604. <https://doi.org/10.1523/JNEUROSCI.0277-14.2014>
- Chelazzi, L., Perlato, A., Santandrea, E., Della Libera, C., 2013. Rewards teach visual selective attention. *Vision Research, Visual Attention 2013 Volume II* 85, 58–72. <https://doi.org/10.1016/j.visres.2012.12.005>

- Clark, V.P., Hillyard, S.A., 1996. Spatial Selective Attention Affects Early Extrastriate But Not Striate Components of the Visual Evoked Potential. *Journal of Cognitive Neuroscience* 8, 387–402. <https://doi.org/10.1162/jocn.1996.8.5.387>
- Cox, R.W., 1996. AFNI: software for analysis and visualization of functional magnetic resonance neuroimages. *Comput. Biomed. Res.* 29, 162–173. <https://doi.org/10.1006/cbmr.1996.0014>
- d’Almeida, O.C., Mateus, C., Reis, A., Grazina, M.M., Castelo-Branco, M., 2013. Long term cortical plasticity in visual retinotopic areas in humans with silent retinal ganglion cell loss. *NeuroImage* 81, 222–230. <https://doi.org/10.1016/j.neuroimage.2013.05.032>
- DeYoe, E.A., Carman, G.J., Bandettini, P., Glickman, S., Wieser, J., Cox, R., Miller, D., Neitz, J., 1996. Mapping striate and extrastriate visual areas in human cerebral cortex. *Proc Natl Acad Sci U S A* 93, 2382–2386.
- Donahue, M.J., Near, J., Blicher, J.U., Jezzard, P., 2010. Baseline GABA concentration and fMRI response. *NeuroImage* 53, 392–398. <https://doi.org/10.1016/j.neuroimage.2010.07.017>
- Dumoulin, S.O., Hoge, R.D., Baker, C.L., Hess, R.F., Achtman, R.L., Evans, A.C., 2003. Automatic volumetric segmentation of human visual retinotopic cortex. *NeuroImage* 18, 576–587. [https://doi.org/10.1016/S1053-8119\(02\)00058-7](https://doi.org/10.1016/S1053-8119(02)00058-7)
- Engel, S.A., Glover, G.H., Wandell, B.A., 1997. Retinotopic organization in human visual cortex and the spatial precision of functional MRI. *Cerebral Cortex* 7, 181–192. <https://doi.org/10.1093/cercor/7.2.181>
- Fize, D., Vanduffel, W., Nelissen, K., Denys, K., d’Hotel, C.C., Faugeras, O., Orban, G.A., 2003. The Retinotopic Organization of Primate Dorsal V4 and Surrounding Areas: A Functional Magnetic Resonance Imaging Study in Awake Monkeys. *J. Neurosci.* 23, 7395–7406. <https://doi.org/10.1523/JNEUROSCI.23-19-07395.2003>
- Gacoin, M., Hamed, S.B., 2022. Fluoxetine degrades luminance perceptual thresholds while enhancing motivation and reward sensitivity. <https://doi.org/10.1101/2022.11.11.516168>
- Gattass, R., Sousa, A.P., Gross, C.G., 1988. Visuotopic organization and extent of V3 and V4 of the macaque. *J. Neurosci.* 8, 1831–1845. <https://doi.org/10.1523/JNEUROSCI.08-06-01831.1988>
- Goodale, M.A., Westwood, D.A., 2004. An evolving view of duplex vision: separate but interacting cortical pathways for perception and action. *Current Opinion in Neurobiology* 14, 203–211. <https://doi.org/10.1016/j.conb.2004.03.002>
- Hammett, S.T., Cook, E., Hassan, O., Hughes, C.-A., Rooslien, H., Tizkar, R., Larsson, J., 2020. GABA, noise and gain in human visual cortex. *Neuroscience Letters* 736, 135294. <https://doi.org/10.1016/j.neulet.2020.135294>
- Heinze, H.J., Mangun, G.R., Burchert, W., Hinrichs, H., Scholz, M., Münte, T.F., Gös, A., Scherg, M., Johannes, S., Hundeshagen, H., Gazzaniga, M.S., Hillyard, S.A., 1994. Combined spatial and temporal imaging of brain activity during visual selective attention in humans. *Nature* 372, 543–546. <https://doi.org/10.1038/372543a0>
- Hou, B.L., Bradbury, M., Peck, K.K., Petrovich, N.M., Gutin, P.H., Holodny, A.I., 2006. Effect of brain tumor neovasculature defined by rCBV on BOLD fMRI activation volume in the primary motor cortex. *NeuroImage* 32, 489–497. <https://doi.org/10.1016/j.neuroimage.2006.04.188>
- Janssens, T., Zhu, Q., Popivanov, I.D., Vanduffel, W., 2014. Probabilistic and Single-Subject Retinotopic Maps Reveal the Topographic Organization of Face Patches in the Macaque Cortex. *Journal of Neuroscience* 34, 10156–10167. <https://doi.org/10.1523/JNEUROSCI.2914-13.2013>
- Jeffery, G., 2001. Architecture of the Optic Chiasm and the Mechanisms That Sculpt Its Development. *Physiological Reviews* 81, 1393–1414. <https://doi.org/10.1152/physrev.2001.81.4.1393>

- Kaulen, N., Rajkumar, R., Régio Brambilla, C., Mauler, J., Ramkiran, S., Orth, L., Sbaihat, H., Lang, M., Wyss, C., Rota Kops, E., Scheins, J., Neumaier, B., Ermert, J., Herzog, H., Langen, K.-J., Lerche, C., Shah, N.J., Veselinović, T., Neuner, I., 2022. mGluR5 and GABAA receptor-specific parametric PET atlas construction—PET/MR data processing pipeline, validation, and application. *Human Brain Mapping* 43, 2148–2163. <https://doi.org/10.1002/hbm.25778>
- Kolster, H., Janssens, T., Orban, G.A., Vanduffel, W., 2014. The Retinotopic Organization of Macaque Occipitotemporal Cortex Anterior to V4 and Caudoventral to the Middle Temporal (MT) Cluster. *J. Neurosci.* 34, 10168–10191. <https://doi.org/10.1523/JNEUROSCI.3288-13.2014>
- Kolster, H., Mandeville, J.B., Arsenault, J.T., Ekstrom, L.B., Wald, L.L., Vanduffel, W., 2009. Visual Field Map Clusters in Macaque Extrastriate Visual Cortex. *J. Neurosci.* 29, 7031–7039. <https://doi.org/10.1523/JNEUROSCI.0518-09.2009>
- Krasnow, B., Tamm, L., Greicius, M.D., Yang, T.T., Glover, G.H., Reiss, A.L., Menon, V., 2003. Comparison of fMRI activation at 3 and 1.5 T during perceptual, cognitive, and affective processing. *NeuroImage* 18, 813–826. [https://doi.org/10.1016/S1053-8119\(03\)00002-8](https://doi.org/10.1016/S1053-8119(03)00002-8)
- Leite, F.P., Tsao, D., Vanduffel, W., Fize, D., Sasaki, Y., Wald, L.L., Dale, A.M., Kwong, K.K., Orban, G.A., Rosen, B.R., Tootell, R.B.H., Mandeville, J.B., 2002. Repeated fMRI Using Iron Oxide Contrast Agent in Awake, Behaving Macaques at 3 Tesla. *NeuroImage* 16, 283–294. <https://doi.org/10.1006/nimg.2002.1110>
- Logothetis, N.K., Wandell, B.A., 2004. Interpreting the BOLD signal. *Annu Rev Physiol* 66, 735–769. <https://doi.org/10.1146/annurev.physiol.66.082602.092845>
- Lyon, D.C., Kaas, J.H., 2002. Evidence for a Modified V3 with Dorsal and Ventral Halves in Macaque Monkeys. *Neuron* 33, 453–461. [https://doi.org/10.1016/S0896-6273\(02\)00580-9](https://doi.org/10.1016/S0896-6273(02)00580-9)
- Macoveanu, J., 2014. Serotonergic modulation of reward and punishment: Evidence from pharmacological fMRI studies. *Brain Research* 1556, 19–27. <https://doi.org/10.1016/j.brainres.2014.02.003>
- Mangun, G.R., Hillyard, S.A., Luck, S.J., 1993. Electro cortical substrates of visual selective attention, in: *Attention and Performance 14: Synergies in Experimental Psychology, Artificial Intelligence, and Cognitive Neuroscience*. The MIT Press, Cambridge, MA, US, pp. 219–243.
- McCabe, C., Mishor, Z., Cowen, P.J., Harmer, C.J., 2010. Diminished Neural Processing of Aversive and Rewarding Stimuli During Selective Serotonin Reuptake Inhibitor Treatment. *Biological Psychiatry* 67, 439–445. <https://doi.org/10.1016/j.biopsych.2009.11.001>
- Mishkin, M., Ungerleider, L.G., 1982. Contribution of striate inputs to the visuospatial functions of parieto-preoccipital cortex in monkeys. *Behavioural Brain Research* 6, 57–77. [https://doi.org/10.1016/0166-4328\(82\)90081-X](https://doi.org/10.1016/0166-4328(82)90081-X)
- Muthukumaraswamy, S.D., Edden, R.A.E., Jones, D.K., Swettenham, J.B., Singh, K.D., 2009. Resting GABA concentration predicts peak gamma frequency and fMRI amplitude in response to visual stimulation in humans. *Proceedings of the National Academy of Sciences* 106, 8356–8361. <https://doi.org/10.1073/pnas.0900728106>
- Ogawa, S., Lee, T.M., Kay, A.R., Tank, D.W., 1990. Brain magnetic resonance imaging with contrast dependent on blood oxygenation. *Proceedings of the National Academy of Sciences* 87, 9868–9872. <https://doi.org/10.1073/pnas.87.24.9868>
- Petersen, S.E., Robinson, D.L., Morris, J.D., 1987. Contributions of the pulvinar to visual spatial attention. *Neuropsychologia* 25, 97–105. [https://doi.org/10.1016/0028-3932\(87\)90046-7](https://doi.org/10.1016/0028-3932(87)90046-7)
- Rajimehr, R., Tootell, R.B.H., 2009. Does Retinotopy Influence Cortical Folding in Primate Visual Cortex? *J Neurosci* 29, 11149–11152. <https://doi.org/10.1523/JNEUROSCI.1835-09.2009>

- Scholl, J., Kolling, N., Nelissen, N., Browning, M., Rushworth, M.F.S., Harmer, C.J., 2017. Beyond negative valence: 2-week administration of a serotonergic antidepressant enhances both reward and effort learning signals. *PLOS Biology* 15, e2000756. <https://doi.org/10.1371/journal.pbio.2000756>
- Sereno, M., Dale, A., Reppas, J., Kwong, K., Belliveau, J., Brady, T., Rosen, B., Tootell, R., 1995. Borders of multiple visual areas in humans revealed by functional magnetic resonance imaging. *Science* 268, 889–893. <https://doi.org/10.1126/science.7754376>
- Stensaas, S.S., Eddington, D.K., Dobbelle, W.H., 1974. The topography and variability of the primary visual cortex in man. *Journal of Neurosurgery* 40, 747–755. <https://doi.org/10.3171/jns.1974.40.6.0747>
- Striem-Amit, E., Ovadia-Caro, S., Caramazza, A., Margulies, D.S., Villringer, A., Amedi, A., 2015. Functional connectivity of visual cortex in the blind follows retinotopic organization principles. *Brain* 138, 1679–1695. <https://doi.org/10.1093/brain/awv083>
- Ungerleider, L.G., Haxby, J.V., 1994. ‘What’ and ‘where’ in the human brain. *Current Opinion in Neurobiology* 4, 157–165. [https://doi.org/10.1016/0959-4388\(94\)90066-3](https://doi.org/10.1016/0959-4388(94)90066-3)
- Ungerleider, L.G., Pessoa, L., 2008. What and where pathways. *Scholarpedia* 3, 5342. <https://doi.org/10.4249/scholarpedia.5342>
- Van Essen, D.C., Newsome, W.T., Maunsell, J.H.R., 1984. The visual field representation in striate cortex of the macaque monkey: Asymmetries, anisotropies, and individual variability. *Vision Research* 24, 429–448. [https://doi.org/10.1016/0042-6989\(84\)90041-5](https://doi.org/10.1016/0042-6989(84)90041-5)
- Vandenberghe, R., Dupont, P., Bruyn, B.D., Bormans, G., Michiels, J., Mortelmans, L., Orban, G.A., 1996. The influence of stimulus location on the brain activation pattern in detection and orientation discrimination: A PET study of visual attention. *Brain* 119, 1263–1276. <https://doi.org/10.1093/brain/119.4.1263>
- Vanduffel, W., Fize, D., Mandeville, J.B., Nelissen, K., Van Hecke, P., Rosen, B.R., Tootell, R.B.H., Orban, G.A., 2001. Visual Motion Processing Investigated Using Contrast Agent-Enhanced fMRI in Awake Behaving Monkeys. *Neuron* 32, 565–577. [https://doi.org/10.1016/S0896-6273\(01\)00502-5](https://doi.org/10.1016/S0896-6273(01)00502-5)
- Vanduffel, W., Fize, D., Peuskens, H., Denys, K., Sinaert, S., Todd, J.T., Orban, G.A., 2002. Extracting 3D from Motion: Differences in Human and Monkey Intraparietal Cortex. *Science* 298, 413–415. <https://doi.org/10.1126/science.1073574>
- Violante, I.R., Ribeiro, M.J., Edden, R.A.E., Guimarães, P., Bernardino, I., Rebola, J., Cunha, G., Silva, E., Castelo-Branco, M., 2013. GABA deficit in the visual cortex of patients with neurofibromatosis type 1: genotype–phenotype correlations and functional impact. *Brain* 136, 918–925. <https://doi.org/10.1093/brain/aws368>
- Wandell, B.A., Winawer, J., 2011. Imaging retinotopic maps in the human brain. *Vision Research, Vision Research 50th Anniversary Issue: Part 1* 51, 718–737. <https://doi.org/10.1016/j.visres.2010.08.004>
- Woldorff, M. g., Fox, P. t., Matzke, M., Lancaster, J. l., Veeraswamy, S., Zamarripa, F., Seabolt, M., Glass, T., Gao, J. h., Martin, C. c., Jerabek, P., 1997. Retinotopic organization of early visual spatial attention effects as revealed by PET and ERPs. *Human Brain Mapping* 5, 280–286. [https://doi.org/10.1002/\(SICI\)1097-0193\(1997\)5:4<280::AID-HBM13>3.0.CO;2-I](https://doi.org/10.1002/(SICI)1097-0193(1997)5:4<280::AID-HBM13>3.0.CO;2-I)

Perspectives of the chapter III

This preliminary study displays promising results and has to be further consolidated. Some potential perspectives would be to study the %SC and activation volume in the dual-choice saccadic task, used to drive the reward-based visual plasticity. Indeed, in this task, there were 27 pairs of targets the monkeys could choose from, each pair corresponding to the combination of specific spatial location associated with a specific pair of high / low reward outcome (or equal outcome). How such a complex task changes the functional activations within the V2 map and drives the monkey's behavioral choice in the control condition (T2) or under fluoxetine (T3) would be of outmost interest.

DISCUSSION & PERSPECTIVES

| | |
|-------------------------|-----|
| General discussion..... | 173 |
| Perspectives..... | 176 |
| References | 183 |

General discussion

The extent of brain plasticity changes throughout the lifespan or following central or peripheral lesions, as well as its neural, cellular and molecular bases. The plasticity inherent to the critical period that occurs in early development is characterized by a high excitability (Bavelier et al., 2010). Once this critical period closes, it cannot be re-opened. However, some degree of plasticity is retained in adulthood (Karni and Bertini, 1997; for review, see Castaldi et al., 2020), yet different from the early development one, and it can be enhanced by various mechanisms. An example accounting for a different form of plasticity and yet efficient in the adulthood, is the neuronal and network plasticity occurring after a lesion, namely a stroke. There, the sensitive period, characterized by molecular (Li et al., 2010; Urban et al., 2012), physiological (Clarkson et al., 2010), and structural changes produces a very distinct plasticity mechanism in the presence of a chronic stroke as compared to a healthy brain. Likewise, forms and strengths of plasticity in the healthy adult brain differ according to the type of intervention, whether purely sensory or more invasive such as electrical stimulations with transcranial direct current stimulation (Frase et al., 2021), optogenetic manipulation of the retina to stimulate the visual cortex (Chaffiol et al., 2022), astrocytes manipulation (Ribot et al., 2021) or neuromodulation (for review, see Hensch and Quinlan, 2018). Whichever they are, these forms of plasticity are all characterized by a more or less strong excitability of the brain, aiming at widening its sensitivity to sensory interventions. These efforts in enhancing the adult brain plasticity testify here of the crucial fundamental and clinical value of this research. Indeed while some sensory impairments such as amblyopia can be cured during the early life critical period (for review, see Daw, 1998; Mitchell and Mackinnon, 2002; Simons, 2005), the restrained nature of adult plasticity makes such interventions in the adult difficult, although not impossible (Bavelier et al., 2010; Baroncelli et al., 2011). To date, while we know how to enhance this plasticity from a behavioral and interventional point of view, its precise neural and network associated mechanisms remain mostly unknown.

The aim of this thesis was thus to investigate the neural mechanisms at play during an enhancement of visual plasticity in the adult brain in response to behavioral and pharmacological manipulations. To address this question, we used awake non-human primate fMRI while assessing behavioral changes associated with the induced visual plasticity. More precisely, we designed a longitudinal study to understand the neural mechanisms associated with a behavioral manipulation alone or when coupled with pharmacology. One strategy to re-instate a form of excitability of the brain is to act on the excitation/inhibition balance by decreasing over all inhibition (Bavelier et al., 2010). In the brain, GABA binding to its receptors is responsible for increased inhibition (Ulrich and Bettler, 2007). Several options exist to decrease GABA_A levels pharmacologically in the brain. The most direct option is to administer its direct antagonist, bicuculline (Straughan et al., 1971). While this first option shows very efficient results, it presents the disadvantage to have negative outcomes such as epilepsy and convulsions. Another one consists in modulating it indirectly thanks to neuromodulators, such as

serotonin, and more particularly serotonin selective reuptake inhibitors (SSRI), since serotonin cannot cross the blood-brain barrier, unlike its precursor, tryptophan (Clark et al., 1954; Tyce, 1990). One particular SSRI, fluoxetine, has been proposed to be a promising neuromodulator involved in adult plasticity enhancement (Maya-Vetencourt et al., 2008). Fluoxetine is already used for its antidepressant properties in humans (Bauer et al., 2008). Thus, it is easily transposable for human therapies involving an enhancement of plasticity.

In chapter I (**study n°1**), we characterized fluoxetine impact on visual perception through behavioral and physiological observations. We here aimed at validating the behavioral effect of fluoxetine on visual plasticity reported in the literature prior to observing its neural mechanisms and to bring another perspective on understanding the low to high-level features involved in such a plasticity. We here first demonstrated that under fluoxetine, monkeys work longer and have increased performances to tasks, mostly due to an enhanced sustained attention (Carter et al., 2005; Scholes et al., 2007; Wingen et al., 2008; Enge et al., 2011; Li et al., 2018). Moreover, these changes in top-down control due to fluoxetine differ with the nature of the task. Indeed, since they are modulated by a wide range of cognitive functions (spatial attention, decision making, temporal expectation, reward processing and reinforcement learning), we chose to study reaction times (RT) in the presence and absence of fluoxetine. Our main result was that monkeys responded faster while under fluoxetine in simple detection tasks, but were slower with the SSRI when the task presented distractors. In this context, the latter task presented a spatial uncertainty, thus a noise. In the light of recent finding on stochastic resonance (Groen et al., 2018), we proposed that the observed paradoxical effect of RT depend on the specific noise function associated with each tasks. We defined that noise as both neuronal noise, possibly effected by fluoxetine due to changes in the excitatory balance in the brain (Yin et al., 2021) and environmental noise due task-related uncertainty (spatial or reward based). Our observation that the ability of discriminating a signal from a spatial distractor, as a function of its distance to expected target position target (Di Bello et al., 2022), worsened with fluoxetine, brings support to this hypothesis. On a neural point of view, since the increase of cortical GABA levels are known to reduce intrinsic noise in the visual cortex (Hammett et al., 2020), we hypothesized that reducing the cortical GABA levels increase this noise and cause the reported behavioral observation. In chapter III (**study n°3**), indirect fMRI observation based on activations levels and volumes, suggest that GABA levels indeed decrease under fluoxetine. Interestingly, GABA decrease to favor excitability has been shown to correlate with faster RT in a context of motor plasticity (Greenhouse et al., 2017) but is hypothesized to slow manual RTs in the presence of an intrinsic noise (Verstraelen et al., 2021). We here provided behavioral and fMRI evidences of this effect of fluoxetine on the visual system.

In chapter I (**study n°1**) we also characterized a decrease of luminance perception in the peripheral vision under fluoxetine both on the high or the low visual field, and reproduced twice on data collected 10 months apart. This observation can be due to the noise increase that we aforementioned.

Additionally, we suggest in the same chapter that this apparent impairment could also trigger compensatory mechanisms to balance it and thus, enhance visual plasticity, in the manner of an ocular dominance plasticity. Nonetheless, the most striking observation of this experiment lies in the dissociation between upper and lower visual fields associated performances. Indeed, we here observed that on a placebo condition, luminance vision was better in the lower visual field than in the upper, and that fluoxetine intake decreased the luminance perception mostly in the lower visual field, although this lower visual field luminance perception still remains better than that in the upper visual field with the SSRI. We provide in chapter II a description of the neural correlates of this observation (**study n°2**). Indeed, we studied the functional connectivity at the three time-points of the longitudinal study, and while we observed no particular dorso-ventral decoupling on the basal state (T1), we reported that fluoxetine coupled to a reward-based training enhanced this decoupling. This decoupling in V2 area is further confirmed in chapter III (**study n°3**): we report that higher activation volumes in dorsal V2 than in its ventral part under SSRI. Although such a dorso-ventral decoupling effect has been reported recently on the hippocampus in a context of fear extinction modulated by the memory (Diniz et al., 2022), no such mechanism of decoupling has been observed yet in the visual system to our knowledge nor has fluoxetine been shown to enhance this effect.

One major result of chapter I (**study n°1**) is the increased sensitivity to reward under fluoxetine. This finding corroborates with the literature (McCabe et al., 2010; Macoveanu, 2014; Scholl et al., 2017) and increased our interest to couple fluoxetine administration with a reward-based attentional learning task that alters the spatial priority map (Chelazzi et al., 2013, 2014). Indeed, as shown in chapter III (**study n°3**), activation strength for dorsal V2 ROIs were stronger for the most rewarding target position in the T3 condition, compared to the T2 condition (and both were stronger than the activations to the least rewarding positions), this in both peripheral detection tasks. In other words, this indicates that the long-lasting effects of the reward-based learning on V2 organization were enhanced by fluoxetine. Moreover, these observations supported the observations in chapter II (**study n°2**). In the latter, we also reported that this left/right hemifield imbalance in favor of the most rewarding side is accompanied by a functional connectivity re-organization between visual areas and higher cognitive level areas such as parietal and pre-frontal areas through a weaker connectivity within the ventral visual stream and a stronger connectivity within the dorsal visual stream. We hypothesize that this reorganization aims at optimizing the decision-making process, and captures the key mechanism by which perceptual learning is enhanced under fluoxetine administration. Indeed, on a cellular level, fluoxetine intake promotes the proliferation of glia in the prefrontal cortex (Kodama et al., 2004), which are known to help myelin formation around axons (Hughes, 2021). While the decrease of myelin promotes plasticity, its increase allows strengthening a given structure and is thus expected to reinforce perceptual learning. During the development, myelination is involved in the closure of the critical period (Fields, 2015). In this particular case, we thus hypothesize that the enhanced plasticity observed in T2 and T3 conditions result from a

reorganization of myelin. Mapping myelin in the brain across time-points, as discussed in the **Perspectives**, would allow to directly test this point. Although we did not show these results in the present manuscript, these data have been acquired during the longitudinal protocol and will serve to address this hypothesis. A fourth time-point of measurement would be interesting to do in order to observe if this plasticity is persistent and for how long, and whether fluoxetine enhanced plasticity remains in time or fades as fluoxetine chronic treatment is stopped. Back on a functional level, pre-frontal brain activations has been shown to be increased with a rise of serotonin level when engaged in repetitive verbal tasks induced by tryptophan modulation (Allen et al., 2006). Furthermore, fluoxetine has also been shown to restore DLPFC activity levels in attention-deficit hyperactivity disorders patient (Chantiluke et al., 2015). These two findings account for an involvement of fluoxetine in high-level cognitive function. Our observations fully support this molecular, behavioral and clinical evidence.

In summary, we provide behavioral, neural and network evidences indicating that fluoxetine does contribute to enhanced plasticity in the adult brain. We further characterize this plasticity by showing that it has two origins: a local change in neural computation in the visual cortex, accounting for part of the bottom up low level changes in visual perception; a network level change dominated by a decrease of the functional connectivity in the ventral visual pathway and an increase of the functional connectivity in the dorsal visual pathway, guided by a reweight of the contribution of the DLPFC to whole brain functional connectivity.

Perspectives

In this PhD thesis, we have investigated the effect of perceptual learning when coupled or not with a neuropharmacological manipulation combining behavioral assessments with fMRI measures. While these studies shed a new light on the neural and network plastic reorganization taking place in the brain and possibly accounting for the behavioral effects we describe, some scientific questions related to these observations remain. In the following, I would like to highlight some of the scientific questions that I believe are worth exploring in continuation of the work presented here. I will highlight the different datasets that I acquired during my thesis work for this purpose, but that are still under investigation. If our predictions are confirmed by the data, this will lead to publications (see **Publication lists**, section **Articles in preparation**, p. 14).

A first set of studies involved the further characterizing of the functional and structural effects of reward-based learning plasticity under fluoxetine. A second set of studies involved the further characterization of the behavioral effects of fluoxetine of several domains of visual perception.

1. Functional and structural effects of fluoxetine on cortical plasticity

1. How does fluoxetine affects cortical networks during the active performance of a dual-choice saccadic task?

In the **three studies** discussed in this thesis manuscript, we present a dual-choice saccadic task that describes decision-making in the presence of a bias spatial priority map (Chelazzi et al., 2014) and which was used to induce the reward-based learning plasticity. We actually collected fMRI data while the two macaques were performing this dual-choice saccadic task. One very interesting perspective would be to investigate more closely the brain activations linked to the choice of one target or another as a function of the second target presented in the pair. Analyzing this information in T2 will allow us to analyze competitive spatial decision-making in the face of complex spatial reward contingencies. Analyzing this information in T3 will further allow us to specify the specific action of fluoxetine in these cognitive processes. This will allow us to link fMRI-based observations with the behavioral observations described in chapter 1. Most literature on the effects of fluoxetine on reward sensitivity focus on the striatal effects of serotonin and their interaction with dopaminergic neuromodulation. Here, we expect to complement this view with specific cortical local and network effects, thus bringing a novel perspective on the role of serotonin (and SSRIs) on cognition.

2. Are GABA levels influenced by the behavioral and pharmacological plasticity induction on the adult visual system?

Our working hypothesis was that fluoxetine induced indirectly changes to the GABA levels and fluoxetine allowed us to assess of the state of the plasticity and of the role of the neuromodulator in the pharmacological enhancement of plasticity. In order to estimate more directly the presence of GABA in a given brain region, we designed a protocol based on MRI GABA spectroscopy. The GABA spectroscopy was done at the 3T MRI, on M1 and M2 under anesthesia. Because most anesthetics interact with GABA (Zoletil or ketamine for anesthesia induction, gas isoflurane to maintain anesthesia), we decided to stay as consistent throughout the three time-points and for both monkeys as possible, so that we could observe differences between our time-points that are not due to the anesthesia method. The principle of in vivo magnetic resonance spectroscopy (MRS) of GABA is to record the magnetic resonance in a given brain region and to compare the obtained spectrum with known spectra of molecules, here the GABA (Puts and Edden, 2012). The MRS sequence we used was the MEGA-PRESS, directed specifically towards regions of interest of 15x8x10mm, in the occipital region (left and right hemispheres). We acquired these data by being careful to repeat the same measurements conditions across time-points. While M1 and M2 were under 1-2% gas isoflurane administered through intubation to maintain their anesthesia, two L11 coils were placed on each macaque temporal regions in addition to a special flexible coil (SP-coil) to fit well all the occipital region in order to obtain the best signal

possible. M1 and M2 were laying on their left side to make this setup possible. The data were preprocessed thanks to FID-A (Simpson et al., 2017), and ANIMA (<https://anima.irisa.fr/>) softwares. This project is an ongoing collaboration with Franck Lambertson (CERMEP - Lyon) and H el ene Ratiney (CREATIS - Lyon).

3. What are the effects of behavioral and pharmacological plasticity induction on the adult (myelin) brain structure?

As aforementioned in the **Discussion**, myelin increases action potential along axons and insulates them. Myelination increases a lot during development (Natu et al., 2019), and is slowed down in adulthood. However, according to observations in mice, some white matter regions of the brain such as the corpus callosum still contain many unmyelinated axons in the adult (Sturrock, 1980). Moreover, activities involving learning and plasticity induce changes in white matter microstructure, hence increasing myelination (Richardson et al., 2011; Zatorre et al., 2012). Following our T2 and T3 manipulations, we thus expected to observe changes in the myelination patterns between visual, frontal and parietal areas. Indeed, if the V1-LIP-FEF network myelination will be reduced to allow dynamic and plastic changes with the addition of new connections or suppression of others. This network could also have a stronger heavy myelination to reinforce old connections and strengthen the network. Thus, myelination is a marker of visual plasticity. Magnetic resonance imaging (MRI) studies that quantify T1w/T2w ratio allow to have an indirect measure of the myelination and of the individual differences in intracortical brain structure following the induction of plasticity (Glasser and Van Essen, 2011; Norbom et al., 2020). Since we had the opportunity to record MRI T1w and T2w contrasts on our anesthetized two adults macaques M1 and M2, we initiated to determine their myelin maps across our three longitudinal time points T1, T2 and T3.

However, this quantitative MRI (qMRI) method is not the most efficient to measure fine grained structural changes induced by plasticity occurring in a macaque adult brain. We thus considered to measure myelin quantitative changes thanks to g-ratio measure (Stikov et al., 2015; Duval et al., 2017; Campbell et al., 2018) which consists in estimating the diameter of axons as thickness indicates myelin presence. Unfortunately, this acquisition method was too long, given that we would acquire it under anesthesia. Another promising method was the myelin water fraction (MWF) measurement (Arshad et al., 2017; Uddin et al., 2018). This method principle is to measure water trapped within myelin bilayers (Laule and Moore, 2018) by measuring differential MR T2 decays in time (TE) of water within an axon (longer T2, the water is less tightly confined) and of water trapped in myelin bilayer (shorter T2, the water is more tightly confined). Thus, the MWF calculation is the ratio of the trapped myelin water (short T2) on the overall water contained in the white matter (short and long T2) (Mackay et al., 1994; Whittall et al., 1997). This method is already widely used to study reading ability (Beaulieu et al., 2020), schizophrenia (Flynn et al., 2003) and ischemic stroke (Borich et al., 2013), so both to understand diseases processes or to monitor therapies. Thus, this method was well designated to follow myelin state

in a macaque adult brain plasticity enhancement. We acquired these data on anesthetized M1 and M2 under 1-2% of gas isoflurane through intubation, in a stereotaxic frame with two L11 coils on each temporal region and one L7 coil on the parietal region. The monkeys sat head first prone in a stereotaxic frame. This setup was the same for all the anesthesia on M1 and M2 (T1w/T2w, MWF and DTI), except for the GABA spectroscopy. Our first results in time points T1, T2 and T3 already show more precision than we obtained with the T1w/T2w ratio, however, some further investigations are still needed, such as comparing the myelination in specific structures of interest across time-points.

4. How does the functional connectivity of these structures under fluoxetine compare to those observed under noradrenaline enhancer (ATX)?

In the **Introduction** part of the present thesis we also discussed of the noradrenergic modulations as a factor of adult plasticity enhancement. Indeed, the central noradrenergic system is responsible for saliency (Rogawski and Aghajanian, 1980), improvement in the treatment of sensory information (Waterhouse and Navarra, 2019), attentional processes/visuo-spatial attention (Reynaud et al., 2019) but also spatial and recognition memory, which were interesting criterion to couple a noradrenergic pharmacology with the reward-based task in the T2 condition. Although we preferred to focus on the serotonergic system in the present thesis, we also acquired resting state fMRI data on monkeys (M1, M2 and a third macaque) under placebo condition and with atomoxetine (ATX) which is an inhibitor of the pre-synaptic transporter of noradrenaline, with no effect on serotonin transporters. We thus plan to investigate these data in a near future. In particular, we hypothesize that both will impact the temporal dynamic of the resting state, as both noradrenaline and serotonin are involved in the wake/sleep cycle.

5. What are the sub-cortical plasticity effects induced by fluoxetine?

Indeed, the aim of this project was to characterize the audio-visual networks (cortical and sub-cortical) in a social context among macaques (**Appendix n°1**) in order to understand what are the neural mechanisms at play when responding to a social stimuli. Thus, this project involved the study of emotional context and of audio-visual integration. Thanks to fMRI we first demonstrated that in a context of audio-visual processing of social stimuli, the auditory perception highly depends on the meaning of the associated visual stimuli and its context (Froesel et al., 2022a). Thus, we studied the sub-cortical structures at play during this cross-modal integration. Three regions involved in audio-visual processing of socio-emotional stimuli were identified: the amygdala, the ventral putamen and the pulvinar (Froesel et al., 2022b). This particular structure is part of the audio-visual integration circuitry and responds to both auditory and visual stimuli according to its subparts division (Arcaro et al., 2015;

Froesel et al., 2021). For example, we shown in this study that the medial pulvinar has a role in the emotional regulation according to the audio-visual presented modalities (Froesel et al., 2022b). This project (**Appendix n°1**) thus binds the study of the social valence induced by fluoxetine we are interested in but also structures involved in the visual plasticity.

Indeed, in line with the present Ph.D. project, the pulvinar has been shown to be a key brain area involved in the visual plasticity (Bourne and Morrone, 2017) and the visual spatial attention (Petersen et al., 1987). Thus, one interesting perspective would be to do sub-cortical FC analyses on the pulvinar in the context of our three time-points T1, T2 and T3, along with the study of other sub-cortical actors of the visual plasticity in the context of this protocol, namely the lateral geniculate nucleus (LGN) and the dorsal raphe nucleus. This perspective is very interesting in the way that it can bind other ongoing projects presented here.

2. Behavioral effects of fluoxetine on visual perception

1. How long-lasting is the plasticity and the enhanced reward sensitivity due to fluoxetine effects?

In **chapter I** of the present manuscript, we described the effect of fluoxetine on reward sensitivity based on an everyday remapping of the spatial priority map induced by a dual-choice saccadic task. These task acquisitions occurred under an acute injection schedule, i.e. day 1 was a placebo condition, day 2 was fluoxetine injection condition and day 3 to 5 were again placebo condition. In the **study n°1** we only compared the condition effect between day 1 and day 2. However, we can also investigate the performances, working duration and learning rate on placebo days following the fluoxetine injection that can be considered as washout days. This would allow to track the effects of fluoxetine in time. As we aforementioned, since the pharmacokinetics of fluoxetine is expected to allow a behavioral effect up to 24-hours following fluoxetine administration (although this is expected to be subject-dependent), behavioral effects continuing beyond 24-hours would sign a persistence of plasticity in time.

2. What are the effects of fluoxetine on learning rate and flexibility?

Still on the same data (**study n°1**), we can also investigate the effect of fluoxetine on learning rate within single session. In addition, we also have training data of monkeys learning this behavioral task in both T2 and T3 condition. Indeed, M1 and M2 first learned this dual-choice task while no differential reward values were associated with the positions. Once they were trained in T2, we applied the statistical learning of the contingency map (overall more rewarding on the right hemifield and less rewarding on the left hemifield). In T3 condition, since they already knew the task, they were trained on the new inverted map (overall more rewarding on the left hemifield and less rewarding on the right hemifield). Although we do not have a final condition with acquisition on contingency map such as in T2 condition,

we can still observe effects of reversal learning by comparing these data with the one acquired for study n°1 and study a flexibility effect induced by fluoxetine. Indeed, this hypothesis emerges due to the fact that I empirically observed that monkeys were learning the new maps faster under fluoxetine condition than on placebo condition.

3. What are the behavioral effects on visual perception of a scotoma-based manipulation of vision under fluoxetine in macaque monkeys?

While designing the present thesis work protocol, we also intended to study the influence of bottom-up attention to enhance the visual plasticity in a fourth time-point. Yet, we decided that this protocol was already consistent and decided to conduct this fourth time-point only behaviorally. As we have seen in the **Introduction** part of the present manuscript, bottom-up attention is the involuntary guidance of attention by a salient stimulus relative to the background (Corbetta and Shulman, 2002; Yantis, 2002; Ibos et al., 2013; Astrand et al., 2015). We thus designed a protocol comprising three phases, which we recorded simultaneously with the tasks presented in **study n°1**. Each session took place according to the following schedule. First, and after having their luminance perception assessed (**study n°1**, same task) M1 and M2 performed a target detection task in the presence of spatial distractors (**study n°1**, same task). Then, they viewed a 1-hour documentary in the presence of a peripheral blurred scotoma, 8° away from their foveal point of view and of 2° of diameter. Finally, they performed again the target detection task in the presence of spatial distractors, thus assessing the behavioral consequences of plasticity induced by this transient scotoma. The results of this repeated task were not presented in the **study n°1**. The macaques were thus free to watch the movie and the transient scotoma would follow their gaze, always at the same position according to their center of fixation. Macaques were head fixated and we used eye-tracking. We also hypothesized that the bottom-up effect would be stronger if the overall scenes were blurred while the peripheral scotoma was clear. We thus acquired our data altering randomly according to the days blurred scotoma vs. clear background and clear scotoma vs. blurred background, changing the side of the scotoma (left/right). We acquired these data both in control condition and under fluoxetine. The control condition for this task consisted in the same two detection tasks before and after the movie, while the movie contained no scotoma.

We thus plan to study both performances of the target detection tasks before and after the movie and we expect to see variations in d' as a function of the type of scotoma used and we expect to see a main effect of fluoxetine. Indeed, in **Study 1**, we saw that fluoxetine administration did not impact d' while it impacted spatial resolution. Moreover, we also seek to understand the saccadic behavior in presence of such scotomic alterations in the visual field, in the absence or with fluoxetine. Is the scotoma ignored completely or solely as a function of whether it was a clear or blurred scotoma? Is the scotoma implicitly taken into account in scene exploration, and does this depends on the social content of the

scenes? Or, on the contrary, are saccades directed toward the scotoma to optimize access to the visual information affected by the scotoma and complete the visual scene? We are currently investigating these questions by comparing placebo and fluoxetine conditions.

4. What are the behavioral effects on visual perception of a scotoma-based manipulation of vision?

A last study that we designed in the frame of my Ph.D. work was the effect of a peripheral scotoma on visual attention on adult humans. Indeed, in this last project, we followed the exact same protocol as the one we described previously with two exceptions: we did not include pharmacological neuromodulation and we used a different peripheral detection task in the presence of a distractor. Indeed, after we assessed the luminance perception of each subjects (15 subjects per condition: control, blurred scotoma, neat scotoma), we presented them with a target detection task in the presence of a distractor. In this task, subjects had to press a button to indicate they detected the target, which consisted in a vertical gabor stimuli. The distractors were other gabor stimuli of the same size, luminance and duration, except that they had different orientations than the target (-60° ; -30° ; 30° ; 60°). Once this task performed, subject viewed the same 1-hour documentary as macaques did, in the same conditions. Finally, they performed again the peripheral detection task in the presence of a distractor. Subjects we required to maintain a steady head position while they were recorded with eye-tracking, 60cm away from a screen. Although we only have preliminary results on this task, we can already observe a differential d' between two conditions (clear scotoma and blurred scotoma), while we saw no effect of the control condition on the target perception. This study still needs to be further analyzed in order to be able to bind the bottom-up mechanisms of attention modulation in humans with those observed in macaques. Although our animal model allowed us to include a pharmacological protocol, we still expect to see similar mechanism that will allow to propose a transposition of our findings with the macaque model to the human vision research field. We indeed hypothesize to observe similarly a decrease in time of the scotoma effect thanks to the study of the post-detection task in time. We also hypothesize to observe a similar pattern in coping with the information lacking in the presence of the clear scotoma on the blurred movie.

5. What are the specific effects of fluoxetine in the social cognition domain?

As we have seen in the **Introduction** of the present manuscript, serotonin has an important role in social interactions and in emotional valence, such as decreasing aggressivity (for review, see Steenbergen et al., 2016) and promoting affiliations (Raleigh et al., 1980) among primates. We thus designed a project to link the scanpaths (the succession of fixations and saccades during spontaneous viewing) of social scenes with and without fluoxetine, with neural activations measured with fMRI. Indeed, since serotonin levels in the brain influences the scanpaths of social scenes among macaques (Gibboni et al., 2009), we hypothesized that fluoxetine can modulate this scanpath. We thus displayed

a 1-hour documentary outside the fMRI to both M1 and M2 while using eye-tracking, in the presence and the absence of fluoxetine. We here first aimed at calculating the heatmaps of their most viewed scenes features in scenes (faces, body), in comparison with non-social scenes. Indeed, this documentary contained a wide range of social situations, such as grooming, aggressions and flights. M1 and M2 viewed this documentary 10 times in both conditions. Then, monkeys viewed this documentary under fluoxetine at the MRI and specific scenes that we manipulated as a control (looming, upside-down and scrambled scenes). Each scene being also associated with an emotional valence, this project opens-up to a new perspective that is in direct link with a project I had the opportunity to be a collaborator of (**Appendix n°1**).

Altogether, based on the data collected during my Ph.D. work several theoretical questions will be addressed to further expand on the main results presented in this manuscript thesis.

References

- Allen, P.P., Cleare, A.J., Lee, F., Fusar-Poli, P., Tunstall, N., Fu, C.H.Y., Brammer, M.J., McGuire, P.K., 2006. Effect of acute tryptophan depletion on pre-frontal engagement. *Psychopharmacology* 187, 486–497. <https://doi.org/10.1007/s00213-006-0444-x>
- Arcaro, M.J., Pinsk, M.A., Kastner, S., 2015. The Anatomical and Functional Organization of the Human Visual Pulvinar. *J. Neurosci.* 35, 9848–9871. <https://doi.org/10.1523/JNEUROSCI.1575-14.2015>
- Arshad, M., Stanley, J.A., Raz, N., 2017. Test–retest reliability and concurrent validity of in vivo myelin content indices: Myelin water fraction and calibrated T1w/T2w image ratio. *Human Brain Mapping* 38, 1780–1790. <https://doi.org/10.1002/hbm.23481>
- Astrand, E., Ibos, G., Duhamel, J.-R., Hamed, S.B., 2015. Differential Dynamics of Spatial Attention, Position, and Color Coding within the Parietofrontal Network. *J. Neurosci.* 35, 3174–3189. <https://doi.org/10.1523/JNEUROSCI.2370-14.2015>
- Baroncelli, L., Maffei, L., Sale, A., 2011. New Perspectives in Amblyopia Therapy on Adults: A Critical Role for the Excitatory/Inhibitory Balance. *Frontiers in Cellular Neuroscience* 5.
- Bauer, M., Monz, B.U., Montejo, A.L., Quail, D., Dantchev, N., Demyttenaere, K., Garcia-Cebrian, A., Grassi, L., Perahia, D.G.S., Reed, C., Tylee, A., 2008. Prescribing patterns of antidepressants in Europe: Results from the Factors Influencing Depression Endpoints Research (FINDER) study. *European Psychiatry* 23, 66–73. <https://doi.org/10.1016/j.eurpsy.2007.11.001>
- Bavelier, D., Levi, D.M., Li, R.W., Dan, Y., Hensch, T.K., 2010. Removing Brakes on Adult Brain Plasticity: From Molecular to Behavioral Interventions. *Journal of Neuroscience* 30, 14964–14971. <https://doi.org/10.1523/JNEUROSCI.4812-10.2010>
- Beaulieu, C., Yip, E., Low, P.B., Mädler, B., Lebel, C.A., Siegel, L., Mackay, A.L., Laule, C., 2020. Myelin Water Imaging Demonstrates Lower Brain Myelination in Children and Adolescents With Poor Reading Ability. *Frontiers in Human Neuroscience* 14.
- Borich, M.R., MacKay, A.L., Vavasour, I.M., Rauscher, A., Boyd, L.A., 2013. Evaluation of white matter myelin water fraction in chronic stroke. *NeuroImage: Clinical* 2, 569–580. <https://doi.org/10.1016/j.nicl.2013.04.006>

- Bourne, J.A., Morrone, M.C., 2017. Plasticity of Visual Pathways and Function in the Developing Brain: Is the Pulvinar a Crucial Player? *Front. Syst. Neurosci.* 11. <https://doi.org/10.3389/fnsys.2017.00003>
- Campbell, J.S.W., Leppert, I.R., Narayanan, S., Boudreau, M., Duval, T., Cohen-Adad, J., Pike, G.B., Stikov, N., 2018. Promise and pitfalls of g-ratio estimation with MRI. *NeuroImage, Microstructural Imaging* 182, 80–96. <https://doi.org/10.1016/j.neuroimage.2017.08.038>
- Carter, O.L., Burr, D.C., Pettigrew, J.D., Vollenweider, F.X., 2005. Using psilocybin to investigate the relationship between attention, working memory and the serotonin 5-HT1A and 5-HT2A receptors. *Journal of Vision* 5, 683. <https://doi.org/10.1167/5.8.683>
- Castaldi, E., Lunghi, C., Morrone, M.C., 2020. Neuroplasticity in adult human visual cortex. *Neuroscience & Biobehavioral Reviews* 112, 542–552. <https://doi.org/10.1016/j.neubiorev.2020.02.028>
- Chaffiol, A., Provansal, M., Joffrois, C., Blaize, K., Labernede, G., Goulet, R., Burban, E., Brazhnikova, E., Duebel, J., Pouget, P., Sahel, J.A., Picaud, S., Arcizet, F., Gauvain, G., 2022. In vivo optogenetic stimulation of the primate retina activates the visual cortex after long-term transduction. *Molecular Therapy - Methods & Clinical Development* 24, 1–10. <https://doi.org/10.1016/j.omtm.2021.11.009>
- Chantiluke, K., Barrett, N., Giampietro, V., Brammer, M., Simmons, A., Rubia, K., 2015. Disorder-dissociated effects of fluoxetine on brain function of working memory in attention deficit hyperactivity disorder and autism spectrum disorder. *Psychological Medicine* 45, 1195–1205. <https://doi.org/10.1017/S0033291714002232>
- Chelazzi, L., E to inova, J., Calletti, R., Lo Gerfo, E., Sani, I., Della Libera, C., Santandrea, E., 2014. Altering Spatial Priority Maps via Reward-Based Learning. *Journal of Neuroscience* 34, 8594–8604. <https://doi.org/10.1523/JNEUROSCI.0277-14.2014>
- Chelazzi, L., Perlato, A., Santandrea, E., Della Libera, C., 2013. Rewards teach visual selective attention. *Vision Research, Visual Attention 2013 Volume II* 85, 58–72. <https://doi.org/10.1016/j.visres.2012.12.005>
- Clark, C.T., Weissbach, H., Udenfriend, S., 1954. 5-HYDROXYTRYPTOPHAN DECARBOXYLASE: PREPARATION AND PROPERTIES. *Journal of Biological Chemistry* 210, 139–148. [https://doi.org/10.1016/S0021-9258\(18\)65440-7](https://doi.org/10.1016/S0021-9258(18)65440-7)
- Clarkson, A.N., Huang, B.S., MacIsaac, S.E., Mody, I., Carmichael, S.T., 2010. Reducing excessive GABA-mediated tonic inhibition promotes functional recovery after stroke. *Nature* 468, 305–309. <https://doi.org/10.1038/nature09511>
- Corbetta, M., Shulman, G.L., 2002. Control of goal-directed and stimulus-driven attention in the brain. *Nat Rev Neurosci* 3, 201–215. <https://doi.org/10.1038/nrn755>
- Daw, N.W., 1998. Critical Periods and Amblyopia. *Archives of Ophthalmology* 116, 502–505. <https://doi.org/10.1001/archophth.116.4.502>
- Di Bello, F., Ben Hadj Hassen, S., Astrand, E., Ben Hamed, S., 2022. Prefrontal Control of Proactive and Reactive Mechanisms of Visual Suppression. *Cerebral Cortex* 32, 2745–2761. <https://doi.org/10.1093/cercor/bhab378>
- Diniz, C.R.A.F., da Silva, L.A., Domingos, L.B., Sonogo, A.B., Moraes, L.R.B., Joca, S., 2022. Fluoxetine acts concomitantly on dorsal and ventral hippocampus to Trk-dependently modulate the extinction of fear memory. *Progress in Neuro-Psychopharmacology and Biological Psychiatry* 113, 110451. <https://doi.org/10.1016/j.pnpbp.2021.110451>

- Duval, T., Lévy, S., Stikov, N., Campbell, J., Mezer, A., Witzel, T., Keil, B., Smith, V., Wald, L.L., Klawiter, E., Cohen-Adad, J., 2017. g-Ratio weighted imaging of the human spinal cord in vivo. *NeuroImage* 145, 11–23. <https://doi.org/10.1016/j.neuroimage.2016.09.018>
- Enge, S., Fleischhauer, M., Lesch, K.-P., Strobel, A., 2011. On the role of serotonin and effort in voluntary attention: Evidence of genetic variation in N1 modulation. *Behavioural Brain Research* 216, 122–128. <https://doi.org/10.1016/j.bbr.2010.07.021>
- Fields, R.D., 2015. A new mechanism of nervous system plasticity: activity-dependent myelination. *Nat Rev Neurosci* 16, 756–767. <https://doi.org/10.1038/nrn4023>
- Flynn, S.W., Lang, D.J., Mackay, A.L., Goghari, V., Vavasour, I.M., Whittall, K.P., Smith, G.N., Arango, V., Mann, J.J., Dwork, A.J., Falkai, P., Honer, W.G., 2003. Abnormalities of myelination in schizophrenia detected in vivo with MRI, and post-mortem with analysis of oligodendrocyte proteins. *Mol Psychiatry* 8, 811–820. <https://doi.org/10.1038/sj.mp.4001337>
- Frase, L., Mertens, L., Krahl, A., Bhatia, K., Feige, B., Heinrich, S.P., Vestring, S., Nissen, C., Domschke, K., Bach, M., Normann, C., 2021. Transcranial direct current stimulation induces long-term potentiation-like plasticity in the human visual cortex. *Transl Psychiatry* 11, 17. <https://doi.org/10.1038/s41398-020-01134-4>
- Froesel, M., Cappe, C., Ben Hamed, S., 2021. A multisensory perspective onto primate pulvinar functions. *Neuroscience & Biobehavioral Reviews* 125, 231–243. <https://doi.org/10.1016/j.neubiorev.2021.02.043>
- Froesel, M., Gacoin, M., Clavagnier, S., Hauser, M., Goudard, Q., Ben Hamed, S., 2022a. Socially meaningful visual context either enhances or inhibits vocalisation processing in the macaque brain. *Nat Commun* 13, 4886. <https://doi.org/10.1038/s41467-022-32512-9>
- Froesel, M., Gacoin, M., Clavagnier, S., Hauser, M., Goudard, Q., Hamed, S.B., 2022b. Macaque amygdala, claustrum and pulvinar support the cross-modal association of social audio-visual stimuli based on meaning. <https://doi.org/10.1101/2022.09.28.509981>
- Gibboni, R., Zimmerman, P., Gothard, K., 2009. Individual differences in scanpaths correspond with serotonin transporter genotype and behavioral phenotype in rhesus monkeys (*Macaca mulatta*). *Frontiers in Behavioral Neuroscience* 3.
- Glasser, M.F., Van Essen, D.C., 2011. Mapping Human Cortical Areas In Vivo Based on Myelin Content as Revealed by T1- and T2-Weighted MRI. *Journal of Neuroscience* 31, 11597–11616. <https://doi.org/10.1523/JNEUROSCI.2180-11.2011>
- Greenhouse, I., King, M., Noah, S., Maddock, R.J., Ivry, R.B., 2017. Individual Differences in Resting Corticospinal Excitability Are Correlated with Reaction Time and GABA Content in Motor Cortex. *J Neurosci* 37, 2686–2696. <https://doi.org/10.1523/JNEUROSCI.3129-16.2017>
- Groen, O. van der, Tang, M.F., Wenderoth, N., Mattingley, J.B., 2018. Stochastic resonance enhances the rate of evidence accumulation during combined brain stimulation and perceptual decision-making. *PLOS Computational Biology* 14, e1006301. <https://doi.org/10.1371/journal.pcbi.1006301>
- Hammett, S.T., Cook, E., Hassan, O., Hughes, C.-A., Rooslien, H., Tizkar, R., Larsson, J., 2020. GABA, noise and gain in human visual cortex. *Neuroscience Letters* 736, 135294. <https://doi.org/10.1016/j.neulet.2020.135294>
- Hensch, T.K., Quinlan, E.M., 2018. Critical periods in amblyopia. *Visual Neuroscience* 35, E014. <https://doi.org/10.1017/S0952523817000219>
- Hughes, A.N., 2021. Glial Cells Promote Myelin Formation and Elimination. *Frontiers in Cell and Developmental Biology* 9.

- Ibos, G., Duhamel, J.-R., Hamed, S.B., 2013. A Functional Hierarchy within the Parietofrontal Network in Stimulus Selection and Attention Control. *J. Neurosci.* 33, 8359–8369. <https://doi.org/10.1523/JNEUROSCI.4058-12.2013>
- Karni, A., Bertini, G., 1997. Learning perceptual skills: behavioral probes into adult cortical plasticity. *Current Opinion in Neurobiology* 7, 530–535. [https://doi.org/10.1016/S0959-4388\(97\)80033-5](https://doi.org/10.1016/S0959-4388(97)80033-5)
- Kodama, M., Fujioka, T., Duman, R.S., 2004. Chronic olanzapine or fluoxetine administration increases cell proliferation in hippocampus and prefrontal cortex of adult rat. *Biological Psychiatry* 56, 570–580. <https://doi.org/10.1016/j.biopsych.2004.07.008>
- Laule, C., Moore, G.R.W., 2018. Myelin water imaging to detect demyelination and remyelination and its validation in pathology. *Brain Pathology* 28, 750–764. <https://doi.org/10.1111/bpa.12645>
- Li, S., Overman, J.J., Katsman, D., Kozlov, S.V., Donnelly, C.J., Twiss, J.L., Giger, R.J., Coppola, G., Geschwind, D.H., Carmichael, S.T., 2010. An age-related sprouting transcriptome provides molecular control of axonal sprouting after stroke. *Nat Neurosci* 13, 1496–1504. <https://doi.org/10.1038/nn.2674>
- Li, X., Chen, W., Pan, K., Li, H., Pang, P., Guo, Y., Shu, S., Cai, Y., Pei, L., Liu, D., Afewerky, H.K., Tian, Q., Zhu, L.-Q., Lu, Y., 2018. Serotonin receptor 2c-expressing cells in the ventral CA1 control attention via innervation of the Edinger–Westphal nucleus. *Nat Neurosci* 21, 1239–1250. <https://doi.org/10.1038/s41593-018-0207-0>
- Mackay, A., Whittall, K., Adler, J., Li, D., Paty, D., Graeb, D., 1994. In vivo visualization of myelin water in brain by magnetic resonance. *Magnetic Resonance in Medicine* 31, 673–677. <https://doi.org/10.1002/mrm.1910310614>
- Macoveanu, J., 2014. Serotonergic modulation of reward and punishment: Evidence from pharmacological fMRI studies. *Brain Research* 1556, 19–27. <https://doi.org/10.1016/j.brainres.2014.02.003>
- McCabe, C., Mishor, Z., Cowen, P.J., Harmer, C.J., 2010. Diminished Neural Processing of Aversive and Rewarding Stimuli During Selective Serotonin Reuptake Inhibitor Treatment. *Biological Psychiatry* 67, 439–445. <https://doi.org/10.1016/j.biopsych.2009.11.001>
- Mitchell, D.E., Mackinnon, S., 2002. The present and potential impact of research on animal models for clinical treatment of stimulus deprivation amblyopia. *Clinical and Experimental Optometry* 85, 5–18. <https://doi.org/10.1111/j.1444-0938.2002.tb03067.x>
- Natu, V.S., Gomez, J., Barnett, M., Jeska, B., Kirilina, E., Jaeger, C., Zhen, Z., Cox, S., Weiner, K.S., Weiskopf, N., Grill-Spector, K., 2019. Apparent thinning of human visual cortex during childhood is associated with myelination. *Proc Natl Acad Sci USA* 116, 20750–20759. <https://doi.org/10.1073/pnas.1904931116>
- Norbom, L.B., Rokicki, J., Alnaes, D., Kaufmann, T., Doan, N.T., Andreassen, O.A., Westlye, L.T., Tamnes, C.K., 2020. Maturation of cortical microstructure and cognitive development in childhood and adolescence: A T1w/T2w ratio MRI study. *Hum Brain Mapp.* <https://doi.org/10.1002/hbm.25149>
- Petersen, S.E., Robinson, D.L., Morris, J.D., 1987. Contributions of the pulvinar to visual spatial attention. *Neuropsychologia* 25, 97–105. [https://doi.org/10.1016/0028-3932\(87\)90046-7](https://doi.org/10.1016/0028-3932(87)90046-7)
- Puts, N.A.J., Edden, R.A.E., 2012. In vivo magnetic resonance spectroscopy of GABA: A methodological review. *Prog Nucl Magn Reson Spectrosc* 60, 29–41. <https://doi.org/10.1016/j.pnmrs.2011.06.001>
- Raleigh, M.J., Brammer, G.L., Yuwiler, A., Flannery, J.W., McGuire, M.T., Geller, E., 1980. Serotonergic influences on the social behavior of vervet monkeys (*Cercopithecus aethiops*)

- sabaeus). *Experimental Neurology* 68, 322–334. [https://doi.org/10.1016/0014-4886\(80\)90089-8](https://doi.org/10.1016/0014-4886(80)90089-8)
- Reynaud, A.J., Froesel, M., Guedj, C., Ben Hadj Hassen, S., Cléry, J., Meunier, M., Ben Hamed, S., Hadj-Bouziane, F., 2019. Atomoxetine improves attentional orienting in a predictive context. *Neuropharmacology* 150, 59–69. <https://doi.org/10.1016/j.neuropharm.2019.03.012>
- Ribot, J., Breton, R., Calvo, C.-F., Moulard, J., Ezan, P., Zapata, J., Samama, K., Moreau, M., Bemelmans, A.-P., Sabatet, V., Dingli, F., Loew, D., Milleret, C., Billuart, P., Dallérac, G., Rouach, N., 2021. Astrocytes close the mouse critical period for visual plasticity. *Science* 373, 77–81. <https://doi.org/10.1126/science.abf5273>
- Richardson, W.D., Young, K.M., Tripathi, R.B., McKenzie, I., 2011. NG2-glia as Multipotent Neural Stem Cells: Fact or Fantasy? *Neuron* 70, 661–673. <https://doi.org/10.1016/j.neuron.2011.05.013>
- Rogawski, M.A., Aghajanian, G.K., 1980. Modulation of lateral geniculate neurone excitability by noradrenaline microiontophoresis or locus coeruleus stimulation. *Nature* 287, 731–734. <https://doi.org/10.1038/287731a0>
- Scholes, K.E., Harrison, B.J., O’Neill, B.V., Leung, S., Croft, R.J., Pipingas, A., Phan, K.L., Nathan, P.J., 2007. Acute Serotonin and Dopamine Depletion Improves Attentional Control: Findings from the Stroop Task. *Neuropsychopharmacol* 32, 1600–1610. <https://doi.org/10.1038/sj.npp.1301262>
- Scholl, J., Kolling, N., Nelissen, N., Browning, M., Rushworth, M.F.S., Harmer, C.J., 2017. Beyond negative valence: 2-week administration of a serotonergic antidepressant enhances both reward and effort learning signals. *PLOS Biology* 15, e2000756. <https://doi.org/10.1371/journal.pbio.2000756>
- Simons, K., 2005. Amblyopia Characterization, Treatment, and Prophylaxis. *Survey of Ophthalmology* 50, 123–166. <https://doi.org/10.1016/j.survophthal.2004.12.005>
- Simpson, R., Devenyi, G.A., Jezzard, P., Hennessy, T.J., Near, J., 2017. Advanced processing and simulation of MRS data using the FID appliance (FID-A)—An open source, MATLAB-based toolkit. *Magnetic Resonance in Medicine* 77, 23–33. <https://doi.org/10.1002/mrm.26091>
- Steenbergen, L., Jongkees, B.J., Sellaro, R., Colzato, L.S., 2016. Tryptophan supplementation modulates social behavior: A review. *Neuroscience & Biobehavioral Reviews* 64, 346–358. <https://doi.org/10.1016/j.neubiorev.2016.02.022>
- Stikov, N., Campbell, J.S.W., Stroh, T., Lavelée, M., Frey, S., Novek, J., Nuara, S., Ho, M.-K., Bedell, B.J., Dougherty, R.F., Leppert, I.R., Boudreau, M., Narayanan, S., Duval, T., Cohen-Adad, J., Picard, P.-A., Gasecka, A., Côté, D., Pike, G.B., 2015. In vivo histology of the myelin g-ratio with magnetic resonance imaging. *NeuroImage* 118, 397–405. <https://doi.org/10.1016/j.neuroimage.2015.05.023>
- Straughan, D.W., Neal, M.J., Simmonds, M.A., Collins, G.G.S., Hill, R.G., 1971. Evaluation of Bicuculline as a GABA Antagonist. *Nature* 233, 352–354. <https://doi.org/10.1038/233352a0>
- Sturrock, R.R., 1980. Myelination of the mouse corpus callosum. *Neuropathol Appl Neurobiol* 6, 415–420. <https://doi.org/10.1111/j.1365-2990.1980.tb00219.x>
- Tyce, G.M., 1990. Origin and metabolism of serotonin. *J Cardiovasc Pharmacol* 16 Suppl 3, S1-7.
- Uddin, M.N., Figley, T.D., Marrie, R.A., Figley, C.R., Group, for the C.S., 2018. Can T1w/T2w ratio be used as a myelin-specific measure in subcortical structures? Comparisons between FSE-based T1w/T2w ratios, GRASE-based T1w/T2w ratios and multi-echo GRASE-based myelin water fractions. *NMR in Biomedicine* 31, e3868. <https://doi.org/10.1002/nbm.3868>

- Ulrich, D., Bettler, B., 2007. GABAB receptors: synaptic functions and mechanisms of diversity. *Current Opinion in Neurobiology, Signalling mechanisms* 17, 298–303. <https://doi.org/10.1016/j.conb.2007.04.001>
- Urban, E.T.R., Bury, S.D., Barbay, H.S., Guggenmos, D.J., Dong, Y., Nudo, R.J., 2012. Gene expression changes of interconnected spared cortical neurons 7 days after ischemic infarct of the primary motor cortex in the rat. *Mol Cell Biochem* 369, 267–286. <https://doi.org/10.1007/s11010-012-1390-z>
- Verstraelen, S., Cuypers, K., Maes, C., Hehl, M., Van Malderen, S., Levin, O., Mikkelsen, M., Meesen, R.L.J., Swinnen, S.P., 2021. Neurophysiological modulations in the (pre)motor-motor network underlying age-related increases in reaction time and the role of GABA levels – a bimodal TMS-MRS study. *NeuroImage* 243, 118500. <https://doi.org/10.1016/j.neuroimage.2021.118500>
- Vetencourt, J.F.M., Sale, A., Viegi, A., Baroncelli, L., De Pasquale, R., F. O’Leary, O., Castrén, E., Maffei, L., 2008. The Antidepressant Fluoxetine Restores Plasticity in the Adult Visual Cortex. *Science* 320, 385–388. <https://doi.org/10.1126/science.1150516>
- Waterhouse, B.D., Navarra, R.L., 2019. The locus coeruleus-norepinephrine system and sensory signal processing: A historical review and current perspectives. *Brain Research, Behavioral Consequences of Noradrenergic Actions in Sensory Networks* 1709, 1–15. <https://doi.org/10.1016/j.brainres.2018.08.032>
- Whittall, K.P., Mackay, A.L., Graeb, D.A., Nugent, R.A., Li, D.K.B., Paty, D.W., 1997. In vivo measurement of T2 distributions and water contents in normal human brain. *Magnetic Resonance in Medicine* 37, 34–43. <https://doi.org/10.1002/mrm.1910370107>
- Wingen, M., Kuypers, K.P.C., van de Ven, V., Formisano, E., Ramaekers, J.G., 2008. Sustained attention and serotonin: a pharmacofMRI study. *Human Psychopharmacology: Clinical and Experimental* 23, 221–230. <https://doi.org/10.1002/hup.923>
- Yantis, S., 2002. Stimulus-Driven and Goal-Directed Attentional Control, in: Cantoni, V., Marinaro, M., Petrosino, A. (Eds.), *Visual Attention Mechanisms*. Springer US, Boston, MA, pp. 125–134. https://doi.org/10.1007/978-1-4615-0111-4_12
- Yin, Y.-Y., Wang, Y.-H., Liu, W.-G., Yao, J.-Q., Yuan, J., Li, Z.-H., Ran, Y.-H., Zhang, L.-M., Li, Y.-F., 2021. The role of the excitation:inhibition functional balance in the mPFC in the onset of antidepressants. *Neuropharmacology* 191, 108573. <https://doi.org/10.1016/j.neuropharm.2021.108573>
- Zatorre, R.J., Fields, R.D., Johansen-Berg, H., 2012. Plasticity in gray and white: neuroimaging changes in brain structure during learning. *Nat Neurosci* 15, 528–536. <https://doi.org/10.1038/nn.3045>

APPENDICES

| | |
|-----------------------------------------------------------------------------------------------------|-----|
| Appendix 1 : Cortical and subcortical neural bases of audio-visual social processing in macaques .. | 192 |
| References | 192 |
| Appendix 2: Effect of early social deprivation on the development of <i>Macaca mulatta</i> | 253 |
| References | 253 |
| Appendix 3: Diffusion imaging..... | 257 |
| References | 257 |

Appendix 1 : Cortical and subcortical neural bases of audio-visual social processing in macaques

As mentioned in the **Perspectives**, this project lies on the neural audio-visual integration to understand social contexts, in macaques. Indeed, reacting to a social group reaction requires several cognitive functions to respond to our senses. Thanks to fMRI, this project highlighted the underlying neural basis of audio-visual perception of social stimuli while investigating its effect in a social contextualisation. Based on heart-rate estimates, obtained thanks to the eulerian video magnification (EVM, article 1), and neuromimaging, it is here shown that on a cortical level, macaque monkeys associate affiliative facial expressions or social scenes with corresponding affiliative vocalizations, aggressive expressions or scenes with corresponding aggressive vocalizations and escape visual scenes with scream vocalizations, while suppressing vocalizations that are incongruent with the visual context. This process is influenced by both an emotional and a cognitive attentional network that inhibit the processing of context-irrelevant vocalizations (article 2). On a sub-cortical level, three regions involved in audio-visual processing of socio-emotional stimuli have been identified: the amygdala, the ventral putamen and the pulvinar. The amygdala and the ventral putamen are activated by visual, auditory congruent and audio-visual stimuli and the pulvinar is activated in a task-dependent manner and show a clear sensory activation gradient. This structure is known to be a key brain area involved in the visual plasticity (Bourne and Morrone, 2017) and the visual spatial attention (Petersen et al., 1987). Thus, one interesting perspective would be to continue further functional connectivity analysis on the T1, T2 and T3 data presented in this manuscript, in the light of the findings of **Appendix 1**.

References

- Bourne, J.A., Morrone, M.C., 2017. Plasticity of Visual Pathways and Function in the Developing Brain: Is the Pulvinar a Crucial Player? *Front. Syst. Neurosci.* 11. <https://doi.org/10.3389/fnsys.2017.00003>
- Petersen, S.E., Robinson, D.L., Morris, J.D., 1987. Contributions of the pulvinar to visual spatial attention. *Neuropsychologia* 25, 97–105. [https://doi.org/10.1016/0028-3932\(87\)90046-7](https://doi.org/10.1016/0028-3932(87)90046-7)



OPEN

Automated video-based heart rate tracking for the anesthetized and behaving monkey

Mathilda Froesel^{1,3}, Quentin Goudard^{1,3}, Marc Hauser², Maëva Gacoin¹ & Suliann Ben Hamed¹

Heart rate (HR) is extremely valuable in the study of complex behaviours and their physiological correlates in non-human primates. However, collecting this information is often challenging, involving either invasive implants or tedious behavioural training. In the present study, we implement a Eulerian video magnification (EVM) heart tracking method in the macaque monkey combined with wavelet transform. This is based on a measure of image to image fluctuations in skin reflectance due to changes in blood influx. We show a strong temporal coherence and amplitude match between EVM-based heart tracking and ground truth ECG, from both color (RGB) and infrared (IR) videos, in anesthetized macaques, to a level comparable to what can be achieved in humans. We further show that this method allows to identify consistent HR changes following the presentation of conspecific emotional voices or faces. EVM is used to extract HR in humans but has never been applied to non-human primates. Video photoplethysmography allows to extract awake macaques HR from RGB videos. In contrast, our method allows to extract awake macaques HR from both RGB and IR videos and is particularly resilient to the head motion that can be observed in awake behaving monkeys. Overall, we believe that this method can be generalized as a tool to track HR of the awake behaving monkey, for ethological, behavioural, neuroscience or welfare purposes.

Tracking variations in autonomous responses has proven to be invaluable in the study of complex behaviours and their physiological correlates in non-human primates¹. These include tracking changes in pupil diameter²⁻⁵, in skin conductance⁶, social blinks⁷, blink rates^{8,9}, nose temperature¹⁰ and heart rate (HR)^{11,12}. HR measure is of particular relevance in diverse cognitive contexts. For example, it has been shown that HR increases when monkeys watch videos with high affective content¹³ and during learning process^{14,15}. In spite of this, very few methods currently allow to easily, reliably and non-invasively track HR in awake behaving untrained monkeys. The aim of the present study is to fill this methodological gap.

The classical tools already available on the market to extract heart rate, such as electrocardiograms (ECG) or pulse oximeters, require a direct contact of electrodes or captors with the skin. Indeed, ECG detects changes in voltage generated by the cardiac muscles and requires to place electrodes on a shaved skin. The pulse oximetry method measures oxygen saturation and pulsations of blood thanks to photoplethysmography (PPG). PPG consists in detecting luminosity variations of the skin that are directly related to changes in blood flow^{16,17}. It also involves placing a captor on the subject, usually on the fingers. For both these methods, signal quality can deteriorate in time, due to a displacement of the electrodes or the captor. In addition, when dealing with adult human subjects, this may introduce experimental biases due to the fact that subjects possibly becomes aware of the scope of the study. In young infants or animals, placing the captor or maintaining it all throughout the experiment may turn out to be challenging if not impossible. In monkeys, recording HR either involves ECG or PPG under sedation¹⁸⁻²⁰ or implanting a telemetry device for HR measure during behaviour^{21,22}. PPG recording or HR measures using captors embedded in a wearable jacket is also an option^{11,23,24}. However, this requires intensive monkey training and might bias HR measures due to discomfort or stress.

Ballistocardiography has proven efficient in tracking human HR in open field situation, such as the home, analysing whole body movement using machine learning methods²⁵⁻²⁷. This method is based on the mechanical effect of blood ejection from the heart on hole body posture. More recently, methods allowing to extract HR at a distance from human subjects have been developed based on video image processing²⁸⁻³⁰. Imaging

¹Institut des Sciences Cognitives Marc Jeannerod, UMR5229 CNRS, Université de Lyon, 67 Boulevard Pinel, 69675 Bron Cedex, France. ²Risk-Eraser, LLC, PO Box 376, West Falmouth, MA 02574, USA. ³These authors contributed equally: Mathilda Froesel and Quentin Goudard. ✉email: mathilda.froesel@isc.cnrs.fr; quentin.goudard@isc.cnrs.fr; benhamed@isc.cnrs.fr

photoplethysmogram (iPPG), detects, as is the case for PPG, variation of skin light absorption/reflection properties^{31–33}. Indeed, heartbeat induces blood flow in all the body including the face skin. This results in a change in the skin reflectance^{34–38}. These changes in human skin reflectance can be tracked from webcam^{39,40} or smartphone⁴¹ video quality images associated with ICA signal processing techniques.

These methods appear highly relevant to non-human primate research and welfare, as cognitive processes, emotional states or welfare indicators such as stress can only be inferred by indirect measures. However, one of the major challenges in this context is the fact that changes in skin reflectance are more difficult to detect in monkeys due to reduced glabrous facial skin surface. In spite of this limitation, Unakafov et al.⁴² have successfully applied HR tracking in awake macaques in combination with discrete Fourier and wavelet transform based iPPG. While this study is of great interest, it falls short of two objectives that are useful to behavioural and experimental studies in non-human primates. First, Unakafov et al.⁴² do not address IR video-based heart rate estimation, although for example, a lot of neuroscience studies require video recording in light controlled environments. Second, they do not evaluate the sensitivity of their method in the awake behaving monkey and its ability to track subtle changes in heart rate, for example during the processing of emotional stimuli.

Here, we present an alternative indirect HR tracking method in the monkey, using Eulerian Video Magnification (EVM)³⁰. A major advantage of this approach relative to iPPG is its resilience to subject motion²⁹. We have further associated EVM video extraction with wavelet transformation based analyses, that has also been shown to be motion tolerant on poor quality human webcam video data⁴³. In a first step, we show that EVM-based HR tracking has a high temporal coherence with ground truth ECG data, whether extracted from RGB video images or IR video images (that are often used in neuroscience experimental protocols) and that EVM-based HR estimate is very close to ECG-based HR estimate. For both types of video quality, we show that temporal coherence between EVM-based heart tracking and ground truth ECG is not significantly different between humans and monkeys. Last, we describe the dependence of temporal coherence between EVM-based heart tracking and ground truth ECG on the localization of the specific facial region EVM is performed onto. In a second step, we apply EVM-based heart tracking to the awake monkey and we show that this measure allows to identify consistent HR changes following the presentation of conspecific emotional voices or faces. Overall, we believe that this method can be generalized as a tool to track HR of the awake behaving monkey, for ethological, behavioural or welfare purposes.

Material and methods

Subjects. *Monkeys.* Three rhesus monkeys (*Macaca mulatta*) participated at this study. They were aged between 9 and 17 years (2 males: monkeys T and S, 1 female: monkey Z). The project was authorized by the French Ministry for Higher Education and Research (project no. 2016120910476056 and 2015090114042892) in agreement with the French implementation of European Directive 2010/63/UE. This authorization was based on the ethical evaluation by the local Committee on the Ethics of Experiments in Animals (C2EA) CELYNE registered at the national level as C2EA number 42 and the National Ethics of Experiments in Animals board of the French Ministry of Higher Education, Research and Innovation. In order to meet the ethical requirement of reduction, following the recommendation of the ethical committee, we describe our finding and perform our statistical tests in two monkeys.

Humans. Two human participants were included in this study and were covered by a broader project authorization (ID RCB 2018-A03438-47).

Monkey anaesthesia. Monkeys were lightly anesthetized with Zoletil (Tiletamine-Zolazepam, Virbac, 10 mg/kg) so as to avoid head movements. During the video and ECG acquisitions, monkeys were gently resting on their side, under constant physiological monitoring.

Monkey Behavioural task. During these sessions, monkeys were awake and sat in a sphinx position in a plastic monkey chair and head restrained to avoid movement. They faced a screen (1920 × 1200 pixels and a refresh rate of 60 Hz) placed 54 cm from their eyes on which stimuli were presented by an experimental control and stimulus delivery software (EventIDE). The auditory stimuli were displayed by a Sensimetrics S14 insert earphones and set up. Monkeys were required to fixate the centre of the screen all throughout the recording blocks. Eye fixation was controlled thanks to an EyeLink video eye tracker (EyeLink). Recording blocks consisted in 2 alternations of 16 s of fixation and 16 s of emotional stimuli presentation (alternations of 450 ms stimuli of the same sensory and emotional category, differing in specific identity). In one type of recording blocks, fixations alternated with highly emotional auditory content (screams). In a second type of recording blocks, fixations alternated with highly emotional visual content (4° × 4° aggressive faces). In total, 54 fixation to scream transitions (30 for monkey T and 24 for monkey S), and 57 fixation to aggressive faces (30 for monkey T and 27 for monkey S) were collected. The auditory stimuli and part of the visual stimuli were recorded in Cayo Santiago, Puerto Rico and kindly produced by Marc Hauser. The other visual stimuli were created in our own lab.

Electrocardiogram recordings. Electrocardiographic signal (ECG) was recorded thanks to a Biopac-System. In humans, two electrodes were placed on the subject's thoracic cage, on each side of the heart, while the reference electrode was placed on the abdomen, close to the stomach.

In macaques, two electrodes were placed on the subject's thoracic cage, on each side of the heart, while the reference electrode was placed close to the groin on a shaved skin. ECG signal was recorded at a frequency of 2 kHz, in order to have a well-defined QRS waveform.

Video recordings. We used a USB camera with a variable framerate (maximum frame rate of 30 frames per second), and a spatial resolution of 640×480 pixels. The camera had two working modes depending of light intensity. At high light intensity level, the camera was a color (RGB) device. At low light intensity level, the camera was an infrared (IR) device.

When comparing EVM-based HR tracking to ground truth ECG HR estimation in monkeys (monkey T and monkey Z), the animals were anesthetized and laying on their side. The video recording was targeted to the face. When comparing EVM-based HR tracking to ground truth ECG HR estimation in humans (subject H1 and H2), subjects were requested to gently and steadily gaze at the camera and video recording were targeted to the face. For each monkey and human subject, we collect ten minutes of videos in full light (RGB mode) or in the dark (IR mode).

When analysing the effect of emotional stimuli on EVM-based HR tracking, we recorded IR videos while monkeys T and S were performing the above described task.

ECG and video time series were synchronized using the AcqKnowledge software. Specifically, the AcqKnowledge software was used to record the ECG signal and send start and stop synchronization triggers to the video recording system.

HR extraction from recorded video. *Definition of Region of Interest (ROI).* In order to optimize HR extraction, the first processing step involves defining, in the recorded video a region of interest (ROI) to feed in the rest of the processing pipeline (Fig. 1A). Because subsequent processing involves estimating variations in skin luminosity, ROIs should be placed on the face. The optimal location on the face is further discussed in the result section. The video is cropped around this ROI and the output is fed into a first EVM processing step.

Eulerian Video Magnification—step one. The Eulerian video magnification algorithm or EVM³⁰ allows to magnify variations in frame to frame video information and can thus be used amongst other things to amplify skin colour variations due to blood circulation. It involves both a spatial and a temporal processing such that any variation in pixel properties through time and space is amplified. This can be modelled as follows: on a 1D signal, let $I(x,t)$ be the intensity of the signal at pixel x and sampling time t . The displacement function, $\delta(t)$, represents at a given time the distance of the pixel from its original position. Thus the intensity of the pixel of interest can be written as

$$I(x, t) = f(x + \delta(t))$$

where at the initial condition $t=0$, the intensity of the pixel x takes the value:

$$I(x, 0) = f(x)$$

The EVM process consists in adding an amplified displacement function to the original intensity signal of gain α . Considering that the signal is within the selected range of frequencies of an ideal band-pass filter, the intensity signal generated by the EVM is defined as:

$$\hat{I}(x, t) = f(x + (1 + \alpha)\delta(t))$$

Outside the selected frequency range, the intensity signal is set to identity: $\hat{I}=I$. This results in the selective amplification of movement information in the 1D signal within the frequency range of interest. This procedure can be generalized to a 2D signal such as a video. The input video is decomposed into several spatial frequency bands. The same temporal filter is applied to all these bands. The most relevant spatial frequency band to the signal of interest (here, HR detection) is amplified and the result of this amplification is added to the initial video signal. Amplification factor (α) and temporal filtering parameters are hand-optimized by the experimenters to maximize the identification of the signal of interest.

Specifically, we use the EVM functions for Matlab (<https://people.csail.mit.edu/mrub/evm/>), and run it on our ROI-cropped video, defining a spatial filtering by a Gaussian blur and a down sample, as well as a temporal filtering by a band pass filter matching the expected range of HR estimates (e.g. 90 to 200 bpm^{12,44,45}). The output of this first EVM processing round is a video in which luminosity changes due to HR are enhanced (Fig. 1A).

HR approximation. The ROI pixels with highest frequency power are further extracted, all video colour time series are averaged and a wavelet transform is used to select frequency with highest peak in these selected pixels (Fig. 1B).

HR estimation—step two. In order to obtain a more precise estimate of HR in time, the EVM is run onto the selected ROI-cropped video a second time, and a band pass temporal filtering better matching the individual subject HR range is applied (Fig. 1A). A second HR estimation is run as described in Fig. 1B and the HR approximation paragraph above.

Signal processing. *ECG-based HR* Inter-peak intervals were extracted from the raw ECG signal and pulse rate were estimated in time by computing a running average over the inter-peak times series (Fig. 2b, averaging window size = 20 s).

EVM-based HR Instantaneous HR estimates are defined as maximal power frequencies at each time step of the wavelet transform. EVM-based HR is estimated in time by computing a running average over the instantaneous HR times series (Fig. 2c, averaging window size = 20 s).

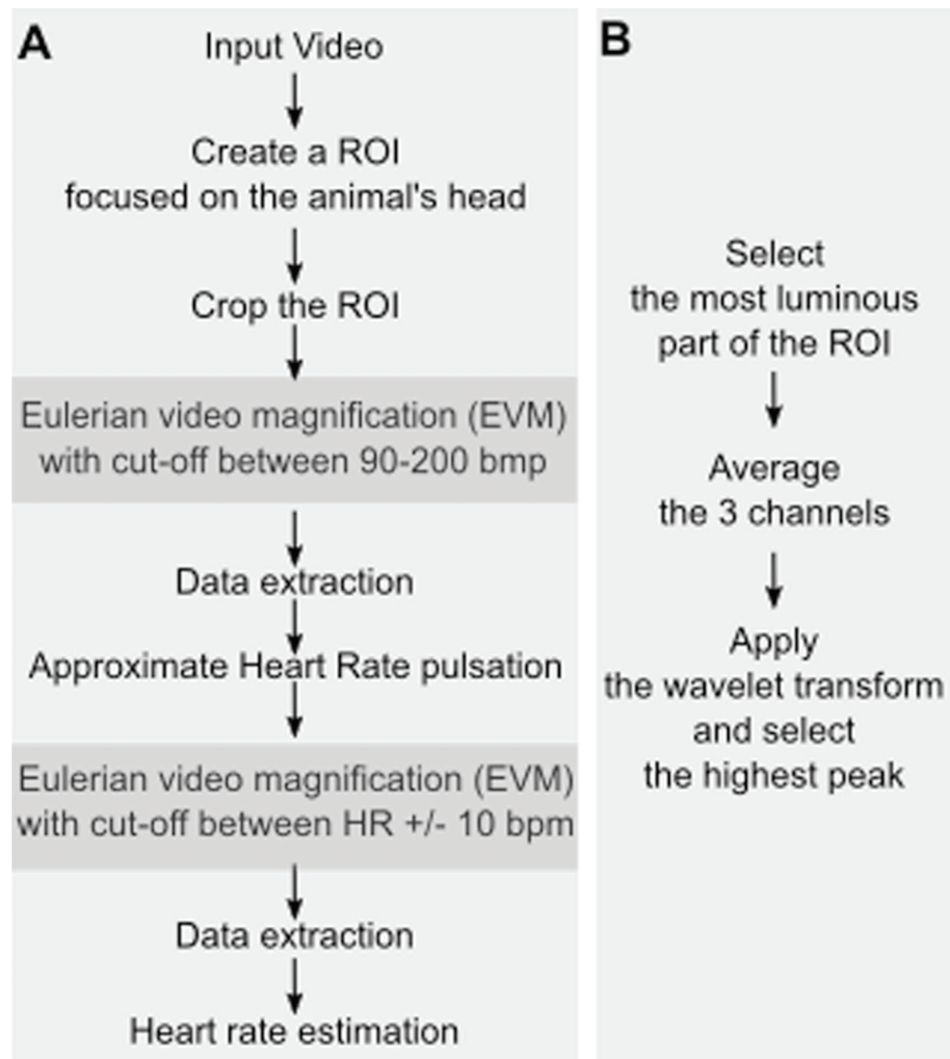


Figure 1. (A) *HR video extraction pipeline.* A Region of interest (ROI) is defined on the video input, ideally placed in a hairless skin region, such as the face. The video is cropped around this ROI selection and serves as input to the Eulerian video magnification (EVM) algorithm (see text for specifications). The result is a video in which luminosity changes due to HR are enhanced. A first HR approximation is extracted from this video (as described in B). In order to obtain a more precise HR estimate, this approximated HR is used as a parameter for a second EVM processing round. (B) *HR approximation.* Average time series are extracted from the ROI pixels of highest luminosity, for each color channel, and their frequency power profile is extracted using a wavelet transform. Peak frequency is taken as the estimate of HR.

ECG–EVM temporal coherence In order to statistically assess the extent to which ECG-based and EVM-based HR measures co-vary in time, we perform a wavelet coherence analysis that estimates instantaneous coherence in time and for all frequencies of interest (Fig. 3). Reported temporal coherence is the average of maximum temporal coherence in time, across all frequency ranges. The wavelet coherence improves the time–frequency localization of spatial correlation patterns. It is also particularly well suited to non-stationary and noisy physiological data⁴⁶.

Stimulus triggered changes in EVM-based HR EVM-based HR is estimated for each run and each monkey the pulse rate along the entire recording blocks. HR time series are extracted around the onset of the stimulus of interest (i.e. scream or aggressive face, [− 16 s 16 s]) and realigned to stimulus event presentation (0 s time reference). Individual time series are baseline corrected ([− 13 – 3 s]) and mean \pm s.e. is computed in time. Pre ([− 13 – 3 s]) and post-stimulus ([3 13 s]) HR estimates are compared using a non-parametric Wilcoxon test.

Ethical standards statement. *Monkeys.* Three rhesus monkeys (*Macaca mulatta*) participated at this study. They were aged between 9 and 17 years (2 males: monkeys T and S, 1 female: monkey Z). The project was authorized by the French Ministry for Higher Education and Research (Project No. 2016120910476056 and 2015090114042892) in agreement with the French implementation of European Directive 2010/63/UE. This authorization was based on the ethical evaluation by the local Committee on the Ethics of Experiments in Animals

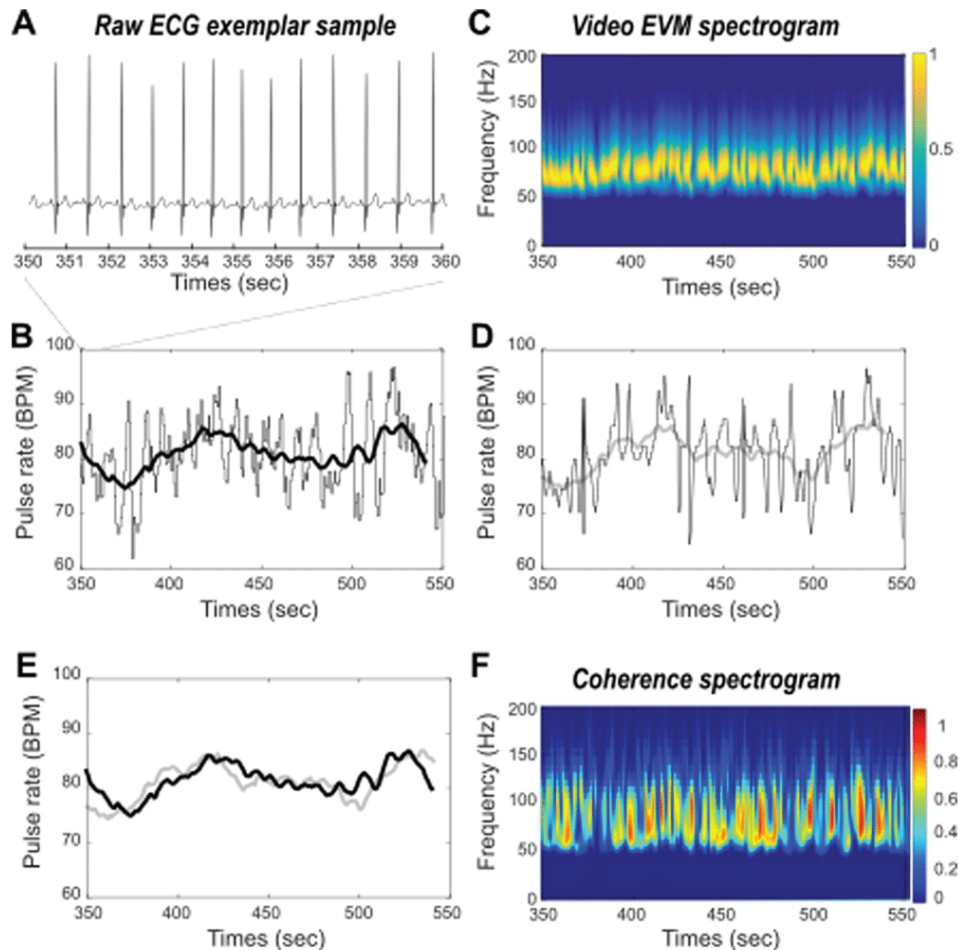


Figure 2. Comparing ECG and EVM HR estimates. **(A)** Raw ECG exemplar sample. **(B)** ECG inter-peak interval estimate (gray) and pulse rate running average (black) in time. **(C)** Time frequency spectrogram of EVM processed video data. Highest power frequency band (yellow) corresponds to the HR estimate. **(D)** EVM peak frequency estimate (gray) and corresponding pulse rate running average (light gray) in time. **(E)** Overlay of ECG (black) and EVM (light gray) based running average pulse rates estimates in time. **(F)** Coherence between ECG and EVM HR estimates.

(C2EA) CELYNE registered at the national level as C2EA number 42 and the National Ethics of Experiments in Animals board of the French Ministry of Higher Education, Research and Innovation. All experiments on non-human primates were performed in accordance with relevant guidelines and regulations.

Humans. Two human participants were included in this study and were covered by a broader project authorization (ID RCB 2018-A03438-47). All individual data was anonymized. All human experiments were performed in accordance with relevant guidelines and regulations. All experimental protocols were approved by the CNRS (research institution acting as promotor) and the CPP-Sud-Est (acting as licensing committee). Informed consent was obtained from all participants.

Analysis. All statistical analyses are non-parametric Wilcoxon rank-sum tests that do not assume normally distributed data. This tests the hypothesis according to which the medians of two independent data distributions are close to each other. Such non-parametric statistical tests are usually considered as more stringent than parametric statistical tests. The effect size Cohen's d was calculated by dividing the mean difference between HR before and after the stimulus by the global standard deviation during the run. When the Cohen's d is equal to 0.2, the effect is considered as small effect, 0.5 as medium and 0.8 and more as large.

Results

Comparing EVM-based HR estimation to ground truth ECG. In order to validate the EVM-based HR measure, we compared the inter-pulse signal estimated using the EVM approach (Fig. 1) to ground truth ECG-based inter-pulse estimation. Figure 2A represents a sample of our ground truth recording measure in a human subject, and the corresponding inter-peak estimation (Fig. 2B, gray) and pulse rate running average on a

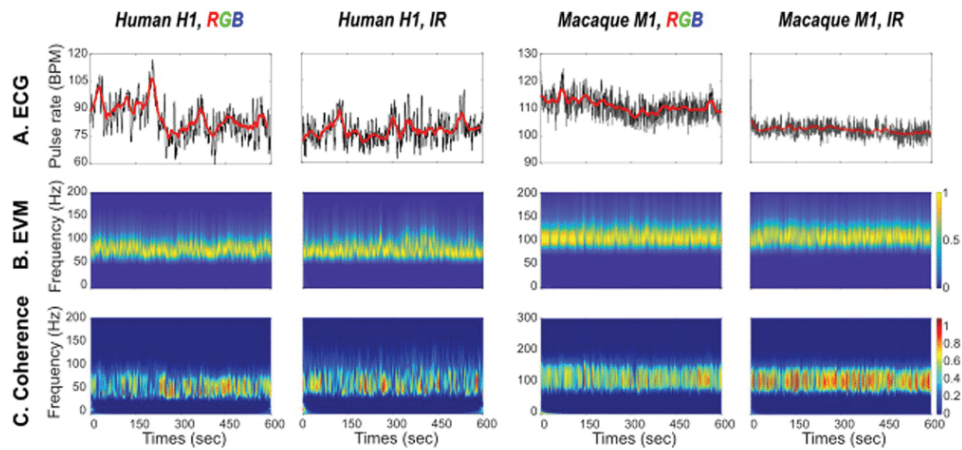


Figure 3. HR estimation in humans (panels 1 & 2) and monkey (panels 3 & 4) based on RGB (panels 1 & 3) and IR (panels 2 & 4). **(A)** ECG HR ground truth. **(B)** EVM HR estimate. **(C)** Coherence between ECG and EVM HR estimates.

longer recording period (Fig. 2B, black). Figure 2C represents, during the exact same time period, the frequency over time, the EVM-based time frequency output of our EVM processing pipeline (Fig. 1). HR induced rhythmic changes in the recorded video flow are clearly observed in the 70 to 90 Hz frequency range (Fig. 2C, yellow saturation epochs). At each time point, EVM-based instantaneous HR peak frequencies are extracted resulting in an EVM-based pulse rate estimation in time (Fig. 2D, gray, running average, light gray). The ECG-based (Fig. 2E, back) and EVM-based running averages (Fig. 2E, gray) strongly co-vary in time. In order to statistically assess the extent to which ECG-based and EVM-based HR measures co-vary in time, we perform a wavelet coherence analysis that estimates instantaneous coherence in time and for all frequencies of interest (Fig. 2F). This statistics computes, at each time point of the time series, and each frequency, the degree of coherence between the two signals of interest. On this specific recording, average temporal coherence between ECG-based and EVM-based HR estimates is 0.5 (s.d. = 0.22).

EVM-based HR estimation performs better in monkeys than in humans, whether using color (RGB) or infrared (IR) videos. EVM-based HR estimation has already been validated with human RGB data³⁰. Here, we confirm that HR can be estimated from human RGB (Fig. 3, first column) as well as IR videos (Fig. 3, second column). We further show that EVM-based HR estimation can also be achieved from anesthetized macaque RGB (Fig. 3, third column) as well as IR videos (Fig. 3, fourth column). For each type of video, each column represents ECG-based inter-pulse estimation and corresponding running average (upper row), normalized EVM-based pulse rate power estimation (middle row) and temporal coherence between ECG-based and EVM-based HR estimates (lower row).

Table 1 further summarizes pulse rate statistics for each type of recording. Differences between ECG and EVM-based HR estimations range between 0.07 BPM and 8.28 BPM (mean = 0.85, s.d. = 4.01). Both methods reach very similar signal variability (mean s.d.: ECG: 2.9275; EVM: 2.6575). Average coherence between the two signals is 0.51 (s.d. = 0.08). Importantly, coherence between ECG-based and EVM-based HR estimates tend to be higher in monkeys (mean = 0.5763, s.d. = 0.05) than in humans (mean = 0.4554, s.d. = 0.05, unilateral Wilcoxon, $p = 0.06$, Effect size: Cohen's $d = 2.418$). Overall, this is thus evidence for the fact that EVM can be used to provide a reliable non-invasive measure of HR estimation in the anesthetized preparation.

Effect of ROI selection on EVM-based HR estimation. During the EVM signal analysis, a ROI must be defined in order to optimize HR extraction. This ROI is usually placed in the most luminous part of the video, in order to record the luminosity variabilities as precisely as possible and thus have the best EVM-based HR estimation. (see Fig. 1B). Although coherence between ECG and EVM-based HR estimations is always higher than 0.45, it can reach up to 0.55 when adequately placed on the face. Figure 4A represents the initial video frame recorded in an anesthetized monkey. Figure 4B represents coherence between ECG and EVM-based HR estimations computed over 10×10 independent ROIs covering the video frame presented in Fig. 4A. Coherence is overall higher in the glabrous skin parts of the face (eyes and eye lids, snout and mouth), although important variations can still be observed between different parts of this glabrous skin. The skin around the eyes and the snout appear to be most informative in relation with heart-rate extraction. Focusing on the face regions (Fig. 4C) and defining 270 smaller pixels in this region produces local pixels of maximal coherence at the bottom of the snout. However, on average, these smaller voxels do not produce higher coherence between ECG and EVM-based HR estimations than larger voxels as presented in Fig. 4B.

EVM-based HR estimation tracks changes in HR in the awake behaving monkey. The main objective of this paper is to provide a non-invasive alternative to ECG and pulse oximeter HR tracking method

| | | ECG-based pulse rate | | EVM-based pulse rate | | Coherence coefficient |
|----------|-----|----------------------|------|----------------------|------|-----------------------|
| | | Mean | S.D. | Mean | S.D. | |
| Human 1 | RGB | 84.10 | 5.64 | 80.83 | 2.9 | 0.48 |
| | IR | 77.95 | 2.9 | 77.88 | 2.3 | 0.4656 |
| Human 2 | RGB | 84.76 | 4 | 76.48 | 3.3 | 0.377 |
| | IR | 81.35 | 2.88 | 82.08 | 4.61 | 0.499 |
| Monkey 1 | RGB | 109.5 | 1.74 | 105.79 | 1.49 | 0.554 |
| | IR | 102.5 | 0.89 | 105.5 | 1.88 | 0.66 |
| Monkey 2 | RGB | 178.35 | 1.94 | 182.26 | 2.95 | 0.5676 |
| | IR | 167.16 | 3.43 | 168.05 | 1.83 | 0.5236 |

Table 1. Pulse rate estimation statistics from ECG and EVM time series and corresponding temporal coherence.

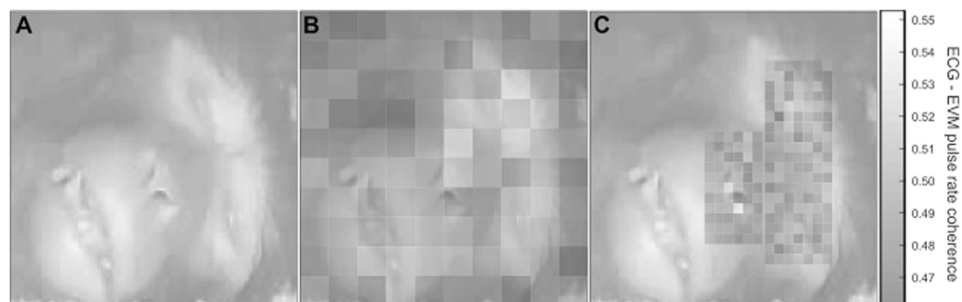


Figure 4. Effect of ROI size and localization on ECG-EVM pulse rate coherence. (A) Reference monkey face on which is superimposed ECG-EVM coherence maximum power based on a 10×10 pixel matrix covering the entire face (B) or smaller pixels covering the eyes and muzzle (C). Note that B and C share the same color scale.

for monkeys during typical behavioral tasks, with no behavioral training requirements. During such tasks, HR measures have been shown to co-vary with cognitive^{47,48} or emotional processes¹³. A non-invasive HR tracking alternative thus needs to be able to track subtle changes in HR while monkeys are actively performing a task. Here, we required two monkeys to maintain eye fixation on a central cross for reward, while stimulating them with either monkey screams (Fig. 5A, auditory negative emotion) or with a static aggressive monkey picture (Fig. 5B, visual negative emotion). Meanwhile, we recorded their faces thanks to an IR video system. The videos were EVM-processed as described in Fig. 1, placing a ROI between the two eyes, at the base of the snout, allowing to obtain an optimal estimate of HR. Then, we synchronized the latter with events, characterized by the sensory stimuli and corrected it with respect to the pre-event baseline (baseline corrected), such thus we could report the HR changes induced by stimulus presentation, irrespective of other possible modulatory effects. Both the monkey screams (Fig. 5A, pre-post comparison, Wilcoxon $p=0.03$, Effect size: Cohen's $d=0.3943$) and the aggressive monkey faces (Fig. 5B, $p=0.001$, Effect size: Cohen's $d=2.05$) induce a small but systematic change in HR. The onset of these systematic changes are of the order of a few seconds and are compatible with the reported latency of HR changes during emotional processing¹³.

Discussion

Overall, we demonstrate that EVM combined with wavelet transform analyses allows to reliably extract HR estimates from both RGB and IR videos of both anesthetized and awake macaque monkeys. These HR estimates are directly comparable to ground truth ECG HR estimate, as they have the same temporal stability and show a high temporal coherence with these reference signals. These EVM-based HR estimates also show a higher similarity with ECG in monkeys than in human subjects (max difference in BPM: human: 8.28 BPM; monkeys: 3.91 BPM) probably due to the fact that monkeys were under anaesthesia while human subjects were awake. Irrespective of anaesthesia and quite remarkably, coherence between EVM-based and ECG-based HR estimates tended to be higher when extracted from monkey videos than from humans. While this could still be due to improved stability of the face in the video stream in the anesthetized preparation, it is still noteworthy, as human faces have more glabrous as well as a thinner skin, thus allowing for a better capture of superficial vascular changes. In any case, reporting this temporal coherence measure is crucial as it indicates that EVM-based HR estimation is sufficiently sensitive to track actual physiological variation of HR in time. These EVM-based HR estimates compare to those reported in a previous study extracting monkey HR from videos using imaging photoplethysmogram⁴². Importantly, and in contrast with this previous study, EVM-based HR estimates can be reliably obtained both from RGB and IR videos.

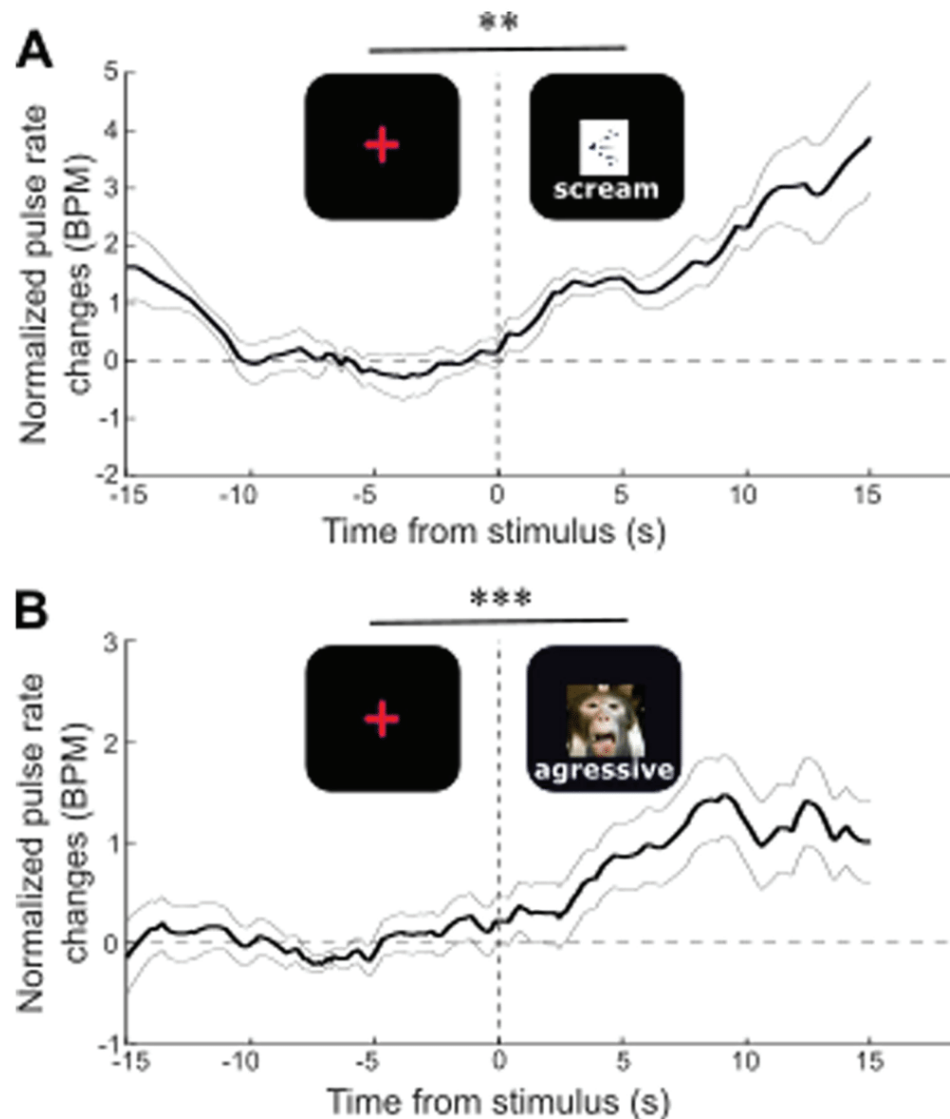


Figure 5. EVM HR estimate modulation (mean \pm s.e.) by (A) monkey screams (Wilcoxon test comparing pre-stimulus $[-400 - 100$ ms] and post-stimulus $[100 - 400]$ epochs, $p=0.03$) and (B) monkey aggressive faces ($p=0.001$).

Our present work addresses one crucial aspect of highest relevance to behavioural and cognitive studies in non-human primates, namely HR estimation in awake behaving monkeys. Here, using our EVM-based HR estimation method, we reproduce the observation that emotional sensory stimuli, whether it be auditory or visual, induce HR changes in monkeys¹³. Reported HR changes can thus be specifically associated to stimulus emotional informational content rather than to visual stimulus presentation. This is an important point as local luminosity changes due to for example visual stimuli presentation have been shown to affect plethysmographic signals⁴⁹ but not ambient light⁵⁰. Indeed, HR has been shown to be modulated in a variety of tasks: emotional or valence tasks^{13,51–53}, attentional tasks^{48,54–56} as well as learning tasks⁴⁷. Tracking this physiological parameter non-invasively, is methodologically easier, brings no stress and thus improves animal welfare while experimenting, saves training time and minimizes possible measure biasing factors (for example when animals are training to accept pulse oximetry measures). In addition, HR measure has been shown to covary with pupil dilation, typically controlled by the autonomic nervous system⁵⁷. Pupil dilation has been shown to vary as a function of reward^{57,58}, surprise⁵⁹, vigilance for social distractors⁶⁰, arousal⁶¹ and systemic pharmacological neuromodulation⁵. Last, HR can be a crucial parameter to assess behaviour following a drug induction⁶² or a lesion¹⁵. Overall, this ability to track changes in HR measure in an experimental context, that we demonstrate here, is thus of major implications to behavioural, cognitive and neuroscience experiments in awake macaque monkeys. This method is less expensive and requires no training. It can thus now be recommended and implemented as a control measure in most such awake macaque experiments.

In order to improve HR detection from videos, a recent paper suggests to use neural networks to detect and enhance the ROI from which the signal is extracted⁶³. This technique can be implemented to detect moving

animals in open fields or working animals in less restrained environments than ours, provided a high-resolution fast frame rate camera is used. This would be an important add-on to our work as HR and HR variation in monkeys in their home cage, during their time in the experimental setup or in open zoo spaces is considered as a good health state and stress marker^{12,44,45}. For example, Hassimoto et al.⁶⁴ tracked the first 3 months of acclimation of rhesus monkeys in a new laboratory environment and they demonstrate a decrease of HR following this stressful period⁶⁴.

In summary, the method we describe here is an easy and reliable non-invasive alternative for HR estimation both in anesthetized and awake monkeys. It has several notable advantages. It is very easy to set up as it only requires a decent recording camera and a computer to implement the processing pipeline. It is stable over time and does not require any specific training from the animal due to its absence of body sensors. It works in a classical behavioural task environment and is resilient to luminosity changes. Its major disadvantage lies in the fact that it doesn't, as it stands, allow real-time tracking of HR or the tracking of HR in freely moving subjects. Once these two limitations are overcome, the method will be usable during veterinary or health visits whether under sedation or light anaesthesia, under minimal contention condition, or even in home cage or open field environments.

The generalization of this method to experimental and ethology animal facilities can be considered as a contribution to animal welfare. During actual cognitive, behavioural or neuroscience experiments it can be considered as a refinement measure as well as a crucial physiological control parameter to include in the data analyses or in the framework of data sharing consortia^{65,66}. By extension, we expect that this method can also be applied on young infants in neurodevelopment studies, where pulse oximetry HR tracking can turn out to be extremely challenging.

Conclusion

Overall, the non-invasive video-based HR extraction method described here generalizes to experimental situations that have not been addressed by previous studies. First, it successfully extracts non-human primate HR estimates both from RGB videos, as previously achieved by others, as well as from IR videos. Second, we show that this method is very robust to small head movements, successfully tracking HR in the awake behaving monkey. Third, we show that this method is sufficiently sensitive to track HR variations during the exposition of non-human primates to emotional visual and auditory stimuli. It thus represents a non-invasive low cost and easy to implement HR tracking method that can be used in multiple anesthetized and awake monkey behavioural, veterinary and experimental set-ups. Association with automated face detection algorithms is further expected to generalize this method to open-field situations, thus representing a real breakthrough in the study of monkey behaviour and well-being.

Received: 25 June 2020; Accepted: 8 October 2020

Published online: 21 October 2020

References

- Bradley, M. M., Sapigao, R. G. & Lang, P. J. Sympathetic ANS modulation of pupil diameter in emotional scene perception: effects of hedonic content, brightness, and contrast. *Psychophysiology* **54**, 1419–1435 (2017).
- Bradley, M. M., Miccoli, L., Escrig, M. A. & Lang, P. J. The pupil as a measure of emotional arousal and autonomic activation. *Psychophysiology* **45**, 602–607 (2008).
- Henderson, R. R., Bradley, M. M. & Lang, P. J. Emotional imagery and pupil diameter. *Psychophysiology* **55**, e13050 (2018).
- Macatee, R. J., Albanese, B. J., Schmidt, N. B. & Cougle, J. R. The moderating influence of heart rate variability on stressor-elicited change in pupillary and attentional indices of emotional processing: An eye-Tracking study. *Biol. Psychol.* **123**, 83–93 (2017).
- Reynaud, A. J. et al. Atomoxetine improves attentional orienting in a predictive context. *Neuropharmacology* **150**, 59–69 (2019).
- Nakasone, A., Prendinger, H. & Ishizuka, M. Emotion recognition from electromyography and skin conductance. In *Proc. of the 5th international workshop on biosignal interpretation*. **2005**, 219–222 (2005).
- Ballesta, S., Mosher, C. P., Szep, J., Fischl, K. D. & Gothard, K. M. Social determinants of eyeblinks in adult male macaques. *Sci. Rep.* **6**, 1–8 (2016).
- Cléry, J. et al. The prediction of impact of a looming stimulus onto the body is subserved by multisensory integration mechanisms. *J. Neurosci.* **37**, 10656–10670 (2017).
- Guipponi, O., Odouard, S., Pinède, S., Wardak, C. & Ben Hamed, S. fMRI cortical correlates of spontaneous eye blinks in the nonhuman primate. *Cereb. Cortex* **25**, 2333–2345 (2015).
- Kuraoka, K. & Nakamura, K. The use of nasal skin temperature measurements in studying emotion in macaque monkeys. *Physiol. Behav.* **102**, 347–355 (2011).
- Hassimoto, M., Harada, T., Kaga, N., Murano, H. & Obata, M. Accurate evaluation of QT interval in conscious rhesus monkeys (*Macaca mulatta*) by use of Holter ECG. *J. Electrocardiol.* **35**, 333–342 (2002).
- Grandi, L. C. & Ishida, H. The physiological effect of human grooming on the heart rate and the heart rate variability of laboratory non-human primates: a pilot study in male rhesus monkeys. *Front. Vet. Sci.* **2**, 50 (2015).
- Bliss-Moreau, E., Machado, C. J. & Amaral, D. G. Macaque cardiac physiology is sensitive to the valence of passively viewed sensory stimuli. *PLoS ONE* **8**, e71170 (2013).
- Uchiyama, H., Ohtani, N. & Ohta, M. The evaluation of autonomic nervous system activation during learning in rhesus macaques with the analysis of the heart rate variability. *J. Vet. Med. Sci.* **69**, 521–526 (2007).
- Mitz, A. R., Chacko, R. V., Putnam, P. T., Rudebeck, P. H. & Murray, E. A. Using pupil size and heart rate to infer affective states during behavioral neurophysiology and neuropsychology experiments. *J. Neurosci. Methods* **279**, 1–12 (2017).
- Challoner, A. V. & Ramsay, C. A. A photoelectric plethysmograph for the measurement of cutaneous blood flow. *Phys. Med. Biol.* **19**, 317–328 (1974).
- Kamal, A. A., Harness, J. B., Irving, G. & Mearns, A. J. Skin photoplethysmography—a review. *Comput. Methods Progr. Biomed.* **28**, 257–269 (1989).
- Huss, M. K., Ikeno, F., Buckmaster, C. L. & Albertelli, M. A. Echocardiographic and electrocardiographic characteristics of male and female squirrel monkeys (*Saimiri* spp.). *J. Am. Assoc. Lab. Anim. Sci. JAALAS* **54**, 25–28 (2015).
- Yamaoka, A., Koie, H., Sato, K., Kanayama, T. & Taira, M. Standard electrocardiographic data of young Japanese monkeys (*Macaca fuscata*). *J. Am. Assoc. Lab. Anim. Sci. JAALAS* **52**, 491–494 (2013).

20. Sun, X. *et al.* Decreases in electrocardiographic R-wave amplitude and QT interval predict myocardial ischemic infarction in rhesus monkeys with left anterior descending artery ligation. *PLoS ONE* **8**, e71876 (2013).
21. Hoffmann, P. *et al.* Vascular origin of vildagliptin-induced skin effects in Cynomolgus monkeys: pathomechanistic role of peripheral sympathetic system and neuropeptide Y. *Toxicol. Pathol.* **42**, 684–695 (2014).
22. Chui, R. W., Derakhchan, K. & Vargas, H. M. Comprehensive analysis of cardiac arrhythmias in telemetered cynomolgus monkeys over a 6 month period. *J. Pharmacol. Toxicol. Methods* **66**, 84–91 (2012).
23. Derakhchan, K., Chui, R. W., Stevens, D., Gu, W. & Vargas, H. M. Detection of QTc interval prolongation using jacket telemetry in conscious non-human primates: comparison with implanted telemetry. *Br. J. Pharmacol.* **171**, 509–522 (2014).
24. Kremer, J. J. *et al.* Comparison of ECG signals and arrhythmia detection using jacketed external telemetry and implanted telemetry in monkeys. *J. Pharmacol. Toxicol. Methods* **1**, e47 (2011).
25. Brüser, C., Stadlthanner, K., de Waele, S. & Leonhardt, S. Adaptive beat-to-beat heart rate estimation in ballistocardiograms. *IEEE Trans. Inf. Technol. Biomed. Publ. IEEE Eng. Med. Biol. Soc.* **15**, 778–786 (2011).
26. Brüser, C., Stadlthanner, K., Brauers, A. & Leonhardt, S. Applying machine learning to detect individual heart beats in ballistocardiograms. *Conf. Proc. Annu. Int. Conf. IEEE Eng. Med. Biol. Soc. IEEE Eng. Med. Biol. Soc. Annu. Conf.* **2010**, 1926–1929 (2010).
27. Choe, S.-T. & Cho, W.-D. Simplified real-time heartbeat detection in ballistocardiography using a dispersion-maximum method. (2017).
28. Madan, C. R., Harrison, T. & Mathewson, K. E. Noncontact measurement of emotional and physiological changes in heart rate from a webcam. *Psychophysiology* **55**, e13005 (2018).
29. Alghoul, K., Alharthi, S., Osman, H. A. & Saddik, A. E. Heart rate variability extraction from videos signals: ICA vs. EVM comparison. *IEEE Access* **5**, 4711–4719 (2017).
30. WuHao-Yu, *et al.* Eulerian video magnification for revealing subtle changes in the world (ACM Trans. Graph, TOG, 2012).
31. Huelsbusch, M. & Blazek, V. Contactless mapping of rhythmical phenomena in tissue perfusion using PPGL. In *Medical Imaging 2002: Physiology and Function from Multidimensional Images* vol. 4683 110–117 (International Society for Optics and Photonics, 2002).
32. Takano, C. & Ohta, Y. Heart rate measurement based on a time-lapse image. *Med. Eng. Phys.* **29**, 853–857 (2007).
33. Verkrusse, W., Svaasand, L. O. & Nelson, J. S. Remote plethysmographic imaging using ambient light. *Opt. Express* **16**, 21434–21445 (2008).
34. Tsumura, N. *et al.* Image-based skin color and texture analysis/synthesis by extracting hemoglobin and melanin information in the skin. In *ACM SIGGRAPH 2003 Papers* 770–779 (ACM, 2003).
35. Jakovels, D., Kuzmina, I., Berzina, A. & Spigulis, J. RGB imaging system for monitoring of skin vascular malformation's laser therapy. In *Biophotonics: Photonic Solutions for Better Health Care III* vol. 8427 842737 (International Society for Optics and Photonics, 2012).
36. Jakovels, D., Kuzmina, I., Berzina, A., Valeine, L. & Spigulis, J. Noncontact monitoring of vascular lesion phototherapy efficiency by RGB multispectral imaging. *J. Biomed. Opt.* **18**, 126019 (2013).
37. Anderson, R. R. & Parrish, J. A. The optics of human skin. *J. Invest. Dermatol.* **77**, 13–19 (1981).
38. Angelopoulou, E. Understanding the color of human skin. In *Human Vision and Electronic Imaging VI* vol. 4299 243–251 (International Society for Optics and Photonics, 2001).
39. Poh, M.-Z., McDuff, D. J. & Picard, R. W. Non-contact, automated cardiac pulse measurements using video imaging and blind source separation. *Opt. Express* **18**, 10762–10774 (2010).
40. Poh, M.-Z., McDuff, D. J. & Picard, R. W. Advancements in noncontact, multiparameter physiological measurements using a webcam. *IEEE Trans. Biomed. Eng.* **58**, 7–11 (2011).
41. Kwon, S., Kim, H. & Park, K. S. Validation of heart rate extraction using video imaging on a built-in camera system of a smartphone. In *2012 Annual International Conference of the IEEE Engineering in Medicine and Biology Society* 2174–2177 (2012). <https://doi.org/10.1109/EMBC.2012.6346392>.
42. Unakafov, A. M. *et al.* Using imaging photoplethysmography for heart rate estimation in non-human primates. *PLoS ONE* **13**, e0202581 (2018).
43. Bousefsaf, F., Maaoui, C. & Pruski, A. Continuous wavelet filtering on webcam photoplethysmographic signals to remotely assess the instantaneous heart rate. *Biomed. Signal Process. Control* **8**, 568–574 (2013).
44. Tsumura, N., Koto, M., Komatsu, H. & Adachi, J. Effects of repeated chair restraint on physiological values in the rhesus monkey (*Macaca mulatta*). *Jikken Dobutsu* **39**, 361–369 (1990).
45. Clarke, A. S., Mason, W. A. & Mendoza, S. P. Heart rate patterns under stress in three species of macaques. *Am. J. Primatol.* **33**, 133–148 (1994).
46. Chavez, M. & Cazelles, B. Detecting dynamic spatial correlation patterns with generalized wavelet coherence and non-stationary surrogate data. *Sci. Rep.* **9**, 7389 (2019).
47. Zeki Al Hazzouri, A., Haan Mary, N., Deng, Y., Neuhaus, J. & Yaffe, K. Reduced heart rate variability is associated with worse cognitive performance in elderly Mexican Americans. *Hypertension* **63**, 181–187 (2014).
48. Siennicka, A. *et al.* Resting heart rate variability, attention and attention maintenance in young adults. *Int. J. Psychophysiol.* **143**, 126–131 (2019).
49. Lewandowska, M., Rumiński, J., Kocejko, T. & Nowak, J. Measuring pulse rate with a webcam—a non-contact method for evaluating cardiac activity. In *2011 Federated Conference on Computer Science and Information Systems (FedCSIS)* 405–410 (2011).
50. Sun, Y. *et al.* Use of ambient light in remote photoplethysmographic systems: comparison between a high-performance camera and a low-cost webcam. *J. Biomed. Opt.* **17**, 037005 (2012).
51. Kreibitz, S. D. Autonomic nervous system activity in emotion: a review. *Biol. Psychol.* **84**, 394–421 (2010).
52. Bauer, R. M. Physiologic measures of emotion. *J. Clin. Neurophysiol. Off. Publ. Am. Electroencephalogr. Soc.* **15**, 388–396 (1998).
53. Lang, P. J. The emotion probe: studies of motivation and attention. *Am. Psychol.* **50**, 372–385 (1995).
54. Petrie Thomas, J. H., Whitfield, M. F., Oberlander, T. F., Synnes, A. R. & Grunau, R. E. Focused attention, heart rate deceleration, and cognitive development in preterm and full-term infants. *Dev. Psychobiol.* **54**, 383–400 (2012).
55. Gazzellini, S. *et al.* Association between attention and heart rate fluctuations in pathological worriers. *Front. Hum. Neurosci.* **10**, 648 (2016).
56. Duschek, S., Muckenthaler, M., Werner, N. & del Paso, G. A. R. Relationships between features of autonomic cardiovascular control and cognitive performance. *Biol. Psychol.* **81**, 110–117 (2009).
57. Varazzani, C., San-Galli, A., Gilardeau, S. & Bouret, S. Noradrenaline and dopamine neurons in the reward/effort trade-off: a direct electrophysiological comparison in behaving monkeys. *J. Neurosci. Off. J. Soc. Neurosci.* **35**, 7866–7877 (2015).
58. Satterthwaite, T. D. *et al.* Dissociable but inter-related systems of cognitive control and reward during decision making: evidence from pupillometry and event-related fMRI. *NeuroImage* **37**, 1017–1031 (2007).
59. Lavin, C., San Martín, R. & Rosales Jubal, E. Pupil dilation signals uncertainty and surprise in a learning gambling task. *Front. Behav. Neurosci.* **7**, 218 (2014).
60. Ebitz, R. B., Pearson, J. M. & Platt, M. L. Pupil size and social vigilance in rhesus macaques. *Front. Neurosci.* **8**, 100 (2014).
61. Kennerley, S. W. & Wallis, J. D. Reward-dependent modulation of working memory in lateral prefrontal cortex. *J. Neurosci.* **29**, 3259–3270 (2009).

62. Bloch, S., Pradayrol, E. B. & Mirsky, A. F. Heart rate and respiratory rate changes during drug-induced impairment in a conditioned avoidance task in monkeys. *Pharmacol. Biochem. Behav.* **1**, 29–34 (1973).
63. Pursche, T., Clauß, R., Tibken, B. & Möller, R. Using neural networks to enhance the quality of ROIs for video based remote heart rate measurement from human faces. In *2019 IEEE International Conference on Consumer Electronics (ICCE)* 1–5 (2019).
64. Hassimoto, M., Harada, T. & Harada, T. Changes in hematology, biochemical values, and restraint ECG of rhesus monkeys (*Macaca mulatta*) following 6-month laboratory acclimation. *J. Med. Primatol.* **33**, 175–186 (2004).
65. Milham, M. P. *et al.* An open resource for non-human primate imaging. *Neuron* **100**, 61–74.e2 (2018).
66. Margulies, D. S. *et al.* Accelerating the evolution of nonhuman primate neuroimaging. *Neuron* **105**, 600–603 (2020).

Author contributions

Conceptualization, S.B.H. M.F. and Q.G.; Stimuli preparation, M.H., M.F. Q.G. M.G; Data Acquisition, M.F. Q.G. M.G.; Methodology, Q.G., M.F. and S.B.H; Investigation, M.F., Q.G. and S.B.H.; Writing–Original Draft, M.F. S.B.H. and Q.G; Writing–Review and Editing, S.B.H., M.F., Q.G; Funding Acquisition, S.B.H.; Supervision, S.B.H.

Funding

This work was funded by the French National Research Agency (ANR) ANR-16-CE37-0009-01 Grant.

Competing interests

The authors declare no competing interests.

Additional information

Correspondence and requests for materials should be addressed to M.F., Q.G. or S.B.H.

Reprints and permissions information is available at www.nature.com/reprints.

Publisher's note Springer Nature remains neutral with regard to jurisdictional claims in published maps and institutional affiliations.



Open Access This article is licensed under a Creative Commons Attribution 4.0 International License, which permits use, sharing, adaptation, distribution and reproduction in any medium or format, as long as you give appropriate credit to the original author(s) and the source, provide a link to the Creative Commons licence, and indicate if changes were made. The images or other third party material in this article are included in the article's Creative Commons licence, unless indicated otherwise in a credit line to the material. If material is not included in the article's Creative Commons licence and your intended use is not permitted by statutory regulation or exceeds the permitted use, you will need to obtain permission directly from the copyright holder. To view a copy of this licence, visit <http://creativecommons.org/licenses/by/4.0/>.

© The Author(s) 2020

Socially meaningful visual context either enhances or inhibits vocalisation processing in the macaque brain

Received: 24 May 2021

Accepted: 3 August 2022

Published online: 19 August 2022

 Check for updates

Mathilda Froesel¹✉, Maëva Gacoin¹, Simon Clavagnier¹, Marc Hauser²,
Quentin Goudard¹ & Suliann Ben Hamed¹✉

Social interactions rely on the interpretation of semantic and emotional information, often from multiple sensory modalities. Nonhuman primates send and receive auditory and visual communicative signals. However, the neural mechanisms underlying the association of visual and auditory information based on their common social meaning are unknown. Using heart rate estimates and functional neuroimaging, we show that in the lateral and superior temporal sulcus of the macaque monkey, neural responses are enhanced in response to species-specific vocalisations paired with a matching visual context, or when vocalisations follow, in time, visual information, but inhibited when vocalisation are incongruent with the visual context. For example, responses to affiliative vocalisations are enhanced when paired with affiliative contexts but inhibited when paired with aggressive or escape contexts. Overall, we propose that the identified neural network represents social meaning irrespective of sensory modality.

Brain structure and function have evolved in response to social relationships, both within and between groups, in all mammals. For example, across species, brain size and gyrification has been shown to increase with average social group size^{1–3}, as well as meta-cognitive abilities⁴. Within a given species, functional connectivity within the so-called social brain has been shown to be stronger in macaques living in larger social groups⁵. In this context, successful social interactions require the proper interpretation of social signals⁶, whether visual (body postures, facial expressions, inter-individual interactions) or auditory (vocalisation).

In humans, the core language system is amodal, in the sense that our phonology, semantics and syntax function in the same way whether the input is auditory (speech) or visual (sign). In monkeys and apes, vocalisations are often associated with specific facial expressions and body postures⁷. This raises the question of whether and how auditory and visual information are integrated to interpret the meaning of a given situation, including emotional states and functional behavioural responses. For example, macaque monkeys scream as an indication of fear, triggered by potential danger from conspecifics or

heterospecifics. In contrast, macaques coo during positive social interactions, involving approach, feeding and group movement^{8,9}. To what extent, does hearing a scream generate a visual representation of the individual(s) involved in such an antagonistic situation, as opposed to a positive social situation? Does seeing an antagonistic situation set up an expectation that screams, but not coos, will be produced?

Face, voice, and social scene processing in monkeys have been individually explored, to some extent, from the behavioural^{10–13} and neuronal points of view^{14–35}. Audio-visual integration during naturalistic social stimuli has recently been shown in specific regions of the monkey face-patch system³⁶, the voice-patch system^{37–40}, as well as in the prefrontal voice area⁴¹. However, beyond combining sensory information, social perception also involves integrating contextual, behavioural and emotional information^{42,43}. In this context, how macaque monkeys associate specific vocalisations with specific social visual scenes based on their respective meaning has scarcely been explored. Our goal is to help fill this gap.

This study used video-based heart rate monitoring and functional magnetic resonance in awake behaving monkeys to show that rhesus

¹Institut des Sciences Cognitives Marc Jeannerod, UMR5229 CNRS Université de Lyon, 67 Boulevard Pinel, 69675 Bron Cedex, France. ²Risk-Eraser, LLC, PO Box 376, West Falmouth, MA 02574, USA. ✉e-mail: mathilda.froesel@isc.cnrs.fr; benhamed@isc.cnrs.fr

monkeys (*Macaca mulatta*) systematically associate the meaning of a vocalisation with the meaning of a visual scene. Specifically, they associate affiliative facial expressions or social scenes with corresponding affiliative vocalisations, aggressive facial expressions or social scenes with corresponding aggressive vocalisations, and escape visual scenes with scream vocalisations. In contrast, vocalisations that are incompatible with the visual information are fully suppressed, indicating a top-down regulation over the processing of sensory input.

Results

In the following, we investigate whether and how macaques associate visual and auditory stimuli based on their semantic content, and we characterize the neuronal bases underlying this audio-visual integration. We obtained neural and autonomic data from two macaques using functional magnetic resonance brain imaging and video-based heart rate tracking. We designed six variants of a unique task in which we systematically manipulated the general semantics or meaning of the context as specified by visual information and presented as independent runs in the sessions. Each context, and so each independent run, combined visual stimuli of identical social content with either semantically congruent or incongruent monkey vocalisations presented together with the visual stimuli or not. The semantic context was set by the social content of the visual stimuli presented within a given variant of the task. As a result, auditory stimuli could be readily identified as congruent or incongruent with the context defined by the visual stimuli even when presented alone. On each block of trials, the

monkeys could be exposed to either visual stimuli only (Vi), auditory congruent stimuli only (AC), auditory incongruent stimuli only (AI), audio-visual congruent stimuli (VAC) or audio-visual incongruent stimuli (VAI), in a block design (Fig. 1A). Importantly, paired contexts shared the same auditory stimuli, but opposite social visual content (Fig. 1B), thus opposite semantic content and meaning. All contexts were presented randomly in independent runs and at least once during each scanning session. We report group fMRI and group heart-rate analyses. All reported statistics are based on non-parametric tests.

Auditory whole brain activations depend on semantic congruence with visual context

Combining the F+ and F- face contexts (Fig. 2, see Supplementary Fig. 1A for individual monkey maps and Supplementary Fig. 2), which include faces expressing lipsmacks or aggressive threats, we find in the visual contrast, robust bilateral activation ($p < 0.05$ FWE) in the extrastriate cortex, along the superior temporal sulcus (STS) as well as in the prefrontal cortex, as expected from previous studies^{17,24,44}. Activations were also observed in the posterior part of the fundus of the intraparietal sulcus at an uncorrected level ($p < 0.001$). Supplementary Fig. 3 represents these activation patterns overlaid with the CIVM non-human primate atlas parcellation and corresponding percentage signal change (%SC) for each area described in Supplementary Table 1 for the visual, auditory congruent and auditory incongruent vs. fixation contrasts. Please note that receiving coils were placed so as to optimize temporal and prefrontal cortex signal-to-noise ratio (SNR). As a result,

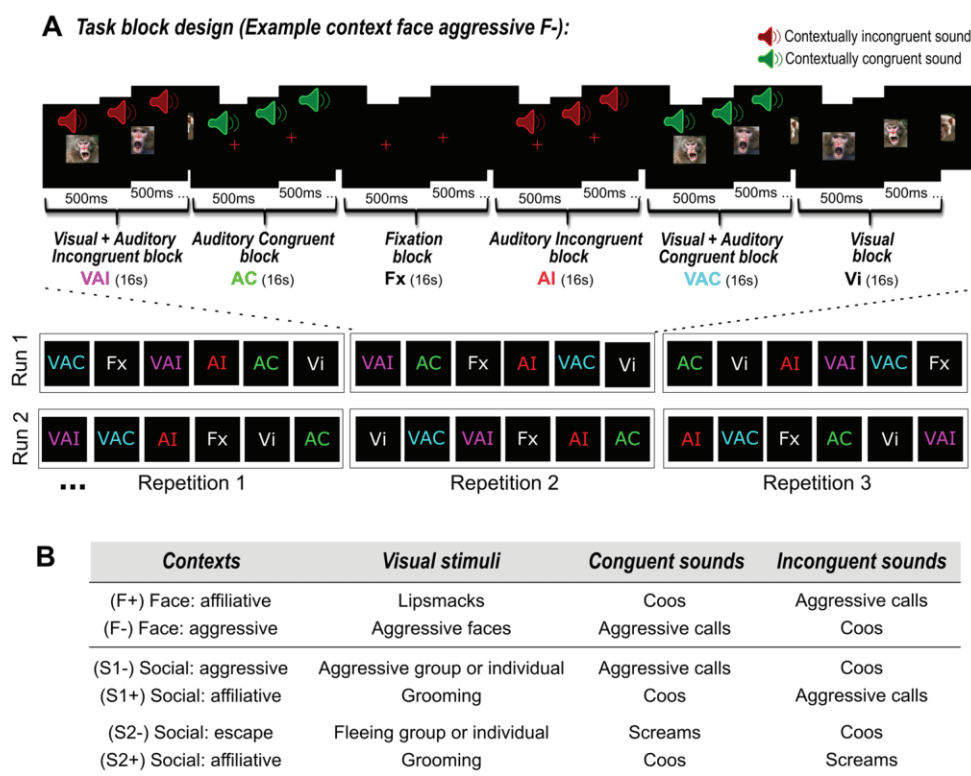


Fig. 1 | Description of experimental design and the six different contexts used in the study. **A** Experimental design. Example of an aggressive face (F-) context. Each run was composed of three randomized repetitions of six different blocks of 16 s. The six blocks could be either visual stimuli only (Vi), auditory congruent stimuli only (AC), auditory incongruent stimuli only (AI), audio-visual congruent stimuli (VAC) or audio-visual incongruent stimuli (VAI), or fixation with no sensory stimulation (Fx). Block presentation was pseudo-randomized and counter-balanced so that, across all repetitions and all runs of given context, each block was, on average, preceded by the same number of blocks from the other conditions. Initial blocks were either a visual block (Vi, VAC, VAI), or a fixation block followed by

a visual block (Vi, VAC or VAI), such that context was set by visual information early on in each run. Each sensory stimulation block contained a rapid succession of 500 ms stimuli. Each run started and ended with 10 seconds of fixation.

B Description of contexts. Six different contexts were used. Each context combined visual stimuli of identical social content with either semantically congruent or incongruent monkey vocalisations. Pairs of contexts shared the same auditory stimuli, but opposite social visual content (F+ vs. F-; S1+ vs. S1-; S2+ vs. S2-). Each run corresponded to one of the semantic contexts described above. Visual stimuli were extracted from videos collected by the Ben Hamed lab, as well as by Marc Hauser on Cayo Santiago, Puerto Rico.

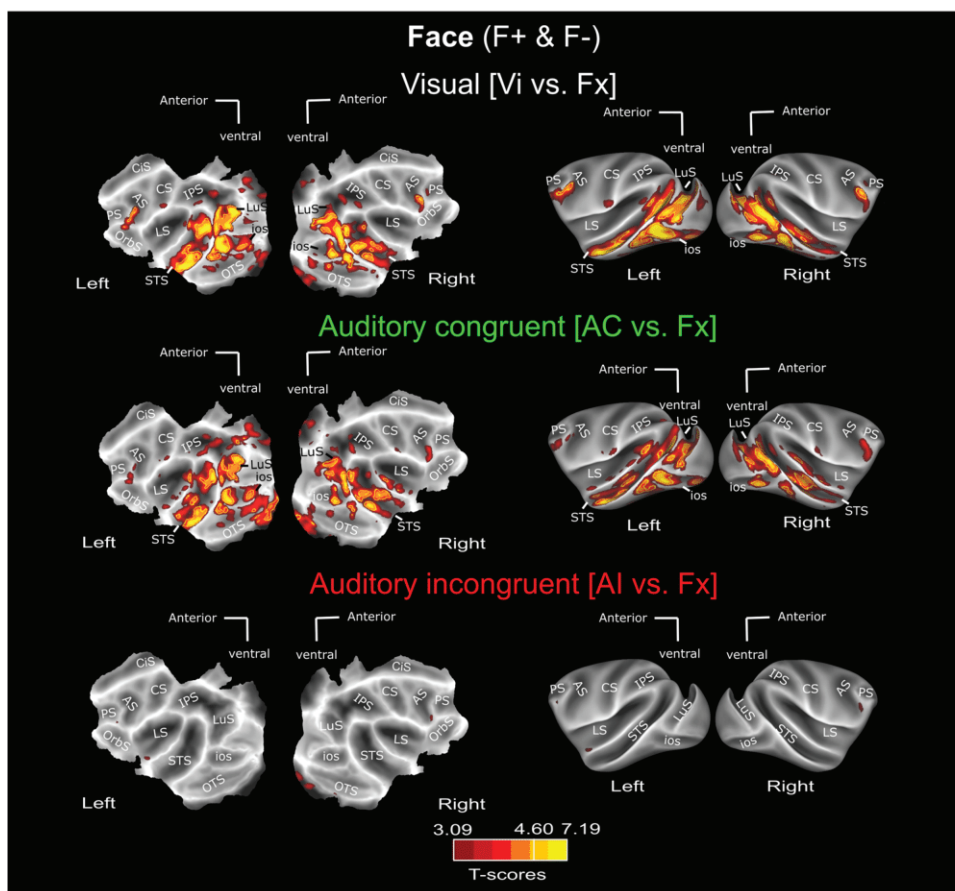


Fig. 2 | Whole-brain activation FACE contexts (F+ & F-): main contrasts. Whole-brain activation maps of the F+ (face affiliative) and F- (face aggressive) runs, cumulated over both monkeys, for the visual (white, Vi vs. Fx), auditory congruent (green, AC vs. Fx) and auditory incongruent (red, AI vs. Fx). Note that the AC and AI conditions contain exactly the same sound samples (coos and aggressive calls). Darker shades of red indicate level of significance at $p < 0.001$ uncorrected, t -score > 3.09 . Lighter shades of yellow and brown outlines indicate level of

significance at $p < 0.05$ FWE correction, t -score > 4.6 , DF [1, 5200]. ios Inferior Occipital Sulcus, LS Lateral Sulcus, STS Superior Temporal Sulcus, CiS Cingulate Sulcus, LuS Lunate Sulcus, IPS Intraparietal Sulcus, PS Precentral Sulcus, CS Central Sulcus, AS Arcuate Sulcus, OrbS Orbital Sulcus. See Supplementary Fig. S1 for individual monkey data. Corresponding size effects are presented in Supplementary Figs. S2, S6 and main Fig. 6.

no activations can be seen in the occipital cortex (see temporal SNR maps in Supplementary Fig. 4 and precise mean and std signal evaluation in occipital cortex and STS; Please note that in spite of these lower SNR in the occipital cortex, %SC based on an atlas defined ROIs are occasionally significant for the Visual vs. Fixation contrast, and (less so) for the Auditory congruent vs. Fixation contrast, in V1, V2, V3 and V4: see Supplementary Tables 1–3). The congruent auditory versus fixation contrast, which combined aggressive calls and coos from the two different contexts, leads to activation within the inferior bank of the lateral sulcus, both at corrected ($p < 0.05$ FWE) and uncorrected levels ($p < 0.0001$), as described in previous studies^{22,26,29}. Importantly, this contrast also leads to the same robust bilateral activations as the visual contrast: the extra-striate cortex, along the superior temporal sulcus (STS) ($p < 0.05$ FWE), as well as in the prefrontal and intraparietal cortex ($p < 0.0001$ uncorrected). Percent signal change at local peak activations in the lateral sulcus and superior temporal sulcus are presented in Supplementary Fig. 2. Supplementary Fig. 5 (left) represents the distribution of AC – AI/AC + AI (Supplementary Fig. 5A) and AC – V/AC + V (Supplementary Fig. 5B) modulation indexes across ROIs, thus precisely quantifying the effect strength. These activations are significantly higher than those observed for the incongruent vocalisations, whether the congruent auditory stimuli are coos (Fig. 3B, Supplementary Figs. 2, 6 for the effect strengths of the t -score maps) or aggressive calls (Fig. 3C), although congruent coos led to significantly higher activations than congruent aggressive calls (Supplementary

Fig. 6). Supplementary Fig. 7 represents the activation patterns of Fig. 3 overlaid with the CIVM non-human primate atlas parcellation and corresponding percentage signal change (%SC) for each area are described in Supplementary Table 2 for the visual, auditory congruent and auditory incongruent vs. fixation contrasts. In contrast, when we present the exact same aggressive calls and coos, the incongruent auditory versus fixation contrast leads to minimal activation, if any (Fig. 2, see Supplementary Fig. 1 for individual monkey data and Supplementary Figs. 2, 6 for the effect strengths of the t -score maps). Again, this doesn't depend on whether the incongruent sounds are aggressive calls (Fig. 3D) or coos (Fig. 3E). This pattern of activation therefore confirms that auditory activation does not depend on the acoustic morphology or function of the vocalisation. Rather, it depends on whether the vocalisations are congruent or not to the semantic content of the visual stimuli.

These observations are reproduced in a different set of contexts, in which the visual stimuli involve social scenes (grooming, aggression or escape) with either semantically congruent or incongruent vocalisations (Fig. 4 for all social contexts on group data, see Supplementary Fig. 1B for individual monkey data, Supplementary Fig. 8 for S+ and S- group data social contexts presented independently, and Supplementary Figs. 9, 10 for effect strengths in representative ROIs of the t -score map. Supplementary Fig. 11 represents these activation patterns overlaid with the CIVM non-human primate atlas parcellation; corresponding percentage signal change (%SC) for each area is

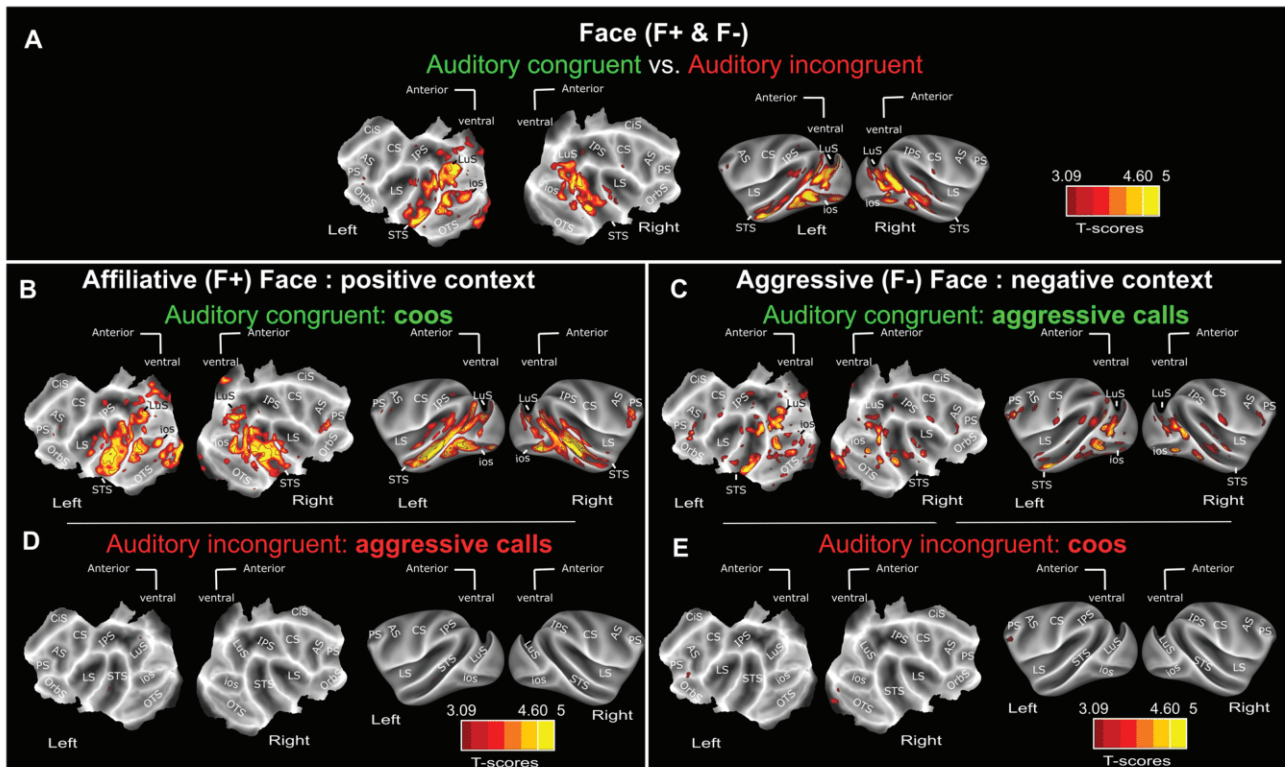


Fig. 3 | Auditory activations depend on semantic congruence with visual context. **A** Whole-brain activation maps of the F+ (face affiliative) and F- (face aggressive) runs, for the auditory congruent vs auditory incongruent (relative to the visual context) contrast. Whole-brain activation map for the F+ (face affiliative) **(B)** auditory congruent (coos, dark green, AC vs. Fx) and **(D)** auditory incongruent (aggressive calls, dark red, AI vs. Fx) conditions. Whole-brain activation map for the F- (face aggressive) **(C)** auditory congruent (aggressive calls, green, AC vs. Fx) and

(E) auditory incongruent (coos, red, AI vs. Fx) conditions. Darker shades of red indicate level of significance at $p < 0.001$ uncorrected, t -score > 3.09 . Lighter shades of yellow and brown outlines indicate level of significance at $p < 0.05$ FWE correction, t -score > 4.6 , $DF = [1, 2604]$ for F+ and F- $DF = [1, 2618]$ and $DF [1, 5200]$ for Face (F+ & F-). ios Inferior Occipital Sulcus, LS Lateral Sulcus, STS Superior Temporal Sulcus, CIS Cingulate Sulcus, LuS Lunate Sulcus, IPS Intraparietal Sulcus, PS Precentral Sulcus, CS Central Sulcus, AS Arcuate Sulcus, OrbS Orbital Sulcus.

described in Supplementary Table 3 for the visual, auditory congruent and auditory incongruent vs. fixation contrasts. To further quantify the effect strength of congruency on auditory processing, we computed an AC - AI/AC + AI modulation index (Supplementary Fig. 5A) for both face and social contexts. In both lateral and superior temporal sulci and both types of contexts, this index reveals a significantly higher activation for auditory congruent vocalisation than auditory incongruent stimuli. It is worth noting that, in 66% of the instances, both AI and AC conditions are preceded by blocks involving visual stimulation (Vi, VAC and VAI). Because this was the case for both AI and AC conditions, the absence of auditory activations in the AI vs. Fx contrast and the presence of temporal and occipital activations in the AC vs. Fx contrast cannot be interpreted as a trace of the activations resulting from the previous blocks. Instead, this pattern of responses should be considered as a process that results from the structure of the task. Indeed, the AC - AI/AC + AI modulation index progressively grows stronger within any given run, as visual stimulation reinforces context-related information. This supports the idea that the observed enhancement of AC relative to AI is context-dependent (Fig. 5A). In addition, this modulation index is not significantly different whether the auditory stimuli were presented right after a block containing visual information or separated in time from it (Fig. 5B).

Taken together, these results indicate that audio-visual semantic associations are implemented in a specific cortical network involved in the processing of both visual face and social stimuli as well as voice stimuli. This network is composed of prefrontal and temporal areas, but also, of visual striate and extrastriate visual areas (see Supplementary note attached to Supplementary Tables 1-3. An important question is thus whether these neuronal computations impact the

behaviour or the physiology of the monkeys. In the following section, we investigate how heart rate changes in response to auditory-visual stimuli that are either congruent or incongruent with the social situation.

Heart rate variations depend on semantic congruence with visual context

In this study, monkeys were required to fixate the centre of the screen while the different auditory and visual stimuli were presented. As a result, it was not possible to analyse whether gaze is spontaneously affected by the different stimulus categories. It was, however, possible to analyse heart-rate variation using a video-based method developed by our team⁴⁵. Figure 6 focuses on heart rate variation in response to the auditory sound categories in the different contexts. Heart rate responses, described in Fig. 6 of Froesel et al. 2020, are typically slow to build up (several seconds). As a result, quantifications of heart rate information were carried out in the second half of the block (last 8 s).

We observe a main context effect on heart rate measures (Fig. 6A, Friedman non-parametric test, $\chi^2_{(253)} = 437.8$, $p < 0.001$), such that overall heart rate (HR) varies in response to a specific sound, as a function of the type of run being used. Differences in HR are observed between face runs and the two types of social runs, most probably due to the identity of the visual and auditory stimuli, and how they are processed by the monkeys. While this pattern is interesting, we focus here on the observed differences in HR between the positive and negative contexts of runs involving identical stimuli. For the paired contexts (F+ /F- and S1+/S1-) both types of sounds (i.e. coos and aggressive calls) are associated with higher heart rate in the positive contexts than in the negative contexts (Wilcoxon paired non-

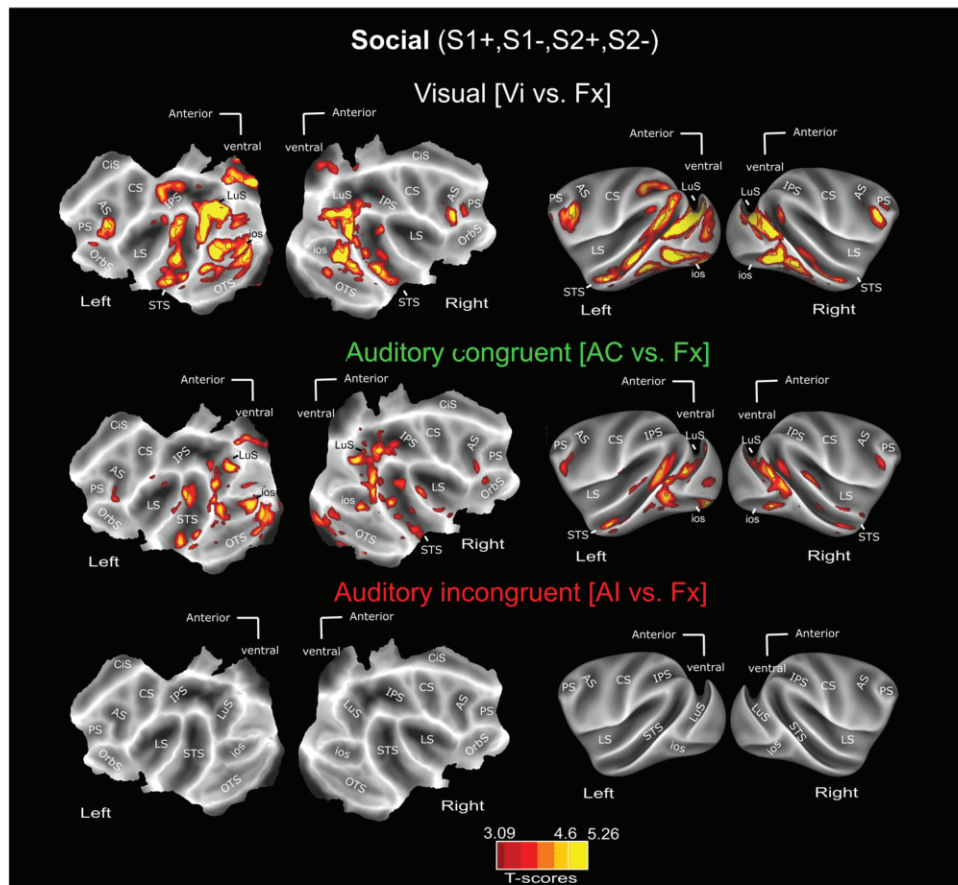


Fig. 4 | Whole-brain activation Social contexts (S1+, S1-, S2+ & S2-): main contrasts. Whole-brain activation maps of the S1+, S2+ (social affiliative 1 & 2), S1- (social aggressive) and S2- (social escape) runs, cumulated over both monkeys, for the visual (white, Vi vs. Fx), auditory congruent (green, AC vs. Fx) and auditory incongruent (red, AI vs. Fx). Note that the AC and AI conditions contain exactly the same sound samples (coos, aggressive calls and screams). Darker shades of red

indicate level of significance at $p < 0.001$ uncorrected, t -score 3.09. Lighter shades of yellow and brown outlines indicate level of significance at $p < 0.05$ FWE correction, t -score > 4.6 , $DF = [1, 10344]$. ios Inferior Occipital Sulcus, LS Lateral Sulcus, STS Superior Temporal Sulcus, C1S Cingulate Sulcus, IPS Intraparietal Sulcus, PS Precentral Sulcus, CS Central Sulcus, AS Arcuate Sulcus, LuS Lunate Sulcus, OrbS Orbital Sulcus.

parametric test, aggressive calls between the F+ and F- contexts: $Z = 13.77$, $p < 0.001$, Cohen's $d = 16.3$ and S1+ and S1-: $Z = 13.82$, $p < 0.001$, Cohen's $d = 91.6$; Coos between the F+ and F-: $Z = 13.87$, $p < 0.001$, Cohen's $d = 47.05$, S1+ and S1-: $Z = 13.78$, $p < 0.001$, Cohen's $d = 17.42$). Screams are also associated with higher heart rate in the positive context than in the negative context (S2+/S2-: Wilcoxon paired non-parametric test, $Z = 13.77$, $p < 0.001$, Cohen's $d = 4.01$). A reverse effect is observable for coos in the negative context containing screams (S2+/S2-), i.e. heart rate is higher in the negative context than in the positive context (Wilcoxon paired non-parametric test, $Z = 13.78$, $p < 0.001$, Cohen's $d = 5.987$). Although heart rate measures vary from one context to the other, in all contexts, congruent auditory stimuli (Fig. 6A, green) is systematically associated with lower heart rates than incongruent auditory stimuli (Fig. 6A, red, Friedman non-parametric test, Face: $\chi^2_{(253)} = 271.442$, $p < 0.001$; Social 1: $\chi^2_{(253)} = 295.34$, $p < 0.001$; Social 2: $\chi^2_{(253)} = 174.66$, $p < 0.001$, Wilcoxon paired non-parametric test: F+ : $Z = 13.98$, $p < 0.001$, Cohen's $d = 4.5$, F-: $Z = 9.77$, $p = 0.012$, Cohen's $d = 3.9$; S1+ : $Z = 13.76$, $p < 0.001$, Cohen's $d = 19.7$, S1-: $Z = 13.72$, $p < 0.001$, Cohen's $d = 18.66$, S2+ : $Z = 13.82$, $p < 0.001$, Cohen's $d = 8.1$, S2-: $Z = 13.77$, $p < 0.001$, Cohen's $d = 2.92$). This effect is more pronounced for the social contexts (S1+/S1- and S2+/S2-) than for the face contexts (Fig. 6B, F+/F-, Wilcoxon, $F = 17.45$, $p < 0.001$, Cohen's $d = 1.81$). This suggests an intrinsic difference between the processing of faces and social scenes. This effect is also more pronounced for contexts involving affiliative visual stimuli (F+, S1+ and S2+) than for contexts involving aggressive or escape visual stimuli (Fig. 6B. F-, S1-

and S2-, Wilcoxon non-parametric test, $F = 13.20$, $p < 0.001$, Cohen's $d = 1.73$). This latter interaction possibly reflects an additive effect between the semantics and emotional valence of the stimuli. Indeed, affiliative auditory stimuli are reported to decrease heart rate relative to aggressive or alarm stimuli⁴⁶. As a result, emotionally positive stimuli would enhance the semantic congruence effect, while emotionally negative stimuli would suppress the semantic congruence effect. Overall, these observations indicate that semantic congruence is perceptually salient, at least implicitly. Importantly, the temporal dynamics of heart rate changes appear to mirror hemodynamic signal modulation in the identified functional network. Because changes in heart rate might affect measured fMRI responses⁴⁷, we re-ran the analyses presented in Figs. 2-4 using heart rate as a regressor of non-interest in addition to head motion and eye position (Supplementary Fig. 12). Observed activations remained unchanged, thus indicating that the reported activations are not an artefact of changes in heart rate. In order to further estimate the degree of coupling between heart rate and brain activations, we run a GLM using heart rate as a regressor of interest. No activations could be observed including at uncorrected levels.

Visual auditory gradients across the lateral sulcus (LS) and superior temporal sulcus (STS)

While LS demonstrates stronger activation for socially congruent auditory stimuli relative to visual stimuli, the STS appears to be equally activated by both sensory modalities. To better quantify this effect, we

Evolution of AC-AI/AC+AI modulation index as a function of

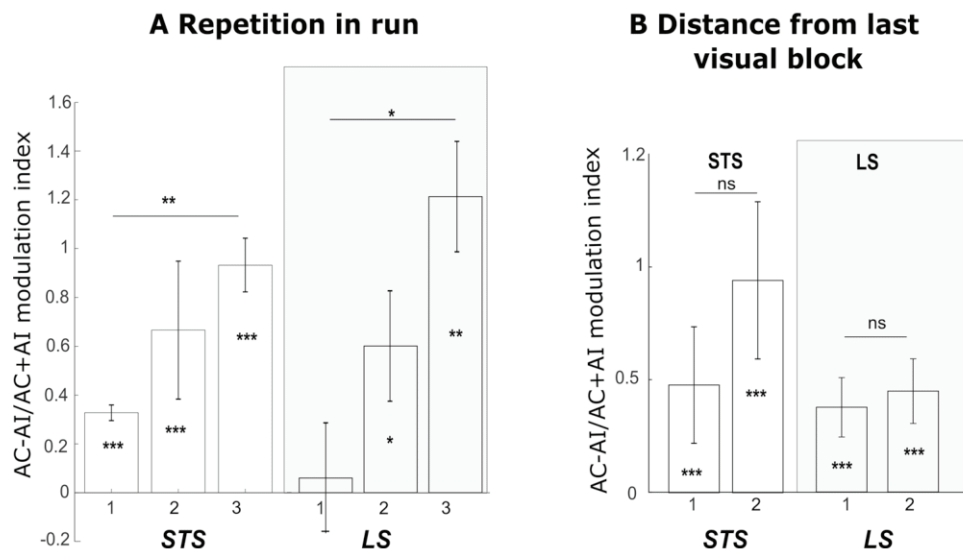


Fig. 5 | Distribution of AC-AI/AC+AI modulation index as a function of repetition in run and distance from last visual block. Distribution of modulation index of percentage signal change (%SC) for the AC condition relative to fixation baseline compared to the AI condition relative to fixation baseline (AC - AI/AC + AI), as a function of repetition order in the run (A) or as a function of the distance from the last visual block (B), for each of the STS and LS, and each of the face and social runs, computed on individual ROIs across all runs. In (A), 1: first occurrence of AC or AI, 2: second occurrence, 3: third occurrence. In (B), 1: AC or AI just following a block with visual stimuli presentations, 2: AC or AI presented two blocks away from a block

with visual stimuli presentations. Statistical differences relative to baseline or across conditions are indicated as follows: ***, $p < 0.001$; **, $p < 0.01$; *, $p < 0.05$; n.s., $p > 0.05$ (Wilcoxon two-sided non-parametric test: (A) STS 1: $n = 14$, $Z = 3.21$, $p = 1.6e-06$; 2: $n = 14$, $Z = 3.41$, $p = 6.4e-04$; 3: $n = 14$, $Z = 4.78$, $p = 1.7e-06$; 1-2: $Z = 1.58$, $p = 0.11$; 1-3: $Z = 4.16$, $p = 0.003$; 2-3: $Z = 1.81$, $p = 0.06$. LS: 1: $n = 10$, $Z = 1.57$, $p = 0.11$; 2: $n = 10$, $Z = 2.38$, $p = 0.02$; 3: $n = 10$, $Z = 4.38$, $p = 0.01$; 1-2: $Z = 1.77$, $p = 0.07$; 1-3: $Z = 2.3$, $p = 0.02$; 2-3: $Z = 0.86$, $p = 0.38$. B STS: 1: $n = 196$, $Z = 3.26$, $p = 6.7e-12$; 2: $n = 196$, $Z = 3.62$, $p = 6.9e-12$; 1-2: $Z = 1.58$, $p = 0.19$; LS: 1: $Z = 3.18$, $p = 5.1e-12$; 2: $Z = 3.28$, $p = 6.7e-10$; 1-2: $Z = 0.05$, $p = 0.8$). Data are presented as median \pm s.e.

define regions of interest (ROIs, 1.5 mm spheres) at local peak activations in the auditory congruent (AC vs Fx) contrast, in the face contexts (Fig. 7A, see Supplementary Fig. 13 for a precise localization of each of these local maxima on corresponding brain anatomy). These peaks match peak activations in the social contexts auditory congruent (AC vs Fx) contrast. This latter social context contrast reveals two additional peaks in the right LS which were used to define two additional ROIs (right LS4 and LS6). Overall, 8 ROIs are thus defined in the right STS, 6 in the left STS, 4 in the left LS and 6 in the right LS. The numbering of these ROIs was adjusted so as to match mirror positions across hemispheres. Figure 7B presents median percentage signal change (%SC) for each independent ROI, in the left and right hemispheres, on each of the face and social contexts. Overall, STS ROIs and LS ROIs had similar %SC profiles across the face and social contexts (LS: FACE $F_{(9,320)} = 0.585$, $p = 0.867$; SOCIAL $F_{(9,702)} = 1.008$, $p = 0.432$ and STS: FACE $F_{(13, 507)} = 1.283$, $p = 0.225$; SOCIAL $F_{(13,1014)} = 1.629$; $p = 0.078$). No interhemispheric difference could be noted (LS: FACE $F_{(1,40)} = 0.136$; $p = 0.714$; SOCIAL: $F_{(1,78)} = 0.727$; $p = 0.396$ and STS: FACE $F_{(1, 40)} = 0.014$; $p = 0.906$; SOCIAL: $F_{(1,78)} = 0.544$; $p = 0.463$). Note that these observations are preserved when ROIs are defined in an independent set of data identifying face-related activation local maxima from a purely visual task (see Supplementary Fig. 14 and its associated note).

In the STS, in both of the face (F+ and F-) and social contexts (S1+, S1-, S2+ and S2-), %SC in the visual condition relative to fixation across all ROIs is not significantly different from %SC in the auditory congruent condition relative to fixation although a trend can be noted, (Fig. 8, left, Wilcoxon two-sided non-parametric test: FACE: AC vs V: $Z = 1.68$, $p = 0.09$. SOCIAL: AC vs V: $Z = 2.4$, $p = 0.051$). The STS thus appears equally responsive to visual and auditory social stimuli (%SC of all contexts are significantly different from fixation %SC, Wilcoxon non-parametric test, FACE: AC: $Z = 16.14$, $p < 0.001$; V: $Z = 19.35$, $p < 0.001$; SOCIAL: AC: $Z = 11.49$, $p < 0.01$; V: $Z = 14.87$, $p < 0.001$). In

contrast, in the LS, %SC in the visual condition relative to fixation across all ROIs is significantly different from %SC in the auditory congruent condition relative to fixation, (Fig. 8, left, two-sided Wilcoxon non-parametric test, FACE: AC vs V: $Z = 3.97$, $p < 0.01$; SOCIAL: AC vs V: $Z = 4.7$, $p < 0.01$). This result therefore suggests a strong auditory preference for LS (%SC of all auditory congruent are significantly different from fixation, Wilcoxon non-parametric test, FACE: $Z = 11.65$, $p < 0.001$; SOCIAL: $Z = 5.86$, $p < 0.01$), although LS is also significantly activated by the visual stimuli in the face context (V: $Z = 4.84$, $p < 0.01$). Last, V and AC activations were significantly weaker in the social context relative to the face context (AC: STS: $Z = 7.17$, $p < 0.001$; LS: $Z = 4.9$, $p < 0.001$; V: STS: $Z = 6.54$, $p < 0.001$; LS: $Z = 4.32$, $p < 0.001$). This is most probably due to the fact that both visual (faces vs. social scenes) and auditory stimuli (coos + aggressive calls vs. coos + aggressive calls + screams) were different between the two contexts. This could have resulted in low level sensory differences in stimulus processing due to differences in spatial and auditory frequency content. Alternatively, these differences might have generated a different engagement from the monkeys in the task for faces and scenes. Yet, another possibility is that the non-human primate brain does not process in exactly the same way the association of social auditory stimuli with facial expressions and with scenes. This will have to be further explored. Overall, therefore, LS appears preferentially sensitive to auditory stimuli whereas the STS appears more responsive to visual than auditory stimuli. In Supplementary Fig. 5B, we show the modulation index of AC versus Vi for both sulci and type of context.

Visual-auditory integration in the STS during the social contexts

When processed in the brain, sensory stimuli from different modalities are combined such that the neuronal response to their combined processing is different from the sum of the neuronal responses to each one of them. This process is called multisensory integration⁴⁸ and is more pronounced when unimodal stimuli are ambiguous or difficult to

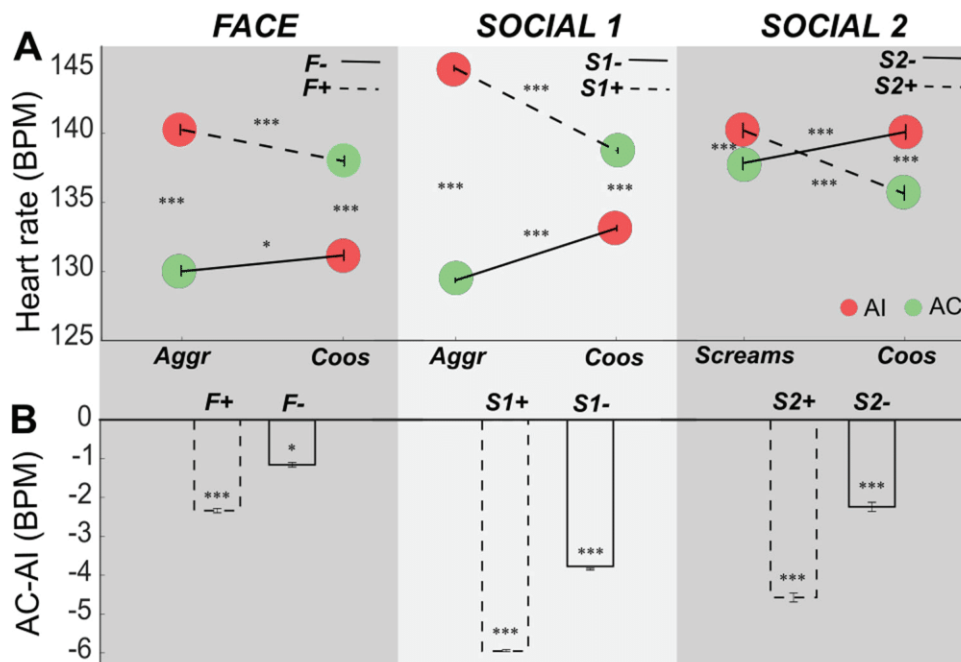


Fig. 6 | Context-related heart rate (BMP) variations. **A** Absolute heart rate (BPM, beats per minute) during the congruent (green) and incongruent (red) auditory blocks of each task. Dashed lines correspond to the positive affiliative context (F+, S1+ and S2+) as defined by the visual stimuli, whereas continuous lines refer to the negative aggressive (F- and S1-) or escape contexts (S2-). Contexts are defined by pairs involving the same vocalisation categories but different visual stimuli, as defined in Fig. 1b. There is a general context effect on heart rate (Friedman non-parametric test, $\chi^2_{(253)} = 437.8, p = 6.7e-286$). There is a significant difference of HR for a same sound as a function of the context (Wilcoxon paired two-sided non-parametric test, all $n = 127$, aggressive calls between the F+ and F- contexts: $Z = 13.77, p = 3.6e-43$, Cohen's $d = 16.3$ and S1+ and S1-: $Z = 13.82, p = 1.8e-43$, Cohen's $d = 91.6$; Coos between the F+ and F-: $Z = 13.87, p = 9.1e-44$, Cohen's $d = 47.05$, S1+ and S1-: $Z = 13.78, p = 3.5e-43$, Cohen's $d = 17.42$ and S2+ and S2- contexts: $Z = 13.78, p = 3.6e-43$, Cohen's $d = 5.987$ and for screams between S2+ and S2- contexts: $Z = 13.77, p = 3.6e-43$, Cohen's $d = 4.01$). Each context pair shows significantly higher

heart rates for incongruent auditory stimuli compared to congruent auditory stimuli (Friedman non-parametric test, Face: $\chi^2_{(253)} = 271.442, p = 2.8e-82$; Social 1, $\chi^2_{(253)} = 295.34, p = 1.3e-87$; Social 2, $\chi^2_{(253)} = 174.66, p = 5.4e-78$). This is also true for each individual context (Wilcoxon paired two-sided non-parametric test. F+ : $Z = 13.98, p = 9.1e-49$, Cohen's $d = 4.5$, F- : $Z = 9.77, p = 0.012$, Cohen's $d = 3.9$, S1+ : $Z = 13.76, p = 4.4e-49$, Cohen's $d = 19.7$, S1- : $Z = 13.72, p = 4e-49$, Cohen's $d = 18.66$, S2+ : $Z = 13.82, p = 3.6e-49$, Cohen's $d = 8.1$, S2- : $Z = 13.77, p = 4.4e-49$, Cohen's $d = 2.92$). **B** Difference between AC and AI bloc (medians \pm s.e). All significantly different from zero (Wilcoxon paired two-sided non-parametric test. F+ : $n = 127, Z = 13.98, p = 4.4e-5$, Cohen's $d = 4.5$, F- : $n = 127, Z = 9.77, p = 0.012$, Cohen's $d = 3.9$, S1+ : $n = 127, Z = 13.76, p = 2.4e-04$, Cohen's $d = 19.7$, S1- : $n = 127, Z = 13.72, p = 2e-04$, Cohen's $d = 18.66$, S2+ : $n = 127, Z = 13.82, p = 4.3e-05$, Cohen's $d = 8.1$, S2- : $n = 127, Z = 13.77, p = 2.4e-04$, Cohen's $d = 2.92$). Note that for every item, Cohen's d coefficient is higher than 0.8. Each effect size is therefore considered as large. ***, $p < 0.001$; **, $p < 0.01$; *, $p < 0.05$; n.s., $p > 0.05$.

perceive^{49,50}. The question here, therefore, is whether and how the LS and the STS combine visual and auditory social stimuli as a function of their semantic congruency. Multisensory integration is not straightforward to assess based on fMRI signals. A minimal criterion here would be to have significant %SC differences between the bimodal conditions and both of the unimodal conditions. Figure 9 shows the whole brain activation maps obtained for the two visual-auditory conditions, congruent (VAC, Fig. 9A) and incongruent (VAI, Fig. 9B) contrasted with fixation, as well as for the visual condition (vs. fixation) and the auditory condition (vs. fixation). These contrasts are presented for both face (Fig. 9, left panel) and the social contexts (Fig. 9, right panel). Figure 9C presents the contrast between the incongruent and congruent visuo-auditory conditions (VAI vs VAC).

Overall, in the face context, activations in the audio-visual conditions are not significantly different from the visual and auditory conditions alone (Fig. 9A, B, left panel). Likewise, no significant difference can be seen between the congruent and incongruent visuo-auditory conditions (Fig. 9C, left panel). Supplementary Fig. 15 compares %SC for the bimodal and unimodal conditions across all STS selected ROIs and all LS selected ROIs. Neither reach the minimal criteria set for multisensory integration. In the social context, activation in the audio-visual conditions show local significant differences relative to the visual and auditory conditions alone (Fig. 9A, B, right panel). When comparing the %SC for the bimodal and unimodal conditions across all STS selected ROIs and all LS selected ROIs, the STS ROIs reach the minimal criteria set for multisensory integration,

as their %SC is significantly different from each of the bimodal conditions and each of the unimodal conditions (Wilcoxon non-parametric test, AC vs VAC: $Z = 5.35, p < 0.01$; AC vs VAI: $Z = 4.06, p < 0.01$; V vs VAC: $Z = 2.64, p < 0.01$; V vs VAI: $Z = 2.48, p < 0.01$). Thus, multisensory integration appears to take place, specifically in the STS, and during the social context, possibly due to the higher ambiguity in interpreting social static scenes relative to faces (Supplementary Fig. 15). Importantly, and while most significant activations in the bimodal vs. unimodal auditory conditions are located within the audio-visual vs. fixation network, a bilateral activation located in the anterior medial part of the LS deserves attention. Indeed, this activation, encompassing part of the insula and of anterior SII/PV, is identified both in the congruent and incongruent auditory conditions and might be involved in the interpretation of semantic congruence between the visual and auditory stimuli. This possibility is addressed in the Discussion that follows.

Discussion

Based on heart rate estimates and fMRI, our results show that rhesus monkeys systematically associate affiliative facial expressions or social scenes with corresponding affiliative vocalisations, aggressive facial expressions or social scenes with corresponding aggressive vocalisations, and escape visual scenes with scream vocalisations. In contrast, vocalisations that are incompatible with the visual information are fully suppressed, suggesting a top-down regulation over the processing of sensory input. In other words, rhesus monkeys correctly associate the

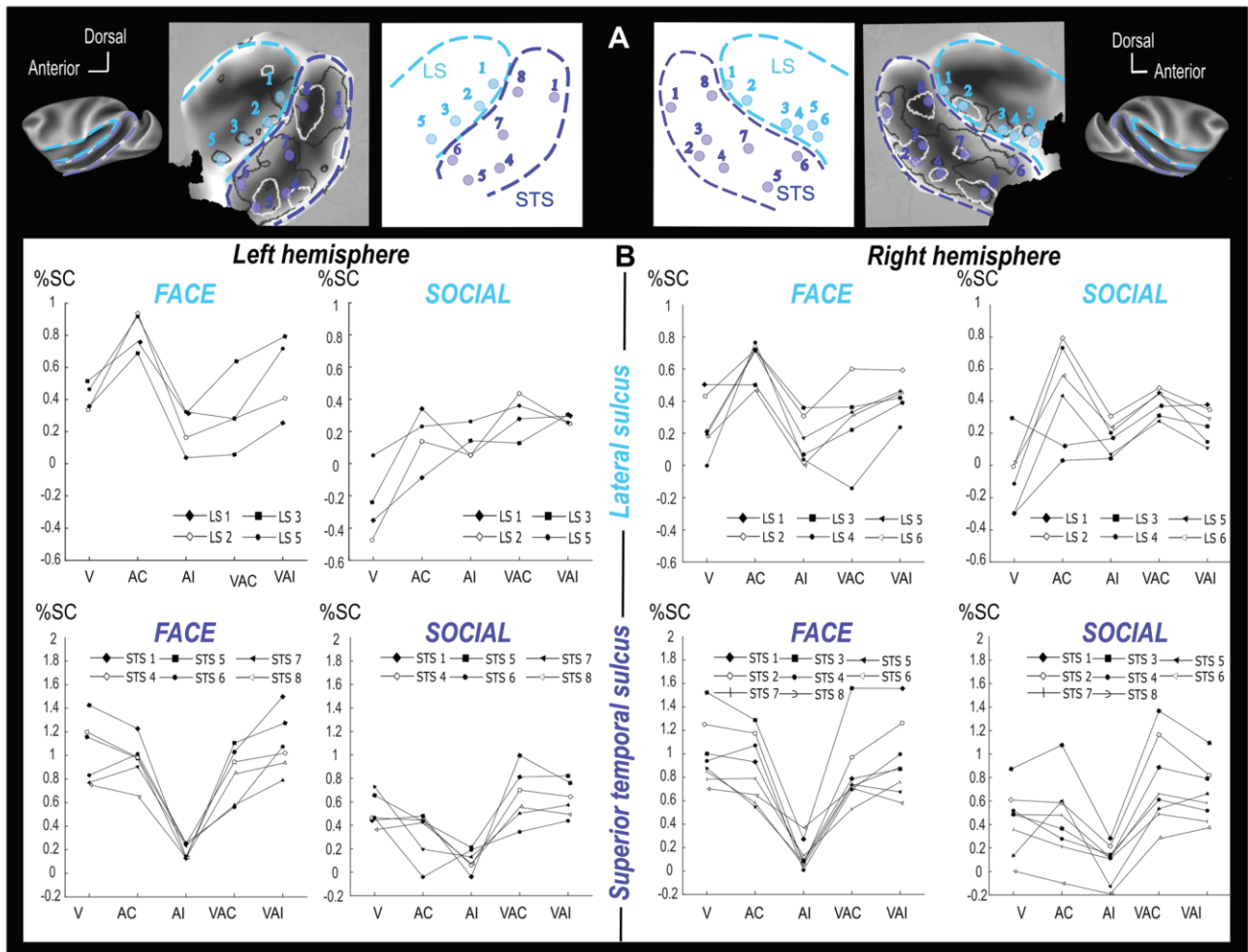


Fig. 7 | Percentage of signal change (%SC) for selected left and right hemisphere ROIs in the lateral sulcus (light blue) and in the superior temporal sulci (dark blue). **A** ROIs are 1.5 mm spheres located at local peak activations. Left and right hemisphere numbering associate mirror ROIs. ROI location in the each of the left and right STS and LS is described in the bottom flat maps. **B** %SC (median) are

presented for each ROI (eight in right STS, six in left STS, four in left and six in right lateral sulcus) and each contrast of interest (V visual vs fixation, AC auditory congruent vs fixation, AI auditory incongruent vs fixation, VAC visuo-auditory congruent vs fixation, VAI visuo-auditory incongruent vs fixation).

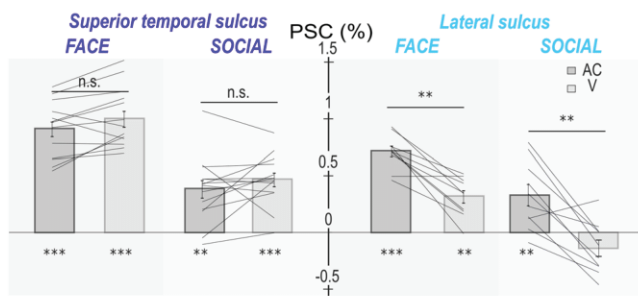


Fig. 8 | Percentage of signal change (PSC) across all lateral sulcus (light blue) and superior temporal sulci (dark blue) ROIs of both hemispheres, comparing the auditory and visual contexts (median ± s.e., single lines correspond to the PSC computed over single ROIs from the group analysis; n = 14 ROIs for STS and n = 10 ROIs for LS). Statistical differences relative to fixation are between contexts and indicated as follows: ***, $p < 0.001$; **, $p < 0.01$; n.s., $p > 0.05$ (Wilcoxon two-sided non-parametric test). STS: FACE: AC: $n = 560$, $Z = 16.14$, $p = 4.1e-57$; V: $n = 560$, $Z = 19.35$, $p = 1.8e-68$; AC vs V: $Z = 1.68$, $p = 0.09$. SOCIAL: AC: $n = 1106$, $Z = 11.49$, $p = 0.0011$; V: $n = 1106$, $Z = 14.87$, $p = 1.5e-49$; AC vs V: $Z = 2.4$, $p = 0.051$. LS: FACE: AC: $n = 400$, $Z = 11.65$, $p = 2.4e-31$; V: $n = 400$, $Z = 4.84$, $p = 0.002$; AC vs V: $Z = 3.97$, $p = 0.01$. SOCIAL: AC: $n = 790$, $Z = 5.86$, $p = 0.002$; V: $n = 790$, $Z = -0.7$, $p = 0.45$; AC vs V: $Z = 4.7$, $p = 0.0013$.

meaning of a vocalisation with the meaning of a visual scene. This audio-visual, semantic binding with contextual information relies on a core functional network involving the superior temporal sulcus (STS) and the lateral sulcus (LS). LS regions of interest (ROIs) have a preference for auditory and audio-visual congruent stimuli while STS ROIs respond equally to auditory, visual and audio-visual congruent stimuli. Multisensory integration is only identified in the STS and only in the social condition in which visual information is expected to be more ambiguous than in the face condition. These observations are highly robust as they are reproduced over six sets of independent behavioural contexts, involving distinct associations of visual and auditory social information.

Interpretation of social scenes and vocalisation by macaque monkeys

As is the case for human oral communication, monkey vocalisations are expected to be interpreted as a function of their emotional or contextual meaning. For example, a monkey scream indicates potential danger, is associated with fear and calls for escape and flight from the dangerous context. In contrast, coos are produced during positive social interactions and often elicit approach^{8,9}. Here, we show that when two different types of vocalisations are presented together with a social visual stimulus, the heart rate of the monkeys is significantly lower when the vocalisation is congruent with the visual scene than

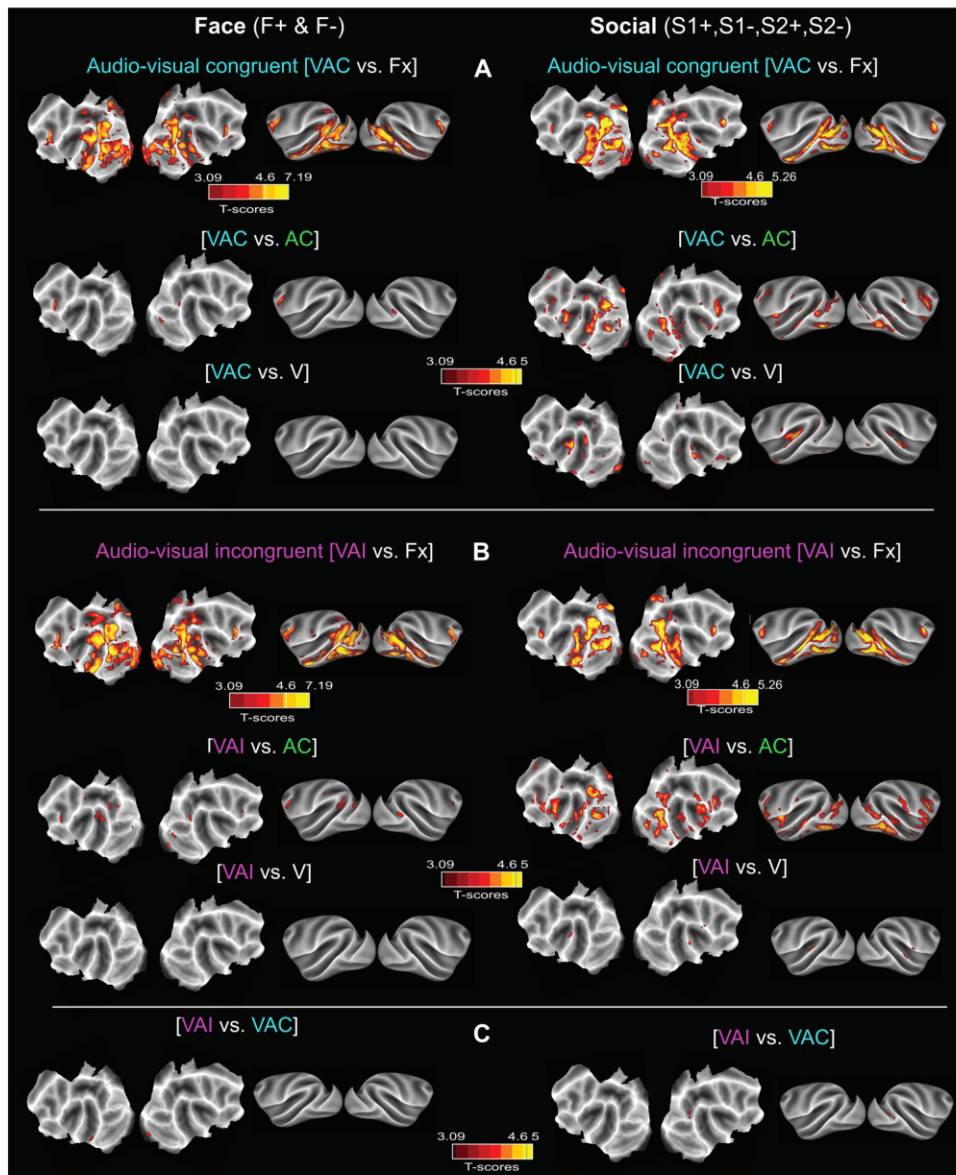


Fig. 9 | Whole-brain activations for the Face (F+ & F-) and Social contexts (S1+, S1-, S2+ & S2-): bimodal versus unimodal contrasts. **A** Whole-brain activation maps of the F+ (face affiliative) and F- (face aggressive) runs (left panel) and the S1+, S2+ (social affiliative 1 & 2), S1- (social aggressive) and S2- (social escape) runs (right panel) for the congruent audio-visual stimulation (blue). Contrasts from top to bottom: audio-visual vs. fixation, audio-visual vs. auditory congruent and audio-

visual vs. visual. **B** Same as in (A) but for the incongruent audio-visual stimulation (pink). **C** Whole-brain activation maps for the audio-visual incongruent vs. audio-visual congruent contrast. All else as in (A). Darker shades of red indicate level of significance at $p < 0.001$ uncorrected, t -score > 3.09 . Lighter shades of yellow and brown outlines indicate level of significance at $p < 0.05$ FWE correction, t -score > 4.6 . $DF = [1, 5200]$ for Face and $DF = [1, 10344]$ for Social.

when the vocalisation is incongruent with the scene. Likewise, we show that the activity of the voice processing network is dramatically suppressed in response to the incongruent vocalisation. This pattern of activation provides neurobiological evidence that macaques infer meaning from both social auditory and visual information and are able to associate congruent information. In the network of interest, activations are not significantly different between the auditory, visual or audio-visual conditions. Most interestingly, aggressive calls are associated with both aggressive faces and aggressive social scenes, whereas coos are associated with both lipsmacks and inter-individual social grooming. We thus propose that these networks represent social meaning irrespective of sensory modality, thereby implying that social meaning is amodally represented. We hypothesize that such representations are ideal candidate precursors to the lexical categories that trigger, when activated, a coherent set of motor, emotional and social repertoires.

Audio-visual association based on meaning and multisensory integration

The strict definition of multisensory integration involves the combination of sensory inputs from different modalities under the assumption of a common source^{51,52}. In this context, it has been shown that multisensory integration speeds up reaction times and enhances perception⁵³⁻⁵⁷, including when processing lip movement during speech⁵⁸⁻⁶⁰. Multisensory processes are also at play to predict the consequences of one modality onto another, i.e. in the temporal domain⁶¹⁻⁶⁴. At the neuronal level, multisensory integration is defined as a process whereby the neuronal response to two sensory inputs is different from the sum of the neuronal responses to each on its own^{48,65}. In the present study, the auditory and visual stimuli are associated based on their meaning (e.g., coos are associated with grooming) and possible contingency (e.g., screams are associated with escape scenes). Thus the audio-visual association described here goes

beyond the strict definition of two sensory inputs produced by a common source.

Additionally, by task design, two levels of audio-visual congruency can be defined. Level one is a first order congruency, defined within the audio-visual blocks, such that the auditory information can either be congruent (VAC) or incongruent (VAI) to the visual information. Level two is second order congruency, defined at the level of the run, such that given the visual information presented in a given run, the pure auditory blocks can either be defined as congruent (AC) or incongruent (AI) to the general visual context of this specific run, even if not simultaneously presented with the visual information. In order to probe whether first order congruency gives rise to multisensory integration, we applied the less stringent multisensory integration criteria used in fMRI studies, testing if audio-visual responses are statistically higher or lower than each of the uni-sensory conditions^{66–70}. Face-voice integration has been described in the auditory cortex (CL, CM, in awake and anaesthetised monkeys; AI only in awake monkeys) and the STS^{40,71}, and to a lesser extent in specific face-patches³⁶. This latter study is worth noting as their experimental design matched, in important ways, our own, including audio-visual, visual only or auditory only stimuli. They used both monkey movies with a perfect match between visual and auditory stimulation in the audio-visual stimulus and created a computer-generated animated macaque avatar with the explicit intention of having synchronisation between the vocalisation and facial movements of the avatar. The study was thus explicitly testing multisensory integration under the hypothesis that the visual and auditory stimuli were associated with a common source. The audio-visual stimuli thus achieved a double congruence: they were temporally synchronised such that facial movements predicted vocalisations and as a consequence, they matched in semantic content. In the present study, our aim was to study the second type of congruence, i.e. semantic congruence. Our audio-visual stimuli were therefore not synchronised, but the two stimuli, when presented at the same time could be congruent (or incongruent) in semantic terms. The face-voice or scene-voice multisensory integration described by Khandhadia et al. is of a different nature to the one we report here. More specifically, in the present data, enhancement of the audio-visual response can only be seen in the contexts involving visual scenes. The parsimonious interpretation of these observations is that face-vocalisation binding was easier than scene-vocalisation binding and resulted in signal saturation, in agreement with the fact that neuronal multisensory integration is more pronounced for low saliency stimuli. The most significant difference between our study and that of Khandhadia et al. pertains to the second order congruency, an issue we discuss next.

Second order congruency is set by the visual information defining any given experimental run and results in major differences in how congruent and incongruent sounds are processed including in the absence of any visual stimulation. Congruent auditory information results in enhanced cortical activations relative to previous reports. Indeed, auditory activations have already been described in the STS^{22,23,25,29,40,71,72}. However, and specific to our task design, the STS auditory activations described here in response to the congruent auditory stimuli are as strong as the visual responses (though with a trend to being slightly significantly weaker) and extend into the extrastriate visual cortex, thus suggesting cross-modal enhancement. In contrast, we show in this study an inhibition of irrelevant auditory information as a function of the context set by visual information. This process of filtering incongruent social auditory stimuli relative to social visual stimuli has already been shown at the behavioural level. Specifically, adults are shown to reliably filter out irrelevant social auditory information as a function of visual information while children below age 11 found this more challenging⁷³. This was even more marked for children below age 7. This capacity of adults to filter irrelevant information is thought to arise from cross modal inhibition.

Such cross-modal inhibition has for example been described in the auditory cortex in response to visual and auditory stimuli presented simultaneously. Importantly, such cross-modal inhibition has been shown to switch on or off as a function of the context⁷⁴. Accordingly, functional interactions between the visual and auditory networks can either result in an enhancement or in a suppression of cortical activity depending on the task and the presented stimuli⁷⁵. The results we present here go beyond these early observations, as the inhibition of the irrelevant auditory stimulus does not take place at the time of presentation of the visual stimulus but when presented on its own, as the context is not set on a single trial basis but rather in well segregated behavioural runs. We hypothesize that our observations rely on a generalized form of cross-modal inhibition. This will have to be tested experimentally.

As discussed above, a specificity of our task design is that it creates, within each run, an implicit association between a set of social visual stimuli and their auditory match, possibly based on past learned sensory-motor associations and the development of internal models of what vocalisations are produced in a given visual context. This is very reminiscent of the recent description of auditory fMRI activations to learned sound sequences in the motor cortex of the macaque brain⁷⁶. These auditory responses were only present in monkeys who had received an audio-motor training and were only present in response to the learned sound and were absent for other sounds. The authors propose that an internal model of auditory perception associating a given auditory set of stimuli with a given motor repertoire (and thus motor structure) was created by the training. We here argue that likewise, our current observations arise from the fact that macaques have, throughout their lifespan, associated specific macaque calls with specific social visual experiences, and that our specific task design allows to reveal this internal model. It is an open question as to how this mapping develops in young rhesus monkeys, and what experience is necessary.

It is worth noting that our results go against the predictive coding theory. This theory posits that the brain is constantly generating and updating an internal model of the environment. This model generates predictions of sensory input and compares these to actual sensory input^{77,78}. Prediction errors are then used to update and revise the internal model⁷⁹. In the context of predictive coding, when viewing an affiliative face, monkeys are expected to predict affiliative vocalisations. As a result, aggressive vocalisations in the context of affiliative faces are expected to generate prediction errors and hence higher activations than those observed for the affiliative vocalisations. This is not what our data show: when, viewing affiliative faces, there are enhanced responses to affiliative vocalisation and suppressed responses to aggressive vocalisations. This effect actually builds up as visual contextual information is reinforced through the run and is present in both the STS and the LS, i.e. at the early stages of auditory processing. Thus, these observations are inconsistent with the predictive coding experimental predictions. They suggest, instead, that the monkeys implement an active matching or association between the visual and the auditory social information, similar to a match to sample task, based on their life-long social experiences. In match to sample fMRI and EEG studies in humans⁸⁰ and electrophysiology studies in non-human primates^{81,82}, responses to the probe matching the sample is significantly higher than the response to a non-match probe, thus describing a match enhancement⁸³. This is very similar to what we describe here, if considering the visual context as the probe and the auditory stimuli as the match and non-match probes. Further work is required to confirm this hypothesis.

An important question is how context is implemented into LS and STS. The STS is involved in multisensory integration and is shown to play a modulatory role on lateral sulcus functions during audio-visual stimulations^{38,40,72}. However, the mechanisms subserving the observed selective cross modal inhibition of auditory processing based on the

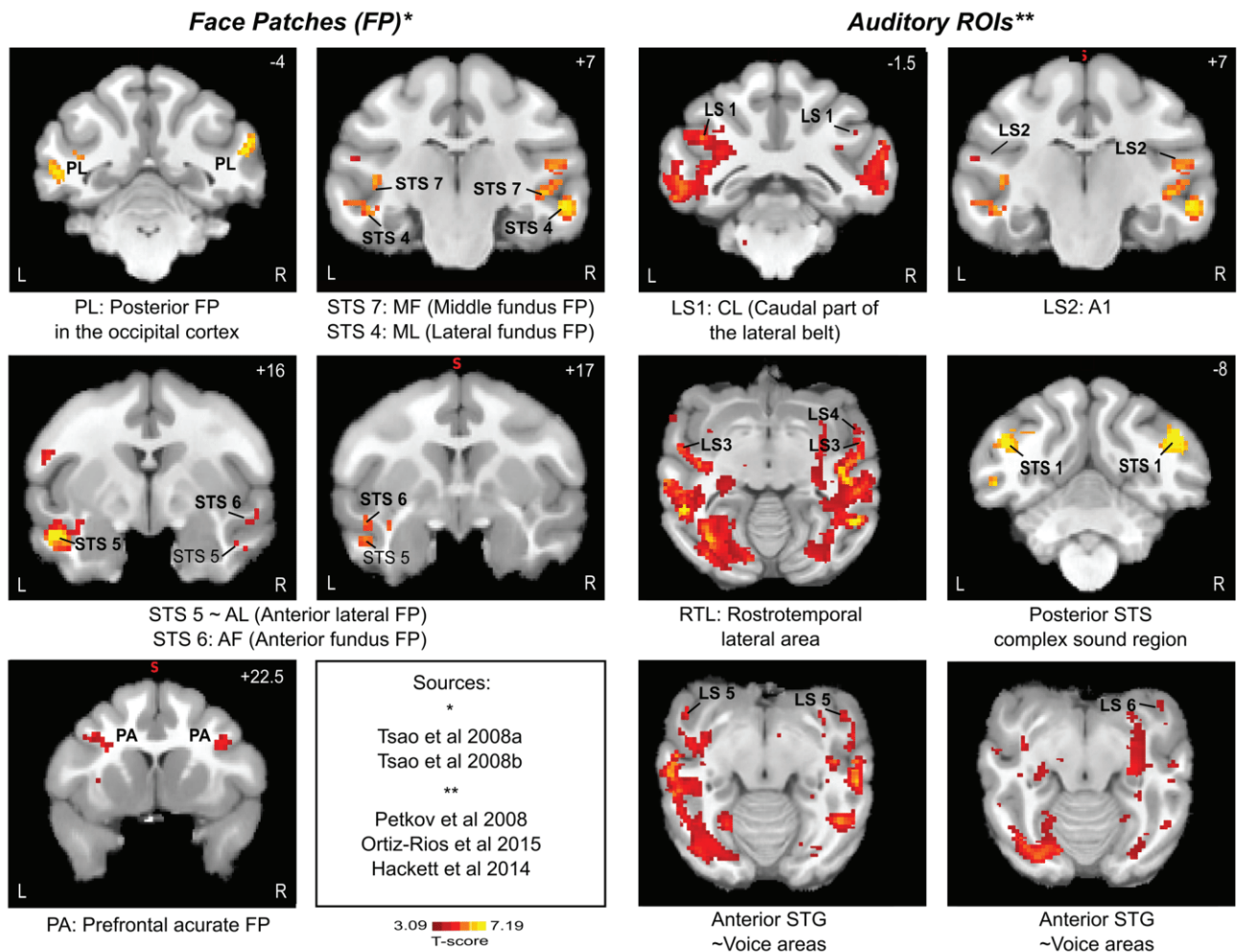


Fig. 10 | Correspondence between task-related ROIs and face patches (left panels) and voice areas (right panels). Color-scale runs start at $p < 0.001$ uncorrected levels. Task related ROIs are numbered as in Fig. 7. PA prefrontal accurate, AM anterior medial, AF anterior fundus, AL anterior lateral, MF middle fundus, ML middle lateral, PL a posterior face patch in the occipital cortex, CL Caudal part of the lateral belt, A1 primary auditory cortex, RTL Rostrotemporal lateral area, STS Superior Temporal Sulcus, STG Superior Temporal Gyrus. *: Sources for face patch localization. **: Sources for voice areas.

middle lateral, PL a posterior face patch in the occipital cortex, CL Caudal part of the lateral belt, A1 primary auditory cortex, RTL Rostrotemporal lateral area, STS Superior Temporal Sulcus, STG Superior Temporal Gyrus. *: Sources for face patch localization. **: Sources for voice areas.

visual context are implemented not just during audio-visual blocks but throughout any given run. As a result, they are expected to originate from a higher order cortical region exerting a top-down control on both the LS and the STS. The prefrontal cortex is a choice region in this respect, as it connects to LS⁸⁴⁻⁸⁶ and STS^{87,88} and has been shown to play a crucial role in working memory and the top-down modulation of perception^{89,90}. LS and STS are also connected to the cingulate cortex and orbitofrontal cortex^{91,92}. These cortical regions that are involved in the processing of social interactions from visual cues and are thus in a position to provide feedback to the LS and STS based on the social dimension of the stimuli^{13,93-96}. Lastly, LS and STS are also connected to the limbic system^{91,92,97}. Accordingly, conspecific vocalisations activate a network recruiting, in addition to the voice patches, visual areas such as V4, MT, STS areas TE and TEO, as well as areas from the limbic and paralimbic system, including the hippocampus, the amygdala and the ventromedial prefrontal cortex (vmPFC)¹⁸. All of these regions are expected to contribute (most probably in coordination) to setting the context based on which auditory information is considered either as congruent or incongruent. These possibilities will have to be addressed experimentally.

Audio-visual association based on social meaning possibly recruits the face and voice patches

Face processing is highly specialized in the primate brain²⁰. In the macaque brain, it recruits a specific system called the face patch

system, composed of interconnected areas, identified by both fMRI^{14,15,17,21,24,27,28,35,98-100} and single cell recording^{24,101,102}. This system recruits areas in the superior temporal sulcus, as well as in the prefrontal and orbito-frontal cortex. Specific limbic and parietal regions are also recruited together with this core system during, respectively, the emotional and attentional processing of faces³³. The core face patches are divided into five STS areas (Anterior medial, AM; anterior fundus, AF; anterior lateral, AL; middle fundus, MF and middle lateral ML) and the PL (posterior lateral patch), a posterior face patch in the occipital cortex^{35,103}. Based on a review of the literature, and anatomical landmark definitions, we associate the activation peaks identified in the present study with these five face patches (Fig. 10). Correspondence is unambiguous and the STS 4 ROIs matches ML, STS 7 matches MF, STS 5 matches AL and STS 6 matches AF. The occipital face patch PL is also identified in the general contrast maps as well as the frontal area defined in the literature as PA (prefrontal accurate)⁴⁴. It is worth noting that in our experimental design, these face patches are activated both during the purely auditory congruent condition as well as during the visual conditions. Such activations are not reported by others during purely auditory conditions, indicating that this network is recruited during audio-visual association based on meaning. In the right hemisphere, two supplementary STS activations are reported, STS 2 and STS 3. They are located posterior to the putative ML face patch and ventral to the gaze following patch reported in the dorsal posterior infero-temporal cortex¹⁰⁴ and possibly coincide with an area

in the middle superior temporal cortex that has been recently described as modulated by the predictability of social interactions¹⁰⁵, though this would have to be tested explicitly.

The auditory processing circuit is proposed to be organized in two main networks, a ventral and a dorsal network (see for review^{84,106,107}), such that the auditory ventral stream, also called the pattern or “what” stream, is activated by conspecific vocalisations whereas the dorsal stream, also called spatial or “where” stream, is involved in the spatial location of sounds^{25,32}. Similarly, to face patches, voice processing by the “what” auditory stream, also involves a system of voice patches (for review, see¹⁰⁸). In macaques, voice specific areas include the anterior superior temporal gyrus (aSTG), the orbitofrontal cortex (OFC) and a part of the STS close to the lateral sulcus^{16,22,23,26,29,39}. This functional dissociation is observable as early as in the lateral belt such that its caudal part (CL) is selectively associated with sound location while the anterior part (AL) is more linked to sound identity such as vocalisations^{106,109,110}. Again, based on a review of the literature, and anatomical landmark definitions, we associate the activation peaks identified in the present study with these voice patches (Fig. 10). This network is composed of prefrontal and temporal areas, but also, of visual striate and extrastriate visual areas (see Supplementary note attached to Supplementary Tables 1–3). Correspondence is unambiguous and the LS 1 ROI can be associated to CL (i.e. dorsal sound processing pathway) and LS2 to core primary auditory area A1. Within the ventral sound processing pathway, LS 4 ROI can be associated to area AL, LS 5 to rostro-temporal lateral area (RTL) and LS 6 to the rostro-temporal polar field (RTp). Last, LS 6 is compatible with the anterior most voice STG area described by Petkov and colleagues²⁶. The voice patch system also involves the ventral dorsolateral prefrontal cortex or vlPFC³¹, located in the inferior dimple at the boundary between area 45a and 46¹¹¹. This cortical region has been proposed to play a key role in the cognitive control of vocalisations as well as in the interpretation of call meaning¹¹². Microstimulations further indicate that this prefrontal voice patch is functionally connected with the putative macaque homologue of human’s Broca area 44¹¹³. In the present study, the ventral prefrontal activation, while matching nicely with the PA face patch, only partially overlaps with the prefrontal voice patch, suggesting a possible functional specialization. Taken together, these results strongly suggest that the association between vocalisation meaning and social visual stimuli recruits the face and voice patch system.

Visual fMRI activations have already been described in the LS, in the primary auditory cortex and in the non-primary core (belt)¹¹⁴. This observation has been confirmed using single cell recording studies¹¹⁵. An important question to be addressed by single unit recording studies is whether the STS auditory activations correspond to neuromodulatory LFP modulations or to actual spiking activity. Quite interestingly, while we identify an audio-visual gradient between the LS and the STS, the LS showing higher activations for voice as compared to visual social stimuli, and the STS showing a preference for visual stimuli compared to auditory stimuli, no clear gradient of auditory or visual activations can be identified either within the STS or within the LS. This suggests that voice-social visual associations rely on the activity of the entire network, rather than on some of its subparts.

Visual and auditory responses in the lateral sulcus and superior temporal sulcus

Expectedly, the LS activations in response to auditory stimuli are higher than its activations to visual stimuli (Fig. 8). This most probably arises from the fact that while the primary function of the LS is auditory processing, it receives (visual) input from the adjacent STS^{38,116}. In contrast, based on the ROIs defined in the audio-visual face task, STS appears to be equally responsive to auditory and visual stimuli (Fig. 8, trend to significance), although $AC - V/AC + V$ modulation indexes are significantly negative (Supplementary Fig. S5). When ROIs are defined

on the basis of a purely visual task, STS visual responses are significantly higher than STS auditory responses (Supplementary Fig. 14). Overall, this suggests the existence, within the STS, of specialized regions involved in the visuo-auditory association of social stimuli. While large areas of the STS become responsive to auditory stimuli during visuo-auditory association of social stimuli—perhaps due to a direct projection from the LS to the STS⁸⁸—only some regions are activated to almost a similar level by both sensory modalities. These regions could contribute to the amodal representation of social stimuli.

To conclude, our experiments demonstrate, using indirect measures (heart rate and hemodynamic brain response), that macaque monkeys are able to associate social auditory and visual information based on their abstract meaning. This supports the idea that non-human primates display advanced social competences, amodally represented, that may have paved the way, evolutionary, for human social cognition, including its linguistic representations and expressions.

Methods

Subjects and surgical procedures

Two male rhesus monkeys (*Macaca mulatta*) participated in the study (T, 15 years, 10 kg and S, 12, 11 kg). The animals were implanted with a Peek MRI-compatible headset covered by dental acrylic. The anaesthesia for the surgery was induced by Zoletil (Tiletamine-Zolazepam, Virbac, 5 mg/kg) and maintained by isoflurane (Belamont, 1–2%). Post-surgery analgesia was ensured thanks to Temgesic (buprenorphine, 0.3 mg/ml, 0.01 mg/kg). During recovery, proper analgesic and antibiotic coverage was provided. The surgical procedures conformed to European and National Institutes of Health Guidelines for the Care and Use of Laboratory Animals.

Experimental setup

During the scanning sessions, monkeys sat in a sphinx position in a plastic monkey chair¹¹⁷ facing a translucent screen placed 60 cm from the eyes. Visual stimuli were retro-projected onto this translucent screen. Their head was restrained and the auditory stimuli were displayed by Sensimetrics MRI-compatible S14 insert earphones. The monkey chair was secured in the MRI with safety rubber stoppers to prevent any movement. Eye position (X, Y, right eye) was recorded thanks to a pupil-corneal reflection video-tracking system (EyeLink at 1000 Hz, SR-Research) interfaced with a program for stimulus delivery and experimental control (EventIDE®). Monkeys were rewarded for maintaining fixation into a $2 \times 2^\circ$ tolerance window around the fixation point.

General run design

On each run, monkeys were required to fixate a central cross on the screen (Fig. 1A). Runs followed a block design. Each run started with 10 s of fixation in the absence of sensory stimulation followed by three repetitions of a pseudo-randomized sequence containing six 16 s blocks: fixation (Fx), visual (Vi), auditory congruent (AC), auditory incongruent (AI), congruent audio-visual (VAC) and incongruent audio-visual (VAI) (Fig. 1A). The pseudo-randomization was implemented such that each block in each repetition was presented in a randomized order. Thus monkeys could not anticipate the sequence of stimuli. In addition, the initial blocks were either a visual block (Vi, VAC, VAI), or a fixation block followed by a visual block (Vi, VAC or VAI), such that context was set by visual information early on in each run. As a result, pure auditory blocks were always presented after a visual block and could thus be defined as congruent or incongruent to the visual information characterizing the block. Pseudo-randomization was also implemented such that, across all repetitions and all runs for a given context, each block was, on average, preceded by the same number of blocks from the other conditions. Quite crucially to the results

presented in this work, in 66% of the times, both AI and AC conditions were preceded by blocks involving visual stimulation (Vi, VAC and VAI). Last, each block (except the fixation block) consisted in an alternation of 500 ms stimuli (except for lipsmacks, 1 s dynamic stimuli succession) of the same semantic category (see Stimuli section below), in the visual, auditory or audio-visual modalities. In each block, 32 stimuli were presented randomly (16 for lipsmack). Each run ended by 10 s of fixation in the absence of any sensory stimulations.

Face and social contexts

Six audio-visual contexts were presented to both monkeys, organized in runs as described above (Fig. 1A). Each context combined visual stimuli of identical social content with either semantically congruent or incongruent monkey vocalisations with the predominant visual stimuli (Fig. 1B). Runs always started by a block condition involving visual stimulations, thus setting the social context of the task and, as a result, defining auditory congruent and incongruent auditory stimuli. Given the structure of our task, two levels of congruency can be defined. A first order congruency is defined within the audio-visual blocks, such that the auditory information can either be congruent (VAC) or incongruent (VAI) to the visual information. The second order of congruency is defined at the level of the run, such that, given the visual information presented in a given run, the pure auditory blocks can either be defined as congruent (AC) or incongruent (AI) in this specific run, even if not simultaneously presented with the visual information. The face affiliative context (F+) combined lipsmacks with coos and aggressive calls. The face aggressive context (F-) combined aggressive faces with coos and aggressive calls. The first social affiliative context (S1+) combined grooming scenes with coos and aggressive calls. The second social affiliative context (S2+) combined grooming scenes with coos and screams. The social aggressive context (S1-) combined aggressive group or individual scenes with coos and aggressive calls. The social escape context (S2-) combined fleeing groups or individual scenes with coos and screams. Importantly, pairs of contexts (F+ & F-; S1+ & S1-; S2+ & S2-) shared the same vocalisations, but opposite social visual content (i.e. opposite semantic content, defining either a positive or a negative context). All contexts were presented randomly and at least once during each scanning sessions.

Stimuli

Vocalisations were recorded from semi-free-ranging rhesus monkeys during naturally occurring situations by Marc Hauser. Detailed acoustic and functional analyses of this repertoire has been published elsewhere (e.g.,^{8,9}). Field recordings were then processed, restricting to selection of experimental stimuli to calls that were recorded from known individuals, in clearly identified situations, and that were free of competing noise from the environment. Exemplars from this stimulus set have already been used in several imaging studies^{16,31,32,41,118}. All stimuli were normalized in intensity. The frequency ranges varied between the different types of stimuli as shown in Supplementary Fig. 16. For each of the three vocalisation categories, we used 10 unique exemplars coming from matched male and female individuals, thus controlling for possible effects due to gender, social hierarchy or individual specificity. Coos are vocalisations typically produced during affiliative social interactions, including grooming, approach, coordinated movement, and feeding. Aggressive calls are typically used by a dominant animal toward a subordinate, often as a precursor to an actual physical attack. Screams are produced by subordinates who are either being chased or attacked, or as they are witnessing others in the same condition. Face (lipsmacks and aggressive facial expression) and social scene (group grooming, aggressive individual alone or in group/escaping individual or group) stimuli were extracted from videos collected by the Ben Hamed lab, as well as by Marc Hauser on Cayo Santiago, Puerto Rico. Images were normalized for average intensity

and size. All stimuli were 4° × 4° in size. However, we decided to keep them in colour to get closer to natural stimuli even if it produced greater luminosity disparity between the different stimuli preventing us to use pupil diameter as a physiological marker. Only unambiguous facial expressions and social scenes were retained (Supplementary Fig. 16 and Fig. 1). A 10% blur was applied to all images, in the hope of triggering multisensory integration processes (but see result section). For each visual category, 10 stimuli were used.

Scanning procedures

The in-vivo MRI scans were performed on a 3 T Magnetom Prisma system (Siemens Healthineers, Erlangen, Germany). For the anatomical MRI acquisitions, monkeys were first anesthetized with an intramuscular injection of ketamine (10 mg/kg). Then, the subjects were intubated and maintained under 1–2% of isoflurane. During the scan, animals were placed in a sphinx position in a Kopf MRI-compatible stereotaxic frame (Kopf Instruments, Tujunga, CA). Two L11 coils were placed on each side of the skull and a L7 coil was placed on the top of it. T1-weighted anatomical images were acquired for each subject using a magnetization-prepared rapid gradient-echo (MPRAGE) pulse sequence. Spatial resolution was set to 0.5 mm, with TR = 3000 ms, TE = 3.62 ms, Inversion Time (TI) = 1100 ms, flip angle = 8°, bandwidth = 250 Hz/pixel, 144 slices. T2-weighted anatomical images were acquired per monkey, using a Sampling Perfection with Application optimized Contrasts using different flip angle Evolution (SPACE) pulse sequence. Spatial resolution was set to 0.5 mm, with TR = 3000 ms, TE = 366.0 ms, flip angle = 120°, bandwidth = 710 Hz/pixel, 144 slices. Functional MRI acquisitions were as follows. Before each scanning session, a contrast agent, composed of monocrySTALLINE iron oxide nanoparticles, Molday ION™, was injected into the animal's saphenous vein (9–11 mg/kg) to increase the signal to noise ratio^{117,119}. We acquired gradient-echoecho-planar images covering the whole brain (TR = 2000 ms; TE = 18 ms; 37 sagittal slices; resolution: 1.25 × 1.25 × 1.38 mm anisotropic voxels, flip angle = 90°, bandwidth = 1190 Hz/pixel) using an eight-channel phased-array receive coil; and a loop radial transmit-only surface coil (MRI Coil Laboratory, Laboratory for Neuro- and Psychophysiology, Katholieke Universiteit Leuven, Leuven, Belgium, see¹²⁰). The coils were placed so as to maximise the signal on the temporal and prefrontal cortex. As a result, signal-to-noise was low in the occipital cortex (see Supplementary Fig. 4).

Data description

In total, 76 runs were collected in 12 sessions for monkey T and 65 runs in 9 sessions for monkey S. Based on the monkey's fixation quality during each run (85% within the eye fixation tolerance window) we selected 60 runs from monkey T and 59 runs for monkey S in total, i.e. 10 runs per task, except for one task of monkey S.

Data analysis

Data were pre-processed and analysed using AFNI (Cox, 1996), FSL (Jenkinson et al., 2012; Smith et al., 2013), SPM software (version SPM12, Wellcome Department of Cognitive Neurology, London, UK, <https://www.fil.ion.ucl.ac.uk/spm/software/>), JIP analysis toolkit (<http://www.nitrc.org/projects/jip>) and Workbench (<https://www.humanconnectome.org/software/get-connectome-workbench>). The T1-weighted and T2-weighted anatomical images were processed according to the HCP pipeline^{121,122} and were normalized into the MY19 Atlas¹²³. Functional volumes were corrected for head motion and slice time and skull-stripped. They were then linearly realigned on the T2-weighted anatomical image with flirt from FSL, the image distortions were corrected using nonlinear warping with JIP. A spatial smoothing was applied with a 3-mm FWHM Gaussian Kernel. A representative example of time courses is presented in Supplementary Fig. 17.

Fixed effect individual analyses were performed for each monkey, with a level of significance set at $p < 0.05$ corrected for multiple

comparisons (FWE, t -scores 4.6) and $p < 0.001$ (uncorrected level, t -scores 3.09). Head motion and eye movements were included as covariate of no interest. Because of the contrast agent injection, a specific MION hemodynamic response function (HRF)¹⁷ was used instead of the BOLD HRF provided by SPM. The main effects were computed over both monkeys. In most analyses, face contexts and social contexts were independently pooled.

ROI analyses were performed as follows. ROIs were determined from the auditory congruent contrast (AC vs Fx) of face contexts with the exception of two ROIs of the right lateral sulcus (LS4 and LS6) that were defined from the same contrast of social contexts. ROIs were defined as 1.5 mm diameter spheres centred around the local peaks of activation. In total, eight ROIs were selected in the right STS, six from the left STS, four in the left LS and six in the right LS. Supplementary Fig. 13 shows the peak activations defining each selected ROI; so as to confirm the location of the peak activation on either of the inferior LS bank, the superior STS bank or the inferior STS bank. For each ROI, the activity profiles were extracted with the Marsbar SPM toolbox (marsbar.sourceforge.net) and the mean percent of signal change (\pm standard error of the mean across runs) was calculated for each condition relative to the fixation baseline. %SC were compared using non-parametric two-sided tests.

Behaviour and heart rate

During each run of acquisition, videos of the faces of monkeys S and T were recorded in order to track heart rate variations (HRV) as a function of contexts and blocks⁴⁵. We focus on heart rate variations between auditory congruent and incongruent stimuli. For each task, we extracted HRV during AC and AI blocs. As changes in cardiac rhythm are slow, analyses were performed over the second half (8 s of each block). This has been done for each run of each task, grouping both monkeys. Because the data were not normally distributed (Kolmogorov–Smirnov Test of Normality), we carried out Friedman tests and non-parametric post hoc tests.

Reporting summary

Further information on research design is available in the Nature Research Reporting Summary linked to this article.

Data availability

The data that support the findings of this study are available from the corresponding author upon reasonable request. Data are still being analysed for other purposes and cannot be made publically available at this time. A Source Data file provides the raw data used to create all of the figures of this paper except the whole brain fMRI contrast maps. Source data are provided with this paper.

Code availability

The code that supports the findings of this study is available from the corresponding author upon reasonable request. The code is still being used for other purposes and cannot be made publically available at this time.

References

1. Fox, K. C. R., Muthukrishna, M. & Shultz, S. The social and cultural roots of whale and dolphin brains. *Nat. Ecol. Evol.* **1**, 1699–1705 (2017).
2. Shultz, S. & Dunbar, R. Encephalization is not a universal macro-evolutionary phenomenon in mammals but is associated with sociality. *Proc. Natl Acad. Sci.* **107**, 21582–21586 (2010).
3. Van Essen, D. C. & Dierker, D. L. Surface-based and probabilistic atlases of primate cerebral cortex. *Neuron* **56**, 209–225 (2007).
4. Devaine, M. et al. Reading wild minds: a computational assay of Theory of Mind sophistication across seven primate species. *PLOS Comput. Biol.* **13**, e1005833 (2017).
5. Mars, R. B. et al. On the relationship between the “default mode network” and the “social brain”. *Front. Hum. Neurosci.* **6**, 189 (2012).
6. Ghazanfar, A. A. & Hauser, M. D. The neuroethology of primate vocal communication: substrates for the evolution of speech. *Trends Cogn. Sci.* **3**, 377–384 (1999).
7. Parr, L. A., Waller, B. M. & Fugate, J. Emotional communication in primates: implications for neurobiology. *Curr. Opin. Neurobiol.* **15**, 716–720 (2005).
8. Gouzoules, S., Gouzoules, H. & Marler, P. Rhesus monkey (*Macaca mulatta*) screams: representational signalling in the recruitment of agonistic aid. *Anim. Behav.* **32**, 182–193 (1984).
9. Hauser, M. D. & Marler, P. Food-associated calls in rhesus macaques (*Macaca mulatta*): I. Socioecological factors. *Behav. Ecol.* **4**, 194–205 (1993).
10. Gothard, K. M., Erickson, C. A. & Amaral, D. G. How do rhesus monkeys (*Macaca mulatta*) scan faces in a visual paired comparison task? *Anim. Cogn.* **7**, 25–36 (2004).
11. Gothard, K. M., Brooks, K. N. & Peterson, M. A. Multiple perceptual strategies used by macaque monkeys for face recognition. *Anim. Cogn.* **12**, 155–167 (2009).
12. Rendall, D., Rodman, P. S. & Emond, R. E. Vocal recognition of individuals and kin in free-ranging rhesus monkeys. *Anim. Behav.* **51**, 1007–1015 (1996).
13. Sliwa, J., Duhamel, J.-R., Pascalis, O. & Wirth, S. Spontaneous voice–face identity matching by rhesus monkeys for familiar conspecifics and humans. *Proc. Natl Acad. Sci.* **108**, 1735–1740 (2011).
14. Aparicio, P. L., Issa, E. B. & DiCarlo, J. J. Neurophysiological organization of the middle face patch in macaque inferior temporal cortex. *J. Neurosci.* **36**, 12729–12745 (2016).
15. Arcaro, M. J., Schade, P. F., Vincent, J. L., Ponce, C. R. & Livingstone, M. S. Seeing faces is necessary for face-domain formation. *Nat. Neurosci.* **20**, 1404–1412 (2017).
16. Cohen, Y. E., Theunissen, F., Russ, B. E. & Gill, P. Acoustic features of rhesus vocalizations and their representation in the ventrolateral prefrontal cortex. *J. Neurophysiol.* **97**, 1470–1484 (2007).
17. Eifuku, S. Neural representations of perceptual and semantic identities of individuals in the anterior ventral inferior temporal cortex of monkeys. *Jpn. Psychol. Res.* **56**, 58–75 (2014).
18. Gil-da-Costa, R. et al. Toward an evolutionary perspective on conceptual representation: Species-specific calls activate visual and affective processing systems in the macaque. *Proc. Natl Acad. Sci.* **101**, 17516–17521 (2004).
19. Gil-da-Costa, R. et al. Species-specific calls activate homologs of Broca’s and Wernicke’s areas in the macaque. *Nat. Neurosci.* **9**, 1064–1070 (2006).
20. Hesse, J. K. & Tsao, D. Y. The macaque face patch system: a turtle’s underbelly for the brain. *Nat. Rev. Neurosci.* 1–22, <https://doi.org/10.1038/s41583-020-00393-w> (2020).
21. Issa, E. B. & DiCarlo, J. J. Precedence of the eye region in neural processing of faces. *J. Neurosci.* **32**, 16666–16682 (2012).
22. Joly, O. et al. Processing of vocalizations in humans and monkeys: a comparative fMRI study. *NeuroImage* **62**, 1376–1389 (2012).
23. Joly, O., Ramus, F., Pressnitzer, D., Vanduffel, W. & Orban, G. A. Interhemispheric differences in auditory processing revealed by fMRI in awake Rhesus monkeys. *Cereb. Cortex* **22**, 838–853 (2012).
24. Moeller, S., Freiwald, W. A. & Tsao, D. Y. Patches with Links: a unified system for processing faces in the Macaque temporal lobe. *Science* **320**, 1355–1359 (2008).
25. Ortiz-Rios, M. et al. Functional MRI of the vocalization-processing network in the macaque brain. *Front. Neurosci.* **9**, 113 (2015).
26. Petkov, C. I. et al. A voice region in the monkey brain. *Nat. Neurosci.* **11**, 367–374 (2008).

27. Pinsk, M. A., DeSimone, K., Moore, T., Gross, C. G. & Kastner, S. Representations of faces and body parts in macaque temporal cortex: a functional MRI study. *Proc. Natl Acad. Sci. U. S. A.* **102**, 6996–7001 (2005).
28. Pinsk, M. A. et al. Neural representations of faces and body parts in macaque and human cortex: a comparative fMRI study. *J. Neurophysiol.* **101**, 2581–2600 (2009).
29. Poremba, A. et al. Functional mapping of the primate auditory system. *Science* **299**, 568–572 (2003).
30. Poremba, A. et al. Species-specific calls evoke asymmetric activity in the monkey's temporal poles. *Nature* **427**, 448–451 (2004).
31. Romanski, L. M., Averbach, B. B. & Diltz, M. Neural representation of vocalizations in the primate ventrolateral prefrontal cortex. *J. Neurophysiol.* **93**, 734–747 (2005).
32. Russ, B. E., Ackelson, A. L., Baker, A. E. & Cohen, Y. E. Coding of auditory-stimulus identity in the auditory non-spatial processing stream. *J. Neurophysiol.* **99**, 87–95 (2008).
33. Schwiedrzik, C. M., Zarco, W., Everling, S. & Freiwald, W. A. Face patch resting state networks link face processing to social cognition. *PLoS Biol.* **13**, e1002245 (2015).
34. Sliwa, J. & Freiwald, W. A. A dedicated network for social interaction processing in the primate brain. *Science* **356**, 745–749 (2017).
35. Tsao, D. Y., Freiwald, W. A., Knutsen, T. A., Mandeville, J. B. & Tootell, R. B. H. Faces and objects in macaque cerebral cortex. *Nat. Neurosci.* **6**, 989 (2003).
36. Khandhadia, A. P., Murphy, A. P., Romanski, L. M., Bizley, J. K. & Leopold, D. A. Audiovisual integration in macaque face patch neurons. *Curr. Biol.* <https://doi.org/10.1016/j.cub.2021.01.102> (2021).
37. Ghazanfar, A. A. The multisensory roles for auditory cortex in primate vocal communication. *Hear. Res.* **258**, 113–120 (2009).
38. Ghazanfar, A. A., Maier, J. X., Hoffman, K. L. & Logothetis, N. K. Multisensory integration of dynamic faces and voices in rhesus monkey auditory cortex. *J. Neurosci.* **25**, 5004–5012 (2005).
39. Perrodin, C., Kayser, C., Logothetis, N. K. & Petkov, C. I. Natural asynchronies in audiovisual communication signals regulate neuronal multisensory interactions in voice-sensitive cortex. *Proc. Natl Acad. Sci.* **112**, 273–278 (2015).
40. Perrodin, C., Kayser, C., Logothetis, N. K. & Petkov, C. I. Auditory and visual modulation of temporal lobe neurons in voice-sensitive and association cortices. *J. Neurosci. J. Soc. Neurosci.* **34**, 2524–2537 (2014).
41. Romanski, L. M. Integration of faces and vocalizations in ventral prefrontal cortex: Implications for the evolution of audiovisual speech. *Proc. Natl Acad. Sci.* **109**, 10717–10724 (2012).
42. Freiwald, W. A. Social interaction networks in the primate brain. *Curr. Opin. Neurobiol.* **65**, 49–58 (2020).
43. Ghazanfar, A. A. & Santos, L. R. Primate brains in the wild: the sensory bases for social interactions. *Nat. Rev. Neurosci.* **5**, 603–616 (2004).
44. Tsao, D. Y., Schweers, N., Moeller, S. & Freiwald, W. A. Patches of face-selective cortex in the macaque frontal lobe. *Nat. Neurosci.* **11**, 877–879 (2008).
45. Froesel, M., Goudard, Q., Hauser, M., Gacoin, M. & Ben Hamed, S. Automated video-based heart rate tracking for the anesthetized and behaving monkey. *Sci. Rep.* **10**, 17940 (2020).
46. Kreibitz, S. D. Autonomic nervous system activity in emotion: a review. *Biol. Psychol.* **84**, 394–421 (2010).
47. Chang, C., Cunningham, J. P. & Glover, G. H. Influence of heart rate on the BOLD signal: the cardiac response function. *NeuroImage* **44**, 857–869 (2009).
48. Avillac, M., Ben Hamed, S. & Duhamel, J.-R. Multisensory integration in the ventral intraparietal area of the macaque monkey. *J. Neurosci.* **27**, 1922–1932 (2007).
49. Alais, D. & Burr, D. The Ventriloquist effect results from near-optimal bimodal integration. *Curr. Biol.* **14**, 257–262 (2004).
50. Ernst, M. O. & Banks, M. S. Humans integrate visual and haptic information in a statistically optimal fashion. *Nature* **415**, 429–433 (2002).
51. Lee, H. & Noppeney, U. Temporal prediction errors in visual and auditory cortices. *Curr. Biol.* **24**, R309–R310 (2014).
52. Stein, B. E., Stanford, T. R. & Rowland, B. A. Development of multisensory integration from the perspective of the individual neuron. *Nat. Rev. Neurosci.* **15**, 520–535 (2014).
53. Grant, K. W. & Seitz, P. F. The use of visible speech cues for improving auditory detection of spoken sentences. *J. Acoust. Soc. Am.* **108**, 1197–1208 (2000).
54. Lehmann, S. & Murray, M. M. The role of multisensory memories in unisensory object discrimination. *Cogn. Brain Res.* **24**, 326–334 (2005).
55. Murray, M. M. et al. Grabbing your ear: rapid auditory–somatosensory multisensory interactions in low-level sensory cortices are not constrained by stimulus alignment. *Cereb. Cortex* **15**, 963–974 (2005).
56. Raab, D. H. Division of psychology: statistical facilitation of simple reaction times*. *Trans. N. Y. Acad. Sci.* **24**, 574–590 (1962).
57. Welch, R. B., Dutton-Hurt, L. D. & Warren, D. H. Contributions of audition and vision to temporal rate perception. *Percept. Psychophys.* **39**, 294–300 (1986).
58. Navarra, J. & Soto-Faraco, S. Hearing lips in a second language: visual articulatory information enables the perception of second language sounds. *Psychol. Res.* **71**, 4–12 (2007).
59. Shahin, A. J. & Miller, L. M. Multisensory integration enhances phonemic restoration. *J. Acoust. Soc. Am.* **125**, 1744–1750 (2009).
60. Van Wassenhove, V., Grant, K. W. & Poeppel, D. Visual speech speeds up the neural processing of auditory speech. *Proc. Natl Acad. Sci.* **102**, 1181–1186 (2005).
61. Cléry, J., Guipponi, O., Odouard, S., Wardak, C. & Ben Hamed, S. Impact prediction by looming visual stimuli enhances tactile detection. *J. Neurosci.* **35**, 4179–4189 (2015).
62. Cléry, J. et al. The prediction of impact of a looming stimulus onto the body is subserved by multisensory integration mechanisms. *J. Neurosci.* **37**, 10656–10670 (2017).
63. Cléry, J. C. et al. Looming and receding visual networks in awake marmosets investigated with fMRI. *NeuroImage* **215**, 116815 (2020).
64. Guipponi, O., Odouard, S., Pinède, S., Wardak, C. & Ben Hamed, S. fMRI cortical correlates of spontaneous eye blinks in the nonhuman primate. *Cereb. Cortex* **25**, 2333–2345 (2015).
65. Stein, B. E., Stanford, T. R., Ramachandran, R., Perrault, T. J. & Rowland, B. A. Challenges in quantifying multisensory integration: alternative criteria, models, and inverse effectiveness. *Exp. Brain Res.* **198**, 113 (2009).
66. Beauchamp, M. S. See me, hear me, touch me: multisensory integration in lateral occipital-temporal cortex. *Curr. Opin. Neurobiol.* **15**, 145–153 (2005).
67. Gentile, G., Petkova, V. I. & Ehrsson, H. H. Integration of visual and tactile signals from the hand in the human brain: an fMRI study. *J. Neurophysiol.* **105**, 910–922 (2010).
68. Pollick, F., Love, S. & Latinus, M. Cerebral correlates and statistical criteria of cross-modal face and voice integration. *Seeing Perceiving* **24**, 351–367 (2011).
69. Tyll, S. et al. Neural basis of multisensory looming signals. *NeuroImage* **65**, 13–22 (2013).
70. Werner, S. & Noppeney, U. Superadditive responses in superior temporal sulcus predict audiovisual benefits in object categorization. *Cereb. Cortex* **20**, 1829–1842 (2010).
71. Ghazanfar, A. A., Chandrasekaran, C. & Logothetis, N. K. Interactions between the superior temporal sulcus and auditory cortex

- mediate dynamic face/voice integration in rhesus monkeys. *J. Neurosci.* **28**, 4457–4469 (2008).
72. Barraclough, N. E., Xiao, D., Baker, C. I., Oram, M. W. & Perrett, D. I. Integration of visual and auditory information by superior temporal sulcus neurons responsive to the sight of actions. *J. Cogn. Neurosci.* **17**, 377–391 (2005).
 73. Ross, P. et al. Children cannot ignore what they hear: incongruent emotional information leads to an auditory dominance in children. *J. Exp. Child Psychol.* **204**, 105068 (2021).
 74. Laurienti, P. J. et al. Deactivation of sensory-specific cortex by cross-modal stimuli. *J. Cogn. Neurosci.* **14**, 420–429 (2002).
 75. Lewis, J. W., Beauchamp, M. S. & DeYoe, E. A. A comparison of visual and auditory motion processing in human cerebral cortex. *Cereb. Cortex* **10**, 873–888 (2000).
 76. Archakov, D. et al. Auditory representation of learned sound sequences in motor regions of the macaque brain. *Proc. Natl Acad. Sci.* **117**, 15242–15252 (2020).
 77. Friston, K. The free-energy principle: a unified brain theory? *Nat. Rev. Neurosci.* **11**, 127–138 (2010).
 78. Rao, R. P. N. & Ballard, D. H. Predictive coding in the visual cortex: a functional interpretation of some extra-classical receptive-field effects. *Nat. Neurosci.* **2**, 79–87 (1999).
 79. Millidge, B., Seth, A. & Buckley, C. L. Predictive coding: a theoretical and experimental review. *ArXiv210712979 Cs Q-Bio* (2022).
 80. Druzgal, T. J. & D’Esposito, M. A neural network reflecting decisions about human faces. *Neuron* **32**, 947–955 (2001).
 81. Miller, E. K. & Desimone, R. Parallel neuronal mechanisms for short-term memory. *Science* **263**, 520–522 (1994).
 82. Suzuki, W. A., Miller, E. K. & Desimone, R. Object and place memory in the macaque entorhinal cortex. *J. Neurophysiol.* **78**, 1062–1081 (1997).
 83. Suzuki, W. A. & Eichenbaum, H. The neurophysiology of memory. *Ann. N. Y. Acad. Sci.* **911**, 175–191 (2000).
 84. Rauschecker, J. P. & Tian, B. Mechanisms and streams for processing of “what” and “where” in auditory cortex. *Proc. Natl Acad. Sci.* **97**, 11800–11806 (2000).
 85. Romanski, L. M. et al. Dual streams of auditory afferents target multiple domains in the primate prefrontal cortex. *Nat. Neurosci.* **2**, 1131–1136 (1999).
 86. Saleem, K. S., Miller, B. & Price, J. L. Subdivisions and connective networks of the lateral prefrontal cortex in the macaque monkey. *J. Comp. Neurol.* **522**, 1641–1690 (2014).
 87. Seltzer, B. & Pandya, D. N. Frontal lobe connections of the superior temporal sulcus in the rhesus monkey. *J. Comp. Neurol.* **281**, 97–113 (1989).
 88. Seltzer, B. & Pandya, D. N. Parietal, temporal, and occipital projections to cortex of the superior temporal sulcus in the rhesus monkey: A retrograde tracer study. *J. Comp. Neurol.* **343**, 445–463 (1994).
 89. Fuster, J. M. Physiology of executive functions: The perception-action cycle. in *Principles of frontal lobe function* 96–108 (Oxford University Press, 2002). <https://doi.org/10.1093/acprof:oso/9780195134971.003.0006>.
 90. Goldman-Rakic, P. S. Regional and cellular fractionation of working memory. *Proc. Natl Acad. Sci.* **93**, 13473–13480 (1996).
 91. Kondo, H., Saleem, K. S. & Price, J. L. Differential connections of the temporal pole with the orbital and medial prefrontal networks in macaque monkeys. *J. Comp. Neurol.* **465**, 499–523 (2003).
 92. Saleem, K. S., Kondo, H. & Price, J. L. Complementary circuits connecting the orbital and medial prefrontal networks with the temporal, insular, and opercular cortex in the macaque monkey. *J. Comp. Neurol.* **506**, 659–693 (2008).
 93. Cléry, J. C., Hori, Y., Schaeffer, D. J., Menon, R. S. & Everling, S. Neural network of social interaction observation in marmosets. *eLife* **10**, e65012 (2021).
 94. Roberts, A. C. Primate orbitofrontal cortex and adaptive behaviour. *Trends Cogn. Sci.* **10**, 83–90 (2006).
 95. Rudebeck, P. H., Buckley, M. J., Walton, M. E. & Rushworth, M. F. S. A role for the macaque anterior cingulate gyrus in social valuation. *Science* **313**, 1310–1312 (2006).
 96. Rushworth, M. F. S., Behrens, T. E. J., Rudebeck, P. H. & Walton, M. E. Contrasting roles for cingulate and orbitofrontal cortex in decisions and social behaviour. *Trends Cogn. Sci.* **11**, 168–176 (2007).
 97. Amaral, D. & Price, J. L. Amygdalo-cortical projections in the monkey (*Macaca fascicularis*). *J. Comp. Neurol.* <https://doi.org/10.1002/CNE.902300402> (1984).
 98. Afraz, A., Boyden, E. S. & DiCarlo, J. J. Optogenetic and pharmacological suppression of spatial clusters of face neurons reveal their causal role in face gender discrimination. *Proc. Natl Acad. Sci.* **112**, 6730–6735 (2015).
 99. Freiwald, W. A. & Tsao, D. Y. Functional compartmentalization and viewpoint generalization within the macaque face-processing system. *Science* **330**, 845–851 (2010).
 100. Hadj-Bouziane, F., Bell, A. H., Knusten, T. A., Ungerleider, L. G. & Tootell, R. B. H. Perception of emotional expressions is independent of face selectivity in monkey inferior temporal cortex. *Proc. Natl Acad. Sci.* **105**, 5591–5596 (2008).
 101. Grimaldi, P., Saleem, K. S. & Tsao, D. Anatomical connections of the functionally defined ‘face patches’ in the macaque monkey. *Neuron* **90**, 1325–1342 (2016).
 102. Tsao, D. Y., Freiwald, W. A., Tootell, R. B. H. & Livingstone, M. S. A cortical region consisting entirely of face-selective cells. *Science* **311**, 670–674 (2006).
 103. Tsao, D. Y., Moeller, S. & Freiwald, W. A. Comparing face patch systems in macaques and humans. *Proc. Natl Acad. Sci.* **105**, 19514–19519 (2008).
 104. Marciniak, K., Atabaki, A., Dicke, P. W. & Thier, P. Disparate substrates for head gaze following and face perception in the monkey superior temporal sulcus. *eLife* **3**, e03222 (2014).
 105. Roumazeilles, L. et al. Social prediction modulates activity of macaque superior temporal cortex. 2021.01.22.427803 <https://www.biorxiv.org/content/10.1101/2021.01.22.427803v1>; <https://doi.org/10.1101/2021.01.22.427803> (2021).
 106. Kuśmierk, P. & Rauschecker, J. P. Selectivity for space and time in early areas of the auditory dorsal stream in the rhesus monkey. *J. Neurophysiol.* **111**, 1671–1685 (2014).
 107. Rauschecker, J. P. & Scott, S. K. Maps and streams in the auditory cortex: nonhuman primates illuminate human speech processing. *Nat. Neurosci.* **12**, 718–724 (2009).
 108. Belin, P. Similarities in face and voice cerebral processing. *Vis. Cogn.* **25**, 658–665 (2017).
 109. Kuśmierk, P. & Rauschecker, J. P. Functional specialization of medial auditory belt cortex in the alert rhesus monkey. *J. Neurophysiol.* **102**, 1606–1622 (2009).
 110. Tian, B., Reser, D., Durham, A., Kustov, A. & Rauschecker, J. P. Functional specialization in rhesus monkey auditory cortex. *Science* **292**, 290–293 (2001).
 111. Petrides, M. & Pandya, D. N. Comparative cytoarchitectonic analysis of the human and the macaque ventrolateral prefrontal cortex and corticocortical connection patterns in the monkey. *Eur. J. Neurosci.* **16**, 291–310 (2002).
 112. Romanski, L. M. & Averbeck, B. B. The primate cortical auditory system and neural representation of conspecific vocalizations. *Annu. Rev. Neurosci.* **32**, 315–346 (2009).
 113. Rocchi, F. et al. Common fronto-temporal effective connectivity in humans and monkeys. *Neuron* **109**, 852–868.e8 (2021).
 114. Kayser, C., Petkov, C. I., Augath, M. & Logothetis, N. K. Functional imaging reveals visual modulation of specific fields in auditory cortex. *J. Neurosci.* **27**, 1824–1835 (2007).

115. Kayser, C., Petkov, C. I. & Logothetis, N. K. Visual modulation of neurons in auditory cortex. *Cereb. Cortex* **18**, 1560–1574 (2008).
116. Calvert, G. A. Crossmodal processing in the human brain: insights from functional neuroimaging studies. *Cereb. Cortex* **11**, 1110–1123 (2001).
117. Vanduffel, W. et al. Visual motion processing investigated using contrast agent-enhanced fMRI in awake behaving monkeys. *Neuron* **32**, 565–577 (2001).
118. Belin, P. et al. Human cerebral response to animal affective vocalizations. *Proc. R. Soc. B Biol. Sci.* <https://doi.org/10.1098/rspb.2007.1460> (2007).
119. Leite, F. P. et al. Repeated fMRI using iron oxide contrast agent in awake, behaving macaques at 3 Tesla. *NeuroImage* **16**, 283–294 (2002).
120. Kolster, H., Janssens, T., Orban, G. A. & Vanduffel, W. The retinotopic organization of macaque occipitotemporal cortex anterior to V4 and caudovernal to the middle temporal (MT) cluster. *J. Neurosci. J. Soc. Neurosci.* **34**, 10168–10191 (2014).
121. Autio, J. A. et al. Towards HCP-Style macaque connectomes: 24-Channel 3T multi-array coil, MRI sequences and preprocessing. *NeuroImage* **215**, 116800 (2020).
122. Glasser, M. F. et al. The minimal preprocessing pipelines for the Human Connectome Project. *NeuroImage* **80**, 105–124 (2013).
123. Donahue, C. J. et al. Using diffusion tractography to predict cortical connection strength and distance: a quantitative comparison with tracers in the monkey. *J. Neurosci.* **36**, 6758–6770 (2016).

Acknowledgements

S.B.H. were funded by the French National Research Agency (ANR) ANR-16-CE37-0009-01 grant and the LABEX CORTEX funding (ANR-11-LABX-0042) from the Université de Lyon, within the program Investissements d’Avenir (ANR-11-IDEX-0007) operated by the French National Research Agency (ANR). We thank Fidji Francioly and Laurence Boes for animal care, Julian Amengual and Justine Cléry for their rich scientific exchanges during data collection and analyses, Franck Lambertson and Danièle Ibarrola for their MRI methodological support and Holly Rayson for her help on visual stimuli collection. We thank Serge Pinède for technical assistance on the project.

Author contributions

Conceptualization, S.B.H., M.F.; Stimuli preparation, M.H., M.F., Q.G., M.G.; Data Acquisition, M.F., M.G.; Methodology, M.F., S.C., Q.G., and S.B.H.; Investigation, M.F. and S.B.H.; Writing – Original Draft, M.F. and S.B.H.; Writing – Review & Editing, S.B.H., M.F., M.H.; Funding Acquisition, S.B.H.; Supervision, S.B.H.

Competing interests

The authors declare no competing interests.

Ethics declaration

Animal experiments were authorized by the French Ministry for Higher Education and Research (project no. 2016120910476056 and 1588-2015090114042892) in accordance with the French transposition texts of Directive 2010/63/UE. This authorization was based on ethical evaluation by the French Committee on the Ethics of Experiments in Animals (C2EA) CELYNE registered at the national level as C2EA number 42.

Additional information

Supplementary information The online version contains supplementary material available at

<https://doi.org/10.1038/s41467-022-32512-9>.

Correspondence and requests for materials should be addressed to Mathilda Froesel or Suliann Ben Hamed.

Peer review information *Nature Communications* thanks Josef Rauschecker, Wim Vanduffel and the other, anonymous, reviewer(s) for their contribution to the peer review of this work. Peer reviewer reports are available.

Reprints and permission information is available at <http://www.nature.com/reprints>

Publisher’s note Springer Nature remains neutral with regard to jurisdictional claims in published maps and institutional affiliations.

Open Access This article is licensed under a Creative Commons Attribution 4.0 International License, which permits use, sharing, adaptation, distribution and reproduction in any medium or format, as long as you give appropriate credit to the original author(s) and the source, provide a link to the Creative Commons license, and indicate if changes were made. The images or other third party material in this article are included in the article’s Creative Commons license, unless indicated otherwise in a credit line to the material. If material is not included in the article’s Creative Commons license and your intended use is not permitted by statutory regulation or exceeds the permitted use, you will need to obtain permission directly from the copyright holder. To view a copy of this license, visit <http://creativecommons.org/licenses/by/4.0/>.

© The Author(s) 2022

Macaque amygdala, claustrum and pulvina support the cross-modal association of social audio-visual stimuli based on meaning

Mathilda Froesel¹, Maëva Gacoin¹, Simon Clavagnier¹, Marc Hauser², Quentin Goudard¹, Suliann Ben Hamed¹

1. Institut des Sciences Cognitives Marc Jeannerod, UMR5229 CNRS Université de Lyon, 67 Boulevard Pinel, 69675 Bron Cedex, France
2. Risk-Eraser, LLC, PO Box 376, West Falmouth, MA, 02574, USA

Corresponding author: mathilda.froesel@isc.cnrs.fr and benhamed@isc.cnrs.fr

Abstract

Social communication draws on several cognitive functions such as perception, emotion recognition and attention. In a previous study, we demonstrated that macaques associate audio-visual information when processing their species-specific communicative signals. Specifically, cortical activation is inhibited when there is a mismatch between vocalisations and social visual information whereas activation is enhanced in the lateral sulcus, superior temporal sulcus as well as a larger network composed of early visual and prefrontal areas when vocalisations and social visual information match. Here, we use a similar task and functional magnetic resonance imaging to assess the role of subcortical structures. We identify three subcortical regions involved in audio-visual processing of species-specific communicative signal: the amygdala, the claustrum and the pulvina. Like the cortex, these subcortical structures are not activated when there is a mismatch between visual and acoustic information. In contrast, the amygdala and claustrum are activated by visual, auditory congruent and audio-visual stimulations. The pulvina responds in a task-dependent manner, along a specific spatial sensory gradient. Anterior pulvina responds to auditory stimuli, medial pulvina is activated by auditory, audio-visual and visual stimuli and the dorsal lateral pulvina only responds to visual stimuli in a pure visual task. The medial pulvina and the amygdala are the only subcortical structures integrating audio-visual social stimuli. We propose that these three structures belong to a multisensory network that modulates the perception of visual socioemotional information and vocalizations as a function of the relevance of the stimuli in the social context.

Significance Statement

Understanding and correctly associating socioemotional information across sensory modalities, such that happy faces predict laughter and escape scenes screams, is essential when living in complex social groups. Using functional magnetic imaging in the awake macaque, we identify three subcortical structures – amygdala, claustrum and pulvina - that only respond to auditory

information that matches the ongoing visual socioemotional context, such as hearing positively valenced coo calls and seeing positively valenced grooming monkeys. We additionally describe task-dependent activations in the pulvinar, organizing along a specific spatial sensory gradient, supporting its role as a network regulator.

Running title: Audiovisual processing in amygdala, claustrum & pulvinar

Conflict of interest statement: The authors declare no conflict interests or competing financial interests.

Contributions: Conceptualization, S.B.H., M.F.; Stimuli preparation, M.F, Q.G, M.G, M.H; Data Acquisition, M.F., M.G.; Methodology, M.F., S.C., Q.G., and S.B.H; Investigation, M.F. and S.B.H.; Writing – Original Draft, M.F. and S.B.H.; Writing – Review & Editing, S.B.H., M.F.; Funding Acquisition, S.B.H.; Supervision, S.B.H.

Acknowledgements

S.B.H. were funded by the French National Research Agency (ANR) ANR-16-CE37-0009-01 grant and the LABEX CORTEX funding (ANR-11-LABX-0042) from the Université de Lyon, within the program Investissements d’Avenir (ANR-11-IDEX-0007) operated by the French National Research Agency (ANR). We thank Fidji Francioly and Laurence Boes for animal care, Franck Lambertson and Danièle Ibarrola for their MRI methodological support and Holly Rayson for their help on visual and auditory stimuli collection.

Keywords

Audio-visual, multisensory, pulvinar, amygdala, claustrum, fMRI, macaque, socioemotional

Introduction

In a wide variety of species, social communication often involves sending and receiving systems that must integrate information across different modalities, recruiting multiple processes such as sensory perception, emotion processing and attention. In a previous study, we demonstrate thanks to cardiac recordings (Froesel et al., 2020) and functional magnetic resonance imaging (fMRI) that macaques associate communicatively salient audio-visual information based on the social context set by visual information. This process is mediated by a network of face and voice patches in the superior temporal sulcus and lateral sulcus (Froesel et al., 2022). Here, using the same task and data, we identify the relevant subcortical structures in cross-modal association.

Given that the task involves functionally meaningful communicative signals that are emotionally salient, we predicted strong amygdala activation. This subcortical nucleus contains face-selective neurons that are globally activated both by face identity and facial expressions (Nakamura et al., 1992; Fitzgerald et al., 2006; Pessoa et al., 2006; Sergerie et al., 2008; Livneh et al., 2012; Todorov, 2012). Specifically, affiliative facial expressions induce a decrease of firing rates in the amygdala, while threatening faces induce an increase in firing rates (Gothard et al., 2007). Overall, beyond face processing, the amygdala is part of a social perception network and is proposed to play a central role in emotional encoding during complex social interactions (Leonard et al., 1985; Barraclough and Perrett, 2011), including during cross-modal sensory emotional processing (Dolan et al., 2001; Kuraoka and Nakamura, 2007). In addition to the amygdala, the pulvinar, the largest nucleus of the thalamus, is also involved in face processing, emotion regulation and multisensory integration (Moeller et al., 2008; Pessoa, 2010a; Froesel et al., 2021). Last, the claustrum is also activated following face patches stimulation and is proposed to play a role in face perception (Moeller et al., 2008). We thus hypothesize that all of these sub-cortical structures are activated by visual and auditory social stimuli and may play a part in multisensory integration. Social perception also involves integrating contextual, behavioural, and emotional information (Ghazanfar and Santos, 2004; Freiwald, 2020). We thus predict that the audio-visual association of social information is impacted by the functional context and mediated by both these sub-cortical structures.

Here, we describe fMRI study in awake macaques performing a passive audio-visual task manipulating the congruency of cross-modal social information across six different emotional contexts, together with a passive visual task manipulating monkey facial expressions. We show, in parallel to our previous report of cortical activation, that sub-cortical activations are determined by whether monkey vocalisations match or mismatch the faces or actions associated with them. As predicted, the subcortical structures identified included the amygdala, claustrum and pulvinar. As we reported in cortical activations, these regions are modulated by the task context. Auditory activations are significant for auditory stimuli that are congruent with the visual context, but not for incongruent stimuli, indicating that inhibitory or facilitatory feedback on the context filtering auditory stimuli extends to subcortical areas. We further report three novel observations. First, the amygdala and the claustrum respond to all of visual, auditory and audio-visual stimuli, demonstrating their involvement in audio-visual integrative processes. However, only the amygdala demonstrates multisensory integration. Second, the pulvinar is activated along a sensory gradient that is determined by stimulation modality (visual, auditory or audio-visual) or

context. Anterior pulvinar is only activated by auditory stimulations. Medial pulvinar is activated by visual, auditory and audio-visual congruent stimuli. The dorsal lateral pulvinar is only activated by visual stimuli in the pure visual task (For review, see Froesel et al., 2021). Third, the functional activations observed in the medial pulvinar are similar to those observed in the amygdala and claustrum, thus suggesting a coordinated role of these three sub-cortical structures in multisensory social processing. Medial pulvinar is also the only pulvinar subregion that expresses multisensory integration. Overall, our observations shed a new light on how functionally meaningful, multimodal social signal are processed by subcortical structures.

Material and methods

Subjects and surgical procedures

Two male rhesus monkeys (*Macaca mulatta*) participated in the study (T, 15 years, 10kg and S, 12 years, 11kg). The animals were implanted with a Peek MRI-compatible headset covered by dental acrylic. The anaesthesia for the surgery was induced by Zoletil (Tiletamine-Zolazepam, Virbac, 5 mg/kg) and maintained by isoflurane (Belamont, 1–2%). Post-surgery analgesia was ensured thanks to Temgesic (buprenorphine, 0.3 mg/ml, 0.01 mg/kg). During recovery, proper analgesic and antibiotic coverage was provided. The surgical procedures conformed to European and National Institutes of Health Guidelines for the Care and Use of Laboratory Animals. The project was authorized by the French Ministry for Higher Education and Research (project no. 2016120910476056 and 1588-2015090114042892) in accordance with the French transposition texts of Directive 2010/63/UE. This authorization was based on ethical evaluation by the French Committee on the Ethics of Experiments in Animals (C2EA) CELYNE registered at the national level as C2EA number 42.

Experimental setup

During the scanning sessions, monkeys sat in a sphinx position in a plastic monkey chair (Vanduffel et al., 2001) facing a translucent screen placed 60 cm from the eyes. Visual stimuli were retro-projected onto this translucent screen. Their head was restrained and the auditory stimuli were displayed by Sensimetrics MRI-compatible S14 insert earphones. The monkey chair was secured in the MRI with safety rubber stoppers to prevent any movement. Eye position (X, Y, right eye) was recorded thanks to a pupil-corneal reflection video-tracking system (EyeLink at 1000 Hz, SR-Research) interfaced with a program for stimulus delivery and experimental control (EventIDE®). Monkeys were rewarded for maintaining fixation into a 2x2° tolerance window around the fixation point.

General audio-visual run design

On each run, monkeys were required to fixate a central cross on the screen (Figure 1A). Runs followed a block design. Each run started with 10 s of fixation in the absence of sensory stimulation followed by three repetitions of a pseudo-randomized sequence containing six possible 16 s blocks: fixation (Fx), visual (Vi), auditory congruent (AC), auditory incongruent (AI), congruent audio-visual (VAC) and incongruent audio-visual (VAI). Each block (except the fixation block) consisted of alternating 500 ms stimuli (except for lipsmacks, 1s dynamic stimuli succession) of the same semantic category (see Stimuli section below), in the visual, auditory or

audio-visual modalities. Each block ended with 10 s of fixation in the absence of sensory stimulation. Note that within any one run the visual stimulations were prevalent and always reflecting the same emotional content, thus setting the emotional context of the run. The initial blocks always contained a visual stimulation (V, VAC or VAI) such that pure auditory blocks could be defined as congruent or incongruent relative to the visual context set by previous blocks.

Face and social task design

Six audio-visual contexts were presented to both monkeys, organized in runs as described above (Figure 1B). Each run combined visual stimuli of identical social content with either semantically congruent or incongruent monkey vocalisations (Figure 1B). The face affiliative context (F+) combined lipsmacks with coos and aggressive calls. The face aggressive context (F-) combined aggressive faces with coos and aggressive calls. The first social affiliative context (S1+) combined grooming scenes with coos and aggressive calls. The second social affiliative context (S2+) combined grooming scenes with coos and screams. The social aggressive context (S1-) combined aggressive group or individual scenes with coos and aggressive calls. The social escape context (S2-) combined fleeing groups or individual scenes with coos and screams. Importantly, pairs of contexts (F+ & F-; S1+ & S1-; S2+ & S2-) shared the same auditory conditions, but opposite social visual content.

Pure Visual runs design

The design of the visual runs was similar to that of the audio-visual run design, organized in blocks, except for the fact that all blocks were pure visual blocks and varied as a function of facial emotions. The six possible 16 s blocks were: fixation (Fx), lipsmack (Lip), scared monkey faces (Sca), aggressive monkey faces (Aggr), neutral monkey faces (Neu) and scrambled monkey faces (Scr). As for the audio-visual runs each block consisted in an alternation of 500 ms stimuli (except for lip smacks, 1s dynamic stimuli succession) of the same emotional category (see Figure 1C).

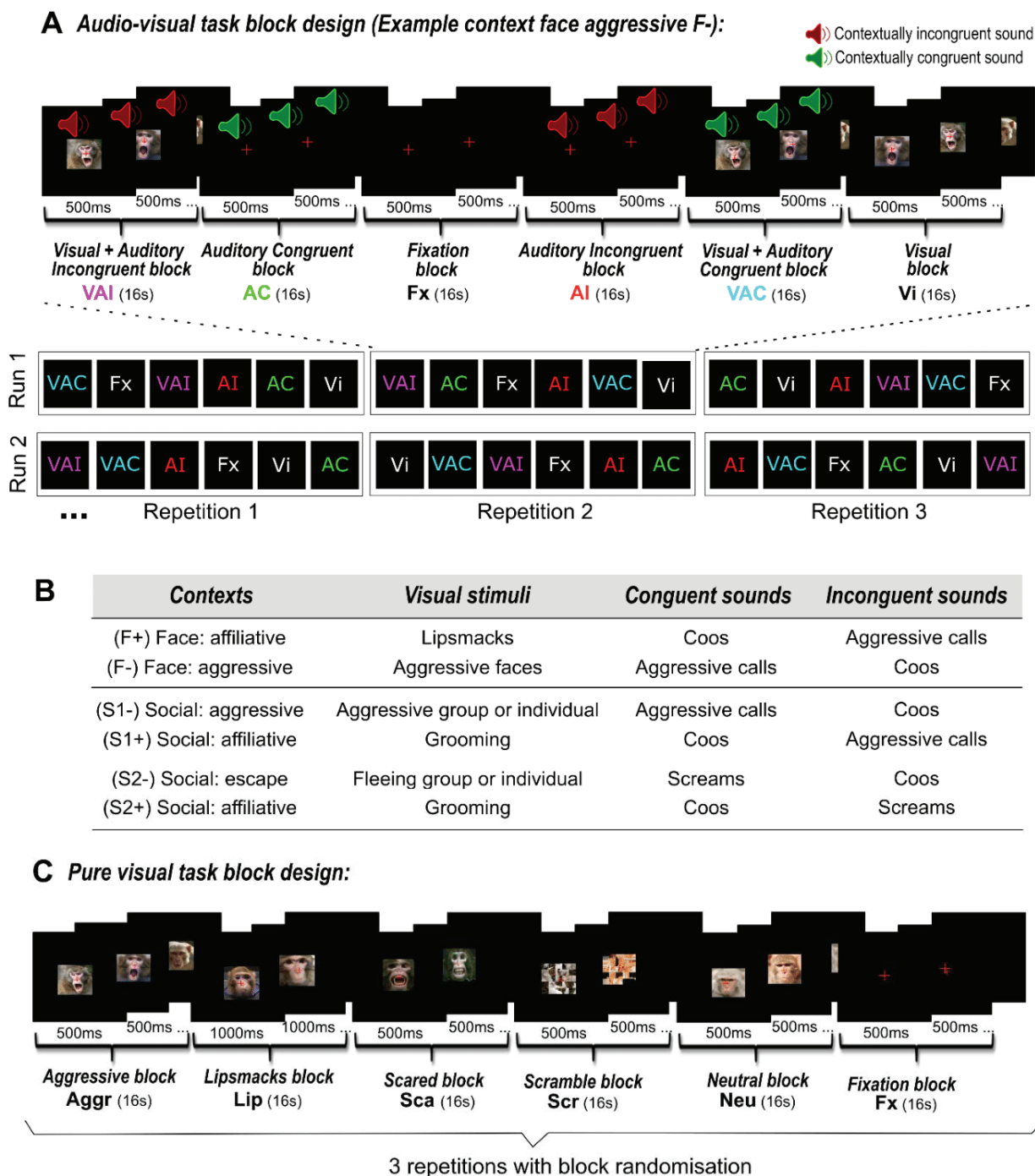


Figure 1. Experimental designs. Each sensory stimulation block contained a rapid succession of 500ms stimuli (with the exception of the lipsmack for the pure visual task). Each run started and ended with 10s of fixation regardless of the task type. **A)** Experimental design of the audio-visual task. Example of an aggressive face (F-) context. One run represents one context set up by the visual stimuli and contains three randomized repetitions of six different blocks of 16s. The six blocks displayed were either visual stimuli only (Vi), auditory congruent stimuli only (AC), auditory incongruent stimuli only (AI), audio-visual congruent stimuli (VAC) or audio-

visual incongruent stimuli (VAI), or fixation with no sensory stimulation (Fx). Blocks were pseudo randomized in order that each block was, on average, preceded by the same number of blocks from the other conditions and that each run started with a block of a visual information (V, VAC or VAI). **B)** Description of the contexts. Six contexts were displayed. Each context combined visual stimuli of identical social content with either semantically congruent or incongruent monkey vocalisations. Pairs of contexts shared the same auditory stimuli, but opposite social visual content (F+ vs. F-; S1+ vs. S1-; S2+ vs. S2-). Each run corresponded to one of the semantic contexts described above. **C)** Experimental design of the pure visual task. In one run six different blocks were displayed three times randomly. The six possible 16 s blocks were: fixation (Fx), lipsmack (Lip), scared monkey faces (Sca), aggressive monkey faces (Aggr), neutral monkey faces (Neu) and scrambled monkey faces (Scr). Visual stimuli were extracted from videos collected by the Ben Hamed lab, as well as by Marc Hauser on Cayo Santiago, Puerto Rico.

Stimuli

Vocalisations were recorded by Marc Hauser from semi-free-ranging rhesus monkeys during naturally occurring situations. Detailed acoustic and functional analyses of this repertoire has been published elsewhere (e.g., Gouzoules et al., 1984; Hauser & Marler, 1993). Field recordings were then processed, restricting selection of experimental stimuli to calls that were recorded from known individuals, in clearly identified situations, and that were free of competing noise from the environment. Exemplars from this stimulus set have already been used in several imaging studies (Belin et al., 2007; Cohen et al., 2007; Romanski, 2012; Romanski et al., 2005; Russ et al., 2008). As in our previous study (Froesel et al., 2022), all stimuli were normalized in luminance and colour but the frequency ranges varied between the different types of stimuli as shown in the supplementary Figure 4. For each of the three vocalisation categories, we used 10 unique exemplars coming from matched male and female individuals for each category in order to control for possible gender, social hierarchy or individual effects. Coos are affiliative vocalisations, aggressive calls are used as a precursor of a physical attack and screams are produced by subordinate being chased or attacked by a dominant. Facial expression (lipsmacks and aggressive facial expression) and social scene (group grooming, aggressive individual alone or in group / escaping individual or group) stimuli were extracted from videos collected by the Ben Hamed lab, as well as by Marc Hauser on Cayo Santiago, Puerto Rico. Images were normalized for average intensity and size. All stimuli were 4° x 4° in size. We decided to keep them in colour to get closer to natural stimuli even if it produced greater luminosity disparity between the different stimuli preventing us to use pupil diameter as a physiological marker. Only unambiguous facial expressions and social scenes were retained. A 10% blur was applied to all images, in the hope of triggering multisensory integration processes (Stein and Meredith, 1993)(but see result section). For each visual category, 10 stimuli were used. The scrambling of the images was performed by EventIDE (<https://www.okazolab.com/okazolab.com/>) and applied to each visual stimuli displayed from the task.

Scanning Procedures

The in-vivo MRI scans were performed on a 3T Magnetom Prisma system (Siemens Healthineers, Erlangen, Germany). For the anatomical MRI acquisitions, monkeys were first

anesthetized with an intramuscular injection of ketamine (10 mg/kg). Then, the subjects were intubated and maintained under 1-2% of isoflurane. During the scan, animals were placed in a sphinx position in a Kopf MRI-compatible stereotaxic frame (Kopf Instruments, Tujunga, CA). Two L11 coils were placed on each side of the skull and a L7 coil was placed on the top of it. T1-weighted anatomical images were acquired for each subject using a magnetization-prepared rapid gradient-echo (MPRAGE) pulse sequence. Spatial resolution was set to 0.5 mm, with TR=3000 ms, TE=3.62 ms, Inversion Time (TI)=1100 ms, flip angle=8°, bandwidth=250 Hz/pixel, 144 slices. T2-weighted anatomical images were acquired per monkey, using a Sampling Perfection with Application optimized Contrasts using different flip angle Evolution (SPACE) pulse sequence. Spatial resolution was set to 0.5 mm, with TR=3000 ms, TE=366.0 ms, flip angle=120°, bandwidth=710 Hz/pixel, 144 slices. fMRI acquisitions were as follows. Before each scanning session, a contrast agent, composed of monocrySTALLINE iron oxide nanoparticles, Molday ION™, was injected into the animal's saphenous vein (9-11 mg/kg) to increase the signal to noise ratio (Vanduffel et al., 2001; Leite et al., 2002). We acquired gradient-echoechoplanar images covering the whole brain (TR=2000 ms; TE=18 ms; 37 sagittal slices; resolution: 1.25x1.25x1.38 mm anisotropic voxels) using an eight-channel phased-array receive coil; and a loop radial transmit-only surface coil (MRI Coil Laboratory, Laboratory for Neuro- and Psychophysiology, Katholieke Universiteit Leuven, Leuven, Belgium, see Kolster et al., 2014). The coils were placed so as to maximise the signal on the temporal lobe.

Data description

In total, for the audio-visual runs (155 pulses), 76 runs were collected in 12 sessions for monkey T and 65 runs in 9 sessions for monkey S. For the pure visual runs (155 pulses), 13 runs were collected in 8 sessions for monkey T and 12 runs in 5 sessions for monkey S. Based on the monkey's fixation quality during each run (85% within the eye fixation tolerance window), we selected 60 runs from monkey T and 59 runs for monkey S in total, i.e. 10 runs per task, except for one task of monkey S for audio-visual runs and 11 pure visual runs for S and 13 for T.

Data analysis

Data were pre-processed and analysed using AFNI (Cox, 1996), FSL (Jenkinson et al., 2012; Smith et al., 2013), SPM software (version SPM12, Wellcome Department of Cognitive Neurology, London, UK, <https://www.fil.ion.ucl.ac.uk/spm/software/>), JIP analysis toolkit (<http://www.nitrc.org/projects/jip>) and Workbench (<https://www.humanconnectome.org/software/get-connectome-workbench>). The T1-weighted and T2-weighted anatomical images were processed according to the HCP pipeline (Glasser et al., 2013; Autio et al., 2020) and were normalized into the MY19 Atlas (Donahue et al., 2016). Functional volumes were corrected for head motion, slice timed referred on the middle image of the run and skull-stripped. They were then linearly realigned on the T2-weighted anatomical image with flirt from FSL, the image distortions were corrected using nonlinear warping with JIP. A spatial smoothing was applied with a 3-mm FWHM Gaussian Kernel.

Fixed effect individual analyses were performed for each monkey, with a level of significance set at $p < 0.05$ corrected for multiple comparisons (FWE, t-scores 4.6) and $p < 0.001$ (uncorrected level, t-scores 3.09). Head motion and eye movements were included as covariate of no interest.

Because of the contrast agent injection, a specific MION hemodynamic response function (HRF) (Vanduffel et al., 2001) was used instead of the BOLD HRF provided by SPM. The main effects were computed over both monkeys. In most analyses, face blocked conditions and social blocked conditions were independently pooled.

ROI analyses were performed as follows. The anterior pulvinar, claustrum ROIs were determined from the auditory congruent contrast (AC vs Fx) and the medial pulvinar and the amygdala ROIs from the audio-visual contrast (VAC vs FX) of face context (Figure 2). PLvl and Pldm ROIs were extracted from the pure visual runs (all conditions vs fixation contrast; figure 4). ROIs were defined as 1 mm diameter spheres centred around the local peaks of activation. To note, there was no overlap between the different clusters. For each ROI, the activity profiles were extracted with the Marsbar SPM toolbox (marsbar.sourceforge.net) and the mean percent of signal change (+/- standard error of the mean across runs) was calculated for each condition relative to the fixation baseline. As the face context includes both aggressive and lipsmack expressions, we decided for pure visual runs to combine these two expressions conditions and focus on this combination for the analysis to be comparable to the PSC results from the audio-visual runs. %SC were compared using Friedman non-parametric tests and Wilcoxon non-parametric paired tests.

Results

In Froesel et al., 2022, we characterized cortical activations underlying the association of social visual and auditory stimuli based on their semantic content or meaning in the broad sense. Cortical regions were active when visual and auditory information were congruent, but inactive when this information was incongruent. Here, we identify subcortical structures -the amygdala, the claustrum and the pulvinar- that also respond to the congruence of the auditory and visual stimuli. In addition, we show that among subcortical regions, only the amygdala and the medial pulvinar implement multisensory integration.

Sub-cortical activations: amygdala, ventral putamen and pulvinar.

A small group of sub-regions are significantly activated during one or several of the unimodal or bimodal conditions presented to the monkeys in the different types of runs. Indeed, in a general contrast analysis, the claustrum (Claus) and the anterior (PuA) and medial (PuM) pulvinar nuclei are activated by the Auditory congruent vs. Fixation contrast (Figure 2, top row). The amygdala (AMG) is activated by the Visual vs. Fixation contrast (Figure 2, middle left panel). The inferior (PuI) and medial (PuM) pulvinar nuclei are activated by the Audio-visual incongruent vs. Fixation contrast (Figure 2, middle right panel). The amygdala (AMG), claustrum (Claus) and medial (PuM) pulvinar nucleus are activated by the Audio-visual congruent vs. Fixation contrast (Figure 2, bottom row). All of the activations are bilateral in at least one contrast except for the amygdala. Supplemental figure S1 represents the SNR map for the coronal section at the level of the pulvinar.

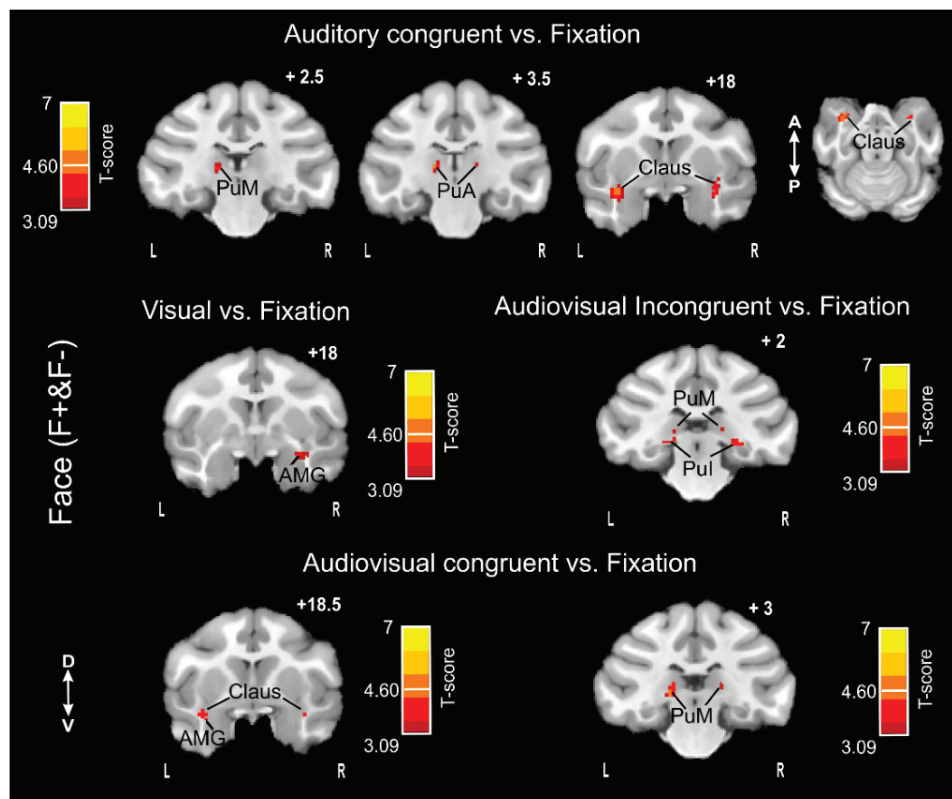


Figure 2: Whole-brain FACE blocked conditions (F+ & F-) activations: main contrasts. Whole-brain activation maps of the F+ (face affiliative) and F- (face aggressive) runs, cumulated over both monkeys, for the visual, auditory congruent, audio-visual congruent and audio-visual incongruent contrasts. Darker shades of red indicate level of significance at $p < 0.001$ uncorrected, t-score 3.09. Lighter shades of yellow indicate level of significance at $p < 0.05$ FWE, t-score 4.6.

We defined functional ROIs based on these sub-cortical activations and we computed the percent of signal change relative to fixation (%SC) for all conditions, cumulated over identical block conditions of either the face contexts (Figure 3, left), or the social scenes contexts (Figure 3, right). For all ROIs, and both face and social contexts, there was no significant activation relative to the fixation baseline in response to the auditory incongruent blocks. All other blocks led to consistent significant activations, except for inferior and anterior pulvinar, in the visual blocks of both face and social scene contexts, and the ventral putamen, in the visual blocks of social scene contexts.

Amygdala and claustrum audio-visual activations

In the amygdala and the claustrum, %SC in response to the auditory incongruent blocks relative to fixation, was statistically significantly lower than the %SC in all other conditions (i.e., V, AC, VAC and VAI), in both the face and the social contexts (figure 3, two top panels, except for the claustrum, in the social scene where AI was not significantly different from V and AC). The pattern of response in these two sub-cortical structures was thus very close to that reported in Froesel et al. (2022) at the cortical level. Interestingly, the amygdala shows a higher activation

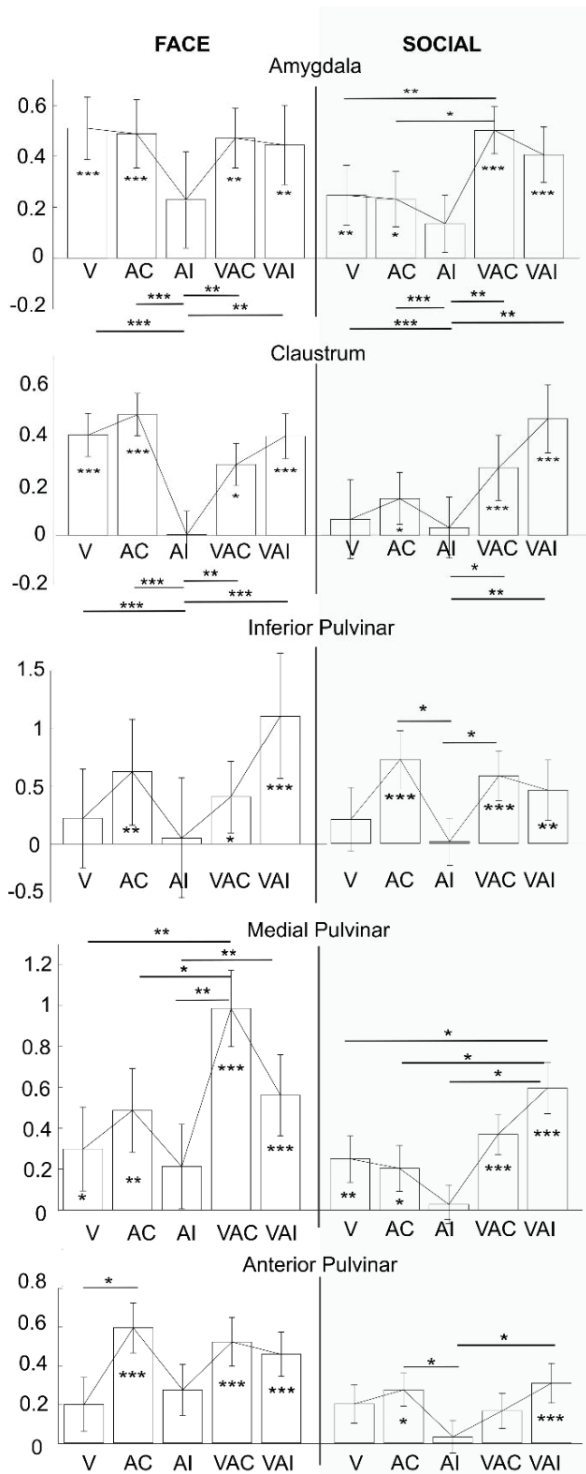
following audio-visual congruent stimulation, i.e. in the bimodal stimulation, than for unimodal stimulation, i.e. visual only and auditory only contexts, in the social context. This was similar to what we previously described in the superior temporal sulcus in Froesel et al. (2022), suggesting a functional interaction between these two regions.

Pulvinar audio-visual activations

Quite unexpectedly, in the three different pulvinar ROIs (inferior, medial and anterior), although there was no significant %SC in response to the auditory incongruent condition relative to fixation, in most cases, no statistically significant difference could be observed between the %SC in this condition and the other conditions (i.e., V, AC, VAC and VAI), in neither the face context nor the social context (figure 3, three bottom panels), except for the medial pulvinar. Indeed, in medial pulvinar, marked significant differences could be observed between the %SC in the AI condition and in the VAC and/or VAI conditions in both types of context (FACE: Friedman non-parametric test, $X^2_{(4)} = 19.26$, $p < 0.001$, $n=80$, post hoc: VAC-AI: $Z=1.9$, $p < 0.01$, VAI-AI: $Z=1.37$, $p < 0.01$; SOCIAL: Friedman non-parametric test, $X^2_{(4)} = 10.54$, $p = 0.03$, $n=158$; post hoc: VAI-AI: $Z=2$, $p=0.048$).

PuM was also the only pulvinar subregion to respond to visual stimulation presented alone (FACE: V: $Z=2.04$, $p=0.04$; V: $Z=2.9$, $p=0.003$). In addition, and paralleling amygdala activation, the medial pulvinar showed a higher activation in bimodal (VAC) versus unimodal conditions (V and AC), specifically to the face context (FACE: Friedman non-parametric test, $X^2_{(4)} = 19.26$, $p < 0.001$, $n=80$, post hoc: V-VAC: $Z=1.6$, $p < 0.01$, AC-VAC: $Z=1.2$, $p=0.02$).

This leads to the noteworthy and unexpected observation that, in this task, the inferior and anterior pulvinar preferentially respond in the auditory conditions, i.e. AC, VAC and VAI conditions rather than in the visual condition, while PuM singles out responding to all



conditions and exhibiting a form of high-level multisensory integration.

Figure 3: Percentage of signal change (%SC) for FACE tasks (F+ & F-) and for Social tasks (S1+, S1-, S2+ & S2-) across sub cortical ROIs, amygdala, claustrum, inferior pulvinar, medial pulvinar and anterior pulvinar of both hemispheres, comparing the auditory, visual and audio-visual conditions. Statistical differences relative to fixation and between conditions are indicated as follows: ***, $p < 0.001$; **, $p < 0.01$; *, $p < 0.05$ (Wilcoxon non-parametric test). See table 1 for quantitative effect sizes. **AMG:** *FACE*: V: $Z=4.8$, $p < 0.001$; AC: $Z=3.79$, $p < 0.001$; AI: $Z=1.17$, $p=0.2$; VAC: $Z=2.9$, $p=0.003$; VAI: $Z=2.62$, $p=0.009$. Friedman non-parametric test, $X^2_{(4)} = 20.83$, $p < 0.001$, $n=80$, post hoc: V-AI: $Z=2.16$, $p < 0.001$, AC-AI: $Z=1.75$, $p < 0.001$, VAC-AI: $Z=1.74$, $p < 0.01$, VAI-AI: $Z=1.4$, $p < 0.01$). *SOCIAL*: V: $Z=2.9$, $p=0.0036$; AC: $Z=1.9$, $p=0.05$; AI: $Z=1.03$, $p=0.29$; VAC: $Z=5.6$, $p < 0.001$; VAI: $Z=4.7$, $p < 0.001$. Friedman non-parametric test, $X^2_{(4)} = 32.77$, $p < 0.001$, $n=158$; post hoc: VAC-V: $Z=2.36$, $p=0.01$; VAC-AC: $Z=2.25$, $p=0.022$; AI-V: $Z=3.09$, $p=0.0019$; VAC-AI: $Z=2.52$, $p=0.01$). **Claus:** *FACE*: V: $Z=3.79$, $p < 0.001$; AC: $Z=3.8$, $p < 0.001$; AI: $Z=0$, $p=0.9$; VAC: $Z=2.04$, $p=0.0412$; VAI: $Z=4.37$, $p=0.009$. Friedman non-parametric test, $X^2_{(4)} = 24.83$, $p < 0.001$, $n=80$, post hoc: V-AI: $Z=2.4$, $p < 0.001$, AC-AI: $Z=2.9$, $p < 0.001$, VAC-AI: $Z=1.77$, $p < 0.01$, VAI-AI: $Z=2.6$, $p < 0.01$). *SOCIAL*: V: $Z=1.45$, $p=0.14$; AC: $Z=2.28$, $p=0.022$; AI: $Z=0.2$, $p=0.83$; VAC: $Z=4.57$, $p < 0.001$; VAI: $Z=5.40$, $p < 0.001$. Friedman non-parametric test, $X^2_{(4)} = 26.82$, $p < 0.001$, $n=158$; post hoc: VAC-AI: $Z=2.23$, $p=0.025$; VAI-AI: $Z=2.58$, $p=0.009$). **PuI:** *FACE*: V: $Z=0.87$, $p=0.38$; AC: $Z=3.2$, $p=0.0013$; AI: $Z=1.45$, $p=0.14$; VAC: $Z=2.3$, $p=0.012$; VAI: $Z=5.25$, $p < 0.001$. Friedman non-parametric test, $X^2_{(4)} = 6.48$, $p=0.1$, $n=80$). *SOCIAL*: V: $Z=1.24$, $p=0.2$; AC: $Z=4.78$, $p < 0.001$; AI: $Z=0$, $p=1$; VAC: $Z=3.74$, $p < 0.001$; VAI: $Z=2.70$, $p=0.006$. Friedman non-parametric test, $X^2_{(4)} = 19.25$, $p < 0.001$, $n=158$, post hoc: AC-AI: $Z=2.6$, $p=0.009$; VAC-AI: $Z=1.9$, $p=0.049$). **PuM:** *FACE*: V: $Z=2.04$, $p=0.04$; AC: $Z=2.6$, $p < 0.01$; AI: $Z=1.7$, $p=0.08$; VAC: $Z=5.25$, $p < 0.001$; VAI: $Z=3.79$, $p < 0.001$. Friedman non-parametric test, $X^2_{(4)} = 19.26$, $p < 0.001$, $n=80$, post hoc: V-VAC: $Z=1.6$, $p < 0.01$, AC-VAC: $Z=1.2$, $p=0.02$, VAC-AI: $Z=1.9$, $p < 0.01$, VAI-AI: $Z=1.37$, $p < 0.01$). *SOCIAL*: V: $Z=2.9$, $p=0.003$; AC: $Z=2.01$, $p=0.037$; AI: $Z=1.03$, $p=0.29$; VAC: $Z=3.95$, $p < 0.001$; VAI: $Z=3.96$, $p < 0.001$. Friedman non-parametric test, $X^2_{(4)} = 10.54$, $p=0.03$, $n=158$; post hoc: VAI-V: $Z=1.86$, $p=0.05$; VAI-AC: $Z=1.9$, $p=0.049$, VAI-AI: $Z=2$, $p=0.048$). **PuA:** *FACE*: V: $Z=1.16$, $p=0.24$; AC: $Z=4.08$, $p < 0.001$; AI: $Z=1.45$, $p=0.14$; VAC: $Z=4.37$, $p < 0.001$; VAI: $Z=3.79$, $p < 0.001$. Friedman non-parametric test, $X^2_{(4)} = 11.59$, $p=0.02$, $n=80$, post hoc: V-AC: $Z=1.7$, $p=0.04$). *SOCIAL*: V: $Z=1.45$, $p=0.14$; AC: $Z=2.28$, $p=0.02$; AI: $Z=0.2$, $p=0.8$; VAC: $Z=1.87$, $p=0.06$; VAI: $Z=4.36$, $p < 0.001$. Friedman non-parametric test, $X^2_{(4)} = 18$, $p=0.0012$, $n=158$, post hoc: AC-AI: $Z=1.88$, $p=0.05$; VAI-AI: $Z=1.9$, $p=0.049$).

Amygdala, claustrum and pulvinar activations in a purely visual task

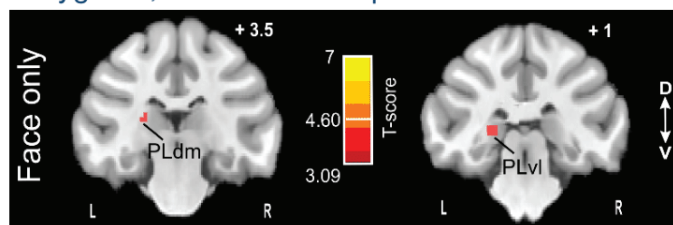


Figure 4: Pulvinar (and whole-brain activation) in a pure visual task: (lipsmacks + aggressive) conditions vs. fixation contrasts. Whole-brain activation maps of the pure visual task cumulated over both monkeys, for lipsmack +

aggressive blocks versus fixation contrast. Darker shades of red indicate level of significance at $p < 0.001$ uncorrected, t-score 3.09. Lighter shades of yellow indicate level of significance at $p < 0.05$ FWE, t-score 4.6.

Because macaque pulvinar has been repeatedly observed to be involved in visual processing, we hypothesized that this specific pulvinar response pattern is a task effect and reflects a spatial segregation of pulvinar sensory responses. To test this, we investigated pulvinar activations in a pure visual task, in which only monkey faces were presented in blocks of consistent emotional categories. In order to match the visual categories used in the main audio-visual task, the following, we only used the lipsmacks and aggressive categories. Clear lateralized left visual activations could be identified in the lateral pulvinar (figure 4, dorsally: PLdm and ventrally: PLvl), at a location very distinct from the ROIs activated in the audio-visual tasks. In this same task and same contrast, the claustrum was also significantly activated (figure 5A) but not the amygdala, although a %SC analysis using a priori defined ROIs extracted from the audio-visual task show that both subcortical structures are highly activated during these pure visual runs (figure 5B; AMG: $Z=4.27$; $p < 0.001$; Claus: $Z=5.8$, $p < 0.001$). Overall, this indicates that while the amygdala and the claustrum are involved in the processing of social cues in both visual and audio-visual contexts, the spatial organization of the pulvinar activations vary between the two types of sensory contexts. This is explored in more details in the next section.

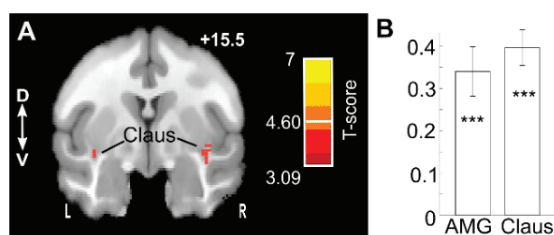


Figure 5: Claustrum (and whole-brain activation) in a pure visual task: (lipsmacks + aggressive) conditions vs. fixation contrasts. (A) Whole-brain activation maps of the pure visual task cumulated over both monkeys, for lipsmack + aggressive blocks versus fixation contrast. Darker shades of red indicate level of significance at $p < 0.001$ uncorrected, t-score 3.09. Lighter shades of yellow indicate level of significance at $p < 0.05$ FWE, t-score 4.6. (B) Percent signal change of lipsmack + aggressive blocks versus fixation contrast in the amygdala (AMG) and the claustrum (Claus) ROIs defined in the audio-visual task described in Figure 2. AMG: $Z=4.27$; $p < 0.001$; Claus: $Z=5.8$, $p < 0.001$.

Gradient of multi and unimodal pulvinar activations

The pulvinar is involved in several sensory processes (for review, see Froesel et al., 2021). How this sensory information from multiple modalities is organized remains poorly understood. In the following, we describe a spatial gradient of sensory responses within the pulvinar, from pure auditory responses (Figure 6A, red), audio-visual responses (Figure 6A&B, blue, see supplemental figure S2 for individual monkey maps), and pure visual responses (Figure 6B, green). More specifically, pure auditory activations are located in anterior pulvinar (PuA), anterior and medial to the audio-visual activations which are located in medial pulvinar (PuM), with a slight overlap between the two activated ROIs. The pure visual activations in the visual task are located in two distinct lateral pulvinar ROIs (Figure 6B, sagittal view, green), lateral to the PuM audio-visual ROIs (Figure 6B, blue), that coincide with PLvl and PLdm (Figure 4), again with a slight overlap between the audio-visual and the visual ROIs. It is worth noting that this gradient was present in each monkey (supplemental figure S2).

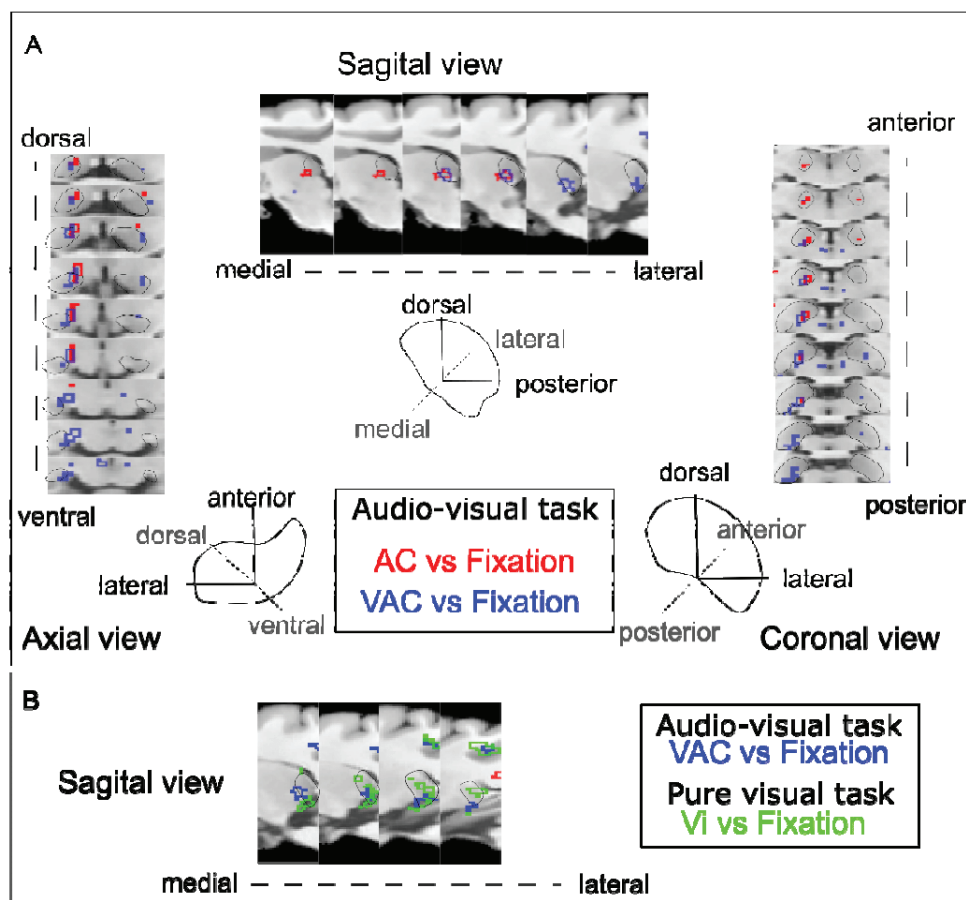


Figure 6: Pulvinal (and whole-brain) activations in FACE (F+ & F-) audio-visual and pure visual tasks. A) Whole-brain activation maps of the FACE context cumulated over both monkeys, for auditory congruent (red) and audio-visual congruent (blue) contrasts vs. fixation. Axial, sagittal and coronal view are shown, zooming on the pulvinal. The activation outline in red and blue correspond to activation thresholds at the level of significance $p < 0.001$ uncorrected, t -score 3.09. B) Whole-brain activation maps of the FACE context cumulated over both monkeys, audio-visual congruent condition of the audio-visual task (blue) and visual condition (aggressive + lipsmack faces) of the pure visual task (green).

Importantly, this very clear functional sensory gradient within the pulvinal is task specific. Indeed, the visual ROIs identified during the pure visual task are not activated during the audio-visual task using the exact same stimuli, and vice versa (Figure 7A&B). All pulvinal ROIs except the anterior pulvinal (PuA) are significantly activated relative to fixation during the pure visual task (Figure 7A; Pul: $Z=3.19$, $p < 0.001$; PuM: $Z=2.6$, $p=0.007$; PuA: $Z=1.86$; $p=0.062$). In contrast, only the ventro-lateral pulvinal ROI (PLvl) retains this significant visual response in the visual only condition of the audio-visual task, although both tasks involve the same visual conditions (Figure 7B; $Z=2.1$, $p=0.02$). These results suggest that pulvinal visual responses (except for PLvl) are not fully driven by sensory input and are modulated by general task context.

PLvl also retains significant %SC in the visuo-auditory condition (Figure 7B, VAC: $Z=2.4$, $p=0.01$) but not in the AC condition ($Z=1.16$, $p=0.24$), suggesting that the VAC significance is

driven by the visual component of the VAC condition. Although we did not run a pure auditory task, the inferior and anterior pulvinar ROIs contrast with PLvl and appear to be driven by auditory stimulation as their %SC is significant for both the auditory (Figure 7B, AC: Pul: $Z=3.2$, $p=0.0013$; PuA: $Z=2.6$, $p<0.01$) and visuo-auditory condition (VAC: Pul: $Z=2.3$, $p=0.011$; PuA: $Z=4.37$, $p<0.001$), but not in the visual condition (V: Pul: $Z=0.87$, $p=0.38$; PuA: $Z=1.16$, $p=0.24$). Medial pulvinar ROI (PuM) stands out in that is activated by all of the visual conditions whether in the pure visual task (Figure 7A, V: $Z=2.6$, $p=0.007$) or the audio-visual task (Figure 7B, V: $Z=2.04$, $p=0.04$), the auditory condition of the audio-visual task (Figure 7B, AC: $Z=2.6$, $p<0.01$) and the audio-visual condition of the audio-visual task (Figure 7B, VAC: $Z=5.25$, $p<0.001$). Notably, the %SC in the VAC condition is significantly higher than the %SC in the V and AC conditions of the audio-visual task (Friedman non-parametric test, $X^2_{(4)} = 19.26$, $p<0.001$, $n=80$, post hoc: V-VAC: $Z=1.6$, $p<0.01$, AC-VAC: $Z=1.2$, $p=0.02$), strongly suggesting that the medial pulvinar, PuM ROI, in contrast with the other ROIs, is integrating visual and auditory information.

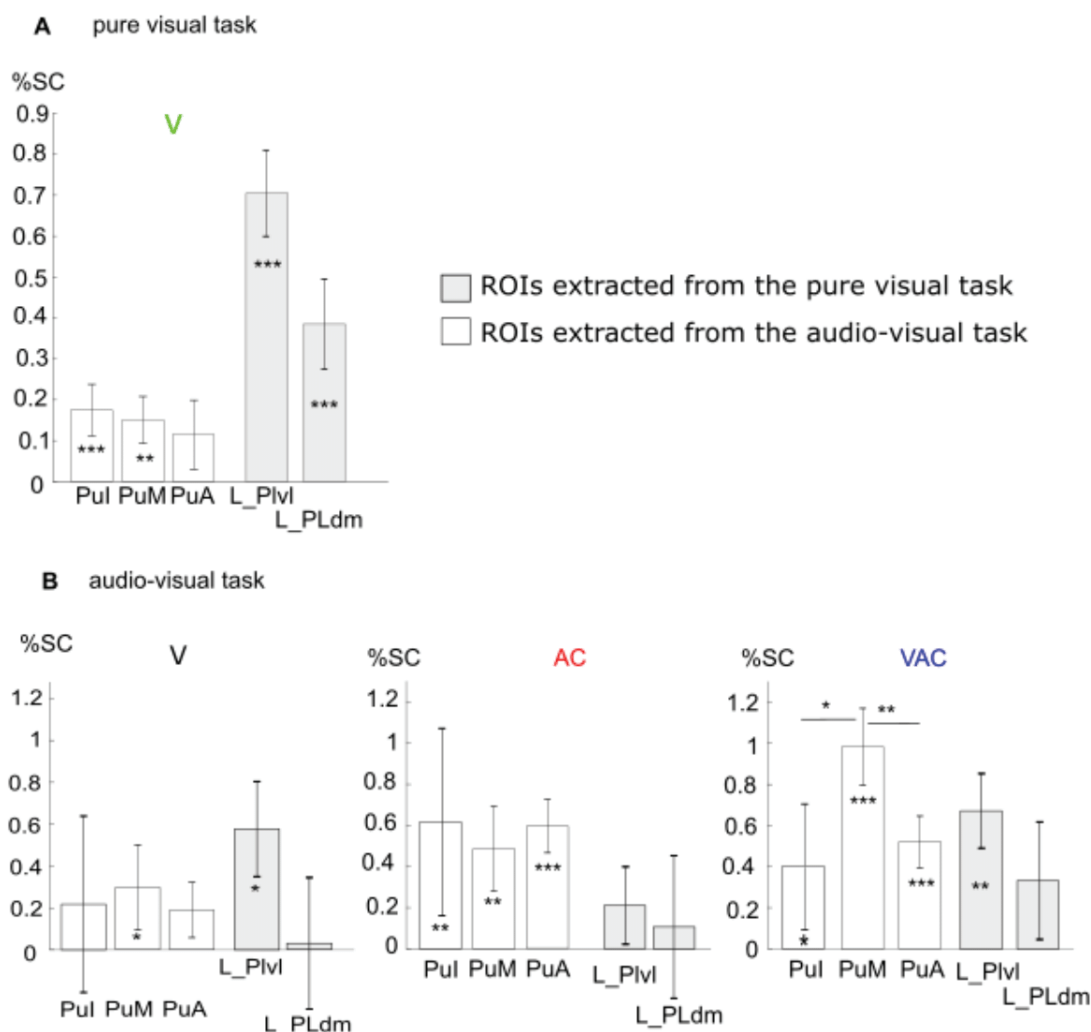


Figure 7: Percentage of signal change in selected pulvinar ROIs, the pure visual task (A) and the audio-visual task (B). Statistical differences relative to fixation and between conditions are indicated as follows: ***, $p < 0.001$; **, $p < 0.01$ (Wilcoxon non-parametric test). Selected ROIs are: Inferior pulvinar (Pul, bilateral), Medial pulvinar (PuM, bilateral), Anterior pulvinar (PuA, bilateral) and Lateral pulvinar (PLdm and PLvl, left). ROIs defined in the audio-visual task are in white. ROIs defined in the pure visual task are in gray. V: visual vs fixation; AC: auditory congruent vs fixation and VAC: audio-visual congruent vs fixation. (A) Pul: $Z=3.19$, $p < 0.001$; PuM: $Z=2.6$, $p=0.007$; PuA: $Z=1.86$, $p=0.062$; PLdm: $Z=2.66$, $p < 0.001$; PLvl: $Z=3.99$, $p < 0.001$. Friedman non-parametric test, $X^2_{(4)} = 3.94$, $p = 0.4$, $n=96$. (B) V: Pul: $Z=0.87$, $p=0.38$; PuM: $Z=2.04$, $p=0.04$; PuA: $Z=1.16$, $p=0.24$; PLdm: $Z=0.29$, $p=0.7$; PLvl: $Z=2.1$, $p=0.02$. Friedman non-parametric test, $X^2_{(4)} = 7.67$, $p = 0.1$, $n=80$. AC: Pul: $Z=3.2$, $p=0.0013$; PuM: $Z=2.6$, $p < 0.01$; PuA: $Z=2.6$, $p < 0.01$; PLdm: $Z=0.8$, $p=0.38$; PLvl: $Z=1.16$, $p=0.24$. Friedman non-parametric test, $X^2_{(4)} = 7.87$, $p = 0.09$, $n=80$. VAC: Pul: $Z=2.3$, $p=0.011$; PuM: $Z=5.25$, $p < 0.001$; PuA: $Z=4.37$, $p < 0.001$; PLdm: $Z=3.2$, $p=0.0013$; PLvl: $Z=2.4$, $p=0.01$. Friedman non-parametric test, $X^2_{(4)} = 9.82$, $p = 0.03$, $n=80$. Pul-PuM: $Z=2.1$, $p=0.02$; PuM-PuA: $Z=2.4$, $p=0.01$.

Discussion

Overall, three key subcortical structures contribute to the audio-visual association of functionally significant communicative signal: the amygdala, claustrum and pulvinar. Activation patterns in the pulvinar were not predicted based on prior research and shed new light on the functional organization of this subcortical nucleus. The medial part of the nucleus and the amygdala demonstrate multisensory integration similar to what we report in the superior temporal sulcus in a previous study using the same data (Froesel et al., 2022). It is worth noting that the amygdala, claustrum and pulvinar correspond to the three subcortical regions activated by face patch stimulations. It has been proposed that these regions correspond to a bottlenecks for the communication between face patches (Moeller et al., 2008). This interpretation is supported by a tracer studies showing that individual patches receive input from these three subcortical structures (Grimaldi et al., 2016) as well as by resting-state fMRI, alone or in association with single cell recording studies (Schwiedrzik et al., 2015; Zaldivar et al., 2022). The amygdala, claustrum and pulvinar are thus a part of a subcortical network involved in face processing. In this study, we extend their role to the processing of species-specific vocalizations and their association with socioemotional visual information. The degree of specificity is not yet established, requiring tests with other species' vocalisations, facial expressions, and social scenes.

Audio-visual association of social stimuli in the amygdala and the claustrum

The amygdala and claustrum are activated by all visual, auditory congruent and audio-visual (congruent and incongruent) stimuli where auditory congruence or incongruence is defined by the visual context set in each presentation. Both these subcortical structures thus follow a response pattern that is similar to that observed at the cortical level (Froesel et al., 2022). In addition, they both are also activated by emotional facial expressions during a pure visual task.

visual association task. Third, only the medial pulvinar and the ventral lateral pulvinar respond to visual social stimuli irrespective of context. It is also worth noting that this gradient does not follow the classical sub divisions defined based on its cytoarchitectonic properties, i.e. inferior pulvinar, lateral pulvinar and medial pulvinar (supplemental figures S3 and S4) (Walker, 1938; Olszewski et al., 1952; Gutierrez et al., 1995; Stepniewska and Kaas, 1997).

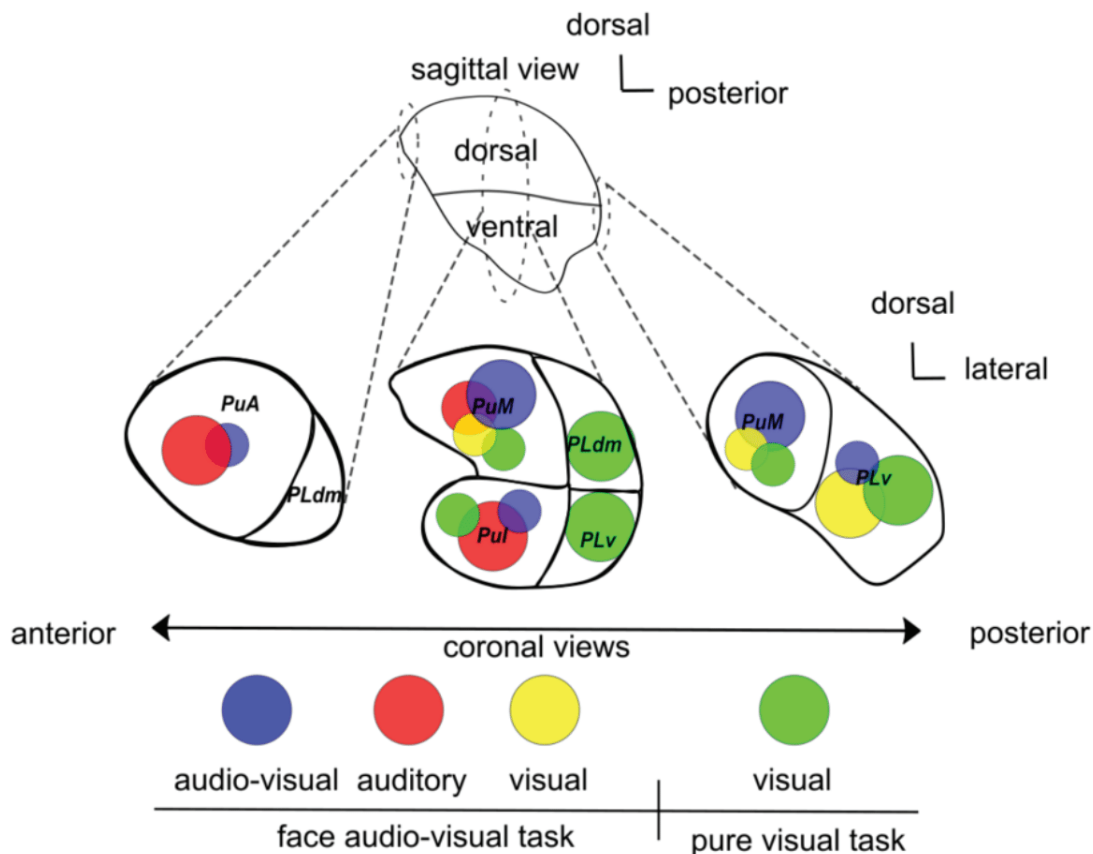


Figure 8: Summary of the activations within the pulvinar as a function of the task and sensory of stimulation. The circle size is largest in the regions of nucleus that present a higher activation. All circles correspond to significant activations or %SC.

Pulvinar and Face perception

The lateral part of monkey pulvinar has been proved to contain face responsive neurons and the medial part is shown to be responsive to human facial expressions (Maier et al., 2010; Nguyen et al., 2013). Our observations from the pure visual task bring full support to this observation (figure 8, green circles). Using resting-state analysis, it has been found that the dorsal pulvinar, i.e. dorsal lateral and medial pulvinar, is functionally connected with face patches (Schwiedrzik et al., 2015). This is also the case for the ventral pulvinar. Generally speaking, the more anterior face patches connect to more anterior parts of the pulvinar thus defining an antero-posterior functional connectivity gradient between the superior temporal sulcus and the pulvinar (Grimaldi et al., 2016). In addition, the stimulation of the two face patches AL and ML (respectively anterior lateral and medial lateral) of the superior temporal sulcus elicits activation in the inferior pulvinar

(Moeller et al., 2008). Overall, this suggests that the entire pulvinar is potentially responsive to faces, these face responses being recruited differentially as a function of task and context.

Our study showed that a task implicitly calling for an association between auditory and visual social information, activates the medial as well as the ventro-lateral pulvinar. The pure visual task additionally activates the dorso-lateral and the inferior pulvinar. This is in agreement with the human pulvinar lesion literature, whereby a patient presenting with an entirely damaged unilateral pulvinar was not able to recognize fearful expressions in the contralesional field, while patients with damage limited to the anterior and lateral pulvinar showed no deficits in fear recognition (Ward et al., 2007). These results suggested fear recognition is mediated by the medial pulvinar. We propose to link these observations to the role of the pulvinar in emotional regulation, as discussed next. Additionally, the medial pulvinar is the unique pulvinar nucleus that presents audio-visual integration. This result supports the idea that this subregion implements multisensory integration (Froesel et al., 2021). As is the case for the amygdala, recent studies report multisensory integration in this brain structure. A macaque single cell recording study describes sub-additive and suppressive multisensory integration in the medial pulvinar (Vittek et al., 2022) while a recent human fMRI study of the pulvinar region describes multisensory enhancement during natural narrative speech perception (Ross et al., 2022). Here, we show that audio-visual integration can also be observed when the stimuli are matching only on semantic criterions and not classical multisensory matching. It follows the hypothesis formulated by Ross et al (2022) that multisensory enhancement in more naturalistic contexts involving understanding of semantics, recruits more than the typical multisensory network, notably the amygdala and the pulvinar. Given the fact that the medial pulvinar is highly connected with the limbic system and areas involved in the regulation of emotions such as anterior cingulate cortex, the temporal cortex, the temporo-parietal junction, the insula, the frontal parietal opercular cortex (Yeterian and Pandya, 1997; Rosenberg et al., 2009), together with the amygdala with which it is also connected (Jones and Burton, 1976), these structures are proposed to coordinate cortical networks to evaluate the biological significance of affective visual stimuli (Pessoa, 2010b). Their recruitment during audio-visual binding based on socioemotional context supports this hypothesis.

Lateralisation

In the pulvinar, a processing bias in the left pulvinar has already been demonstrated in humans, which has been interpreted in the light of the role of the pulvinar in the attentional function (Padmala et al., 2010). In their monkey rsfMRI study, Schwiedrzik et al determined that the pulvinar, amygdala, hippocampus, caudate nucleus, claustrum and other sub cortical structures are functionally connected with face patches (Schwiedrzik et al., 2015). In addition, their left pulvinar activations were more widespread than the right activations. In our present study, activations during the pure visual context are exclusively identified in the left pulvinar. A left hemisphere bias for processing species-specific vocalisation was reported in a field study of rhesus monkeys (Hauser and Andersson, 1994). All this taken together with the fact that the SNR is not higher on the left than on the right (see supplemental figure S4), raises the possibility of functional lateralization bias in the monkey pulvinar. This will have to be further explored.

Conclusion

In this study, we suggest that of the amygdala, claustrum, pulvinar play an essential role in multisensory integration of communicatively significant information. In addition, we demonstrate that there is a sensory audio-visual processing gradient within the pulvinar that is task dependent. We show that the medial pulvinar and amygdala, but not the claustrum, can be considered as audio-visual associators of social stimuli. We propose that these three sub cortical structures are part of an amodal network that modulates sensory perception as a function of the social context.

References

- Autio JA et al. (2020) Towards HCP-Style macaque connectomes: 24-Channel 3T multi-array coil, MRI sequences and preprocessing. *NeuroImage* 215:116800.
- Barracough NE, Perrett DI (2011) From single cells to social perception. *Philos Trans R Soc B Biol Sci* 366:1739–1752.
- Belin P, Fecteau S, Charest I, Nicastro N, Hauser MD, Armony JL (2007) Human cerebral response to animal affective vocalizations. *Proc R Soc B Biol Sci* Available at: <https://royalsocietypublishing.org/doi/abs/10.1098/rspb.2007.1460> [Accessed April 15, 2021].
- Cohen YE, Theunissen F, Russ BE, Gill P (2007) Acoustic Features of Rhesus Vocalizations and Their Representation in the Ventrolateral Prefrontal Cortex. *J Neurophysiol* 97:1470–1484.
- Dolan RJ, Morris JS, Gelder B de (2001) Crossmodal binding of fear in voice and face. *Proc Natl Acad Sci* 98:10006–10010.
- Domínguez-Borràs J, Guex R, Méndez-Bértolo C, Legendre G, Spinelli L, Moratti S, Frühholz S, Mégevand P, Arnal L, Strange B, Seeck M, Vuilleumier P (2019) Human amygdala response to unisensory and multisensory emotion input: No evidence for superadditivity from intracranial recordings. *Neuropsychologia* 131:9–24.
- Donahue CJ, Sotiropoulos SN, Jbabdi S, Hernandez-Fernandez M, Behrens TE, Dyrby TB, Coalson T, Kennedy H, Knoblauch K, Essen DCV, Glasser MF (2016) Using Diffusion Tractography to Predict Cortical Connection Strength and Distance: A Quantitative Comparison with Tracers in the Monkey. *J Neurosci* 36:6758–6770.
- Fitzgerald DA, Angstadt M, Jelsone LM, Nathan PJ, Phan KL (2006) Beyond threat: Amygdala reactivity across multiple expressions of facial affect. *NeuroImage* 30:1441–1448.
- Freiwald WA (2020) Social interaction networks in the primate brain. *Curr Opin Neurobiol* 65:49–58.
- Froesel M, Cappe C, Ben Hamed S (2021) A multisensory perspective onto primate pulvinar functions. *Neurosci Biobehav Rev* Available at: <https://www.sciencedirect.com/science/article/pii/S0149763421001044> [Accessed March 1, 2021].

- Froesel M, Gacoin M, Clavagnier S, Hauser M, Goudard Q, Ben Hamed S (2022) Socially meaningful visual context either enhances or inhibits vocalisation processing in the macaque brain. *Nat Commun* 13:4886.
- Froesel M, Goudard Q, Hauser M, Gacoin M, Ben Hamed S (2020) Automated video-based heart rate tracking for the anesthetized and behaving monkey. *Sci Rep* 10:17940.
- Gadziola MA, Grimsley JMS, Shanbhag SJ, Wenstrup JJ (2012) A novel coding mechanism for social vocalizations in the lateral amygdala. *J Neurophysiol* 107:1047–1057.
- Ghazanfar AA, Santos LR (2004) Primate brains in the wild: the sensory bases for social interactions. *Nat Rev Neurosci* 5:603–616.
- Glasser MF, Sotiropoulos SN, Wilson JA, Coalson TS, Fischl B, Andersson JL, Xu J, Jbabdi S, Webster M, Polimeni JR, Van Essen DC, Jenkinson M (2013) The minimal preprocessing pipelines for the Human Connectome Project. *NeuroImage* 80:105–124.
- Gothard KM (2020) Multidimensional processing in the amygdala. *Nat Rev Neurosci* 21:565–575.
- Gothard KM, Battaglia FP, Erickson CA, Spitler KM, Amaral DG (2007) Neural Responses to Facial Expression and Face Identity in the Monkey Amygdala. *J Neurophysiol* 97:1671–1683.
- Gouzoules S, Gouzoules H, Marler P (1984) Rhesus monkey (*Macaca mulatta*) screams: Representational signalling in the recruitment of agonistic aid. *Anim Behav* 32:182–193.
- Grimaldi P, Saleem KS, Tsao D (2016) Anatomical Connections of the Functionally Defined “Face Patches” in the Macaque Monkey. *Neuron* 90:1325–1342.
- Gutierrez C, Yaun A, Cusick CG (1995) Neurochemical subdivisions of the inferior pulvinar in macaque monkeys. *J Comp Neurol* 363:545–562.
- Hauser MD, Andersson K (1994) Left hemisphere dominance for processing vocalizations in adult, but not infant, rhesus monkeys: field experiments. *Proc Natl Acad Sci U S A* 91:3946–3948.
- Hauser MD, Marler P (1993) Food-associated calls in rhesus macaques (*Macaca mulatta*): I. Socioecological factors. *Behav Ecol* 4:194–205.
- Jones EG, Burton H (1976) A projection from the medial pulvinar to the amygdala in primates. *Brain Res* 104:142–147.
- Kolster H, Janssens T, Orban GA, Vanduffel W (2014) The retinotopic organization of macaque occipitotemporal cortex anterior to V4 and caudoventral to the middle temporal (MT) cluster. *J Neurosci Off J Soc Neurosci* 34:10168–10191.
- Kuraoka K, Nakamura K (2007) Responses of Single Neurons in Monkey Amygdala to Facial and Vocal Emotions. *J Neurophysiol* 97:1379–1387.

- Leite FP, Tsao D, Vanduffel W, Fize D, Sasaki Y, Wald LL, Dale AM, Kwong KK, Orban GA, Rosen BR, Tootell RBH, Mandeville JB (2002) Repeated fMRI using iron oxide contrast agent in awake, behaving macaques at 3 Tesla. *NeuroImage* 16:283–294.
- Leonard CM, Rolls ET, Wilson FA, Baylis GC (1985) Neurons in the amygdala of the monkey with responses selective for faces. *Behav Brain Res* 15:159–176.
- Livneh U, Resnik J, Shohat Y, Paz R (2012) Self-monitoring of social facial expressions in the primate amygdala and cingulate cortex. *Proc Natl Acad Sci U S A* 109:18956–18961.
- Maier RS, Hori E, Tomaz C, Ono T, Nishijo H (2010) The monkey pulvinar neurons differentially respond to emotional expressions of human faces. *Behav Brain Res* 215:129–135.
- Moeller S, Freiwald WA, Tsao DY (2008) Patches with Links: A Unified System for Processing Faces in the Macaque Temporal Lobe. *Science* 320:1355–1359.
- Morrow J, Mosher C, Gothard K (2019) Multisensory Neurons in the Primate Amygdala. *J Neurosci Off J Soc Neurosci* 39:3663–3675.
- Nakamura K, Mikami A, Kubota K (1992) Activity of single neurons in the monkey amygdala during performance of a visual discrimination task. *J Neurophysiol* 67:1447–1463.
- Nguyen MN, Hori E, Matsumoto J, Tran AH, Ono T, Nishijo H (2013) Neuronal responses to face-like stimuli in the monkey pulvinar. *Eur J Neurosci* 37:35–51.
- Olszewski J, Assistant Professor of Neuro-anatomy D of N, Neuro-surgery MU (1952) The thalamus of the Macaca, mulatta. An atlas for use with the stereotaxic instrument. *Thalamus Macaca Mulatta Atlas Use Ster Instrum* Available at: <https://www.cabdirect.org/cabdirect/abstract/19522203025> [Accessed December 6, 2018].
- Padmala S, Lim S-L, Pessoa L (2010) Pulvinar and Affective Significance: Responses Track Moment-to-Moment Stimulus Visibility. *Front Hum Neurosci* 4 Available at: <https://www.frontiersin.org/articles/10.3389/fnhum.2010.00064/full> [Accessed June 14, 2019].
- Pessoa L (2010a) Emotion and Cognition and the Amygdala: From “what is it?” to “what’s to be done?” *Neuropsychologia* 48:3416–3429.
- Pessoa L (2010b) Emotion and Cognition and the Amygdala: From “what is it?” to “what’s to be done?” *Neuropsychologia* 48:3416–3429.
- Pessoa L, Japee S, Sturman D, Ungerleider LG (2006) Target Visibility and Visual Awareness Modulate Amygdala Responses to Fearful Faces. *Cereb Cortex* 16:366–375.
- Remedios R, Logothetis NK, Kayser C (2010) Unimodal Responses Preval within the Multisensory Claustrum. *J Neurosci* 30:12902–12907.
- Romanski LM (2012) Integration of faces and vocalizations in ventral prefrontal cortex: Implications for the evolution of audiovisual speech. *Proc Natl Acad Sci* 109:10717–10724.

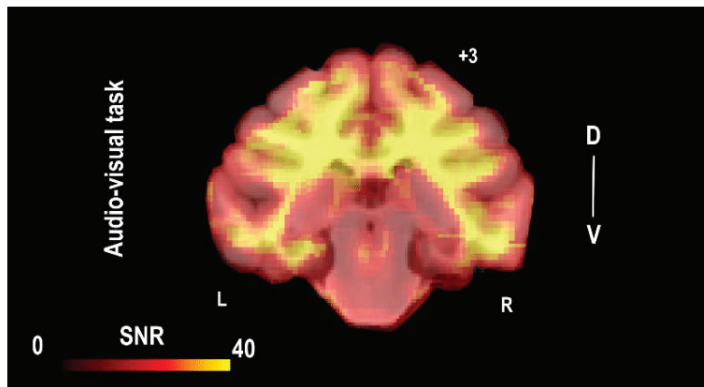
- Romanski LM, Averbeck BB, Diltz M (2005) Neural Representation of Vocalizations in the Primate Ventrolateral Prefrontal Cortex. *J Neurophysiol* 93:734–747.
- Rosenberg DS, Mauguière F, Catenoix H, Faillenot I, Magnin M (2009) Reciprocal Thalamocortical Connectivity of the Medial Pulvinar: A Depth Stimulation and Evoked Potential Study in Human Brain. *Cereb Cortex* 19:1462–1473.
- Ross LA, Molholm S, Butler JS, Bene VAD, Foxe JJ (2022) Neural correlates of multisensory enhancement in audiovisual narrative speech perception: a fMRI investigation. *NeuroImage*:119598.
- Russ BE, Ackelson AL, Baker AE, Cohen YE (2008) Coding of Auditory-Stimulus Identity in the Auditory Non-Spatial Processing Stream. *J Neurophysiol* 99:87–95.
- Schwiedrzik CM, Zarco W, Everling S, Freiwald WA (2015) Face Patch Resting State Networks Link Face Processing to Social Cognition. *PLOS Biol* 13:e1002245.
- Sergerie K, Chochol C, Armony JL (2008) The role of the amygdala in emotional processing: A quantitative meta-analysis of functional neuroimaging studies. *Neurosci Biobehav Rev* 32:811–830.
- Smith JB, Lee AK, Jackson J (2020) The claustrum. *Curr Biol* 30:R1401–R1406.
- Stein BE, Meredith MA (1993) *The merging of the senses*. Cambridge, MA, US: The MIT Press.
- Stepniewska I, Kaas JH (1997) Architectonic subdivisions of the inferior pulvinar in New World and Old World monkeys. *Vis Neurosci* 14:1043–1060.
- Todorov A (2012) The role of the amygdala in face perception and evaluation. *Motiv Emot* 36:16–26.
- Vanduffel W, Fize D, Mandeville JB, Nelissen K, Hecke PV, Rosen BR, Tootell RBH, Orban GA (2001) Visual Motion Processing Investigated Using Contrast Agent-Enhanced fMRI in Awake Behaving Monkeys. *Neuron* 32:565–577.
- Vittek A-L, Juan C, Nowak LG, Girard P, Cappe C (2022) Multisensory integration in neurons of the medial pulvinar of macaque monkey. :2022.03.21.485176 Available at: <https://www.biorxiv.org/content/10.1101/2022.03.21.485176v1> [Accessed September 19, 2022].
- Walker AE (1938) The thalamus of the chimpanzee: IV. Thalamic projections to the cerebral cortex. *J Anat* 73:37–93.
- Ward R, Calder AJ, Parker M, Arend I (2007) Emotion recognition following human pulvinar damage. *Neuropsychologia* 45:1973–1978.
- Yeterian EH, Pandya DN (1997) Corticothalamic connections of extrastriate visual areas in rhesus monkeys. *J Comp Neurol* 378:562–585.
- Zaldivar D, Koyano KW, Ye FQ, Godlove DC, Park SH, Russ BE, Bhik-Ghanie R, Leopold DA (2022) Brain-wide functional connectivity of face patch neurons during rest. *Proc Natl Acad Sci* 119:e2206559119.

Supplemental data

| ROIS | Context | Visual (V) | Auditory congruent (AC) | Auditory Incongruent (AI) | Visuo-auditory congruent (VAC) | Visuo-auditory congruent (VAI) |
|-------------------|---------|------------|-------------------------|---------------------------|--------------------------------|--------------------------------|
| Amygdala | FACE | Z=4.8 | Z=3.79 | Z=1.17 | Z=2.9 | Z=2.62 |
| | SOCIAL | Z=2.9 | Z=1.9 | Z=1.03 | Z=5.6 | Z=4.7 |
| Caudate | FACE | Z=3.79 | Z=3.8 | Z=0 | Z=2.04 | Z=4.37 |
| | SOCIAL | Z=1.45 | Z=2.28 | Z=0.2 | Z=4.57 | Z=5.40 |
| Inferior Pulvinar | FACE | Z=0.87 | Z=3.2 | Z=1.45 | Z=2.3 | Z=5.25 |
| | SOCIAL | Z=1.24 | Z=4.78 | Z=0 | Z=3.74 | Z=2.70 |
| Medial Pulvinar | FACE | Z=2.04 | Z=2.6 | Z=1.7 | Z=5.25 | Z=3.79 |
| | SOCIAL | Z=2.9 | Z=2.01 | Z=1.03 | Z=3.95 | Z=3.96 |
| Anterior Pulvinar | FACE | Z=1.16 | Z=4.08 | Z=1.45 | Z=4.37 | Z=3.79 |
| | SOCIAL | Z=1.45 | Z=2.28 | Z=0.2 | Z=1.87 | Z=4.36 |

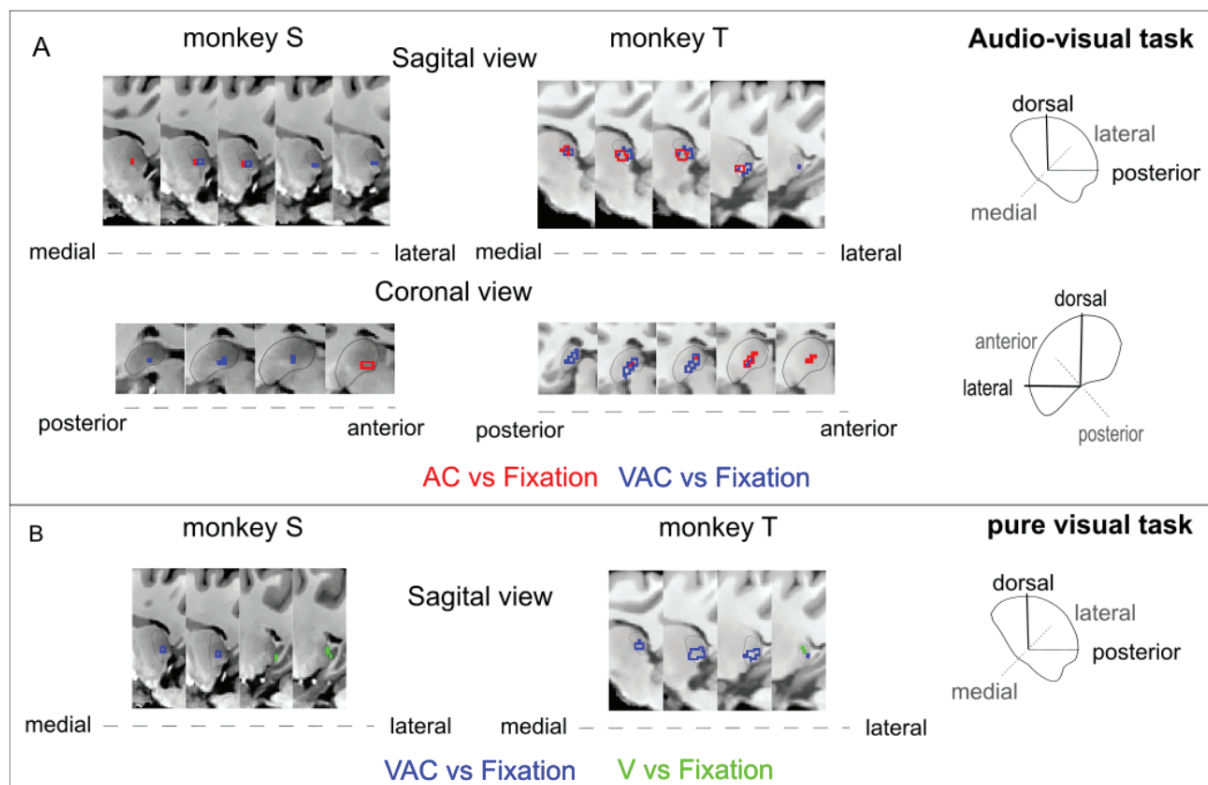
Supplementary Table 1: Effect sizes of the activations (percent signal change). Effect sizes of the Wilcoxon test performed on the percent signal changed. Significant results are presented in bold. This is a companion table to Figure 3.

bioRxiv preprint doi: <https://doi.org/10.1101/2022.09.28.509981>; this version posted September 30, 2022. The copyright holder for this preprint (which was not certified by peer review) is the author/funder, who has granted bioRxiv a license to display the preprint in perpetuity. It is made available under aCC-BY-NC-ND 4.0 International license.

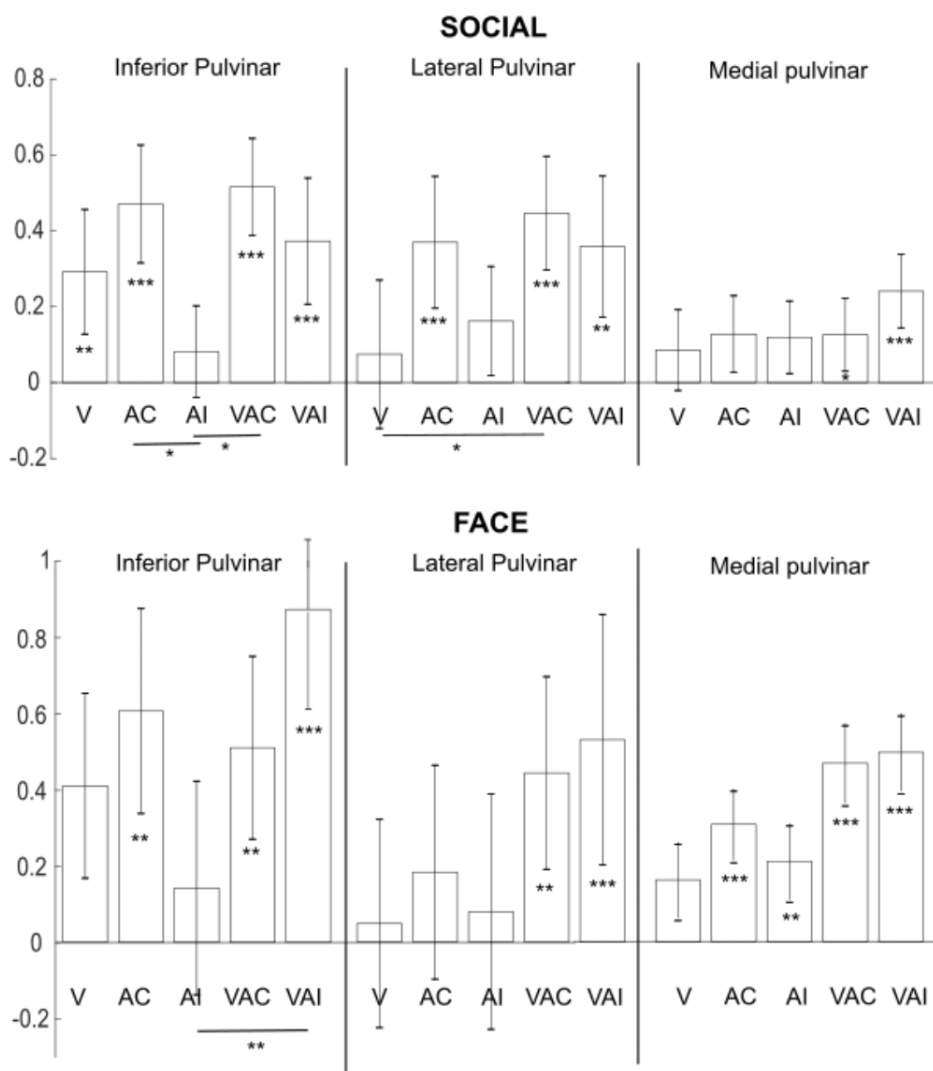


Supplemental figure S1: group SNR map for the audio-visual task.

bioRxiv preprint doi: <https://doi.org/10.1101/2022.09.28.509981>; this version posted September 30, 2022. The copyright holder for this preprint (which was not certified by peer review) is the author/funder, who has granted bioRxiv a license to display the preprint in perpetuity. It is made available under aCC-BY-NC-ND 4.0 International license.



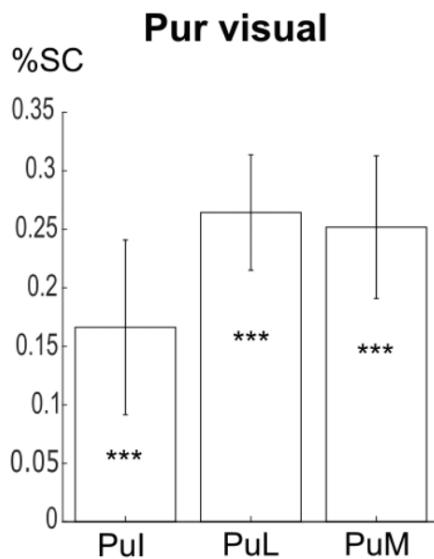
Supplemental figure S2: Pulvinar (and whole-brain) activations in FACE (F+ & F-) audio-visual and pure visual tasks per monkey. A) Whole-brain activation maps of the FACE context for both monkeys (monkey S and T), for auditory congruent (red) and audio-visual congruent (blue) contrasts vs. fixation. Axial, sagittal and coronal view are shown, zooming on the pulvinar. The activation outline in red and blue correspond to activation thresholds at the level of significance $p < 0.001$ uncorrected, t-score 3.09, DF [1, 2600], and $p < 0.05$ uncorrected, t-score 1.64 DF [1,2600] for monkey S. B) Whole-brain activation maps of the FACE context cumulated over both monkeys, audio-visual congruent condition of the audio-visual task (blue) and visual condition (aggressive + lipsmack faces) of the pure visual task (green). Note that even if the significance threshold for both monkeys are not the same, the gradient is present.



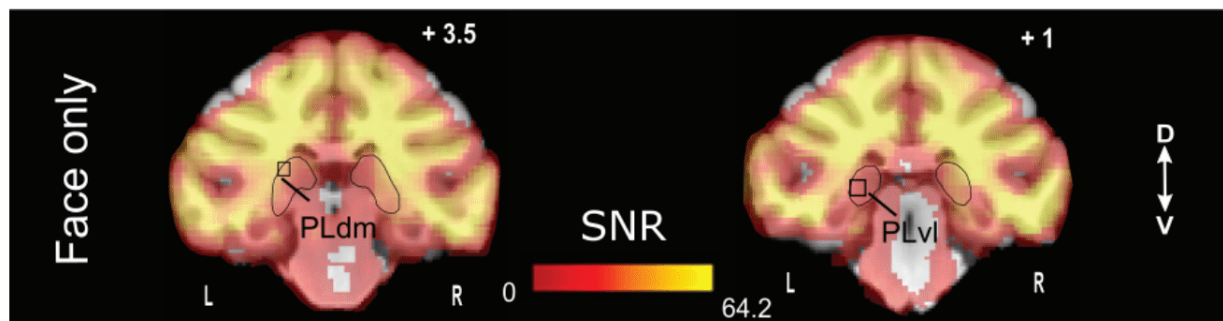
*Supplemental figure S3: Percentage of signal change (%SC) in anatomical defined pulvinar ROIs for the audio-visual task for social and face contexts. Statistical differences relative to fixation and between conditions are indicates as follows: ***, $p < 0.001$; **, $p < 0.01$ (Wilcoxon non-parametric test). V: visual vs fixation, AC: auditory congruent vs fixation; AI: auditory incongruent vs fixation; VAC: audio-visual congruent vs fixation; VAI: audio-visual incongruent vs fixation. SOCIAL : Pul : V : $Z=2.70$, $p=0.007$; AC: $Z=4.16$, $p < 0.001$; AI: 1.24 , $p=0.21$, VAC: 5.4 , $p < 0.001$, VAI : 3.53 $p < 0.001$. Friedman non-parametric test, $X^2_{(4)} = 16.34$, $p=0.0026$, $n=158$, post hoc: V-AC: $Z=1.96$, $p=0.049$, AC-AI: $Z=2.48$, $p=0.013$. PuL : V= 0.8 , $p=0.4$, AC : 3.32 , $p < 0.001$; AI : 1.87 , $p=0.06$; VAC : 3.74 , $p < 0.001$; VAI : 2.9 , $p=0.0036$. Friedman non-parametric test, $X^2_{(4)} = 10.57$, $p=0.032$, $n=158$, post hoc: V-VAC: $Z=2.15$, $p=0.031$. PuM : V : $Z=1.39$, $p=0.29$; AC : $Z=1.45$, $p=0.14$, AI : $Z=1.66$, $p=0.09$; VAC : $Z=2.08$, $p=0.03$; VAI : $Z=3.53$, $p < 0.001$. Friedman non-parametric test, $X^2_{(4)} = 5.72$, $p=0.22$, $n=158$. FACE: Pul : V : $Z=0.87$, $p=0.38$; AC: $Z=3.2$, $p=0.0013$; AI: 1.45 , $p=0.14$; VAC: 3.21 , $p=0.0013$, VAI : 5.25 , $p < 0.001$. Friedman non-parametric test, $X^2_{(4)} = 11.59$, $p=0.02$, $n=80$, post hoc: V-AC: $Z=1.96$, $p=0.049$, AC-AI: $Z=2.48$,*

bioRxiv preprint doi: <https://doi.org/10.1101/2022.09.28.509981>; this version posted September 30, 2022. The copyright holder for this preprint (which was not certified by peer review) is the author/funder, who has granted bioRxiv a license to display the preprint in perpetuity. It is made available under aCC-BY-NC-ND 4.0 International license.

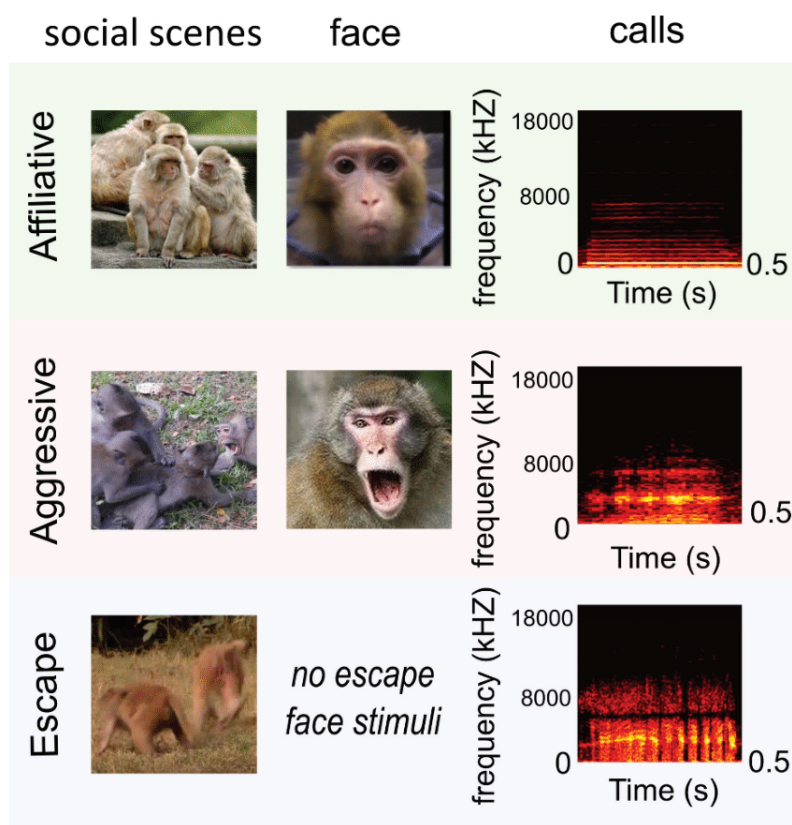
$p=0.013$. PuL : V=0.29, $p=0.77$; AC : 1.46, $p=0.15$; AI : 0.29, $p=0.77$; VAC : 3.21, $p=0.0013$; VAI : 3.5, $p<0.001$. Friedman non-parametric test, $X^2_{(4)} = 8.6$, $p=0.07$, $n=80$, post hoc: V-VAC: $Z=2.15$, $p=0.031$. PuM : V : $Z=1.1$, $p=0.24$; AC : $Z=4.08$, $p<0.001$; AI : $Z=3.2$, $p=0.001$; VAC : $Z=4.9$, $p<0.001$; VAI : $Z=3.2$, $p=0.0013$. Friedman non-parametric test, $X^2_{(4)} = 7.45$, $p=0.11$, $n=80$.



Supplemental figure S4: Percentage of signal change (%SC) in anatomical defined pulvinar ROIs for the pure visual task. Statistical differences relative to fixation and between conditions are indicated as follows: ***, $p<0.001$; **, $p<0.01$ (Wilcoxon non-parametric test: PuL: $Z=3.99$, $p<0.001$; PuL: 6.12, $p<0.001$; PuM: 3.73, $p<0.001$). PuL: inferior pulvinar; PuL: lateral pulvinar and PuM: medial pulvinar.



Supplemental figure S5: SNR map for the purely visual task both animals



Supplementary Figure S6: Example of visual and auditory stimuli. At the right are shown examples of visual stimuli used for social and face contexts. On the left, congruent calls spectrograms are associated to the visual stimuli are shown. The affiliative call is a coo, the aggressive congruent auditory stimulus is an aggressive call and the escape call is a scream. Stimuli were not strictly normalized in terms of in low visual and auditory feature properties, thus making their social meaning the dominant cue across the different stimuli of a given category.

Appendices – Appendix 1

bioRxiv preprint doi: <https://doi.org/10.1101/2022.09.28.509981>; this version posted September 30, 2022. The copyright holder for this preprint (which was not certified by peer review) is the author/funder, who has granted bioRxiv a license to display the preprint in perpetuity. It is made available under a [CC-BY-NC-ND 4.0 International license](#).

Stimuli were extracted from videos collected by the Ben Hamed lab, as well as by Marc Hauser on Cayo Santiago, Puerto Rico.

Appendix 2: Effect of early social deprivation on the development of *Macaca mulatta*

As a side project of the present thesis, I had the opportunity to collaborate on another longitudinal MRI study that aims at study the behavioral and neural basis of early social deprivation in the rhesus macaque (**Appendix n°2**). To achieve this project, both behavioral and neuroimaging data have been acquired on two groups of rhesus macaques. The first group was composed of 10 macaques reared by their mothers and the second group by 10 macaques reared in a nursery of peers. The latter group was thus deprived from early social experiences, which are mostly mother-infant interactions in macaques (Ferrari et al., 2009). To quantify repetitive and restrictive behavior, characteristics to developmental impairments, such as those observed in the autism spectrum disorder (Hoksbergen et al., 2005; Sonuga-Barke et al., 2017; Bos et al., 2010), social interactions and polymorphisms, videos and blood samples were collected. In order to characterize underlying neural mechanisms of such a development, we recorder MRI images at three time points (2,5 years, corresponding to childhood; 3,5 years corresponding to adolescence; 4,5 corresponding to young adulthood).

On this project, I was in charge of MRI scanning (T1, T2, DTI and resting-state with MION injection) and the monitoring of gas-induced anesthesia with isoflurane administered by intubation. Further, I will investigate the obtained resting state data and study the functional connectivity (FC) of regions specific to the visual system development, such as the lateral geniculate nucleus, the intra-parietal sulcus or early visual areas with the rest of the brain. Moreover, since a pendent of this project consists in behaviors measures and hierarchy assessment, I will also study the FC of the dorsal raphe with the rest of the brain, to possibly link a visual system network design development with the hierchical status of the macaque. Indeed, since the retinotopic organization in the developing brain has been investigated (Arcaro and Livingstone, 2017), yet little is known about the development of the visual system in a context of social early adversity in the macaque. Since we referred to the critical period throughout this thesis manuscript, we are highly interested to compare our FC results of an enhanced visual plasticity in the adult with a visual plasticity induced by social impairments, all the more that fluoxetine in juvenile rhesus macaques under fluoxetine facilitates their social interactions (Golub et al., 2016).

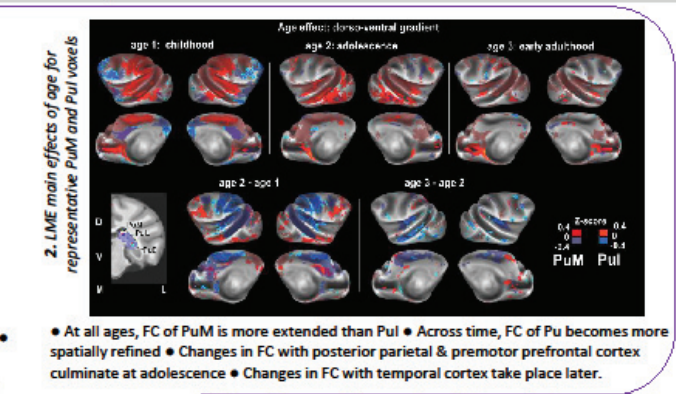
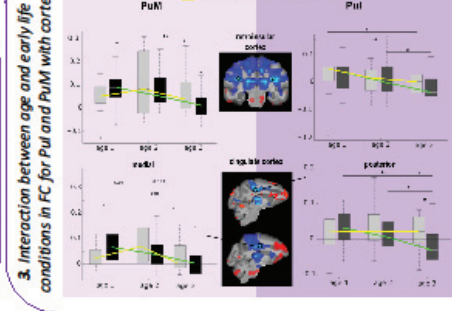
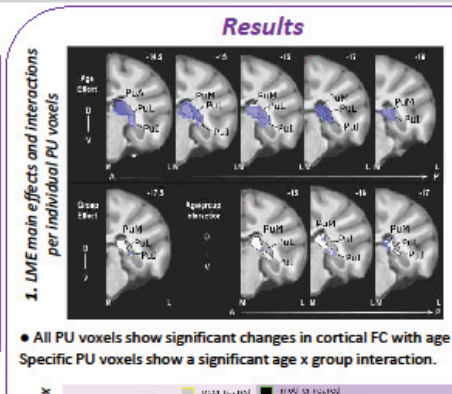
References

- Arcaro, M.J., Livingstone, M.S., 2017. A hierarchical, retinotopic proto-organization of the primate visual system at birth. *eLife* 6, e26196. <https://doi.org/10.7554/eLife.26196>
- Bos, K.J., Zeanah, C.H., Jr, Smyke, A.T., Fox, N.A., Nelson, C.A., III, 2010. Stereotypies in Children With a History of Early Institutional Care. *Archives of Pediatrics & Adolescent Medicine* 164, 406–411. <https://doi.org/10.1001/archpediatrics.2010.47>

- Ferrari, P.F., Paukner, A., Ionica, C., Suomi, S.J., 2009. Reciprocal Face-to-Face Communication between Rhesus Macaque Mothers and Their Newborn Infants. *Current Biology* 19, 1768–1772. <https://doi.org/10.1016/j.cub.2009.08.055>
- Golub, M.S., Hogrefe, C.E., Bulleri, A.M., 2016. Peer social interaction is facilitated in juvenile rhesus monkeys treated with fluoxetine. *Neuropharmacology* 105, 553–560. <https://doi.org/10.1016/j.neuropharm.2016.02.025>
- Hoksbergen, R., Laak, J. ter, Rijk, K., van Dijkum, C., Stoutjesdijk, F., 2005. Post-Institutional Autistic Syndrome in Romanian Adoptees. *J Autism Dev Disord* 35, 615–623. <https://doi.org/10.1007/s10803-005-0005-x>
- Sonuga-Barke, E.J.S., Kennedy, M., Kumsta, R., Knights, N., Golm, D., Rutter, M., Maughan, B., Schlotz, W., Kreppner, J., 2017. Child-to-adult neurodevelopmental and mental health trajectories after early life deprivation: the young adult follow-up of the longitudinal English and Romanian Adoptees study. *The Lancet* 389, 1539–1548. [https://doi.org/10.1016/S0140-6736\(17\)30045-4](https://doi.org/10.1016/S0140-6736(17)30045-4)

Introduction
 The pulvinar (PU) is a complex thalamic nucleus involved in high cognitive functions (Froesel et al. 2021). PU subregions are associated with different developmental trajectories; e.g. the inferior PU (Pul) is adult-like in function and cortical connectivity rapidly stabilizes after birth, whereas medial PU (PuM) maturation is more protracted and subject to individual variability. Adult anatomo-functional PU properties are associated with attention deficit & hyperactivity disorder (ADHD), autism spectrum disorders (ASD) & schizophrenia.
PU functional connectivity with cortex:
 1. Changes from childhood to adulthood?
 2. Impact of early social adversity on development?

Materials and method
Two groups: Peer-reared (n=9) and mother reared (n=11; control) rhesus macaques.
Methods: 3T resting-state fMRI under controlled gas anesthesia.
Assessment time points: Childhood (2,63y+/-0,06). Adolescence (3,75y +/-0,2). Early adulthood (4,9y +/-0,23).
Analysis: Linear Mixed-Effects Modelling (LME) on functional connectivity (FC) metrics.



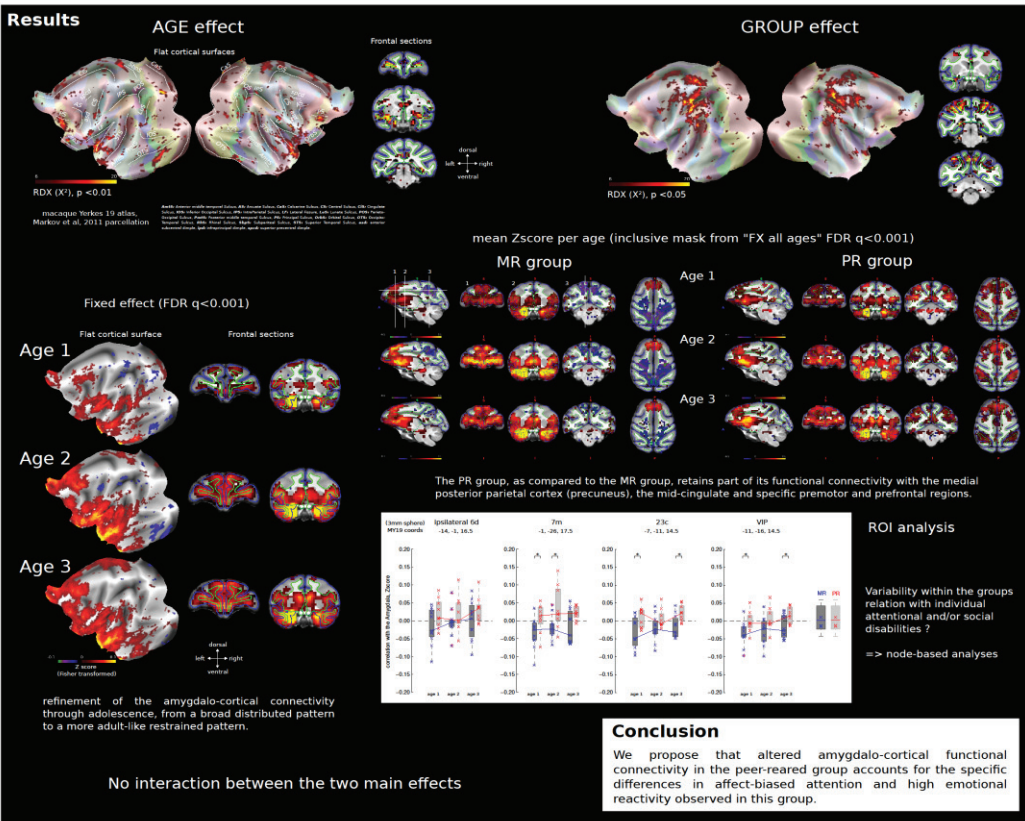
Discussion & Conclusion
 PuM is associated with multiple high level cognitive functions including action, decision-making and emotion regulation, while Pul is mostly involved in sensory perception. Here, developmental trajectories of PU FC with cortex varied between PuM and Pul. We found distinct developmental trajectories of PU with parietal, premotor, prefrontal and temporal cortex, initiated either before or after adolescence. Early adversity perturbed these trajectories, targeting specific functional networks. While developmental trajectories were mostly linear in mother-reared individuals, peer-reared individuals showed both stable (no change) or inverted U-shaped trajectories, indicating puberty related-brain changes in this group.

Froesel, M., Cappe, C., & Ben Hamed, S. (2021). A multisensory perspective onto primate pulvinal functions. *Neuroscience & Biobehavioral Reviews*. <https://doi.org/10.1016/j.neubiorev.2021.02.043> S03-021

Introduction
 Neuroimaging of the non-human social primate brain has been instrumental to forge our current understanding of primate social cognition. However, little is known to date on how this cognitive function develops from childhood into adolescence, and how early social adversity (ESA) interferes with typical brain functional developmental trajectories. Here, we used a longitudinal neuroimaging protocol and collected anesthetized resting-state fMRI data in 21 juvenile monkeys. We focus on the amygdala, a subcortical structure which plays a key role in socioemotional and attentional processing.

Material and Methods
 3T Resting state MRI acquisitions under anesthesia + MION injection
Control group : 11 Mother-reared (MR) macaques
ESA group : 9 Peer-reared (PR) macaques (Rayson et al, 2021)
3 Time points : - Childhood (age 1: 2,63y +/- 0,06)
 - Adolescence (age 2: 3,75y +/- 0,2)
 - Early adulthood (age 3: 4,9y +/- 0,23)
MRI anatomical procedure
 2 T1w + 1 T2w whole brain images
 Processing method using Matlab, AFNI, FSL, Freesurfer, ANTs and Connectome workbench (Adapted from Autio et al, 2020 and Seitz et al, 2017)
Resting state MRI procedure
 4 runs of 526 EPI images (28 slices, 1.5x1.5x1.6mm, TR = 1.7s, TE = 17ms)
 Processing method (using Matlab, AFNI and FSL)
 - Despiking - Slice time correction - Motion correction - Bias field correction
 - Non linear transformation to the individual reference T1w image and Skull-stripping
 - Non linear transformation to M19 atlas
 - Detrend - bandpass filter (0.01-0.1Hz), censoring - Regressing out head motion, mean white matter signal and ventricles signal
 - Blurring at 3 mm - Signal normalisation
 - Hand classification and removal of ICA noise component with MELODIC
FC Analysis :
 Left and Right Amygdala :

Seed-based correlation analysis per each run + Fisher's-to-Z score transformation
 T Test.
 "Right-to-left" transformation of Right Amygdala results.
Linear Mixed-Effects Modelling Approach analysis
 Random intercept and random slope : Age x Group + (1/Monkey)
 Random effects (RDX) : AGE, GROUP and AGExGROUP



Appendix 3: Diffusion imaging

In order to have another structural point of view on these structures across time-points, we also acquired diffusion imaging data. Diffusion imaging is a non-invasive MR technique which principle is to study the water molecules displacement in a given structure. Thus, in brain tissues, water molecules diffusion is dependent of the microstructure and of the organization of the living tissues. Thanks to differential orientations of the magnetic field gradient, the diffusion weighting (b-value) can be applied to specific directions (b-vector). Hence, if the water diffusivity is weak in a specific structure, the diffusion-weighting (DW) – MRI images will appear hyper signal, while if the diffusivity is strong, DW-MRI images will be in hypo signal. Acquiring different b-vectors (at least 6 non-collinear DWI-MRI images) and one non- DW image, permit to estimate diffusion tensor imaging (DTI). In order to avoid any susceptibilities and distortions, we acquired the diffusion imaging data at each time-points prior to injecting the MION contrast agent and after ensuring by blood sampling that the iron blood concentration was at a normal physiological level. In order to possibly detect any structural changes due to the plasticity induction, we used a 3D-multishot Echo Planar Imaging (3D-msEPI) sequence, developed in the team on anesthetized macaques (Tounekti et al., 2018). We will investigate these data in a close future. I was trained on macaque anesthesia at the MRI on this protocol, a competence I further used along my Ph.D. thesis for myelin mapping acquisitions or GABA spectroscopy, but also when participating in other projects, such as the macaques development project (Appendix 2) . Another project I took part related to diffusion imaging acquisition is the optimization of the previously developed 3D-msEPI sequence (Tounekti et al., 2018) by triggering MRI pulses synchronized with the macaque heart beat in order to reduce the susceptibilities ghosting artifacts induced by cardiovascular pulsations (**Appendix 3**). Once the cardiac cycle is known, the image diffusion acquisition can be trigger precisely during the diastolic period. This method allowed improving greatly the DTI imaging resolution by getting an artifact-free high-resolution DW-MRI imaging. Although I did not acquired data for my Ph.D. project thanks to this method, I nonetheless contributed here too to 8 macaques anesthesia and to this crucial maintenance of a stable cardiac rhythm while keeping track of their physiological constant to keep them sane, all along the acquisitions duration.

References

Tounekti, S., Troalen, T., Bihan-Poudec, Y., Froesel, M., Lamberton, F., Ozenne, V., Cléry, J., Richard, N., Descoteaux, M., Ben Hamed, S., Hiba, B., 2018. High-resolution 3D diffusion tensor MRI of anesthetized rhesus macaque brain at 3T. *NeuroImage* 181, 149–161. <https://doi.org/10.1016/j.neuroimage.2018.06.045>

High Resolution Triggered Three-Dimensional Diffusion MRI of Anesthetized Rhesus Macaque Brain

Yann Bihan-Poudec^{1,2}, Slimane Tounekti^{1,3}, Thomas Troalen⁴, Mathilda Froesel^{1,2}, Franck Lambertson^{5,6}, Maëva Gacoin^{1,2}, Nathalie Richard^{1,2}, Suliann Ben Hamed^{1,2} and Bassem Hiba^{1,2}

¹Institut des Sciences Cognitives Marc Jeannerod, CNRS UMR 5229, Université Lyon 1, Lyon, France

²Université Claude Bernard Lyon I, Villeurbanne, France

³Department of Radiology, Thomas Jefferson University, Philadelphia, PA, United States

⁴Siemens Healthcare SAS, Avenue des Fruitiers, Saint-Denis, France

⁵Cermep, Imagerie du Vivant Lyon, France

⁶SFR Santé Lyon-Est, CNRS UMS3453, INSERM US7, Université Lyon 1, Lyon, France

Corresponding Author:

Dr. Bassem Hiba

Institut des Sciences Cognitives - Marc Jeannerod, CNRS UMR 5229

67 Boulevard Pinel, 69676 Bron cedex

E-mail : bassem.hiba@cnrs.fr

Phone: +33 (0)4 37 91 12 25

Short title : Triggered 3D-dMRI of Macaque Brain

Word count : 3903

Number of figures : 6

Number of tables : 2

Keywords

- High resolution brain imaging
- Macaque brain
- Diffusion MRI
- Triggered diffusion MRI
- 3D Multi-shot EPI

Abstract

The macaque brain is a key model for neuroscience and medical research due to its strong homologies with the human brain. This study investigates the value of triggered 3D Echo-Planar-Imaging to achieve diffusion-MRI of anesthetized macaque brain with the high spatial-resolution typically used in post-mortem studies. The effects of cardiovascular-pulsations are also characterized by comparing triggered and untriggered diffusion-MRI.

Diffusion-MRI data were collected from 4 macaques at 3 Tesla. Cardiovascular-pulsations induce intershot phase-errors with a nonlinear spatial-distribution on diffusion-weighted images. These phase-errors are associated with signal loss and ghosting artifacts particularly in the brainstem, thalamus and cerebellum. Cardiovascular-triggering addresses these phase-errors and recovers images quality, diffusion tensor maps definition and tractography results. Triggered 3D Echo-Planar-Imaging provides diffusion tensor data of macaque brain with a spatial-resolution up to 400 microns, a resolution never achieved in-vivo before with this degree of quality. At this resolution, several substructures of the macaque brain, invisible at the standard resolution become discernible.

In conclusion, this study highlights the value of triggered 3D echo-planar imaging to provide high spatial resolution diffusion-MRI of the in-vivo macaque brain. To be suitable for routine studies, this pulse sequence must be coupled with appropriate techniques to significantly reduce acquisition duration.

1. Introduction

Diffusion Magnetic Resonance Imaging (dMRI) is a powerful tool for probing the microstructure and the connectivity of living cerebral tissues in normal and pathological conditions. Several reports have highlighted the benefits of high-resolution dMRI to characterize small anatomical structures of the brain (1,2) □, to enhance dMRI-based white-matter tractography (3,4) □, and also to define new prognostic biomarkers of pathological, pharmacological or physiological conditions (5) □.

When high-resolution dMRI is needed, the readout duration of echo-train collected using the standard 2D signal-shot Echo-Planar-Imaging (2D-ssEPI) becomes too long, which makes ssEPI very vulnerable to several artifacts (T_2^* decay, geometric distortions, susceptibility and eddy currents) and limits its ability to achieve high-resolution images. To avoid these undesirable effects, high-resolution dMRI can be performed using a multi-shot EPI (msEPI). In each shot, a fraction of the Fourier-space is recorded with a phase-error, induced by the head rigid-motions or by cardio-vascular pulsations occurring between spins excitation and echo-train acquisition. If not corrected, the inter-shot phase inconsistencies amplified by the application of diffusion-encoding gradients can result in serious artifacts on the diffusion-weighted (DW)-images (6,7) □. Additional inter-shot phase-errors are cumulated when a 3D sampling of Fourier-space is employed in order to enhance the Signal-to-Noise Ratio (SNR) (8-10) □. Thus, the large diffusion-weighting gradient pulses, which sensitize magnetic-resonance (MR)-signal to the microscopic diffusion of water spins, amplify inter-shot phase errors induced by the head rigid-motions and by the cardiovascular pulsations, and thus lead to aliasing artifact and/or signal loss when 3D-msEPI is used to collect dMRI data. 3D-msEPI must therefore always be coupled with an appropriate inter-shot phase errors correction strategy in order to obtain artifact-free dMRI data.

The first aim of this study is to investigate the benefits of 3D-msEPI acquisitions with cardiovascular triggering to achieve high-quality dMRI data of anesthetized macaque brain with a spatial resolution similar to those usually performed post-mortem. Indeed, in order to take full advantage of dMRI of the monkey brain, which has very strong functional and structural homologies with the human brain, several *ex-vivo* studies have reported very high-resolution dMRI of fixed macaque brain (see supplementary data S1). The spatial-resolution commonly used for *ex-vivo* studies is about 0.4 mm. While post-mortem dMRI is a major achievement and has brought important advances to the field, it does not maintain the non-invasive aspect of dMRI and excludes a wide range of longitudinal non-human primates studies in pharmacology and neurosciences. In addition, water diffusivity and core physiological properties of grey and white matter change as a result of brain fixation and the natural degradation of *ex-vivo* biological tissues (11)□.

Only two reports have described cerebral dMRI in anesthetized macaque at sub-millimetric cubic resolution. Janssens et al. developed a high sensitivity 8-channel array coils whose loops were implanted directly onto the skull of a macaque monkey. Using these invasive coils, diffusion tensor imaging (DTI) data of anesthetized macaque brain were collected at an isotropic spatial resolution of 0.7 mm (12)□. More recently, our group has non-invasively achieved DTI data of anesthetized macaque brain with an isotropic spatial-resolution of 0.5 mm using a 3D-msEPI dMRI pulse sequence (13)□. The study by Tounekti et al. also revealed the sensitivity of high spatial resolution 3D-msEPI dMRI of anesthetized macaque brain to the cardiac pulsation effects.

Human cerebral dMRI studies typically assume random translation and rotation of the head, whose effects on DW-images have been characterized as a phase-error with linear spatial dependence (6, 14, 15)□. Although cardiovascular pulsatility affects not only 3D-msEPI acquisitions but also standard 2D-ssEPI acquisitions (16, 17)□, the phase-errors it induces on brain DW-images have not been precisely characterized independently of the effects of rigid head motion. such a characterization could be crucial to develop and evaluate correction methods. To

our knowledge, only one study by O'Halloran et al. has attempted to characterize the effects of cardiovascular-pulsations on 2D-EPI dMRI data at a low spatial-resolution ($3.4 \times 3.4 \times 10 \text{ mm}^3$) and a low $b=250 \text{ s.mm}^{-2}$ after having corrected the effects of the head rigid-motions using an appropriate algorithm (18)□.

Thus, the second aim of this study is to accurately characterize intershot phase-errors induced by the cardio-vascular pulsations on anesthetized macaque brain DW-images collected at high-spatial resolution and with a standard diffusion-weighting ($b=1000$ to 1500 s.mm^{-2}). Imaging anesthetized Rhesus macaques, with the head carefully restrained in a stereotaxic frame, presents the advantage of significantly reducing the rigid bulk motion. We can thus focus on the characterization and the compensation of the physiological motion effects on 3D-msEPI dMRI. In this study, cerebral DW-images with a spatial-resolution of up to 400 microns were collected in anesthetized monkeys using 3D-msEPI. The effects of cardiovascular-pulsations were then analyzed by comparing triggered and untriggered DW-data.

2. Methods

This study was authorized by the French Ministry for Higher Education and Research (project no. 2016120910476056) in accordance with the French transposition texts of Directive 2010/63/UE. Four Rhesus monkeys were involved in this study (M1 is a 16 year old female weighing 7.02 kg; while M2 M3, and M4 are 14, 12, and 7 year old males weighing 7.20, 9.08, and 9.15 kg respectively). For each experiment, the subject was first injected with an intramuscular glycopyrrolate (Robinul-V, Vetoquinol, 5 mg/kg), and 10 min later, with ketamine (Ketamine 1000, Virbac, 10 mg/kg) to induce anesthesia. The monkey was then intubated and maintained with isoflurane at a concentration between 1.5 and 1.75%, and at a respiratory frequency of 20 resp/min. Electrocardiogram (ECG) electrodes were placed on the subject's thoracic cage and a pulse oximeter on its toe. The subject was finally placed in a sphinx position within a stereotaxic frame. Physiological parameters

(temperature and respiratory, heart, blood oxygenation and expired CO₂ rates) were monitored. The heart rate was maintained stable throughout the dMRI scan by adjusting the isoflurane concentration, respiratory volume and the temperature of the warming blanket.

dMRI scans were performed on a 3T Magnetom Prisma system (Siemens Healthineers, Germany). The whole-body coil was used for the Radio-Frequency (RF) transmission and three Siemens surface coils for MR-signal reception. Two 11 cm loop coils were placed on both sides of the head and a 7 cm loop coil on the top of the head ((13), Figure 1).

2.1. Triggered 3D-msEPI dMRI

A 3D-msEPI dMRI pulse sequence was used in this study (13) □. EPI readouts were used to scan the k -space in k_x and k_y . MR-signal collected from the slab was phase-encoded along k_z to generate a 3D k -space. The Stejskal-Tanner preparation scheme was then introduced to create diffusion-weighting (19) □. A binomial RF pulse was used to selectively excite water protons only (20) □. To reduce the echo-train duration (ETD) and echo-time (TE), each k_z plan (k_{xy} -space) was sampled through numerous interleaved segments, each sampled with one EPI-readout (13) □. Partial-Fourier was used in k_y to reduce the ETD and the TE, and in k_z to shorten acquisition time. Finally, an 1D echo-navigator, of 3 k_y lines at the central k -space, is acquired for each shot before the diffusion preparation. It was used to estimate and to correct for the shift between forwarded and reflected EPI-echoes. The k -space orientations k_x , k_y and k_z were set respectively to left-right, posterior-anterior and inferior-superior directions based on the brain frame, which Corresponding respectively to the X , Z and Y axis of the MR scanner. The 3D-msEPI dMRI pulse sequence was used in triggered mode, such that Fourier-space partition sampling was time-locked to a specific period of the cardiac cycle. Since ECG-signal is very vulnerable to electromagnetic interference, the peripheral-pulse oximeter was used for the gating of dMRI-acquisition. ECG-signal was only used before each scan to estimate the delay required to achieve peripheral gating. A

trigger-delay of 70% of the interval elapsed between two successive R-waves of the QRS signal on the electrocardiogram (R - R interval) is used in this study (See supplementary data S2). dMRI-acquisition was triggered once every two cardiac cycles leading to a repetition-time (TR) value between 1 and 2 s which is the efficient range of TR for 3D-dMRI acquisitions (21)□.

2.2. Diffusion-MRI acquisitions

Two sets of dMRI acquisitions were performed with two complementary goals:

2.2.1 Investigate the value of triggered 3D-msEPI for high-resolution DTI (Acq 1)

Triggered DTI data with a spatial-resolution of $0.4 \times 0.4 \times 0.4 \text{ mm}^3$ were collected in three monkeys (M1, M2 and M3). For each DTI data-set, twenty-one axial DW-images were acquired with a $b=1000 \text{ s.mm}^{-2}$ applied along non-collinear diffusion-encoding vectors generated using an electrostatic repulsion model (22)□. Supplementary data S3 contains the diffusion direction vectors used for these acquisitions. A b_0 -image, without diffusion-weighting, and a b_0 -image with a reversed phase-encoding direction (posterior-anterior) were also collected. The DTI was repeated twice in M3 monkey, once without and once with cardiovascular-triggering. The DTI acquisition and the physiological parameters are summarized in tables 1 and 2 (Acq. 1).

2.2.2. Investigate the effects of cardiovascular-pulsations on DW-images (Acq 2)

The aim of this second experiment was to characterize the intershot phase-errors induced by blood and cerebrospinal fluid (CSF) pulsations on DW-images. Eight repetitions of triggered and eight repetitions of untriggered DW-images were collected using 3D-msEPI in one macaque (Acq. 2 of tables 1 and 2). A relatively high diffusion-weighting ($b=1500 \text{ s.mm}^{-2}$) was applied to encode the water diffusivity along the inferior-superior orientation of the macaque brain which

corresponds to the Y axis of the MR scanner. This specific direction was chosen because it produces a high level of ghost artifacts and signal loss (21)□.

2.3. Data-processing

DW-images were reconstructed using the Gadgetron library (23)□ with a noise pre-whitening (24) and an iterative Cuppen/projection onto convex sets algorithm for partial-Fourier reconstruction before the inverse Fourier-transform (25)□. Off-resonance and eddy-currents effects of DTI-data were corrected using the Topup and Eddy tools from the FMRIB-Software Library (26,27)□. The tensor metrics maps (Fractional Anisotropy (FA), Mean Diffusivity (MD), Axial Diffusivity (AD) and Radial Diffusivity (RD)) were computed with Mrtrix3 (28)□. A denoising step was applied on DTI data data using the dwidenoise command of MRtrix3 (29).

Deterministic tractography of the medial cerebellum peduncle (MCP) and the inferior cerebellar peduncle (ICP) was performed using triggered and untriggered DTI data of M3. A sphere was defined as seeding region to generate 100,000 streamlines. A step size of 0.2 mm, an angle of 25° , and a FA cutoff of 0.28 were used for each tractogram.

2.4. Data analyses and statistics

The SNRs values of the Acq. 2 were computed as the ratio between the mean intensity assessed in a Region-Of-Interest (ROI) and the standard-deviation of the noise assessed in the image background (30). ROIs manually drawn on the right hemisphere, on the left hemisphere or central part of the brain are denoted hereafter with the subscript “l”, “r” and “c” respectively. White-Matter (WM) ROIs were manually drawn in the Splenium of the Corpus-Callosum (SCCl, SCCr and SCCc), in the Genu of the Corpus-Callosum (GCCc), in the Anterior Commissure (ACc), in the Posterior Thalamic Radiation (PTRl and PTRr) and in the Cingulum (CGL and CGr). Gray Matter (GM) ROIs were drawn in the Thalamus (THl and THr), in the Supramarginal Gyrus (SMGl and SMGr), in the Precentral Gyrus (PGL and PGr), in the central part of the Superior Temporal Gyrus (STGl and STGr), in the Inferior

part of the Superior Temporal Gyrus (iSTG1 and iSTGr) and in the Middle Temporal Gyrus (MTG1 and MTGr).

The ghosting artifacts of acquisition 1 were also evaluated as the Ghost to Signal Ratio (GSR) (2, 8), computed as:

$$\text{GSR} = S_g / S_b$$

where S_b and S_g are the mean-values of signal assessed in two ROIs drawn in the splenium of the corpus-callosum and in its ghost respectively.

Statistical analyses were performed with the R package. An ANOVA-2 test was performed to analyze effects of ROIs and triggering conditions for WM- and GM-ROIs. A unilateral non-parametric Wilcoxon test was then applied as post-hoc test for each ROI to compare the SNRs of the triggered and the untriggered-images.

3. Results

3.1. High-resolution DTI of macaque brain using triggered 3D-msEPI

Figure 1 presents axial views of DTI maps achieved with an isotropic spatial-resolution of 400 microns for 3 monkeys. The quality of these maps illustrates the feasibility of high-resolution DTI of anesthetized macaque brain using triggered 3D-msEPI.

The comparison between the triggered and untriggered diffusion-tensor maps of M3 shows that the benefits of the triggering are detectable mainly in the regions of the brain affected by cardiovascular-pulsations (brainstem, cerebellum and thalamus). For example, Figure 2 shows that the triggered cFA map reveals some substructures of the brainstem, such as Commissure of the Superior Colliculus (CSC), Superior Colliculus (SC), Central Gray of the Mid-brain (CGM), Medial Longitudinal Fasciculus (MLF), Decussation of the Superior Cerebellar Peduncle (DSCP), Anterior Pretectal Nucleus (ATP), Pontine Nuclei (Pn), Third Ventricle (3rd VT) and Reticulotegmental nucleus (RtTG), which remain difficult to delineate on the untriggered cFA map and indistinguishable at the standard DTI resolution of 1-2 mm. The brainstem sub-structures were defined according to the Neuromaps atlas (31,32). Axial views of triggered and untriggered cFA maps of M3 are also presented in the supplementary data S4.

Similarly, cardiovascular triggering appears to be highly beneficial to recover and better delineate the cerebellum WM bundles. Visually, an abnormal anisotropy of water diffusivity is observable on untriggered cFA map for a large anterior part of the cerebellum with a blue appearance (Figure 3). This abnormal anisotropy, oriented along the brain inferior-superior direction, could be induced by tissue displacements occurring in the same direction during cardiac cycle (18,21)□. The MCP and ICP tracks generated by tractography using the triggered dMRI data (Figure 4) were in agreement with those obtained ex-vivo by Calabrese et al (33)□. While the corresponding tracks, obtained using untriggered data, present numerous false-positives (Figure 4, red arrows) and true-negatives (Figure 4, pink arrows).

3.2. Effects of cardiovascular-pulsations on DW-images

Figure 5 illustrates the impact of cardiovascular-pulsations on macaque brain DW-images collected with a $b=1500 \text{ s.mm}^{-2}$ applied through the inferior-superior orientation. Cardiovascular pulsations corrupt phase-maps by a phase-error which presents a nonlinear spatial distribution and mainly localized in specific regions of the brain such as the brainstem, cerebellum and thalamus (Figure 5. A and C, untriggered phase-map). These phase-errors are negligible and have little to no effect on triggered phase-maps (Figure 5. A and C, triggered phase-map). Figure 5. B shows that in comparison with triggered DW-images, untriggered DW-images are corrupted by ghosting effects (green arrow) and also by signal dropout observed in brain regions suffering from nonlinear phase-errors ((brainstem (Figure 5. B, red arrow), cerebellum and thalamus (Figure 5. B, yellow arrow)). The measured GSR values revealed that triggering the 3D-msEPI significantly decreased the ghost level (from $16.5 \pm 10\%$ for the 8 non-triggered DW-images to $4.7 \pm 4.2\%$ for the 8 triggered DW-images ($p=0.007$)). Figure 5. D shows axial and coronal views of the ratio map between the mean of the 8 triggered DW-images and the mean of the 8 untriggered DW-images. This map illustrates the benefits of triggering to recover the signal dropout introduced by cardiovascular-pulsations in the brainstem, cerebellum and thalamus regions.

The signal recovery, achieved by the cardiovascular trigger, is confirmed by the ROI analysis summarized in Figure 6. Triggered DW-images present significantly higher SNR values in WM (2-way ANOVA trigger condition×ROIs: main effect of trigger condition $p=2.0 \times 10^{-16}$, main effect of ROI condition $p=2.0 \times 10^{-16}$). The superior SNR detected in triggered data is mainly driven by a SNR recovery occurring in the SCC ($p=7.8 \times 10^{-5}$, Mann-Whitney post-hoc test), and in the AC ($p=1.5 \times 10^{-5}$).

⁹). No significant effect of triggering in term of SNR was detectable in PTRl, PTRr, CGI, CGr and GCC. For GM-ROIs, a significant SNR recovery was only observed in the thalamus ROI of triggered DW-images (1-way ANOVA, main effect of trigger condition $p=3.0\times 10^{-4}$, Mann-Whitney post-hoc test, $p=5.0\times 10^{-4}$). No significant SNR differences were observed between triggered and untriggered data in the cortical GM-ROIs (2-way ANOVA trigger condition \times ROIs: main effect of trigger condition $p=0.33$, main effect of ROIs $p=2.0\times 10^{-16}$).

4. Discussion

This study proves the feasibility of high-resolution dMRI of anesthetized macaque monkey brain using triggered 3D-msEPI. To our knowledge, the spatial-resolution of 400 microns is the highest ever achieved in-vivo. In terms of voxel size, the resolution reached in this study (0.064 mm^3), is twice as high as the highest resolution (voxel size of 0.125 mm^3) reported in recent literature (13) \square .

Such a resolution of 0.4 mm allows the visualization and the investigation of very fine substructures of the brain, like that in the brainstem (Figure 2) and in the cerebellum (Figure 3), which are undetectable at the slandered resolution of 1-2 mm. Note that achieving dMRI with such spatial resolution is a very challenging issue, not only because of the small voxel size and thus the low SNR, but also because of the strong increase in TE and ETD, which exacerbates the T2/T2* decay and motion effects.

Cardiovascular-triggering enhances the diffusion-tensor maps sharpness and recovers its capacities to depict fine cerebral structure in the brainstem (Figure 2), in the cerebellum (figure 3) and in the thalamus (Supplementary data S4). No visual difference between triggered and untriggered diffusion-tensor maps was observed in other regions of the brain less affected by elastic tissue deformation.

Interestingly, cardiovascular pulsations could affect the tractography of white matter bundles that cross the brainstem, the cerebellum and the thalamus. For example, a miss-estimation of the fiber orientation distributions (FOD) was observed in the cerebellum region when untriggered dMRI is used (Figure 3). This leads to an increase of the false positive and the true negative tracts of the medial cerebellum peduncle and the inferior cerebellar peduncle. In contrast, these two bundles reconstructed using triggered data are similar to those ex-vivo tracted by Calabrese et al (33) \square .

Although the cardiovascular triggering of 3D-msEPI provides a clear improvement to the quality of DW-images, it also presents certain drawbacks. First, the cardiovascular triggering forces the TR to be a multiple of the R-R interval, which may increase the total acquisition time. Second, the R-R interval must be stable over the relatively long acquisition time. In this study, both of isoflurane concentration and animal temperature were regularly adjusted to maintain a constant R-R interval throughout the dMRI scans (Table 2). The mean standard deviation of the heart rate for all the triggered acquisitions achieved in this study is 1.4%.

Pulsatile brain tissue displacements, referred to here as nonrigid motions, result from the dynamics of blood and CSF flow during the cardiac cycle (34,35)□. In human, the largest movements occur during the systolic period of the cardiac cycle, mostly impacting the brainstem, with a peak velocity of the parenchyma in these regions reaching ~ 2 mm/s in the cranio-caudal direction. During this period, thalamic tissues are also compressed at velocities inferior to 1.5 mm/s in the cranio-caudal and medio-lateral directions (35)□. In the diastolic period, the brain recovers slowly its initial form.

The present study highlights the benefits of minimizing the effects of pulsatile displacements of brain tissue during the 3D-msEPI dMRI of anesthetized macaque brain by cardiovascular triggering. Since dMRI is performed on anesthetized macaques with the head held in a stereotactic frame, the intershot phase-errors induced by cardiovascular pulsatility were characterized in the almost complete absence of rigid head movements. Indeed, additional investigations not presented here were carried out in 3 anesthetized macaques (M2, M3 and M4) in order to estimate the amplitude of residual rigid movements of the head restrained in a stereotaxic frame. For each monkey, 3 acquisitions were performed in sagittal, coronal and axial orientations respectively to collect 197 volumes of 3 slices of the brain field of view (FOV=160×102 mm²; voxel-size=1.7×1.7×2.5 mm³) using a 2D-ssEPI pulse sequence (TR/TE=304/23.8 ms). The transformation matrices between successive images were computed among the 197 volumes using SPM (SPM12, <http://www.fil.ion.ucl.ac.uk/spm>) implemented in Matlab 9.1 (MathWorks, Inc., Natick, MA). These investigations confirm the negligibility of rigid movements (translations of 0.04±0.03 mm, 0.07±0.04 mm and 0.13±0.22 mm in left-right, posterior-anterior and inferior-superior orientations respectively, and rotations of 0.05±0.1°, 0.03±0.007° and 0.03±0.003° around left-right, posterior-anterior and inferior-superior axes respectively). These translation and rotation values were comparable to those measured using the 2D-EPI on an immobile phantom. The minor translation of the macaque brain in the inferior-

superior orientation (0.13 ± 0.22 mm) could be induced by mechanic vibrations or by residual respiratory effects.

This study shows that elastic pulsatile deformations of brain tissue introduce inter-shots inconsistencies to dMRI data collected using untriggered 3D-msEPI, which lead to phase-errors with nonlinear spatial dependence on the phase-maps (Figure 5, A and C). These phase-errors corrupt DW-images by ghosting artifacts and by MR-signal losses mainly located in brainstem, cerebellum and thalamus (Figure 5, B and D).

Several strategies have been developed for estimating and correcting phase-errors in multi-shot dMRI (8, 36, 37) □. In practice, model-based algorithms used to estimate inter-shot phase-errors work well for linear phase components induced by rigid head motion, but cannot reliably estimate nonlinear phase-errors induced by cardiac pulsatility (2) □. In this context, the anesthetized macaque brain could represent an interesting model to optimize multi-shot phase correction methods and to evaluate their effectiveness.

A pilot study, we conducted on the anesthetized macaque brain to determine the optimal delay between the R-wave and the trigger pulse, shows that nonlinear phase-errors are at their minimum amplitudes when data are collected either at the early beginning of the cardiac cycle (Trigger delay=0 s) or during the end-diastolic period of the cardiac cycle (Trigger delay=70–90% of the R-R interval) (see supplementary data S5). This range of optimal trigger delay is consistent with previous human studies (21, 38) □.

Quantitatively, the SNR measurements performed on the 8 triggered and the 8 untriggered DW-images collected at a spatial resolution of 0.5 mm and with $b=1500$ s.mm⁻² reveal significant signal dropout of WM and GM localized only in the brainstem, cerebellum and thalamus (Figure. 6). Cardiovascular triggering of 3D-msEPI reduced also the mean GSR value of the 8 untriggered DW-images from $16.5\pm 10\%$ to $4.7\pm 4.2\%$. The slight residual ghosts detected on triggered DW-images could be induced by mechanical vibrations generated in the MRI scanner during the data

acquisition, by B_0 -inhomogeneities and/or by Eddy currents (39) □. Such residual ghosts have been observed in phantom (Kiwi) images obtained using 3D-msEPI (GSR of $4.6 \pm 1.8\%$).

The very long acquisition time is the major drawback of a whole brain 3D-msEPI dMRI. In this study, 2h were needed to encode DTI data with 22 diffusion directions at the resolution of $0.4 \times 0.4 \times 0.4 \text{ mm}^3$. Such a long scan is impractical for routine neuroimaging studies and unfeasible for medical imaging. Various strategies could be employed to reduce the 3D-msEPI dMRI duration. In contrast to 2D-EPI, parallel imaging techniques can reduce 3D-EPI sampling of the Fourier-space simultaneously in both K_y and k_z directions, which could lead to a considerable reduction in acquisition time. For example, Narsude et al. have demonstrated the feasibility and the interest of 10-fold (2-fold in K_y and 5-fold in k_z) acceleration of 3D-msEPI for functional MRI (40) □. Furthermore, combining parallel imaging with other techniques to accelerate triggered 3D-msEPI dMRI, such as multi-slab method (9, 36, 41) □, zoomed field-of-view (42, 43), and/or simultaneous multi-slice (44) □, could lead to interesting trade-off between spatial-resolution, angular-resolution and acquisition time for human and primate applications.

5. Conclusion

Cardiovascular pulsations induce intershot phase-errors with a nonlinear spatial distribution on DW images of anesthetized macaque brains. These phase-errors are associated with MR-signal losses as well as with ghosting artifacts on the DW-images and with deteriorations of the DTI maps and of the tractography results, particularly in the brainstem, thalamus and cerebellum regions.

This study highlights the interest of triggered 3D-msEPI to address the effects of cardiovascular-pulsations and to provide in-vivo DW-images of the macaque brain with an isotropic spatial-resolution up to 400 microns.

To be suitable for imaging the human brain, the triggered 3D-mSEPI MRI approach must be coupled with appropriate techniques allowing the correction of head rigid movements and a significant acceleration of the acquisition.

6- References

1. Crombe A, Planche V, Raffard G, et al. Deciphering the microstructure of hippocampal subfields with in vivo DTI and NODDI: Applications to experimental multiple sclerosis. *Neuroimage* 2018;172:357–368 doi: 10.1016/j.neuroimage.2018.01.061.
2. Zhang H, Wang C, Chen W, et al. Deep learning based multiplexed sensitivity-encoding (DL-MUSE) for high-resolution multi-shot DWI. *Neuroimage* 2021;244:118632 doi: 10.1016/j.neuroimage.2021.118632.
3. Kamali A, Hasan KM, Adapa P, et al. Distinguishing and quantification of the human visual pathways using high-spatial-resolution diffusion tensor tractography. *Magn. Reson. Imaging* 2014;32:796–803 doi: 10.1016/j.mri.2014.04.002.
4. Steele CJ, Anwander A, Bazin P, et al. Human Cerebellar Sub-millimeter Diffusion Imaging Reveals the Motor and Non-motor Topography of the Dentate Nucleus. 2016:1–12 doi: 10.1093/cercor/bhw258.
5. Planche V, Panatier A, Hiba B, et al. Selective dentate gyrus disruption causes memory impairment at the early stage of experimental multiple sclerosis. *Brain. Behav. Immun.* 2017;60:240–254 doi: 10.1016/j.bbi.2016.11.010.
6. Anderson AW, Gore JC. Analysis and correction of motion artifacts in diffusion weighted imaging. *Magn. Reson. Med.* 1994;32:379–387 doi: 10.1002/mrm.1910320313.
7. Atkinson D, Porter DA, Hill DLG, Calamante F, Connelly A. Sampling and reconstruction effects due to motion in diffusion-weighted interleaved echo planar imaging. *Magn. Reson. Med.* 2000;44:101–109 doi: 10.1002/1522-2594(200007)44:1<101::AID-MRM15>3.0.CO;2-S.
8. Chang H-C, Hui ES, Chiu P-W, Liu X, Chen N. Phase correction for three-dimensional (3D) diffusion-weighted interleaved EPI using 3D multiplexed sensitivity encoding and reconstruction (3D-MUSER). *Magn. Reson. Med.* 2018;79:2702–2712 doi: 10.1002/mrm.26944.
9. Engström M, Skare S. Diffusion-Weighted 3D Multislab Echo Planar Imaging for High Signal-to-Noise Ratio Efficiency and Isotropic Image Resolution. *Magn. Reson. Med.* 2013;70:1507–1514 doi: 10.1002/mrm.24594.
10. Van AT, Hernando D, Sutton BP. Motion-induced phase error estimation and correction in 3D diffusion tensor imaging. *IEEE Trans. Med. Imaging* 2011;30:1933–1940 doi: 10.1109/TMI.2011.2158654.
11. D’Arceuil H, De Crespigny A. The effects of brain tissue decomposition on diffusion tensor imaging and tractography. *Neuroimage* 2007;36:64–68 doi: 10.1016/j.neuroimage.2007.02.039.
12. Janssens T, Keil B, Farivar R, et al. An implanted 8-channel array coil for high-resolution macaque MRI at 3T. *Neuroimage* 2012;62:1529–1536 doi: 10.1016/j.neuroimage.2012.05.028.

13. Tounekti S, Troalen T, Bihan-Poudec Y, et al. High-resolution 3D diffusion tensor MRI of anesthetized rhesus macaque brain at 3T. *Neuroimage* 2018;181:149–161 doi: 10.1016/j.neuroimage.2018.06.045.
14. Norris DG. Implications of bulk motion for diffusion-weighted imaging experiments: Effects, mechanisms, and solutions. *J. Magn. Reson. Imaging* 2001;13:486–495 doi: 10.1002/jmri.1072.
15. Trouard TP, Sabharwal Y, Altbach MI, Gmitro AF. Analysis and comparison of motion-correction techniques in Diffusion-Weighted Imaging. *J. Magn. Reson. Imaging* 1996;6:925–935 doi: 10.1002/jmri.1880060614.
16. Skare S, Andersson JLR. On the effects of gating in diffusion imaging of the brain using single shot EPI. *Magn. Reson. Imaging* 2001;19:1125–1128 doi: 10.1016/S0730-725X(01)00415-5.
17. Bopp MHA, Yang J, Nimsy C, Carl B. The effect of pulsatile motion and cardiac-gating on reconstruction and diffusion tensor properties of the corticospinal tract. *Sci. Rep.* 2018;8:11204 doi: 10.1038/s41598-018-29525-0.
18. O'Halloran RL, Holdsworth S, Aksoy M, Bammer R. Model for the correction of motion-induced phase errors in multishot diffusion-weighted-MRI of the head: Are cardiac-motion-induced phase errors reproducible from beat-to-beat? *Magn. Reson. Med.* 2012;68:430–440 doi: 10.1002/mrm.23245.
19. Stejskal EO, Tanner JE. Spin diffusion measurements: spin echoes in the presence of a time-dependent field gradient. *J. Chem. Phys.* 1965;42:288–292.
20. Hauger O, Dumont E, Chateil J-F, Moinard M, Diard F. Water Excitation as an Alternative to Fat Saturation in MR Imaging: Preliminary Results in Musculoskeletal Imaging. *Radiology* 2002;224:657–663 doi: 10.1148/radiol.2243011227.
21. Nunes RG, Jezard P, Clare S. Investigations on the efficiency of cardiac-gated methods for the acquisition of diffusion-weighted images. *J. Magn. Reson.* 2005;177:102–110 doi: 10.1016/j.jmr.2005.07.005.
22. Caruyer E, Lenglet C, Sapiro G, Deriche R. Design of multishell sampling schemes with uniform coverage in diffusion MRI. *Magn. Reson. Med.* 2013;69:1534–1540 doi: 10.1002/mrm.24736.
23. Hansen MS, Sørensen TS. Gadgetron: An open source framework for medical image reconstruction. *Magn. Reson. Med.* 2013;69:1768–1776 doi: 10.1002/mrm.24389.
24. Hansen MS, Kellman P. Image reconstruction: An overview for clinicians. *J. Magn. Reson. Imaging* 2015;41:573–585 doi: 10.1002/jmri.24687.
25. Haacke E., Lindskog E., Lin W. A fast, iterative, partial-fourier technique capable of local phase recovery. *J. Magn. Reson.* 1991;92:126–145 doi: 10.1016/0022-2364(91)90253-P.
26. Andersson JLR, Skare S, Ashburner J. How to correct susceptibility distortions in spin-echo echo-planar images: Application to diffusion tensor imaging. *Neuroimage* 2003;20:870–888 doi: 10.1016/S1053-8119(03)00336-7.

27. Andersson JLR, Sotiropoulos SN. An integrated approach to correction for off-resonance effects and subject movement in diffusion MR imaging. *Neuroimage* 2016;125:1063–1078 doi: 10.1016/j.neuroimage.2015.10.019.
28. Tournier JD, Calamante F, Connelly A. MRtrix: Diffusion tractography in crossing fiber regions. *Int. J. Imaging Syst. Technol.* 2012;22:53–66 doi: 10.1002/ima.22005.
29. Veraart J, Novikov DS, Christiaens D, Ades-aron B, Sijbers J, Fieremans E. Denoising of diffusion MRI using random matrix theory. *Neuroimage* 2016;142:394–406 doi: 10.1016/j.neuroimage.2016.08.016.
30. Dietrich O, Raya JG, Reeder SB, Reiser MF. Measurement of SNR in MR images. *J Magn Reson Imaging* 2007;26:375–385 doi: 10.1002/jmri.20969.
31. Rohlfing T, Kroenke CD, Sullivan E V., et al. The INIA19 Template and NeuroMaps Atlas for Primate Brain Image Parcellation and Spatial Normalization. *Front. Neuroinform.* 2012;6 doi: 10.3389/fninf.2012.00027.
32. Dubach MF, Bowden DM. BrainInfo online 3D macaque brain atlas: a database in the shape of a brain. In: *Society for Neuroscience Annual Meeting.* ; 2009. pp. 17–21.
33. Calabrese E, Badea A, Coe CL, et al. A diffusion tensor MRI atlas of the postmortem rhesus macaque brain. *Neuroimage* 2015;117:408–416 doi: 10.1016/j.neuroimage.2015.05.072.
34. Greitz D, Wirestam R, Franck A, Nordell B, Thomsen C, Stfihlberg F. Pulsatile brain movement and associated hydrodynamics studied by magnetic resonance phase imaging. *Neuroradiology* 1992;34:370–380 doi: 10.1007/BF00596493.
35. Poncelet BP, Wedeen VJ, Weisskoff RM, Cohen MS. Brain parenchyma motion: measurement with cine echo-planar MR imaging. *Radiology* 1992;185:645–651 doi: 10.1148/radiology.185.3.1438740.
36. Bruce IP, Chang HC, Petty C, Chen NK, Song AW. 3D-MB-MUSE: A robust 3D multi-slab, multi-band and multi-shot reconstruction approach for ultrahigh resolution diffusion MRI. *Neuroimage* 2017;159:46–56 doi: 10.1016/j.neuroimage.2017.07.035.
37. Zhang Z, Huang F, Ma X, Xie S, Guo H. Self-feeding MUSE: A robust method for high resolution diffusion imaging using interleaved EPI. *Neuroimage* 2015;105:552–560 doi: 10.1016/j.neuroimage.2014.10.022.
38. Holdsworth SJ, Skare S, Newbould RD, Guzmán R, Blevins NH, Bammer R. Readout-segmented EPI for rapid high resolution diffusion imaging at 3T. *Eur. J. Radiol.* 2008;65:36–46 doi: 10.1016/j.ejrad.2007.09.016.
39. Alhamud A., Taylor PA, van der Kouwe AJW, Meintjes EM. Real-time measurement and correction of both B0 changes and subject motion in diffusion tensor imaging using a double volumetric navigated (DvNav) sequence. *Neuroimage* 2016;126:60–71 doi: 10.1016/j.neuroimage.2015.11.022.

40. Narsude M, Gallichan D, Van Der Zwaag W, Gruetter R, Marques JP. Three-dimensional echo planar imaging with controlled aliasing: A sequence for high temporal resolution functional MRI. *Magn. Reson. Med.* 2016;75:2350–2361 doi: 10.1002/mrm.25835.
41. Wu W, Koopmans PJ, Frost R, Miller KL. Reducing slab boundary artifacts in three-dimensional multislab diffusion MRI using nonlinear inversion for slab profile encoding (NPEN). *Magn. Reson. Med.* 2016;76:1183–1195 doi: 10.1002/mrm.26027.
42. Gaggl W, Jesmanowicz A, Prost RW. High-resolution reduced field of view diffusion tensor imaging using spatially selective RF pulses. *Magn. Reson. Med.* 2014;72:1668–1679 doi: 10.1002/mrm.25092.
43. Jeong E-K, Kim S-E, Guo J, Kholmovski EG, Parker DL. High-resolution DTI with 2D interleaved multislice reduced FOV single-shot diffusion-weighted EPI (2D ss-rFOV-DWEPI). *Magn. Reson. Med.* 2005;54:1575–1579 doi: 10.1002/mrm.20711.
44. Setsompop K, Fan Q, Stockmann J, et al. High-resolution in vivo diffusion imaging of the human brain with generalized slice dithered enhanced resolution: Simultaneous multislice (gSlider-SMS). *Magn. Reson. Med.* 2018;79:141–151 doi: 10.1002/mrm.26653.

Acknowledgements: The authors would like to thank Mr. Maurin Sylvain for his precious help regarding the IT infrastructure.

Author contributions: Y.B-P. acquired the MRIs, reconstructed and analyzed the dMRI data, performed the statistical analyses, and contributed to the study design and the writing of the first draft. S.T developed the dMRI pulse sequence and contributed to the MRI acquisitions. T.T. contributed to the development of the pulse sequence and the design of the dMRI acquisition protocols. M.F. contributed to the MRI acquisitions and the anatomical and statistical analyses. F.L. contributed to the development of the pulse sequence and the design of the dMRI acquisition protocols. M.G contributed to the MRI acquisitions. N.R contributed to the reconstruction and analyses of the dMRI data. S.B.H. obtained the funding and contributed to the MRI acquisitions and the anatomical and statistical analyses. B.H. conceived the study, obtained the funding, designed the data acquisition and analyses and wrote the 1st draft. All authors contributed to the writing and have approved the final version of the manuscript.

Data availability statement: The datasets can be made available from the corresponding author on reasonable request.

Funding: This work was supported by public grants from the French Agence Nationale de la Recherche programs (TRAIL, ANR-10-LABX-57 to B.H. and ANR-19-CE37-0023-01 to S.B.H.). Y.B-P, MF and SBH were supported by a grant from the French Agence Nationale de la Recherche (ANR-16-CE37-0009-1 to S.B.H.).

Competing interests: Thomas Troalen is a Siemens Healthineers employee supporting MRI research customers for scientific and clinical developments. He is involved in the project referred to this manuscript as he supports the project for the MRI sequence developed in-house as well as the MR protocol setup.

Tables:

Table 1: dMRI pulse sequence parameters for each acquisition.

| <i>dMRI acquisitions</i> | <i>Resolution (mm³)</i> | <i>Matrix size (pixels)</i> | <i>b-value (s/mm²)</i> | <i># of shots</i> | <i>TR (R-R)</i> | <i>TE (ms)</i> | <i>k_y partial Fourier</i> | <i>k_z partial Fourier</i> | <i># of subjects</i> |
|--------------------------|------------------------------------|-----------------------------|-----------------------------------|-------------------|-----------------|----------------|--------------------------------------|--------------------------------------|----------------------|
| Acq. 1 | 0.4×0.4×0.4 | 304×254×128 | 1000 | 4 | 2 | 82 | 0.63 | 0.75 | 3 |
| Acq. 2 | 0.5×0.5×1.0 | 250×212×112 | 1500 | 3 | 2 | 74 | 0.75 | 0.75 | 1 |

Table 2: Summary of all the acquisitions performed in this study. The Mean±SD of the heart rate are presented for each acquisition.

| <i>dMRI Acquisitions</i> | <i>Subject</i> | <i>Isoflurane concentration (%)</i> | <i>Trig</i> | <i>Cardiac rate (bpm)</i> | <i>TR (ms)</i> | <i>Total acquisition time</i> |
|--------------------------|----------------|-------------------------------------|-------------|---------------------------|----------------|-------------------------------|
| Acq. 1 | M1 | 1.55-1.7 | Yes | 111 ± 1.1 | 2×RR | 1h53mn54 |
| | M2 | 1.5-1.75 | Yes | 114 ± 2.0 | 2×RR | 1h57mn45 |
| | M3 | 1.5-2 | No | 109 ± 2.3 | 1200 | 2h6mn57 |
| | M3 | 1.5-1.75 | Yes | 115 ± 1.7 | 2×RR | 1h58mn3 |
| Acq. 2 | M4 | 1.5 | No | 118 ± 0.5 | 1000 | 17mn |
| | M4 | 1.5 | Yes | 119 ± 1.6 | 2×RR | 17mn7 |

Figure 1: Axial views of diffusion tensor maps (colored Fractional Anisotropy (cFA), Mean Diffusivity (MD), Axial Diffusivity (AD) and Radial Diffusivity (RD)) of 3 anesthetized macaque brains (M1, M2 and M3) achieved using triggered 3D multi-shot EPI at an isotropic spatial-resolution of 400 microns and with $b=1000 \text{ s.mm}^{-2}$. Color scales are indicated on the right.

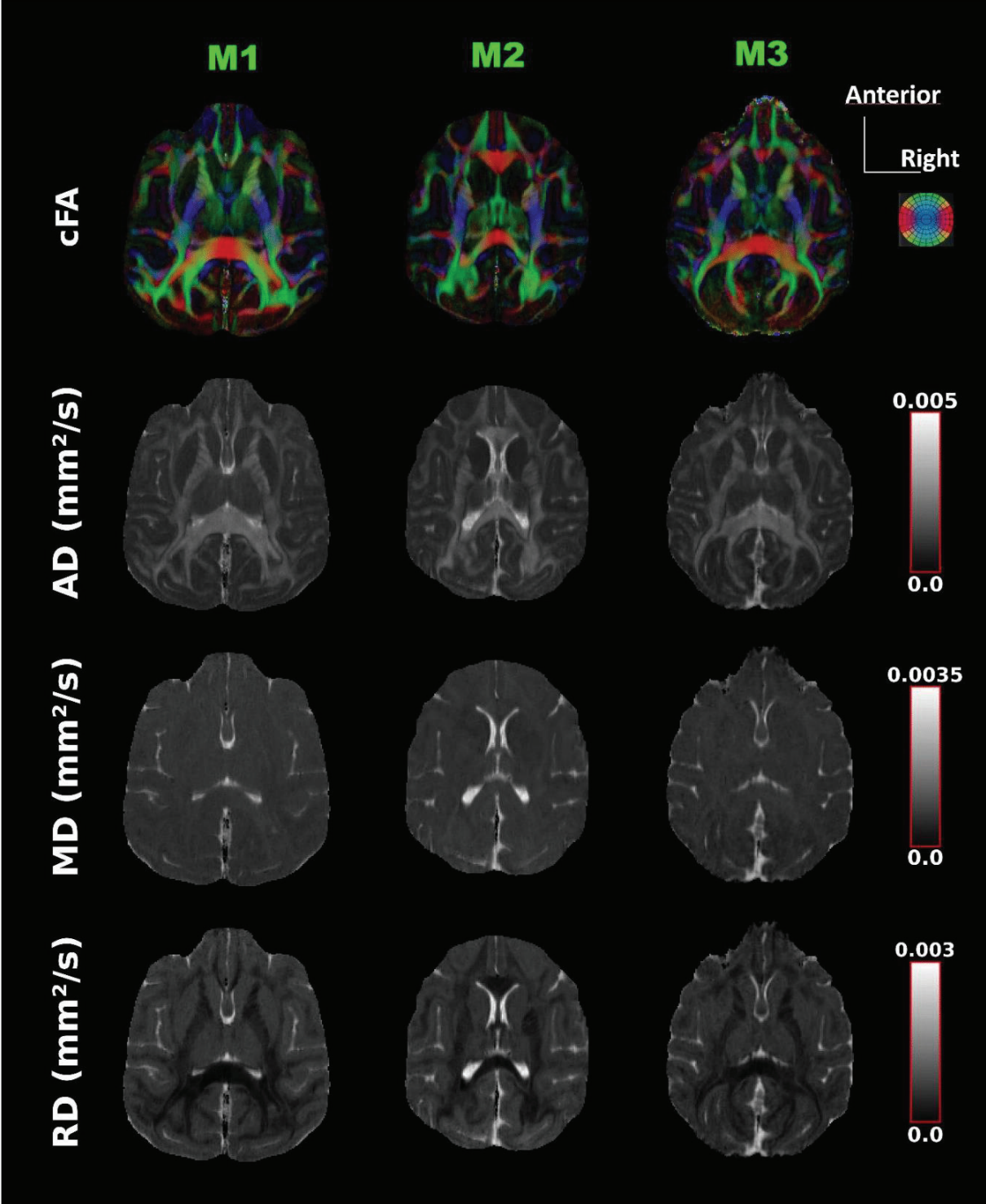


Figure 2: Coronal views of triggered and untriggered Fractional Anisotropy (FA) and colored Fractional Anisotropy (cFA) maps of macaque brain achieved with an isotropic resolution of 400 microns and the corresponding slices of the Neuromap atlas. The zoom shows that the triggered cFA map reveals some substructures of the brainstem, such as Commissure of the Superior Colliculus (CSC), Superior Colliculus (SC), Central Gray of the Mid-brain (CGM), Medial Longitudinal Fasciculus (MLF), Decussation of the Superior Cerebellar Peduncle (DSCP), Anterior Pretectal Nucleus (ATP), Pontine Nuclei (Pn), Third Ventricule (3rd VT) and Reticulotegmental nucleus (RtTG), which remain difficult to delineate on the untriggered cFA map and indistinguishable at the standard DTI resolution of 1–2 mm. To locate the coronal sections in the brain, landmarks are identified: the Intraparietal Sulcus (IPS), Middle Temporal Gyrus (MTG), Medial Pulvinar (PM), Lateral Pulvinar (PL) and Inferior Pulvinar (PI).

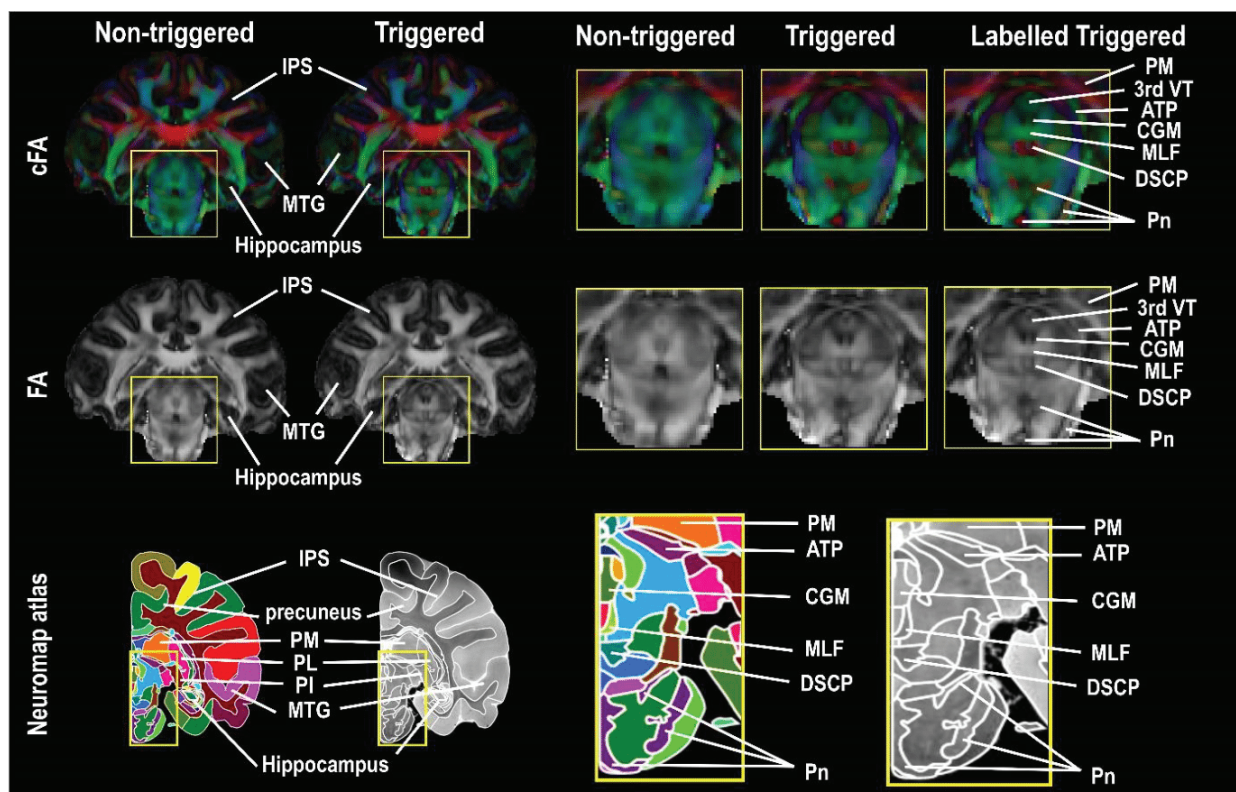


Figure 3: Sagittal views of triggered and untriggered cFA (colored Fractional Anisotropy) maps of macaque brain achieved with spatial resolution of 400 microns. A focus on the cerebellum reveals a blurring covering the complex anatomy of the cerebellum's white matter when DTI maps are generated using untriggered 3D multi-shot EPI.

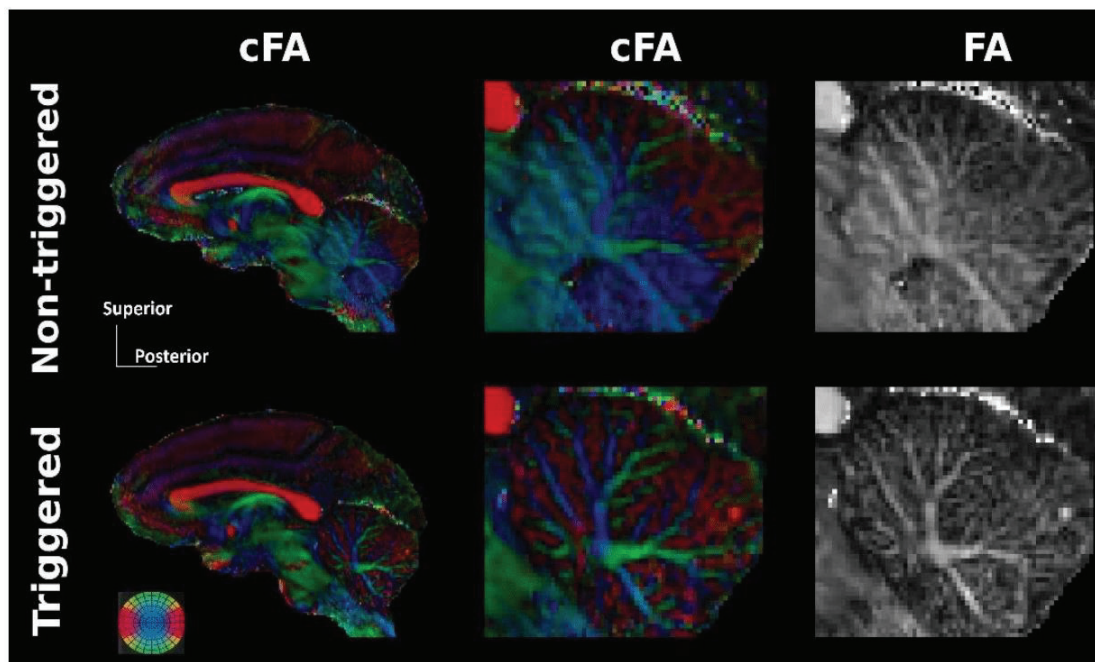


Figure 4: Tractograms of macaque middle cerebellum Peduncle (MCP) and inferior cerebellum Peduncle (ICP). In comparison to the triggered tractograms, the red and the pink arrows indicate respectively the false positives and true negatives generated by the untriggered data.

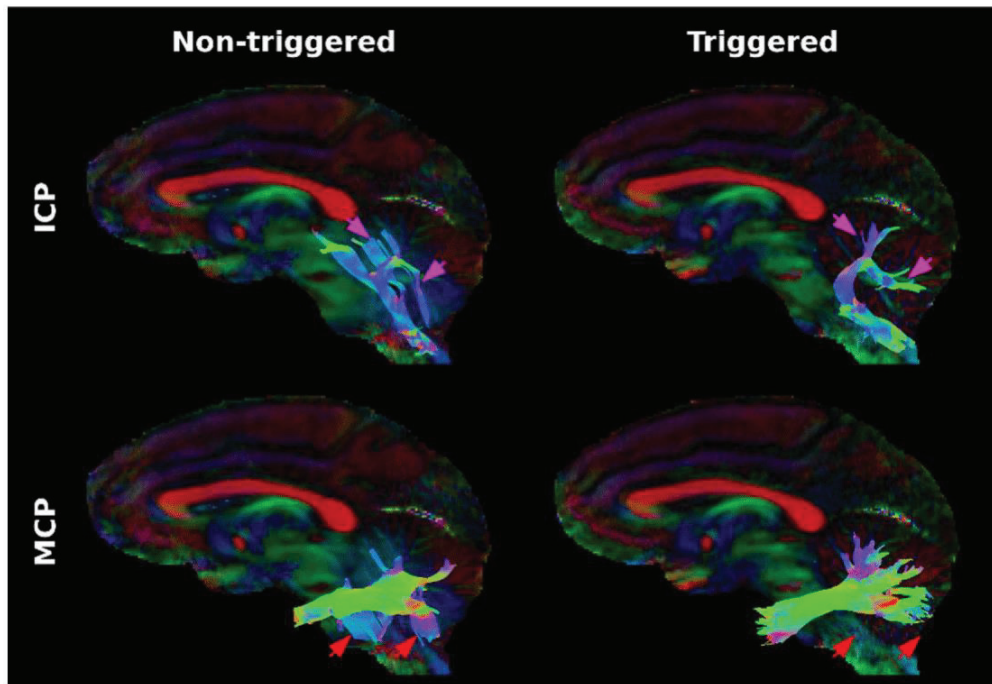


Figure 5: Coronal and axial views of phase-maps (A) and magnitude-maps (B) of anesthetized macaque brain acquired with a $b=1500 \text{ s. mm}^{-2}$ using 3D-msEPI. Untriggered magnitude-maps suffer from significant signal losses (yellow and red arrows) and ghosting artifacts (green arrow). The phase curves, corresponding to the red line defined on A show the intershot phase-errors with nonlinear space dependence, induced by the cardiovascular pulsations only on the untriggered images (C). The triggered to untriggered magnitude ratio map illustrates the signal loss due to cardiovascular-pulsations (D).

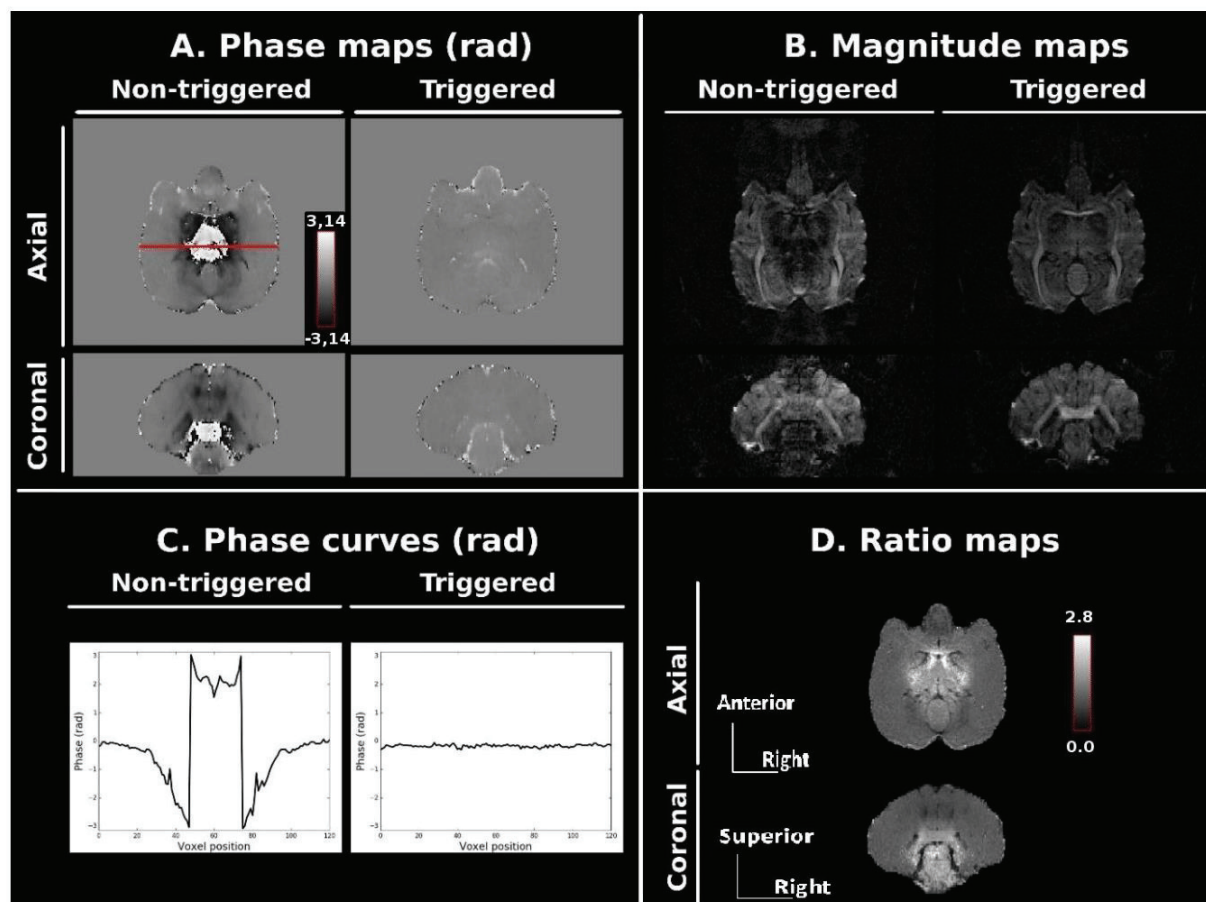
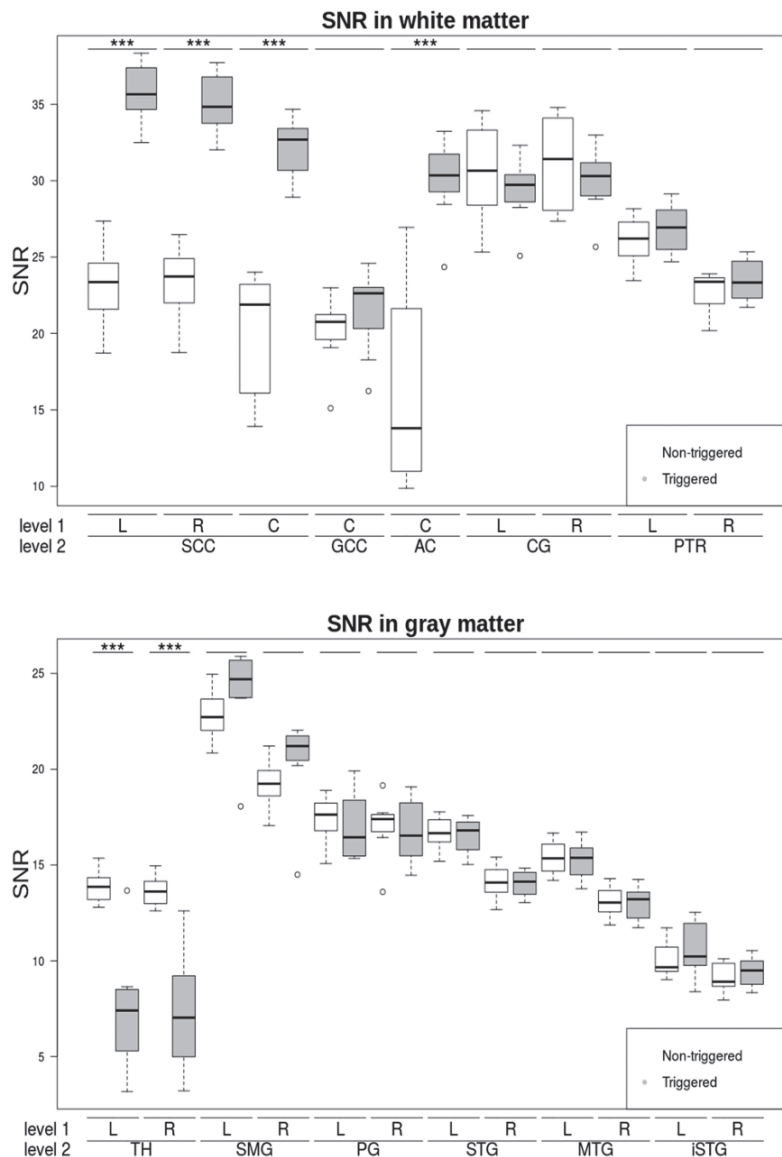


Figure 6: Mean and standard deviation values of SNR assessed from 8 triggered and the 8 untriggered DW-images of macaque brain acquired with a $b=1500 \text{ s.mm}^{-2}$ and with a spatial resolution of 500 microns for white-matter ROIs (Splenum of the Corpus Callosum (SCC), Genu of the Corpus Callosum (GCC), Anterior Commissure (AC), Cingulum (CG), and Posterior Thalamic Radiation (PTR)) and for gray-matter ROIs (Thalamus (TH), Supramarginal Gyrus (SMG), Precentral Gyrus (PG), Superior Temporal Gyrus (STG) and Middle Temporal Gyrus (MTG)). The hemispheric position is indicated by L (left), R (right) and C (center). (*): $p\text{-value} < 0.05$, (*): $p\text{-value} < 0.01$ and (***) : $p\text{-value} < 0.001$ were obtained with a Wilcoxon



statistical test between the non-triggered (white boxplots) and the triggered (gray

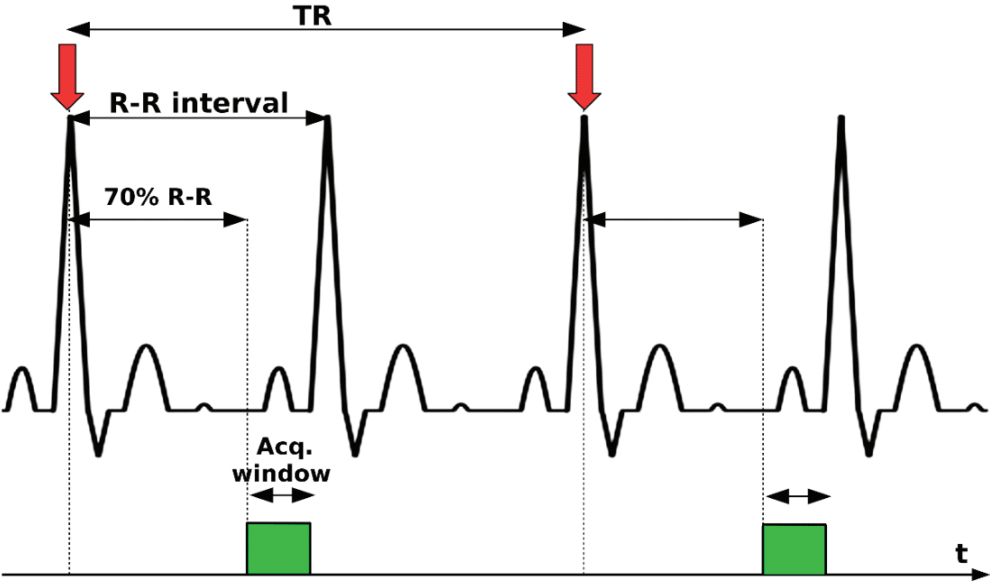
boxplots) SNR.

Supplementary Data

Supplementary Data S1. Ex-vivo and sub-millimetric in-vivo dMRI studies performed in macaque monkey models.

| Reference | Resolution (mm) | Diffusion directions | B-value (s.mm⁻²) | Acquisition time (h) | B0-field (Tesla) | Study type |
|-----------------------------|------------------------|-----------------------------|------------------------------------|-----------------------------|-------------------------|-------------------|
| D'Arceuil et al., 2007 (1) | 0.425 | 20 | 4025 | 25 | 4.7 | Ex-vivo |
| Wedeen et al., 2008 (2) | 0.512 | 515 | Up to 40000 | 36 | 4.7 | Ex-vivo |
| Calabrese et al., 2014 (3) | 0.4 | 120 | 4000 | – | 7 | Ex-vivo |
| Thomas et al., 2014 (4) | 0.25 | 121 | 4800 | 71 | 7 | Ex-vivo |
| Reveley et al., 2015 (5) | 0.25 | 126 | 4800 | 61 | 7 | Ex-vivo |
| Calabrese et al., 2015 (6) | 0.15 | 20 | 1500 | 46 | 7 | Ex-vivo |
| Azadbakht et al., 2015 (7) | 0.43 | 120 | 8000 | 27 | 4.7 | Ex-vivo |
| Donahue et al., 2016 (8) | 0.43 | 120 | 8000 | 27 | 4.7 | Ex-vivo |
| Catani et al., 2017 (9) | 0.5 | 61 | 4310 | – | 4.7 | Ex-vivo |
| Schilling et al., 2019 (10) | 0.3 | 31 | 1200 | 50 | 9.4 | Ex-vivo |
| Janssens et al., 2012 (11) | 0.7 | 256 | 1000 | 3 | 3 | In-vivo |
| Tounekti et al., 2018 (12) | 0.5 | 30 | 1000 | 2.2 | 3 | In-vivo |
| Current study | 0.4 | 22 | 1000 | 2 | 3 | In-vivo |

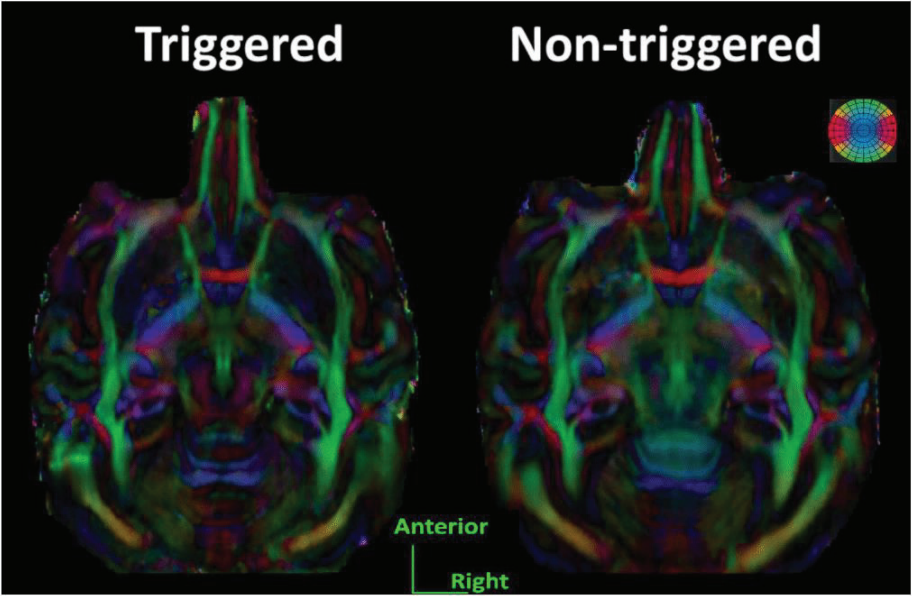
Supplementary Data S2. Triggering schema used with 3D multishot EPI diffusion MRI pulse sequence. Each EPI shot is gated in the end-diastolic phase of cardiac cycle, at a delay corresponding to 70% of the R-R interval (green). The acquisition was triggered once every two cardiac cycles.



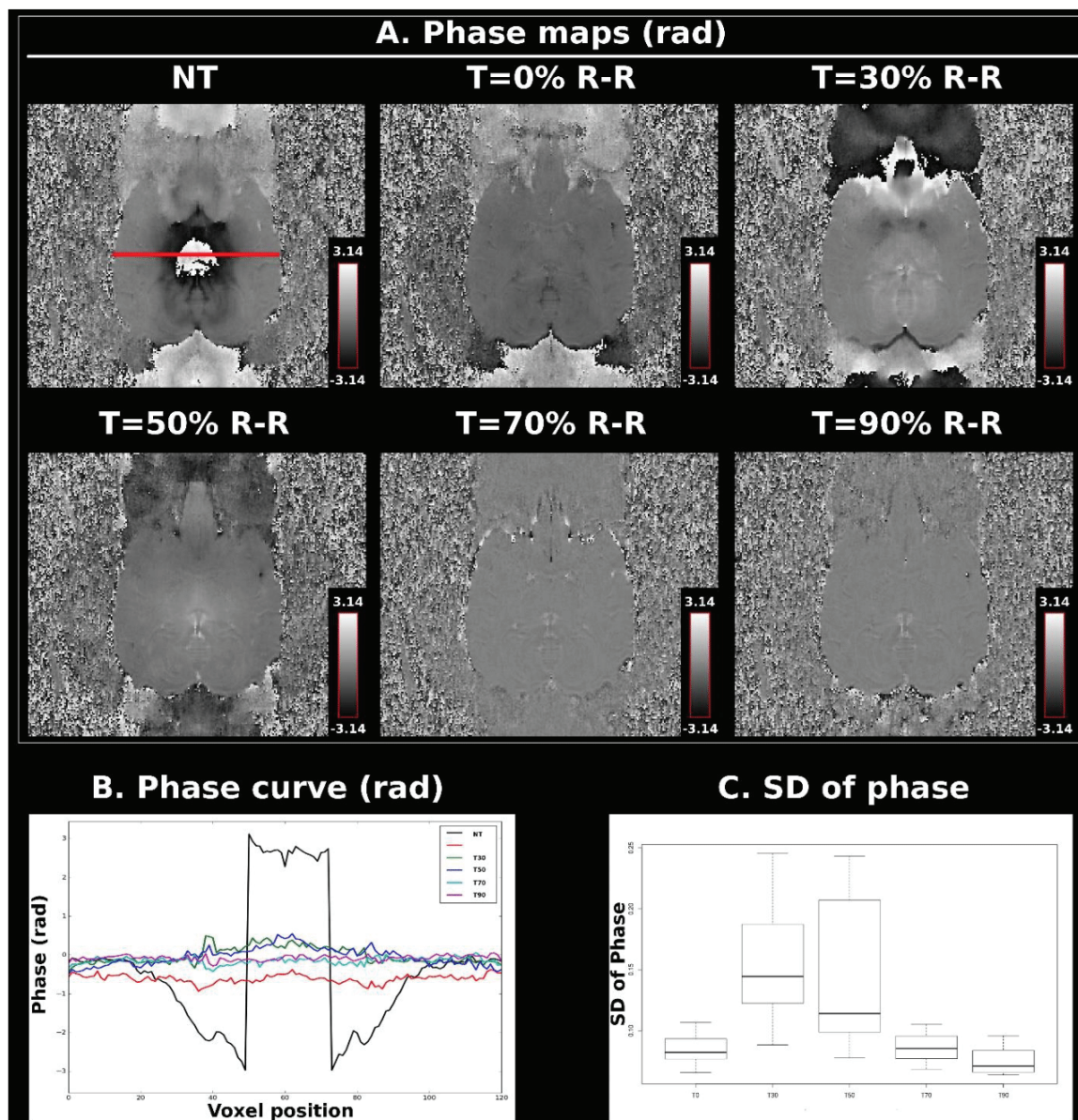
Supplementary Data S3. The diffusion direction vectors used for the DTI acquisition (Table 2).

| Diffusion vector | X | Y | Z |
|-------------------------|----------|----------|----------|
| 1 | 0.061 | 0.958 | 0.281 |
| 2 | -0.989 | 0.096 | -0.114 |
| 3 | -0.132 | -0.272 | 0.953 |
| 4 | -0.616 | 0.448 | 0.648 |
| 5 | -0.647 | -0.711 | 0.276 |
| 6 | -0.569 | -0.182 | -0.802 |
| 7 | -0.453 | 0.788 | -0.417 |
| 8 | -0.023 | -0.54 | -0.841 |
| 9 | 0.826 | 0.183 | -0.533 |
| 10 | 0.096 | 0.85 | -0.518 |
| 11 | 0.754 | 0.554 | 0.353 |
| 12 | 0.714 | -0.694 | -0.088 |
| 13 | 0.523 | -0.356 | 0.775 |
| 14 | 0.409 | -0.095 | -0.908 |
| 15 | 0.451 | 0.883 | 0.131 |
| 16 | -0.836 | 0.375 | -0.402 |
| 17 | 0.352 | -0.827 | -0.438 |
| 18 | 0.468 | 0.526 | -0.71 |
| 19 | 0.948 | 0.315 | -0.038 |
| 20 | 0.172 | 0.098 | 0.98 |
| 21 | 0.181 | -0.977 | 0.109 |

Supplementary Data S4. Axial views of triggered and untriggered colored fractional anisotropy (cFA) maps of macaque brain achieved with an isotropic spatial resolution of 400 microns.



Supplementary Data S5. A. The phase maps of the additional DW-images, collected using the Acq.1 protocol without triggering (NT) and with the trigger delay set at $T=0\%$, 30% , 50% , 70% and 90% of the R-R interval respectively, show the drastic decrease in nonlinear phase errors produced thanks to cardiovascular triggering. B. Phase curves plotted for the red line, defined through the brain on the non-triggered phase map. C. The values of the standard deviations, computed for the phase curves plotted in B and averaged over the 8 repeats, show that the nonlinear phase errors reach minimum values with a trigger delay of 0% , 70% or 90% of the R-R interval.



References to supplementary **Data**

1. D'Arceuil HE, Westmoreland S, de Crespigny AJ. An approach to high resolution diffusion tensor imaging in fixed primate brain. *Neuroimage* 2007;35:553–565 doi: 10.1016/j.neuroimage.2006.12.028.
2. Wedeen VJ, Wang RP, Schmahmann JD, et al. Diffusion spectrum magnetic resonance imaging (DSI) tractography of crossing fibers. *Neuroimage* 2008;41:1267–1277 doi: 10.1016/j.neuroimage.2008.03.036.
3. Calabrese E, Badea A, Coe CL, Lubach GR, Styner MA, Johnson GA. Investigating the tradeoffs between spatial resolution and diffusion sampling for brain mapping with diffusion tractography: Time well spent? *Hum. Brain Mapp.* 2014;35:5667–5685 doi: 10.1002/hbm.22578.
4. Thomas C, Ye FQ, Irfanoglu MO, et al. Anatomical accuracy of brain connections derived from diffusion MRI tractography is inherently limited. *Proc. Natl. Acad. Sci.* 2014;111:16574–16579 doi: 10.1073/pnas.1405672111.
5. Reveley C, Seth AK, Pierpaoli C, et al. Superficial white matter fiber systems impede detection of long-range cortical connections in diffusion MR tractography. *Proc. Natl. Acad. Sci.* 2015;112:E2820–E2828 doi: 10.1073/pnas.1418198112.
6. Calabrese E, Badea A, Coe CL, et al. A diffusion tensor MRI atlas of the postmortem rhesus macaque brain. *Neuroimage* 2015;117:408–416 doi: 10.1016/j.neuroimage.2015.05.072.
7. Azadbakht H, Parkes LM, Haroon HA, et al. Validation of high-resolution tractography against in Vivo tracing in the macaque visual cortex. *Cereb. Cortex* 2015;25:4299–4309 doi: 10.1093/cercor/bhu326.
8. Donahue CJ, Sotiropoulos SN, Jbabdi S, et al. Using Diffusion Tractography to Predict Cortical Connection Strength and Distance: A Quantitative Comparison with Tracers in the Monkey. *J. Neurosci.* 2016;36:6758–6770 doi: 10.1523/jneurosci.0493-16.2016.
9. Catani M, Robertsson N, Beyh A, et al. Short parietal lobe connections of the human and monkey brain. *Cortex* 2017;97:339–357 doi: 10.1016/j.cortex.2017.10.022.
10. Schilling KG, Nath V, Hansen C, et al. Limits to anatomical accuracy of diffusion tractography using modern approaches. *Neuroimage* 2019;185:1–11 doi: 10.1016/j.neuroimage.2018.10.029.
11. Janssens T, Keil B, Farivar R, et al. An implanted 8-channel array coil for high-resolution macaque MRI at 3T. *Neuroimage* 2012;62:1529–1536 doi: 10.1016/j.neuroimage.2012.05.028.
12. Tounekti S, Troalen T, Bihan-Poudec Y, et al. High-resolution 3D diffusion tensor MRI of anesthetized rhesus macaque brain at 3T. *Neuroimage* 2018;181:149–161 doi: 10.1016/j.neuroimage.2018.06.045.